

**APPLYING ARYLTRIFLUOROBORATES AS PET IMAGING AGENTS**

by

YING LI

M.Sc., Nanjing University, 2006

B.Sc. (Honours), Nanjing University, 2003

A THESIS SUBMITTED IN PARTIAL FULFILLMENT OF THE  
REQUIREMENTS FOR THE DEGREE OF

DOCTOR OF PHILOSOPHY

in

THE FACULTY OF GRADUATE STUDIES

(Chemistry)

THE UNIVERSITY OF BRITISH COLUMBIA

(Vancouver)

January 2012

© Ying Li, 2012

## Abstract

This dissertation is focused on applying aryltrifluoroborates ( $\text{ArBF}_3\text{s}$ ) as PET imaging agents. Several aspects of this new  $^{18}\text{F}$ -labeling technique are addressed. These include the hydrolytic stability of heteroaryltrifluoroborates ( $\text{HetArBF}_3\text{s}$ ), the fluoridation of arylboronic acids/esters and the radiosyntheses of several  $^{18}\text{F}$ - $\text{ArBF}_3$  labeled biomolecules for potential PET imaging applications. The solvolysis of several *N*- $\text{HetArBF}_3\text{s}$  under physiological conditions was studied with  $^{19}\text{F}$  NMR spectroscopy in Chapter 2. All the *N*- $\text{HetArBF}_3\text{s}$  tested therein displayed excellent solvolytic stability under physiological conditions. It is expected that these  $\text{HetArBF}_3\text{s}$  can be further applied as  $^{18}\text{F}$ -labeled PET imaging agents.

In Chapter 3, a rapid fluoridation was carried out under conditions with low fluoride concentrations in a short reaction time ( $\sim$  one hour). Via TLC-fluorescent densitometry,  $^{19}\text{F}$  NMR spectroscopy, and radio-HPLC, the fluoridation of different arylboronic acids/esters was investigated. It was found that the fluoridation occurs relatively rapidly in the presence of 3 to 5 equivalents of fluoride in acidic aqueous  $\text{CH}_3\text{CN}$  at room temperature. Under such conditions, radiochemical yields of 20-30% can be achieved. It was also noticed that arylboronates with acid-sensitive protecting groups could undergo fluoridations rapidly comparable to the arylboronic acids.

In Chapter 4, marimastat, an MMP inhibitor, was labeled with an  $^{18}\text{F}$ - $\text{ArBF}_3$  to image breast cancer in mice. An unoptimized isolated radiochemical yield of  $\sim$  1.5% and specific activities of 0.179 and 0.396  $\text{Ci}/\mu\text{mol}$  were obtained within two hours including packaging. The blocking experiment suggested that the tumor uptake of  $\text{Mar-}^{18}\text{F-ArBF}_3$  was MMP specific. This one-step aqueous fluoridation was also applied to label a urea-based PSMA inhibitor (Chapter 5) and RGD-containing cyclopeptides (Chapter 8). Radiochemical yields ranging from 10% to 25% were obtained within one hour and good HPLC separation was achieved. In addition, a one-pot two-step labeling strategy was developed in Chapter 6 to label acid-sensitive biomolecules with  $^{18}\text{F}$ - $\text{ArBF}_3\text{s}$ . The copper(I) catalyzed 1,3-dipolar cycloaddition was successfully used to conjugate  $^{18}\text{F}$ - $\text{ArBF}_3\text{s}$  with biomolecules including oligonucleotides (Chapter 6), folate (Chapter 7), and a cyclic RGD-peptide (Chapter 8) with radiochemical yields of 20-30% over two steps in one hour.

## Preface

The projects presented in this dissertation are done in collaboration with many people. Therefore, “we” and “our” are used in many parts of this thesis. Throughout the whole dissertation, Dr. David M. Perrin and I designed most of the projects and set the goals of this thesis together. I have performed the majority of the work presented in this dissertation, and any contribution from other people is described in this section. Papers already published or manuscripts based on the work in this thesis were co-written by Dr. Perrin and me. Former students in the Perrin lab carried out a small number of the reactions presented as data in this thesis and their contribution will be stated in this part.

The study presented in Chapter 2 was published in *J. Fluorine Chem.* in 2008 as “Hydrolytic Stability of Nitrogenous-Heteroaryltrifluoroborates under Aqueous Conditions at Neutral pH”. In this work, Dr. Ali Asadi prepared boronate ester **2.4**. I synthesized all the other boronic acids/esters and prepared all the heteroaryltrifluoroborates (HetArBF<sub>3</sub>s). I also performed the <sup>19</sup>F NMR experiments and data analysis.

The work in Chapter 4 was published in *Cancer Res.* in 2010 as “Novel Matrix Metalloproteinase Inhibitor [<sup>18</sup>F]Marimastat-Aryltrifluoroborate as a Probe for *in vivo* Positron Emission Tomography Imaging in Cancer” and *Med. Chem. Comm.* in 2011 as “Towards kit-like <sup>18</sup>F-labeling of marimastat, a noncovalent inhibitor drug for *in vivo* PET imaging cancer associated matrix metalloproteases” respectively in collaboration with Dr. Christopher M. Overall. Dr. Perrin and Dr. Overall initiated this collaboration in order to image breast cancer with marimastat-<sup>18</sup>F-aryltrifluoroborate (Mar-<sup>18</sup>F-ArBF<sub>3</sub>) **4.15**. Dr. Curtis Harwig designed and accomplished the initial synthesis of marimastat-arylboronate **4.14** and the fluorescent marimastat-FITC **4.19**. Dr. Richard Ting did the initial radiolabeling experiments. I also synthesized **4.14** and all the other hydroxamic acids tested in this chapter. I developed the HPLC method for the isolation of **4.15** and performed the ferriin test and acid stability studies. I also studied the radiolabeling conditions to prepare Mar-<sup>18</sup>F-ArBF<sub>3</sub> **4.15**. Dr. David Perrin performed the radiolabeling experiments and formulation for the animal imaging experiments. Dr. Ulrich auf dem Keller, Dr. Caroline L. Bellac, Dr. Philipp F. Lange, and Dr. Reinhild Kappelhoff carried out all

the biological experiments including the inhibition assay and binding test; Dr. Yuanmei Lou and Dr. Shoukat Dedhar prepared the animal models including tumor cell implantations, while Drs. auf dem Keller and Bellac along with Ms. Siobhan McCormick carried out the tail vein injections and PET scan experiments. Dr. Francois Benard assisted in the imaging reconstruction; Dr. Tom J. Ruth, Dr. Mike Adam, and Dr. Paul Schaffer at TRIUMF provided supervision in the hot lab. Mr. Wade English and Ms. Linda Graham operated the cyclotron to generate  $^{18}\text{F}$ -fluoride from  $^{18}\text{O}\text{-H}_2\text{O}$ . Dr. Mike Adam trapped and released  $^{18}\text{F}$ -fluoride from the anion exchange column and also concentrated the fluoride solution under helium flow. Mr. James A. H. Inkster performed the radio-HPLC purifications on the Waters system. Mr. Peter Tian, an undergraduate NSERC summer student whom I supervised, helped to synthesize some **4.14** for studies at the Center for Probe Development and Commercialization (CPDC).

For other chapters, I performed all the experiments, including the syntheses of precursors,  $^{19}\text{F}$  NMR studies, and radiolabeling experiments. Ms. Shiqing Tang, an exchange student from Singapore whom I supervised, helped to synthesize BODIPY-boronate **3.6**, the precursor **5.8** for the urea-based PSMA inhibitor, and some precursors for RGD-peptide synthesis. Ms. Angela Leung, an undergraduate 425 student whom I supervised, scaled up the synthesis of **3.6** and studied the fluoridation of **3.6** under various conditions by TLC-fluorescent densitometry.

All the radiolabeling experiments carried out at the CPDC were in collaboration with Dr. John Valliant and Dr. Karin Stephenson. Dr. Ryan Simms collected and transported the  $^{18}\text{F}$ -fluoride solution from the cyclotron site to the  $^{18}\text{F}$ -hot lab and assisted me with the radiolabeling experiments and radio-UPLC analysis. For the radiolabeling experiments undertaken in collaboration with Dr. Tom Ruth, Dr. Paul Schaffer, and Dr. Mike Adam at TRIUMF, I performed all the experiments and Dr. Hua Yang helped with the set-up of the radio-HPLC system.

All the high-resolution mass spectrometry was performed by Mr. David Wong and Mr. Marshall Lapawa. Mr. Marshall Lapawa also performed the MALDI-TOF experiments. Dr. Yun Ling and Mr. Derek Smith helped with the ESI-LCMS experiments. Dr. David Perrin and I co-wrote the manuscripts for *J. Fluorine Chem.* and *Med. Chem. Comm.*

# Table of contents

<b>Abstract</b> .....	<b>ii</b>
<b>Preface</b> .....	<b>iii</b>
<b>Table of contents</b> .....	<b>v</b>
<b>List of tables</b> .....	<b>xiii</b>
<b>List of figures</b> .....	<b>xiv</b>
<b>List of schemes</b> .....	<b>xviii</b>
<b>List of abbreviations and symbols</b> .....	<b>xx</b>
<b>Acknowledgements</b> .....	<b>xxvi</b>
<b>Dedication</b> .....	<b>xxix</b>
<b>Chapter 1 Introduction</b> .....	<b>1</b>
1.1 Molecular imaging.....	1
1.2 Molecular imaging with PET.....	4
1.2.1 How does PET work? .....	4
1.2.2 Choices of PET radionuclides .....	6
1.3 <sup>18</sup> F-Labeling techniques.....	8
1.3.1 Production of <sup>18</sup> F-fluoride/fluorine.....	8
1.3.2 Radiosyntheses involving electrophilic <sup>18</sup> F-F <sub>2</sub> .....	8
1.3.3 Radiosyntheses with nucleophilic <sup>18</sup> F-fluoride.....	10
1.3.3.1 To form the C- <sup>18</sup> F bond via nucleophilic reactions- the conventional technique for <sup>18</sup> F-labeling .....	10
1.3.3.2 Newly developed methods to prepare <sup>18</sup> F-labeled molecules.....	12
1.4 Applying ArBF <sub>3</sub> s as PET imaging agents.....	16
1.4.1 Specific activity .....	17
1.4.2 Radiochemical yields and synthesis time .....	19
1.4.3 Solvolytic stability of ArBF <sub>3</sub> s.....	20
1.5 The goal of this dissertation.....	22
<b>Chapter 2 Hydrolytic defluoridation of <i>N</i>-HetArBF<sub>3</sub>s at neutral pH</b> .....	<b>24</b>
2.1 Introduction .....	24
2.2 Results .....	25
2.2.1 Synthesis.....	25

2.2.2	Solvolytic studies of <i>N</i> -HetArBF <sub>3</sub> s.....	27
2.3	Discussion.....	30
2.3.1	Synthesis.....	30
2.3.2	Solvolytic studies of <i>N</i> -HetArBF <sub>3</sub> s.....	30
2.4	Conclusion.....	34
2.5	Materials and methods.....	34
2.5.1	Preparation of several heteroarylboronic acids.....	35
2.5.2	General protocols to prepare <i>N</i> -HetArBF <sub>3</sub> s.....	38
2.5.3	Kinetics of the hydrolytic defluoridation of <i>N</i> -HetArBF <sub>3</sub> s.....	39
<b>Chapter 3</b>	<b>Fluoridation of arylboronates .....</b>	<b>40</b>
3.1	Introduction .....	40
3.2	Results .....	43
3.2.1	Synthesis.....	44
3.2.2	Fluoridation studies based on BODIPY-boronate <b>3.6</b> .....	47
3.2.2.1	Test of organic solvents for the fluoridation.....	47
3.2.2.2	Examination on acids for the fluoridation of <b>3.6</b> .....	49
3.2.2.3	Fluoride concentrations for the fluoridation of <b>3.6</b> .....	50
3.2.2.4	Reaction temperatures for the fluoridation of <b>3.6</b> .....	51
3.2.2.5	The content of the organic solvent for the fluoridation of <b>3.6</b> .....	52
3.2.2.6	Acid concentrations for the fluoridation of <b>3.6</b> .....	52
3.2.2.7	Effects of the ionic strength on the fluoridation of <b>3.6</b> .....	54
3.2.2.8	Kinetic studies on the fluoridation of <b>3.6</b> .....	56
3.2.3	Fluoridation studies by <sup>19</sup> F NMR spectroscopy .....	56
3.2.4	The <sup>18</sup> F-fluoridation of boronates .....	59
3.3	Discussion.....	62
3.3.1	Synthesis .....	62
3.3.2	The fluoridation of BODIPY-boronate <b>3.6</b> .....	63
3.3.3	Fluoridation studies by <sup>19</sup> F NMR spectroscopy .....	66
3.3.4	<sup>18</sup> F-Fluoridations of boronates.....	66
3.4	Conclusion.....	68
3.5	Materials and methods.....	69
3.5.1	Synthesis.....	70

3.5.2	General procedures of the fluoridation .....	80
<b>Chapter 4</b>	<b>Radiosynthesis of matrix metalloproteinase inhibitor</b>	
	<b>marimastat-<sup>18</sup>F-ArBF<sub>3</sub> to image breast cancer .....</b>	<b>82</b>
4.1	Introduction .....	82
4.1.1	Matrix metalloproteinases .....	82
4.1.2	MMP inhibitors.....	83
4.1.2.1	Endogenous MMP inhibitors.....	83
4.1.2.2	Synthetic MMP inhibitors.....	84
4.1.3	Imaging MMPs .....	86
4.1.4	Towards <i>in vivo</i> imaging of breast cancer with Mar- <sup>18</sup> F-ArBF <sub>3</sub> targeting MMPs .....	89
4.2	Results .....	90
4.2.1	Synthesis .....	90
4.2.2	The <i>in vitro</i> stability of MarArBF <sub>3</sub> <b>4.15</b> .....	92
4.2.3	The stability study of hydroxamic acids under acidic conditions.....	93
4.2.4	<i>In vitro</i> enzyme inhibition assays of marimastat derivatives.....	96
4.2.5	Fluorescent marimastat-FITC and <i>in vitro</i> cell imaging.....	99
4.2.6	Radiosyntheses of Mar- <sup>18</sup> F-ArBF <sub>3</sub> <b>4.15</b> .....	100
4.2.6.1	The radiosynthesis of Mar- <sup>18</sup> F-ArBF <sub>3</sub> <b>4.15</b> .....	100
4.2.6.2	The radiosynthesis to image MMPs in breast cancer .....	102
4.2.7	<i>In vivo</i> PET imaging of MMPs in murine breast carcinomas.....	105
4.2.8	Several factors influencing the radiosynthesis of Mar- <sup>18</sup> F-ArBF <sub>3</sub> <b>4.15</b> ..... .....	106
4.3	Discussion.....	111
4.3.1	Synthesis .....	111
4.3.2	The <i>in vitro</i> stability of MarArBF <sub>3</sub> <b>4.15</b> .....	113
4.3.3	The acid stability of hydroxamic acids.....	114
4.3.4	<i>In vitro</i> enzyme inhibitory activity of MarArBF <sub>3</sub> <b>4.15</b> .....	116
4.3.5	Cell binding assays with fluorescent marimastat-FITC.....	117
4.3.6	<i>In vivo</i> PET imaging of MMPs in murine breast carcinomas.....	118
4.3.7	Some factors related to the <sup>18</sup> F-fluoridation of marimastat-boronate <b>4.14</b> . .....	120
4.4	Conclusion .....	122

4.5	Materials and methods .....	123
4.5.1	Synthesis .....	124
4.5.2	Defluoridation study of MarArBF <sub>3</sub> (4.15) .....	135
4.5.3	Ferrioin test .....	135
4.5.4	The acid stability of hydroxamic acids studied by NMR spectroscopy .....	135
4.5.5	Enzyme inhibition assays .....	135
4.5.6	Assays for fluorescent marimastat-FITC .....	136
4.5.6.1	Binding assay of marimastat-FITC with MMPs .....	136
4.5.6.2	Cell assay for MMP14 by marimastat-FITC .....	136
4.5.7	Radiolabeling marimastat-boronate .....	137
4.5.8	MicroPET imaging .....	139
<b>Chapter 5 Radiosynthesis of an <sup>18</sup>F-ArBF<sub>3</sub> labeled PSMA inhibitor for prostate cancer imaging .....</b>		<b>140</b>
5.1	Introduction .....	140
5.1.1	Prostate cancer .....	140
5.1.2	Biomarkers for prostate cancer .....	140
5.1.3	PSMA and molecular imaging of prostate cancer .....	142
5.1.4	Labeling the urea-based PSMA inhibitor with an <sup>18</sup> F-ArBF <sub>3</sub> .....	146
5.2	Results .....	147
5.2.1	Synthesis .....	147
5.2.2	HPLC conditions for urea-ArBF <sub>3</sub> 5.10 .....	151
5.2.2.1	HPLC analysis of urea-ArBF <sub>3</sub> 5.10 .....	151
5.2.2.2	The fluoridation analyzed by ESI-LCMS .....	152
5.2.3	The radiosynthesis of urea- <sup>18</sup> F-ArBF <sub>3</sub> 5.10 .....	153
5.3	Discussion .....	155
5.3.1	Synthesis .....	155
5.3.2	The HPLC analysis of urea-ArBF <sub>3</sub> 5.10 .....	159
5.3.3	Radiosyntheses of urea- <sup>18</sup> F-ArBF <sub>3</sub> 5.10 .....	160
5.4	Conclusion and future perspectives .....	163
5.5	Materials and methods .....	163
<b>Chapter 6 Applying copper(I) catalyzed click chemistry to label oligonucleotides with <sup>18</sup>F-ArBF<sub>3</sub>s .....</b>		<b>176</b>

6.1	Introduction .....	176
6.1.1	Click chemistry .....	176
6.1.2	The copper(I) catalyzed 1,3-dipolar cycloaddition applied in radiopharmaceutical chemistry .....	182
6.1.3	Imaging oligonucleotides .....	185
6.1.4	Radiolabeling oligonucleotides with $^{18}\text{F}$ -ArBF <sub>3</sub> s via the copper(I) catalyzed 1,3-dipolar cycloaddition .....	189
6.2	Results .....	192
6.2.1	The derivatization of oligonucleotides .....	192
6.2.2	Synthesis of alkynes .....	194
6.2.3	Click reactions between 5'-N <sub>3</sub> - <sup>31/32</sup> P-ONs and alkynes .....	196
6.2.4	The $^{18}\text{F}$ -labeling of oligonucleotides via click chemistry .....	203
6.2.5	Specific activity .....	209
6.3	Discussion .....	212
6.3.1	The derivatization of oligonucleotides .....	212
6.3.2	Synthesis of alkynes .....	214
6.3.3	Click reactions between 5'-N <sub>3</sub> - <sup>31/32</sup> P-ONs and alkynes .....	216
6.3.4	The one-pot two-step $^{18}\text{F}$ -labeling of oligonucleotides .....	218
6.3.5	Specific activity .....	221
6.4	Conclusion .....	224
6.5	Materials and methods .....	224
6.5.1	The derivatization of oligonucleotides .....	226
6.5.2	Synthesis .....	229
6.5.3	Click reactions between alkynylArBF <sub>3</sub> <b>6.2</b> and 5'-N <sub>3</sub> - <sup>31/32</sup> P-ONs .....	232
6.5.4	The $^{18}\text{F}$ -radiolabeling of boronic acid <b>3.11</b> .....	232
6.5.5	Click reactions on 5'-N <sub>3</sub> - <sup>31/32</sup> P-ONs with alkynyl- $^{18}\text{F}$ -ArBF <sub>3</sub> <b>6.2</b> .....	233
<b>Chapter 7</b>	<b>Labeling folate with <math>^{18}\text{F}</math>-ArBF<sub>3</sub>s .....</b>	<b>234</b>
7.1	Introduction .....	234
7.1.1	Folate and folate receptors .....	234
7.1.2	Folate and molecular imaging .....	238
7.1.3	Labeling folate with ArBF <sub>3</sub> s .....	241
7.2	Results .....	243
7.2.1	Synthesis of Pte-Glu[(PEG) <sub>2</sub> N <sub>3</sub> ]-OH <b>7.10</b> .....	243

7.2.2	Click reactions between Pte-Glu[(PEG) <sub>2</sub> N <sub>3</sub> ]-OH <b>7.10</b> and alkynes.....	245
7.2.3	Radiolabeling folate with the <sup>18</sup> F-ArBF <sub>3</sub> via click chemistry.....	247
7.3	Discussion.....	251
7.3.1	Synthesis of Pte-Glu[(PEG) <sub>2</sub> N <sub>3</sub> ]-OH <b>7.10</b> .....	251
7.3.2	Click reactions between Pte-Glu[(PEG) <sub>2</sub> N <sub>3</sub> ]-OH <b>7.10</b> and alkynes.....	252
7.3.3	Radiolabeling folate with the <sup>18</sup> F-ArBF <sub>3</sub> via click chemistry.....	253
7.4	Conclusion and perspectives.....	254
7.5	Materials and methods.....	255
<b>Chapter 8</b>	<b>Preparation of <sup>18</sup>F-ArBF<sub>3</sub> labeled RGD-peptides for cancer</b>	
<b>imaging</b>	<b>.....</b>	<b>262</b>
8.1	Introduction .....	262
8.1.1	Integrin $\alpha_v\beta_3$ and RGD.....	262
8.1.2	$\alpha_v\beta_3$ Antagonists based on RGD sequences .....	263
8.1.3	RGD-containing peptides as drug delivery vehicles .....	264
8.1.4	RGD-peptides in molecular imaging.....	266
8.1.5	Labeling RGD-containing peptides with ArBF <sub>3</sub> s .....	270
8.2	Results .....	270
8.2.1	Preparation of the RGD-containing peptides.....	270
8.2.2	The one-step fluoridation of RGD-boronates .....	276
8.2.2.1	The HPLC conditions for RGD-ArBF <sub>3</sub> s.....	276
8.2.2.2	The one-step radiolabeling of RGD-boronates.....	277
8.2.3	One-pot two-step syntheses of RGD-ArBF <sub>3</sub> s via click chemistry.....	277
8.2.3.1	The one-pot two-step synthesis via click chemistry to prepare an RGD-ArBF <sub>3</sub> .....	278
8.2.3.2	The one-pot two-step <sup>18</sup> F-labeling to prepare an RGD-ArBF <sub>3</sub> .....	279
8.3	Discussion.....	280
8.3.1	Synthesis.....	280
8.3.2	The fluoridation to prepare RGD-ArBF <sub>3</sub> s .....	282
8.3.2.1	The one-step fluoridation of RGD-boronates .....	282
8.3.2.2	The one-pot two-step labeling of an RGD-peptide with the ArBF <sub>3</sub> .....	283
8.4	Conclusion and future perspectives.....	285
8.5	Methods and materials.....	285

8.5.1	Synthesis .....	286
8.5.2	The fluoridation of RGD-peptides .....	301
8.5.3	Preparation of the $^{18}\text{F}$ -ArBF <sub>3</sub> labeled RGD-peptides .....	302
<b>Chapter 9</b>	<b>Discussion and conclusion .....</b>	<b>305</b>
9.1	Discussion .....	305
9.1.1	Defluoridation and fluoridation: rapid preparation and slow decomposition of $^{18}\text{F}$ -ArBF <sub>3</sub> s .....	305
9.1.1.1	The stability of ArBF <sub>3</sub> s .....	305
9.1.1.2	The fluoridation to prepare ArBF <sub>3</sub> s .....	306
9.1.2	One-step labeling or one-pot two-step labeling to prepare $^{18}\text{F}$ -ArBF <sub>3</sub> s? .....	307
9.1.3	Specific activity of $^{18}\text{F}$ -ArBF <sub>3</sub> s .....	309
9.2	Perspectives .....	311
9.2.1	Are $^{18}\text{F}$ -alkyltrifluoroborates suitable for PET imaging? .....	311
9.2.2	Developing new protecting groups to facilitate the fluoridation of boronates .....	312
9.2.3	Alternative one-pot two-step strategies .....	313
9.2.4	Where is $^{19}\text{F}$ -fluoride in the irradiated $^{18}\text{O}\text{H}_2$ from? .....	314
9.3	Conclusion .....	315
<b>Bibliography</b> .....		<b>317</b>
<b>Appendices</b> .....		<b>339</b>
Appendix A.	Preparation of various solutions .....	339
Appendix B.	HPLC information .....	340
Appendix B.1.	HPLC systems .....	340
Appendix B.2.	HPLC C18 columns .....	340
Appendix B.3.	HPLC programs .....	340
Appendix C.	HPLC chromatograms .....	344
Appendix D.	The kinetic study on the solvolysis of <i>N</i> -HetArBF <sub>3</sub> s by $^{19}\text{F}$ NMR spectroscopy .....	358
Appendix E.	NMR spectra .....	363
Appendix E.1.	NMR spectra for Chapter 2 .....	363
Appendix E.2.	NMR spectra for Chapter 3 .....	369
Appendix E.3.	NMR spectra for Chapter 4 .....	392

Appendix E.4. NMR spectra for Chapter 5 .....	414
Appendix E.5. NMR spectra for Chapter 6 .....	430
Appendix E.6. NMR spectra for Chapter 7 .....	437
Appendix E.7. NMR spectra for Chapter 8 .....	446

## List of tables

Table 1.1 A summary of imaging modalities. <sup>4, 10</sup> .....	4
Table 1.2 Some positron-emitting radionuclides for PET. <sup>20-22</sup> .....	6
Table 2.1 The kinetic data for the solvolysis of <i>N</i> -HetArBF <sub>3</sub> s .....	29
Table 3.1 A check-list of the boronates studied for the fluoridation in this chapter. ...	43
Table 4.1 <sup>18</sup> F-Radiosyntheses of Mar- <sup>18</sup> F-ArBF <sub>3</sub> <b>4.15</b> under various conditions. ....	109
Table 6.1 The calculation for the specific activity of <b>ON2</b> - <sup>18</sup> F-ArBF <sub>3</sub> . .....	211
Table 7.1 A summary of the click reactions between <b>6.2</b> and <b>7.10</b> under radioactive conditions.....	247
Table 9.1 A summary of the radiosyntheses of several bioligands in this dissertation. ....	307

## List of figures

Figure 1.1 An illustration of positron annihilation. ....	5
Figure 1.2 Hammett plot in the form of $\log(k) = \sigma\rho + \log(k_0)$ . <sup>85</sup> .....	21
Figure 1.3 The structures of boronic acid/ester <b>3.1</b> and <b>3.8</b> that will be used in this dissertation. ....	22
Figure 2.1 The <sup>19</sup> F NMR study of <i>para</i> -pyridinyltrifluoroborate (TFB-2.1) dissociation in 200 mM phosphate buffer (pH 6.89). ....	27
Figure 2.2 Proposed energy diagram of hydroxide-fluoride exchange for step 1 of mechanism A. ....	33
Figure 3.1 Screening organic solvents for the fluoridation of <b>3.6</b> . ....	47
Figure 3.2 The structure of the oxidatively-deboronated product from <b>3.6</b> . ....	48
Figure 3.3 Examination on acids used in the fluoridation of <b>3.6</b> . ....	49
Figure 3.4 Effect of fluoride concentrations on the fluoridation of <b>3.6</b> . ....	50
Figure 3.5 Study on the temperature dependence of the fluoridation of <b>3.6</b> . ....	51
Figure 3.6 Investigation of organic solvent content affecting the fluoridation of <b>3.6</b> . ....	52
Figure 3.7 Concentrations of HCl used in the fluoridation of <b>3.6</b> . ....	53
Figure 3.8 Concentrations of TsOH used in the fluoridation of <b>3.6</b> . ....	53
Figure 3.9 Addition of concentrated acids to the fluoridation of <b>3.6</b> . ....	54
Figure 3.10 The study of salt effects on the fluoridation to prepare BODIPY-ArBF <sub>3</sub> <b>3.2</b> . ....	55
Figure 3.11 The kinetic study of the fluoridation of BODIPY-boronate <b>3.6</b> in CH <sub>3</sub> CN or NMP. ....	56
Figure 3.12 The fluoridation of <b>3.7</b> studied by <sup>19</sup> F NMR spectroscopy. ....	57
Figure 3.13 The <sup>19</sup> F NMR study on the fluoridation of <b>3.10</b> . ....	58
Figure 3.14 The kinetic study on the <sup>18</sup> F-fluoridation of <b>3.16</b> . ....	60
Figure 3.15 The radio-HPLC chromatogram of the <sup>18</sup> F-fluoridation of <b>3.11</b> ....	60
Figure 3.16 The radio-HPLC traces of the <sup>18</sup> F-radiolabeling of <b>3.19</b> , <b>3.20</b> , <b>3.21</b> and <b>3.23</b> . ....	61
Figure 4.1 Some synthetic MMPiS. ....	85
Figure 4.2 Structures of some representative radiolabeled MMPiS. ....	87
Figure 4.3 HPLC chromatograms of <b>4.14</b> and <b>4.15</b> . ....	92
Figure 4.4 The hydrolysis of MarArBF <sub>3</sub> <b>4.15</b> in 1 × PBS (pH 7.4) monitored by <sup>19</sup> F NMR spectroscopy. ....	93

Figure 4.5 The study on the acid stability of <b>4.17</b> with the ferrioin test analyzed by UV-vis spectroscopy. ....	94
Figure 4.6 The acid stability of <b>4.17</b> studied by <sup>1</sup> H NMR spectroscopy. ....	94
Figure 4.7 The acid stability of <b>4.18</b> studied by <sup>1</sup> H NMR spectroscopy. ....	95
Figure 4.8 The determination of the concentration of MarArBF <sub>3</sub> <b>4.15</b> by the ferrioin test. ....	97
Figure 4.9 The MMP2 inhibition assay with marimastat compounds. ....	98
Figure 4.10 The specificity of marimastat-FITC <b>4.19</b> and the <i>in vitro</i> cell image of MMPs. ....	99
Figure 4.11 The autoradiographic TLC analysis of the <sup>18</sup> F-fluoridation to prepare Mar- <sup>18</sup> F-ArBF <sub>3</sub> <b>4.15</b> . ....	101
Figure 4.12 The test of reductant additives to the <sup>18</sup> F-fluoridation of marimastat-boronate <b>4.14</b> . ....	101
Figure 4.13 Radio-HPLC chromatograms of the fluoridation to prepare Mar- <sup>18</sup> F-ArBF <sub>3</sub> <b>4.15</b> . ....	103
Figure 4.14 Radio-HPLC chromatograms of the 2 <sup>nd</sup> synthesis of Mar- <sup>18</sup> F-ArBF <sub>3</sub> <b>4.15</b> . ....	104
Figure 4.15 <i>In vivo</i> PET imaging of murine breast carcinomas targeting MMPs. ....	105
Figure 4.16 The radio-UPLC chromatogram of the <sup>18</sup> F-radiolabeling reaction of marimastat- boronate <b>4.14</b> . ....	107
Figure 4.17 Identification of the byproduct in the <sup>18</sup> F-fluoridation to prepare Mar- <sup>18</sup> F-ArBF <sub>3</sub> <b>4.15</b> . ....	110
Figure 5.1 Examples for some synthesized PSMA inhibitors. <sup>232, 234, 236</sup> ....	144
Figure 5.2 Several radiolabeled PSMA inhibitors reviewed in this chapter. ....	145
Figure 5.3 NMR spectra of urea-ArBF <sub>3</sub> <b>5.10</b> . ....	150
Figure 5.4 The ESI-LCMS of urea-ArBF <sub>3</sub> <b>5.10</b> . ....	151
Figure 5.5 The ESI-LCMS analysis of the fluoridation to prepare urea-ArBF <sub>3</sub> <b>5.10</b> . ....	152
Figure 5.6 The radio-HPLC chromatogram of the <sup>18</sup> F-fluoridation of urea-boronate <b>5.9</b> in HCO <sub>2</sub> NH <sub>4</sub> /CH <sub>3</sub> CN solvent system. ....	153
Figure 5.7 The radio-HPLC chromatograms of the radiosynthesis of urea- <sup>18</sup> F-ArBF <sub>3</sub> <b>5.10</b> . ....	154
Figure 5.8 The HPLC traces of the deprotection of <b>5.8</b> and <b>5.20</b> with TFA. ....	157
Figure 5.9 Studies on the deprotection of <b>5.20</b> in neat TFA. ....	158
Figure 5.10 The proposed mechanism of the fluoridation of the benzopinacol protected boronate. ....	162
Figure 6.1 The 1,3-dipolar cycloadditions. ....	178

Figure 6.2 The proposed mechanism of the copper(I)-catalyzed alkyne-azide dipolar cycloaddition by Sharpless <i>et al.</i> <sup>261, 280</sup> .....	180
Figure 6.3 The autoradiographic gel image of the derivatization of 5'- <sup>31/32</sup> P-ON. ....	193
Figure 6.4 The HPLC chromatograms at 229 nm of alkynylArBF <sub>3</sub> <b>6.2</b> (black) and the fluoridation of alkynylarylboronic acid <b>3.11</b> (red). ....	195
Figure 6.5 A radio-HPLC chromatogram of the <sup>18</sup> F-fluoridation of alkynylarylboronic acid <b>3.11</b> . ....	196
Figure 6.6 The autoradiographic gel image of the click reactions between the gel-purified 5'-N <sub>3</sub> - <sup>31/32</sup> P-ONs and alkynes. ....	197
Figure 6.7 The study of the concentrations of Cu(II)-TBTA for the click reaction between 5'-N <sub>3</sub> - <sup>31/32</sup> P-ON2 and alkynylArBF <sub>3</sub> <b>6.2</b> . ....	199
Figure 6.8 The kinetics of the click reaction between 5'-N <sub>3</sub> - <sup>31/32</sup> P-ON2 and alkynylArBF <sub>3</sub> <b>6.2</b> . ....	200
Figure 6.9 The click reaction between 5'-N <sub>3</sub> - <sup>31/32</sup> P-ON1 and alkynylArBF <sub>3</sub> <b>6.2</b> . ....	201
Figure 6.10 The one-pot two-step reaction to label oligonucleotide 5'-N <sub>3</sub> - <sup>31/32</sup> P-ON1. ....	202
Figure 6.11 The autoradiographic gel images of the click reactions between alkynes and 5'-N <sub>3</sub> - <sup>31/32</sup> P-ON1. ....	204
Figure 6.12 The resolution of various oligonucleotides in 10% polyacrylamide gel. ....	205
Figure 6.13 The radio-HPLC chromatogram of the preparation of alkynyl- <sup>18</sup> F-ArBF <sub>3</sub> <b>6.2</b> and the autoradiographic gel images of click reactions with 5'-N <sub>3</sub> - <sup>31/32</sup> P-ON1. ....	206
Figure 6.14 The HPLC chromatograms of the crude click reaction with 5'-N <sub>3</sub> - <sup>31</sup> P-ON2. ....	208
Figure 6.15 The UV absorption spectra of the sample collected from the radio-HPLC. ....	210
Figure 6.16 The mechanism of the derivatization of oligonucleotides by Knorre's protocol. <sup>351</sup> .....	213
Figure 6.17 The UV absorption of the decayed sample of the HPLC collected 5'- <sup>31</sup> P-ON2- <sup>18</sup> F-ArBF <sub>3</sub> can be corrected by deconvolution of the UV spectrum. ....	223
Figure 7.1 The folate receptor-mediated endocytosis. ....	237
Figure 7.2 The structure of EC145. <sup>413-416</sup> .....	238
Figure 7.3 Several radiolabeled folate conjugates. <sup>302, 387, 425-427</sup> .....	239
Figure 7.4 The preparation of Pte-Glu[(PEG) <sub>2</sub> N <sub>3</sub> ]-OCH <sub>3</sub> <b>7.9</b> using different coupling reagents. ....	245
Figure 7.5 The click reaction between <b>6.4</b> and <b>7.10</b> monitored by HPLC. ....	246
Figure 7.6 The click reaction between <b>6.2</b> and <b>7.10</b> monitored by HPLC. ....	246

Figure 7.7 The one-pot two-step radiolabeling of folate from alkynyl- $^{18}\text{F}$ -ArBF $_3$ <b>6.2</b> via click chemistry. ....	248
Figure 7.8 The one-pot two-step radiosynthesis of folate- $^{18}\text{F}$ -ArBF $_3$ . ....	250
Figure 7.9 The radio-HPLC chromatograms of the one-pot two-step radiolabeling of folate with the $^{18}\text{F}$ -ArBF $_3$ via click chemistry. ....	250
Figure 8.1 The macrolactamization of H $_2$ N-Asp(O $^t$ Bu)- <i>D</i> -Phe-Lys(N $_3$ )-Arg(Pbf)-Gly-OH ( <b>8.2a</b> ). ....	272
Figure 8.2 The test of different coupling reagents to conjugate boronate <b>3.1</b> to peptide 8.5. ....	273
Figure 8.3 The HPLC traces of the RGD-ArBF $_3$ s. ....	276
Figure 8.4 The radio-HPLC traces of the one-step $^{18}\text{F}$ -fluoridation of RGD-boronates <b>8.7</b> and <b>8.13</b> . ....	277
Figure 8.5 The HPLC chromatogram of the click reaction between <b>8.4</b> and <b>6.2</b> . ....	278
Figure 8.6 The LCMS chromatograms and ESI-spectra of the click reaction between <b>6.2</b> and <b>8.4</b> . ....	279
Figure 8.7 The radio-HPLC traces of the one-pot two-step labeling reaction to prepare RGD- $^{18}\text{F}$ -ArBF $_3$ . ....	280
Figure 9.1 The structures of possible pursued protecting groups for boronic acids. ....	313

## List of schemes

Scheme 1.1 The scheme of the nuclear reactions to produce $^{18}\text{F}$ -fluorine/fluoride. ....	8
Scheme 1.2 Radiosyntheses of $^{18}\text{F}$ -FDG via electrophilic reactions. <sup>37, 40, 45</sup> .....	9
Scheme 1.3 Examples of fluorodestannylation to prepare functional $^{18}\text{F}$ -labeled reagents. <sup>49, 50</sup> .....	10
Scheme 1.4 The radiosynthesis of $^{18}\text{F}$ -FDG via a nucleophilic substitution. <sup>51</sup> .....	11
Scheme 1.5 The nucleophilic aromatic substitution to prepare $^{18}\text{F}$ -labeled compounds. ....	11
Scheme 1.6 Reactions of diaryliodonium salts with $^{18}\text{F}$ -fluoride. <sup>63-65</sup> .....	11
Scheme 1.7 The radiosynthesis of $^{18}\text{F}$ - <i>N,N,N',N'</i> -tetramethylphosphorodiamidic fluoride. <sup>66</sup> .....	12
Scheme 1.8 $^{18}\text{F}$ -Labeled NOTA-octreotide with $\text{Al}^{18}\text{F}$ . <sup>69</sup> .....	13
Scheme 1.9 $^{18}\text{F}$ -Radiosyntheses of silicon-based building blocks. <sup>71-73, 76</sup> .....	14
Scheme 1.10 The radiosynthesis of $^{18/19}\text{F}$ - $\text{ArBF}_3\text{S}$ . <sup>78</sup> .....	16
Scheme 2.1 The proposed kinetic scheme of the $\text{ArBF}_3$ solvolysis. ....	24
Scheme 2.2 Synthesis of several heteroarylboronic acids. ....	26
Scheme 2.3 Proposed mechanisms of the hydrolysis of $\text{HetArBF}_3\text{S}$ . ....	32
Scheme 3.1 Proposed mechanism of the fluoridation of arylboronate esters. ....	40
Scheme 3.2 Synthetic scheme of BODIPY-boronate <b>3.6</b> and BODIPY- $\text{ArBF}_3$ <b>3.2</b> . ...	44
Scheme 3.3 Synthetic scheme of boronates protected with 1,8-diaminonaphthalene. ....	45
Scheme 3.4 Synthesis of DiDiAN protected boronates. ....	45
Scheme 3.5 Synthesis of boronates containing a piperazine linker. ....	46
Scheme 4.1 Synthesis of marimastat-boronate <b>4.14</b> and $\text{MarArBF}_3$ <b>4.15</b> . ....	91
Scheme 4.2 The proposed mechanism of the deboronation of marimastat-boronate <b>4.14</b> . ....	112
Scheme 4.3 The proposed mechanism of the solvolysis of $\text{MarArBF}_3$ <b>4.15</b> . ....	114
Scheme 4.4 Chelation between the hydroxamic acid and $\text{Fe}^{3+}$ . <sup>172</sup> .....	115
Scheme 5.1 Synthesis of urea-borate <b>5.9</b> following the literature protocol. ....	147
Scheme 5.2 Modified synthetic route of urea-borate <b>5.9</b> . ....	149
Scheme 5.3 The proposed deboronation mechanism of the benzopinacol protected boronate in neat TFA. ....	159
Scheme 6.1 Examples of some copper-free cycloaddition reactions. ....	180
Scheme 6.2 The scheme of the one-pot two-step method to label biomolecules with	

an $^{18}\text{F}$ -ArBF <sub>3</sub> via the copper(I) catalyzed alkyne-azide cycloaddition. ....	190
Scheme 6.3 The scheme of the oligonucleotide derivatization. <sup>341</sup> .....	192
Scheme 6.4 Synthetic scheme of alkynes. ....	194
Scheme 7.1 The mechanism of the thymidylate synthesis. <sup>359</sup> .....	235
Scheme 7.2 Synthesis of Pte-Glu[(PEG) <sub>2</sub> N <sub>3</sub> ]-OH <b>7.10</b> . ....	243
Scheme 7.3 The proposed mechanism of the synthesis of pteric acid <b>7.8</b> . ....	251
Scheme 8.1 Synthetic scheme of the cyclic RGD pentapeptides. ....	271
Scheme 8.2 Synthesis of <i>cyclo</i> [Arg-Gly-Asp-D-Phe-Lys(suc-piperazinyboronate)] 8.13 and the corresponding RGD-ArBF <sub>3</sub> <b>8.19</b> . ....	274
Scheme 8.3 Synthesis of the fluorescent RGD-peptides <b>8.20</b> and <b>8.21</b> . ....	275
Scheme 9.1 Potential one-pot two-step labeling alternatives to label molecules with ArBF <sub>3</sub> s. ....	314

## List of abbreviations and symbols

$\alpha$	$\alpha$ -particle, He <sup>2+</sup>
$\beta^+$	positron
$\gamma$	gamma ray
$\epsilon$	extinction coefficient
$\delta$	chemical shift
$\lambda$	wavelength
$\rho$	reaction constant
$\sigma$	substituent value
°C	degrees centigrade
(Boc) <sub>2</sub> O	di- <i>tert</i> -butyl dicarbonate
(PyS) <sub>2</sub>	dipyridyl disulfide
5,10-CH <sub>2</sub> -H <sub>4</sub> PteGlu	5,10-methylenetetrahydrofolate
A <sub>260 nm</sub>	absorbance at 260 nm
A	deoxyadenosine
AcCl	acetyl chloride
Ala (A)	<i>L</i> -alanine
APS	ammonium persulfate
ArBF <sub>3</sub>	aryltrifluoroborate
ArB(OH) <sub>2</sub>	arylboronic acid
Ar	argon
Arg (R)	<i>L</i> -arginine
Asn (N)	<i>L</i> -asparagine
Asp (D)	<i>L</i> -aspartic acid
ATP	adenosine-5'-triphosphate
AU	absorbance unit
Av	avidin
Boc	<i>tert</i> -butyloxycarbonyl
BODIPY	boron-dipyromethene
BOS	beginning of synthesis
br	broad
Bt	biotin
BTES	bis( <i>tert</i> -butyltriazolyl) triazolylethylene sulfonate
BuLi	butyllithium
BuMgBr	butylmagnesium bromide
C	deoxycytidine
Cbz	carbobenzyloxy
Cbz-Osu	<i>N</i> -(benzyloxycarbonyloxy) succinimide
CDI	carbonyldiimidazole
Ci	curie
CPDC	Center for Probe Development and Commercialization
cpm	count per minute

CT	computed tomography
CTA	cetyltrimethylammonium
CTAB	cetyltrimethylammonium bromide
Cy	cyanine dye
Cys (C)	<i>L</i> -cysteine
d	deuteron
d	doublet
Dap	2,3-diaminopropionic acid
DBU	1,8-diazabicycloundec-7-ene
dC	deoxyribocytosine
DCC	<i>N,N'</i> -dicyclohexylcarbodiimide
DDQ	2,3-dichloro-5,6-dicyanobenzoquinone
DEPC	diethylpyrocarbonate
DHFR	dihydrofolate reductase
DiDiAN	2,7-dimethoxy-1,8-diaminonaphthalene
DIPEA	diisopropylethylamine
DMA	<i>N,N</i> -dimethylacetamide
DMAP	4-dimethylaminopyridine
DMF	<i>N,N</i> -dimethylformamide
DMSO	dimethyl sulfoxide
DNA	deoxynucleic acid
DOPA	3,4-dihydroxylphenylalanine
DOTA	1,4,7,12-tetraazacyclododecane
<i>D</i> -Phe (f)	<i>D</i> -phenylalanine
DPPA	diphenylphosphonic azide
dTMP	thymidine monophosphate
DTPA	diethylenetriamine pentaacetic acid
DTT	dithiothreitol
dTTP	thymidine triphosphate
dUMP	deoxyuridine monophosphate
EC <sub>50</sub>	half maximal effective concentration
ECM	extracellular matrix
EDC	1-ethyl-3-(3-dimethylaminopropyl)carbodiimide
EDTA	ethylenediaminetetraacetic acid
EOS	end of synthesis
EPCA	early prostate cancer antigen
eq.	equivalent
ESI-HRMS	electrospray ionization-high resolution mass spectrometry
ESI-LRMS	electrospray ionization-low resolution mass spectrometry
ESI-MS	electrospray ionization-mass spectrometry
Et	ethyl
FACS	fluorescence-activated cell-sorting
FBA	fluorobenzylamine
FDA	US Food & Drug Administration

FDG	2-deoxy-2-fluoroglucose
FITC	fluorescein isothiocyanate
Fmoc	fluorenylmethyloxycarbonyl
Fmoc-OSu	fluorenylmethyloxycarbonyl succinimide
FmocCl	fluorenylmethyloxycarbonyl chloride
FR	folate receptor
FR(-)	FR negative
FR(+)	FR positive
RFC	reduced-folate carrier
G	deoxyguanosine
G	Gibbs free energy
G4	generation 4 polyamidoamine dendrimer
Gln (Q)	<i>L</i> -glutamine
Glu (E)	<i>L</i> -glutamic acid
Gly (G)	<i>L</i> -glycine
GRO	G-rich oligonucleotide
H <sub>2</sub> PteGlu	dihydrofolate
H <sub>4</sub> PteGlu	tetrahydrofolate
HBTU	<i>O</i> -benzotriazole- <i>N,N,N',N'</i> -tetramethyl-uronium hexafluorophosphate
HetArBF <sub>3</sub>	heteroaryltrifluoroborate
HFIP	hexafluoro-2-propanol
His (H)	<i>L</i> -histidine
HOAc	acetic acid
HOBt	<i>N</i> -hydroxybenzotriazole
HPLC	high performance liquid chromatography
HPMA	<i>N</i> -(2-hydroxypropyl)methacrylamide
hr	hour
HUVEC	human umbilical vascular endothelial cells
HYNIC	6-hydrazinonicotinic acid
Hz	Hertz
IC <sub>50</sub>	half maximal inhibitory concentration
<i>J</i>	coupling constant
Ile (I)	<i>L</i> -isoleucine
<i>iso</i> -Bu	iso-butyl
K2.2.2	Kryptofix 222 (4,7,13,16,21,24-hexaoxa-1,10-diazabicyclo[8,8,8]-hexacosane)
K <sub>D</sub>	dissociation constant
K <sub>i</sub>	inhibitory constant
k <sub>obs</sub>	observed rate constant
LCMS	liquid chromatography mass spectrometry
Leu (L)	<i>L</i> -leucine
Lys (K)	<i>L</i> -lysine
m	multiplet
M	molar

mAb	monoantibody
MALDI-TOF	matrix-assisted laser desorption time-of-flight
MarArBF <sub>3</sub>	marimastat-aryltrifluoroborate
mAU	milli-absorbance unit
Me	methyl
Met (M)	<i>L</i> -methionine
mg	milligram
MHz	megahertz
min	minute
mL	milliliter
mM	millimolar
MMP	matrix metalloproteinase
MMPI	matrix metalloproteinase inhibitor
mol	mole
Mp	melting point
MR	magnetic resonance
mV	milliVolt
MV	MegaVolt
μL	microliter
n	neutron
ND	not determined
NHS	<i>N</i> -hydroxysuccinimide
NIRF	near infrared fluorescence
nm	nanometer
NMM	<i>N</i> -methylmorpholine
NMP	<i>N</i> -methylpyrrolidone
NMR	nuclear magnetic resonance
NOTA	1,4,7-triazacyclonane-1,4,7-triacetic acid
ONs	oligonucleotides
p	proton
PAGE	polyacrylamide gel electrophoresis
Pbf	2,2,4,6,7-pentamethyldihydrobenzofuran-5-sulfonyl
PBS	phosphate buffer saline
PCA3 <sup>DD3</sup>	prostate cancer gene 3
PCR	polymerase chain reaction
PEG	polyethyleneglycol
PET	positron emission tomography
Phe (F)	<i>L</i> -phenylalanine
PMB	<i>para</i> -methoxybenzyl
PNK	polynucleotide kinase
<i>ppm</i>	parts per million
Pro (P)	<i>L</i> -proline
PSA	prostate-specific antigen
PSMA	prostate-specific membrane antigen

Pte		pterotic
PteGlu		pteroyl-glutamic acid (folic acid)
PTX		paclitaxel
Py		pyridine
PyBOP	(benzotriazol-1-yl-oxytripyrrolidinophosphonium hexafluorophosphate)	
pz		pyrazolyl
QF24	(7-methoxycoumarin-4-yl)acetyl-Pro-Leu-Gly-Leu-[3-(2,4-dinitrophenyl)- <i>L</i> -2,3-diaminopropionyl]-Ala-Arg-NH <sub>2</sub>	
quant.		quantitatively
rC		cytidine
RCY		radiochemical yield
R <sub>f</sub>		retention factor
RNA		ribonucleic acid
RNase		ribonuclease
RP-HPLC		reverse phase high performance liquid chromatography
rt		room temperature
<i>s</i>		singlet
SA		specific activity
SDS		sodium dodecyl sulfate
<i>sec</i> -BuLi		<i>sec</i> -butyllithium
SELEX		systematic evolution of ligands by exponential enrichment
Ser (S)		<i>L</i> -serine
SFB		<i>N</i> -succinimidyl-4-fluorobenzoate
siRNA		short/small interfering RNA
S <sub>N</sub> 1		unimolecular nucleophilic substitution
S <sub>N</sub> 2		bimolecular nucleophilic substitution
SPECT		single proton emission computed tomography
sst		somatostatin
T		thymidine
<i>t</i>		time
<i>t</i>		triplet
<i>t</i> <sub>1/2</sub>		half-life
T4 PNK		T4 polynucleotide kinase
TBE		Tris-borate-EDTA
TBTA		<i>tris</i> -[(1-benzyl-1 <i>H</i> -1,2,3-triazol-yl)methyl]amine
TBTU		<i>O</i> -(benzotriazol-1-yl)- <i>N,N,N',N'</i> -tetramethyluronium tetrafluoroborate
<sup>t</sup> Bu		<i>tert</i> -butyl
<sup>t</sup> BuOH		<i>tert</i> -butanol
TEA		triethylamine
TEAA		triethylammonium acetate
Tf		triflyly/triflate/trifluoromethanesulfonate
TFA		trifluoroacetic acid
TFAA		trifluoroacetic anhydride
TFB		trifluoroborate

THF	tetrahydrofuran
Thr (T)	<i>L</i> -threonine
TIC	the total ion current chromatography
TIMP	tissue-localized inhibitor of metalloproteinases
TLC	thin layer chromatography
TMEDA	tetramethylethylenediamine
TMS	trimethylsilyl
Tol	toluene
$t_R$	retention time
Tris	tris(hydroxymethyl)aminomethane
Trp (W)	<i>L</i> -tryptophan
Trt	trityl
TS	transition state
TsOH	toluenesulfonic acid
Tyr (Y)	<i>L</i> -tyrosine
UPLC	ultra-performance liquid chromatography
UV-vis	ultraviolet-visible
Val (V)	<i>L</i> -valine
VEGF	vascular endothelial growth factor

## Acknowledgements

It has been a long journey to reach this point. Thanks to all the help and support, personally and academically from many kind people around me, I can be here now.

First of all, I would like to acknowledge my supervisor Dr. David M. Perrin. It would not have been possible for me to get involved in these great projects described in this dissertation without him. As a young scientist in the imaging field, Dave led me into this important and fascinating research area. His passion about great science always helps us out during times of difficulty. His persistence and enormous efforts are the major driving force to push everything forward. His critical comments and advice have been extremely helpful through the preparation of this thesis. Besides setting high scientific standards, he has also provided me a great deal of freedom to explore many aspects of the projects and offered me opportunities to present my work in many conferences, which have been great scientific experiences in these six years. In addition, I'd also like to acknowledge all members in my supervisory committee, Dr. Jennifer A. Love, Dr. Stephen G. Withers, and Dr. Chris Orvig, for their advice on the projects.

Moreover, I would like to acknowledge my previous fellow graduate students, Dr. Curtis Lam, Dr. Christopher Hipolito, and Dr. David J. Dietrich for their efforts in proof-reading my thesis. Their advice clearly helped to improve this thesis. Besides, all of them have been very helpful and supportive during my stay in the Perrin lab. I really appreciate their friendship and support.

Special thanks to several people who have been involved in this work. Dr. Richard Ting initiated this project in 2005 and thereafter has made numerous discoveries, which provided the foundation of this project. Richard has helped me a lot to understand many key things/concepts in this field since I took over the project. Dr. Curtis Harwig gave me useful advice for the synthesis, and discussion with him was always fruitful. Thank you very much. There were several undergraduate students having worked with me in this project. Ms. Shiqing Tang, Ms. Liqun Wang, Ms. Angela Leung, and Mr. Peter Tian have contributed to the project by making several precursors. It was quite enjoyable working with them.

I must acknowledge our collaborators, to only some of whom it is possible to give

particular mention here. Dr. Christopher M. Overall, Dr. Ulrich auf dem Keller, Dr. Caroline L. Bellac, and Dr. Philipp F. Lange were our biological support for the marimastat project (Chapter 4). It was pleasant to work with them. And special thanks should go to Dr. Caroline L. Bellac, who I have harassed a lot during my thesis preparation for all those biological details. She is so nice and patient to respond to all my questions and requests. Thank you very much. I would like to thank all the people I have talked to and worked with at TRIUMF. It is impossible to have the work done without them. Dr. Tom Ruth, Dr. Mike Adam, Dr. Salma Jivan, and Dr. Paul Schaffer provided me training and guidance to work with radioactive materials and also helped to schedule our radiolabeling experiments. Mr. Wade English and Ms. Linda Graham have operated the cyclotron to produce  $^{18}\text{F}$ -fluoride for our experiments. I need to thank Dr. Hua Yang for her assistance on the radio-HPLC, frequently taking care of my radioactive waste and useful discussion on my radiolabeling work. I would like to thank Ms. Christine Takhar, Ms. Kathleen Genge, and (soon-to-be) Dr. James Inkster for their patience and help with my radiolabeling work undertaken at TRIUMF. On the other hand, we were fortunate to collaborate with Dr. John Valliant and Dr. Karin Stephenson at the CPDC. They provided us  $^{18}\text{F}$ -fluoride for about two weeks in 2010, which was a really productive period. I would like to especially thank Dr. Ryan Simms at the CPDC, who patiently assisted me with the radiolabeling work. I would also like to acknowledge Dr. Francois Benard from the BC Cancer Agency (BCCA) for his input to the imaging work of marimastat. I would like to thank Dr. Kuo-Shyan Lin, Dr. Jinhe Pan, Ms. Maral Pourghiasian, Ms. Jennifer Greene, and Mr. Jean-Pierre Appiah for their help on the labeling work at the BCCA.

I would like to thank all my talented colleagues in the lab. It is because of them that my PhD life is more joyful. To Dr. Jason Thomas, Dr. Jonathan May, Dr. Marcel Hollenstein, Dr. Ali Asadi, Mr. Justin Lo, Mr. Jack Huang, (soon-to-be) Dr. Marie Willaing Johannsen, (soon-to-be) Dr. Erkai Liu, Dr. Liang Zhao, Mr. Henry Chen, Mr. Daniel Walker, Mr. Abid Hasan, Mr. Zhibo Liu, Mr. Wenbo Liu, Ms. Yajun Wang, Mr. Jerome Lozada, (soon-to-be) Dr. Antoine Blanc, Dr. Marleen Renders, and many undergraduate students ever working in the lab, thank you all.

I would like to acknowledge the staff from the facilities in Chemistry Department, especially the staff in the NMR and Mass labs, who have helped a lot during my Ph.D study. Thank you to Dr. Paul Zhicheng Xia, Ms. Zorana Danilovic, Ms. Maria Ezhova,

and Mr. Jason Traer for their assistance with the NMR spectroscopy. Thank you to Dr. Yun Ling, Mr. Marshall Lapawa, Mr. David Wong, and Mr. Derek Smith for their advice and assistance with the mass spectrometry. I would also like to acknowledge the supporting staff in the department. They are Ms. Sheri Harbour, Ms. Lani Collins, Mr. Milan Coshizza, Mr. Des Lovrity, Ms. Jane Cua, Mr. Bojan Zimonjia, Mr. Xinhui Huang, Mr. John Ellis, Mr. Patrick Olsthoorn, Mr. Nate Kumar, Ms. Helen Bottriell, Ms. Bev Evans, Ms. Tram Nguyen, and Ms. Marjan Molouk-Zadeh.

Also, I would like to take this opportunity to acknowledge my dear friends, physically in Vancouver or not. Qin, I guess I finally have accomplished both of our dreams. Huiying, Yuan (Li), Yan (Cai), Dan (Yu), Liang, Feng, Yuan (Ren), Xiaozhe, Arwen, Jian, Yan (Xu), Zhifeng, Qiao, Hui, Zhan, Xiufeng, Peng, Xuan, Yong, Kuan, Chengguang, Yan (Liu), and Dan (Wang), thank you all for your great friendship.

Mostly, in the end, I am extremely grateful to my family. Without your support and understanding, I will not be able to pursue my Ph.D dreams. Thank you, Dad and Mum, for raising me up and educating me to be an honest, determined and strong person who is able to take the challenges and be persistent at tough times. Thank you, my parents-in-law, for your consideration and support during these years and your forgiveness to my childishness. Most of most, I would like to thank my husband, Yi, for his unequivocal support and encouragement throughout, as always, for which my mere expression of thanks likewise does not suffice.

To everyone listed above and showing up in my life, thank you all. You made me!

## **Dedication**

*This dissertation is dedicated to my beloved grandparents, who passed away during my graduate studies.*

# Chapter 1 Introduction

While significant progress has been made in our understanding of various biological processes at the molecular levels in the past decades, the causes of many malignant diseases still remain unknown. The remarkable advances from various noninvasive imaging techniques that allow the direct visualization of *in vivo* processes, however, have provided better understanding about disease progression for suitable treatment, and significant *in vivo* information to evaluate tested drugs for improved pharmacokinetics, pharmacodynamics, specificity, and stability at a timely manner.<sup>1-4</sup> Both drug development and therapies, therefore, have benefited from this newly emerging field: molecular imaging science. A brief review about molecular imaging will be presented in this chapter.

## 1.1 Molecular imaging

Molecular imaging is a multi-disciplinary field, which has been defined as noninvasive, quantitative, and reproducible visualization of biological processes and targeted macromolecules in living organisms.<sup>1</sup> It is now playing increasingly important roles in diagnosis, therapeutic evaluation, and drug development. There are two important elements for molecular imaging: i) the concentration and/or detectable properties of a molecular probe can be changed due to the biological process/distribution, and ii) a suitable technique is available to track the probe *in vivo*.<sup>1, 5</sup> Molecular imaging is therefore expected to provide characteristic and quantitative information about biological processes at cellular and subcellular levels in intact living subjects.<sup>4</sup> There are generally two categories of probes used in molecular imaging: direct and indirect probes, which target the biomarkers differently via either the concentration or the functionality of the biomarkers.<sup>1</sup> In addition, based on different reporter modalities, there are many molecular imaging approaches extensively applied in animal studies or in clinical trials, such as optical imaging, ultrasound imaging, magnetic resonance imaging (MRI), X-ray computed tomography (CT), and radionuclide imaging including positron emission tomography (PET) and single photon emission computed tomography (SPECT).<sup>4-6</sup>

**Optical imaging** includes fluorescence imaging<sup>7</sup> and bioluminescence imaging.<sup>8</sup> Fluorescence imaging relies on the detection of fluorescent light that is emitted upon the excitation of fluorophores, which can be endogenously produced or exogenously administered.<sup>4, 6, 7</sup> Bioluminescence imaging is based on the enzymatic reactions that release light, which can be detected to indicate aspects of a biological process.<sup>4, 8</sup> Both of these optical imaging methods benefit from high sensitivity (up to  $10^{-15}$  M), low instrumentation cost, general availability, and compatibility with high-throughput capabilities. They are quick and easy to perform. Nevertheless, both modalities suffer from high degrees of light scattering *in vivo* and absorption by overlying tissues, which limits their use in deep tissue detection.<sup>4, 6</sup> Autofluorescence from normal tissues is another drawback of fluorescence imaging. Generally, optical imaging is most often used for preclinical studies in small animals.

**Ultrasound imaging** examines the reflection of high-frequency sound waves from tissues to construct *real-time* ultrasound images to monitor the structure and movement of the body's internal organs and to measure the blood flow.<sup>4, 6</sup> It has been found that ultrasound imaging might be useful to study microcirculation, angiogenesis, and neovascularization of tumors.<sup>9</sup> Ultrasound imaging is inexpensive, simple, and rapid to perform, but its poor tissue penetration and high dependence on operators' skill and experience highly limit its application to intravascular structures. It is more regarded as a qualitative tool, since it has limited sensitivity to detect the contrast agents.<sup>6</sup>

**Magnetic resonance imaging** (MRI), based on the energy absorbed and emitted in the magnetic field, measures the rates of relaxation of hydrogen atoms or other atoms in high magnetic fields.<sup>6</sup> As water is abundant in living beings, most MRI contrast agents based on paramagnetic metals have been designed to interact with water and perturb the magnetic properties of hydrogen atoms. Since the relaxation of hydrogen atoms bound to water is different in tissues that retain the targeted contrast agents, MRI is a powerful imaging technique that provides anatomical images with high resolution and is also able to map the contrast agents *in vivo*. However, its sensitivity is as low as  $10^{-3}$  to  $10^{-4}$  M; the acquisition time is long and the available contrast agents are limited.<sup>4, 10, 11</sup>

**X-ray computed tomography** (CT) is based on the differentiable absorption of X-rays

by different tissues,<sup>4, 6</sup> and provides high resolution anatomical images. Since X-ray absorption is determined by the density of the tissues, CT is limited to providing information on soft tissues. In spite of its low detection sensitivity and lack of readily available targeted probes, CT is highly significant when used in combination with other imaging techniques such as MRI,<sup>12</sup> SPECT,<sup>13</sup> and PET.<sup>14</sup>

**Single photon emission computed tomography** (SPECT) detects  $\gamma$ -rays directly emitted by radioisotopes and reconstructs the localization of the contrast agents carrying the radioisotopes *in vivo* noninvasively.<sup>4, 6, 15</sup> Since a collimator is installed between the detector and the imaging subject to allow only  $\gamma$ -rays of characteristic energies to pass through and be detected, photons with different energies can be differentiated and SPECT is thus able to provide the information of multiple radionuclides (2 ~ 3) simultaneously.<sup>4, 6</sup> Notwithstanding the use of radionuclides, the sensitivity of SPECT is compromised by the collimator, which absorbs a large quantity of  $\gamma$ -rays emitted from the radionuclides. In turn, relatively high administered doses of the radiotracer and long scanning time are usually prerequisites for generating high quality SPECT images.<sup>4, 6, 10</sup>

**Positron emission tomography** (PET) detects  $\gamma$ -rays with the energy of 511 keV, which are released upon the annihilation of positrons. PET proceeds with high sensitivity ( $10^{-11}$  ~  $10^{-12}$  M) while small doses of radioactivity are required for the image acquisition, since nearly all the incidents can be directly measured by the detector.<sup>4, 16</sup> PET imaging is also independent of the depth where the radioactive compound locates, and it is regarded as quantitative in that the signals are proportional to the concentration of the radioligand in the tissue. PET, however, has a functional limitation of spatial resolution, which relies on the size of the single detector component.<sup>4</sup> Moreover, with the requirement of an expensive cyclotron to produce most of the PET-radionuclides and of PET scanners, PET imaging remains one of the most costly diagnostic techniques.

The molecular imaging techniques have been briefly reviewed above. Several aspects including the advantages and disadvantages of these imaging modalities are listed in Table 1.1. Clearly, each technique carries its advantages and disadvantages. Currently, besides the application of the single imaging modality for diagnosis, the combination of different imaging techniques is a promising direction of molecular imaging to provide

more accurate measurement in monitoring *in vivo* processes. On the other hand, since the development of PET imaging agents is the goal of this dissertation, a more detailed review about PET imaging is given in the following section.

**Table 1.1 A summary of imaging modalities.**<sup>4, 10</sup>

<i>Modality</i>	<i>Resolution (mm)</i>	<i>Spatial temporal</i>	<i>Penetration depth</i>	<i>Sensitivity (M)</i>	<i>Advantages</i>	<i>Disadvantages</i>
Fluorescence	2-3	Sec to min	< 1 mm	10 <sup>-9</sup> -10 <sup>-12</sup>	High-throughput screening High sensitivity	Low penetration depth Limited clinical translation*
Bioluminescence	3-5	Sec to min	1-2 mm	10 <sup>-15</sup> -10 <sup>-17</sup>		
Ultrasound	0.05-0.5	Sec to min	mm-cm	-	Clinical translation High spatial and temporal resolution Low cost	Operator dependency Low penetration depth Lack of targeted probes Targeted imaging limited to vascular compartment
CT	0.025-0.2	Min	No limitation	-	High spatial resolution Unlimited depth penetration Clinical translation	No target-specific imaging Use of X-radiation Poor soft-tissue contrast
MRI	0.025-0.1	Min to hr	No limitation	10 <sup>-3</sup> -10 <sup>-5</sup>	Superior spatial resolution Clinical translation	Imaging time Costs
SPECT	0.5-1.5	Min	No limitation	10 <sup>-10</sup> -10 <sup>-11</sup>	High sensitivity Multiple isotope imaging Availability of tracers and instruments	Attenuation-associated accuracy limit Size of reporter probes Limited spatial resolution
PET	3-7	10 s to min	No limitation	10 <sup>-11</sup> -10 <sup>-12</sup>	High sensitivity High throughput Attenuation correction	Fundamentally limited spatial resolution Lack of clinical translation Costs

\* Clinical translation refers to availability of anatomical information.

## 1.2 Molecular imaging with PET

### 1.2.1 How does PET work?

PET, as mentioned in the previous section, relies on the detection of  $\gamma$ -rays created during the annihilation of positrons. As shown in Figure 1.1, positrons, positively charged electrons, are released from the decay of positron-emitting radionuclides (PET-radionuclides).<sup>17</sup> When positrons, which are antimatter particles, collide with negatively charged electrons, which are abundant in all matter, this collision results in the annihilation, in which both the positron and the electron disappear and two  $\gamma$ -ray photons are produced. These photons, with energy of 511 keV, correspond to the resting masses of

the positron and electron, following the laws of conservation of electric charge/linear and angular momentum/total energy. The two photons are released simultaneously in the 180° direction to each other and can be detected by the detector surrounding the subject. The positron might travel a short distance from where the decay of the radionuclide occurs, and the average net trajectory (positron range) is always determined by the positron energy in the emission, which is a characteristic decay property of the corresponding radionuclide. By recording many pairs of the coincident  $\gamma$ -ray photons, a spatial distribution of the radioactivity can be constructed through the use of computed tomography as a function of time to provide PET images.

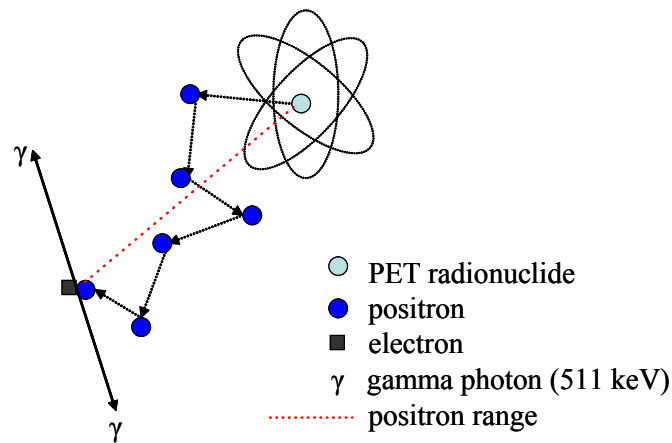


**Figure 1.1 An illustration of positron annihilation.**

A positron is emitted from the radionuclide during the decay process. Since the positron possesses momentum, it travels (shown as the black dot line) through elastic collision until it collides with an electron to release two  $\gamma$ -photons with 511 keV at two opposite directions.

The spatial resolution of a PET scan highly depends on the size of the detector and the positron range.<sup>18,19</sup> The detector size actually determines the intrinsic resolution of most scintillation detectors. In addition, the distance that a positron travels in the tissue, before it is annihilated via capturing an electron, also affects the resolution. The site of positron emission is always distant from the site of the annihilation as shown in Figure 1.1. This distance is defined as the positron range. Although the positron range is an average value, it is directly related to the positron energy in H<sub>2</sub>O or tissues. Higher positron energy always results in a longer positron range. As the detector actually records signals, which directly relate to the site of the annihilation, a longer positron range always results in poorer spatial resolution. Therefore, for a good image, PET-radionuclides with low positron energies are always preferred.

## 1.2.2 Choices of PET radionuclides

The increased use of PET imaging depends on the development of new imaging probes. Every probe consists of both a functionally targeting moiety and a radionuclide. There are many positron-emitting radioisotopes, and several frequently used ones are listed in Table 1.2 with their radioactive properties presented. There are several criteria to consider when choosing a PET radioisotope for PET imaging studies:<sup>20</sup> a), a reasonable half-life that allows the preparation of the radiotracers and the *in vivo* clearance of the radiotracer; b), suitable positron energy that affords high image resolution; c), acceptable radiation dosimetry to the subject; d) availability of the isotope in sufficient amounts and in high specific activities from a cyclotron or a generator; and e), one or more reliable and reproducible methods to incorporate the radionuclides into the bioligands with high radiochemical yields.

**Table 1.2 Some positron-emitting radionuclides for PET.**<sup>20-22</sup>

Nuclide	$t_{1/2}$ (min)	SA* (Ci/ $\mu$ mol)	Decay (% $\beta^+$ )	$\beta^+$ energy (keV)**		$\beta^+$ range in Water (mm)	
				Max.	Mean	Max.	Mean
<sup>11</sup> C	20.4	9220	99.77	960.1	385.6	4.1	1.1
<sup>15</sup> O	2.04	91730	100	1700	n/a	5.4	n/a
<sup>18</sup> F	109.8	1710	96.7	633.5	249.8	2.4	0.6
<sup>64</sup> Cu	768	245	17.87	652.9	278.1	2.9	0.64
<sup>68</sup> Ga	68.3	2766	87.7	1899.1	836	8.2	2.9
<sup>86</sup> Y	884	213	12.4	1253.5	440	5.2	1.8
			5.6	1578	696	6.5	2.9
<sup>124</sup> I	6048	31	11.0	1532.3	685.9	6.3	2.3
			12.0	2135	973.6	8.7	3.5

NOTE: The most characteristic emissions of positron for each radionuclide have been indicated. \*SA is specific activity; \*\* $\beta^+$  is positron.

Among the radionuclides listed in Table 1.2, <sup>11</sup>C-carbon is one of the radionuclides often used for PET studies and clinical trials. Although its short half-life of 20.3 minutes imposes a strict limitation on radiotracer preparation and imaging data acquisition, the radiation dose administered to the patients and the production chemists is intrinsically reduced. Additionally, as carbon is one of the key elements in various compounds, <sup>11</sup>C-labeled radiotracers would retain largely the biological nature of the leading compounds by simply replacing <sup>12</sup>C-carbon to <sup>11</sup>C-carbon.<sup>23</sup> The <sup>11</sup>C-radiochemistry has

been expanded and developed to provide many new  $^{11}\text{C}$ -imaging compounds and some of the  $^{11}\text{C}$ -labeled radiotracers are currently under clinical evaluation.<sup>23-25</sup>

Another radionuclide that has received a large amount of attention is copper-64.<sup>26</sup> The longer half-life allows its transport from one site to another (within hours of driving/flying etc.), and it is also useful to localize  $^{64}\text{Cu}$ -radiolabeled tracers, such as antibodies and macromolecules, the clearance of which requires longer time. The radionuclide  $^{64}\text{Cu}$ -copper has been incorporated into functional molecules via various chelating ligands and some  $^{64}\text{Cu}$ -labeled compounds have provided promising imaging results.<sup>26-28</sup> Despite the fact that  $^{64}\text{Cu}$  is an emerging PET isotope, only 17.9% of its decay accounts for positron emission. Due to the low positron yield, longer acquisition times<sup>29</sup> or higher administration doses<sup>17</sup> may be required to accumulate enough data to achieve reasonable image quality.

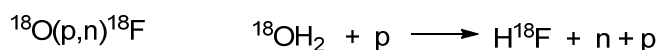
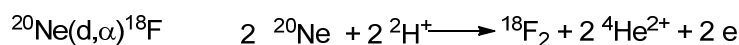
Gallium-68 ( $^{68}\text{Ga}$ ) has been recognized as an attractive alternative radionuclide in PET imaging.<sup>30</sup> In addition to its moderate half-life (68.3 min), a high positron yield (87.7%), and the relatively low mean positron energy, its production from  $^{68}\text{Ge}$  in the commercially available generator accelerates the development of  $^{68}\text{Ga}$ -labeled radiotracers. By coordination with a variety of ligands, several  $^{68}\text{Ga}$ -labeled peptides such as  $[\text{Tyr}^3]\text{octreotide}$  and bombesin have entered preclinical evaluations and encouraging results have been obtained.<sup>30</sup>

In addition, there are also many  $^{18}\text{F}$ -labeled PET imaging agents under investigation in the field. Some of them have exhibited high potential for clinical uses in cancer diagnosis.<sup>31</sup> This is because of the optimal properties of fluorine-18, which conform to various requirements to achieve good qualities of PET images.<sup>17, 31</sup> Fluorine-18 has a half-life of 109.8 minutes, weak positron energy, and a clean decay process (96.7%). It can be produced with high specific activities in a cyclotron efficiently. All these attributes make fluorine-18 one of the ideal isotopes for PET imaging development in terms of resolution and dosimetry.

## 1.3 <sup>18</sup>F-Labeling techniques

### 1.3.1 Production of <sup>18</sup>F-fluoride/fluorine

The radionuclide <sup>18</sup>F-fluoride/fluorine can be produced in a cyclotron via two nuclear reactions as shown in Scheme 1.1.<sup>32</sup> Fluorine-18 was first produced in the form of <sup>18</sup>F-F<sub>2</sub> gas from the bombardment of neon gas with 5 MV deuterons, described as the nuclear reaction of [<sup>20</sup>Ne(d,α)<sup>18</sup>F], by Snell and co-workers.<sup>33</sup> Later, <sup>18</sup>O-target<sup>a</sup> was developed as a more widely used method for both <sup>18</sup>F-F<sub>2</sub> and <sup>18</sup>F-fluoride via proton bombardment following [<sup>18</sup>O(p,n)<sup>18</sup>F].<sup>34-36</sup> The <sup>18</sup>O(p,n)<sup>18</sup>F nuclear reaction with <sup>18</sup>O-enriched water is the most used nuclear reaction to produce <sup>18</sup>F-fluoride with high specific activities.



**Scheme 1.1** The scheme of the nuclear reactions to produce <sup>18</sup>F-fluorine/fluoride.

For <sup>18</sup>O(p,n)<sup>18</sup>F, the nuclear reaction for the irradiation of <sup>18</sup>O-enriched water is demonstrated.

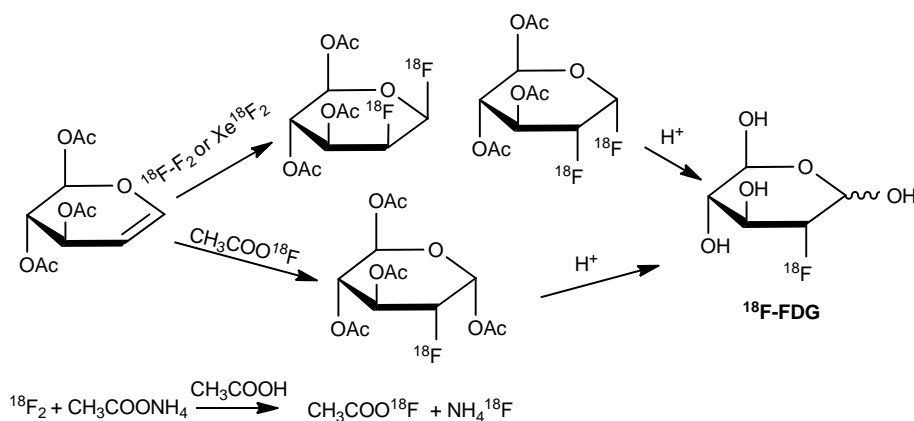
Radiosyntheses, however, are constrained by radiation safety concerns, short half-lives of the radioisotopes, and the need for high specific activities. Short total radiosynthesis time and reasonable high radiochemical yields are necessary for the preparation of radiopharmaceuticals. To reduce the operation of radiation with regard to safety and production concerns, fewer steps, radioisotope incorporation at a later stage and simpler purification procedures are always favored.<sup>17</sup> The two different forms of <sup>18</sup>F-fluorine produced in the cyclotron demonstrate dramatically different chemical reactivities. Hence different chemical reactions have been employed to incorporate <sup>18</sup>F-fluorine into molecules for PET imaging applications.<sup>16, 17</sup> In the following part, chemistry involving <sup>18</sup>F-fluorine incorporation is described.

### 1.3.2 Radiosyntheses involving electrophilic <sup>18</sup>F-F<sub>2</sub>

Electrophilic <sup>18</sup>F-fluorine has been applied to reactions involving electronically enriched molecules, such as alkenes and arenes. <sup>18</sup>F-Fluorine gas (<sup>18</sup>F-F<sub>2</sub>),<sup>37-39</sup> xenon

<sup>a</sup> <sup>18</sup>O-Target is the target with oxygen-18.

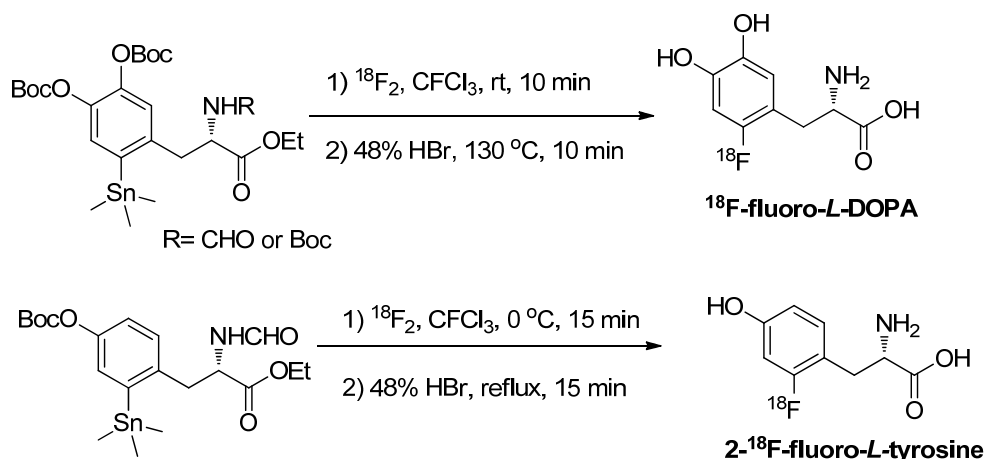
difluoride ( $\text{Xe}^{18}\text{F}_2$ ),<sup>40-44</sup> and  $^{18}\text{F}$ -acetylhypofluoride ( $\text{CH}_3\text{CO}_2^{18}\text{F}$ )<sup>39, 45, 46</sup> are used for the electrophilic fluorination.<sup>47</sup> Using different electrophilic  $^{18}\text{F}$ -fluorine reagents via electrophilic addition reactions, the radiosyntheses of 2-deoxy-2- $^{18}\text{F}$ -fluoroglucose ( $^{18}\text{F}$ -FDG), which is widely used in clinic to investigate various diseases by monitoring glucose mechanism, are summarized in Scheme 1.2.<sup>37, 40, 45</sup> By the electrophilic addition of  $^{18}\text{F}$ -reagents to the double bond, an  $^{18}\text{F}$ -fluorinated intermediate is obtained. Following an acid treatment, the desired product  $^{18}\text{F}$ -FDG is prepared. In addition to the electrophilic addition reactions to introduce  $^{18}\text{F}$ -fluorine, electrophilic aromatic substitutions have also been developed.<sup>47-49</sup> Particularly, the fluorodestannylation reaction has been applied to prepare useful imaging tracers such as  $^{18}\text{F}$ -fluoro-*L*-DOPA<sup>50</sup> and  $^{18}\text{F}$ -fluoro-*L*-tyrosine<sup>49</sup> regioselectively from trialkyltin derivatives, as indicated in Scheme 1.3.  $^{18}\text{F}$ -Fluoro-*L*-DOPA is known to target the cerebral dopamine metabolism for imaging neurodegenerative diseases, and  $^{18}\text{F}$ -fluoro-*L*-tyrosine images protein synthesis.



**Scheme 1.2** Radiosyntheses of  $^{18}\text{F}$ -FDG via electrophilic reactions.<sup>37, 40, 45</sup>

Electrophilic addition using either  $\text{Xe}^{18}\text{F}_2$  or  $^{18}\text{F}_2$  always provides stereometric intermediates, while at most 50% of  $^{18}\text{F}$ -fluorine can be incorporated to the final radiolabeled compounds. Moreover,  $^{18}\text{F}$ -fluorine production from the nuclear reaction always requires the addition of  $^{19}\text{F}$ - $\text{F}_2$ , which limits the specific activity to a few  $\text{mCi}/\mu\text{mol}$  ( $< 20 \text{ mCi}/\mu\text{mol}$ ).<sup>17, 51</sup> However, as for the synthesis of  $^{18}\text{F}$ -fluoro-*L*-DOPA, the electrophilic fluorodestannylation remains the synthesis of choice due to its simplicity compared with the synthetic route involving  $^{18}\text{F}$ -fluoride nucleophilic

reactions.



Scheme 1.3 Examples of fluorodestannylation to prepare functional  $^{18}\text{F}$ -labeled reagents.<sup>49, 50</sup>

### 1.3.3 Radiosyntheses with nucleophilic $^{18}\text{F}$ -fluoride

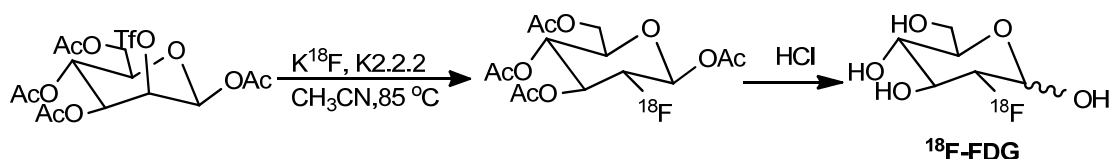
In contrast to the production of  $^{18}\text{F}\text{-F}_2$ ,  $^{18}\text{F}$ -fluoride can be routinely prepared with very high specific activities ( $\sim 5\text{-}14 \text{ Ci}/\mu\text{mol}$ ).<sup>16, 17, 52</sup> Although  $^{18}\text{F}$ -fluoride is highly hydrophilic and its hydrated form is quite inert, it can be converted to a very nucleophilic species by routine manipulations. Briefly,  $^{18}\text{F}$ -fluoride is activated by the removal of water and the addition of metal ion chelating agents such as Kryptofix-222 (K2.2.2).<sup>17, 22</sup> In this section, the incorporation of  $^{18}\text{F}$ -fluoride will be reviewed. Two categories of labeling methods, based on the construction of  $\text{C-}^{18}\text{F}$  and  $\text{X-}^{18}\text{F}$  (X is any atom rather than carbon) bonds, will be described.<sup>16, 53</sup>

#### 1.3.3.1 To form the $\text{C-}^{18}\text{F}$ bond via nucleophilic reactions- the conventional technique for $^{18}\text{F}$ -labeling

The majority of  $^{18}\text{F}$ -labeled radiopharmaceuticals are synthesized by nucleophilic substitutions on aliphatic substrates and aromatic compounds. Some of the  $^{18}\text{F}$ -labeled radiotracers have been routinely prepared by this method and used on a daily basis for diagnostics. The nucleophilicity of  $^{18}\text{F}$ -fluoride is usually activated by the addition of K2.2.2 in anhydrous solvent (DMSO or  $\text{CH}_3\text{CN}$ ) at elevated temperatures ( $120\text{-}150 \text{ }^\circ\text{C}$ ).<sup>17</sup>

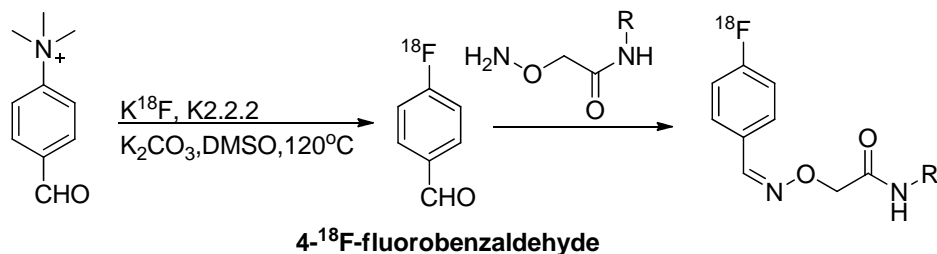
Most of the  $^{18}\text{F}$ -labeled aliphatic compounds are prepared from substrates with good

leaving groups such as halides and sulfonates (tosylate, mesylate or triflate).<sup>50</sup> The best known example might be the radiosynthesis of <sup>18</sup>F-FDG shown in Scheme 1.4.<sup>51</sup> The precursor 1,3,4,6-tetra-*O*-acetyl-2-trifluoromethanesulfonyl-β-*D*-mannopyranose is first fluoridated in the presence of K<sup>18</sup>F, K2.2.2 at ~ 80 °C for about 5 minutes under basic anhydrous conditions. Then the additive K2.2.2 and salts are removed by passing through a C18 sep-pak cartridge. The removal of acetyl groups under acidic conditions gives <sup>18</sup>F-FDG with high efficiency. By using a large quantity of precursors, the radiochemical yield of this reaction was determined to be 99% via radio-thin layer chromatography (TLC). Many <sup>18</sup>F-labeling compounds have been prepared in a similar manner.<sup>54-57</sup>

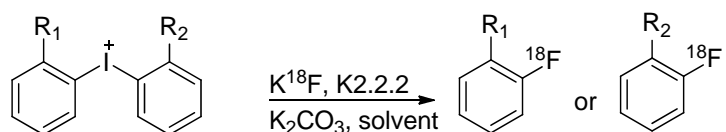


**Scheme 1.4** The radiosynthesis of <sup>18</sup>F-FDG via a nucleophilic substitution.<sup>51</sup>

Aromatic nucleophilic substitutions, on the other hand, involve leaving groups (such as halides, nitro groups, and trimethylamine) and electron withdrawing groups (such as cyano, nitro, and acyl groups) at the *para*- or *ortho*-position to the leaving group on the aromatic ring are always required to activate the ring for the reaction.<sup>17, 58-60</sup> For example, a simple <sup>18</sup>F-prosthetic group 4-<sup>18</sup>F-fluorobenzaldehyde is frequently prepared following substitution as shown in Scheme 1.5. Once the <sup>18</sup>F-synthon is prepared, it is rapidly incorporated to bioactive molecules via an oxime ether formation reaction.<sup>61, 62</sup>



**Scheme 1.5** The nucleophilic aromatic substitution to prepare <sup>18</sup>F-labeled compounds.



**Scheme 1.6** Reactions of diaryliodonium salts with <sup>18</sup>F-fluoride.<sup>63-65</sup>

In addition, diaryliodonium salts were reported as precursors for <sup>18</sup>F-fluoroarenes

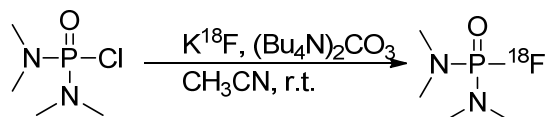
without electron withdrawing groups, as shown in Scheme 1.6.<sup>63</sup> The fluoridation can be accomplished in one step with good yields. A recent study revealed that the regioselectivity in the reaction of unsymmetrical diaryliodoniums could be controlled by the *ortho*-substituents.<sup>64, 65</sup>

From the examples illustrated for the C-<sup>18</sup>F bond formation with nucleophilic <sup>18</sup>F-fluoride, extremely anhydrous anionic <sup>18</sup>F-fluoride, elevated temperatures, protecting-group chemistry, and additives such as K2.2.2 are almost always required. These often lead to tedious multistep syntheses, problems for purification, and incompatibility to many biomolecules. Ideally, a one-step labeling strategy to incorporate <sup>18</sup>F-fluoride at room temperature under aqueous conditions is favored.

### 1.3.3.2 Newly developed methods to prepare <sup>18</sup>F-labeled molecules

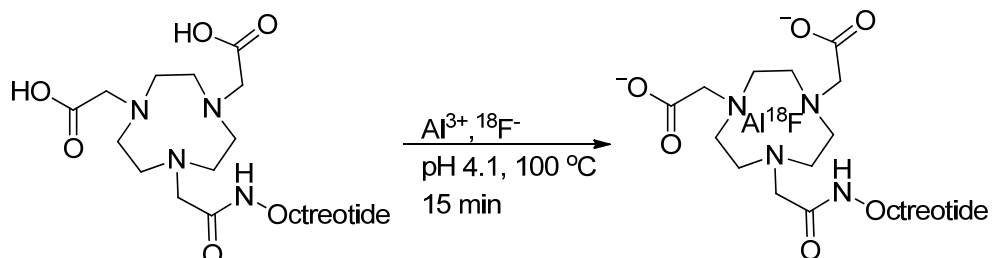
Several newly developed methods have provided possible alternatives for the incorporation of <sup>18</sup>F-fluoride, in the fashion dramatically different from the conventional C-<sup>18</sup>F bond formation. In this section, a brief introduction to the formation of a P-<sup>18</sup>F bond,<sup>66</sup> Al-<sup>18</sup>F complexes,<sup>67-70</sup> an Si-<sup>18</sup>F bond,<sup>71-77</sup> and a B-<sup>18</sup>F bond<sup>78-82</sup> will be presented.

**The P-<sup>18</sup>F bond formation** was reported by Studenov and co-workers in 2005.<sup>66</sup> It was described therein that a substitution reaction between <sup>18</sup>F-fluoride and *N,N,N',N'*-tetramethylphosphorodiamidic chloride in anhydrous CH<sub>3</sub>CN could yield the <sup>18</sup>F-labeled phosphorodiamidic compound with a high radiochemical yield of 96%. Instead of K2.2.2, tetrabutylammonium carbonate was added to activate <sup>18</sup>F-fluoride as a phase transfer agent (Scheme 1.7). Though the radiosynthesis ensued with a high radiochemical yield and efficiency, the <sup>18</sup>F-labeled compound underwent relatively rapid defluoridation in aqueous conditions, as about 25% of the P-<sup>18</sup>F bond decomposed within 30 minutes. Unfortunately, ever since then, no further investigation on improving the stability of the phosphorofluoridates has been reported.



Scheme 1.7 The radiosynthesis of <sup>18</sup>F-*N,N,N',N'*-tetramethylphosphorodiamidic fluoride.<sup>66</sup>

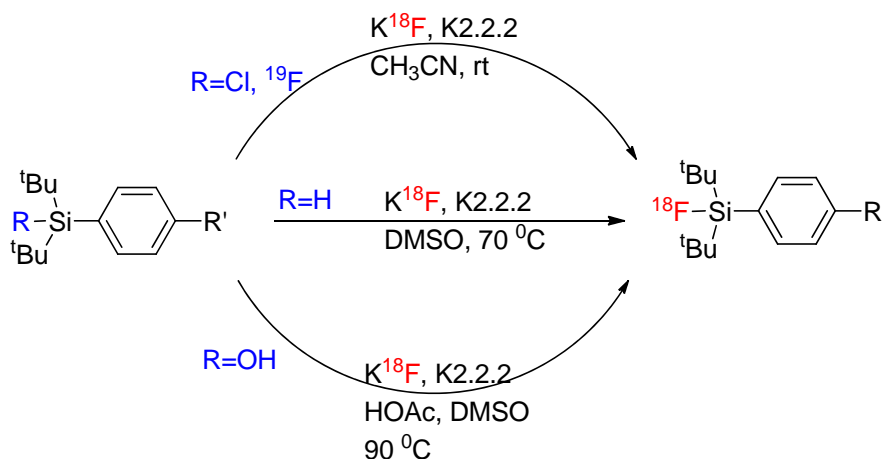
**<sup>18</sup>F-Fluoride-aluminum-chelates (Al-<sup>18</sup>F)** have been developed in the McBride group to label thermostable peptides such as haptin-peptides<sup>67, 68, 70</sup> and octreotide<sup>69</sup> for *in vivo* imaging studies. On the basis of fluoride-metal interactions, McBride and colleagues first tested the stability of the Al<sup>18</sup>F complexes with various chelating groups.<sup>67</sup> They found that peptides with the ligand 1,4,7-triazacyclonane-1,4,7-triacetic acid (NOTA) yielded Al<sup>18</sup>F complexes with the highest *in vivo* stability. It was also discovered in the same report that two of the carboxylic groups are critically required to stabilize the complex. With modifications of the NOTA ligands and optimization of the labeling conditions, both the radiochemical yield and labeling efficiency were improved.<sup>68</sup> The radiosynthesis via this method is usually undertaken in aqueous sodium acetate solution (pH 4.5) at around 100 °C and is complete within 15 minutes in high yields. It is expected this labeling technique might be expanded to biomolecules with low thermostability via one-pot two-step radiosyntheses using useful prosthetic groups. The chelation of Al<sup>18</sup>F with NOTA-octreotide is shown in Scheme 1.8 as an example of this labeling method.<sup>69</sup>



**Scheme 1.8** <sup>18</sup>F-Labeled NOTA-octreotide with Al<sup>18</sup>F.<sup>69</sup>

**The Si-<sup>18</sup>F bond formation** has received a great deal of attention recently. Synthetically, fluoride has frequently been used to remove silyl protecting groups, especially the sterically hindered ones.<sup>83</sup> This might be due to the strong bond energy of the Si-F bond. In fact, dating back to 1985, the first preparation of <sup>18</sup>F-trimethylsilyl fluoride (<sup>18</sup>F-TMS-F) was reported by Rosenthal *et al.*, who treated TMS-Cl with <sup>18</sup>F-trimethylammonium fluoride in aqueous CH<sub>3</sub>CN to give <sup>18</sup>F-TMS-F with a radiochemical yield of 80% (decay corrected).<sup>84</sup> <sup>18</sup>F-TMS-F, however, decomposed quickly *in vivo*, resulting primarily in bone uptake as imaged in mice. It was not until recently that the formation of the Si-<sup>18</sup>F bond came back to the stage to provide potential <sup>18</sup>F-labeled radiopharmaceuticals, with a better understanding of the stability of the <sup>18</sup>F-fluorosilyl compounds.<sup>71-73</sup> Schirmacher and colleagues found that the hydrolytic

stability of  $^{18}\text{F}$ -fluorosilanes can be highly improved through sterics by introducing bulky substituents such as the *tert*-butyl group to the silicon atom.<sup>71</sup> Consequently, the di-*tert*-butylphenyl- $^{18}\text{F}$ -fluorosilane exhibited high *in vitro* and *in vivo* stability. Moreover, the di-*tert*-butylphenyl- $^{18}\text{F}$ -fluorosilane can be prepared in the presence of K2.2.2 in anhydrous  $\text{CH}_3\text{CN}$  at room temperature by either the isotopic exchange reaction or the substitution reaction of the related chlorosilane compound with  $^{18}\text{F}$ -fluoride, as indicated in Scheme 1.9. Since it is of great synthetic challenge to conjugate biomolecules to the hydrolytically labile chlorosilanes, Schirmacher and co-workers have thereafter mainly focused on the development of an elegant isotopic exchange reaction to prepare  $\text{Si-}^{18}\text{F}$  compounds, in spite of the fact that this represents a carrier-added experiment whereby the specific activity may be compromised.<sup>74, 75, 77</sup> On the other hand, also indicated in Scheme 1.9, Ametamey and colleagues reported alternative ways to prepare the di-*tert*-butylphenyl fluorosilane from the corresponding silanol or silane.<sup>72, 73</sup> The resulting di-*tert*-butylphenyl- $^{18}\text{F}$ -fluorosilane based bioconjugates, albeit with high preparative yields and good hydrolytic stability, are of high lipophilicity, which results predominantly in excretion by the liver. Modification of the silyl molecule will therefore be necessary to decrease its hydrophobicity for favored *in vivo* distribution and also improved clearance.

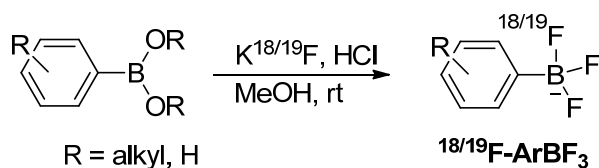


Scheme 1.9  $^{18}\text{F}$ -Radiosyntheses of silicon-based building blocks.<sup>71-73, 76</sup>

**The formation of the B- $^{18}\text{F}$  bond** was reported as another fluoride capturing technique by Perrin and co-workers in 2005.<sup>78</sup> By radiolabeling biotinylated *p*-aminophenylboronyl pinacolate under acidic conditions, Ting *et al.* were able to show  $^{18}\text{F}$ -fluoride

incorporation through the formation of an  $^{18}\text{F}$ -aryltrifluoroborate ( $^{18}\text{F}$ -ArBF<sub>3</sub>) in the presence of  $^{19}\text{F}$ -fluoride using avidin magnetic particles to separate the  $^{18}\text{F}$ -labeled biotin from the unreacted  $^{18}\text{F}$ -fluoride.<sup>78</sup> It was therein pointed out that the specific activity of the  $^{18}\text{F}$ -ArBF<sub>3</sub> is three times that of the source  $^{18}\text{F}$ -fluoride. Via a systematic study on the *in vitro* solvolytic stability of a series of ArBF<sub>3</sub>s, it was recognized that the hydrolytic stability of ArBF<sub>3</sub>s can be controlled by different substituents on the aryl region and several potential ArBF<sub>3</sub>s with high hydrolytic stability were identified for further studies.<sup>80, 85</sup> Furthermore, the *in vivo* stability of one  $^{18}\text{F}$ -ArBF<sub>3</sub> was confirmed by an animal study on the clearance and biodistribution of the biotin- $^{18}\text{F}$ -ArBF<sub>3</sub> conjugate.<sup>79</sup> Recently, Tsien and colleagues reported the work in combination of  $^{18}\text{F}$ -PET and near infrared fluorescence (NIRF).<sup>81</sup> Their “boron/optical multimodality beacon”, called  $^{18}\text{F}$ -BOMB, is based on the conjugation of the  $^{18}\text{F}$ -ArBF<sub>3</sub>/NIRF fluorophores to Lymphoseek to detect the distribution of the sentinel lymph node. We also have reported *in vivo* imaging work with an  $^{18}\text{F}$ -ArBF<sub>3</sub> conjugated to marimastat, which is a broad-spectrum MMP inhibitor that might find use in breast cancer diagnosis.<sup>86</sup> In addition to the efforts directed towards  $^{18}\text{F}$ -ArBF<sub>3</sub>s as PET imaging compounds, an isotopic exchange method has been reported to construct the B- $^{18}\text{F}$  bond for  $^{18}\text{F}$ -tetrafluoroborate ( $^{18}\text{F}$ -BF<sub>4</sub><sup>-</sup>) by Jauregui-Osoro *et al.* to detect the human sodium-iodide symporter.<sup>82, 87</sup> They incubated  $^{18}\text{F}$ -fluoride with NaBF<sub>4</sub> under acidic conditions at 120 °C for 20 minutes. The radiochemical yield (not decay corrected) of the isotopic exchange reaction was about 10%. Although both methods described here represent the radiosynthesis of boron compounds with the B- $^{18}\text{F}$  bond from carrier-added  $^{18}\text{F}$ -fluoride,  $^{18}\text{F}$ -ArBF<sub>3</sub>s provide extensive flexibility to label various functional molecules targeting different bioprocesses. The negative charge on  $^{18}\text{F}$ -ArBF<sub>3</sub>s may provide added advantage in that the labeled molecules have increased hydrophilicity. Moreover, the specific activity of  $^{18}\text{F}$ -ArBF<sub>3</sub>s is triple that of  $^{18}\text{F}$ -fluoride. This originates from the stoichiometric ratio (1:3) of  $^{18}\text{F}$ -ArBF<sub>3</sub>s to the bound fluorine atoms, which can compensate for any decrease in the specific activity of  $^{18}\text{F}$ -fluoride from the carrier addition. However, when considering the labeling conditions for  $^{18}\text{F}$ -ArBF<sub>3</sub>s, it is realized that the acidic conditions might be detrimental to various biomolecules, which might not survive low pHs. An alternative involving a one-pot two-step synthesis may

enable labeling the acid-sensitive molecules with  $^{18}\text{F}$ -ArBF<sub>3</sub>s.



**Scheme 1.10** The radiosynthesis of  $^{18/19}\text{F}$ -ArBF<sub>3</sub>s.<sup>78</sup>

Although several  $^{18}\text{F}$ -incorporation techniques have been introduced above, there is still no perfect labeling technique so far to accommodate all the requirements for radiosyntheses, such as rapid labeling reactions, high radiochemical yields, high specific activities, and a one-step radiosynthesis to obtain the final product. Every method contains one or more drawbacks. Novel labeling methods thus are desired. Meanwhile current techniques should be optimized to achieve better radiosyntheses with high radiochemical yields and specific activities.

## 1.4 Applying ArBF<sub>3</sub>s as PET imaging agents

In the previous section, it was mentioned that a good radiosynthetic scheme should minimize the number of radiosynthetic steps and shorten the synthesis time, while ensuring a reasonable radiochemical yield and a high specific activity. Moreover, the radiolabeled compounds need to possess good *in vitro* and most importantly *in vivo* stability, low lipophilicity for optimal clearance, and high *in vivo* target specificity.<sup>16, 17</sup> As ArBF<sub>3</sub>s are anionic,<sup>78, 79</sup> the ArBF<sub>3</sub> labeled biomolecules would have higher hydrophilicity, which in turn should lead to rapid *in vivo* clearance of the  $^{18}\text{F}$ -ArBF<sub>3</sub> labeled compounds. The moiety carrying  $^{18}\text{F}$ -atom should not impede the bioactivity of the biomolecules such as target specificity, and several  $^{18}\text{F}$ -ArBF<sub>3</sub> labeled compounds have not been observed to influence the affinity of biomolecules for their targets.<sup>79, 81, 86</sup> Nevertheless, the clearance and excretion of the labeled compound is likely to be enhanced due to the decreased lipophilicity derived from the negatively charged nature of ArBF<sub>3</sub>s. In this section, several aspects will be addressed in order to apply  $^{18}\text{F}$ -ArBF<sub>3</sub>s as potential PET imaging agents, including the specific activity, the radiochemical yield and solvolytic stability of  $^{18}\text{F}$ -ArBF<sub>3</sub>s.

### 1.4.1 Specific activity

Specific activity, an important factor for imaging assays, is defined as the amount of radioactivity given by a certain amount of a radiolabeled compound.<sup>16, 88</sup> Mathematically, it is the amount of radioactivity per micromole of the radiolabeled compound, as shown in Equation 1.1. Based on this definition, the theoretical specific activity of the carrier-free radionuclide can be calculated from the decay half-life of the radionuclide.

**Equation 1.1**      Specific activity =  $\frac{\text{Radioactivity (Ci)}}{\text{Amount of radiolabeled compound } (\mu\text{mol})}$

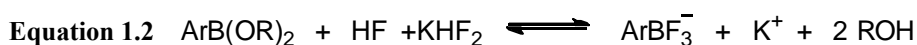
Practically, however, it is often impossible to obtain a carrier-free, 100% radiolabeled compound from a radiosynthesis, particularly in the case of <sup>18</sup>F-fluoride. This is because the radionuclide is almost always contaminated with its stable isotope. Consequently, the highest practical specific activity is much lower than the theoretical number. Taking <sup>18</sup>F-fluoride for example, the calculated theoretical specific activity is 1710 Ci/μmol. In contrast, the specific activity of <sup>18</sup>F-fluoride is usually measured to be < 40 Ci/μmol, according to Equation 1.1.<sup>16, 17, 52</sup> Usually <sup>18</sup>F-labeled imaging agents are produced at much lower specific activities.

Since most PET imaging agents are based on receptor binding, the radiotracer with a low specific activity would have to compete with the non-radiolabeled compounds (either the cold form or the decayed form), and less uptake of the radiolabeled compound will be expected. This is particularly true in cases with relatively low levels of receptors, in which case a significant percentage of receptors are occupied by the non-labeled compound. A significant amount of work has supported this hypothesis.<sup>89, 90</sup> For instance, Frost and co-workers<sup>89</sup> quantified the human opiate receptor *in vivo* via imaging experiments with high specific activities and low specific activities. The brain images clearly suggested that the radioactivity uptake by brain was highly reduced by the <sup>11</sup>C-labeled ligand with low specific activities. Partial saturation of the receptors was regarded to account for the suppression.

As for the case of any <sup>18</sup>F-radiolabeling experiments introduced in the previous section, the specific activity of an <sup>18</sup>F-labeled compound at any given time can be calculated if the specific activity of the source <sup>18</sup>F-fluoride is known. This is due to at least two

reasons. First of all, since  $^{18}\text{F}$ -fluoride has an insignificant kinetic isotopic effect compared to  $^{19}\text{F}$ -fluoride, it has the same physicochemical and biochemical properties as  $^{19}\text{F}$ -fluoride. In other words,  $^{18}\text{F}$ -fluoride and  $^{19}\text{F}$ -fluoride have the same opportunity to react in the same fashion in a radioreaction, and therefore the specific activity of  $^{18}\text{F}$ -fluoride can be directly transferred to that of the  $^{18}\text{F}$ -labeled compound. Secondly,  $^{18}\text{F}$ -fluoride and all the  $^{18}\text{F}$ -labeled species decay at the same rate, which implies that the specific activity at any given time could be calculated from the source  $^{18}\text{F}$ -fluoride via a first order decay function.

For example, for the no-carrier-added nucleophilic substitution reaction to prepare  $^{18}\text{F}$ -FDG as shown in Scheme 1.4, if the  $^{18}\text{F}$ -fluoride solution is the only source of  $^{19}\text{F}$ -fluoride, and if we started with a radioactivity of 50 mCi at a specific activity of 2 Ci/ $\mu\text{mol}$  (at  $t = 0$  min), there is 25 nmol of  $^{19}\text{F}$ -fluoride present. After radiosynthesis and separation to give the pure  $^{18}\text{F}$ -FDG (containing both anomers) at  $t = 55$  minutes ( $t_{1/2}$  for  $^{18}\text{F}$  is  $\sim 110$  min), no matter what the radiochemical yield is, the specific activity of the purified  $^{18}\text{F}$ -labeled compound is 1.41 Ci/ $\mu\text{mol}$  at  $t = 55$  minutes, calculated via the first order decay kinetics.



When it comes to  $^{18}\text{F}$ - $\text{ArBF}_3\text{s}$ , Equation 1.2 briefly demonstrates the overall preparation of  $^{18}\text{F}$ - $\text{ArBF}_3\text{s}$ , though the reaction most likely proceeds stepwise. From the reaction, one boronic acid/ester molecule reacts with one HF molecule and one molecule of  $\text{KHF}_2$  to give one  $\text{ArBF}_3$  anion. The specific activity of the  $^{18}\text{F}$ - $\text{ArBF}_3$  is three times that of  $^{18}\text{F}$ -fluoride, which can be derived as following:

**Equation 1.3**

$$\text{Amount (ArBF}_3) = \text{Amount (F)}/3$$

$$\begin{aligned} \text{Specific activity (ArBF}_3) &= \frac{\text{Radioactivity (Ci)}}{\text{Amount (ArBF}_3) [\mu\text{mol}]} = \frac{\text{Radioactivity (Ci)}}{\text{Amount (F)}/3 [\mu\text{mol}]} \\ &= 3 \times \frac{\text{Radioactivity (Ci)}}{\text{Amount (F) } [\mu\text{mol}]} = 3 \times \text{Specific activity } (^{18}\text{F}) \end{aligned}$$

In  $^{18}\text{F}$ -fluoride generated from the  $^{18}\text{O}$ - $\text{H}_2\text{O}$  irradiation, trace amounts of  $^{19}\text{F}$ -fluoride are always present, but the amount of  $^{19}\text{F}$ -fluoride varies from one cyclotron to another.<sup>52</sup> As a result, there is actually no good correlation to determine the specific activity for

$^{18}\text{F}$ -fluoride. Conventionally, the specific activity is determined by the incorporation of  $^{18}\text{F}$ -fluoride to afford an  $^{18}\text{F}$ -labeled compound, whose amount can be determined by methods such as UV absorption at a certain wavelength.<sup>91</sup> Another possible method to estimate the specific activity is via the addition of a relatively large amount of carrier  $^{19}\text{F}$ -fluoride, which outweighs  $^{19}\text{F}$ -fluoride that normally contaminates the original  $^{18}\text{F}$ -fluoride solution. Generally, if a substantial amount of carrier  $^{19}\text{F}$ -fluoride is added to  $^{18}\text{F}$ -fluoride (no-carrier-added) and well mixed with  $^{18}\text{F}$ -fluoride, the specific activity of the carrier-added  $^{18}\text{F}$ -fluoride can be calculated as (the amount of the radioactivity of  $^{18}\text{F}$ -fluoride)/(the amount of carrier  $^{19}\text{F}$ -fluoride + the amount of  $^{19}\text{F}$ -fluoride present in the original  $^{18}\text{F}$ -fluoride solution + the amount of  $^{18}\text{F}$ -fluoride). Since a large amount of carrier  $^{19}\text{F}$ -fluoride is added, both the amount of  $^{19}\text{F}$ -fluoride from the original  $^{18}\text{F}$ -fluoride solution and that of  $^{18}\text{F}$ -fluoride itself become negligible. The specific activity of the carrier-added  $^{18}\text{F}$ -fluoride can be simplified to (the amount of the radioactivity of  $^{18}\text{F}$ -fluoride)/(the amount of carrier  $^{19}\text{F}$ -fluoride).

For instance, if there is 200 mCi of  $^{18}\text{F}$ -fluoride from  $^{18}\text{O}$ - $\text{H}_2\text{O}$  irradiation and 800 nmol of  $^{19}\text{F}$ -fluoride is added (maybe in the form of  $\text{KHF}_2$ ) at  $t = 0$  minute, the specific activity of  $^{18}\text{F}$ -fluoride (at  $t = 0$  min) is 0.25 Ci/ $\mu\text{mol}$ . Assuming that it takes 55 minutes for the radiosynthesis and purification to prepare an  $^{18}\text{F}$ - $\text{ArBF}_3$ , then at  $t = 55$  minutes, the specific activity of  $^{18}\text{F}$ -fluoride is 0.177 Ci/ $\mu\text{mol}$ . But for the specific activity of the  $^{18}\text{F}$ - $\text{ArBF}_3$  at  $t = 55$  minutes, it should be 0.531 Ci/ $\mu\text{mol}$ .

It is appreciated that the addition of carrier  $^{19}\text{F}$ -fluoride suppresses the specific activity of  $^{18}\text{F}$ -fluoride while the formation of  $^{18}\text{F}$ - $\text{ArBF}_3$ s compensates to some extent for the loss with a tripling of the specific activity. Thus, it is possible to adjust the specific activity by controlling for the amount of added carrier  $^{19}\text{F}$ -fluoride. Furthermore, optimal reaction conditions might favor the formation of  $^{18}\text{F}$ - $\text{ArBF}_3$ s in the presence of a smaller amount of  $^{19}\text{F}$ -fluoride or even under no-carrier-added conditions.

#### **1.4.2 Radiochemical yields and synthesis time**

Though the yield is not always the top concern for radiosyntheses, it is important to be able to prepare radiolabeled compounds with “enough” radioactivity for animal imaging

experiments. Due to radiation safety, the radiosynthesis in the presence of lower initial radioactivity (< 200 mCi) is always favored. Therefore, a relatively good radiochemical yield is needed to provide enough radiolabeled compound for imaging applications. Most of the  $^{18}\text{F}$ -labeling experiments have been reported with radiochemical yields in the range of 5% to 95%.<sup>17, 53</sup> In addition, it has also been addressed in the previous sections that radiosyntheses in a timely manner are preferred to prepare radiolabeled compounds and thus fewer steps are required.<sup>17</sup>

Although  $\text{ArBF}_3\text{s}$  have been applied in synthetic chemistry for a long time, especially in transition-metal catalyzed cross-coupling reactions for the C-C bond formation, their preparation, particularly at relatively low concentrations of boronates and fluoride, is still not well understood. In part, this is because in the past a very large amount of fluoride has always been used to drive the reaction to completion. In contrast, in order to apply  $^{18}\text{F}$ - $\text{ArBF}_3\text{s}$  as PET imaging agents with a relatively high specific activity, the addition of a huge amount of carrier  $^{19}\text{F}$ -fluoride cannot be entertained without compromising the specific activity of the imaging agent. In addition, while a large excess of fluoride can favor the production of  $\text{ArBF}_3\text{s}$ , the yield in terms of fluoride incorporation would drop abruptly. This means that not only the specific activity will be compromised by the addition of a large amount of carrier fluoride, but the radiochemical yield is also sacrificed. Therefore, a systematic study on the fluoridation of organoboronic acids/esters is extremely important for the further development and optimization of this labeling technique.

### 1.4.3 Solvolytic stability of $\text{ArBF}_3\text{s}$

Besides the importance of the radiolabeling technique to fulfill most of the requirements of radiosyntheses, the radiolabeled compounds must be sufficiently stable *in vivo* to be developed as useful imaging agents. To determine the factors that might influence the solvolytic stability of  $\text{ArBF}_3\text{s}$ , Perrin and co-workers measured the hydrolytic rates for a series of  $\text{ArBF}_3\text{s}$  with different substituents on the aromatic system by  $^{19}\text{F}$  NMR spectroscopy or  $^{18}\text{F}/^{19}\text{F}$  TLC autoradiography.<sup>85</sup> In the  $^{19}\text{F}$  NMR study, they did not observe any steady-state intermediate during the solvolysis for any of the  $\text{ArBF}_3\text{s}$  investigated. More importantly, the kinetic data revealed a general trend of the influence

of different substituents on the solvolytic stability of  $\text{ArBF}_3\text{s}$ . Specifically, electron withdrawing groups, at the *para*- and *meta*-positions to the trifluoroborate group, enhance the solvolytic stability of  $\text{ArBF}_3\text{s}$ , while electron donating groups at the *para*-position accelerate the solvolysis of  $\text{ArBF}_3\text{s}$ . Perrin and colleagues then were able to plot the kinetic data with the substituent constants ( $\sigma$ ) to get a Hammett plot as shown in Figure 1.2. Among the  $\text{ArBF}_3\text{s}$  studied therein, the  $\text{ArBF}_3\text{s}$  from two boronates (**3.1** and **3.8**) were found to be especially stable and thus they have potential use for conjugation to biomolecules for PET imaging studies. The structures of the boronate synthons are shown in Figure 1.3. Via the carboxylic group, the boronate can be conjugated to various biomolecules.

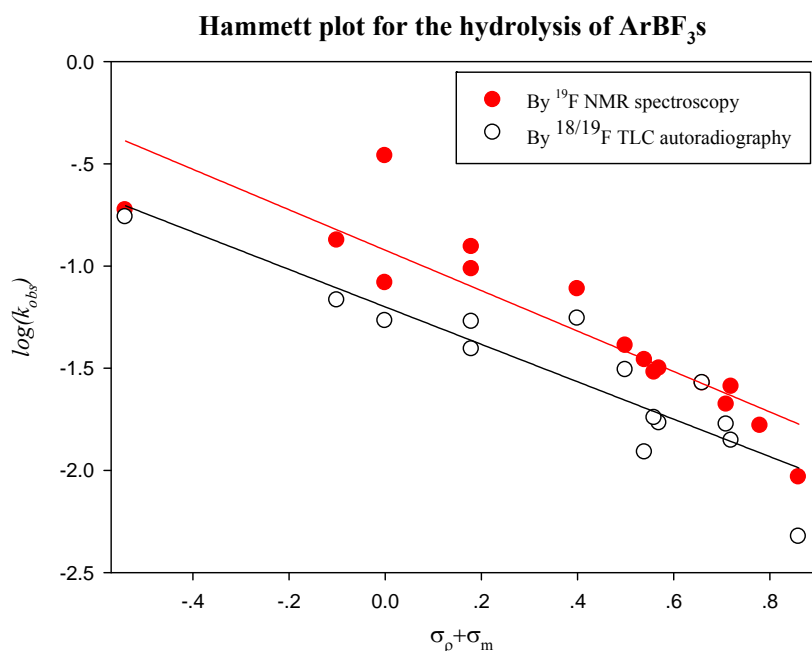


**Figure 1.2 Hammett plot in the form of  $\log(k) = \sigma\rho + \log(k_0)$ .**<sup>85</sup> Data for the  $^{18/19}\text{F}$  exchange TLC experiment ( $\circ$ ) and the  $^{19}\text{F}$  NMR fluoride dissociation experiment ( $\bullet$ ) were plotted against  $\sigma$ . The linear regression analysis of the  $^{18/19}\text{F}$  exchange TLC experiment ( $\circ$ ) (black line) gave the reaction constant for trifluoroborate isotopic exchange,  $\rho = -1.20 \pm 0.06$  and  $R^2 = 0.818$ . The linear regression analysis of the  $^{19}\text{F}$  NMR fluoride dissociation experiment ( $\bullet$ ) (red line) gave the reaction constant for trifluoroborate fluoride loss,  $\rho = -0.92 \pm 0.07$  and  $R^2 = 0.807$ .

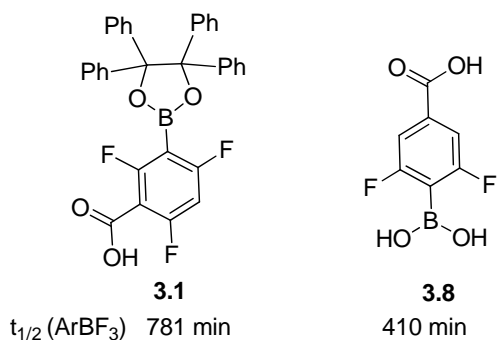


**Figure 1.3** The structures of boronic acid/ester **3.1** and **3.8** that will be used in this dissertation. The  $t_{1/2}$  (the half-life of the defluoridation of the corresponding  $\text{ArBF}_3\text{s}$ ) was measured via  $^{19}\text{F}$  NMR spectroscopy in 192 mM phosphate buffer (pH 7).<sup>85</sup>

## 1.5 The goal of this dissertation

Based on all the aspects discussed above for applying  $\text{ArBF}_3\text{s}$  as PET imaging agents, this dissertation attempts to further understand the process of the fluoridation of boronates to prepare the radiolabeled  $^{18}\text{F}\text{-ArBF}_3\text{s}$  in the presence of a low concentration and small amounts of fluoride. This thesis focuses on the conjugation of the arylboronic acid/ester to several biofunctional molecules for both radiolabeling and animal imaging studies.

Based on the study from Ting *et al.*,<sup>85</sup> the electronic properties on the aromatic system is significant for the solvolytic stability of  $\text{ArBF}_3\text{s}$ . As electron withdrawing groups were found to stabilize  $\text{ArBF}_3\text{s}$  against hydrolysis under physiologic conditions, the investigation of heteroaryltrifluoroborates ( $\text{HetArBF}_3\text{s}$ ) was expected to provide  $\text{ArBF}_3\text{s}$  with higher stability since the  $\pi$ -deficient heteroaromatic systems provide high opportunities to further stabilize the corresponding  $\text{HetArBF}_3\text{s}$ . As the aromatic structure containing  $-\text{CH}=\text{N}-$  unit(s) is considered to be  $\pi$ -deficient<sup>92</sup> and the inductive effect from the endocyclic nitrogen is considerable, the hydrolytic stability of several  $N\text{-HetArBF}_3\text{s}$  has been studied in this dissertation in order to discover more stable  $\text{ArBF}_3\text{s}$ . This work will be presented in Chapter 2.

A systematic fluoridation study based on boronates **3.1** and **3.8**, including their derivatives, will be described in Chapter 3. In this chapter, we used TLC-fluorescent densitometry,  $^{19}\text{F}$  NMR spectroscopy, and radio-HPLC to analyze the fluoridation. Several reaction factors were investigated to achieve a reproducible, high yielding, and

low carrier-added radiosynthesis of  $^{18}\text{F}$ -ArBF<sub>3</sub>s.

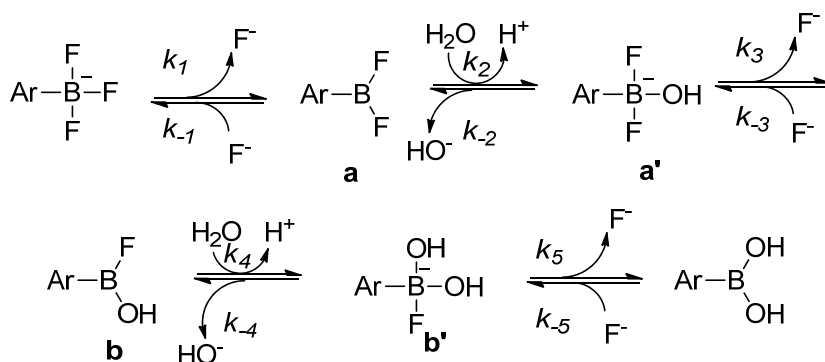
In this dissertation, boronate **3.1** has been conjugated to the matrix metalloproteinase (MMP) inhibitor marimastat (Chapter 4), a urea-based prostate-specific membrane antigen (PSMA) inhibitor (Chapter 5), and cyclic pentapeptides containing the Arg-Gly-Asp (RGD) sequence (Chapter 8). These boronates were all  $^{18}\text{F}$ -labeled under carrier-added conditions. The animal imaging work with marimastat- $^{18}\text{F}$ -ArBF<sub>3</sub> **4.15** is included in Chapter 4.

To further explore this labeling technique to a broader application in terms of labeling biomolecules, an alkynyl prosthetic  $^{18}\text{F}$ -ArBF<sub>3</sub> **6.2** has been prepared for the subsequent copper(I) catalyzed click reaction to radiolabel biomolecules with  $^{18}\text{F}$ -ArBF<sub>3</sub>s. The radiolabeling of oligonucleotides (Chapter 6), folate (Chapter 7), and an RGD-containing cyclic pentapeptide (Chapter 8) has been undertaken using this newly developed one-pot two-step radiosynthesis.

# Chapter 2 Hydrolytic defluoridation of *N*-HetArBF<sub>3</sub>s at neutral pH

## 2.1 Introduction

Organotrifluoroborates are the more air-stable equivalents of boronic acids/esters.<sup>93, 94</sup> These organotrifluoroborates have been increasingly used for synthetic reactions, including transition-metal catalyzed cross-coupling reactions to construct C-C bonds<sup>95-106</sup> or C-X bonds.<sup>107</sup> Moreover, aryltrifluoroborates (ArBF<sub>3</sub>s) have also been proposed to be useful as PET imaging agents.<sup>78</sup> To understand better the solvolysis of ArBF<sub>3</sub>s, a systematic study was carried out and a Hammett plot was obtained to show that the rate constants of the solvolytic defluoridation of ArBF<sub>3</sub>s correlate with standard  $\sigma$ -values (the coefficient of correlation  $\rho$  is  $\sim -1$ ) by Perrin and co-workers.<sup>85</sup> This means that the solvolysis of ArBF<sub>3</sub>s can be retarded by introducing electron withdrawing substituents into the aromatic system yet enhanced in the presence of electron donating groups. Meanwhile, the solvolytic mechanism was proposed therein. It was believed that the reaction undergoes a stepwise process to lose the fluorine atoms following an S<sub>N</sub>1 mechanism, while the empty orbital on the boron is quickly occupied by the hydroxide to give intermediates as shown in Scheme 2.1.



**Scheme 2.1** The proposed kinetic scheme of the ArBF<sub>3</sub> solvolysis.

The steps are all regarded reversible. **a** and **a'** are the difluoro-species; **b** and **b'** are the monofluoro-species.

In contrast, compared with the relatively large pool of reactions involving aryl-, alkenyl-, and alkyltrifluoroborates, there are fewer examples of the coupling reactions

with heteroaryltrifluoroborates (HetArBF<sub>3</sub>S).<sup>96-98, 100, 103-105, 107</sup> This might be due to the less systematic understanding of the performance of HetArBF<sub>3</sub>S during the cross-coupling reactions. In fact, for the Pd-catalyzed cross-coupling reactions with ArBF<sub>3</sub>S, it is believed that defluoridation is necessary to provide a small amount of boronic acid or monofluoroboronate-species in order to facilitate transmetallation of the aryl moiety in H<sub>2</sub>O miscible solvents containing a small amount of H<sub>2</sub>O.<sup>98, 100, 103</sup> Hence, the study of the solvolytic stability of these HetArBF<sub>3</sub> synthons can provide important information to predict their synthetic reactivity in the transition-metal catalyzed cross-coupling reactions. In addition, HetArBF<sub>3</sub>S might possess the desired hydrolytic properties for PET imaging applications. The relatively low electron density, which is normally ascribed to heteroaromatic systems, is regarded as the favored property for stabilizing HetArBF<sub>3</sub>S. Therefore, in this chapter, we prepared some nitrogen-containing HetArBF<sub>3</sub>S and studied their stability under physiological conditions by <sup>19</sup>F NMR spectroscopy. The results demonstrate that the *N*-heteroaromatic ring systems greatly retard the defluoridation of the HetArBF<sub>3</sub>S under buffered aqueous conditions at near neutral pH. Several *N*-HetArBF<sub>3</sub>S are found to display extraordinary hydrolytic resistance and therefore have very promising applications as PET imaging agents.

## 2.2 Results

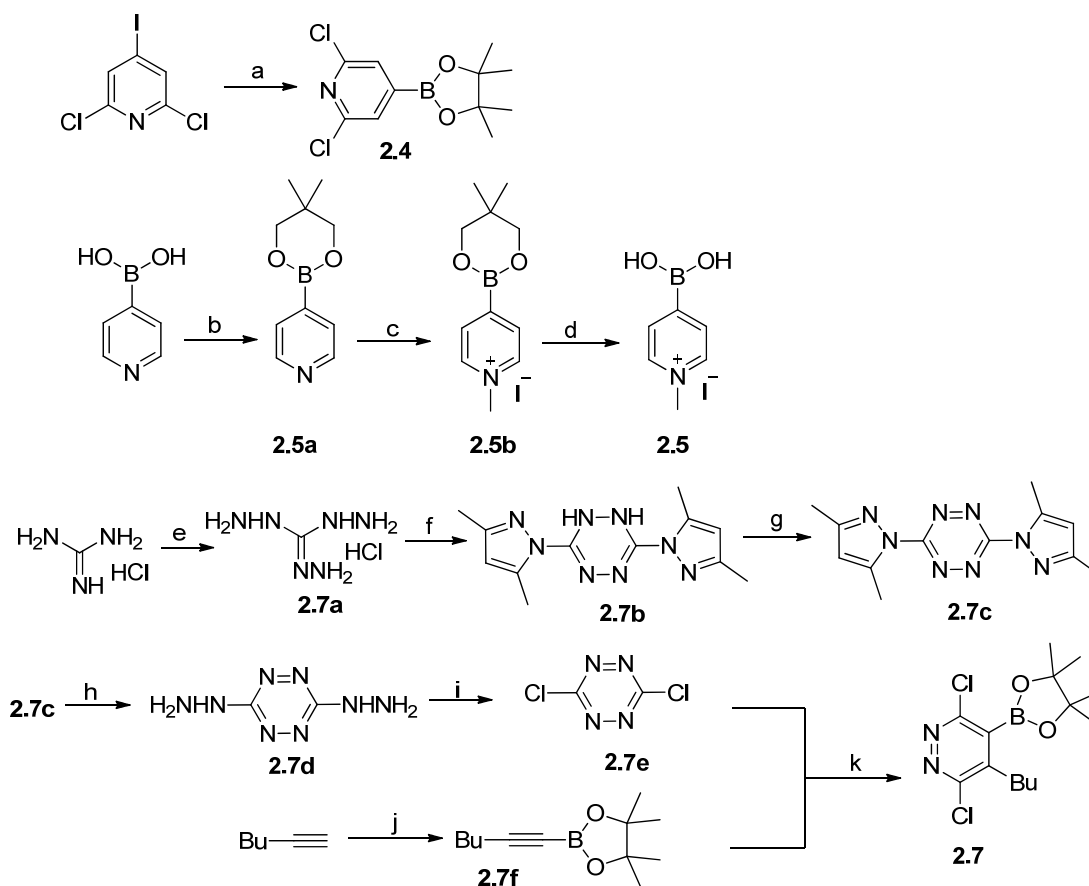
### 2.2.1 Synthesis

The heteroarylboronic acids/esters, which were converted to HetArBF<sub>3</sub>S, were either purchased or synthesized. The synthesis of three heteroarylboronic acids/esters has been summarized in Scheme 2.2. First, 2,6-dichloro-4-iodo-pyridine was treated with BuLi under a halo-lithium exchange reaction, the reaction mixture was quenched with B(OCH<sub>3</sub>)<sub>3</sub>; pinacol was added to protect the newly produced boronic acid to give **2.4** as one of the desired boronate esters.<sup>a</sup> In order to obtain *N*-methyl-4-pyridineboronic acid iodide **2.5**, 4-pyridinylboronic acid was first protected with 2,3-dimethyl-1,3-propanediol, and *N*-methylated with MeI. The protecting group on boronate **2.5b** was then removed to afford the desired product **2.5** with an overall yield of 74% over three

---

<sup>a</sup> Dr. Ali Asadi made this compound.

steps.



**Scheme 2.2 Synthesis of several heteroarylboronic acids.**

(a), i. BuLi, Et<sub>2</sub>O, -78 °C, ii. B(OCH<sub>3</sub>)<sub>3</sub>, -78 °C, 2 hr, iii. pinacol and HOAc, 74%; (b), 2,2-dimethyl-1,3-propanediol, 1,4-dioxane, molecular sieves, reflux, 18 hr, quant.; (c), MeI, CH<sub>3</sub>CN, reflux, overnight; (d), water/acetone, rt, 1 d, 74% over three steps; (e), hydrazine monohydrate, 1,4-dioxane, reflux, 89%; (f), 2,4-pentanedione, H<sub>2</sub>O, 70 °C, overnight, 80%; (g), NO/NO<sub>2</sub>, DMF, rt, 4 hr, 72%; (h), hydrazine monohydrate, CH<sub>3</sub>CN, reflux, 1.5 hr, 73%; (i), trichloroisocyanuric acid, CH<sub>3</sub>CN, 0 °C to rt, 1 hr, 46%; (j), i. BuLi, -78 °C, 0.5 hr, ii. 2-isopropoxy-4,4,5,5-tetramethyl-1,3,2-dioxaborolane, -78 °C, 2 hr, iii. HCl in Et<sub>2</sub>O, -78 °C, 20 min, 37% over three steps; (k), xylenes, reflux, 24 hr, 14%.

Finally, a Diels-Alder reaction was used to prepare dichloropyridazinylboronate **2.7** from dichlorotetrazine **2.7e** and alkynylboronate **2.7f**. Hexyne was first treated with BuLi to give acetylide anions, which were quenched with B(OCH<sub>3</sub>)<sub>3</sub>. The boronate intermediate was further protected with pinacol to give **2.7f**, which was purified via vacuum distillation. Meanwhile, 1,4-dichlorotetrazine **2.7e** was synthesized from guanidinium chloride over five steps. Triaminoguanidinium chloride **2.7a**, obtained from the hydrazinolysis of guanidinium chloride, was reacted with 2,4-pentanedione in H<sub>2</sub>O at 70 °C to afford 1,2-dihydro-1,2,4,5-tetrazine **2.7b**, which was oxidized by NO/NO<sub>2</sub> to

afford 1,2,4,5-tetrazine **2.7c**. The dimethylpyrazole groups on **2.7c** were replaced by hydrazine to provide 3,6-dihydrazino-1,2,4,5-tetrazine **2.7d**. Tetrazine **2.7d** underwent an electrophilic substitution with trichloroisocyanuric acid to give 1,4-dichlorotetrazine **2.7e**. The Diels-Alder reaction between **2.7e** and **2.7f** was undertaken in xylenes at 140 °C for 24 hours to give **2.7**. The overall yield to prepare **2.7** starting from guanidinium chloride was 2.4%.

Then all the heteroarylboronic acids/esters were incubated with excess of  $\text{KHF}_2$  to prepare the corresponding  $N\text{-HetArBF}_3\text{s}$ . The  $N\text{-HetArBF}_3\text{s}$  were generally purified from free fluoride by flash chromatography with a small silica gel column using 5%  $\text{NH}_4\text{OH}/\text{EtOH}$  as the elution buffer. Gratifyingly nearly all of the heteroarylboronic acids/esters showed very good conversions.

## 2.2.2 Solvolytic studies of $N\text{-HetArBF}_3\text{s}$

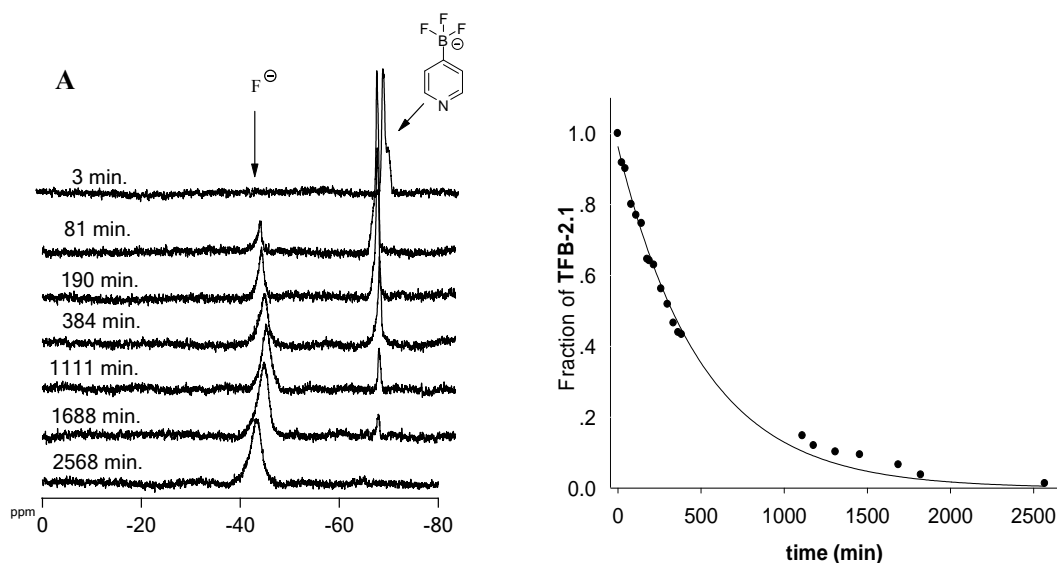


**Figure 2.1** The  $^{19}\text{F}$  NMR study of *para*-pyridinyltrifluoroborate (TFB-2.1) dissociation in 200 mM phosphate buffer (pH 6.89).

A,  $^{19}\text{F}$  NMR spectra of *para*-pyridinyltrifluoroborates TFB-2.1 dissociation; B, the exponential plot of trifluoroborate fraction against time as measured by  $^{19}\text{F}$  NMR spectroscopy with the  $^{19}\text{F}$ -signal of trifluoroacetic acid as the standard reference (0 ppm),  $k_{\text{obs}} = (1.8 \pm 0.20) \times 10^{-3} \text{ min}^{-1}$ ,  $R^2 = 0.9940$ .

The solvolytic stability of various  $N\text{-HetArBF}_3\text{s}$  in buffered aqueous solution at neutral pH was studied by  $^{19}\text{F}$  NMR spectroscopy. In general, it has been found that all the  $N\text{-HetArBF}_3\text{s}$  studied herein have relatively long half-lives ( $t_{1/2} \geq 300 \text{ min}$ ) at room temperature in the phosphate buffer (pH  $\sim 7$ ). An example of the  $^{19}\text{F}$  NMR spectroscopic

assay for the solvolysis of *para*-pyridinyltrifluoroborate **TFB-2.1** is shown in Figure 2.1. This assay monitors the loss of  $\text{HetArBF}_3$  peak ( $\delta \sim -65 \text{ ppm}$ , referenced to trifluoroacetic acid at  $0 \text{ ppm}$ ) and simultaneously the increase of the free fluoride peak ( $\delta \sim -42 \text{ ppm}$ ). The  $^{19}\text{F}$  NMR spectra showed that there were no other obvious fluorine-containing intermediates (monofluoro- or difluoro-species) in the reaction on the time scale of the  $^{19}\text{F}$  NMR data acquisition. The data analysis for the hydrolytic kinetics is therefore simplified due to the absence of any intermediate, since  $^{19}\text{F}$ -signals were used to construct a kinetic curve for the solvolysis. Typically, the percentage of the fluoride remaining on the *N*- $\text{HetArBF}_3$  vs. time was best fitted to a standard first order rate process for all decomposition experiments, while the overall fluoride amount<sup>a</sup> was considered constant for each experiment. The data suggested a single rate-determining step, which is regarded to the loss of the first fluoride atom on the *N*- $\text{HetArBF}_3$ . This controls the overall rate of the decomposition.

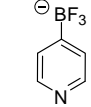
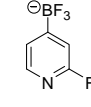
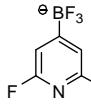
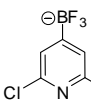
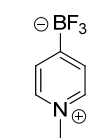
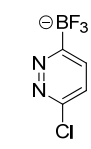
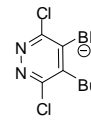
The study of the kinetics for the defluoridation of *para*-pyridinyltrifluoroborate (**TFB-2.1**) via  $^{19}\text{F}$  NMR spectroscopy, shown in Figure 2.1, exhibited a solvolytic decomposition half-life of 385 minutes at  $\text{pH} \sim 7$ . At higher pHs, the solvolytic rate of *para*-pyridinyltrifluoroborate **TFB-2.1** was slightly enhanced, with half-lives of 210 minutes at  $\text{pH} 8$  and 187 minutes at  $\text{pH} 9$ . These results encouraged us to extend the solvolytic studies at  $\text{pH} \sim 7$  to several readily prepared *N*- $\text{HetArBF}_3$ s as summarized in Table 2.1. In brief, introducing one exocyclic halogen atom as fluorine to the pyridine ring, such as 2-fluoro-4-pyridinyltrifluoroborate (**TFB-2.2**), whose fluorine atom is at the *meta*-position to the  $\text{BF}_3$  group, showed little-to-no enhancement to the hydrolytic stability compared with that of **TFB-2.1**. However, when two halogen atoms, i.e. fluorine or chlorine, are introduced to 2- and 6-positions of the pyridine ring of the *N*- $\text{HetArBF}_3$ s (2,6-dihalopyridinyltrifluoroborates **TFB-2.3** and **TFB-2.4**), the solvolysis was largely impeded. Since fluorine is more electronegative than chlorine, it is not surprising that the difluoropyridinyltrifluoroborate **TFB-2.3** ( $t_{1/2} \sim 19 \text{ hr}$ ) is more stable than the dichloro-version **TFB-2.4** ( $t_{1/2} \sim 14 \text{ hr}$ ). When the zwitterionic *para*-*N*-methylpyridinium trifluoroborate (**TFB-2.5**) was tested, the hydrolytic stability was further enhanced to give a half-life of approximately 4 days under the same conditions at room temperature.

---

<sup>a</sup> The overall fluoride only contains the fluoride in the form of  $\text{ArBF}_3$  or free fluoride.

Furthermore, pyridazinyltrifluoroborates **TFB-2.6** and **TFB-2.7**, which contain two endocyclic nitrogen atoms and exocyclic chlorine atoms, displayed extraordinary stability against hydrolytic decomposition. Even at elevated temperatures (37 and 50 °C), the decomposition process was so slow that half-lives were measured in days.

**Table 2.1** The kinetic data for the solvolysis of *N*-HetArBF<sub>3</sub>s

Compound no.	Structure	Temperature	<i>k</i> (min <sup>-1</sup> )	<i>t</i> <sub>1/2</sub> (min)
<b>TFB-2.1</b>		22 ± 2 °C	(1.8 ± 0.20) × 10 <sup>-3</sup>	385 ± 43
		22 ± 2 °C <sup>a</sup>	(3.3 ± 0.20) × 10 <sup>-3</sup>	210 ± 12
		22 ± 2 °C <sup>b</sup>	(3.7 ± 0.10) × 10 <sup>-3</sup>	187 ± 5
		22 ± 2 °C <sup>c</sup>	(1.9 ± 0.20) × 10 <sup>-3</sup>	365 ± 38
<b>TFB-2.2</b>		22 ± 2 °C	(1.9 ± 0.07) × 10 <sup>-3</sup>	364 ± 13
<b>TFB-2.3</b>		22 ± 2 °C	(0.6 ± 0.02) × 10 <sup>-3</sup>	1155 ± 31
<b>TFB-2.4</b>		22 ± 2 °C	(8.0 ± 0.21) × 10 <sup>-4</sup>	866 ± 22
<b>TFB-2.5</b>		22 ± 2 °C	(1.1 ± 0.03) × 10 <sup>-4</sup>	6177 ± 158
		37 ± 2 °C	(5.2 ± 0.20) × 10 <sup>-4</sup>	1329 ± 51
		50 ± 2 °C	(1.3 ± 0.06) × 10 <sup>-3</sup>	527 ± 24
<b>TFB-2.6</b>		22 ± 2 °C	ND <sup>d</sup>	ND
		37 ± 2 °C	(3.7 ± 0.31) × 10 <sup>-5</sup>	18698 ± 1563
		50 ± 2 °C	(1.2 ± 0.05) × 10 <sup>-4</sup>	5996 ± 240
<b>TFB-2.7</b>		22 ± 2 °C	(4.3 ± 0.11) × 10 <sup>-5</sup>	16187 ± 404
		37 ± 2 °C	(1.1 ± 0.03) × 10 <sup>-4</sup>	6478 ± 150
		50 ± 2 °C	(3.4 ± 0.07) × 10 <sup>-4</sup>	2069 ± 41

**Note:** The hydrolytic study was undertaken in 200 mM phosphate buffer at pH 6.87 or otherwise noted; <sup>a</sup>The hydrolytic study was undertaken in 200 mM phosphate buffer at pH 8.01; <sup>b</sup>The hydrolytic study was undertaken in 200 mM phosphate buffer at pH 9.00; <sup>c</sup>The hydrolytic study was undertaken in 200 mM phosphate buffer at pH 6.87 in the presence of 10 mM KF; <sup>d</sup>ND stands for “not-determined” since the reaction rate was too slow to monitor.

More interestingly, when studied in the presence of free fluoride (10 mM), the hydrolytic defluoridation rate of *para*-pyridinyltrifluoroborate (**TFB-2.1**) was not significantly influenced. This may imply that at relatively high dilution these potential intermediates such as *mono*- and/or *bis*-fluoroborates tend to decompose rather than revert back to  $\text{HetArBF}_3\text{s}$  under the solvolytic conditions at  $\text{pH} \sim 7$ .

## 2.3 Discussion

### 2.3.1 Synthesis

Three heteroarylboronic acids/esters were prepared in this chapter for the corresponding  $N\text{-HetArBF}_3\text{s}$ . Boronates **2.4** and **2.5** were synthesized with a reasonable yield of  $\sim 74\%$ ; however, the overall yield of the synthesis of **2.7** was only 2.4% over six steps from guanidium chloride. The very low yielding steps were the chlorination with trichloroisocyanuric acid for tetrazine **2.7e** and the subsequent Diels-Alder reaction. Although the electrophilic substitution with trichloroisocyanuric acid was rapid, there seemed to be extensive loss during the work-up including the sublimation. For the Diels-Alder cycloaddition, it is possible that both the electron poor “diene” (tetrazine **2.7e**) and the electron poor “dienophile” (alkynylboronate **2.7f**) do not quite favor the electron demanding for the (inverse) Diels-Alder reactions. Even though the reaction was driven in terms of the production of  $\text{N}_2$  following the [2+4] cycloaddition, the first Diels-Alder reaction was slow and under the given conditions a relatively low yield was obtained. Since the preparation of the heteroarylboronic acids/esters was not the focus of the project, no further optimization was developed. Then heteroarylboronic acids/esters were treated with excess of  $\text{KHF}_2$  to prepare  $N\text{-HetArBF}_3\text{s}$ , some of which required a bit longer time to achieve full conversions of the boronic acids/esters.

### 2.3.2 Solvolytic studies of $N\text{-HetArBF}_3\text{s}$

The results of the solvolytic study suggest that  $N\text{-HetArBF}_3\text{s}$  are a class of compounds with high kinetic stability against hydrolytic defluoridation. Additional exocyclic electron-withdrawing groups on the heteroaromatic system can further improve the hydrolytic stability of  $N\text{-HetArBF}_3\text{s}$ . The inductive effect of both the endocyclic heteroatoms and the exocyclic electron withdrawing substituents (e.g. fluorine and

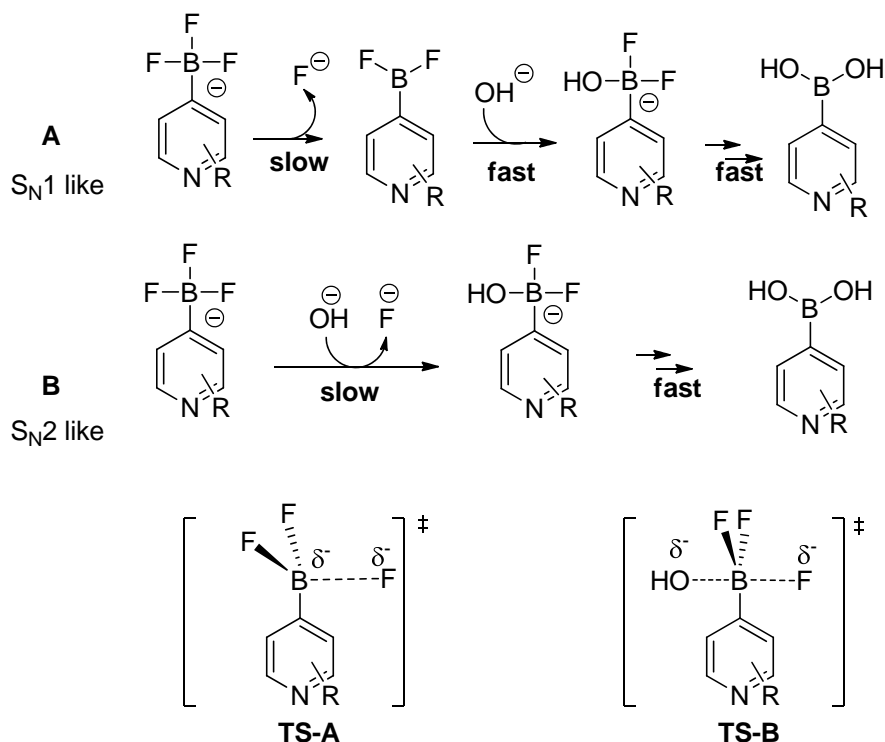
chlorine) accounts for this increased stability. However, pyridinyltrifluoroborate **TFB 2.2** with only one fluoride on 2-position did not demonstrate any significant enhancement to the hydrolytic stability compared with **TFB-2.1**, and there is no immediately forthcoming explanation for this. When comparing **TFB-2.6** with **TFB-2.7**, they are very structurally similar but the position of the boron atom relative to the heteroatom might make a big difference for the ring electron properties. When the trifluoroborate group is next to the endocyclic nitrogen as for **TFB-2.6**, the defluoridation process is much slower than the other pyridazinyl compound **TFB-2.7**, which has two chlorine substituents. Even though the two chlorine substituents at 3- and 6-positions exert a very high inductive effect, **TFB-2.7** with the trifluoroborate group at the 4-position hydrolyzed nearly three times as rapidly as **TFB-2.6** under the same conditions. This suggests that the “in ring” nitrogen atoms greatly improve the stability of the trifluoroborate group at the 3-position. Moreover, although at elevated temperatures, the *N*-HetArBF<sub>3</sub>s demonstrated faster solvolysis than at room temperature, several *N*-HetArBF<sub>3</sub>s such as **TFB-2.5**, **TFB-2.6**, and **TFB-2.7** still exhibited promising stability at higher temperatures under the same buffered conditions.<sup>a</sup> Among the *N*-HetArBF<sub>3</sub>s studied in this chapter, it was found that pyridazinyltrifluoroborates displayed extreme kinetic stability to solvolysis. These data suggest the potential use of these pyridazinyltrifluoroborates as <sup>18</sup>F-PET imaging compounds but may also help to predict their poor reactivity to be used as substrates in transition-metal catalyzed cross-coupling reactions.

It is possible to propose the mechanism of the hydrolytic defluoridation based on the <sup>19</sup>F NMR studies. For all the data we have obtained, no fluorinated intermediate was ever observed in addition to the *N*-HetArBF<sub>3</sub> and the product, namely free fluoride. This would imply very short half-lives of the possible intermediates, as shown in Scheme 2.1, on the NMR time scale. This leads us to hypothesize that the mechanism of *N*-HetArBF<sub>3</sub> solvolysis involves the loss of the first fluoride as the rate-determining step, while the two subsequent fluorides are lost rapidly. This single rate-determining step is thus sufficient to explain the entire defluoridation process, consistent with the first order decay process observed with <sup>19</sup>F NMR data. Based on this hypothesis, two possible

---

<sup>a</sup> Since pH changes due to temperatures, the same buffer was used for all the temperatures without pH corrections.

mechanisms are proposed in Scheme 2.3. Since no  $^{19}\text{F}$ -related intermediates were observed by  $^{19}\text{F}$  NMR spectroscopy for any compound studied herein, the second and third hydroxide-fluoride exchange processes should be very rapid. Moreover, when exogenous fluoride source was added to the reaction, the hydrolytic process was not affected. This also suggests that loss of the second and third fluorine atoms is probably more kinetically favored under such conditions.



**Scheme 2.3** Proposed mechanisms of the hydrolysis of HetArBF<sub>3</sub>s.

**A** is the S<sub>N</sub>1 like mechanism and **B** is the S<sub>N</sub>2 like mechanism for the loss of the first fluoride; **TS-X** is the transition state for the slow step of either proposed mechanism.

Both the mechanisms shown in Scheme 2.3 propose a slow first step to lose the first fluoride, which is the rate-limiting step, and then fast subsequent steps, based on the observation. Mechanism **A** suggests the rate-determining B-F bond breakage is via an S<sub>N</sub>1-like mechanism, which is independent of the nucleophile concentration, where the nucleophile can be water or hydroxide. Alternatively, mechanism **B** is an S<sub>N</sub>2-like process, whose transition state involves a pentacoordinate boron, with the hydroxide ion attacking the boron atom and pushing away one of the fluoride ions. The kinetic data of *para*-pyridinyltrifluoroborate **TFB-2.1** at various pHs, shows that the values of  $\log(k_{\text{obs}})$

for solvolysis are not dramatically changed.<sup>a</sup> Data suggest that the reaction is pH-independent at slightly basic conditions, which corroborates the S<sub>N</sub>1 like mechanism A as the most possible mechanism.

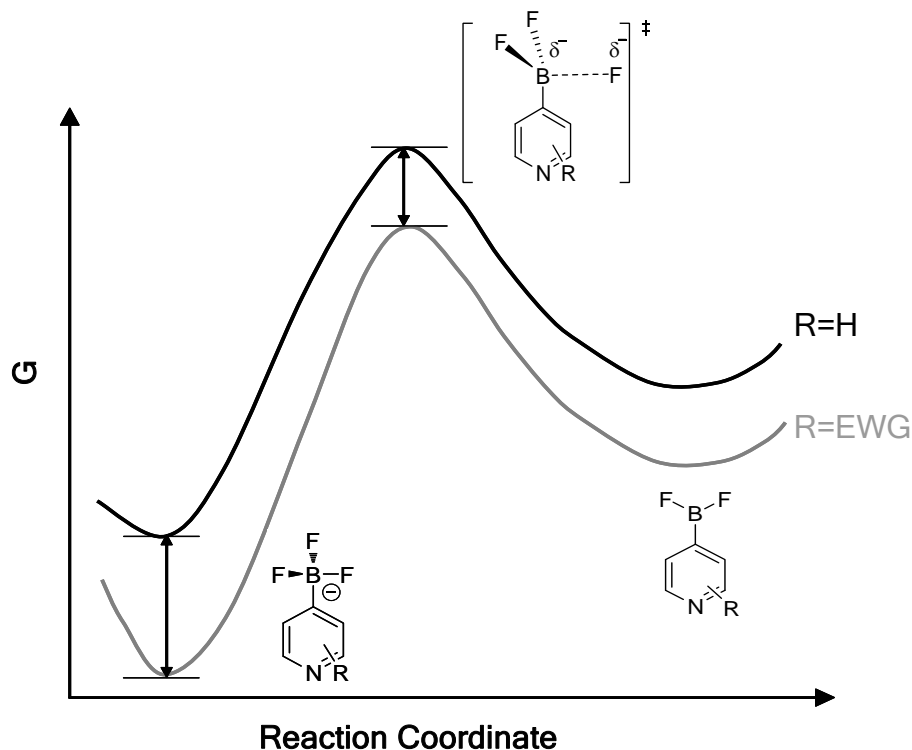


**Figure 2.2 Proposed energy diagram of hydroxide-fluoride exchange for step 1 of mechanism A.** The electron withdrawing groups (EWG) can largely stabilize ground states while the stabilizing effect is much weaker for transition states.

With regard to the overall reaction coordinate, the relative stability (free energies) of both the ground state and the transition state are important. The stabilizing effect from the electron withdrawing elements against hydrolysis increases the energy barrier between the ground state and the transition state. This might be interpreted by decreasing more of the free energy of the ground state or increasing more of the free energy of the transition state. The electron withdrawing groups discussed here exhibit strong inductive effects, which serve to decrease the  $\pi$ -electron density available on the aromatic system and therefore to stabilize any negative charges in the system. Considering the experimental observations of the kinetic studies, it seems that the stabilizing effect of the ground state by the electron withdrawing groups is more than that of the transition state.

<sup>a</sup> The magnitudes of the rate constants among the conditions discussed are the same.

As at the ground state, the negative charge can be stabilized by the aromatic system via the inductive effect of the electron withdrawing substituents. The overall stabilization of the negative charge by the aromatic system at the transition state is less efficient than that at the ground state. As a result, a slightly less stabilizing effect with electron withdrawing groups should be expected for the transition state, as shown in Figure 2.2. Correspondingly, the energy gap between the ground state and the transition state is increased by the presence of electron withdrawing groups. As a result, the solvolysis is more obstructed.

## 2.4 Conclusion

In this chapter, we have studied the hydrolytic stability of several *N*-HetArBF<sub>3</sub>S by <sup>19</sup>F NMR spectroscopy. The *N*-HetArBF<sub>3</sub>S displayed very strong stability against hydrolytic decomposition. To develop new PET imaging compounds based on fluorine-18 chemistry, the *N*-HetArBF<sub>3</sub>S studied herein exhibit very favorable hydrolytic stability compared with the physical half-life of fluorine-18. In regard to the metal catalyzed coupling reactions, these *N*-HetArBF<sub>3</sub>S might not be good substrates. This hydrolytic study suggests that these HetArBF<sub>3</sub>S should be exceptional candidate components for *in vivo* PET imaging studies.

## 2.5 Materials and methods

All chemicals were purchased from Sigma-Aldrich or Alfa-Aesar. Deuterated solvents were obtained from Cambridge Isotope Laboratories. Analytical thin layer chromatography was run on Silica Gel 60 F<sub>254</sub> Glass TLC plates from EMD Chemicals, and SiliaFlash F60 from Silicycle was used for flash chromatography. Melting points were not corrected. All nuclear magnetic resonance (NMR) spectra were recorded at room temperature on a Bruker Avance 300 or 400 MHz spectrometer. Chemical shifts ( $\delta$ ) are reported in *ppm*; all coupling constants (*J*) are reported in Hertz (Hz). Unless specified, <sup>1</sup>H NMR spectra are referenced to the tetramethylsilane peak ( $\delta = 0.00$  *ppm*), <sup>13</sup>C NMR spectra are referenced to the chloroform peak ( $\delta = 77.23$  *ppm*), and <sup>19</sup>F NMR spectra are referenced to neat trifluoroacetic acid ( $\delta = 0.00$  *ppm*,  $-78.3$  *ppm* relative to CFCl<sub>3</sub>). Due to the presence of <sup>19</sup>F contamination in the NMR spectrometer probe,

baseline for samples less than 20 mM in  $^{19}\text{F}$ -fluoride concentration had to be adjusted by the multipoint linear baseline correction using MestReC 4.9.9.9. This correction did not affect the absolute chemical shifts or integration ratios of  $^{19}\text{F}$  signals. Low-resolution ESI mass spectrometry (ESI-LRMS) was performed on a Waters ZQ with a single quadrupole detector, attached to a Waters-2695 HPLC. High-resolution ESI mass spectra (ESI-HRMS) were obtained on a Waters-Micromass LCT with a time-of-flight (TOF) detector.

### 2.5.1 Preparation of several heteroarylboronic acids

#### 2,6-Dichloro-4-(4,4,5,5-tetramethyl-1,3,2 dioxaboryl)pyridine (2.4)<sup>108</sup>

Briefly, 2,6-dichloro-4-iodo-pyridine (1.4 g, 10 mmol) at  $-78\text{ }^{\circ}\text{C}$  was added to a hexane solution of BuLi (8.0 mL, 15 mmol) in dry  $\text{Et}_2\text{O}$  (30 mL). After 30 min at  $-78\text{ }^{\circ}\text{C}$ , the mixture was treated with  $\text{B}(\text{OCH}_3)_3$  (1.25 mL, 11.0 mmol) and the reaction was stirred for 1 hr. The temperature was then allowed to rise slowly over 2 hr up to rt, then pinacol (1.6 g, 13 mmol) was added and 10 min later AcOH (0.60 mL, 10.5 mmol) was added. The resulting mixture was filtered through Celite, which was then washed with ether, and the combined filtrates were evaporated under reduced pressure. The desired product was crystallized from cyclohexane. Yield: 74%.  $^1\text{H}$  NMR (300 MHz,  $\text{CDCl}_3$ , rt):  $\delta$  (ppm) 1.34 (s, 12 H), 8.06 (s, 2 H);  $^{13}\text{C}$  NMR (75.5 MHz,  $\text{CDCl}_3$ , rt):  $\delta$  (ppm) 24.8, 84.4, 111.9, 128.0, 149.0.

#### *N*-Methyl-4-pyridineboronic acid iodide (2.5)

This compound is prepared following a literature protocol.<sup>109</sup> Briefly, 4-pyridinylboronic acid (0.5 g, 4 mmol) and 2,2-dimethyl-1,3-propanediol (0.4 g, 4 mmol) were dissolved in 1,4-dioxane (25 mL) in the presence of a few chips of 4Å molecular sieves. The mixture was refluxed for 18 hr. The reaction was then cooled down and filtered to remove the molecular sieves. The filtrate was concentrated under vacuum and the residue was dried over high vacuum to give 0.85 g (quantitatively) of a white solid, which was used directly without further purification. The white solid was dissolved in  $\text{CH}_3\text{CN}$  (25 mL) and MeI (2.4 mL, 40.2 mmol) was added. The resulting solution was refluxed overnight, and concentrated under vacuum. To the yellowish residue, 1:1

water/acetone (30 mL) was added and the slurry was stirred at rt for 1 day. The mixture was then filtered and the filtrate was concentrated under reduced pressure. The product was precipitated from MeOH/Et<sub>2</sub>O to give a pale yellow powder as the desired product. Yield: 1.0 g, 74% over three steps. <sup>1</sup>H NMR (400 MHz, *d*<sub>6</sub>-DMSO, rt): δ (*ppm*) 4.20 (s, 3 H), 7.54 (d, *J* = 6.16 Hz, 2 H), 8.55 (d, *J* = 6.24 Hz, 2 H); <sup>13</sup>C NMR (100.6 MHz, *d*<sub>6</sub>-DMSO, rt): δ (*ppm*) 48.79, 50.05, 132.12, 144.30.

### **Triaminoguanidine monohydrochloride(2.7a)**

This compound is prepared following a literature protocol with some modifications.<sup>110</sup> Hydrazine monohydrate (3.21 g, 68.2 mmol) was added to a suspension of guanidine hydrochloride (1.91 g, 20.0 mmol) in 1,4-dioxane (10 mL) at rt. The mixture was then refluxed until ammonia was no longer released<sup>a</sup>. The reaction mixture was cooled to rt, filtered, washed with 1,4-dioxane and dried to give a white powder as the target molecule. Yield: 2.49 g, 89%. Mp: 215-216 °C (Lit. 230 °C); <sup>13</sup>C NMR (75.5MHz, D<sub>2</sub>O, rt): δ (*ppm*) 159.78; ESI-LRMS: [M-Cl]<sup>+</sup>: 104.9 (100%).

### **3,6-Bis(3,5-dimethylpyrazol-1-yl)-1,2-dihydro-1,2,4,5-tetrazine(2.7b)**

This compound is prepared following a literature protocol with some modifications.<sup>110</sup> 2,4-Pentanedione (20.4 g, 0.2 mol) was dropwise added to triaminoguanidine monohydrochloride **2.7a** (4.06 g, 0.1 mol) in H<sub>2</sub>O (100 mL) at rt. The mixture was stirred at 70 °C overnight. After the reaction was cooled down, the orange mixture was filtered. The solid was washed with water, and dried to provide pure **2.7b**. Yield: 10.85 g, 80%. Mp: 130-131 °C (Lit. 150 °C); <sup>1</sup>H NMR (300 MHz, *d*<sub>6</sub>-DMSO, rt): δ (*ppm*) 2.17 (s, 6 H), 2.39 (s, 6 H), 6.14 (s, 2 H), 8.82 (s, 2 H); <sup>13</sup>C NMR (75.5 MHz, *d*<sub>6</sub>-DMSO, rt): δ (*ppm*) 12.90, 13.21, 109.39, 141.65, 145.24, 149.35; ESI-LRMS: [M+H]<sup>+</sup>, 273.2 (100%), 273.4 (15%).

### **3,6-Bis(3,5-dimethylpyrazol-1-yl)-1,2,4,5-tetrazine(2.7c)**

This compound is prepared following a literature protocol with some modifications.<sup>110</sup> NO/NO<sub>2</sub> was produced by adding 50 wt% sulfuric acid (78 mL, 0.55 mol) dropwise to 0.6 N sodium nitrite (100 mL, 60 mmol); the resulting gas was bubbled into **2.7b** (2.26g,

<sup>a</sup> The ammonia could be detected with a stripe of pH paper with moisture.

8.3 mmol) in DMF (40 mL) at rt for 4 hr. Then iced water (100 mL) was poured into the reaction to result in a purple precipitate. The reaction mixture was filtered, washed with cold water, and dried to give the desired product. Yield: 1.61 g, 72%. Mp: 216-218 °C (Lit. 223-224 °C); <sup>1</sup>H NMR (300 MHz, *d*<sub>6</sub>-DMSO, rt): δ (*ppm*) 2.27 (s, 6 H), 2.58 (s, 6 H), 6.35 (s, 2 H); <sup>13</sup>C NMR (75.5 MHz, *d*<sub>6</sub>-DMSO, rt): δ (*ppm*) 14.07, 14.27, 111.59, 143.71, 153.19, 159.38; ESI-LRMS: [M+Na]<sup>+</sup>: 293.2 (100%), 294.2 (15%).

### **3,6-Dihydrazino-1,2,4,5-tetrazine(2.7d)**

This compound is prepared following a literature protocol.<sup>111</sup> Hydrazine monohydrate (1.3 g, 26 mmol) was added slowly to a slurry of **2.7c** (3.2 g, 12 mmol) in CH<sub>3</sub>CN (30 mL). The resulting dark red solution was then heated to reflux for 1.5 hr. After the mixture was cooled down to rt, the slurry was filtered and the solid was washed with CH<sub>3</sub>CN to afford the desired product. Yield: 1.22 g, 73%. Mp: 137-138 °C. <sup>13</sup>C NMR (75.5 MHz, *d*<sub>6</sub>-DMSO, rt): δ(*ppm*) 164.22; ESI-LRMS: [M+H]<sup>+</sup>: 143.1 (100%).

### **3,6-Dichloro-1,2,4,5-tetrazine (2.7e)**

To 3,6-dihydrazino-1,2,4,5-tetrazine **2.7d** (1.28 g, 9.00 mmol) in CH<sub>3</sub>CN (35 mL) at 0 °C was added dropwise with CH<sub>3</sub>CN (25 mL) solution of trichloroisocyanuric acid (4.08 g, 18 mmol) for 30 min.<sup>112</sup> The reaction mixture was then allowed to warm up to rt over 20 min. After filtration, the filtrate was concentrated in vacuum to give the crude product. Pure orange red crystals as the product were obtained via sublimation. Yield: 0.63 g, 46%. <sup>13</sup>C NMR (75.5 MHz, CDCl<sub>3</sub>, rt): δ (*ppm*) 167.24; ESI-LRMS: [M+H]<sup>+</sup>: 149.8 (100%).

### **2-(1-Hexyn-1-yl)-4,4,5,5-tetramethyl-1,3,2-dioxaborolane (2.7f)**

This compound is prepared following a literature protocol with some modifications.<sup>113</sup> *n*-Hexyne (2 g, 24 mmol) in anhydrous Et<sub>2</sub>O (24 mL) was cooled to -78 °C and then 1.6 M BuLi (15.2 mL, 24.32 mmol) in hexane was added. The resulting slurry was stirred for 0.5 hr. 2-Isopropoxy-4,4,5,5-tetramethyl-1,3,2-dioxaborolane (4.58 g, 24.6 mmol) in anhydrous Et<sub>2</sub>O (24 mL) was added quickly to the mixture and the reaction was stirred at -78 °C for another 2 hr. The reaction mixture was later warmed up to ambient temperature and stirred for an additional hour. The mixture was then cooled to -78 °C and the reaction was quenched by adding 4.5 M hydrochloric acid in dry Et<sub>2</sub>O (5.4 mL, 24.3

mmol). The slurry was stirred for an additional 20 min and then warmed back to rt. After filtration, the solvent was removed under vacuum, and the desired product was obtained via distillation at 75-80 °C over 1-1.5 mmHg. Yield: 1.86 g, 37%. <sup>1</sup>H NMR (300 MHz CDCl<sub>3</sub>, rt): δ (ppm) 0.86 (t, *J* = 7.16 Hz, 3 H), 1.23 (s, 12 H), 1.28~1.50 (m, 4 H), 2.22 (t, *J* = 6.93 Hz, 2 H); <sup>13</sup>C NMR (75.5 MHz, CDCl<sub>3</sub>, rt): δ (ppm) 13.61, 19.30, 21.99, 24.41, 24.64, 24.75, 30.23, 67.39, 82.51, 83.16, 84.08.

#### **4-Butyl-3,6-dichloro-5-(4,4,5,5-tetramethyl-1,3,2-dioxaborolan-2-yl)pyridazine (2.7)**

Compound **2.7f** (0.32g, 1.9 mmol) and tetrazine **2.7e** (0.15 g, 1.3 mmol) was dissolved in xylenes (7 mL). The solution was refluxed under N<sub>2</sub> flow for 24 hr.<sup>112</sup> The solvent was then removed under vacuum and the desired product was obtained as light red oil via flash chromatography (EtOAc:hexanes 1:30). Yield: 69.0 mg, 14%. <sup>1</sup>H NMR (300 MHz, CDCl<sub>3</sub>, rt): δ (ppm) 0.95 (t, *J* = 7.24 Hz, 3 H), 1.40 (s, 12 H), 1.43 (m, 2 H), 1.55 (m, 2 H), 2.69 (t, *J* = 8.10 Hz, 2 H); <sup>13</sup>C NMR (75.5 MHz, CDCl<sub>3</sub>, rt): δ (ppm) 13.68, 22.94, 24.70, 31.47, 33.43, 85.83, 147.72, 156.54, 157.48; ESI-HRMS: calcd. for C<sub>14</sub>H<sub>22</sub>BCl<sub>2</sub>N<sub>2</sub>O<sub>2</sub><sup>+</sup>: 331.1151, found: 331.1146.

### **2.5.2 General protocols to prepare *N*-HetArBF<sub>3</sub>s**

General protocol: the heteroarylboronic acid/ester, KHF<sub>2</sub>, and acetic acid were mixed in aqueous CH<sub>3</sub>CN or MeOH or DMSO (depends on the solubility of the boronic acid/ester) to make the final cocktail with 5 mM of boronic acid/ester, 200 mM of KHF<sub>2</sub>, and 1.8 M of HOAc. The mixture was stored at rt and the reaction was monitored by TLC (NH<sub>4</sub>OH/EtOH 1:9). Mostly, the reactions were left for 2 days to ensure a 100% conversion to the HetArBF<sub>3</sub>s. The HetArBF<sub>3</sub>s were purified prior to use either by a silica gel packed pasteur pipette column with 5% (V/V) NH<sub>4</sub>OH/EtOH<sup>a</sup> or by extraction of the organic portion of pinacol or protodeboronated byproducts with suitable organic solvents after the removal of the reaction solvent. Products that corresponded to the HetArBF<sub>3</sub>s were characterized by ESI-HRMS.

HRMS data for the HetArBF<sub>3</sub>s are shown below:

---

<sup>a</sup> 5 volumes of concentrated NH<sub>4</sub>OH (aq) was mixed with 95 volumes of EtOH to make 5% (V/V) NH<sub>4</sub>OH/EtOH.

- TFB-2.1:** calcd. for C<sub>5</sub>H<sub>4</sub>BNF<sub>3</sub><sup>-</sup>: 146.0389, found: 146.0385;
- TFB-2.2:** calcd. for C<sub>5</sub>H<sub>3</sub>BNF<sub>4</sub><sup>-</sup>: 164.0295, found: 164.0292;
- TFB-2.3:** calcd. for C<sub>5</sub>H<sub>2</sub>BNF<sub>5</sub><sup>-</sup>: 182.0200, found: 182.0196;
- TFB-2.5:** calcd. for C<sub>6</sub>H<sub>7</sub>BNF<sub>3</sub>K<sup>+</sup>: 200.0261, found: 200.0257.

### 2.5.3 Kinetics of the hydrolytic defluoridation of *N*-HetArBF<sub>3</sub>s

HetArBF<sub>3</sub>s, prepared via the fluoridation of the corresponding heteroarylboronic acids/esters and purified by the silica plug using 5% NH<sub>4</sub>OH/EtOH, were studied for their hydrolytic stability in pH ~ 7 phosphate buffer (200 mM) via <sup>19</sup>F NMR spectroscopy. <sup>19</sup>F NMR spectra were recorded on a Bruker 300 MHz spectrometer with a number of time points and the percentage of HetArBF<sub>3</sub>s integral in the overall <sup>19</sup>F integral (the total integral of trifluoroborate (~ -65 ppm) and free fluoride (~ -42 ppm) was calculated and the value was plotted against time following Equation 2.1:

**Equation 2.1** 
$$R_t = R_0 e^{-k_{obs}t}$$

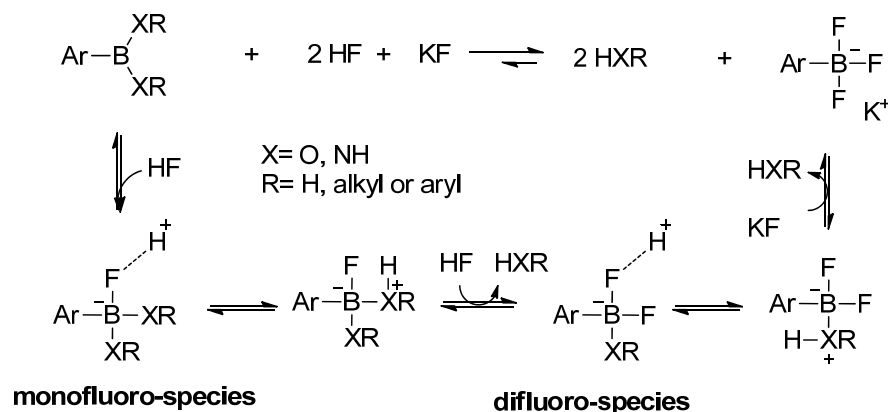
where  $R_t$  and  $R_0$  are the ratios of values corresponding to the HetArBF<sub>3</sub> integral and the total <sup>19</sup>F integral at time  $t$  and  $0$  min, respectively. The half-life of each HetArBF<sub>3</sub> was calculated by dividing the natural *log* of 2 by the observed rate constant  $k_{obs}$ . Since the solvolysis of some HetArBF<sub>3</sub>s proceeded so slow at rt, higher temperatures (37 and 50 °C) were employed. For **TFB-2.1**, the defluoridation was also studied in 200 mM phosphate buffer of pH 8 and pH 9 at rt to understand the effect of higher pHs. Moreover, for the same HetArBF<sub>3</sub> **TFB-2.1**, 10 mM free fluoride was added to the defluoridation pool to help understand the decomposition mechanism. The results are summarized in Table 2.1.

## Chapter 3 Fluoridation of arylboronates

In the previous chapter, a defluoridation study was carried out in search of hydrolytically stable aryltrifluoroborates ( $\text{ArBF}_3\text{s}$ ), whose defluoridation under physiological conditions is sufficiently slow for  $^{18}\text{F}$ -PET imaging applications. In this chapter, we will focus on the study of the fluoridation of arylboronic acids/esters for optimal conditions, under which fast fluoridation can be achieved.

### 3.1 Introduction

From the perspective of radiopharmaceutical development, not only is the *in vivo* and *in vitro* stability of radiolabeled compounds indispensable for their real biodistribution/clearance and good image quality, but it is also very critical to prepare the radiolabeled probes in rapid fashion and via a synthesis with a relatively high radiochemical yield in as few steps as possible. For instance, it has been reported that microwave<sup>114-117</sup> or elevated temperatures<sup>115, 118, 119</sup> have been frequently used to promote the C- $^{18}\text{F}$  covalent bond construction in a short reaction time. Other factors such as solvents, fluoride-activating agents, and leaving groups have also been investigated for certain substrates.<sup>118, 120</sup> Similarly, for the radiosynthesis of  $^{18}\text{F}$ - $\text{ArBF}_3\text{s}$ , optimal conditions should be investigated.



Scheme 3.1 Proposed mechanism of the fluoridation of arylboronate esters.

The conventional way to prepare organotrifluoroborates is to incubate boronic acids/esters in the presence of excess  $\text{KHF}_2$ .<sup>94, 101, 121, 122</sup> A proposed mechanism for the fluoridation of arylboronic acids/esters is shown in Scheme 3.1. Briefly, the reaction

requires at least 3 equivalents of fluoride to give the final product and the fluoridation likely follows a stepwise mechanism. In the first step, fluoride might occupy the empty orbital of the boron atom either by direct attachment or by replacement of H<sub>2</sub>O that may already “sit” in the empty orbital. The heteroatom of the protecting group on the boron is then protonated to become a good leaving group, whereupon another fluoride attacks to displace HXR to give the difluoro-species. A stepwise process results in an organotrifluoroborate.

From the perspective of applying ArBF<sub>3</sub>s in the PET imaging field, the amount of carrier <sup>19</sup>F-fluoride used to prepare <sup>18</sup>F-ArBF<sub>3</sub>s is critical. This is because the specific activity, one of the key factors to guarantee good quality images, will be compromised by the addition of a large amount of carrier <sup>19</sup>F-fluoride. In addition, for a no-carrier-added radiosynthesis, the <sup>18</sup>F-fluoridation of arylboronic acids/esters might proceed under certain conditions that may prove difficult to control due to both low amounts of <sup>18/19</sup>F-fluoride and various unknown contaminants (which might also be critical). Hence it is significantly valuable to study the fluoridation, particularly in small volumes and low amounts of materials, and to understand all the variables that control the rate and efficiency of the reaction.

Although the organotrifluoroborates have now become increasingly more important in organic synthesis, there has not yet been any systematic study on how their formation may proceed. This is particularly due to a) the organoboronates are usually poor chromophores and therefore it is hard to follow their fluoridations by TLC or HPLC quantitatively; b) the reaction itself involves fluoride under acidic conditions, which does not allow directly <sup>19</sup>F NMR acquisition because etching of glass NMR tubes competes for fluoride; c) in most studies that use organotrifluoroborates, a relatively large excess of fluoride is used to prepare them; d) the nature of different protecting groups may influence the fluoridation of organoboronates; and e) although <sup>18</sup>F-fluoride has the same chemical reactivity as <sup>19</sup>F-fluoride, the <sup>18</sup>F-fluoride solution from the source may carry various contaminating elements that could influence the preparation of <sup>18</sup>F-ArBF<sub>3</sub>s under the conditions screened in the cold lab.

In 2008, a fluorescent <sup>18/19</sup>F-labeled ArBF<sub>3</sub> was prepared in our lab.<sup>80</sup> In this work,

Perrin and co-workers were able to prepare *N*-4-aminophenyldi(dimethylpyrro)methane boron difluoride (2,4,6-trifluoro-3-[<sup>18/19</sup>F]-(trifluoroboratephenyl)-methanone (BODIPY-<sup>18/19</sup>F-ArBF<sub>3</sub>) **3.2**. By a fluoride exchange reaction with BODIPY-<sup>18/19</sup>F-ArBF<sub>3</sub> **3.2**, the rate constant of its defluoridation was measured:  $k_{obs} = (1.2 \pm 0.4) \times 10^{-4} \text{ min}^{-1}$ . The fluoridation of compound **3.6** (1.90 mM) monitored by <sup>19</sup>F NMR spectroscopy in the presence of 381 mM F<sup>-</sup> and 95.2 mM HOAc/NaOAc at pH 4.5 in 525 μL MeOH:H<sub>2</sub>O (9:1) was also reported. Although they cleanly and successfully demonstrated the fluoridation of this compound, the reaction was comparatively slow with respect to the decay rate of <sup>18</sup>F-fluorine ( $t_{1/2} = 109.8 \text{ min}$ ). After eight hours, only 75% of boronate **3.6** was converted to the desired product **3.2**. Moreover, the radiolabeling experiment reported therein involved a large amount of carrier <sup>19</sup>F-fluoride, which greatly reduced the specific activity. Although in the paper, it was claimed that using a higher amount of radioactivity could dramatically improve the specific activity, safety issues might restrict the operation. More practically, the addition of a smaller amount of carrier <sup>19</sup>F-fluoride with a lower radioactivity (hundreds of milliCuries) may be more reasonable.

The strong fluorescence of **3.2** or **3.6** on the other hand provides a near-quantitative way to monitor the fluoridation reaction by thin layer chromatography (TLC). In this manner, the optimal conditions, obtained from the fluoridation studies on BODIPY-boronate **3.6**, should be able to directly guide the radiolabeling experiments of other molecules derivatized from the same or similar boronates. Therefore, we herein first studied the fluoridation of BODIPY-boronate **3.6** via TLC-fluorescent densitometry to understand the labeling conditions in non-radioactive experiments, which might imitate conditions used in a radiosynthetic preparation of <sup>18</sup>F-ArBF<sub>3</sub>s at low concentrations of carrier fluoride in small volumes.

Considering the acidic nature of the fluoridation, two acid-sensitive protecting groups 1,8-diaminonaphthalene and 2,7-dimethoxy-1,8-diaminonaphthalene (DiDiAN) **3.14** were introduced to arylboronic acid **3.8** to afford the protected boronates **3.9** and **3.15**, which were further derivatized to give the propargyl amides **3.10** and **3.16**. The fluoridation of these boronates was also studied by <sup>19</sup>F NMR spectroscopy in a relatively larger reaction volume or analyzed by radio-HPLC following reactions in small volumes

under the optimal fluoridation conditions, based on the results of the fluoridation study using BODIPY-boronate **3.6**.

Moreover, the  $^{18}\text{F}$ -fluoridation of biotin-boronate **3.23** demonstrated a much more rapid  $^{18}\text{F}$ -fluoridation than the other derivatives from the same arylboronate ester.<sup>79</sup> It was hypothesized that the piperazinyl bridge between the boronate and the biomolecule might also have somehow accelerated the rate of the fluoridation. To test these hypotheses, a series of boronates (**3.19**, **3.20**, **3.21** and **3.23**) with the piperazine linker were prepared with either 1,1,2,2-tetraphenyl-1,2-ethanediol (benzopinacol) or 1,8-diaminonaphthalene as the protecting groups. Their  $^{18}\text{F}$ -fluoridation was studied under the optimal fluoridation conditions.

## 3.2 Results

**Table 3.1** A check-list of the boronates studied for the fluoridation in this chapter.

Entry	Boronate	Protecting group	Analyzing methods for the fluoridation studies		
			TLC	$^{19}\text{F}$ NMR	Radio-HPLC
1	3.6	Benzopinacol	√		
2	3.7	Benzopinacol		√	
3	3.8	-		√	
4	3.9	DAN		√	
5	3.10	DAN		√	
6	3.11	-			√
7	3.15	DiDiAN		√	
8	3.16	DiDiAN			√
9	3.19	Benzopinacol			√
10	3.20	DAN			√
11	3.21	-			√
12	3.23	Benzopinacol			√

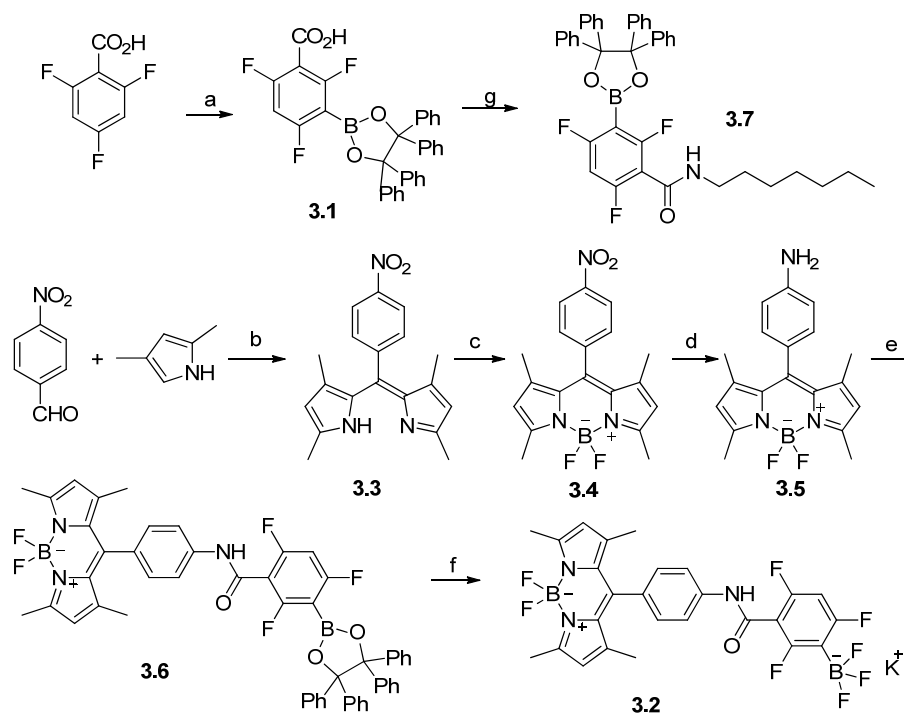
*NOTE:* DAN is 1,8-diaminonaphthalene; DiDiAN is 2,7-dimethoxyl-1,8-diaminonaphthalene.

Several arylboronates were synthesized from **3.1** or **3.8** in this chapter to study the fluoridation via TLC-fluorescent densitometry,  $^{19}\text{F}$  NMR spectroscopy or radio-HPLC. In brief, BODIPY-boronate **3.6** was prepared, and for the fluoridation assays, the fluorescence of **3.6** and that of its fluoridated product **3.2** were measured by fluorescent densitometry after resolution by TLC in order to analyze the extent of the fluoridation under various conditions. Since this method (TLC-fluorescence densitometry) only requires a small amount of material and allows for rapid analysis, we were able to evaluate several reaction factors at least semi-quantitatively. In order to apply the optimal

conditions for the fluoridation of boronate **3.6** to other boronates, several boronate esters protected with either benzopinacol or with acid-sensitive protecting groups, were prepared for the fluoridation that can be analyzed by  $^{19}\text{F}$  NMR spectroscopy or radio-HPLC. The fluoridation of various boronates analyzed by different methods is summarized in Table 3.1.

### 3.2.1 Synthesis

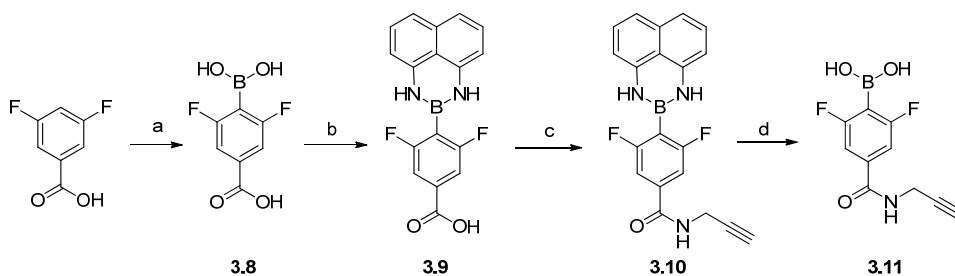
BODIPY-NH<sub>2</sub> **3.5** was prepared according to a literature protocol<sup>123</sup> and then conjugated with boronate **3.1** using DCC as the activating agent to give BODIPY-boronate **3.6** as shown in Scheme 3.2. The overall yield of this four-step synthesis of **3.6** was 4.5%. Meanwhile, the benzopinacol protected heptylamide boronate **3.7** was obtained from a simple amide formation reaction using EDC as the coupling reagent in a yield of 63%.



**Scheme 3.2 Synthetic scheme of BODIPY-boronate **3.6** and BODIPY-ArBF<sub>3</sub> **3.2**.**

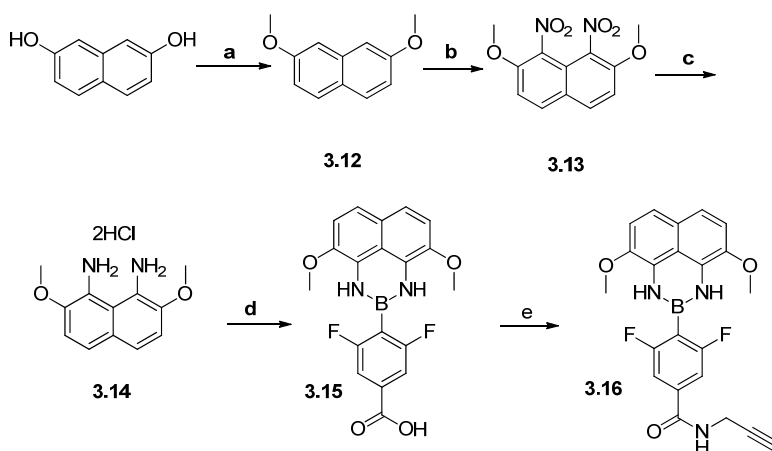
(a), i. BuLi, THF, -78 °C, 15 min, ii. B(OCH<sub>3</sub>)<sub>3</sub>, -78 °C, 3 hr, iii. 4 M HCl, 1,4-dioxane, -78 °C, 10 min, iv. benzopinacol, THF, rt, 2 hr, 47% over four steps; (b), i. TFA (cat.), CH<sub>2</sub>Cl<sub>2</sub>, N<sub>2</sub>, rt, overnight, ii. DDQ, rt, 20 min, 37% over two steps; (c), BF<sub>3</sub>·Et<sub>2</sub>O, DIPEA, PhCH<sub>3</sub>, Ar, rt, 30 min, 33%; (d), 10% Pd/C, THF, H<sub>2</sub>, rt, overnight, 86%; (e), **3.1**, DCC, CH<sub>2</sub>Cl<sub>2</sub>, rt, 48 hr, 43%; (f), KHF<sub>2</sub>, HCl, yields dependent on condition; (g), heptylamine, EDC·HCl, HOBT·H<sub>2</sub>O, CH<sub>2</sub>Cl<sub>2</sub>, rt, overnight, 63%.

1,8-Diaminonaphthalene protected boronates **3.9** and **3.10** were synthesized according to Scheme 3.3. The synthesis started with 3,5-difluorobenzoic acid, which was treated with *sec*-BuLi, quenched with B(OCH<sub>3</sub>)<sub>3</sub>, and subsequently mixed with hydrochloric acid to provide **3.8**. Boronic acid **3.8** was incubated with 1,8-diaminonaphthalene under refluxing to give the protected boronate ester **3.9**, which was further coupled to propargylamine to afford propargyl amide **3.10**. Boronate ester **3.10** was demasked in H<sub>2</sub>SO<sub>4</sub> solution to give **3.11** as the final product of this synthesis. The overall yield to prepare **3.11** from 3,5-difluorobenzoic acid is 40%.



**Scheme 3.3 Synthetic scheme of boronates protected with 1,8-diaminonaphthalene.**

(a), i. TMEDA, *sec*-BuLi, THF, Ar, -78 °C, 2.5 hr; ii. B(OCH<sub>3</sub>)<sub>3</sub>, rt 4 hr; iii. 3 N HCl, 90% over three steps; (b), 1,8-diaminonaphthalene, PhCH<sub>3</sub>/THF, reflux, 4 hr, 67%; (c), EDC·HCl, HOBT·H<sub>2</sub>O, Py, DMF, rt, overnight, 88%; (d), 2 N H<sub>2</sub>SO<sub>4</sub>, THF, rt, overnight, 76%.

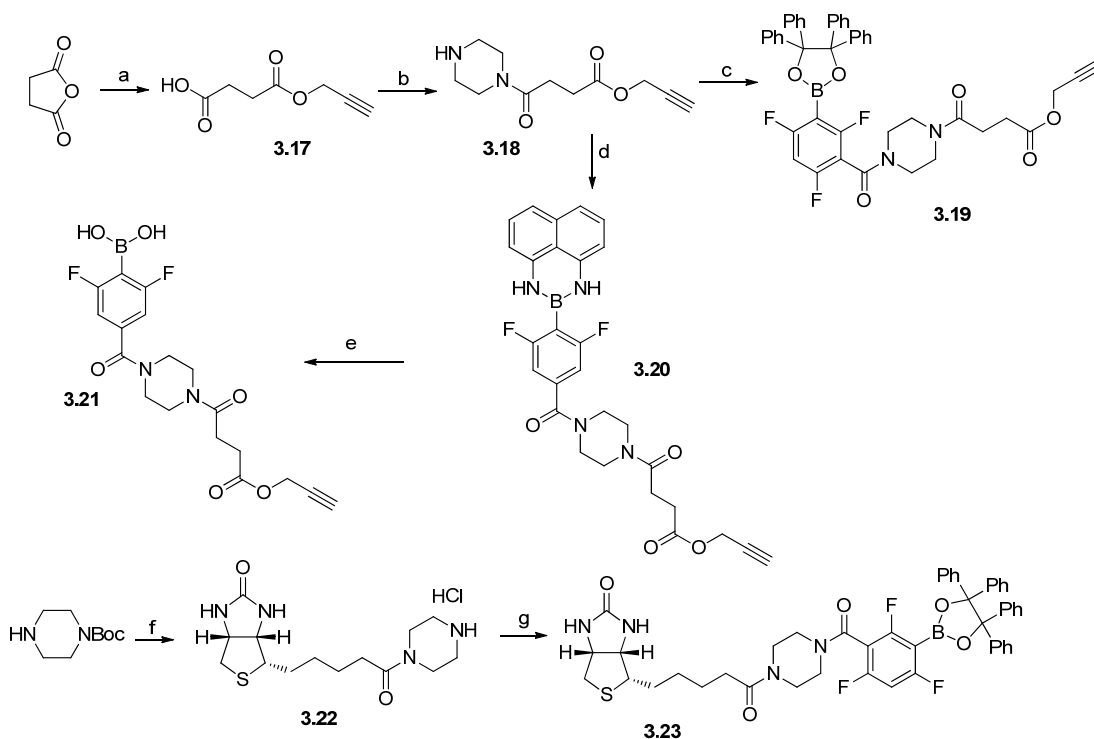


**Scheme 3.4 Synthesis of DiDiAN protected boronates.**

(a), MeI, KOH, DMSO, rt, 24 hr, 85% ; (b), HNO<sub>3</sub>, HOAc, 2 hr, rt, 49%; (c), SnCl<sub>2</sub>·2H<sub>2</sub>O, HCl, MeOH, rt, 77%; (d), **3.8**, THF/Tol, reflux, overnight, 37%; (e), propargylamine, EDC·HCl, HOBT·H<sub>2</sub>O, NEt<sub>3</sub>, THF, rt, overnight, 20%.

We hypothesized that increasing the basicity of diaminonaphthalene through substituent effects could increase its acid liability. Thus, we developed a new protecting group 2,7-dimethoxy-1,8-diaminonaphthalene (DiDiAN) by introducing two electron donating groups to the naphthalene system. Its preparation and introduction to boronic

acid **3.8** is summarized in Scheme 3.4. Methylation of 2,7-dihydroxynaphthalene was first carried out to provide 2,7-dimethoxynaphthalene.<sup>124</sup> Following nitration at 1- and 8-positions<sup>125</sup> and reduction using SnCl<sub>2</sub>/HCl,<sup>125</sup> DiDiAN·2HCl was obtained in an overall yield of 32%. We were able to use this compound to protect the boronic acids to provide **3.15** and **3.16** in reasonable yields. However, the yield of the coupling reaction for propargyl amide **3.16** was as low as 20%.



**Scheme 3.5** Synthesis of boronates containing a piperazine linker.

(a), Propargyl alcohol, DMAP, CH<sub>2</sub>Cl<sub>2</sub>, rt, overnight, 69%; (b), piperazine, DCC, CH<sub>2</sub>Cl<sub>2</sub>, rt, overnight, 23%; (c), **3.1**, EDC·HCl, HOBT·H<sub>2</sub>O, Py, CH<sub>2</sub>Cl<sub>2</sub>, rt, 24 hr, 64%; (d), **3.10**, EDC·HCl, HOBT·H<sub>2</sub>O, Py, THF, rt, 20 hr, 77%; (e), 2 N H<sub>2</sub>SO<sub>4</sub>, THF, rt, overnight, quant; (f), i. *D*-biotin, EDC·HCl, HOBT·H<sub>2</sub>O, NEt<sub>3</sub>, DMF, rt, overnight, 98%, ii. HCl in dioxane/MeOH, rt, 5 hr, quant.; (g), **3.1**, EDC·HCl, HOBT·H<sub>2</sub>O, Py, DMF, rt, overnight, 51%.

To test the fluoridation of boronate esters with different protecting groups under the same conditions (either <sup>18</sup>F<sup>-</sup> or <sup>19</sup>F<sup>-</sup>), we then designed and prepared slightly more complicated compounds **3.19**, **3.20** and **3.21**, which share the same overall structure containing the piperazine linker, as shown in Scheme 3.5. The terminal alkyne residues in **3.19**, **3.20** and **3.21** were expected to afford potential applications to label biomolecules with <sup>18</sup>F-ArBF<sub>3</sub>s. Briefly, succinic anhydride was first mono-esterified with propargyl alcohol in a reasonable yield and the resulting **3.17** was then coupled to piperazine using DCC as the dehydrating reagent. The piperazine derivative **3.18** was then conjugated to

different boronyl-phenylcarboxylic acids to provide **3.19** and **3.20** respectively. Further acid treatment with **3.20** yielded boronic acid **3.21**. In addition, biotin-boronate **3.23** containing the piperazine linker was also prepared to verify the moderate-to-good radiochemical yields observed in previous radiolabeling experiments. Slightly different from the previous report,<sup>79</sup> biotin-piperazine **3.22** was prepared from the Boc-protected piperazine as demonstrated in Scheme 3.5 and this allowed much easier purification. Thus, a higher yield was obtained to prepare **3.23**.

### 3.2.2 Fluoridation studies based on BODIPY-boronate 3.6

The fluoridation of boronate **3.6** was carried out under various conditions. Different factors were studied, including the concentration of the acid/fluoride, solvents, temperatures, and salt effects. Then the reactions were loaded to a silica based TLC plate. Following development in 20% MeOH in CHCl<sub>3</sub>, the reactions were quantitatively analyzed by fluorescent densitometry. In general, this study mimicked radiofluoridation conditions that require a small volume reaction (5 ~ 6 μL) containing 100 nmol of boronate **3.6**. Also, to reflect a desire to minimize the decrease of specific activities, only 8 equivalents of fluoride (800 nmol) in the form of KHF<sub>2</sub> were initially used in the fluoridation for solvent and acid studies.

#### 3.2.2.1 Test of organic solvents for the fluoridation

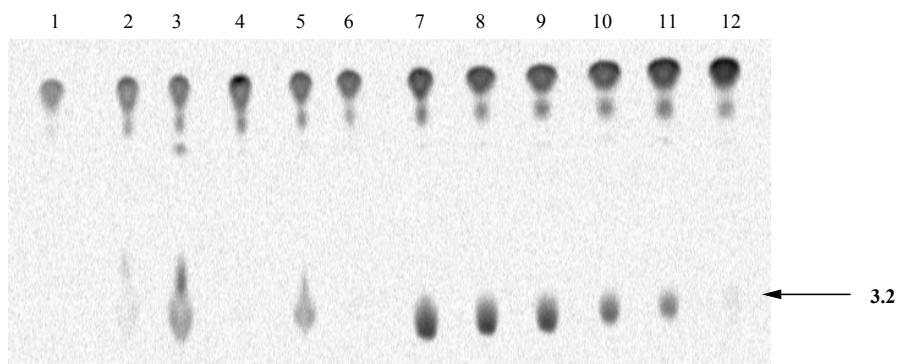


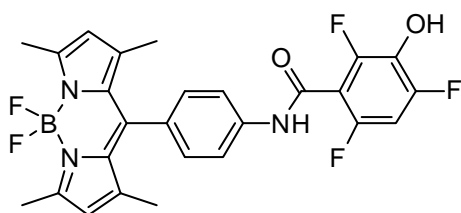
**Figure 3.1 Screening organic solvents for the fluoridation of 3.6.**

The reaction was carried out at rt for 1 hr in the presence of **3.6** (16.67 mM), KHF<sub>2</sub> (66.67 mM) and HCl (0.67 M) in a volume of 6 μL (2:1 organic solvent:H<sub>2</sub>O). Lane 1, only **3.6**; Lane 2, DMA; Lane 3, NMP; Lane 4, DMSO; Lane 5, DMF; Lane 6, acetone; Lane 7, CH<sub>3</sub>CN; Lane 8, THF; Lane 9, 1,4-dioxane; Lane 10, <sup>t</sup>BuOH; Lane 11, EtOH; Lane 12, MeOH.<sup>a</sup>

<sup>a</sup> DMA is dimethylacetamide, NMP is *N*-methyl-2-pyrrolidone, DMF is *N,N*-dimethylformamide.

Solvent plays an important role in every reaction by influencing the energy of the solvated form of starting materials/transition states/products and sometimes even being involved in the reaction. Therefore, a series of water miscible organic solvents were tested for the fluoridation of **3.6**. All the reactions were undertaken in the presence of HCl (0.67 M), **3.6** (16.67 mM), and fluoride (133.3 mM) in the form of KHF<sub>2</sub> in a total reaction volume of 6  $\mu$ L (2:1 organic solvent:H<sub>2</sub>O) at room temperature for one hour. The reactions were then quenched with 5% NH<sub>4</sub>OH in EtOH and 1  $\mu$ L of the quenched reaction was loaded to the TLC plate. After being developed with 20% MeOH in CHCl<sub>3</sub>, the TLC plate was visualized by a Typhoon 9200 Viable Mode Imager. The image acquired is shown in Figure 3.1.

These results suggest that alcoholic solvents, among which <sup>t</sup>BuOH seems the most efficient, are not particularly effective for this reaction. Reactions in polar aprotic solvents such as 1,4-dioxane, THF, and CH<sub>3</sub>CN all gave very high yields under the given conditions, whereas acetone did not prove to be suitable. Reactions in solvents with high boiling points demonstrated relatively poor conversions except for DMF and *N*-methyl-2-pyrrolidone (NMP). The reaction in NMP was comparable to that in 1,4-dioxane, THF, and CH<sub>3</sub>CN. As a result, four suitable solvents were identified for this reaction.



oxidative-deboronated product  
Chemical Formula: C<sub>26</sub>H<sub>21</sub>BF<sub>5</sub>N<sub>3</sub>O<sub>2</sub>  
Molecular Weight: 513.2669

**Figure 3.2** The structure of the oxidatively-deboronated product from **3.6**.

It was also noticed that the quality of 1,4-dioxane is extremely important for its efficiency. When we used 1,4-dioxane that had been stored for a longer time with exposure to the air, a fluorescent byproduct was produced predominantly in the reaction; it was characterized by ESI-LRMS to be the oxidatively-deboronated product ([M-H]<sup>-</sup>: 512.3). As for both 1,4-dioxane and THF, there is possible contamination with peroxide

from the slow oxidation of the ethers by the air. Therefore, we focused our study on CH<sub>3</sub>CN and NMP. For certain cases, fresh THF or 1,4-dioxane can directly replace CH<sub>3</sub>CN under the optimal conditions for the fluoridation.

### 3.2.2.2 Examination on acids for the fluoridation of 3.6

From our experience in preparing ArBF<sub>3</sub>S, the acidity of the reaction is critical for the fluoridation and the addition of acids enhances the reaction rate substantially. Moreover, some acids may play other roles that relate to medium effects and potential complexation with boron. To check whether the fluoridation is influenced by different acids, several acids were studied for the fluoridation of boronate **3.6**. The result, demonstrated in Figure 3.3, first supported our previous observation on the importance of acids in the fluoridation, comparing Lane 1 to other lanes. There was only a small fraction of the starting material converted to the desired product without the acid present in the reaction represented by Lane 1 in Figure 3.3. However, no dramatic difference among reactions with different acids was observed regarding the yields of the reactions. The reaction with HCl showed a slightly better conversion among the mineral acids tested, while that in the presence of TsOH was the best among the reactions employing organic acids. We then decided to further study the fluoridation using either HCl or TsOH as the acid.

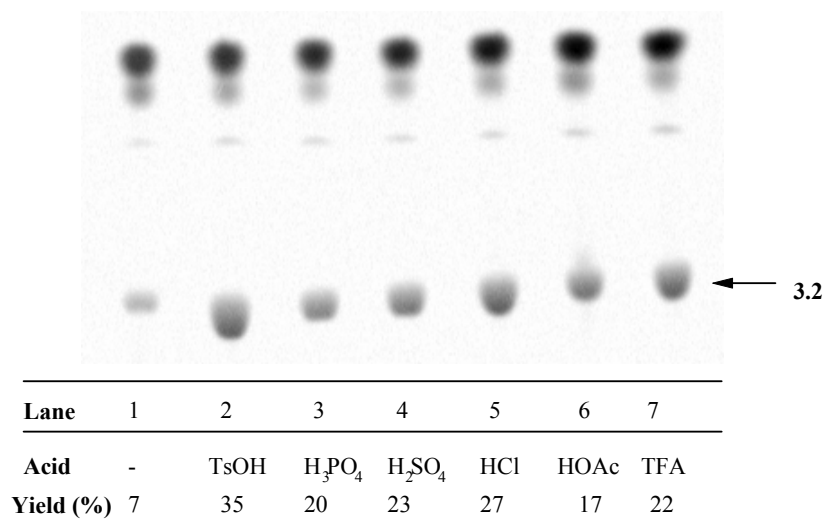


**Figure 3.3 Examination on acids used in the fluoridation of 3.6.**

Each reaction containing **3.6** (16.67 mM) and KHF<sub>2</sub> (66.67 mM) in 2:1 CH<sub>3</sub>CN:H<sub>2</sub>O (6 μL) in the presence of HA at rt for 1 hr. Lane 1, no acid added; Lane 2, 0.625 M TsOH; Lane 3, 0.67 M H<sub>3</sub>PO<sub>4</sub>; Lane 4, 0.33 M H<sub>2</sub>SO<sub>4</sub>; Lane 5, 0.67 M HCl; Lane 6, 0.67 M HOAc; Lane 7, 0.67 M TFA.

### 3.2.2.3 Fluoride concentrations for the fluoridation of 3.6

Logically, increasing the concentration of any reactant in a reaction would normally enhance the reaction rate and the same applies to the fluoridation. Indeed the conventional preparation of organotrifluoroborates has always involved a relatively large excess of free fluoride to guarantee a faster rate and a higher overall conversion of the organoboronic acids. This is due to the fact that the fluoridation of organoboronic acids/esters involves at least three steps as shown in Scheme 3.1, which means the fluoride is captured by the boron sequentially and excess fluoride is always favored to drive the reaction forward. Nevertheless, if a large amount of organoboronic acid/ester is employed, limiting amounts of fluoride may accordingly be trapped by the boron in the first step of the fluoridation to give monofluoroborate species and the overall reaction to prepare  $\text{ArBF}_3\text{s}$  might be disfavored. To maintain a reasonable specific activity of  $^{18}\text{F}$ -fluoride and also to ensure an acceptable radiochemical yield, the fluoride concentration was tested for the fluoridation of **3.6**. As shown in Figure 3.4, within one hour, the reaction with a higher concentration of fluoride always produces more BODIPY- $\text{ArBF}_3$  **3.2**. The reaction can nevertheless occur at a very low concentration of fluoride (16.66 mM of fluoride shown in Lane 2 had a yield of 6%). The reaction yields of Lane 4 (3 eq.) and Lane 5 (4 eq.) were very close to each other and around 23% of **3.6** was consumed within one hour. To guarantee the reaction to proceed with reasonable yields, 4 equivalents of fluoride under similar conditions were used for further studies.

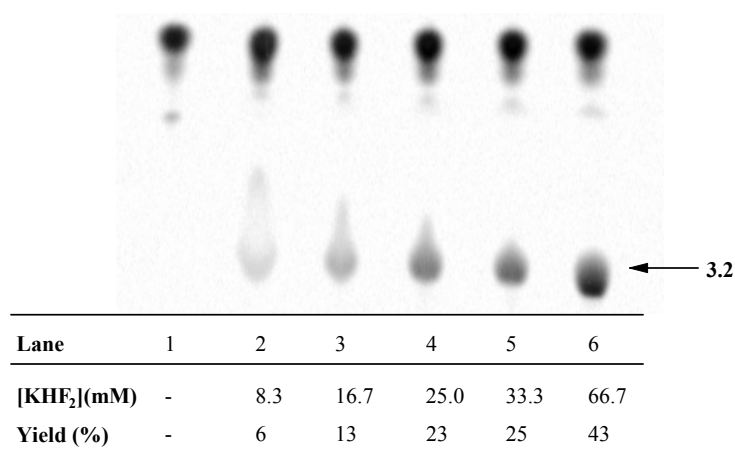


**Figure 3.4 Effect of fluoride concentrations on the fluoridation of 3.6.**

Each reaction containing **3.6** (16.7 mM) and HCl (0.67 M) in 2:1  $\text{CH}_3\text{CN}:\text{H}_2\text{O}$  (6  $\mu\text{L}$ ) in the presence of different concentrations of  $\text{KHF}_2$  at rt for 1 hr. Lane 1, only **3.6**; Lane 2, 8.33 mM  $\text{KHF}_2$ ; Lane 3, 16.7 mM  $\text{KHF}_2$ ; Lane 4, 25.0 mM  $\text{KHF}_2$ ; Lane 5, 33.33 mM  $\text{KHF}_2$ ; Lane 6, 66.7 mM  $\text{KHF}_2$ .

### 3.2.2.4 Reaction temperatures for the fluoridation of 3.6

Temperature is also one of the key factors controlling reaction rates. In most of the cases, a reaction takes less time at a higher temperature. As part of the optimization, temperature was also studied for the fluoridation of BODIPY-boronate **3.6**. Since CH<sub>3</sub>CN has a boiling point of 82 °C and that of NMP is 202 °C, three temperatures were examined: room temperature (~ 20 °C), 30 °C, and 50 °C. Evaporation of CH<sub>3</sub>CN at both 30 °C and 50 °C was very apparent and led to precipitation of the boronate ester. In contrast, the reaction volume in all NMP reactions remained unchanged and the reaction mixture was transparent all the time. As a result, it appears that the reaction in CH<sub>3</sub>CN gave the best yield at room temperature, and higher reaction temperatures seemed to enhance the reaction considerably in aqueous NMP (Figure 3.5). Specifically, the reaction in NMP at 50 °C had a yield (55%) twice that at room temperature (28%), but it also yielded higher quantities of byproducts. In the following studies, the fluoridation of **3.6** in aqueous CH<sub>3</sub>CN was undertaken at room temperature.

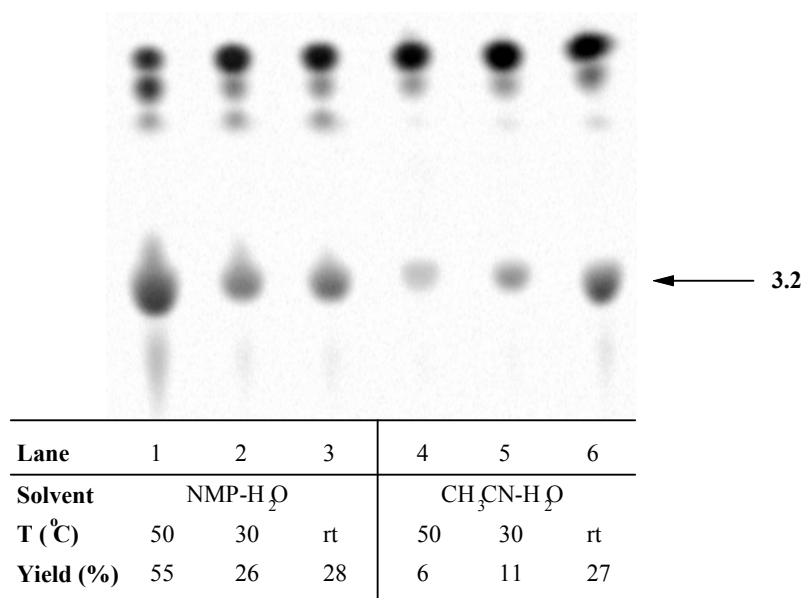


**Figure 3.5 Study on the temperature dependence of the fluoridation of 3.6.**

Each reaction was carried out in the presence of BODIPY-boronate **3.6** (16.67 mM), KHF<sub>2</sub> (33.33 mM), and HCl (2.1 M) in a total volume of 2:1 organic solvent:H<sub>2</sub>O (total in 6 μL) at different temperatures for 1 hr. Lane 1, NMP, 50 °C; Lane 2, NMP, 30 °C; Lane 3, NMP, rt; Lane 4, CH<sub>3</sub>CN, 50 °C; Lane 5, CH<sub>3</sub>CN, 30 °C; Lane 6, CH<sub>3</sub>CN, rt

### 3.2.2.5 The content of the organic solvent for the fluoridation of 3.6

During the experiments executed above, it was noticed that in some assays, BODIPY-boronate **3.6** precipitated upon the addition of aqueous reagents and the yield was significantly lower than those where starting materials were fully dissolved. We then decided to screen the amounts of the organic solvent to 1) provide sufficiently high concentrations for relatively fast fluoridation kinetics, and 2) guarantee a high and effective conversion. It is shown in Figure 3.6 that higher content of CH<sub>3</sub>CN enhances the yield of the reaction. However, the dilution due to a higher amount of the organic solvent also adversely influenced the conversion. From the curve of the conversion against the CH<sub>3</sub>CN content, it appears that ~ 75% aqueous CH<sub>3</sub>CN would be suitable for a good conversion under the same conditions.

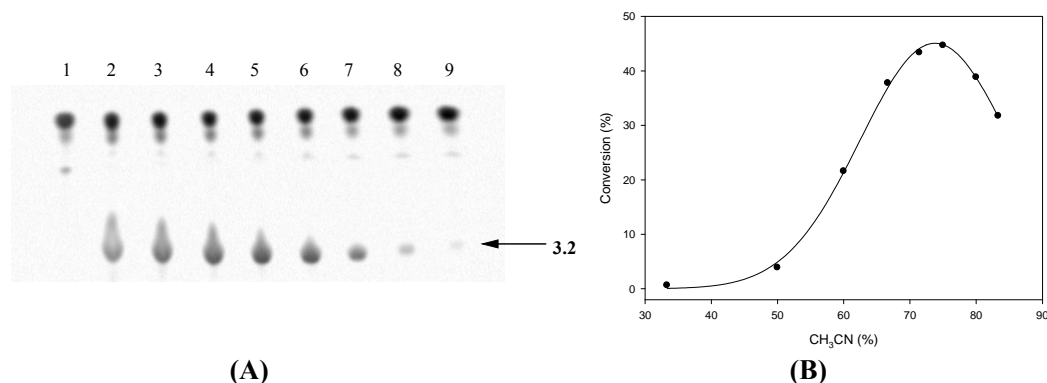


**Figure 3.6 Investigation of organic solvent content affecting the fluoridation of 3.6.**

(A), Each reaction containing 100 nmol of BODIPY-boronate **3.6**, 200 nmol of KHF<sub>2</sub>, and 4 μmol of HCl in 2 μL H<sub>2</sub>O and a different amount of CH<sub>3</sub>CN was incubated at rt for 1 hr. Lane 1, only **3.6**; Lane 2, 10 μL of CH<sub>3</sub>CN; Lane 3, 8 μL of CH<sub>3</sub>CN; Lane 4, 6 μL of CH<sub>3</sub>CN; Lane 5, 5 μL of CH<sub>3</sub>CN; Lane 6, 4 μL of CH<sub>3</sub>CN; Lane 7, 3 μL of CH<sub>3</sub>CN; Lane 8, 2 μL of CH<sub>3</sub>CN; Lane 9, 1 μL of CH<sub>3</sub>CN; (B) The conversion of **3.6** in the presence of different amounts of CH<sub>3</sub>CN and the curve was drawn to illustrate the trend of the changes.

### 3.2.2.6 Acid concentrations for the fluoridation of 3.6

The fluoridation appears much more efficient in the presence of acid, as shown in Figure 3.3. In addition, the reaction proceeds more rapidly in the presence of a higher acid concentration. We therefore studied the acid concentration for this reaction. Figure 3.7B shows a general trend where the reaction yield depends on the concentration of HCl. It seems that there is an optimal acid concentration (~ 1.64 M) in a reaction volume of 6 μL containing 67% organic solvent.

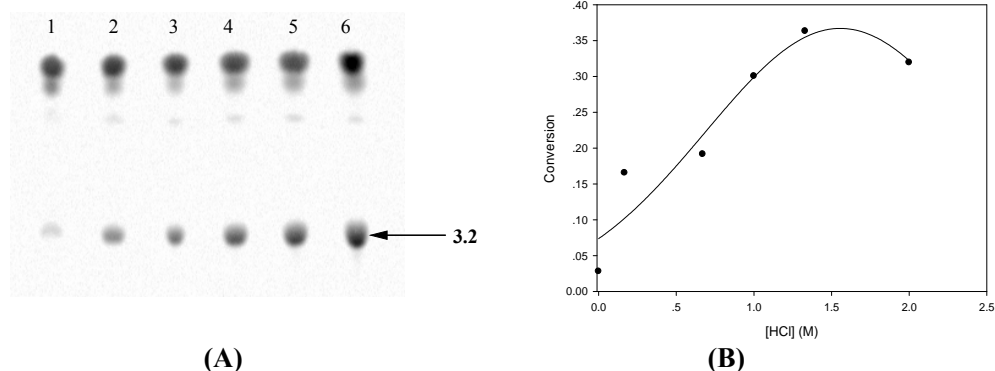


**Figure 3.7 Concentrations of HCl used in the fluoridation of 3.6.**

(A), The TLC analysis of the study on the effect of HCl concentrations for the fluoridation of **3.6**: each reaction containing **3.6** (16.67 mM) and  $\text{KHF}_2$  (33.33 mM) in 2:1  $\text{CH}_3\text{CN}:\text{H}_2\text{O}$  (6  $\mu\text{L}$ ) in the presence of HCl at rt for 1 hr. Lane 1, 0 M HCl; Lane 2, 0.17 M HCl; Lane 3, 0.67 M HCl; Lane 4, 1.00 M HCl; Lane 5, 1.33 M HCl; Lane 6, 2.10 M HCl; (B), the trend for the influence of HCl concentrations on the fluoridation of **3.6** and the data were plotted for eye guidance.

The effect of the TsOH concentration on the fluoridation of **3.6** was also investigated. Because the saturated aqueous solution of TsOH is around 3.6 M, we made a series of stock solutions from 0.5 M to 3.5 M and added that to the reaction in the presence of **3.6** (16.67 mM) and  $\text{KHF}_2$  (33.33 mM). The results in Figure 3.8 imply that, a better conversion in the presence of the same amount of fluoride would be achieved with a higher concentration of TsOH.

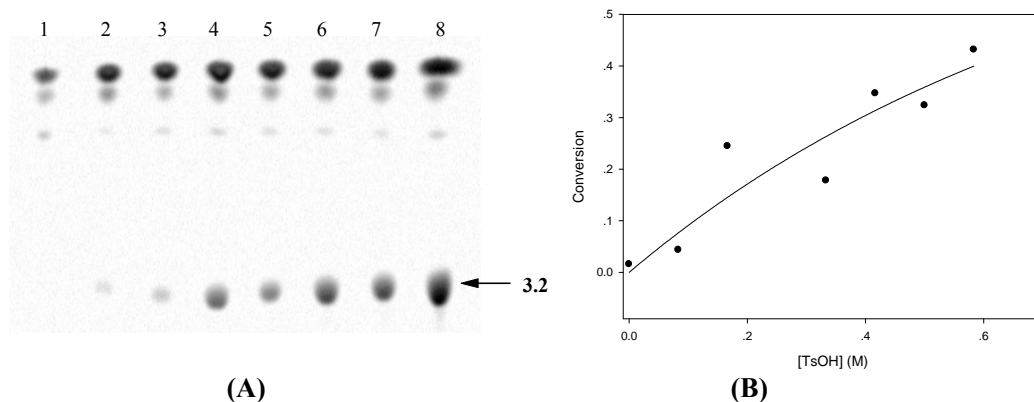


**Figure 3.8 Concentrations of TsOH used in the fluoridation of 3.6.**

(A), The TLC analysis of the study on the effect of TsOH concentrations for the fluoridation of **3.6**: each reaction containing **3.6** (16.67 mM) and  $\text{KHF}_2$  (33.33 mM) in 2:1  $\text{CH}_3\text{CN}:\text{H}_2\text{O}$  (6  $\mu\text{L}$ ) in the presence of TsOH at rt for 1 hr. Lane 1, only **3.6**; Lane 2, 0 M TsOH; Lane 3, 0.083 M TsOH; Lane 4, 0.17 M TsOH; Lane 5, 0.33 M TsOH; Lane 6, 0.42 M TsOH; Lane 7, 0.50 M HCl; Lane 8, 0.58 M TsOH. (B), The trend for the influence of TsOH concentrations on the fluoridation of **3.6** and the data were plotted for eye guidance.

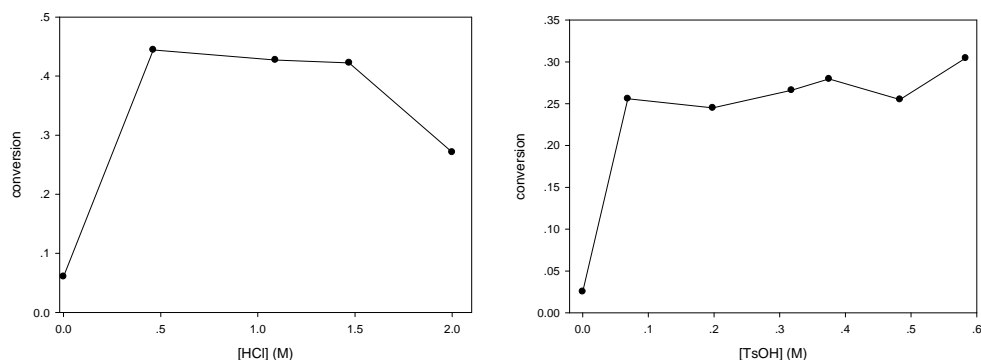


**Figure 3.9 Addition of concentrated acids to the fluoridation of 3.6.**

Reaction conditions: 100 nmol of BODIPY-boronate **3.6** and 200 nmol of  $\text{KHF}_2$  in 4  $\mu\text{L}$  of  $\text{CH}_3\text{CN}$  and 1  $\mu\text{L}$   $\text{H}_2\text{O}$  was added with different amounts of concentrated HCl (left) or 3.5 M aqueous TsOH (right). The reactions were incubated at rt for 1 hr and quenched with 100  $\mu\text{L}$  of 5%  $\text{NH}_4\text{OH}$  in EtOH. The conversion of **3.6** was shown against the final concentration of acid in the reaction and the data were plotted for eye guidance.

Notably however, it is very hard to control the acid concentration of radiofluoridation reactions of arylboronates. Usually, concentrated HCl is directly added to acidify the reaction mixture. Therefore, in order to mimic the addition of the concentrated acid in the radiolabeling experiments, we tried to add different amounts ( $\mu\text{L}$ ) of the concentrated acid (12.6 M HCl or 3.5 M TsOH) to the reaction containing 100 nmol of BODIPY-boronate **3.6** and 400 nmol of  $\text{KHF}_2$  in 5  $\mu\text{L}$  80% aqueous  $\text{CH}_3\text{CN}$ . Though the concentrations of all reactants were changed due to the addition of different volumes of the concentrated acids, we again observed what appeared to be an optimal acid concentration for the reaction in the presence of HCl. In contrast, the reactions acidified with TsOH suggested that once a certain concentration (0.078 M) of TsOH was reached, similar yields after one hour incubation were obtained with different reaction volumes. We realized that with the addition of a different amount of the concentrated acid, the reaction volume was changed and the concentrations of the reactants i.e. **3.6** and  $\text{KHF}_2$  were also affected. Nevertheless, this study suggested that the fluoridation was optimal at  $\sim 1$  M of HCl in a reaction volume of 5.5  $\mu\text{L}$ . It also suggested that HCl and TsOH may have played slightly different roles in the fluoridation based on the data in this section.

### 3.2.2.7 Effects of the ionic strength on the fluoridation of 3.6

In the  $^{18}\text{F}$ -radiofluoridations of arylboronic acids, there are basically two salt sources. One is from the fluoride elution solution, which in our case is  $\text{NaClO}_4$ . The other one is

the sodium chloride that is derived from the acid neutralization of sodium bicarbonate, which co-elutes with  $^{18}\text{F}$ -fluoride from the anion exchange column ( $\text{HCO}_3^-$  form). Therefore, it is important to study the salt effects on the fluoridation to understand whether or not the presence of these salts would influence the reaction.

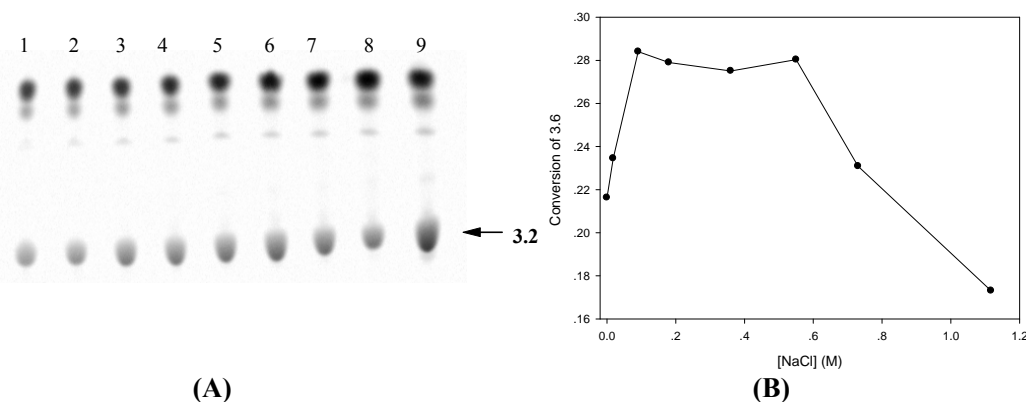


**Figure 3.10 The study of salt effects on the fluoridation to prepare BODIPY-ArBF<sub>3</sub> 3.2.**

(A), TLC analysis of the salt effects on the fluoridation of **3.2**. Each reaction was carried out in the presence of **3.6** (18.18 mM) and  $\text{KHF}_2$  (36.36 mM) in 4:1.5  $\text{CH}_3\text{CN}:\text{H}_2\text{O}$  (5.5  $\mu\text{L}$ ) and  $\text{HCl}$  (1.15 M) at rt for 1 hr with a different salt concentration. Lane 1, 0 M salt; Lane 2, 0.018 M  $\text{NaCl}$ ; Lane 3, 0.091 M  $\text{NaCl}$ ; Lane 4, 0.18 M  $\text{NaCl}$ ; Lane 5, 0.36 M  $\text{NaCl}$ ; Lane 6, 0.55 M  $\text{NaCl}$ ; Lane 7, 0.73 M  $\text{NaCl}$ ; Lane 8, 1  $\mu\text{L}$  of saturated  $\text{NaCl}$  added to make a final reaction volume of 5.5  $\mu\text{L}$ ; Lane 9, 1  $\mu\text{L}$  of saturated  $\text{NaClO}_4$  added to make a final reaction volume of 5.5  $\mu\text{L}$ . (B) The conversion of **3.6** in the presence of different concentrations of  $\text{NaCl}$  based on the TLC analysis shown in (A). The line was drawn to illustrate the trend of the data.

The result shown in Figure 3.10 first suggested that the presence of  $\text{NaClO}_4$  (Lane 9) seemed to enhance the reaction. The concentration of  $\text{NaClO}_4$  used herein was based on the possible concentration of  $\text{NaClO}_4$  that might be achieved by resuspension of  $\text{NaClO}_4$  (1 mg)<sup>a</sup> in 10  $\mu\text{L}$  of the fluoride solution. However, to our surprise, at the expected concentration, a fair amount of the salt remained insoluble and it was then regarded as saturated  $\text{NaClO}_4$  in the fluoride solution. After one hour incubation, a yield of  $\sim 37\%$  was achieved in the presence of  $\text{NaClO}_4$ . On the other hand, various  $\text{NaCl}$  concentrations were tested for the fluoridation. There was a slight enhancement on the conversion of the fluoridation reaction in the presence of salt. It seems that too concentrated or too dilute salt solutions had very minimal effects on the overall yields. The fluoridation in the presence of  $\text{NaCl}$  with a concentration of  $\sim 0.36$  M demonstrated the highest yield in one

<sup>a</sup> The  $^{18}\text{F}$ -fluoride solution was concentrated at  $\sim 110$   $^\circ\text{C}$  under helium flow in the presence of  $\text{NaClO}_4$  (2 mg/mL, a total volume of 1 mL). The residue from this evaporation process was then re-suspended with the  $^{19}\text{F}$ -fluoride solution in the form of  $\text{KHF}_2$ .

hour.

### 3.2.2.8 Kinetic studies on the fluoridation of 3.6

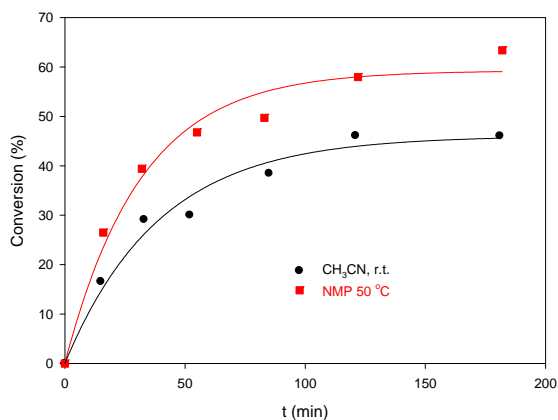


**Figure 3.11** The kinetic study of the fluoridation of BODIPY-boronate 3.6 in CH<sub>3</sub>CN or NMP.

The kinetic study was carried out via a series of reactions that underwent under same conditions at different initiation time but quenched at the same time prior to the development of TLC in 20% MeOH/CHCl<sub>3</sub>. The condition for the kinetic curve represented by (●) was in the presence of BODIPY-boronate 3.6 (18.18 mM), KHF<sub>2</sub> (36.36 mM), and HCl (1.15 M) in a total volume of 5.5 μL (4:1.5 CH<sub>3</sub>CN:H<sub>2</sub>O) at rt. That by (■) was in the presence of BODIPY-boronate 3.6 (16.67 mM), KHF<sub>2</sub> (33.33 mM), HCl (2.1 M) in a total volume of 6 μL (2:1 NMP:H<sub>2</sub>O) at 50 °C. The data were fitted to the equation:  $y = a(1 - e^{-kx})$ . For (●)  $a = 0.47 \pm 0.0024$  and  $k_{\text{obs}} = 0.022 \pm 0.0034 \text{ min}^{-1}$  with  $R^2 = 0.9865$  and for (■)  $a = 0.59 \pm 0.025$  and  $k_{\text{obs}} = 0.032 \pm 0.0045 \text{ min}^{-1}$  with  $R^2 = 0.9777$ .

A kinetic experiment was undertaken for reaction conditions that I estimated to represent an optimal fluoride concentration (4 eq., ~ 66 mM) from section 3.2.2.3, the solvent content (3:1 organic solvent:H<sub>2</sub>O, v/v) from section 3.2.2.5, and the acid concentration (1.09 M of HCl) from section 3.2.2.6 for CH<sub>3</sub>CN. We used a slightly higher volume and more acid for reactions in NMP at 50 °C. It was illustrated in Figure 3.11 that the reactions under both conditions reached apparent equilibrium. Moreover, the data implied that the reaction in CH<sub>3</sub>CN at room temperature gave a yield of ~ 20% after one hour incubation while it reached 44% in aqueous NMP at 50 °C.

### 3.2.3 Fluoridation studies by <sup>19</sup>F NMR spectroscopy

The conditions determined from the previous section provide guidelines for the fluoridation of any benzopinacol protected boronic esters and may also be useful for the fluoridation of other boronic acids/esters. In this section, we used <sup>19</sup>F NMR spectroscopy to investigate the fluoridation of several arylboronic esters that are of great interest for our purpose in developing new PET imaging agents. Since the fluoridation was carried

out under acidic conditions, a reaction with a total volume of approximately 4 mL was first initiated in a plastic falcon tube, and around 150  $\mu\text{L}$  of the reaction was removed and quenched with 150  $\mu\text{L}$  of 33.3%  $\text{NH}_4\text{OH}$  in EtOH prior to the  $^{19}\text{F}$  NMR data acquisition at a specific time point.

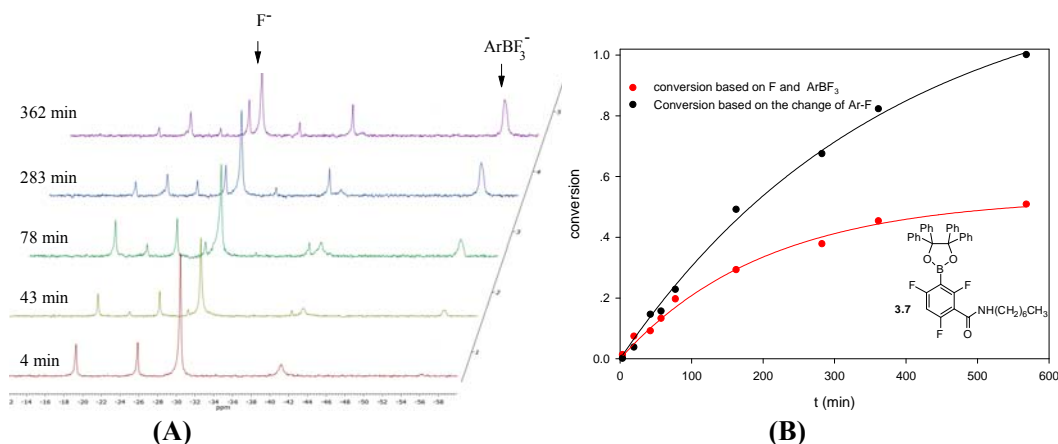


**Figure 3.12** The fluoridation of **3.7** studied by  $^{19}\text{F}$  NMR spectroscopy.

(A), The fluoridation of heptylamide boronate **3.7** monitored by  $^{19}\text{F}$  NMR spectroscopy. The reaction condition was 17.0 mM of **3.7**, 33.33 mM of  $\text{KHF}_2$ , and 1.68 M of  $\text{HCl}$  in 2:1  $\text{CH}_3\text{CN}:\text{H}_2\text{O}$  at rt. 139  $\mu\text{L}$  of the reaction mixture was quenched with 139  $\mu\text{L}$  of 33.3%  $\text{NH}_4\text{OH}$  in EtOH and then the  $^{19}\text{F}$  NMR spectrum of the quenched mixture was recorded on the 282.4 MHz spectrometer at certain time point without locking to any solvent. The time points for the  $^{19}\text{F}$  NMR traces are indicated on the NMR spectra. Other  $^{19}\text{F}$ -signals un-annotated are the aryl-fluoride Ar-F. (B), The kinetic fitting of the fluoridation of boronate **3.7** via first order kinetics. The conversion of the fluoridation was calculated based on -19.23 ppm/-22.63 ppm (black) for the Ar-F or -30.50 ppm/-56.21 ppm (red) for the free fluoride/ $\text{ArBF}_3$ . The data were fitted to the equation:  $y = a(1 - e^{-kx})$ . For the Ar-F:  $k_{\text{obs}} = (2.7 \pm 0.3) \times 10^{-3} \text{ min}^{-1}$ ,  $R^2 = 0.9962$ . For the free fluoride/ $\text{ArBF}_3$ :  $k_{\text{obs}} = (4.9 \pm 0.5) \times 10^{-3} \text{ min}^{-1}$ ,  $R^2 = 0.9921$ .

The fluoridation of heptylamide boronate **3.7**, which is similar to **3.6** bearing the benzopinacol protecting group but much easier and cheaper to make, was studied by  $^{19}\text{F}$  NMR spectroscopy under the conditions optimized in the previous section. The  $^{19}\text{F}$  NMR spectra recorded at certain time points are shown in Figure 3.12A. From the NMR spectra, the free fluoride peak (-30.5 ppm) decreased while the peak at  $\sim -56$  ppm representing the  $\text{ArBF}_3$  gradually increased. The chemical shift change of the aromatic fluoride (Ar-F) suggests that the compound was consumed to give a new product, which was later confirmed by ESI-LRMS to be the corresponding  $\text{ArBF}_3$  ( $[\text{M}]^+$ : 340.4). However, no obvious intermediate was observed in the quenched mixture. From the kinetic data, the reaction was complete around nine hours and it proceeded to around 20% after the first hour. This result is quite consistent with the fluoridation of BODIPY-boronate **3.6**.

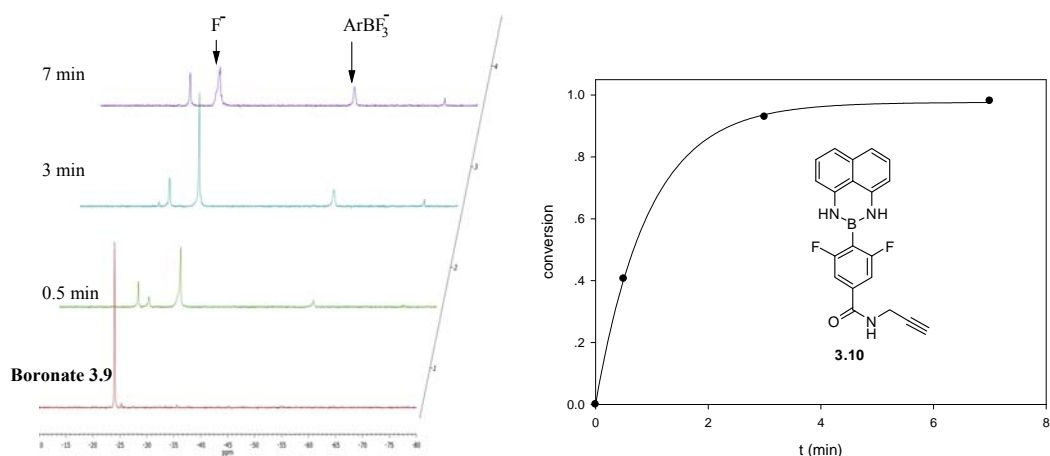


**Figure 3.13** The  $^{19}\text{F}$  NMR study on the fluoridation of **3.10**.

The reaction condition was 17.0 mM of **3.10**, 33.33 mM of  $\text{KHF}_2$ , and 1.68 M of HCl in 2:1 THF:H<sub>2</sub>O at rt. 139  $\mu\text{L}$  of the reaction mixture was quenched with 139  $\mu\text{L}$  of 33.3%  $\text{NH}_4\text{OH}$  in EtOH and then the  $^{19}\text{F}$  NMR spectrum was recorded on the 282.4 MHz spectrometer at certain time point without locking to any solvent. The time points for the  $^{19}\text{F}$  NMR traces indicated from the bottom to the top are: without fluoride treatment, 0.5 min, 3 min, 7 min. The conversion ratio was calculated based on  $-24.63 \text{ ppm}/-26.56 \text{ ppm}$  for the Ar-F and fitted against  $y = a(1 - e^{-kx})$ .  $k_{\text{obs}} = 1.07 \pm 0.02 \text{ min}^{-1}$ ,  $R^2 = 0.9999$ .

1,8-Diaminonaphthalene is another favorable protecting group that has been reported extensively to protect boronic acids and is always removed under acidic conditions.<sup>126-128</sup> 1,8-Diaminonaphthalene protected boronates have very high stability under various conditions including those used in the Pd catalyzed Suzuki reactions and accordingly these boronates can be derivatized via different methods prior to acid treatment to remove the protecting group and hence release the free boronic acids. Since 1,8-diaminonaphthalene is a base, the fluoridation of the boronate protected by this protecting group may occur in a very rapid fashion under acidic conditions. Therefore, boronate esters **3.9** and **3.10** with this protecting group were prepared and their fluoridation was monitored by  $^{19}\text{F}$  NMR spectroscopy. Similar fluoridation conditions were applied to the fluoridation of **3.10**. THF was used instead of  $\text{CH}_3\text{CN}$  as the compound has a higher solubility in THF. It was found that the reaction went to completion very quickly under similar conditions, as indicated in the  $^{19}\text{F}$  NMR traces in Figure 3.13. One thing that might raise concern is the ratio of the fluoride integration from the NMR spectra, which suggested the reaction mixture was with 8.7:1 (instead of 4:1) fluoride to the boronate ratio and this might be caused by the errors in sample preparation since relatively a small amount of **3.10** was weighed for this reaction.

Although the somewhat larger excess of fluoride<sup>a</sup> further accelerated the reaction, we were delighted with the rapid fluoridation rate and high yields with the diamidonaphthalene protected boronate **3.10**. The fluoridation of its precursor **3.9** under similar conditions also displayed a rapid fashion and its half-life was around 1.3 minutes.

To increase the acid sensitivity of the protecting group, the electron donating methoxy groups were introduced to both the 2- and 7-positions of 1,8-diamidonaphthalene to afford DiDiAN, which was expected to be a better leaving group under acidic conditions due to the increasing basicity. We envisioned that the fluoridation of the DiDiAN protected boronate esters should proceed more rapidly. Following the same protocol, DiDiAN was installed on boronic acid **3.8** and the protected boronic acid **3.15** was further conjugated with propargylamine to give the alkyne synthon **3.16** for the click reaction that will be describe in Chapter 6. The <sup>19</sup>F NMR study on the fluoridation of the DiDiAN protected boronate **3.15** indeed exhibited an even higher reaction rate ( $t_{1/2} \sim 0.43$  min).

Based on knowledge of reactions involving electronic and steric effects, if the boronic acid is “naked” (without any protecting groups), there is no steric hindrance involved to prevent the fluoride or water from attacking the boron and consequently the fluoridation should be rapid. Thus we studied the fluoridation of boronic acid **3.8**, which can be prepared in a relatively large amount and reasonable purity. Under the same conditions of the fluoridation as that of **3.10** in THF/H<sub>2</sub>O, the reaction was complete within seconds<sup>b</sup> (data not shown).

### 3.2.4 The <sup>18</sup>F-fluoridation of boronates

I was able to exploit the above findings for <sup>18</sup>F-radiolabeling of some boronates discussed earlier in collaboration with the Center for Probe Development and Commercialization (CPDC) in Hamilton. The DiDiAN protected boronate ester **3.16** was prepared and tested for its <sup>18</sup>F-fluoridation under similar conditions as shown in Figure 3.14. The radio-HPLC chromatograms suggest that the reaction was very fast and

---

<sup>a</sup> Fluoride concentration was the same as other <sup>19</sup>F NMR studies, but the concentration of boronic acid **3.10** was much lower than that of **3.7** in Figure 3.12.

<sup>b</sup> The reaction was mixed for several seconds, quenched with NH<sub>4</sub>OH buffer and then measured for its <sup>19</sup>F NMR spectrum.

equilibrium was reached at around 50 minutes. At equilibrium, around 30%  $^{18/19}\text{F}$ -fluoride was captured by the boron. Based on this, the conversion of boronate ester **3.16** was calculated to be  $\sim 62.5\%$  to yield the  $^{18}\text{F}$ -ArBF<sub>3</sub>.

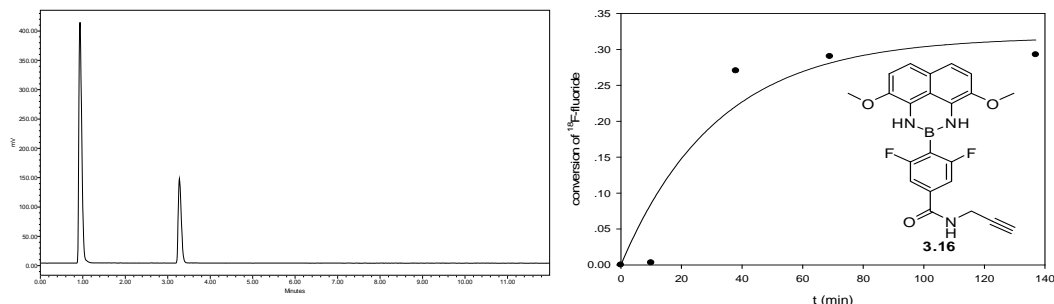


**Figure 3.14** The kinetic study on the  $^{18}\text{F}$ -fluoridation of **3.16**.

The reaction condition: 17.4 mM of **3.16**, 54.4 mM of  $\text{KHF}_2$ , 1.10 M of  $\text{HCl}$  in 70% aqueous THF. Each reaction was 5.75  $\mu\text{L}$  in total and at certain time point was quenched with 5%  $\text{NH}_4\text{OH}$  in 50% aqueous EtOH (100  $\mu\text{L}$ ). The radioactivity for individual reaction was from 5.4 mCi to 6.3 mCi at the beginning of synthesis (BOS). The quenched reaction was then injected into the UPLC with Program 6 and Column III in HPLC System III.<sup>a</sup> The HPLC chromatogram shown in the left was the reaction undertaken for 38 min at rt. The peak at 3.27 min represents the desired  $^{18}\text{F}$ -ArBF<sub>3</sub>. The kinetic curve on the right is the incorporation of  $^{18}\text{F}$ -fluoride based on time, which is fitted with  $y = a(1 - e^{-kx})$  where  $a = 0.3174 \pm 0.0598$  and  $k_{\text{obs}} = 0.0314 \pm 0.018 \text{ min}^{-1}$ ,  $R^2 = 0.8990$ .

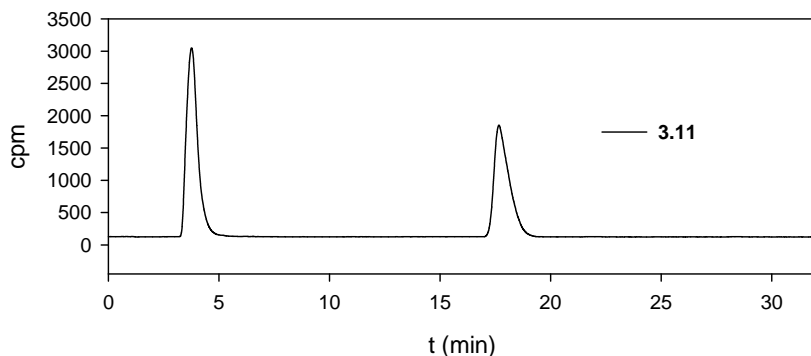


**Figure 3.15** The radio-HPLC chromatogram of the  $^{18}\text{F}$ -fluoridation of **3.11**

The reaction condition: 15.4 mM of **3.11**, 38.5 mM of  $\text{KHF}_2$ , and 0.97 M of  $\text{HCl}$  in 61.5% aqueous THF (6.5  $\mu\text{L}$ ). The reaction (the radioactivity at the BOS: 6.84 mCi) was incubated at rt for 29 min and quenched with 5%  $\text{NH}_4\text{OH}$  in 50% aqueous EtOH. The crude reaction was injected into the HPLC with HPLC Program 7 and Column I in HPLC System IV. The radiochemical yield is 44% ( $t_{\text{R}} = 17.7 \text{ min}$ ) based on the integration of the radio-peak.

We also studied the radiofluoridation of the free boronic acid **3.11** at the CPDC under similar conditions. The radiochemical yields ranged from 40% to 60% in about half an hour. This result was reproduced at TRIUMF. The result displayed in Figure 3.15 represented one of the radiofluoridations of boronic acid **3.11**, which was done recently at TRIUMF. For about 30 minutes, the reaction gave a radiochemical yield of 44% and

<sup>a</sup> The HPLC information can be found in Appendix B.

no intermediate was observed in the radio-HPLC chromatogram.

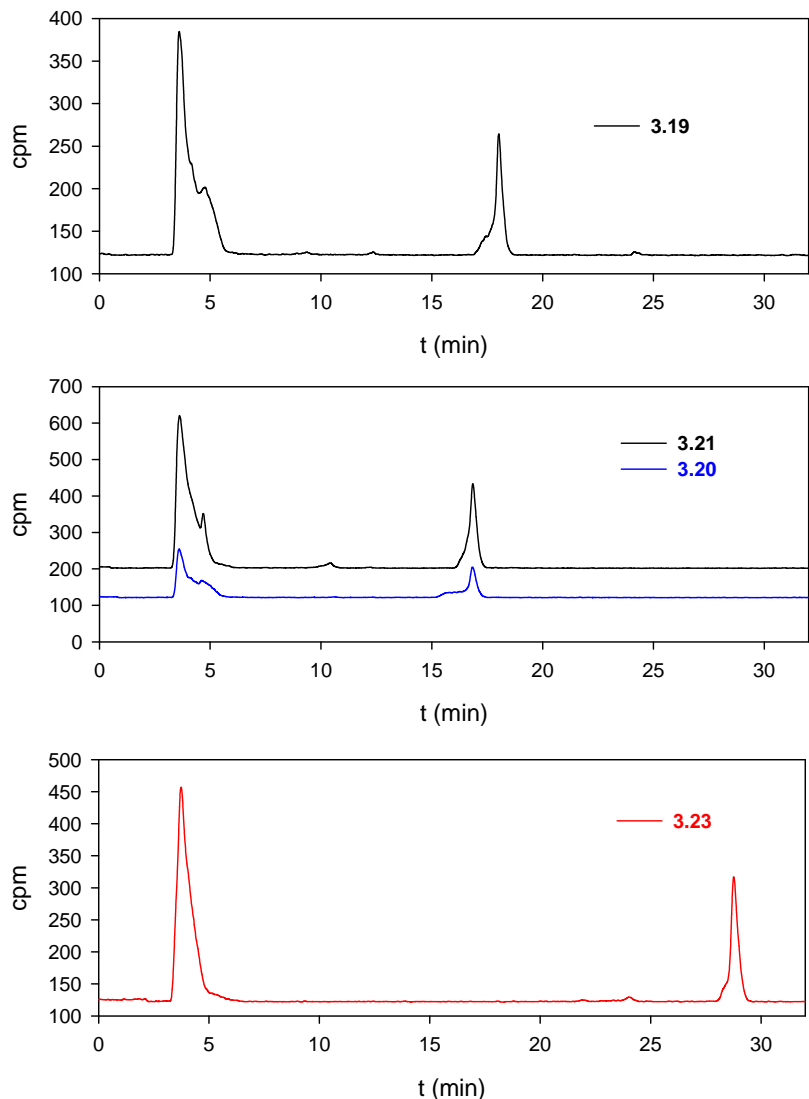


**Figure 3.16** The radio-HPLC traces of the  $^{18}\text{F}$ -radiolabeling of **3.19**, **3.20**, **3.21** and **3.23**.

The reaction condition: 15.4 mM of boronate, 38.5 mM of  $\text{KHF}_2$  and 0.97 M of HCl in 6.5  $\mu\text{L}$  of 61.5% aqueous  $\text{CH}_3\text{CN}$  (for **3.19** and **3.23**) or THF (for **3.20** and **3.21**). The reaction was quenched with 5%  $\text{NH}_4\text{OH}$  in 50% aqueous EtOH and injected into the HPLC with HPLC Program 8 for **3.19**, **3.20** and **3.21** or Program 7 for **3.23** and Column I in HPLC System IV. The radiochemical yield of each reaction: 23% for **3.19** (60 min, 2.03 mCi at the BOS), 30% for **3.20** (66 min, 1.93 mCi at the BOS), 22% for **3.21** (38 min, 3.54 mCi at the BOS) and 25% for **3.23** (63 min, 5.0 mCi at the BOS).

We then tested the  $^{18}\text{F}$ -fluoridation of more structurally complicated compounds **3.19**, **3.20**, **3.21** and **3.23** as shown in Figure 3.16. During these experiments, the boronates with protecting groups as benzopinacol and 1,8-diaminonaphthalene showed slightly different conversion profiles. Boronate **3.20**, with 1,8-diaminonaphthalene as the protecting group, showed a slightly better radiochemical conversion (30%) compared

with the benzopinacol protected **3.19** (23%) and **3.23** (25%) for a reaction of one hour at room temperature, while the free boronic acid **3.21** gave a conversion of 22% after a 38 minute reaction. These discrepancies are discussed below between the NMR data and the radiofluoridations.

## 3.3 Discussion

### 3.3.1 Synthesis

The synthesis of BODIPY-boronate **3.6** was very straightforward as indicated in Scheme 3.2. The construction for the core of BODIPY was achieved with a relatively low but acceptable yield. It was found that the quality of 2,4-dimethylpyrrole is critical for the reaction. Since 2,4-dimethylpyrrole is slightly air-sensitive, the reaction was undertaken under a N<sub>2</sub> atmosphere. On the other hand, the amino group on BODIPY-NH<sub>2</sub> **3.5** that was produced by a Pd/C catalyzed reduction of BODIPY-NO<sub>2</sub> **3.4** is inactivated by the highly conjugated and electron-deficient system, and the coupling reaction with acid **3.1** consequently was very inefficient. In this chapter, the activating agent DCC was used instead of the previously reported EDC·HCl/HOBt·H<sub>2</sub>O coupling<sup>80</sup> to provide a simpler reaction environment and the reaction also gave a better conversion. For both methods, a relatively high amount of a protodeboronated product was detected and this complicated the purification by flash chromatography. The compound was normally purified by flash chromatography, but a preparative TLC was always involved to further resolve the compound from the protodeboronated compound. For some cases, the preparative TLC purified product may still be contaminated with the deboronated byproduct. The purified compound was then stored in aliquots of 100 nmol in 0.5 mL polypropylene PCR tubes at -20 °C for the screening experiments.

1,8-Diaminonaphthalene is a known protecting group for boronic acids.<sup>126, 128</sup> The 1,8-diaminonaphthalene protected boronate esters are reported to be very stable in various conditions and this group can be removed under acidic conditions to release the boronic acids. As the acid sensitivity of the protecting group might facilitate the fluoridation, we prepared 1,8-diaminonaphthalene protected boronates **3.9** and **3.10**. Furthermore, in pursuit of a more acid-sensitive protecting group, DiDiAN was

developed by introducing two methoxy groups onto 1,8-diaminonaphthalene to offer more electron density on the naphthalene ring and hence to increase the basicity of the amino groups to achieve a faster deprotection. Accordingly, **3.15** and **3.16** were prepared. However, the syntheses of **3.15** and **3.16** carrying DiDiAN as the protecting group were with much lower isolated yields than that of the 1,8-diaminonaphthalene protected counterparts **3.9** and **3.10**. Furthermore, through the simple acid treatment with **3.10** in aqueous THF, boronic acid **3.11** was prepared. Based on the  $^{19}\text{F}$  NMR and  $^1\text{H}$  NMR spectra, boronic acid **3.11** was with reasonable purity.

From the previous radiolabeling study of biotin-boronate **3.23**, we have found that the compound with a piperazine linker between the arylboronate and the biotin residue always incorporates  $^{18/19}\text{F}$ -fluoride more efficiently than compounds with linear linkers. Hence, boronic acid/esters **3.19**, **3.20** and **3.21** were designed with the piperazine linker. Moreover, to develop their  $\text{ArBF}_3\text{S}$  as potential prosthetic groups, the terminal alkyne functionality was introduced. Biotin-boronate **3.23** was prepared with some modifications from the reported protocol.<sup>79</sup> The preparation of these compounds followed standard protocols as shown in Scheme 3.5.

### 3.3.2 The fluoridation of BODIPY-boronate **3.6**

Benzopinacol is a very bulky protecting group, which improves the stability of arylboronates during syntheses, purification, and storage. Nevertheless, the fluoridation of benzopinacol protected boronates might be influenced by the steric hindrance imposed by the protecting group. To better understand the fluoridation of the benzopinacol protected boronates, fluorescent BODIPY-boronate **3.6** was used for quantitative fluoridation studies by TLC-fluorescent densitometry. Several factors related to the reaction were investigated.

The effects of various solvents, acids, fluoride/acid concentrations, ionic strengths, and temperatures on the fluoridation of boronate **3.6** were studied on the basis of the semi-quantitative fluorescence. We have found that  $\text{CH}_3\text{CN}$  and NMP are two of the best solvents for this reaction; NMP is suitable for the fluoridation at higher temperatures due to its high boiling point. Reactions in the water miscible ethers such as 1,4-dioxane and

THF also demonstrated very good conversions, but potential presence of peroxides may cause very severe oxidative deboration and thus limits their applications for fluoridation. Nonetheless, the fresh solvents without any peroxide should also be very useful for the fluoridation. To our surprise, alcoholic solvents performed very poorly in the reaction while *t*-BuOH appeared to be the best among the alcoholic solvents. This might be interpreted in terms of their ability to compete with fluoride to fill the empty orbital on the boron.

BODIPY-boronate **3.6** has a very hydrophobic skeleton, which requires high content of the organic solvent to keep the reaction homogeneous. It was actually observed that any precipitation of **3.6** during the fluoridation reaction usually resulted in low yields and this trend was evident in Figure 3.6. It is almost always true that homogeneous reactions are more efficient than the same reactions occurring between multi-phases. Moreover, it was noticed that in testing various solvent content, dilution of the reaction occurred due to the addition of CH<sub>3</sub>CN. This dilution effect may greatly reduce reaction efficiency. As a result, we decided to use 75% organic solvent (CH<sub>3</sub>CN was tested, 8 μL as the total reaction volume) in the reaction, which gave the best results while the reaction remained homogeneous.

All the acids we examined showed very similar effects on the fluoridation. Very interestingly, with TsOH that was tested at a much lower concentration than other acids, the fluoridation of **3.6** exhibited a high conversion. We then further studied the effects of HCl and TsOH on their performance in the fluoridation of **3.6**. Generally, a higher acid concentration favors the fluoridation. The fluoridation with HCl, whose concentration in the reaction was raised to 2 M, showed an optimal concentration of 1.6 M in a reaction volume of 6 μL. Another experiment, wherein different amounts of concentrated acids were added to a 5 μL solution in 80% aqueous CH<sub>3</sub>CN containing BODIPY-boronate **3.6** (100 nmol) and KHF<sub>2</sub> (200 nmol) to initiate the reaction, gave similar results, as shown in Figure 3.7 and Figure 3.9. The optimal concentration of HCl is ~ 1 M in a total reaction volume of 5.5 μL. But that for TsOH is a bit more complicated. It seems that the acid is critical for the reaction, but the dilution effect is very dramatic for reactions using TsOH as the acid.

Since each arylboronate in the reaction requires three fluorine atoms to form an  $\text{ArBF}_3$ , higher fluoride concentration always will ensure a higher conversion of the arylboronate. In contrast, we would like to know how low the concentration of fluoride can go while still ensuring a relatively rapid reaction rate to give acceptable yields and reasonable specific activities for the  $^{18}\text{F}$ -fluoridation. We then investigated the fluoride concentration for the fluoridation. By working with varying equivalents of fluoride to boronate (1-8 eq.), we found that using 4 equivalents of fluoride (66.7 mM), the fluoridation of BODIPY-boronate **3.6** gives a conversion of more than 20% within one hour. This may be good enough to ensure reasonable yields without dramatically decreasing the specific activity.

In the  $^{18}\text{F}$ -radiosynthesis of  $^{18}\text{F}\text{-ArBF}_3\text{S}$ ,  $^{18}\text{F}$ -fluoride is first trapped on an anion exchange column during the radiosynthesis and then released with an elution solution of  $\text{NaClO}_4$  (2 mg/mL). The eluent also contains bicarbonate, which derives from the anionic form of the resin. This bicarbonate would be neutralized to give  $\text{NaCl}$  when  $\text{HCl}$  is used as the acid. Whether or not  $\text{NaCl}$  or  $\text{NaClO}_4$  plays any role in the fluoridation of the boronates is very critical to understanding the radiolabeling reaction. From the results of testing the effect of the salt shown in Figure 3.10, the presence of concentrated  $\text{NaClO}_4$  seems to promote the reaction to some extent. In contrast, there appears to be an optimal concentration of  $\text{NaCl}$  for the reaction, where the  $\text{NaCl}$  concentration is around 0.36 M. Generally however, the effects of salt on the reaction are small.

By combining all the conditions studied above, the kinetic fluoridation study of **3.6** in  $\text{CH}_3\text{CN}$  at room temperature and in  $\text{NMP}$  at  $50\text{ }^\circ\text{C}$  suggested both reactions reached the equilibrium. The reaction in  $\text{NMP}$  at  $50\text{ }^\circ\text{C}$  had a relatively faster reaction rate and gave a yield of  $\sim 44\%$  in one hour. Overall, a small volume reaction containing 100 nmol of arylboronate ester, 4  $\mu\text{L}$  of  $\text{CH}_3\text{CN}$ , 1  $\mu\text{L}$  of 0.2 M  $\text{KHF}_2$  and 0.5  $\mu\text{L}$  of concentrated  $\text{HCl}$  is generally suitable for the radiolabeling experiment at room temperature. However, the use of higher temperatures with  $\text{NMP}$  may provide an alternative for the fluoridation of arylboronates.

### 3.3.3 Fluoridation studies by $^{19}\text{F}$ NMR spectroscopy

$^{19}\text{F}$  NMR spectroscopy, with very high sensitivity, can be used to demonstrate any of the changes based on the  $^{19}\text{F}$ -signals. The reaction conditions summarized in the previous section were directly applied to the  $^{19}\text{F}$  NMR studies but with higher reaction volumes. As we could watch either the changes in the integration values of the Ar-F peaks or the changes in the integration values of the fluoride peak/the  $\text{ArBF}_3$  peak, the  $^{19}\text{F}$  NMR study is suitable for the compounds that can be prepared on a large scale. We focused on several of the simple but potentially useful boronic acids protected with different protecting groups to verify the conditions with regard to the fluoridation. Generally, the arylboronates containing two or three Ar-F's were studied due to the high solvolytic stability of the corresponding  $\text{ArBF}_3\text{s}$  under physiological conditions.<sup>85</sup> The fluoridation under the optimized reaction conditions was very effective, while different protecting groups on the boronates had very strong bearing on the rate and yields of the fluoridation. As shown in Figure 3.12, the fluoridation rate of heptylamide **3.7** with the benzopinacol protecting group is very consistent with the fluoridation studies based on the fluorescent BODIPY-boronate **3.6**, while boronate esters bearing the acid-sensitive protecting groups such as 1,8-diaminonaphthalene and DiDiAN displayed extraordinarily rapid reaction rates under the same conditions. The fluoridation of boronic acid **3.8** appeared complete within seconds upon mixing. Although it was indicated by the  $^{19}\text{F}$  NMR spectra that the actually ratio of fluoride to the boronate ester was higher than expected, which might be due to errors involved in weighing, the reactions occurred in a very rapid fashion and this implied that they should be suitable for the one-step labeling.

### 3.3.4 $^{18}\text{F}$ -Fluoridations of boronates

The key for the whole project is the radiofluoridation of arylboronates to afford  $^{18}\text{F}$ - $\text{ArBF}_3\text{s}$ . A relatively rapid reaction with a high specific activity is always favored. With the conditions determined from the fluoridation study via TLC-fluorescent densitometry analysis and  $^{19}\text{F}$  NMR spectroscopy, several compounds were tested for radiofluoridation. Compounds with the alkynyl residue were used in this study because they could give potential prosthetic synthons to label acid-sensitive probes. We were luckily offered  $^{18}\text{F}$ -fluoride at both the CPDC and TRIUMF. The work at the CPDC

highly supported the fast fluoridation of both boronic acid **3.11** and its DiDiAN protected version **3.16**. The kinetic study for the  $^{18}\text{F}$ -fluoridation of **3.16** exhibited in Figure 3.14 implied a very rapid  $^{18}\text{F}$ -fluoride incorporation to give the  $^{18}\text{F}$ -ArBF<sub>3</sub>. The kinetic curve suggested the reaction reached the equilibrium after ~ 50 minutes. On the other hand, the  $^{19}\text{F}$  NMR studies on the fluoridation of the DiDiAN protected boronate **3.15**, which is the precursor of **3.16**, demonstrated even more rapid kinetics for a reaction that was complete in a short time to give the ArBF<sub>3</sub>. Therefore, we would regard the apparent “equilibrium” of the radiolabeling of **3.16** to also reflect a state of completion. Moreover, while the reaction was rapid with a half-life less than one minute for **3.15** based on the  $^{19}\text{F}$  NMR studies, the radiofluoridation seemed much slower (> 30 min). As suggested in Figure 3.7 and Figure 3.9 of the fluorescence study, the acid concentration is critical for the fluoridation. However, the acid added to the radio-reaction is partially consumed to neutralize the bicarbonate that co-elutes with  $^{18}\text{F}$ -fluoride from the anion exchange column, and consequently the amount of the acid might actually be reduced considerably. As a result, the reaction rate might be decreased accordingly. Since the reaction volume of the radiofluoridation reaction is so small, it is very difficult to accurately control the pH for the reaction, and normally 0.5 to 1  $\mu\text{L}$  of concentrated HCl is added to bring the reaction to low pHs. In contrast to the  $^{19}\text{F}$  NMR spectroscopy studies, the volume of the radiolabeling reaction was only ~ 6  $\mu\text{L}$ , in which case any evaporation of the organic solvent or H<sup>18/19</sup>F would further influence the reaction much more dramatically than reactions in larger volumes with similar concentrations of reactants. In addition, specifically for this reaction, the starting material **3.16** was always found contaminated with some unknown impurities, which could not be fully removed, and this might also cause the observed yields to be lower.

Notwithstanding such discrepancies, boronic acid **3.11** was treated with  $^{18/19}\text{F}$ -fluoride under acidic conditions at room temperature for 30 minutes to give a radiochemical yield of 44%. As with **3.16**, the conversion rate of **3.11** was much slower than the  $^{19}\text{F}$  NMR studies. It is believed that the difference from the large volume reaction to the small volume reaction may play very significant roles as well as the consumption of acid by bicarbonate accounts for the reduced reaction rate and yields.

Three boronates (**3.19**, **3.20** and **3.21**) with similar structures but different protecting groups, along with biotin-boronate **3.23** were prepared to test the difference among the protecting groups. The piperazine linker was used here since it was noticed that the fluoridation of the arylboronates containing this linker (such as biotin-boronate **3.23**) always affords better conversions than those with linear linkers (data not shown). Compounds **3.19** and **3.23** differ from **3.20** and **3.21** in terms of their aromatic system. However, the fluoridation reactions suggested that **3.20**, protected with the acid-sensitive 1,8-diaminonaphthalene underwent a slightly more rapid conversion than **3.19** and **3.23**. This might be due to the bulky nature of benzopinacol, which to some extent blocks the *p*-orbital entry by the attacking fluoride. The fluoridation of **3.21** seemed relatively fast, but when compared with the fluoridation of **3.11** using the same portion of  $^{18}\text{F}$ -fluoride, the conversion was not as high as expected. Nonetheless, the results suggested that the radiofluoridations of **3.19** and **3.23** were generally consistent with the TLC and  $^{19}\text{F}$  NMR studies of similar benzopinacol protected arylboronate esters, and the results of the radiolabeling reactions of **3.20** and **3.21** were similar to those observed in the  $^{19}\text{F}$  NMR study of **3.10**. Moreover, there was indeed some enhancement observed by the introduction of the piperazine linker to the boronate esters compared with the one without the piperazine linker.<sup>a</sup>

### 3.4 Conclusion

In this chapter, the fluoridation of boronates was studied via TLC-fluorescent densitometry,  $^{19}\text{F}$  NMR spectroscopy, and radio-HPLC. The fluoridation conditions were at least partially optimized: boronate (17 mM), HCl (1.64 M), and  $\text{KHF}_2$  (33.33 mM) in aqueous cosolvent (2:1 cosolvent: $\text{H}_2\text{O}$ , 5 ~ 6  $\mu\text{L}$ ) in an apparently homogeneous reaction.  $\text{CH}_3\text{CN}$  and NMP are regarded as appropriate  $\text{H}_2\text{O}$ -miscible solvents for this reaction. The radiofluoridation of the boronates could give radiochemical yields of 20-50% from 30 ~ 60 minutes. To achieve a fast fluoridation rate and a high yield, a new protecting group, DiDiAN, was developed. In spite of its higher basicity to facilitate the fluoridation

---

<sup>a</sup> The fluoridation with RGD-boronate **8.7** with  $^{18/19}\text{F}$ -fluoride from the same source was undertaken the same day and its radiochemical yield was only 11% after incubation for 57 minutes at room temperature under the same fluoridation conditions. Although it is not clear why piperazine seems to accelerate the fluoridation, this linker and other linker system might be worth studying.

of the corresponding boronate ester, the moderate incorporation of this newly developed protecting group to boronic acids and subsequent poor derivatization in attaching the DiDiAN protected boronate to other functional molecules may limit its application. Future optimization of the synthetic protocol may push the application of this protecting group to a new level. In addition, the piperazine linker showed promising effects on the fluoridation to prepare ArBF<sub>3</sub>s. Overall, we identified improved, if not optimal, fluoridation conditions and successfully applied these findings to the radiolabeling syntheses of <sup>18</sup>F-ArBF<sub>3</sub>s, which will be applied in the following chapters in this thesis.

### 3.5 Materials and methods

All chemicals were purchased from Sigma-Aldrich, Oakwood, Acros Organics or Alfa Aesar. Solvents were obtained from Fisher Scientific and used without further treatment unless otherwise noted. When required, the solvents were pretreated following standard protocols.<sup>129</sup> The <sup>18</sup>F-Trap & Release column (HCO<sub>3</sub><sup>-</sup> form, ~ 10 mg) was purchased from ORTG, Inc., or the Sep-Pak Light Accell Plus QMA cartridge (Cl<sup>-</sup> form) 37-50 μm was obtained from Waters. The TLC analysis was performed on aluminium-backed silica gel-60 plates from EMD Chemicals and preparative TLCs and the analysis of all the condition screening was undertaken on Silica Gel 60 F<sub>254</sub> Glass TLC plates from EMD. Flash chromatography was carried out on SiliaFlash F60 (230-400 mesh) silica gel from SiliCycle. ESI-LRMS was performed on a Waters ZQ with a quadrupole detector, attached to a Waters 2695 HPLC. All NMR spectra were recorded on Bruker Avance instruments with results reported as chemical shift (δ) in ppm. <sup>1</sup>H NMR spectra are referenced to the tetramethylsilane peak (δ = 0 ppm), <sup>13</sup>C NMR spectra are referenced to chloroform peak (δ = 77.23 ppm), and <sup>19</sup>F NMR spectra are referenced to neat trifluoroacetic acid (δ = 0 ppm, -78.3 ppm relative to CFCl<sub>3</sub>). The fluorescent images were obtained on an Amersham Typhoon 9200 Imager from GE Healthcare.

**WARNING:** All <sup>18</sup>F-labeling work was done at TRIUMF or at the CPDC. Radiation protection procedures strictly followed the TRIUMF Radiation Safety Regulations. Since this work involves mainly manual handling, fairly high amounts of dosage might be applied; special caution is required to reduce the operating time. A lead brick castle was

built up to shield the radiation. All the materials that came in contact with the source water (the  $^{18}\text{O}$ -water) were collected and decayed separately from other  $^{18}\text{F}$ -contaminated stuffs including gloves, sleeves, vials, tubes and pipette tips prior to disposal.

### 3.5.1 Synthesis

#### 2,4,6-Trifluoro-3-(4,4,5,5-tetraphenyl-1,3,2-dioxaborolan-2-yl)benzoic acid (3.1)

2,4,6-Trifluorobenzoic acid (1.40 g, 7.95 mmol) was dissolved in anhydrous THF (90 mL) and cooled to  $-78\text{ }^{\circ}\text{C}$  over  $\text{N}_2$ . Then 1.6 M BuLi in hexane (11.0 mL, 16.0 mmol) was added dropwise to the solution during 30 min. The resulting red-to-orange slurry was stirred at  $-78\text{ }^{\circ}\text{C}$  for an additional 15 min and  $\text{B}(\text{OCH}_3)_3$  (0.45 mL, 4.04 mmol) was added. The reaction was stirred at the same temperature for 3 hr, and quenched by the addition of 4 M HCl in dioxane (14.0 mL, 56.0 mL). The quenched reaction was further stirred at  $-78\text{ }^{\circ}\text{C}$  for 10 min; 1,1,2,2-tetraphenyl-1,2-ethanediol (3.80 g, 10.4 mmol) in THF (30 mL) was added to the quenched mixture and the resulting mixture was then allowed to warm up to rt and stirred for another 2 hr. The solvent was then removed under vacuum. The residue was resuspended in a toluene/THF cosolvent (3:1, 80 mL) and the solution was concentrated over vacuum. This was repeated a couple of times till the TLC analysis suggested the reaction was done. The final residue was charged with flash chromatography (EtOAc:hexanes 1:9) to give a white solid ( $R_f = 0.14$  in 1:9 MeOH: $\text{CH}_2\text{Cl}_2$ ). Yield: 2.05 g, 47%.  $^{19}\text{F}$  NMR (282.4 MHz,  $\text{CD}_2\text{Cl}_2$ , rt):  $\delta$  (ppm) -23.70 (s, 1 F), -16.83 (s, 1 F), -12.77 (s, 1 F);  $^1\text{H}$  NMR (400 MHz,  $\text{CD}_2\text{Cl}_2$ , rt):  $\delta$  (ppm) 6.93 (t,  $J = 9.40$  Hz, 1 H), 7.13-7.38 (m, 20 H);  $^{13}\text{C}$  NMR (100.6 MHz,  $\text{CD}_2\text{Cl}_2$ , rt):  $\delta$  (ppm) 83.13, 97.03, 101.78, 127.06, 127.32, 127.39, 127.45, 127.49, 128.50, 128.65, 141.98, 144.49; ESI-LRMS:  $[\text{M}+\text{Na}]^+$ : 573.3 (100%).

#### (Z)-2-((3,5-Dimethyl-2H-pyrrol-2-ylidene)(4-nitrophenyl)methyl)-3,5-dimethyl-1H-pyrrole (3.3)

This compound was synthesized according to literature protocol.<sup>123</sup> Under a  $\text{N}_2$  atmosphere, *para*-nitrobenzaldehyde (610 mg, 4.03 mmol) and 2,4-dimethylpyrrole (770 mg, 8.09 mmol) in anhydrous  $\text{CH}_2\text{Cl}_2$  (350 mL) was added with 1 drop of TFA, upon the addition of which the color of the solution changed from bright yellow to golden and

then to brown red. The reaction was allowed to stir at rt under N<sub>2</sub> overnight. DDQ (900 mg, 4.01 mmol) was then added to the reaction in one portion and the reaction was stirred at rt for another 20 min. The reaction was quenched with H<sub>2</sub>O (100 mL). The layers were separated. The CH<sub>2</sub>Cl<sub>2</sub> layer was washed with H<sub>2</sub>O (3 × 100 mL) and brine (1 × 100 mL), and dried over anhydrous Na<sub>2</sub>SO<sub>4</sub>. The solution was then filtered and concentrated over vacuum and the residue was purified via silica gel column chromatography (MeOH:CH<sub>2</sub>Cl<sub>2</sub> 0:100 gradient to 5:95) to give the desired product (*R<sub>f</sub>* = 0.34 in 1:9 MeOH:CH<sub>2</sub>Cl<sub>2</sub>). Yield: 480 mg, 37%. <sup>1</sup>H NMR (400 MHz, CDCl<sub>3</sub>, rt): δ (*ppm*) 1.32 (s, 6 H), 2.40 (s, 6 H), 5.96 (s, 2 H), 7.57 (d, *J* = 8.40 Hz, 2 H), 8.36 (d, *J* = 8.40 Hz, 2 H); <sup>13</sup>C NMR (100.6 MHz, CDCl<sub>3</sub>, rt): δ (*ppm*) 14.99, 16.13, 120.43, 123.97, 130.87, 139.89, 152.72; ESI-LRMS: [M+H]<sup>+</sup>, 322.4 (100%).

### **BODIPY-NO<sub>2</sub> (3.4)**

Compound **3.3** (480 mg, 1.49 mmol) was dissolved in toluene (200 mL) and DIPEA (5 mL, 28.7 mmol) was added to the solution under Ar. BF<sub>3</sub>·Et<sub>2</sub>O (5 mL, 40.5 mmol) was added dropwise and the resulting mixture was stirred at rt for 0.5 hr.<sup>123</sup> Then the reaction was washed with H<sub>2</sub>O (3 × 50 mL) and dried over anhydrous Na<sub>2</sub>SO<sub>4</sub>. The solution was filtered and concentrated over vacuum and the residue was charged to flash chromatography (CH<sub>2</sub>Cl<sub>2</sub>:hexanes 1:1) to give a dark red solid as the desired product (*R<sub>f</sub>* = 0.41 in 1:3 EtOAc:hexanes). Yield: 180 mg, 33%. <sup>19</sup>F NMR (282.4 MHz, CD<sub>2</sub>Cl<sub>2</sub>, rt): δ (*ppm*) -69.55 (q, *J* = 32.10 Hz); <sup>1</sup>H NMR (300 MHz, CD<sub>2</sub>Cl<sub>2</sub>, rt): δ (*ppm*) 1.39 (s, 6 H), 2.54 (s, 6 H), 6.06 (s, 2 H), 7.57 (d, *J* = 8.54 Hz, 2 H), 8.39 (d, *J* = 8.55 Hz, 2 H); <sup>13</sup>C NMR (75.5 MHz, CD<sub>2</sub>Cl<sub>2</sub>, rt): δ (*ppm*) 14.49, 14.57, 121.83, 124.53, 129.85, 130.76, 138.85, 141.86, 143.02, 148.51, 156.58.

### **BODIPY-NH<sub>2</sub> (3.5)**

Compound **3.4** (223 mg, 0.678 mmol) and 10% Pd/C (114 mg) were suspended in THF (40 mL) under a H<sub>2</sub> atmosphere at rt overnight.<sup>123</sup> The reaction was filtered over Celite and the filtrate was concentrated over vacuum. The residue was purified via silica gel flash chromatography (toluene 100%) to give a light orange solid (*R<sub>f</sub>* = 0.39 in 1:1 EtOAc:hexanes). Yield: 197 mg, 86%. <sup>19</sup>F NMR (282.4 MHz, CDCl<sub>3</sub>, rt): δ (*ppm*) -70.22

(q,  $J = 32.85$  Hz);  $^1\text{H}$  NMR (300 MHz,  $\text{CDCl}_3$ , rt):  $\delta$  (ppm) 1.52 (s, 6 H), 2.57 (s, 6 H), 3.95 (s, br, 2 H), 5.99 (s, 2 H), 6.80 (d,  $J = 8.36$  Hz, 2 H), 7.03 (d,  $J = 8.36$  Hz, 2 H);  $^{13}\text{C}$  NMR (100.6 MHz,  $\text{CDCl}_3$ , rt):  $\delta$  (ppm) 14.72, 14.82, 115.59, 121.09, 124.88, 129.12, 142.81, 143.37, 147.19, 155.12; ESI-LRMS:  $[\text{M}+\text{H}]^+$ , 340.2.

### **BODIPY-boronate (3.6)**

Boronate ester **3.1** (55.0 mg, 0.0999 mmol), BODIPY-NH<sub>2</sub> **3.5** (34.0 mg, 0.100 mmol), and DCC (22.7 mg, 0.110 mmol) were dissolved in  $\text{CH}_2\text{Cl}_2$  (10 mL) and the reaction was stirred at rt for 48 hr. The reaction was then filtered and concentrated; the residue was purified by silica gel chromatography ( $\text{CH}_2\text{Cl}_2$ :hexanes 1:1, then 5:3 and then 3:1) to yield an orange solid as the desired product ( $R_f = 0.21$  in 1:3 EtOAc:hexanes). Yield: 37.6 mg, 43%.  $^{19}\text{F}$  NMR (282.4 MHz,  $\text{CD}_2\text{Cl}_2$ , rt):  $\delta$  (ppm) -69.81 (q,  $J = 31.72$  Hz, 2 F), -27.84 (s, 1 F), -21.56 (s, 1 F), -15.64 (s, 1 F);  $^1\text{H}$  NMR (300 MHz,  $\text{CD}_2\text{Cl}_2$ , rt):  $\delta$  (ppm) 1.38 (s, 6 H), 2.53 (s, 6 H), 6.04 (s, 2 H), 6.97 (t,  $J = 9.24$  Hz, 1 H), 7.09-7.30 (m, 20 H), 7.33 (d,  $J = 8.45$  Hz, 2 H), 7.83 (d,  $J = 8.46$  Hz, 2 H), 8.06 (s, 1 H); ESI-LRMS:  $[\text{M}+\text{Na}]^+$ , 894.5 (100%).

### **BODIPY-ArBF<sub>3</sub> (3.2)**

BODIPY-boronate **3.6** (5 mg, 5.7  $\mu\text{mol}$ ) in  $\text{CH}_3\text{CN}$  (1 mL) was added with 0.8 M  $\text{KHF}_2$  (200  $\mu\text{L}$ , 0.16 mmol) and 1 M HCl (50  $\mu\text{L}$ ) in a plastic falcon tube. The resulting mixture was stirred at rt for 5 hr and then quenched with 5%  $\text{NH}_4\text{OH}$  in EtOH (400  $\mu\text{L}$ ). The quenched reaction was concentrated under reduced pressure and the residue was loaded to the preparative TLC plate for purification (MeOH: $\text{CH}_2\text{Cl}_2$  15:85) to afford the desired product ( $R_f = 0.20$  in 1:4 MeOH: $\text{CHCl}_3$ ) for characterization.  $^{19}\text{F}$  NMR (282.4 MHz,  $d_4$ -MeOD, rt):  $\delta$  (ppm) -70.23 (q,  $J = 32.10$  Hz, 2 F), -60.78 (s, 3 F), -41.83 (s, 1 F), -29.44 (s, 1 F), -22.58 (s, 1 F);  $^1\text{H}$  NMR (300 MHz,  $d_4$ -MeOD, rt):  $\delta$  (ppm) 1.51 (s, 6 H), 2.49 (s, 6 H), 6.07 (s, 2 H), 6.66 (t,  $J = 9.44$  Hz, 1 H), 7.31 (d,  $J = 8.42$  Hz, 2 H), 7.90 (d,  $J = 8.38$  Hz, 2 H); ESI-HRMS: calcd. for  $\text{C}_{26}\text{H}_{21}\text{B}_2\text{N}_3\text{OF}_8^-$ : 563.1816, found: 563.1805.

### **2,4,6-Trifluoro-*N*-heptyl-3-(4,4,5,5-tetraphenyl-1,3,2-dioxaborolan-2-yl) benzamide (3.7)**

To boronate **3.1** (62.5 mg, 0.11 mmol), heptylamine (22.0  $\mu\text{L}$ , 0.15 mmol),  $\text{HOBt}\cdot\text{H}_2\text{O}$

(20 mg, 0.13 mmol), and pyridine (38  $\mu$ L, 0.47 mmol) in  $\text{CH}_2\text{Cl}_2$  (15.0 mL) was added EDC·HCl (31 mg, 0.16 mmol). The resulting mixture was stirred at rt overnight and then quenched by the addition of 2.5 N HCl (30 mL). The layers were separated and the aqueous layer was extracted with  $\text{CH}_2\text{Cl}_2$  (3  $\times$  30 mL). The  $\text{CH}_2\text{Cl}_2$  was combined, washed with  $\text{H}_2\text{O}$  (2  $\times$  30 mL) and brine (50 mL), and dried over anhydrous  $\text{Na}_2\text{SO}_4$ . The solution was then filtered and concentrated under reduced pressure to give colorless oil, which was purified by flash chromatography (EtOAc:hexanes 5:95 then 1:9) to give a white solid as the desired product ( $R_f$  = 0.45 in 1:3 EtOAc:hexanes). Yield: 46.4 mg, 63%.  $^{19}\text{F}$  NMR (282.4 MHz,  $\text{CD}_2\text{Cl}_2$ , rt):  $\delta$  (ppm) -28.26 (s, 1 F), -21.89 (s, 1 F), -17.18 (s, 1 F);  $^1\text{H}$  NMR (400 MHz,  $\text{CD}_2\text{Cl}_2$ , rt):  $\delta$  (ppm) 0.90 (m, 3 H), 1.21-1.47 (m, 8 H), 1.60 (m, 2 H), 3.46 (q,  $J$  = 6.68 Hz, 2 H), 5.99 (s, br, 1 H), 6.86 (td,  $J_1$  = 9.30 Hz,  $J_2$  = 1.69 Hz, 1 H), 7.03-7.28 (m, 20 H);  $^{13}\text{C}$  NMR (100.6 MHz,  $\text{CD}_2\text{Cl}_2$ , rt):  $\delta$  (ppm) 13.94, 22.69, 26.90, 29.02, 29.51, 31.85, 40.25, 96.90, 101.00, 101.28, 101.43, 127.12, 127.27, 127.37, 127.44, 128.48, 128.62, 142.01, 164.51; ESI-LRMS:  $[\text{M}+\text{Na}]^+$ , 670.2 (100%).

#### 4-Borono-3,5-difluorobenzoic acid (3.8)

This compound was prepared according the literature procedure.<sup>130</sup> 3,5-Difluorobenzoic acid (2.40 g, 15.2 mmol) and TMEDA (5.0 mL, 33.6 mmol) in anhydrous THF (60.0 mL) were cooled to  $-78$   $^\circ\text{C}$  over a dry-ice/acetone bath under an Ar atmosphere. 1.4 M *sec*-BuLi in hexanes (26.0 mL, 36.4 mmol) was dropwise added to the solution for around 0.5 hr. The resulting mixture was kept stirring at  $-78$   $^\circ\text{C}$  for 2 hr and the reaction was quenched by the addition of  $\text{B}(\text{OCH}_3)_3$  (3.60 mL, 32.3 mmol). The quenched reaction was warmed up to rt and stirred for an additional 4 hr. The reaction was carefully acidified by 3 N HCl (80 mL) and then extracted with EtOAc (3  $\times$  100 mL). The EtOAc layers were combined, washed with  $\text{H}_2\text{O}$  (2  $\times$  50 mL) and brine (1  $\times$  50 mL) and then dried over anhydrous  $\text{Na}_2\text{SO}_4$ . The solution was filtered and concentrated *in vacuo*. Hexanes (300 mL) was added to the residue to give a white precipitate, which was filtered off as the desired product. Yield: 2.76 g, 90%.  $^{19}\text{F}$  NMR (282.4 MHz,  $d_6$ -DMSO, rt):  $\delta$  (ppm) -25.65 (s);  $^1\text{H}$  NMR (300 MHz,  $d_6$ -DMSO, rt):  $\delta$  (ppm) 7.44 (d,  $J$  = 5.57 Hz, 2 H), 8.76 (s, br, 2 H).

### **3,5-Difluoro-4-(1*H*-naphtho[1,8-*de*]-1,3,2-diazaborinyl)benzoic acid (3.9)**

Boronic acid **3.8** (1.50 g, 7.34 mmol) and 1,8-diaminonaphthalene (1.41 g, 8.91 mmol) in THF/PhCH<sub>3</sub> (1:2, 150 mL) were heated to reflux with a Dean-Stark apparatus for 4 hr. The solvent was then removed under vacuum and the residue was subjected to column chromatography (EtOAc:hexanes 1:3 then MeOH:CH<sub>2</sub>Cl<sub>2</sub> 3:97) to give a greenish yellow powder ( $R_f = 0.20$  in 1:9 MeOH:CH<sub>2</sub>Cl<sub>2</sub>). Yield: 1.70 g, 67%. <sup>19</sup>F NMR (282.4 MHz, *d*<sub>6</sub>-DMSO, rt):  $\delta$  (ppm) -23.33; <sup>1</sup>H NMR (300 MHz, *d*<sub>6</sub>-DMSO, rt):  $\delta$  (ppm) 6.41 (d,  $J = 7.01$  Hz, 2 H), 6.91 (d,  $J = 8.23$  Hz, 2 H), 7.03 (m, 2 H), 7.53 (d,  $J = 4.78$  Hz, 2 H), 8.39 (s, 2 H); <sup>13</sup>C NMR (75.5 MHz, *d*<sub>6</sub>-DMSO, rt):  $\delta$  (ppm) 106.33, 112.17, 112.45, 117.43, 120.59, 128.26, 135.78, 136.57, 142.23, 163.75, 165.90, 166.04, 166.18; ESI-LRMS: [M+H]<sup>+</sup>, 342.1 (100%).

### **3,5-Difluoro-4-(1*H*-naphtho[1,8-*de*][1,3,2]diazaborinin-2(3*H*)-yl)-*N*-(prop-2-yn-1-yl)benzamide (3.10)**

Boronate ester **3.9** (162 mg, 0.500 mmol), propargylamine (45  $\mu$ L, 0.703 mmol), pyridine (807  $\mu$ L, 9.99 mmol), and HOBt·H<sub>2</sub>O in DMF (10.0 mL) was added with EDC·HCl (153 mg, 0.798 mmol) and the resulting mixture was stirred at rt overnight. The solvent was then removed under reduced pressure and the residue was charged with flash chromatography (EtOAc:hexanes 1:9 and then 1:4) to give a dark greenish solid as the desired product ( $R_f = 0.33$  in 1:1 EtOAc:hexanes). Yield: 158.7 mg, 88%. <sup>19</sup>F NMR (282.4 MHz, *d*<sub>6</sub>-DMSO, rt):  $\delta$  (ppm) -23.57; <sup>1</sup>H NMR (400 MHz, *d*<sub>6</sub>-DMSO, rt):  $\delta$  (ppm) 3.19 (t,  $J = 2.20$  Hz, 1 H), 4.09 (m, 2 H), 6.45 (d,  $J = 7.28$  Hz, 2 H), 6.93 (d,  $J = 5.26$  Hz, 2 H), 7.07 (t,  $J = 7.80$  Hz, 2 H), 7.57 (d,  $J = 7.28$  Hz, 2 H), 8.38 (s, 2 H), 9.16 (t,  $J = 5.26$  Hz, 1 H); <sup>13</sup>C NMR (100.6 MHz, *d*<sub>6</sub>-DMSO, rt):  $\delta$  (ppm) 29.34, 73.94, 81.43, 106.33, 110.52, 110.81, 117.41, 120.60, 128.28, 136.58, 138.42, 142.29, 166.08; ESI-LRMS: [M+Cl]<sup>-</sup>, 396.4 (100%).

### **(2,6-Difluoro-4-(prop-2-yn-1-ylcarbonyl)phenyl)boronic acid (3.11)**

Boronate ester **3.10** (25.2 mg, 0.0709 mmol) was dissolved in THF (1.4 mL). 2 N H<sub>2</sub>SO<sub>4</sub> (0.3 mL) was added to the solution and the reaction was stirred at rt overnight. Then the solution was diluted with 1 N HCl (10 mL) and extracted with EtOAc (3  $\times$  20

mL). The organic layers were combined, washed with 1 N HCl (1 × 10 mL), and dried over anhydrous Na<sub>2</sub>SO<sub>4</sub>. The solution was then filtered and concentrated under vacuum to give a grey powder, which was used directly in the future without further purification. Yield: 12.7 mg, 76%. <sup>19</sup>F NMR (282.4 MHz, *d*<sub>4</sub>-MeOD, rt): δ (*ppm*) -26.98; <sup>1</sup>H NMR (300 MHz, *d*<sub>4</sub>-MeOD, rt): δ (*ppm*) 2.62 (t, *J* = 2.51 Hz, 1 H), 4.15 (d, *J* = 2.49 Hz, 2 H), 7.42 (d, *J* = 7.50 Hz, 2 H).

### **2,7-Dimethoxynaphthalene (3.12)**

In DMSO (12.0 mL) was added ground KOH (2.80 g, 49.9 mmol) and the resulting mixture was stirred for 5 min. Then 2,7-dihydroxynaphthalene (1.00 g, 6.24 mmol) was added in one portion (the mixture turned dark brown immediately) followed by the addition of MeI (1.60 mL, 25.7 mmol).<sup>124</sup> The mixture was stirred for an additional 24 hr and quenched by H<sub>2</sub>O (15.0 mL). The mixture was filtered and the pellet was thoroughly washed with H<sub>2</sub>O and 50% aqueous ethanol solution (30.0 mL), and dried over vacuum over 5 hr to give a pale yellow powder as the desired product, which was used directly in the following step without further purification. Yield: 1.11g, 85%. For characterization, the powder was further purified by re-crystallization from MeOH/H<sub>2</sub>O to give white needle crystals. <sup>1</sup>H NMR (400 MHz, CDCl<sub>3</sub>, rt): δ (*ppm*) 3.96 (s, 6 H), 7.04 (d, *J* = 10.67 Hz, 2 H), 7.11 (s, 2 H), 7.70 (d, *J* = 8.96 Hz, 2H); <sup>13</sup>C NMR (100.6 MHz, CDCl<sub>3</sub>, rt): δ (*ppm*) 55.43, 105.45, 116.19, 124.46, 129.31, 136.08, 158.38.

### **1,8-Dinitro-2,7-dimethoxynaphthalene(3.13)**

The compound was synthesized via a literature protocol with some modifications.<sup>125</sup> HNO<sub>3</sub> (120 mL) was added to 2,7-dimethoxynaphthalene **3.12** (3.43 g, 18.2 mmol) in HOAc (150 mL). The resulting red solution was stirred at rt for 2 hr and then filtered. The solid was recrystallized with HOAc to give orange-green needle crystals. Yield: 2.51 g, 49%. <sup>1</sup>H NMR (400 MHz, *d*<sub>6</sub>-DMSO, rt): δ (*ppm*) 4.04 (s, 6 H), 7.69 (d, *J* = 9.24 Hz, 2 H), 8.36 (d, *J* = 9.23 Hz, 2 H). <sup>13</sup>C NMR (100.6 MHz, *d*<sub>6</sub>-DMSO, rt): δ (*ppm*) 58.20, 113.57, 116.91, 123.28, 131.24, 134.94, 153.37; ESI-LRMS: [M+Na]<sup>+</sup>, 301.3 (100%).

### 1,8-Diamino-2,7-dimethoxynaphthalene dihydrochloride (DiDiAN·2HCl) (3.14)

The compound **3.14** was prepared via a modified method from the literature procedure.<sup>125</sup> AcCl (100 mL) was dropwise added to MeOH (100 mL) over an ice-water bath for ~ 30 min and the resulting mixture was further stirred at 0 °C for 0.5 hr. Then SnCl<sub>2</sub>·2H<sub>2</sub>O (12.0 g, 53.2 mmol) and 1,8-dinitro-2,7-dimethoxynaphthalene **3.13** (1.45 g, 5.21 mmol) were added in one portion and the suspension was heated to 40 °C for 24 hr. The reaction was cooled to rt. The solution was filtered and the pellet was thoroughly washed with Et<sub>2</sub>O to give a grey powder as the desired product. Yield: 1.16 g, 77%. <sup>1</sup>H NMR (300 MHz, D<sub>2</sub>O, rt): δ (ppm) 3.89 (s, 6 H), 7.17 (d, *J* = 9.17 Hz, 2 H), 7.63 (d, *J* = 9.16 Hz, 2 H). <sup>13</sup>C NMR (75.5 MHz, D<sub>2</sub>O, rt): δ (ppm) 56.59, 111.48, 116.38, 124.23, 124.74, 128.81, 152.33; ESI-LRMS: [M-CH<sub>4</sub>]<sup>+</sup>, 203.3(100%).

### 4-(4,9-Dimethoxy-*IH*-naphtho[1,8-de][1,3,2]diazaborinin-2(3*H*)-yl)-3,5-difluorobenzoic acid (3.15)

2,6-Difluoro-4-carboxylphenylboronic acid **3.8** (450 mg, 2.23 mmol) was treated with DiDiAN·2HCl **3.14** (650 mg, 2.23 mmol) in THF (30 mL)/toluene (60 mL) and the reaction mixture was refluxed with a Dean-Stark apparatus overnight. The solvent was removed under vacuum and the residue was treated with silica gel chromatography (MeOH:CH<sub>2</sub>Cl<sub>2</sub> 1:99 to 5:95) to give the desired product as a purple powder (*R<sub>f</sub>* = 0.22 in 1:9 MeOH:CH<sub>2</sub>Cl<sub>2</sub>). Yield: 320 mg, 37%. <sup>19</sup>F NMR (282 MHz, *d*<sub>6</sub>-DMSO, rt): δ (ppm) -24.34; <sup>1</sup>H NMR (400 MHz, *d*<sub>6</sub>-DMSO, rt): δ (ppm) 3.82 (s, 6 H), 7.05 (q, *J* = 9.57 Hz, 4 H), 7.14 (s, 2 H), 7.52 (d, *J* = 7.76 Hz, 2 H); <sup>13</sup>C NMR (100.6 MHz, *d*<sub>6</sub>-DMSO, rt): δ (ppm) 57.34, 112.25, 112.54, 131.10, 114.52, 117.81, 121.14, 126.75, 127.60, 139.21, 165.94; ESI-HRMS: [M-H]<sup>-</sup>, calcd. for C<sub>19</sub>H<sub>14</sub>BN<sub>2</sub>O<sub>4</sub>F<sub>2</sub><sup>-</sup>: 383.1015, found: 383.1023.

### 4-(4,9-Dimethoxy-*IH*-naphtho[1,8-de][1,3,2]diazaborinin-2(3*H*)-yl)-3,5-difluoro-*N*-(prop-2-yn-1-yl)benzamide (3.16)

The DiDiAN protected boronate ester **3.15** (34 mg, 0.089 mmol), propargylamine (12 μL, 0.177 mmol), HOBT·H<sub>2</sub>O (30 mg, 0.190 mmol), and NEt<sub>3</sub> (54 μL, 0.390 mmol) in THF (5.0 mL) was added with EDC·HCl (40 mg, 0.210 mmol) in one portion; the resulting mixture was stirred at rt for 23 hr. The solvent was removed under reduced

pressure and the residue was charged with flash chromatography (MeOH:CH<sub>2</sub>Cl<sub>2</sub> 0:100 then 0.5:99.5 and then 5:95) to give a dark red solid as the desired product ( $R_f = 0.21$  in 1:1 EtOAc:hexanes). Yield: 7.4 mg, 20%. <sup>19</sup>F NMR (282.4 MHz, *d*<sub>6</sub>-DMSO, rt):  $\delta$  (ppm) -24.34 (s); <sup>1</sup>H NMR (300 MHz, *d*<sub>6</sub>-DMSO, rt):  $\delta$  (ppm) 3.18 (t,  $J = 2.39$  Hz, 1 H), 3.79 (s, 3 H), 3.84 (s, 3 H), 4.10 (s, 2 H), 6.45 (d,  $J = 9.21$  Hz, 1 H), 6.95 (d,  $J = 9.33$  Hz, 1 H), 7.01 (s, 1 H), 7.20 (d,  $J = 18.40$  Hz, 2 H), 7.58 (d,  $J = 8.26$  Hz, 2 H).

#### **4-Oxo-4-(prop-2-ynyloxy)butanoic acid (3.17)**

Propargyl alcohol (2.00 mL, 35.7 mmol), succinic anhydride (4.10 g, 41.1 mmol) and DMAP (0.86 g, 7.0 mmol) in CH<sub>2</sub>Cl<sub>2</sub> (10 mL) was stirred at rt overnight.<sup>131</sup> Then the reaction was poured into 1 N HCl (50 mL) and extracted with CH<sub>2</sub>Cl<sub>2</sub> (3 × 50 mL). The CH<sub>2</sub>Cl<sub>2</sub> layers were combined, washed with 1 N HCl (2 × 50 mL) and brine (50 mL), and dried over anhydrous Na<sub>2</sub>SO<sub>4</sub>. The solution was filtered and concentrated under vacuum to give a pale white solid that had a very good quality to be used directly in the following step. Yield: 3.82 g, 69%. <sup>1</sup>H NMR (400 MHz, CDCl<sub>3</sub>, rt):  $\delta$  (ppm) 2.49 (td,  $J_1 = 2.46$  Hz,  $J_2 = 0.55$  Hz, 1 H), 2.70 (m, 4 H), 4.76 (dd,  $J_1 = 2.38$  Hz,  $J_2 = 1.46$  Hz, 2 H); <sup>13</sup>C NMR (100.6 MHz, CDCl<sub>3</sub>, rt):  $\delta$  (ppm) 28.77, 28.93, 52.50, 75.26, 171.51, 178.23; ESI-LRMS: [M-H+2Na]<sup>+</sup>, 201.3 (100%).

#### **Prop-2-yn-1-yl 4-oxo-4-(piperazin-1-yl)butanoate (3.18)**

DCC (206.0 mg, 1.0 mmol) was added to the CH<sub>2</sub>Cl<sub>2</sub> solution (10 mL) of **3.17** (103 mg, 0.66 mmol) and the solution was stirred at rt for 1 hr. Then piperazine (230.0 mg, 2.60 mmol) was added to the solution and the reaction was incubated at ambient temperature overnight. The reaction was filtered over Celite and washed with H<sub>2</sub>O (50 mL). The aqueous layer was extracted with CH<sub>2</sub>Cl<sub>2</sub> (3 × 50 mL). The CH<sub>2</sub>Cl<sub>2</sub> layers were combined, washed with brine (2 × 50 mL) and dried over anhydrous Na<sub>2</sub>SO<sub>4</sub>. The solution was filtered and concentrated under reduced pressure and the residue was charged with column chromatography (MeOH:CH<sub>2</sub>Cl<sub>2</sub> 3:97 then 1:9) to give colorless oil as the desired product ( $R_f = 0.45$  in 1:9 MeOH:CH<sub>2</sub>Cl<sub>2</sub>). Yield: 34 mg, 23%. <sup>1</sup>H NMR (400 MHz, CDCl<sub>3</sub>, rt):  $\delta$  (ppm) 2.51 (t,  $J = 2.24$  Hz, 1 H), 2.67 (d,  $J = 5.92$  Hz, 2 H), 2.74 (t,  $J = 6.28$  Hz, 2 H), 2.88 (d,  $J = 13.52$  Hz, 4 H), 3.49 (s, 2 H), 3.61 (s, 2 H), 4.72 (d,  $J = 2.32$

Hz, 2 H);  $^{13}\text{C}$  NMR (100.6 MHz,  $\text{CDCl}_3$ , rt):  $\delta$  (ppm) 28.16, 29.52, 43.30, 46.14, 46.51, 46.93, 52.51, 75.29, 78.10, 169.80, 172.78; ESI-LRMS:  $[\text{M}+\text{H}]^+$ , 225.5 (100%).

**Prop-2-yn-1-yl 4-oxo-4-(4-(2,4,6-trifluoro-3-(4,4,5,5-tetraphenyl-1,3,2-dioxaborolan-2-yl)benzoyl)piperazin-1-yl)butanoate (3.19)**

EDC·HCl (15.0 mg, 0.08 mmol) was added to boronate **3.1** (15.0 mg, 0.027 mmol), the amine **3.18** (6.0 mg, 0.027 mmol), HOBt·H<sub>2</sub>O (5.0 mg, 0.033 mmol), and pyridine (10.0  $\mu\text{L}$ , 0.118 mmol) in  $\text{CH}_2\text{Cl}_2$  (1.0 mL) and the resulting solution was stirred at rt for 24 hr. The reaction was quenched by the addition of 3 N HCl (10 mL) and the aqueous was extracted with  $\text{CH}_2\text{Cl}_2$  (3  $\times$  30 mL). The organic layers were combined, washed with brine (10 mL), and dried over anhydrous  $\text{Na}_2\text{SO}_4$ . The solution was filtered and concentrated under vacuum to give an oily residue. The residue was then charged with flash chromatography (MeOH: $\text{CH}_2\text{Cl}_2$  1:99 then 2:98) to afford a white solid as the desired product ( $R_f$  = 0.70 in 1:9 MeOH: $\text{CH}_2\text{Cl}_2$ ). Yield: 12.9 mg, 64%.  $^{19}\text{F}$  NMR (282.4 MHz,  $\text{CD}_2\text{Cl}_2$ , rt):  $\delta$  (ppm) -28.83 (s, 1 F), -22.45 (s, 1 F), -17.30 (s, 1 F);  $^1\text{H}$  NMR (400 MHz,  $\text{CD}_2\text{Cl}_2$ , rt):  $\delta$  (ppm) 2.54 (s, 1 H), 2.68 (m, 4 H), 3.31-4.02 (m, 8 H), 4.70 (s, 2 H), 6.91 (t,  $J$  = 8.82 Hz, 1 H), 7.12-7.28 (m, 20 H); ESI-HRMS: calcd. for  $\text{C}_{44}\text{H}_{36}\text{BN}_2\text{O}_6\text{F}_3\text{Na}^+$ : 779.2516, found: 779.2500.

**Prop-2-yn-1-yl 4-(4-(3,5-difluoro-4-(1H-naphtho[1,8-de][1,3,2]diazaborinin-2(3H)-yl)benzoyl)piperazin-1-yl)-4-oxobutanoate (3.20)**

The 1,8-diaminonaphthalene protected boronate **3.9** (55.0 mg, 0.17 mmol) and **3.18** (29.1 mg, 0.13 mmol) was dissolved in THF (10 mL) with HOBt·H<sub>2</sub>O (29.0 mg, 0.19 mmol) and pyridine (50  $\mu\text{L}$ , 0.58 mmol). To this solution was added EDC·HCl (43.0 mg, 0.22 mmol) in one portion and the resulting reaction was incubated at rt for 20 hr. Then the reaction was poured to 1 N HCl (30 mL) and extracted with  $\text{CH}_2\text{Cl}_2$  (3  $\times$  50 mL). After combination, the  $\text{CH}_2\text{Cl}_2$  layer was washed with H<sub>2</sub>O (2  $\times$  50 mL) and brine (50 mL), and then dried over anhydrous  $\text{Na}_2\text{SO}_4$ . The solution was then filtered and concentrated under reduced pressure. The residue was loaded to a silica gel packed column for flash chromatography (MeOH: $\text{CH}_2\text{Cl}_2$  0.5:99.5 then 1:99) to give a dark

green solid as the desired product ( $R_f = 0.61$  in 1:9 MeOH:CH<sub>2</sub>Cl<sub>2</sub>). Yield: 55.0 mg, 77%. <sup>19</sup>F NMR (282.4 MHz, CDCl<sub>3</sub>, rt):  $\delta$  (ppm) -23.94 (s); <sup>1</sup>H NMR (400 MHz, CD<sub>2</sub>Cl<sub>2</sub>, rt):  $\delta$  (ppm) 2.56 (t,  $J = 2.44$  Hz, 1 H), 2.70 (m, 4 H), 3.40-3.90 (m, 8 H), 4.71 (d,  $J = 2.48$  Hz, 2 H), 6.45 (d,  $J = 7.24$  Hz, 2 H), 6.60 (s, 2 H), 7.03 (d,  $J = 8.32$  Hz, 2 H), 7.07 (d,  $J = 8.24$  Hz, 2 H), 7.16 (t,  $J = 7.78$  Hz, 2 H); ESI-HRMS: calcd. for C<sub>28</sub>H<sub>25</sub>BN<sub>4</sub>O<sub>4</sub>F<sub>2</sub>Na<sup>+</sup>: 553.1835, found: 553.1839.

### **(2,6-Difluoro-4-(4-(4-oxo-4-(prop-2-yn-1-yloxy)butanoyl)piperazine-1-carbonyl)phenyl)boronic acid (3.21)**

Boronate **3.20** (26.5 mg, 0.048 mmol) in THF (5.0 mL) was added with 2 N H<sub>2</sub>SO<sub>4</sub> (3.0 mL) and the resulting mixture was stirred at rt overnight. The mixture was then extracted with EtOAc (3 × 30 mL). The organic layers were combined, washed with brine (3 × 30 mL), and dried over anhydrous Na<sub>2</sub>SO<sub>4</sub>. The solution was filtered and concentrated over vacuum to give a pale green solid, which was used without further purification.<sup>a</sup> Yield: 22.3 mg, 113%. <sup>19</sup>F NMR (282.4 MHz, CDCl<sub>3</sub>, rt):  $\delta$  (ppm) -24.50 (s); <sup>1</sup>H NMR (300 MHz, CDCl<sub>3</sub>, rt):  $\delta$  (ppm) 1.30 (s, 2 H), 2.53 (t,  $J = 2.43$  Hz, 1 H), 2.66-2.86 (m, 4 H), 3.50-3.92 (m, 10 H), 4.75 (d,  $J = 3.24$  Hz, 2 H), 7.02 (t,  $J = 9.24$  Hz, 2 H).

### **Piperazinyl-biotin·HCl (3.22)**

*D*-Biotin (244 mg, 1.0 mmol), *tert*-butyl piperazine-1-carboxylate (223 mg, 1.2 mmol), HOBT·H<sub>2</sub>O (199 mg, 1.3 mmol) and NEt<sub>3</sub> (1.2 mL, 8.6 mmol) in DMF (3 mL) was added with EDC·HCl (259 mg, 1.35 mmol). The resulting mixture was stirred at rt overnight. Then the solvent was removed under vacuum. The residue was charged to a silica gel column for flash chromatography (MeOH:CH<sub>2</sub>Cl<sub>2</sub> 2:98 to 5:95) to give a white solid (402 mg, 98%).<sup>b</sup> The product (100 mg, 0.24 mmol) was dissolved in 4 M HCl in dioxane (6.0 mL, 24 mmol) and then stirred at rt for 5 hr. The solvent was removed over vacuum to give a white solid, which was filtered and used directly without further purification.

<sup>a</sup> The free boronic acid is very fragile under varieties of conditions. And therefore, normally it's not treated with flash chromatography further.

<sup>b</sup> The characterization for this product is <sup>1</sup>H NMR (300 MHz, CDCl<sub>3</sub>, rt)  $\delta$  (ppm) 1.48 (m, 11 H), 1.60-1.83 (m, 4 H), 2.37 (t,  $J = 7.47$  Hz, 2 H), 2.75 (d,  $J = 12.78$  Hz, 1 H), 2.91 (dd,  $J_1 = 12.83$  Hz,  $J_2 = 4.88$  Hz, 1 H), 3.17 (m, 1 H), 3.32-3.52 (m, 6 H), 3.60 (m, 2 H), 4.33 (m, 1 H), 4.52 (m, 1 H), 5.68 (s, 1 H), 6.28 (s, 1 H). ESI-HRMS: calcd. for C<sub>19</sub>H<sub>32</sub>N<sub>4</sub>O<sub>4</sub>NaS<sup>+</sup>: 435.2042, found: 435.2048.

Yield: quant.  $^1\text{H}$  NMR (300 MHz,  $d_4$ -MeOD, rt):  $\delta$  (ppm) 1.50 (m, 2 H), 1.67 (m, 3 H), 1.79 (m, 1 H), 2.50 (m, 2 H), 2.84 (d,  $J = 12.84$  Hz, 1 H), 3.03 (m, 1 H), 3.11-3.46 (m, 7 H), 3.57 (m, 2 H), 3.67 (m, 3 H), 3.74 (m, 1 H), 3.87 (m, 4 H), 4.56 (s, br, 1 H), 4.74 (s, br, 1 H); ESI-HRMS: calcd. for  $\text{C}_{14}\text{H}_{25}\text{N}_4\text{O}_2\text{S}^+$ : 313.1698, found: 313.1689.

### **Biotin-boronate (3.23)**

Boronate **3.1** (155 mg, 0.28 mmol), amine **3.22** (0.24 mmol from previous step), HOBt·H<sub>2</sub>O (46 mg, 0.30 mmol), and pyridine (0.12 mL, 1.50 mmol) in DMF (10 mL) was added with EDC·HCl (61 mg, 0.32 mmol) in one portion. The mixture was stirred at rt overnight. The reaction was diluted with CH<sub>2</sub>Cl<sub>2</sub> (50 mL) and poured into 3 N HCl (30 mL). The layers were separated and the aqueous layer was extracted with CH<sub>2</sub>Cl<sub>2</sub> (2 × 50 mL). The CH<sub>2</sub>Cl<sub>2</sub> layers were combined, further washed with brine (50 mL), and dried over anhydrous Na<sub>2</sub>SO<sub>4</sub>. The solution was filtered and concentrated under reduced pressure. The residue was then loaded to a silica gel column for flash chromatography (MeOH:CH<sub>2</sub>Cl<sub>2</sub> 3:97 to 5:95). Yield: 105 mg, 51%.  $^{19}\text{F}$  NMR (282.4 MHz, CD<sub>2</sub>Cl<sub>2</sub>, rt):  $\delta$  (ppm) -28.94 (s, 1 F), -22.61 (s, 1 F), -17.42 (s, 1 F);  $^1\text{H}$  NMR (400 MHz, CD<sub>2</sub>Cl<sub>2</sub>, rt):  $\delta$  (ppm) 1.50 (m, 2 H), 1.70 (m, 4 H), 2.45 (m, 2 H), 2.76 (m, 1 H), 2.92 (m, 1 H), 3.20 (m, 1 H), 3.31-4.04 (m, 8 H), 4.34 (s, 1 H), 4.51 (s, 1 H), 5.51 (s, 1 H), 6.10 (m, 1 H), 6.94 (t,  $J = 8.46$  Hz, 1 H), 7.01-7.53 (m, 20 H); ESI-HRMS: calcd. for  $\text{C}_{47}\text{H}_{44}\text{BN}_7\text{O}_8\text{F}_2\text{Na}^+$ : 867.2975, found: 867.2961.

### **3.5.2 General procedures of the fluoridation**

100 nmol of BODIPY-boronate ester **3.6** in a 0.5 mL PCR tube was resuspended in the organic solvent (4  $\mu\text{L}$  of CH<sub>3</sub>CN for instance). KHF<sub>2</sub> (1  $\mu\text{L}$  of 200 mM KHF<sub>2</sub> for example), and acid (0.5  $\mu\text{L}$  of concentrated HCl for instance) were added subsequently. The reaction was incubated at certain temperature (rt for example) for a certain reaction time (1 hr for most of the cases). Then the reaction was quenched by the addition of 100  $\mu\text{L}$  of 5% NH<sub>4</sub>OH in EtOH and 1  $\mu\text{L}$  of the quenched reaction was loaded to the TLC plate for the development in 20% MeOH/CHCl<sub>3</sub>. Then the plate was air-dried and scanned with the Typhoon 9200 Viable Mode Imager with the fluorescence mode: filter of 526 SP Fluorescein, Cy2, Alexa Fluor488 and laser of Green (532) at the PMT of 250

V. The images were analyzed by ImageQuant 5.2 and the intensity of the fluorescence was corrected from the background. The kinetic data if available was analyzed with SigmaPlot 10.0.

For the kinetics study by  $^{19}\text{F}$  NMR spectroscopy, the reaction was set up in a 15 mL falcon tube. Generally, boronate (17 mM), HCl (1.64 M) and  $\text{KHF}_2$  (33.33 mM) was mixed in 66.7% aqueous  $\text{CH}_3\text{CN}$  or THF solution. At certain time point, 150  $\mu\text{L}$  of the reaction mixture was quenched with 150  $\mu\text{L}$  of 33%  $\text{NH}_4\text{OH}$  in EtOH and the  $^{19}\text{F}$  NMR spectrum was recorded without solvent locking. The data was then analyzed by MestReNova software and SigmaPlot 10.0.

The radiofluoridation experiments were carried out at either the CPDC in Hamilton or TRIUMF in Vancouver, Canada.  $^{18}\text{F}$ -Fluoride was prepared via the bombardment of  $^{18}\text{O}$ - $\text{H}_2\text{O}$  in the cyclotron and transferred or transported to the labeling site. The  $^{18}\text{F}$ -fluoride was trapped in the anion exchange column with chloride form (at the CPDC) or with bicarbonate form (at TRIUMF). Then the fluoride was released from the column with 2 mg/mL  $\text{NaClO}_4$  (1 mL). The basic eluent<sup>a</sup>, was evaporated at 100 ~ 110 °C under Ar flow. Then  $^{18}\text{F}$ -fluoride was resuspended with 0.125 M  $\text{KHF}_2$  (10 ~ 16  $\mu\text{L}$ ) and 1.25  $\mu\text{L}$  (at the CPDC) or 2  $\mu\text{L}$  (at TRIUMF) was transferred to the solution containing the boronate (100 nmol) and concentrated HCl (0.5  $\mu\text{L}$ ). The reaction was incubated at rt for 30 to 60 min, quenched with 5%  $\text{NH}_4\text{OH}$  ethanolic solution and then injected into the HPLC over  $\text{CH}_3\text{CN}/\text{HCO}_2\text{NH}_4$  solvent system for analysis.

---

<sup>a</sup> The anion form of the anion exchange column at the CPDC is chloride. Therefore, 10~15  $\mu\text{L}$  0.95 M  $\text{NaHCO}_3$  was added to basify the solution.

# Chapter 4 Radiosynthesis of matrix metalloproteinase inhibitor marimastat-<sup>18</sup>F-ArBF<sub>3</sub> to image breast cancer

## 4.1 Introduction

Matrix metalloproteinases (MMPs) are a family of proteinases capable of degrading the protein components of the extracellular matrix (ECM) and membrane basements. MMPs have shown important biological roles in cellular remodeling and reconstruction processes.<sup>132</sup> Moreover, MMPs have been found to be abnormally expressed during many pathological processes.<sup>133</sup> Thus, they have been one of the most targeted systems for drug development and therapies. This chapter will be focused on studies in radiolabeling a marimastat-arylboronate conjugate to give marimastat-<sup>18</sup>F-aryltrifluoroborate (Mar-<sup>18</sup>F-ArBF<sub>3</sub>) in order to image the MMP activity associated with breast cancer. In this introduction section, a brief overview of MMPs, MMP inhibitors, and related radiopharmaceutical agents will be given.

### 4.1.1 Matrix metalloproteinases

MMPs belong to the family of Ca(II) or Zn(II) dependent endopeptidases. There are at least 25 MMPs found in nature, 24 of which are from mammalian cells.<sup>133, 134</sup> The research on MMPs has first disclosed that they play pivotal roles in degrading the ECM to allow cells to interact with their subenvironments.<sup>134</sup> In addition, it has been found that MMPs are also involved in the activation of various cell surface receptors and/or other MMPs, the release of growth factors from either the ECM or the extracellular membranes, shedding of cell adhesion molecules, and creating space for cell migration.<sup>134-136</sup> Hence, they are involved in many biological processes such as ECM remodeling, tissue and organ repair and development, wound healing, and regulation of microenvironments in many MMP dependent diseases and conditions.<sup>132-137</sup>

Generally, the inactive forms of MMPs contain two major domains, a Zn(II) binding catalytic domain and an autoinhibitory pro-domain.<sup>135, 137</sup> The autoinhibitory pro-domain has a conserved sequence containing cysteine at the C-terminus to coordinate with Zn(II)

to inhibit catalysis.<sup>133, 137, 138</sup> The disruption of the Zn(II)-cysteine binding interaction by destabilization or removal of the pro-domain allows Zn(II) to bind to the catalytic domain and therefore activate MMPs.<sup>133, 137, 138</sup> In addition, many MMPs also contain a hemopexin domain that controls aspects of the substrate recognition, enzyme activation, and stabilization of the interaction between the enzyme and the substrate.<sup>135, 137</sup>

MMPs are involved in the degradation of the ECM during the development of embryos, cell migration, tissue developments, and tissue remodeling.<sup>139</sup> They also participate in many pathological processes involving the ECM including inflammation, cellular invasion, tumor aggression and metastasis, vascular diseases, kidney disease, arthritis, and apoptosis.<sup>133, 140</sup> Although the relevance of MMP secretion varies in various cells, diseases, and animals, elevated levels of MMPs have been found in MMP dependent diseases.<sup>133, 134, 139</sup> It has been found that MMPs contribute to all the stages of disease development and thereby they represent important molecular targets for drug development against different MMP dependent diseases.

#### **4.1.2 MMP inhibitors**

Since MMP activity is very important for both normal physiological and abnormal pathological processes, it is very useful to understand how to control and/or suppress their catalytic activity for a variety of reasons: a) to understand their positive functions in wound healing, tissue repair, and tissue remodeling; b) to understand the development of MMP-dependent diseases such as various cancers, inflammation, and atherosclerosis, and c) to stop disease progression or alleviate the malignancy.<sup>132, 133, 136, 137</sup> For this purpose, many MMP inhibitors have been developed. To validate the *in vivo* performance and specificity of various inhibitors, corresponding imaging probes have also been prepared to study the *in vivo* pharmaco-properties and validate target specificity towards various malignant diseases such as cancer.

##### **4.1.2.1 Endogenous MMP inhibitors**

The *in vivo* activity of MMPs following proteolytic activation is precisely controlled and balanced by endogenous MMP inhibitors. The imbalance between MMP enzymes and their natural inhibitors may result in diseases associated with uncontrolled ECM

degradation, such as inflammation, cell growth, and metastasis. For example, the normal balance between MMPs and their natural inhibitors is disrupted due to the overexpression of MMPs in tumor cells or surrounding host cells; this eventually facilitates tumor progression/invasion, metastasis, and angiogenesis. There are several endogenous inhibitors such as  $\alpha_2$ -macroglobulin family members and tissue inhibitors of metalloproteinases (TIMPs).<sup>141-143</sup> TIMPs tend to be broad-spectrum inhibitors of the naturally occurring MMPs found in animals yet exhibit different levels of specificity, and are considered very important in regulating the ECM turnover, tissue remodeling, and cell behaviors.<sup>143</sup> There are four TIMPs encoded in human genomes,<sup>133, 143</sup> and they have been extensively characterized for their structures, biological activity, and functions. Moreover, TIMPs are also found to be important for many biological processes such as cell growth and differentiation, cell migration, antiangiogenesis, and apoptosis.<sup>141-143</sup> Structurally, TIMPs inhibit the activity of MMPs by binding noncovalently to the MMP catalytic site.<sup>138, 141</sup>

#### **4.1.2.2 Synthetic MMP inhibitors**

Synthetic MMP inhibitors (MMPIs) have received a great deal of attention and several candidates are being developed and evaluated for their clinical potential as a means of blocking the activity of the overexpressed MMPs in tumor progression, metastasis, and angiogenesis. Based on their structural features, the synthetic MMPIs have been subdivided into three groups: a) peptidomimetic inhibitors, b) non-peptidomimetic inhibitors, and c) tetracyclines.<sup>138, 144</sup>

By mimicking the sequence of collagen, which is an MMP substrate, peptidomimetic inhibitors carrying a zinc binding group were developed. Among them, the sequence containing the right hand side of the zinc binding groups has proven to be the most useful inhibitors. Especially for the hydroxamate family, the hydroxamate moiety acting as a bidentate ligand can coordinate strongly with the active Zn(II) cation. Among them, the most representative examples are the leading compound, batimastat, and a 2<sup>nd</sup> generation version, marimastat, which were developed by British Biotech. Both compounds showed very potent inhibitory activity against several cancer cell lines. However, batimastat was discontinued in early clinical trials due to poor response in cancer therapy and poor oral

bioavailability.<sup>145</sup> Chemical modifications of batimastat led to marimastat as the first orally bioavailable MMPI with similar inhibitory efficacy. Marimastat has been examined in clinical trials; from phase I and II trials it showed mild to severe dose dependent musculoskeletal toxicity causing joint and muscle pain symptoms, which were reversible upon halting treatment. The clinical evaluation of marimastat was discontinued in the phase III trial where it failed to show a significant difference in progression-free survival or overall survival rates.<sup>145</sup> There is still some ongoing research currently focused on examining the combination of marimastat and chemo/radio-therapeutic agents with very promising results of delaying tumor growth.<sup>146, 147</sup>

Nonpeptidomimetic MMPIs generally comprise sulphonamide inhibitors.<sup>138, 144</sup> Most of the sulphonamides have a hydroxamic acid or a carboxylic acid that also chelates zinc(II). The sulfonamide group is further involved in key hydrogen-bonding interaction with a backbone amide proton within the catalytic site of the enzyme.<sup>144</sup> Clinical trials for the leading compound, prinomastat, were discontinued due to its poor efficacy and toxicity issues with musculoskeletal symptoms.<sup>148</sup> There are also other nonpeptidomimetic MMPIs such as biphenyl compounds and thiol inhibitors.<sup>138, 144</sup> However, patients treated with the leading compounds also showed increasing disease progression and therefore the trials were halted.



**Figure 4.1** Some synthetic MMPIs.

Tetracycline derivatives are another category of MMPIs. Different functional groups as dimethylamino, methyl, ethyl, and hydroxyl groups are introduced to the molecule to obtain the MMP inhibitory properties. The compound COL-3 showed very promising potency to AIDS-related Kaposi Sarcoma.<sup>149, 150</sup> However, the functional mechanism of

this compound remains unclear.

Despite the rapid development of synthetic MMPIs, there are few successful MMPIs available in the treatment of cancer.<sup>138</sup> Several factors might account for this. First, most studies on MMPIs in preclinical development are focused on *in vitro* enzymatic inhibition and *ex vivo* cell assays. Even for *in vivo* experiments, the efficacy and effects of MMPIs are always investigated in animal models with early stages of diseases. As a result, MMPIs have demonstrated the greatest efficacy in early-stage disease. However, clinical trials are usually conducted on patients with advanced disease, who might respond differently to the MMPIs. In order to validate MMPIs for therapeutic trials and also to identify their relevance to specific MMPs in individual patients, MMP imaging probes are required to provide valuable information.

### 4.1.3 Imaging MMPs

Although no MMPI drug is currently prescribed, MMPs are now regarded as one of the most important classes of proteinases relevant to various diseases, especially with regard to a majority of malignant tumors wherein MMPs are overproduced. Although the development of MMPIs has resulted in the development of a variety of candidate drugs, the clinical trials performed so far have mainly yielded disappointing results and many drugs with high potential at early stage have been discontinued. On the other hand, the overexpression of MMPs in cancers compared with healthy tissues potentially makes MMPs ideal molecular targets for *in vivo* imaging.<sup>138, 144</sup> Information from *in vivo* imaging can perhaps provide better understanding to the distribution of *in vivo* MMPs as well as the corresponding proteolytic activity.<sup>138</sup> Moreover, imaging data can also reveal target specificity in an individual patient, which can guide more suitable treatment and suggest a required dose of the MMPI drug to achieve *in vivo* inhibition of MMPs.<sup>138</sup> Hence, many imaging probes have been developed for MMPs. These imaging compounds are mainly derived from MMPIs with high inhibitory activity. Both nonradioactive probes as near-infrared fluorescent probes<sup>151-153</sup> and radioactive probes as PET and SPECT agents<sup>138, 144</sup> have been developed and evaluated. And several radioactive probes, as illustrated in Figure 4.2, will be briefly introduced in the following part.

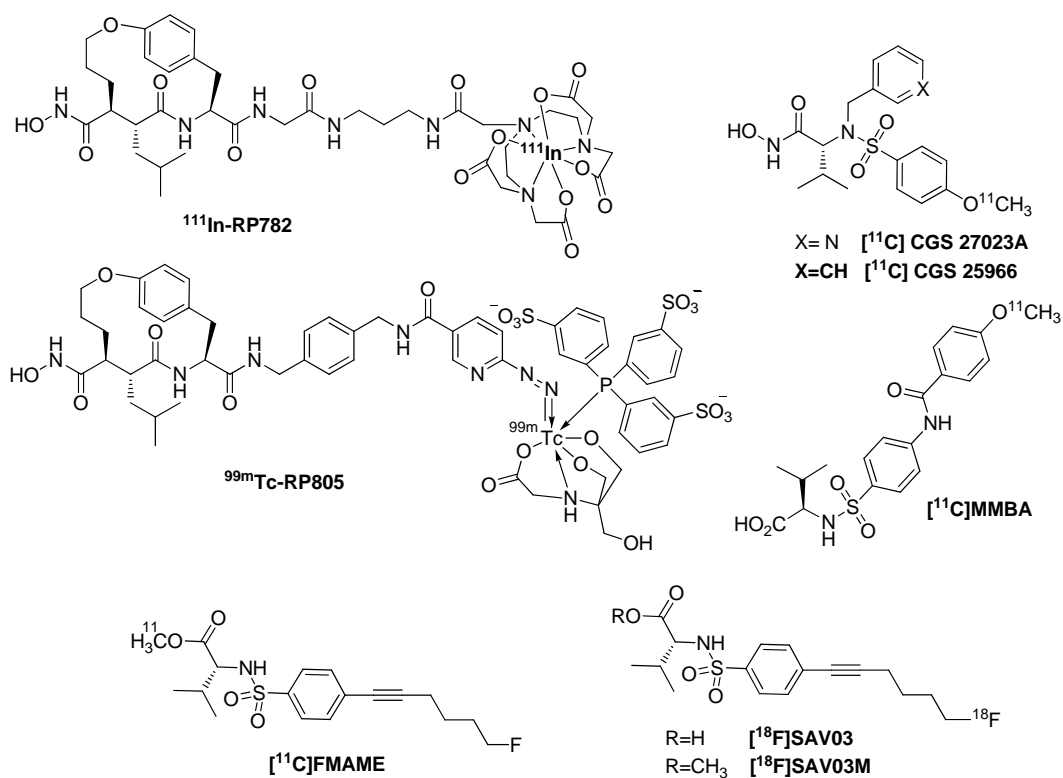


**Figure 4.2 Structures of some representative radiolabeled MMPi.**

Yale University School of Medicine and Bristol-Myers Squibb collaborated to develop the small molecular MMPi labeled with  $^{111}\text{In}$  and  $^{99\text{m}}\text{Tc}$  to *in vivo* localize the MMP activity and track the MMP-mediated post myocardial infarction remodeling.<sup>154</sup> Both compounds  $^{111}\text{In-RP782}$  and  $^{99\text{m}}\text{Tc-RP805}$  contain the macrocyclic hydroxamic acid coupled to either diethylenetriamine pentaacetic acid or 6-hydrazinopyridine-3-carboxylic acid as the binding functionality for radiometals.  $^{99\text{m}}\text{Tc-RP805}$  was found to specifically bind to MMP2 and its inhibition constant  $K_i$  was measured (10.5 nM). One week after surgically induced myocardial infarction in a chosen mouse model, the *in vivo* localization of  $^{111}\text{In-RP782}$  was observed by microautoradiography. The dynamic planar imaging and late dual-isotope micro-SPECT/CT imaging with  $^{201}\text{Tl}$  and  $^{99\text{m}}\text{Tc-RP805}$  displayed favorable *in vivo* biodistribution and clearance kinetics for cardiac imaging. These radiometal labeled MMPi possess important diagnostic applications in localizing the MMP activity and tracking the MMP-mediated post-myocardial infarction in the given animal models.

A  $^{11}\text{C}$ -radiosynthesis, with good radiochemical yields (40-60%) and acceptable specific

activities (0.6-0.8 Ci/ $\mu$ mol at the end of the synthesis) in a short preparation time, was reported for sulfonamidyl hydroxamic acids CGS 27023A<sup>155</sup> and CGS 25966,<sup>156</sup> both of which are potent MMP inhibitors with IC<sub>50</sub>s in the nanomolar range against various MMPs. However, for the radiosynthesis of [<sup>11</sup>C]CGS 25966,<sup>156</sup> the hydroxamic group competed for <sup>11</sup>C-methyl from <sup>11</sup>C-methyltriflate, with desired <sup>11</sup>C-methylation on the phenolic oxygen, providing a modest radiochemical yield of ~ 20%.<sup>155</sup> Further studies indicated that the *O*-methylated hydroxamate analogues of CGS 27023A have similar inhibitory capabilities as the parent compound CGS 27023A.<sup>157</sup> The study of the biodistribution and *in vivo* tumor imaging of [<sup>11</sup>C]CGS 25966 was reported soon after the synthesis.<sup>158</sup> However, the results were a bit disappointing with low tumor-to-muscle and tumor-to-blood ratios, while the tumors were nearly invisible in both breast cancer cell line MCF-7 transfected with IL-1 $\alpha$  implanted athymic mice and MDA-MB-435 implanted athymic mice. [<sup>11</sup>C]FMAME was also prepared with radiochemical yields of 40-55% for imaging.<sup>159</sup> The microPET imaging in the same mouse model with [<sup>11</sup>C]FMAME showed non-specific tumor uptake.

Kuhnast and co-workers radiosynthesized [<sup>11</sup>C]MMBA, a selective and high potent MMP2 and MMP9 inhibitor, via a one-step methylation,<sup>160</sup> Radiochemical yields of 50-60% and specific activities of 0.3-0.7 Ci/ $\mu$ mol were obtained within 40 minutes. The radiolabeled compound has a nanomolar IC<sub>50</sub> and demonstrated good-to-excellent serum stability in normal mice, but there have been no *in vivo* imaging experiments in animal models with elevated MMP levels that are relevant to this compound.

A series of carboxylic acid based MMP inhibitors containing the sulfonamide group were developed for <sup>18</sup>F-labeling with radiochemical yields of 13-43% for a total radiosynthesis time of 60-70 minutes including the preparative HPLC purification.<sup>161</sup> Two radiolabeled compounds with good *in vivo* stability, [<sup>18</sup>F]SAV03 and its methyl ester derivative [<sup>18</sup>F]SAV03M, were further examined for their *in vivo* biodistribution in Ehrlich tumor (breast cancer) bearing mice, in which MMP2 is overexpressed in tumor tissue.<sup>162</sup> The biodistribution of [<sup>18</sup>F]SAV03 with an IC<sub>50</sub> value of 1.9  $\mu$ M demonstrated comparatively high tumor uptake compared with other organs such as muscle, heart, lung, spleen, kidney, and blood. However, the highest radioactivity uptake was observed in the

small intestine and liver, which implied that first-pass effects<sup>a</sup> of [<sup>18</sup>F]SAV03 in the animal largely influence its clearance. In addition, its methyl ester derivative [<sup>18</sup>F]SAV03M, demonstrated a reduced first-pass effect with decreased liver uptake. As a result, higher tumor-specific uptake was observed for [<sup>18</sup>F]SAV03M. Moreover, since the *in vivo* metabolite of [<sup>18</sup>F]SAV03M was found to be primarily [<sup>18</sup>F]SAV03, [<sup>18</sup>F]SAV03M is therefore regarded as a prodrug for tumor imaging. However, the time-dependent increase of bone uptake accompanying during the [<sup>18</sup>F]SAV03M circulation suggested substantial defluoridation of the tracer,<sup>162</sup> which discourages further development of [<sup>18</sup>F]SAV03M for *in vivo* MMP imaging.

Although a great deal of effort has been made to image cancer based on MMP targets, there has been no clear “winner” among MMP imaging agents developed from MMPIs, since most of the results from the imaging studies have been disappointing. Nonetheless, because MMPs are considered to be excellent biomarkers for monitoring tumor progression, development of new and more potent MMPI based imaging tracers might be pivotal to provide useful information to assess the response to therapy, evaluate the drug behavior, and offer indicators of tumor physiology.

#### **4.1.4 Towards *in vivo* imaging of breast cancer with Mar-<sup>18</sup>F-ArBF<sub>3</sub> targeting MMPs**

As introduced in the earlier section, marimastat, a hydroxamic acid MMPI, was developed by British Biotech as the first orally bioavailable, broad-spectrum noncovalent MMPI with a nanomolar IC<sub>50</sub>. Although it was found to be relatively successful in clinical trials phase I and II in spite of dose-dependent musculoskeletal toxicities, it was discontinued in phase III clinical trials due to the fact that it did not provide any improvement compared with other chemotherapeutic agents. On the other hand, the phase III clinical trial involving a large group of patients with advanced cancer indicated that marimastat was safe. Hence, we selected marimastat as a potential molecular probe, onto which a boronic acid can be appended for aqueous <sup>18</sup>F-fluoride capture to develop a noninvasive, clinically safe radiotracer for *in vivo* tumor imaging by detection of the

---

<sup>a</sup> First-pass effect, also called presystemic elimination, refers to drug elimination due to the metabolism and excretion in liver or lung before it reaches the circulation system.<sup>163</sup>

elevated MMP levels. In this chapter, the synthesis and the *in vivo* imaging study of Mar-<sup>18</sup>F-ArBF<sub>3</sub> **4.15** will be described.<sup>a</sup>

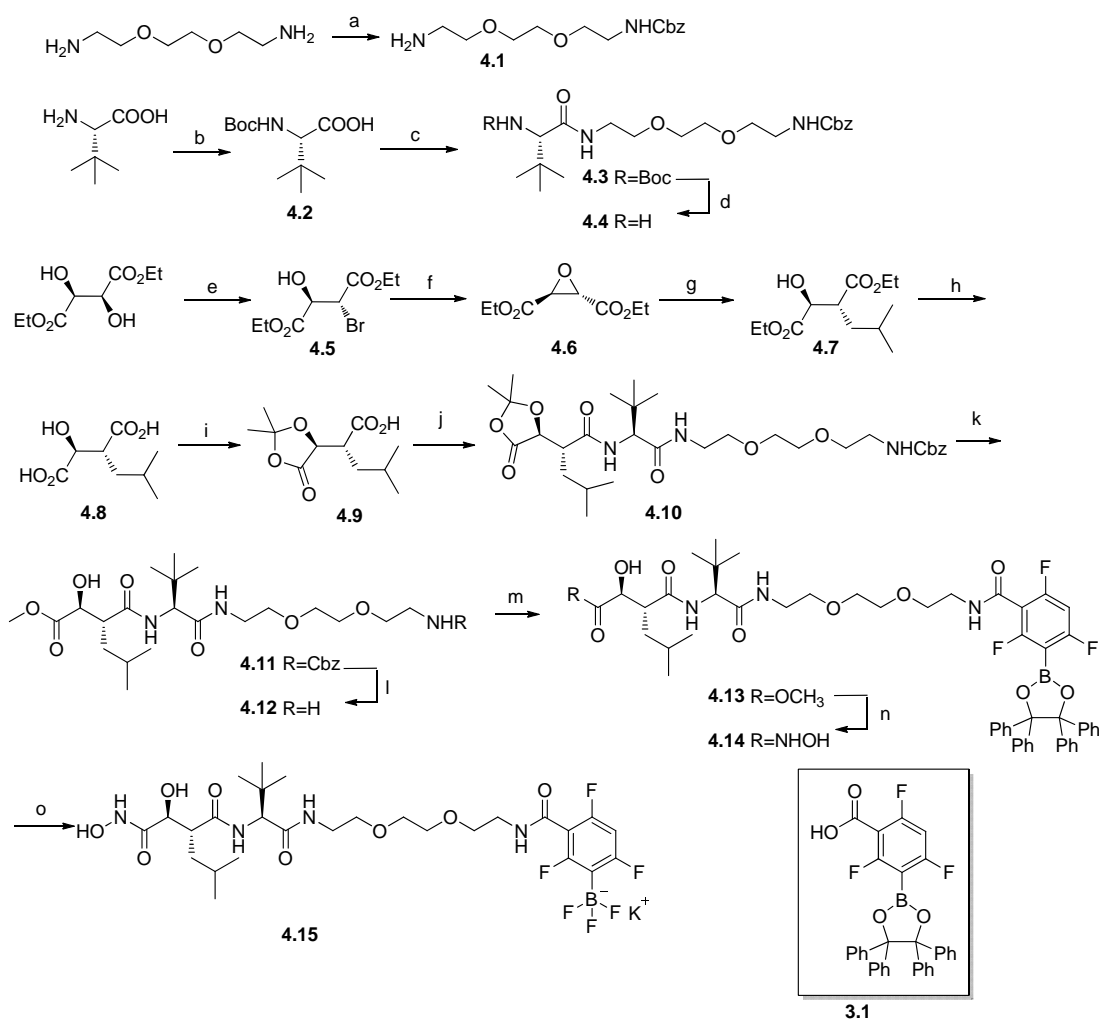
## 4.2 Results

### 4.2.1 Synthesis

Marimastat-boronate ester **4.14** was synthesized as summarized in Scheme 4.1. Briefly, diethyl *D*-tartrate was treated with HBr/HOAc, followed by EtONa to form epoxide **4.6**. Ring opening of epoxide **4.6** was carried out by treating **4.6** with isobutylmagnesium bromide to afford **4.7**. Diethyl ester **4.7** underwent saponification in the presence of NaOH. The formation of a hemiacetal with acetone and a subsequent lactonization on **4.8** gave compound **4.9**. In a simple HBTU coupling reaction, compound **4.9** was PEGylated by *tert*-leucine derivative **4.4** to give compound **4.10**, which was converted to methyl ester **4.11** in MeOH under acidic conditions. The Cbz group of **4.11** was successfully removed by the Pd/C catalyzed hydrogenolysis to give **4.12**, which was then conjugated to boronate **3.1** with EDC/HOBt as the dehydrating agents to afford **4.13**. The hydroxylaminolysis of methyl ester **4.13** with 50% aqueous hydroxylamine in the presence of a catalytic amount of KCN afforded marimastat-boronate ester **4.14** in a moderate yield. MarArBF<sub>3</sub> **4.15** was obtained quantitatively by treating boronate **4.14** with excess KHF<sub>2</sub> in MeOH under acidic conditions and it was purified by either flash chromatography with a small silica gel column packed in a Pasteur pipette or by DMSO extraction. Both the HPLC chromatograms of marimastat-boronate ester **4.14** and MarArBF<sub>3</sub> **4.15** are indicated in Figure 4.3. In brief, marimastat-boronate ester **4.14** was further purified via HPLC in a solvent system of H<sub>2</sub>O/CH<sub>3</sub>CN with 0.1% TFA adduct to remove any possible silica gel contamination from flash chromatography. MarArBF<sub>3</sub> **4.15** was analyzed by HPLC for its purity in a solvent system that initially was composed of H<sub>2</sub>O/MeOH. Since ArBF<sub>3</sub>s were found to undergo relatively fast defluoridation under acidic conditions,<sup>164</sup> no acid adduct was added to the HPLC solvents for the analysis of ArBF<sub>3</sub>s.

---

<sup>a</sup> This work has been done in collaboration with Dr. Christopher M. Overall's lab. The contribution by individuals is stated in the Preface.



**Scheme 4.1 Synthesis of marimastat-boronate 4.14 and MarArBF<sub>3</sub> 4.15.**

(a), CbzOSu, 1,4-dioxane, 0 °C then rt, overnight, 42%; (b), (Boc)<sub>2</sub>CO, NaOH, <sup>t</sup>BuOH/H<sub>2</sub>O, rt, 20 hr, 92%; (c), **4.1**, TBTU, DIPEA, CH<sub>2</sub>Cl<sub>2</sub>, rt, overnight, quant., or HBTU, DIPEA, CH<sub>2</sub>Cl<sub>2</sub>, rt, overnight, 92%; (d), TFA, CH<sub>2</sub>Cl<sub>2</sub>, rt, 2 hr, 87%; (e), i. 30% HBr/HOAc, 0 °C then rt, overnight, ii. AcCl (cat.), EtOH, reflux, 4 hr, 71% over two steps; (f), NaOEt, EtOH, 0 °C, 1 hr, 81%; (g), *iso*-BuMgBr, CuCN, Et<sub>2</sub>O, -30 °C, 1 hr, 34%; (h), 1 N NaOH (aq.), dioxane, rt, overnight, 95%; (i), 2,2-dimethoxypropane, TsOH·H<sub>2</sub>O, rt, overnight, 70%; (j), **4.4**, PyBOP, 2,6-lutidine, CH<sub>2</sub>Cl<sub>2</sub>, rt, overnight, 58%; (k), TsOH·H<sub>2</sub>O, MeOH, reflux, 1 hr, 92%; (l), Pd/C, H<sub>2</sub>, MeOH, rt, 1.5 hr, 97%; (m), **3.1**, EDC·HCl, Py, DMF, rt, overnight, 53%; (n), NH<sub>2</sub>OH, KCN (cat.), MeOH/THF, rt, 6 hr, 58%; (o), KHF<sub>2</sub>, HCl, MeOH, rt, 1 hr, quant.

A model compound, Cbz-PEG-marimastat (Cbz-PEG-Mar) **4.16**, was also prepared under KCN catalyzed hydroxylaminolysis from **4.11** in an isolated yield of 66%. This compound was synthesized to provide a standard solution, which was used to determine the concentration of MarArBF<sub>3</sub> **4.15** via a ferroin test, due to their structural resemblance.

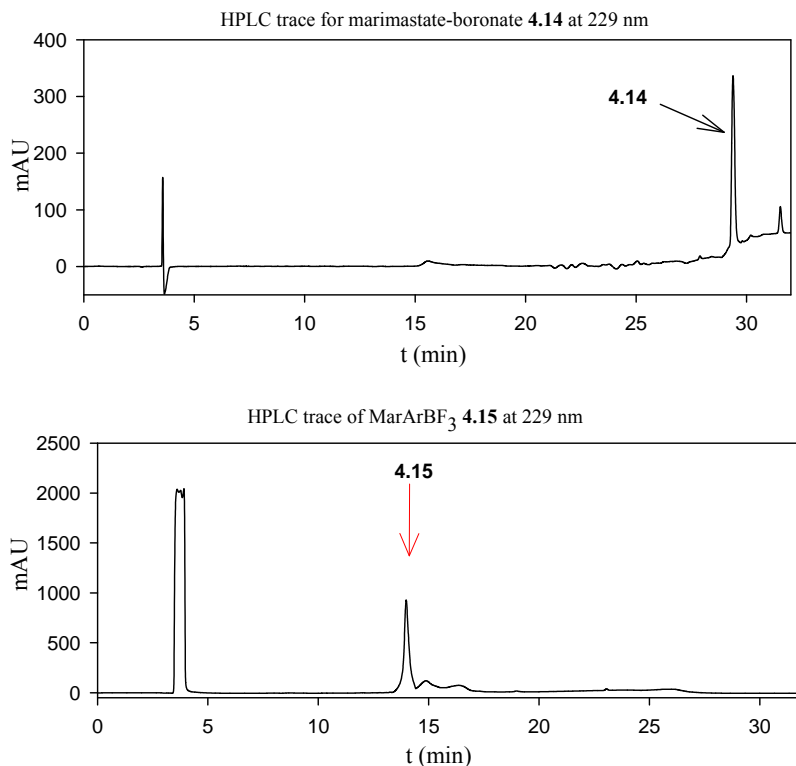


**Figure 4.3 HPLC chromatograms of 4.14 and 4.15.**

The top trace is for marimastat-boronate **4.14** and the lower one is for MarArBF<sub>3</sub> **4.15**. The top one was performed via HPLC Program 1 with Column I and the lower one was by HPLC Program 2 with the same column (Column I) in HPLC System I. For the lower trace, the peak notified with the red arrow was collected and checked with ESI-MS ([M]<sup>-</sup>: 673.6).

## 4.2.2 The *in vitro* stability of MarArBF<sub>3</sub> 4.15

The *in vitro* stability of MarArBF<sub>3</sub> **4.15** under physiological conditions was studied by <sup>19</sup>F NMR spectroscopy as shown in Figure 4.4. The defluoridation process observed for MarArBF<sub>3</sub> **4.15** was similar to those rates described for *N*-HetArBF<sub>3</sub>s in Chapter 2. The ArBF<sub>3</sub> peak at -55.8 ppm slowly disappeared while the free fluoride peak (at pH 7.4) at -42.5 ppm simultaneously increased. There was no appearance of any intermediate during this process, and as expected the solvolyzed product boronic acid subsequently underwent complete protodeboronation as illustrated by the appearance of two aryl fluoride peaks (> -40 ppm) during the experiment. The solvolytic half-life of **4.15** at neutral pH was measured as 1235 ± 50 minutes.

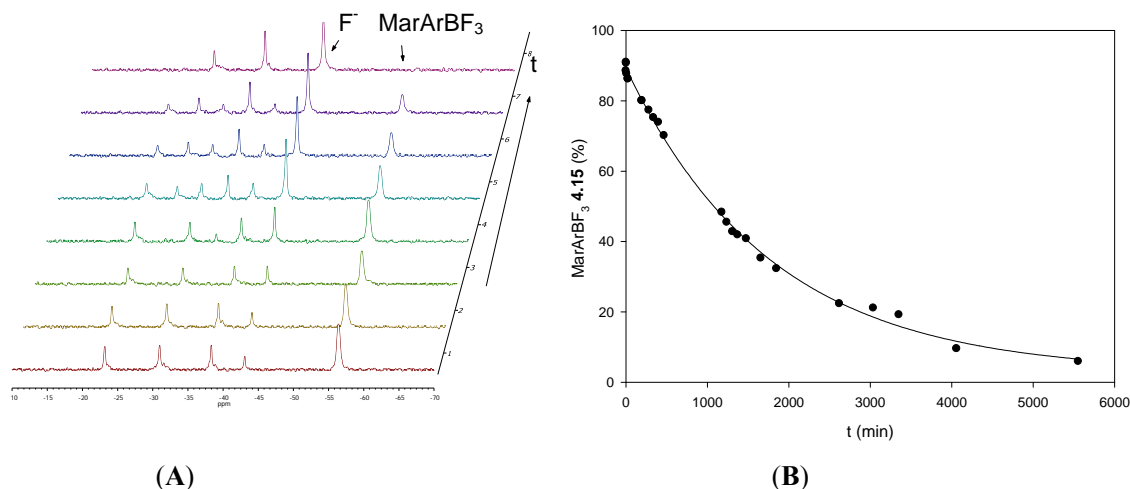


**Figure 4.4** The hydrolysis of MarArBF<sub>3</sub> **4.15** in 1 × PBS (pH 7.4) monitored by <sup>19</sup>F NMR spectroscopy.

(A) <sup>19</sup>F NMR spectra for the solvolysis of MarArBF<sub>3</sub> **4.15** in 1 × PBS (pH ~ 7.4) at rt. The free fluoride is at -42.5 ppm and the fluoride on boron of **4.15** is at -55.8 ppm. (B) The exponential fit of the hydrolysis of MarArBF<sub>3</sub> **4.15** against time with the first order decay process.  $k_{\text{obs}} = (5.61 \pm 0.23) \times 10^{-4} \text{ min}^{-1}$ ,  $R^2 = 0.9971$ .

### 4.2.3 The stability study of hydroxamic acids under acidic conditions

The radiosynthesis of MarArBF<sub>3</sub> **4.15** occurs under acidic conditions. Therefore, good acid stability of the substrates is essential to ensure the bioactivity following the radiolabeling. The MMP inhibitory activity of marimastat is largely determined by the hydroxamic acid functionality, which is the zinc(II) binding group. While there have been reports related to acid catalyzed hydrolysis of several hydroxamic acids at elevated temperatures (45 °C, 55 °C etc.),<sup>165-167</sup> none of them have described the situation at room temperature. Since the preparation of ArBF<sub>3</sub>s occurs under acidic conditions at room temperature, it is very important for us to verify whether the hydroxamic acid group could survive under similar acidic conditions. Hence, we synthesized *N*-hydroxy-2-phenylacetamide **4.17** to study its acid stability on a time scale of one hour at room temperature. Since the ferroin test, which will be introduced shortly, is very rapid and relatively accurate for measuring the concentration of hydroxamic acids, we decided to adopt this test to measure the kinetic changes on the incubation of **4.17** in the acidic solution at a (HCl) concentration comparable to that of a radiolabeling reaction. As indicated in Figure 4.5, very minor changes occurred within the time window of six hours. This suggested that at least for a short period of time, compound **4.17** was stable under acidic conditions.

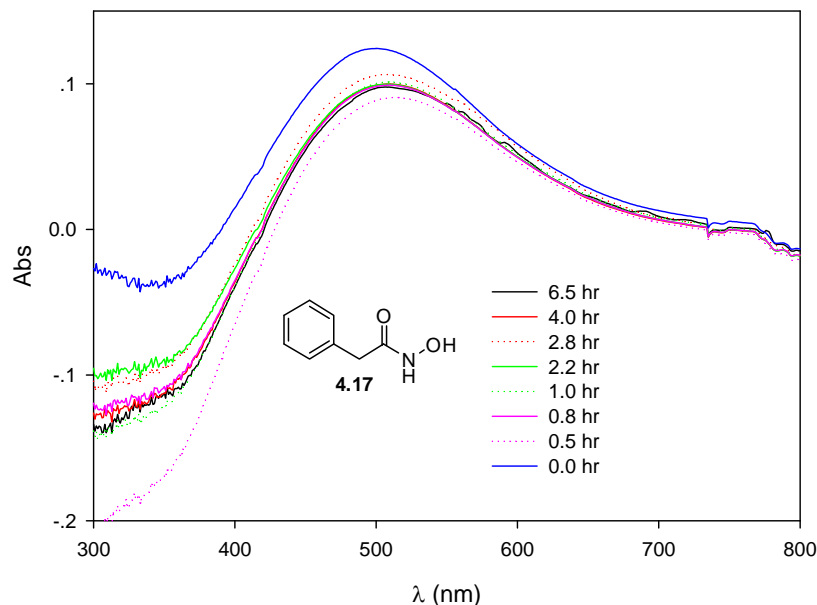


**Figure 4.5** The study on the acid stability of **4.17** with the ferriox test analyzed by UV-vis spectroscopy.

Each assay contained hydroxamic acid (25 mM) and HCl (2 M) in 50% aqueous EtOH. After incubation for a certain time, 10  $\mu$ L of the sample was added to 490  $\mu$ L of FeCl<sub>3</sub> (510  $\mu$ M) in EtOH and the UV absorption spectra (300 to 800 nm) were recorded immediately.

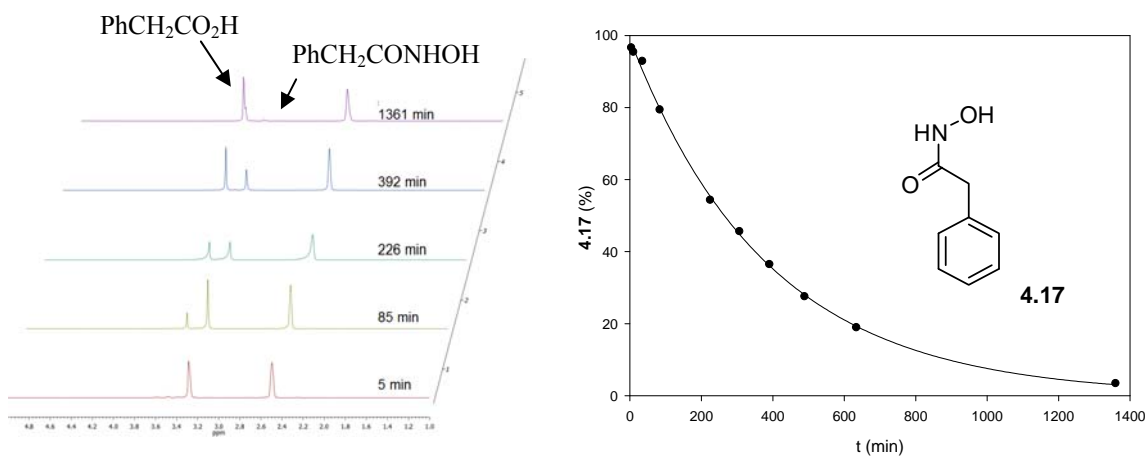


**Figure 4.6** The acid stability of **4.17** studied by <sup>1</sup>H NMR spectroscopy.

The acid catalyzed decomposition of hydroxamic acid **4.17** (21.6 mM) in the presence of D<sub>2</sub>SO<sub>4</sub> (1.7 M) in 1:1 *d*<sub>6</sub>-DMSO:D<sub>2</sub>O was monitored by <sup>1</sup>H NMR spectroscopy (300 MHz). The spectra with a chemical shift range of 1 to 5 ppm are demonstrated here. The reaction time upon the recording of the <sup>1</sup>H NMR spectrum is indicated on the corresponding trace and the percentage of **4.17** in the mixture was calculated based on the integrations of the CH<sub>2</sub> peaks at 3.29 ppm (that of **4.17**) and 3.48 ppm (that of the hydrolyzed product). The NMR spectra from the bottom to the top were from the beginning of the incubation to nearly the end of the experiment. Then the percentage of **4.17** v.s. time was plotted using the equation:  $y = a \cdot e^{-kt}$ , where its decomposition rate constant under this condition was  $k_{\text{obs}} = (2.58 \pm 0.05) \times 10^{-3} \text{ min}^{-1}$ ,  $R^2 = 0.9989$ .

Encouraged by these UV-vis data, we further studied the acid stability of hydroxamic acid **4.17** by <sup>1</sup>H NMR spectroscopy under more forcing acidic conditions, as shown in

Figure 4.6. The need to work in the deuterated solvent resulted in a change to  $d_6$ -DMSO, which might also change the rate of the acid-catalyzed solvolysis. The result indicated that the hydroxamic acid indeed decomposes under acidic conditions and compound **4.17** fully (> 98%) decomposed after 24 hours. To further identify the product, the crude reaction was analyzed by HPLC. It was found that the product shared the same retention time with phenylacetic acid ( $t_R = 13.5$  min via HPLC Program 1 with Column I in HPLC System I). Nevertheless, the rate was relatively slow when compared with the fluoridation process, and at the first hour of incubation, approximately 15% was consumed.

We then synthesized a succinimidyl hydroxamic acid **4.18**, which is more structurally similar to marimastat, and incubated it in the aqueous  $d_6$ -DMSO solution containing  $D_2SO_4$  to monitor its change in the same manner as for compound **4.17**. As demonstrated in Figure 4.7, the hydroxamic acid was slowly converted to another species. However, in contrast to the hydrolysis of **4.17**, which went to completion, that of **4.18** slowed down and appeared to approach equilibrium, as displayed in the kinetic curve, which was plotted based on the change of the peak integration value at 4.08 ppm. From the kinetic data we obtained, there was ~ 15% of the starting material being consumed within a one hour reaction.

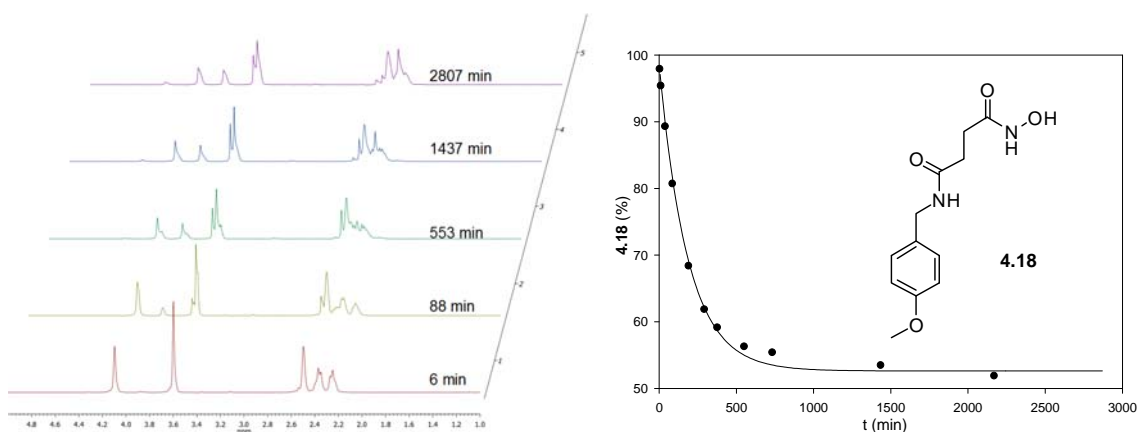


**Figure 4.7** The acid stability of **4.18** studied by  $^1\text{H}$  NMR spectroscopy.

The acid catalyzed hydrolysis of hydroxamic acid **4.18** (21.6 mM) was investigated by  $^1\text{H}$  NMR spectroscopy (300 MHz). The  $^1\text{H}$  NMR spectra with a range of 1 to 5 ppm are demonstrated. The sample contained 21.6 mM of **4.18** in 1.70 M  $D_2SO_4$  in 50% deuterated aqueous  $d_6$ -DMSO. The reaction time upon the recording of the  $^1\text{H}$  NMR spectrum is indicated on the corresponding trace. The percentage of starting material **4.18** was calculated based on the integrations of  $\text{CH}_2\text{N}$  at 4.08 ppm (that of **4.18**) and 3.87 ppm (that of the hydrolyzed product). The percentage of **4.18** against  $t$  (min) was fitted with the equation:  $y = y_0 + a * e^{-kt}$  where  $y_0 = 0.55 \pm 0.0034$  and the hydrolysis rate constant  $k_{\text{obs}} = (6.04 \pm 0.2) \times 10^{-3} \text{ min}^{-1}$ ,  $R^2 = 0.9985$ .

Nevertheless, both of the experiments on **4.17** and **4.18** suggested that at least for a one hour fluoridation reaction of an arylboronic acid under acidic conditions, the hydroxamic acid should be relatively stable and the structure of the marimastat would not be dramatically influenced, which was further confirmed by the enzyme inhibition assays on pure MarArBF<sub>3</sub> **4.15** as featured in the next section.

#### **4.2.4 *In vitro* enzyme inhibition assays of marimastat derivatives**

The *in vitro* bioactivity of any potential imaging agent provides guidelines for researchers to further study the *in vivo* imaging with specific targeting capabilities and other *in vivo* properties. Even though the derivatization at the *C*-terminus of *tert*-leucine residue of marimastat is known not to interfere with the potency or specificity,<sup>168</sup> the enzymatic inhibitory activity of the synthesized marimastat derivatives was measured in MMP assays. One very important parameter for these assays is the concentration of the inhibitor solution. In contrast to other hydroxamic acids, it was nearly impossible to obtain a relatively large amount of MarArBF<sub>3</sub> **4.15** due to the reaction scale and purification process. In addition, because MarArBF<sub>3</sub> **4.15** is composed of weak chromophores, direct and accurate determination of its concentration by spectroscopy methods is difficult. Nevertheless, hydroxamic acids can usually be quantitatively measured via colorimetric methods by taking advantage of their chelating properties with Fe(III) to rapidly give red-brown complexes in solution.<sup>169-171</sup> Although structural differences of the hydroxamates can influence the coordination with Fe(III) and thereby change the spectroscopic read-out, the detection limit of this method is as low as 10<sup>-5</sup> M.<sup>171</sup>

As mentioned earlier, it is difficult to ascertain an accurate concentration value for MarArBF<sub>3</sub> **4.15** by mass. Hence, it is impossible to obtain a calibration curve to determine the concentration of a given MarArBF<sub>3</sub> **4.15** solution. On the other hand, its analogue Cbz-PEG-Mar **4.16** has high structural resemblance to **4.15** and should form the same type of Fe(III)-hydroxamate complex. It is therefore hypothesized that the Fe(III)-**4.16** complex has similar optical properties as the Fe(III)-**4.15** complex. With the same Fe(III) binding group as **4.15** and **4.16**, the commercially purchased marimastat was also used to determine the extinction coefficient of its Fe(III) complex. By

comparing the extinction coefficients of complexes Fe(III)-marimastat and Fe(III)-**4.16**, a direct application of the extinction coefficient of Fe(III)-**4.16** can be directly used to determine the concentration of Fe(III)-**4.15**. The result is demonstrated in Figure 4.8.

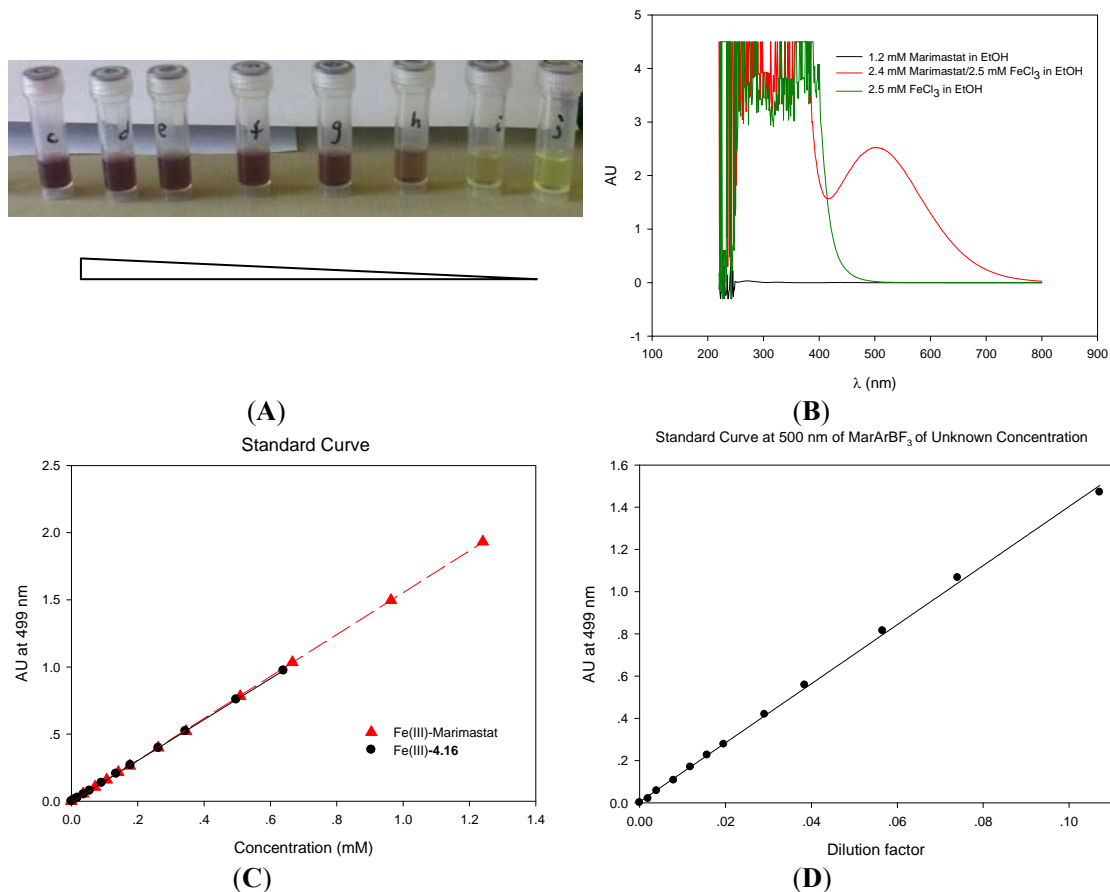


**Figure 4.8** The determination of the concentration of MarArBF<sub>3</sub> **4.15** by the ferroin test.

(A) The color change of FeCl<sub>3</sub> ethanol solution (5 mM) upon the addition of marimastat (6.9 mM), from left to right are the assays containing from a high amount of marimastat to a low amount added; (B), the UV spectra for the ferroin assay on marimastat: the black trace is the UV spectra of marimastat (1.16 mM) in EtOH, the green trace is that of 2.50 mM FeCl<sub>3</sub> in EtOH; the red trace is that of the mixture of marimastat (2.43 mM) and FeCl<sub>3</sub> (2.50 mM) in EtOH; (C) calibration curves for the Fe(III) complexes of hydroxamic acids at 499 nm for both Cbz-PEG-Mar **4.16** (black) and commercial marimastat (red). The extinction coefficients ( $\epsilon$ ) were calculated via the slopes of the linear fitting curves:  $\epsilon(\text{Fe-4.16})$  is  $1526 \pm 2.7 \text{ M}^{-1}\text{cm}^{-1}$  ( $R^2 = 1$ ) and  $\epsilon(\text{Fe-marimastat})$  is  $1560 \pm 4.5 \text{ M}^{-1}\text{cm}^{-1}$  ( $R^2 = 0.9999$ ); (D) a calibration curve for the Fe(III)-MarArBF<sub>3</sub> **4.15** in *d*<sub>4</sub>-MeOD with unknown concentration via the ferroin test. The data were fitted linearly and the slope is  $13.99 \pm 0.146$  ( $R^2 = 0.9989$ ). By using the extinction coefficient determined in C for Fe(III)-**4.16** ( $1526 \pm 2.7 \text{ M}^{-1}\text{cm}^{-1}$ ), the concentration of the stock solution of MarArBF<sub>3</sub> **4.15** was calculated to be  $9.07 \pm 0.095 \text{ mM}$ .

Figure 4.8A shows the color changes that occurred upon the addition of marimastat to the ethanolic Fe(III) solution (5 mM), from light yellow (color of ethanolic Fe(III)) to red-brown (color of the Fe(III)-marimastat complex), which is consistent with a previous

literature report.<sup>171</sup> Figure 4.8B further indicates the different UV-absorption profiles of Fe(III), marimastat, and the Fe(III)-marimastat complex from 200 to 800 nm. From the spectra, the Fe(III)-marimastat complex has a specific absorption between 400 to 800 nm, while neither Fe(III) nor marimastat shows any UV activity in this range. The maximum absorption of different Fe(III)-hydroxamate complexes is found at slightly different wavelengths around 500 nm and we followed a literature procedure to record all absorbance values at 499 nm. On the other hand, to make sure that all the hydroxamic acid being consumed gave only 1:1 Fe(III)-ligand complexes, a large excess of Fe(III) was used in the ferriin test, which results in a high absorption noise between 200 and 400 nm. Different amounts of hydroxamic acid were added to the Fe(III) stock solution for UV-vis absorbance measurement at 499 nm, and a calibration curve was then constructed as shown in Figure 4.8C for the Fe(III) complexes of marimastat (red) and **4.16** (black) respectively. The extinction coefficients are calculated to be  $1526 \pm 3 \text{ M}^{-1}\text{cm}^{-1}$  for Fe(III)-**4.16** and  $1560 \pm 5 \text{ M}^{-1}\text{cm}^{-1}$  for Fe(III)-marimastat. The very close extinction coefficients imply that the UV absorbance of these Fe(III)-complexes at 499 nm is primarily determined by the chelating groups such as the hydroxamic acid and the  $\alpha$ -hydroxyl group. Hence, the extinction coefficient of the complex Fe(III)-**4.16** was used to determine the concentration of a stock solution of MarArBF<sub>3</sub> **4.15** (9.07 mM), as indicated in Figure 4.8D.

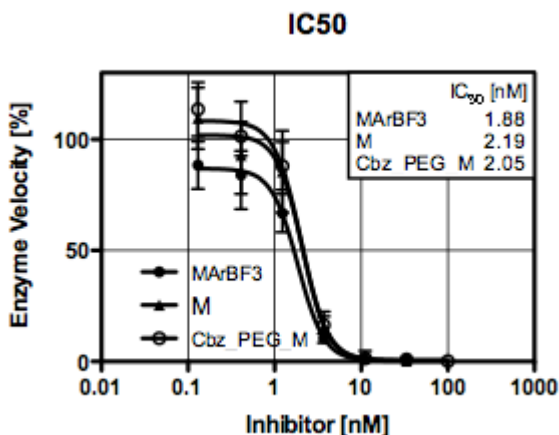


**Figure 4.9 The MMP2 inhibition assay with marimastat compounds.** Commercial marimastat ( $\blacktriangle$ )  $IC_{50} = 2.19 \text{ nM}$ ; MarArBF<sub>3</sub> **4.15** ( $\bullet$ ),  $IC_{50} = 1.88 \text{ nM}$ ; Cbz-PEG-Mar **4.16** ( $\circ$ ),  $IC_{50} = 2.05 \text{ nM}$ .

The marimastat compounds used in the ferriin test were then examined for their

enzymatic inhibitory activity. As shown in Figure 4.9, the activities of all the marimastat compounds tested are within the nanomolar range and are very consistent with literature reports. This also suggests that the acidic conditions for the fluoridation have little influence on the structure of MarArBF<sub>3</sub> **4.15** and therefore its bioactivity (IC<sub>50</sub> ~ 2 nM) is retained under acidic conditions.

#### 4.2.5 Fluorescent marimastat-FITC and *in vitro* cell imaging

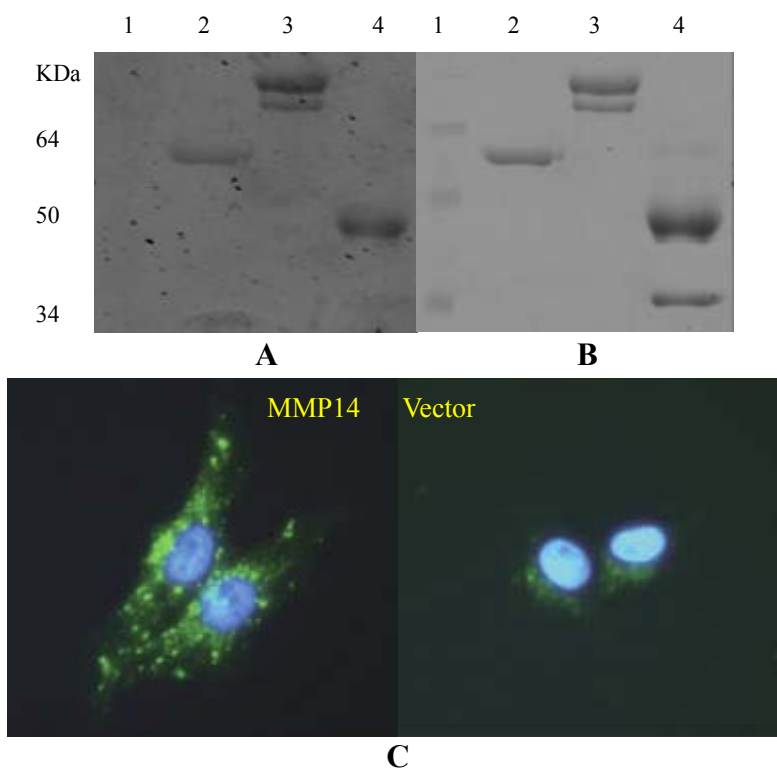


**Figure 4.10** The specificity of marimastat-FITC **4.19** and the *in vitro* cell image of MMPs. Image **A** was the gel image of marimastat-FITC bound MMPs: the recombinant human MMPs 2, 9, and 13, which are 4-aminophenylmercuric acetate-activated MMPs, resolved on 10% SDS-PAGE gel, renatured, incubated with marimastat-FITC **4.19** and washed thoroughly prior to the visualization of the gel. Image **B** was the same gel of **A** that was further stained with Coomassie brilliant blue before gel visualization. Lane 1, the protein size marker; Lane 2, MMP2, Lane 3, MMP9, and Lane 4, MMP13. Image **C**, MDA-MB-231 cells stably transfected with MMP14 and vector were incubated with marimastat-FITC **4.19** (green) and cell nuclei were counterstained with Hoechst blue dye.

In the above section, we demonstrated that the derivatization through the *C*-terminus of *tert*-leucine residue has very little effect on the enzyme inhibitory activities. Prior to the *in vivo* animal imaging, cell binding assays could offer more direct information as to the ability of marimastat to target MMPs. Therefore, the fluorescent marimastat-FITC **4.19**

was synthesized<sup>a</sup> and its IC<sub>50</sub> value was determined to be 2.10 nM via an inhibitory competition assay with a fluorescent MMP substrate QF24.<sup>b</sup>

To start with, the binding of marimastat-FITC **4.19** to MMPs was visualized directly on an SDS-polyacrylamide gel. The gel image as shown in Figure 4.10A clearly suggested specific binding of marimastat-FITC **4.19** to MMPs. Comparing the gel image shown in Figure 4.10A with Figure 4.10B, neither the molecular weight markers nor the band corresponding to a molecular weight around 36 kDa, representing the autolytically cleaved hemopexin domain of MMP13, was labeled with **4.19**. This revealed the active site specificity for the labeling. In addition, as indicated in Figure 4.10C, marimastat-FITC **4.19** specifically labeled MMP14, which is stably transfected in human MDA-MB-231 breast cancer cell lines and is always highly expressed in cancer, while there was nearly no labeling for the vector control cells. This helped us to establish marimastat's *in vitro* affinity and specificity.

## 4.2.6 Radiosyntheses of Mar-<sup>18</sup>F-ArBF<sub>3</sub> **4.15**

### 4.2.6.1 The radiosynthesis of Mar-<sup>18</sup>F-ArBF<sub>3</sub> **4.15**

The radiolabeling of marimastat-boronate **4.14** was first undertaken with a low amount of radioactivity and analyzed by autoradiographic TLC following resolution by 20% MeOH in CHCl<sub>3</sub>. As shown in Figure 4.11, under the given conditions, <sup>18</sup>F-fluoride does not migrate off the baseline of the TLC plate, while Mar-<sup>18</sup>F-ArBF<sub>3</sub> **4.15** has an *R<sub>f</sub>* value of ~ 0.15. Two aqueous cosolvents (CH<sub>3</sub>CN and DMF) were tested for the <sup>18</sup>F-labeling reaction. From the autoradiographic TLC, it is clear that the conversion of **4.14** was better in aqueous CH<sub>3</sub>CN than in aqueous DMF. The radioactivity loaded onto the TLC plate from the crude reaction in CH<sub>3</sub>CN seemed to saturate the phosphorimager screen, while the conversion of the reaction in aqueous DMF was about 15% based on the TLC analysis. Nevertheless, to our surprise, the small silica gel column (~ 8 cm high) was not effective for removing all the unincorporated <sup>18</sup>F-fluoride, while the C18 sep-pak treatment suggested the possibility of rapid solid phase extraction to purify

<sup>a</sup> Dr. Curtis Harwig synthesized **4.19**.

<sup>b</sup> QF24 is (7-methoxycoumarin-4-yl)acetyl-Pro-Leu-Gly-Leu-[3-(2,4-dinitrophenyl)-L-2,3-diaminopropionyl]-Ala-Arg-NH<sub>2</sub>.

### Mar-<sup>18</sup>F-ArBF<sub>3</sub> **4.15**.

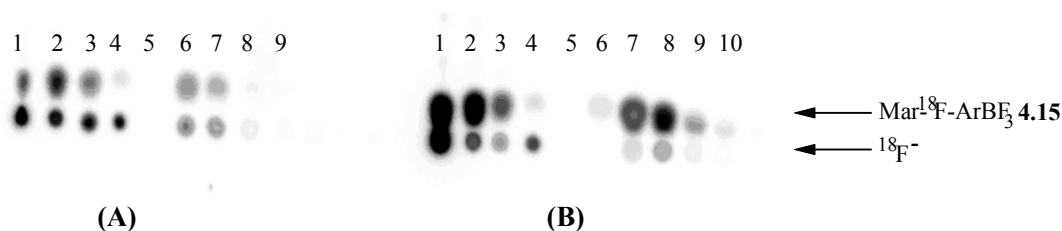


**Figure 4.11** The autoradiographic TLC analysis of the <sup>18</sup>F-fluoridation to prepare Mar-<sup>18</sup>F-ArBF<sub>3</sub> **4.15**.

The <sup>18</sup>F-fluoridation of marimastat-boronate **4.14** was analyzed by TLC developed with 20% MeOH in CHCl<sub>3</sub> and the TLC plate was then visualized by autoradiographic phosphorimaging. (A) The fluoridation to prepare Mar-<sup>18</sup>F-ArBF<sub>3</sub> **4.15** in aqueous DMF; (B) the fluoridation to prepare Mar-<sup>18</sup>F-ArBF<sub>3</sub> **4.15** in aqueous CH<sub>3</sub>CN. Lane 1 was the resolution of the crude reaction; Lanes 2 to 4 were for the fractions (from the first to the third fraction) collected from flash chromatography with a small silica column; Lanes 5 to 10 were for the fractions (from the first to the sixth fraction) from the separation with a C18 sep-pak cartridge. The radiolabeling conditions: marimastat-boronate **4.14** (100 nmol), HCl (4 μmol), <sup>18</sup>F-fluoride containing <sup>19</sup>F-fluoride (200 nmol) in 33.3% aqueous DMF or CH<sub>3</sub>CN, rt, 80 min. The reactions were quenched with 98 μL of 200 mM phosphate buffer (pH 8) and the crude reaction was loaded on a silica column packed in a Pasteur pipette and eluted with 5% NH<sub>4</sub>OH in EtOH. Approximately 200 μL per fraction was collected. Then fractions containing the major radioactivity were combined (the first two fractions represented in Lanes 2), diluted with H<sub>2</sub>O (10 mL) and loaded to a preactivated C18 sep-pak cartridge. The sep-pak cartridge was flushed with 5 mL H<sub>2</sub>O and 40% aqueous CH<sub>3</sub>CN was applied to elute the radioactivity with about 200 μL per fraction. Then the crude and all the fractions from the silica column and the C18 sep-pak cartridge were loaded to a TLC plate, and the TLC plate was developed with 20% MeOH in CHCl<sub>3</sub> at rt. The radioactivity at the BOS<sup>a</sup> for (A): 1.46 mCi and that for (B): 1.86 mCi.

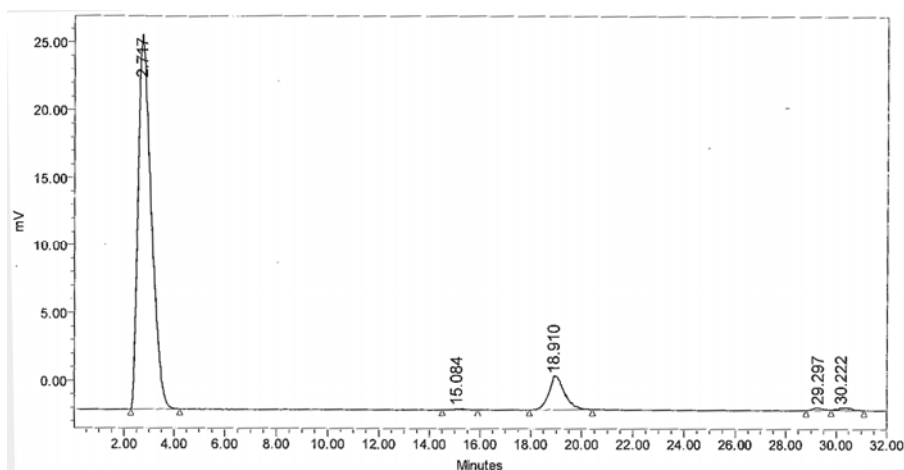


**Figure 4.12** The test of reductant additives to the <sup>18</sup>F-fluoridation of marimastat-boronate **4.14**.

Reaction conditions: marimastat-boronate **4.14** (100 nmol), <sup>18</sup>F-fluoride containing carrier <sup>19</sup>F-fluoride (500 nmol), HCl (8.0 μmol) and reductants (52.2 nmol of ascorbic acid, 20 nmol of DTT and 52.6 nmol of tetrabutylammonium iodide) in 5.25 μL of 50% aqueous CH<sub>3</sub>CN, rt, 74 min. The reaction was quenched with 100 μL of 200 mM phosphate buffer (pH 8). The quenched reaction was loaded to an 8 cm silica gel packed Pasteur pipette and eluted with 5% NH<sub>4</sub>OH in EtOH. Then the collected fraction (first 200 μL fraction) was injected into the radio-HPLC for analysis. The HPLC was performed via HPLC Program 2 (with CH<sub>3</sub>CN as solvent B instead) with Column IV in HPLC System II. The radioactivity at the BOS: 3.15 mCi.

<sup>a</sup> BOS stands for “beginning of the synthesis”

These preliminary results based on the autoradiographic TLC analysis led us to use CH<sub>3</sub>CN as the aqueous cosolvent for the radiofluorination of **4.14**. However, several failures for the <sup>18</sup>F-fluorination of **4.14** at higher radioactivity (at the BOS > 10 mCi) drove us to consider the possibility of radiolysis, which might have been the cause of low radiochemical yields. Hence, we tested the influence of added reductants on the fluorination in order to prevent radiolysis. The result, analyzed by radio-HPLC, shown in Figure 4.12, suggested the reductants, such as ascorbic acid, DTT, and iodide, did not interfere with the reaction, although their exact roles as radioprotectants in this case are unknown. Based on the autoradiographic TLC analysis, the free fluoride seemed to co-elute through the silica column with the product Mar-<sup>18</sup>F-ArBF<sub>3</sub> **4.15**. This advised us to abandon a quick silica plug and directly apply the HPLC isolation to purify the product without any pretreatment to avoid unnecessary radiation exposure from handling the material.

#### 4.2.6.2 The radiosynthesis to image MMPs in breast cancer

Mar-<sup>18</sup>F-ArBrF<sub>3</sub> **4.15** was synthesized from marimastat-boronate **4.14** with <sup>18</sup>F-fluoride in the presence of carrier <sup>19</sup>F-fluoride. HCl was added since the fluorination proceeds under acidic conditions as shown in Chapter 3. Chemoprotectants, including ammonium formate, sodium ascorbate, and potassium iodide, were also added to prevent any possible radiolysis at high radioactivity. The reaction was carried out at room temperature (~ 18 °C) for approximately 90 minutes, quenched with NH<sub>4</sub>OH solution and resolved by HPLC. The radioactivity at the beginning of the synthesis (BOS) was ~ 53 mCi with a specific activity of 0.136 Ci/μmol, and the HPLC purified radiolabeled product contained around 1 mCi after a total radiosynthesis of 126 minutes including the purification and formulation. The specific activity of Mar-<sup>18</sup>F-ArBF<sub>3</sub> **4.15** at the time of packaging was 0.179 Ci/μmol, which was calculated to be three times that of <sup>18</sup>F-fluoride.

From the radio-HPLC chromatogram shown in Figure 4.13B, a major radioactive peak was present at 15.2 minutes, and the radiochemical yield was in excess of 50% based on the radio-HPLC chromatogram. However, the isolated Mar-<sup>18</sup>F-ArBF<sub>3</sub> **4.15** suggested an isolated radiochemical yield of only ~ 1.4%. Meanwhile, it was noticed that the HPLC column remained highly radioactive as measured by a portable Pendulum Geiger counter.

This suggested that a significant portion of the radioactivity might have been retained on the column and what was seen on the radio-HPLC chromatogram represented an “exaggerated” radiochemical yield. In addition, the relatively clean UV-trace as shown in Figure 4.13C suggested good separation of the desired product from other unlabeled materials. In spite of limited infrastructure and equipment at TRIUMF, we were able to re-inject part of the collected fraction to assess the radiochemical purity, however limitations in hardware forced us to use the same column via the same HPLC program approximately one hour after the HPLC purification. As shown in Figure 4.13D, only a small/negligible amount of free  $^{18}\text{F}$ -fluoride in the purified fraction of  $^{18}\text{F}$ -ArBF<sub>3</sub> **4.15** was observed and the source of this trace free fluoride (< 5%) is discussed later.

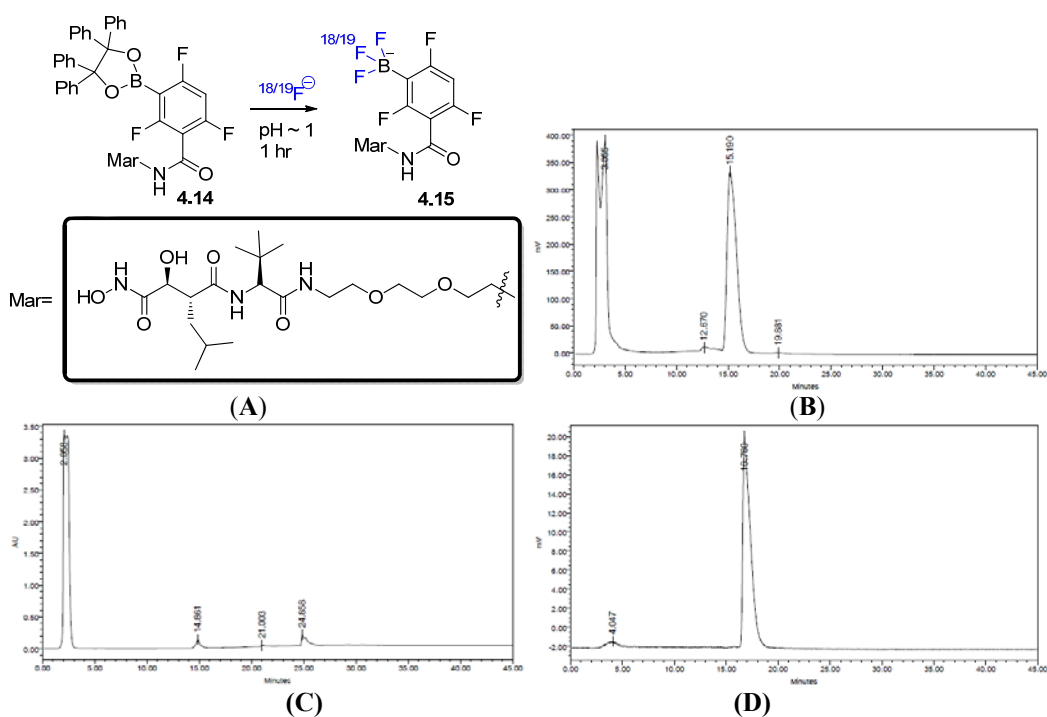


**Figure 4.13 Radio-HPLC chromatograms of the fluoridation to prepare Mar- $^{18}\text{F}$ -ArBF<sub>3</sub> **4.15**.**

**A)** The scheme for the radiosynthesis of Mar- $^{18}\text{F}$ -ArBF<sub>3</sub>; **B)** the HPLC radiochromatogram of the crude reaction (detector at high attenuation); **C)** the UV-chromatogram of the crude reaction at 229 nm; **D)** the analytical HPLC radiochromatogram of the HPLC purified Mar- $^{18}\text{F}$ -ArBF<sub>3</sub> **4.15** collected from HPLC chromatogram **B** (detector at high attenuation). The HPLC was performed via HPLC Program 4 with Column I in HPLC System II. The radiolabeling conditions: marimastat-boronate **4.14** (100 nmol), HCl (6.3  $\mu\text{mol}$ ), sodium ascorbate (2  $\mu\text{mol}$ ), KI (0.4  $\mu\text{mol}$ ),  $^{18}\text{F}$ -fluoride containing  $^{19}\text{F}$ -fluoride (393 nmol) in 44.4% aqueous CH<sub>3</sub>CN, rt, 88 min. The radioactivity at the BOS: 53.4 mCi and the specific activity of  $^{18}\text{F}$ -fluoride at the BOS: 0.136 Ci/ $\mu\text{mol}$ .

A second radiosynthesis was carried out following the same procedure and its radio-HPLC chromatograms are shown in Figure 4.14. Starting with 63 mCi, 950  $\mu\text{Ci}$  of

Mar-<sup>18</sup>F-ArBF<sub>3</sub> **4.15** was obtained at the time of packaging, 105 minutes after the beginning of the synthesis. The isolated radiochemical yield was 1.5%, a value that is much lower than that calculated from the radio-HPLC chromatogram. Similarly, the collected product was re-injected into the HPLC to verify its radiochemical purity. A low attenuation of the radio-detector was used instead of the high attenuation set-up for the analytic radio-HPLC. Consequently, the signal of Mar-<sup>18</sup>F-ArBF<sub>3</sub> **4.15** saturated the detector and the radiochromatogram of Figure 4.14B was off scale. Meanwhile, some <sup>18</sup>F-fluoride was again observed, which suggested some defluoridation of the produced radiotracer or non-perfect separation from the preparative HPLC. Nonetheless, this radiolabeling experiment afforded Mar-<sup>18</sup>F-ArBF<sub>3</sub> **4.15** with a specific activity of 0.396 Ci/μmol at the time of packaging.

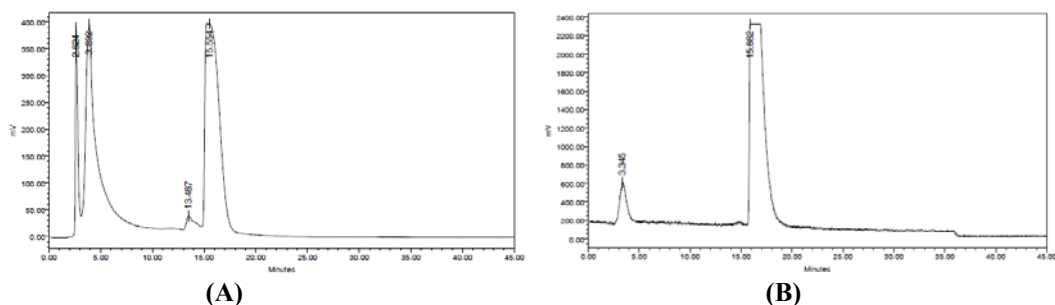


**Figure 4.14 Radio-HPLC chromatograms of the 2<sup>nd</sup> synthesis of Mar-<sup>18</sup>F-ArBF<sub>3</sub> **4.15**.** **A)** The radio-HPLC chromatogram of the crude reaction (detector at high attenuation); **B)** the analytical radio-HPLC chromatogram of the purified Mar-<sup>18</sup>F-ArBF<sub>3</sub> **4.15** collected from HPLC chromatogram **A** (detector at low attenuation). The HPLC was performed via HPLC Program 4 with Column I in HPLC System II. The radiolabeling conditions: marimastat-boronate **4.14** (100 nmol), HCl (6.3 μmol), sodium ascorbate (1.40 μmol), KI (0.28 μmol), HCO<sub>2</sub>NH<sub>4</sub> (0.28 μmol), <sup>18</sup>F-fluoride containing <sup>19</sup>F-fluoride (252 nmol) in 42.9% aqueous CH<sub>3</sub>CN, rt, 69 min. The radioactivity at the BOS: 63 mCi and the specific activity of <sup>18</sup>F-fluoride at the BOS: 0.250 Ci/μmol.

Both radioactive portions of Mar-<sup>18</sup>F-ArBF<sub>3</sub> **4.15** were tail-vein injected into mice with 67NR<sup>a</sup> tumors with or without preblocking to study *in vivo* tumor specificity of this radiolabeled compound. Furthermore, both of the HPLC purified radiotracers were analyzed for the enzymatic inhibitory activity following decay. Their IC<sub>50</sub>s were within the nanomolar range as previously tested, 1.28 nM and 1.68 nM respectively. The collected radiotracer, after complete decay, was also analyzed by ESI-LRMS to demonstrate a mass value corresponding to the desired product with ESI-LRMS: m/z(-) 673.4.

<sup>a</sup> 67NR is one of the breast cancer cells. It forms primary tumors without metastasis.

#### 4.2.7 *In vivo* PET imaging of MMPs in murine breast carcinomas

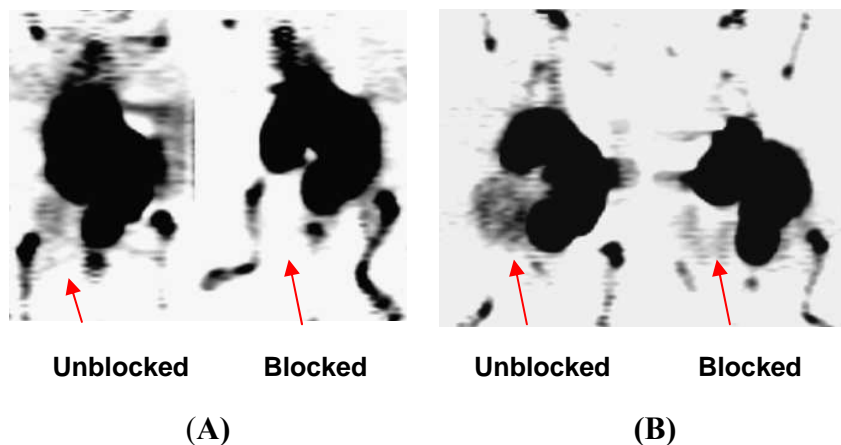


**Figure 4.15** *In vivo* PET imaging of murine breast carcinomas targeting MMPs.

(A), The microPET image of the 67NR breast tumor mice injected with  $\sim 100 \mu\text{Ci}$  of Mar- $^{18}\text{F}$ -ArBF $_3$  **4.15** (with a specific activity of  $0.179 \text{ Ci}/\mu\text{mol}$  at the time of packaging) in PBS via the tail vein either in the unblocked tumor mouse or in the preblocked one with  $300 \text{ nmol}$  of marimastat; (B), the same experiment as for A but the tumor was innoculated on the same date and imaged on day 33 with a specific activity of  $0.396 \text{ Ci}/\mu\text{mol}$  at the time of packaging. The position annotated with the red arrow is the location of the tumor.

Female BALB/c mice (7 to 9 weeks old) with 67NR/CMV-luciferase murine mammary cancer cells were used for *in vivo* PET imaging study with Mar- $^{18}\text{F}$ -ArBF $_3$  **4.15**. Two sets of mice were injected with Mar- $^{18}\text{F}$ -ArBF $_3$  **4.15** in  $1 \times \text{PBS}$  saline with specific activities of  $0.179 \text{ Ci}/\mu\text{mol}$  (Figure 4.15A) and  $0.396 \text{ Ci}/\mu\text{mol}$  (Figure 4.15B) respectively. In each case, one littermate was blocked with unlabeled marimastat. From the PET images shown in Figure 4.15, 60 minutes following tracer injection, we were able to observe low but detectable and specific uptake of Mar- $^{18}\text{F}$ -ArBF $_3$  **4.15** in the primary tumor. The specific tumor uptake was supported by the blocking experiment, in which Mar- $^{18}\text{F}$ -ArBF $_3$  **4.15** was injected in mice pretreated with unlabeled marimastat three times prior to the injection of the radioactive agent. The preblocked mice clearly demonstrated decreased tumor uptake in the same region as the littermates with similar tumor sizes. Meanwhile, bone uptake in the joints was also observed. Other organs such as bladder, stomach, liver, and spleen also demonstrated uptake. Unfortunately, tumor uptake was not improved with a higher specific activity of the radiotracer.

## 4.2.8 Several factors influencing the radiosynthesis of Mar-<sup>18</sup>F-ArBF<sub>3</sub> 4.15

The isolated radiochemical yield from the radiolabeling for tumor imaging was low, as described in section 4.2.6. We figured that there must be some key factors limiting the yields of the <sup>18</sup>F-fluoridation to prepare the ArBF<sub>3</sub>s when using high levels of radioactivity. While the facility at TRIUMF was shut down for renovation, we were fortunate to be offered <sup>18</sup>F-fluoride by Dr. John Valliant and Dr. Karin Stephenson at the CPDC to check several factors that may influence the radiochemical yields for the preparation of Mar-<sup>18</sup>F-ArBF<sub>3</sub> **4.15**. Among these factors, we became concerned with the fact that there was almost always a radioactive byproduct produced in the previous labeling experiments (eluting at around 4 min in the radio-HPLC) as shown in Figure 4.13B and Figure 4.14A. Identifying the source of this byproduct would be of great significance in terms of understanding the labeling reaction.

We first tried to repeat the radiosynthesis at the CPDC. <sup>18</sup>F-Fluoride was trapped on an anion exchange column (a QMA cartridge with Cl<sup>-</sup> form)<sup>a</sup> and then released by NaClO<sub>4</sub> solution (2 mg/mL, 1 mL) to give the resulting radioactive eluent with a pH of 5 ~ 6. We found that upon the addition of KHF<sub>2</sub>, the pH of the solution became more acidic. After the evaporation over N<sub>2</sub> flow at 100 °C in the Pyrex V-vial without pH adjustment, the same procedure was carried out to radiolabel marimastat-boronate **4.14** with this <sup>18/19</sup>F-fluoride mixture. Interestingly, no radioactive product was observed. This suggested that all the free <sup>18</sup>F-fluoride probably was trapped in the glass vial or had gassed off under the slightly acidic conditions during the evaporation to concentrate the <sup>18</sup>F-fluoride solution. Hence, we then added ~ 9.5 μmol of NaHCO<sub>3</sub> to adjust the pH of the <sup>18</sup>F-fluoride eluent to ~ 9 after the addition of carrier fluoride and concentrated the <sup>18</sup>F-fluoride solution over N<sub>2</sub> stream. The basic “dry” <sup>18/19</sup>F-fluoride was then used for the <sup>18</sup>F-fluoridation and gratifyingly a similar radiochemical yield as described in 4.2.6 was obtained (Figure 4.16). An HPLC solvent system (HCO<sub>2</sub>NH<sub>4</sub>/CH<sub>3</sub>CN) in common use at the CPDC was used for our work on labeling marimastat at the CPDC. It was found that, with such a mobile phase, very small amounts of radioactivity were retained on the

<sup>a</sup> The anion exchange column used at TRIUMF to trap <sup>18</sup>F-fluoride is with HCO<sub>3</sub><sup>-</sup> form.

HPLC column over the full HPLC gradient, which suggested that the radio-HPLC chromatogram using this solvent system could provide information of the real radiochemical yield. For instance, the radiosynthesis demonstrated in Figure 4.16 had a radiochemical yield of around 3%.

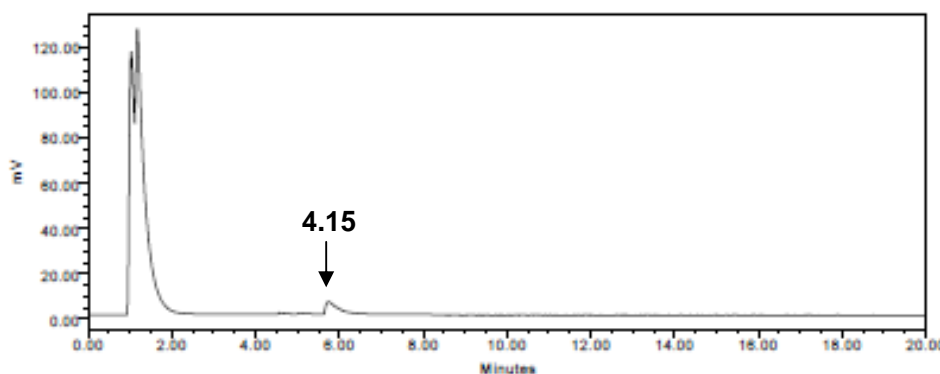


**Figure 4.16** The radio-UPLC chromatogram of the  $^{18}\text{F}$ -radiolabeling reaction of marimastat-boronate **4.14**.

The peak at 5.8 min annotated with an arrow is Mar- $^{18}\text{F}$ -ArBF<sub>3</sub> **4.14**.  $^{18}\text{F}$ -Fluoride was trapped in the QMA anion exchange column (Cl<sup>-</sup> form) and released by the aqueous solution of NaClO<sub>4</sub> (2 mg/mL, 1 mL). NaHCO<sub>3</sub> (9.5 μmol) and  $^{19}\text{F}$ -fluoride (800 nmol, in the form of KHF<sub>2</sub>) were added to give a final pH of 8.5 ~ 9. The solution was concentrated over N<sub>2</sub> flow at 95 °C. The radioactivity after dry-down was resuspended in 6 μL of the aqueous  $^{19}\text{F}$ -fluoride solution (800 nmol) and 1.5 μL of the well-resuspended solution was transferred to marimastat-boronate **4.14** (100 nmol) in 2.5 μL CH<sub>3</sub>CN. The mixture was acidified by 0.5 μL of concentrated HCl, incubated at rt for 1 hr and quenched with 105 μL of 0.83% aqueous NH<sub>4</sub>OH (9.33 mCi at the BOS). 10 μL of the quenched reaction was then injected into the UPLC using HPLC Program 5 with Column III in HPLC System III.

To reduce the radiation exposure and simplify the operation, the  $^{18/19}\text{F}$ -fluoride cocktail was added last to initiate the reaction. It was found that this operation did not influence the radiofluoridation and similar radiochemical yields were obtained. Then several factors with regard to the fluoridation were investigated, including the evaporation conditions and the quality of boronate ester **4.14**. The results have been summarized in Table 4.1. From the table, the quality of marimastat-boronate **4.14** was found to be critical to the radiolabeling reaction. The only two reactions (reactions VI and XII) with marimastat-boronate **4.14**, which had been stored at -20 °C for a long period of time, both gave relatively low radiochemical yields (~ 1-2%) while the newly prepared compound gave much higher yields (average ~ 18%).

On the other hand, it was believed that different dry-down containers might have also resulted in different “qualities” of  $^{18}\text{F}$ -fluoride. Indeed, fluoride is known to react with

glass under acidic conditions via HF to form fluorosilicates and fluoroborates. It was suspected that under neutral to slightly basic conditions, some fluoride loss due to the fluoride-glass reaction might have been occurring during the concentration at elevated temperatures, since it is known that “over-evaporation” often leads to the failure of fluoride incorporation in standard C-<sup>18</sup>F bond forming reactions. To possibly suppress this loss from reactions with glass, containers made of non-glass materials such as polypropylene and glassy carbon, along with Pyrex glass V-vials, were also examined in terms of the <sup>18</sup>F-fluoride dry-down. Based on the failure described above, regarding the importance of the pH values of the <sup>18</sup>F-fluoride solution prior to the solvent evaporation, the <sup>18</sup>F-fluoride solution was basified with KHCO<sub>3</sub> immediately after it was released from the anion exchange column. Moreover, the addition of carrier <sup>19</sup>F-fluoride was also tested to identify whether or not the presence of carrier fluoride during the evaporation process would keep <sup>18</sup>F-fluoride from being consumed by glass.

To accelerate the evaporation process, 1 mL of CH<sub>3</sub>CN was added to the <sup>18</sup>F-fluoride solution to azeotropically remove water. The evaporation of the <sup>18</sup>F-fluoride solution was then carried out at 100 °C under Ar flow, for each test as described in Table 4.1. The evaporation normally took 20 ~ 40 minutes, and the process was always faster in the glass V-vial than in other containers, possibly due to its excellent thermal conductivity. Once all the solvent was removed, <sup>18</sup>F-fluoride was resuspended with the <sup>19</sup>F-fluoride solution. It was also noticed that better resuspension of <sup>18</sup>F-fluoride was actually achieved in the glass V-vials.

The series of tests summarized in Table 4.1 clearly imply that it is not necessary to add carrier fluoride to the <sup>18</sup>F-fluoride eluent prior to the evaporation as long as the solution is kept basic (reactions IX-XII compared with reactions III-VIII). Even for the test on the glassy carbon container, in which the evaporation was undertaken without the addition of <sup>19</sup>F-fluoride or bicarbonate (reactions II), the <sup>18</sup>F-fluoridation of **4.14** succeeded to give the product, albeit with a lower radiochemical yield (11%). This lower yield, which is nonetheless higher than what we first observed at TRIUMF, might be mainly due to some evaporation of H<sup>18</sup>F or because of the insufficient mixing of the 6 μL reaction mixture in the opaque glassy carbon container with a shallow V-shaped bottom. A fluoridation

reaction under more diluted conditions was also carried out. As shown in reaction V with a higher reaction volume (32  $\mu\text{L}$ ) and consequently lowering every reactant's concentration, the radiochemical yield was only 1% after one hour and this implied that the dilution of reactants greatly reduced yields.

**Table 4.1**  $^{18}\text{F}$ -Radiosyntheses of Mar- $^{18}\text{F}$ -ArBF<sub>3</sub> **4.15** under various conditions.

Reaction #	Evaporation Container	Radioactivity at the BOS* (mCi)	t (min)	RCY** (%)
I <sup>a,e</sup>	Falcon tube	6.52	62	21
II <sup>c,l</sup>	Glassy carbon	5.26	63	11
III <sup>a,e</sup>	Glass V-vial	5.63	78	14
IV <sup>a,e</sup>	Falcon tube	2.76	63	15
V <sup>a,d</sup>	Falcon tube	3.02	60	1
VI <sup>a,e,f</sup>	Falcon tube	3.73	65	3
VII <sup>a,e</sup>	Falcon tube	2.84	65	21
VIII <sup>a,b,g</sup>	Glass V-vial	8.79	61	24
IX <sup>b,h,i</sup>	Eppendorf	15.98	60	14
X <sup>b,h,i</sup>	Screw cap tube	13.83	59	17
XI <sup>b,h,j</sup>	Falcon tube	3.65	61	19
XII <sup>b,f,h,k</sup>	Glass V-vial	3.82	57	1

**NOTE:** The evaporation of the  $^{18}\text{F}$ -fluoride eluent that was added with the same volume of  $\text{CH}_3\text{CN}$  was carried out at 100 °C under Ar flow, and 8  $\mu\text{L}$  of 0.125 M  $\text{KHF}_2$  solution (or otherwise noted) was then added to redissolve the residue. The radiosynthesis was carried out similarly as previously described. To simplify the procedure, the  $^{18/19}\text{F}$ -fluoride solution (1.25  $\mu\text{L}$ ) was added the last to the mixture of  $\text{CH}_3\text{CN}$  (4  $\mu\text{L}$ ) solution of freshly purified (or otherwise noted) marimastat-boronate **4.14** (100 nmol) and concentrated HCl (0.5  $\mu\text{L}$ , 6.3  $\mu\text{mol}$ ) in a 500  $\mu\text{L}$  PCR tube (or otherwise noted). The reaction was quenched with 200  $\mu\text{L}$  of 5%  $\text{NH}_4\text{OH}$  in 50% aqueous EtOH and the quenched reaction was injected into the UPLC using HPLC Program 6 with Column III in HPLC System III for analysis. The RCY was determined by the integration percentage of the radio-UPLC traces. \*BOS: beginning of the synthesis; \*\*RCY: radiochemical yield.

- 4  $\mu\text{L}$  of 0.125 M  $\text{KHF}_2$  was added to the  $\text{NaClO}_4$  eluent containing  $^{18}\text{F}$ -fluoride and the pH was adjusted to ~ 8 with 0.95 M  $\text{KHCO}_3$  (~ 6 to 12  $\mu\text{L}$ ) prior to the evaporation.
- The radiosynthesis was undertaken in the presence of a total amount of 625 nmol of  $^{19}\text{F}$ -fluoride.
- No  $^{19}\text{F}$ -fluoride or  $\text{KHCO}_3$  was added to the  $\text{NaClO}_4$  eluent prior to the evaporation of the solvent.
- The reaction was carried out in a total volume of 32  $\mu\text{L}$  (25:7  $\text{CH}_3\text{CN}:\text{H}_2\text{O}$ ) containing 413 nmol of  $^{19}\text{F}$ -fluoride.
- The radiosynthesis was done in the presence of a total of 469 nmol of  $^{19}\text{F}$ -fluoride.
- Marimastat-boronate **4.14** (100 nmol) used was stored at -20 °C for a long time.
- 4  $\mu\text{L}$  of 0.125 M  $\text{KHF}_2$  was added to resuspend the  $^{18}\text{F}$ -fluoride residue after solvent evaporation.
- The evaporation was carried out without carrier  $^{19}\text{F}$ -fluoride at pH ~ 8 in the presence of  $\text{KHCO}_3$ .
- The radiosynthesis was undertaken directly in the evaporation container by adding 4  $\mu\text{L}$  of  $\text{CH}_3\text{CN}$  containing marimastat-boronate **4.14** (100 nmol), 0.5  $\mu\text{L}$  of concentrated HCl (6.3  $\mu\text{mol}$ ), and 1.25  $\mu\text{L}$  of 0.25 M  $\text{KHF}_2$  to the  $^{18}\text{F}$ -fluoride after solvent evaporation.
- 5  $\mu\text{L}$  of 0.25 M  $\text{KHF}_2$  was added to resuspend  $^{18}\text{F}$ -fluoride residue after solvent evaporation.
- 10  $\mu\text{L}$  of 0.25 M  $\text{KHF}_2$  was added to resuspend  $^{18}\text{F}$ -fluoride residue after solvent evaporation.
- The radiosynthesis was undertaken in the presence of a total amount of 500 nmol of  $^{19}\text{F}$ -fluoride.

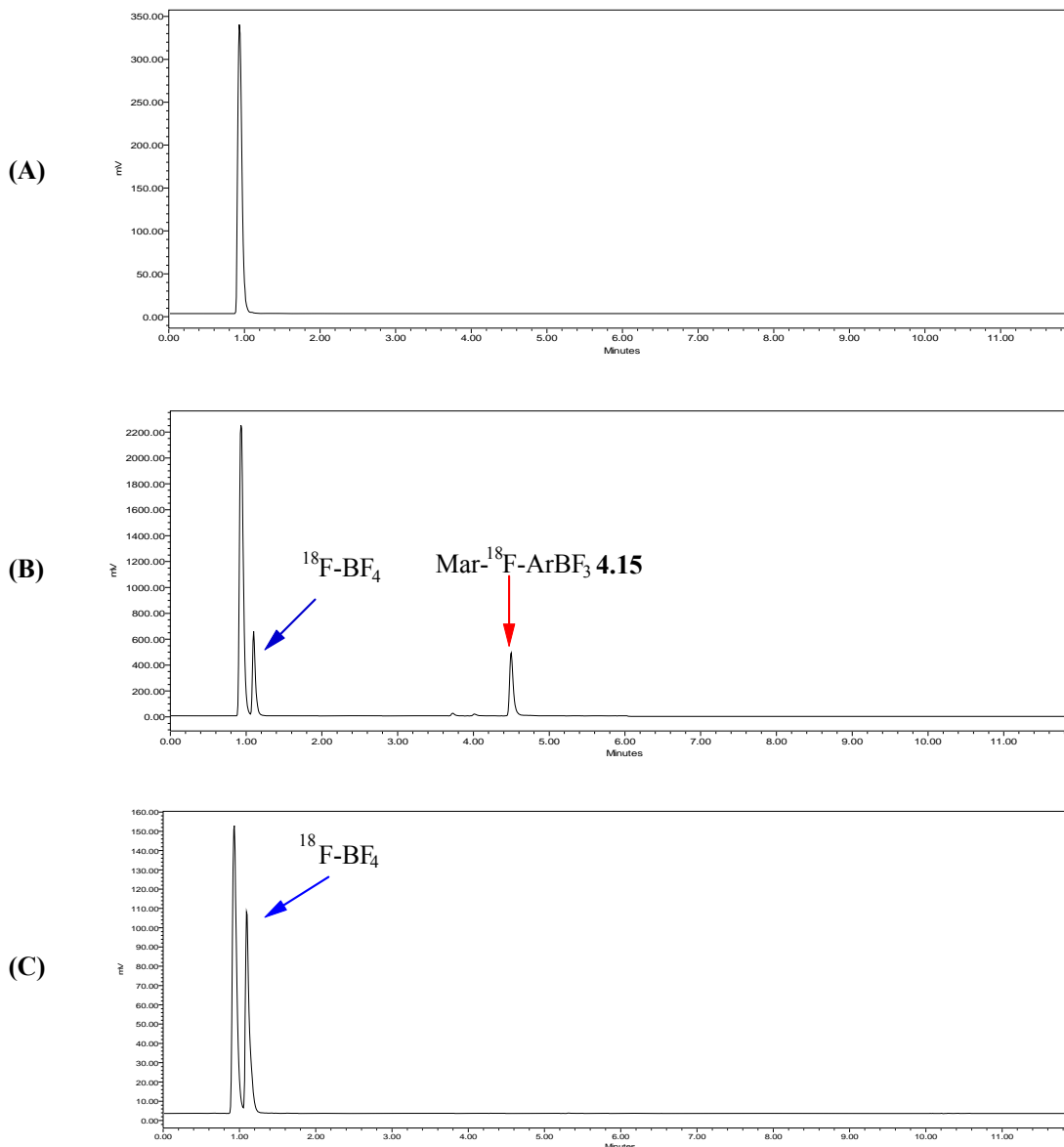


**Figure 4.17 Identification of the byproduct in the  $^{18}\text{F}$ -fluoridation to prepare Mar- $^{18}\text{F}$ -ArBF<sub>3</sub> **4.15**.** (A) The UPLC trace of the reaction in the absence of marimastat-boronate **4.14**; (B) the UPLC trace of reaction III in Table 4.1; (C) the UPLC trace of the radiolabeling of B(OCH<sub>3</sub>)<sub>3</sub>. The reaction conditions: for (A), the  $^{18}\text{F}$ -fluoride solution (containing 469 nmol of  $^{19}\text{F}$ -fluoride), HCl (6.3  $\mu\text{mol}$ ), H<sub>2</sub>O (1.75  $\mu\text{L}$ ), rt, 1 hr (the radioactivity at the BOS: 4.83 mCi); for (B), **4.14** (100 nmol), the  $^{18}\text{F}$ -fluoride solution (containing 469 nmol of  $^{19}\text{F}$ -fluoride), HCl (6.3  $\mu\text{mol}$ ), 69.6% aqueous CH<sub>3</sub>CN (5.75  $\mu\text{L}$ ), rt, 78 min, (the radioactivity at the BOS: 5.63 mCi); for (C),  $^{18}\text{F}$ -fluoride solution (containing 625 nmol of  $^{19}\text{F}$ -fluoride), B(OCH<sub>3</sub>)<sub>3</sub> (326 nmol), HCl (6.3  $\mu\text{mol}$ ) in 69.6% aqueous THF, rt, 56 min (the radioactivity at the BOS: 3.84 mCi). The reactions were quenched with 200  $\mu\text{L}$  5% NH<sub>4</sub>OH in 50% aqueous EtOH prior to the HPLC injection. The UPLC was performed via Program 6 with Column III in HPLC System III. The retention time of Mar- $^{18}\text{F}$ -ArBF<sub>3</sub> **4.15** is 4.5 min and that of  $^{18}\text{F}$ -BF<sub>4</sub><sup>-</sup> is 1.1 min. The peak at 0.9 min is  $^{18}\text{F}$ -fluoride.

Throughout the study on radiolabeling marimastat, a radioactive byproduct other than the desired product Mar- $^{18}\text{F}$ -ArBF<sub>3</sub> **4.15** or free  $^{18}\text{F}$ -fluoride was always present in the

radio-HPLC chromatograms, as shown in Figure 4.13B, Figure 4.14A, and Figure 4.16. In addition, all the radiosyntheses demonstrated in Table 4.1 also produced this very polar product, which eluted at 1.1 minutes directly following  $^{18}\text{F}$ -fluoride that eluted at 0.9 minutes, as the UPLC chromatogram shown in Figure 4.17B for reaction III in Table 4.1. This peak has never been observed in the HPLC with a UV detector, and the radioactive byproduct represented by this peak at 1.1 minutes indicates the advent of a competing reaction accompanying the  $^{18}\text{F}$ -fluoridation of the arylboronate ester. Moreover, when **4.14** had been stored at  $-20\text{ }^{\circ}\text{C}$  for a long time, the radiolabeling of **4.14** gave not only a very poor radiochemical yield (1-2%), but the reaction was also accompanied by this byproduct that was produced in yields of 28-38%. In contrast, the radiolabeling of the newly purified **4.14** had much better  $^{18}\text{F}$ -fluoride incorporation, while the production of this byproduct was much less than that of the desired product. This finding suggests that the radioactive byproduct might be derived from a boronyl-species, which is produced from the deboronation of boronate **4.14** during storage or during the fluoridation.

Although we hypothesized this byproduct might be the  $^{18}\text{F}\text{-BF}_4^-$  anion, we first did a control experiment to examine whether or not this byproduct could be produced in the absence of marimastat-boronate **4.14**. The radio-HPLC trace in Figure 4.17A showed no radioactive peak other than  $^{18}\text{F}$ -fluoride, which indicates that the radioactive byproduct depends on the addition of marimastat-boronate **4.14**. To further test our hypothesis,  $\text{B}(\text{OCH}_3)_3$  was treated with  $^{18/19}\text{F}$ -fluoride under the same conditions for one hour and the radio-HPLC chromatogram shown in Figure 4.17C cleanly produced the radio-peak corresponding to the byproduct that always appears in the radiofluoridation of marimastat-boronate **4.14**. And this supported our hypothesis and suggested the byproduct at 1.1 minutes was  $^{18}\text{F}\text{-BF}_4^-$ .

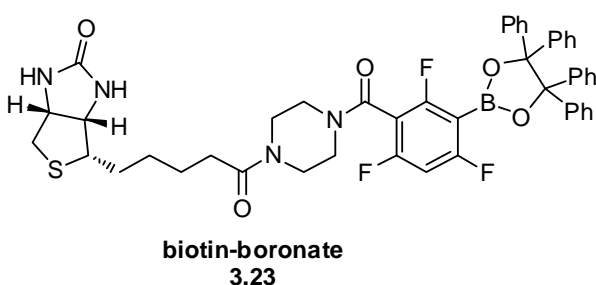
## 4.3 Discussion

### 4.3.1 Synthesis

Marimastat-boronate **4.14** was prepared via a 10-step synthesis in an overall yield of 2.7%. The nucleophilic ring opening of the epoxide to achieve diethyl ester **4.7** is the

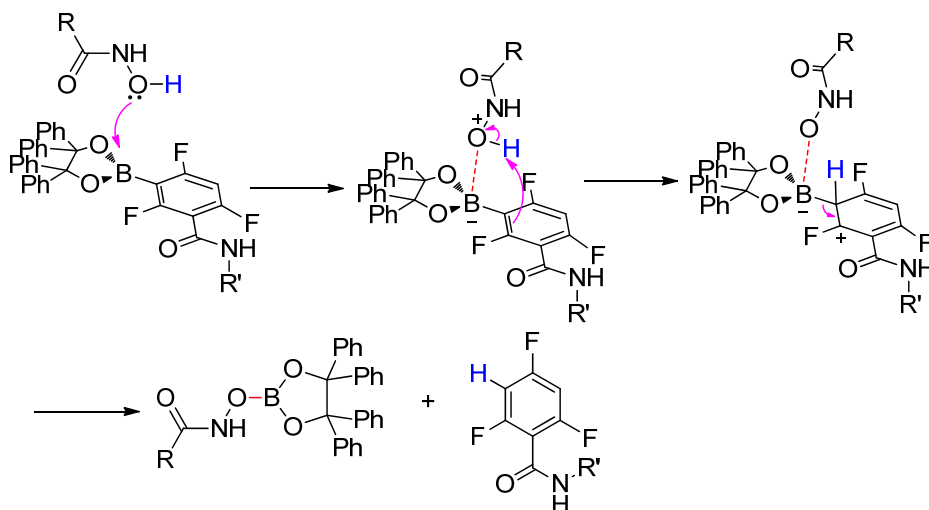
major yield-limiting step. The KCN catalyzed hydroxylaminolysis efficiently converted the methyl ester to the hydroxamic acid. However, there was always some deboronation accompanying the process, and as a result, the yield of the hydroxylaminolysis of **4.13** was compromised. Boronate **4.14** was originally purified by preparative TLC. However, silica gel that is potentially present following TLC purification might compete for fluoride during the fluoridation reaction. This led us to employ semi-preparative reverse phase HPLC (RP-HPLC) to purify marimastat-boronate **4.14** for the radiolabeling experiments. A further modification on the purification was achieved via flash chromatography to give marimastat-boronate **4.14** with good purity, which was characterized by NMR spectroscopy and re-analyzed by RP-HPLC.

Compound **4.14** is relatively stable at lower temperatures ( $\leq -20$  °C). However, slow



deboronation was observed with samples that had been stored for a long period of time. This deboronation during storage is quite abnormal. For example, we prepared and purified biotin-boronate **3.23** via flash chromatography in

February 2009 and stored it at 4 °C since then. The compound was rechecked by HPLC in January 2011; the HPLC trace suggested that biotin-boronate **3.23** was with very good quality of more than 95% purity.



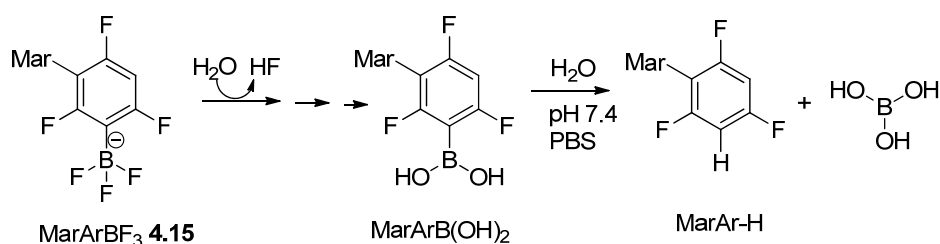
**Scheme 4.2** The proposed mechanism of the deboronation of marimastat-boronate **4.14**.

The difference between the stability of marimastat-boronate **4.14** and biotin-boronate **3.23** highly suggests that the nucleophilic groups on **4.14** such as the hydroxamate and the  $\alpha$ -hydroxyl group might interact with the boron group and promote the cleavage of the C-B bond. The hydroxamate group might serve as a nucleophile, which may add into the boron's empty *p*-orbital *intra*- or *inter*-molecularly allowing the proton to transfer to the benzene ring, which promotes the C-B bond cleavage to give the deboronated product and borate, as proposed in Scheme 4.2. The borate, under radiofluoridation conditions, is rapidly converted to  $^{18}\text{F-BF}_4^-$ , which has been corroborated by the study of the factors influencing the radiosynthesis of **4.15** in section 4.2.8. The deboronation could occur not only during storage but also during the fluoridation reaction itself via an acidic protodeboronation mechanism (not shown), and this would be consistent with the fact that all fluoridations of marimastat-boronate **4.14** tested in this chapter yielded some  $^{18}\text{F-BF}_4^-$  as the byproduct. The identification of the byproduct was based on the chemical correlation via the  $^{18}\text{F}$ -fluoridation of  $\text{B}(\text{OCH}_3)_3$ , which gave  $^{18}\text{F-BF}_4^-$  with the same retention time of the byproduct present in the fluoridation of marimastat-boronate **4.14**. In addition, in the fluoridation of marimastat-boronate **4.14** stored for a very long time (~half a year), a much higher amount of the byproduct  $^{18}\text{F-BF}_4^-$  was produced and this implies that the deboronation of compound **4.14** occurs during storage and it is most likely because of the nucleophilic property of the hydroxamate residue.

### 4.3.2 The *in vitro* stability of MarArBF<sub>3</sub> **4.15**

The half-life of the solvolysis of MarArBF<sub>3</sub> **4.15** was measured as  $1236 \pm 50$  minutes at pH 7.4 in PBS buffer, which equals eleven half-lives of  $^{18}\text{F}$ -fluorine ( $t_{1/2} = 109.8$  min). Its high *in vitro* solvolytic stability suggests it is suitable to be used for *in vivo* studies. Although the hydrolysis followed a first order decay kinetics as shown in Figure 4.4, there was no corresponding arylboronic acid produced during the solvolysis. Instead, a deboronated product was produced, based on the two newly produced Ar-F  $^{19}\text{F}$ -signals (-25 ppm and -33 ppm with an integration ratio of 1:2). This is possibly due to the fast deboronation of the free boronic acid resulting from the solvolytic fluoride loss under the given conditions. We thus hypothesize that the solvolysis of MarArBF<sub>3</sub> **4.15** comprises two independent steps. The first step is the defluoridation of the ArBF<sub>3</sub> to release the

ArB(OH)<sub>2</sub>, which directly undergoes a rapid second step, namely deboronation as shown in Scheme 4.3. The deboronation is assumed to be rapid because there was no hydrolysis product MarArB(OH)<sub>2</sub> present in the <sup>19</sup>F NMR spectra, besides MarArBF<sub>3</sub> **4.15**, free fluoride and the deboronated product MarAr-H. This is possibly the case based on our experience in preparing arylboronic acids such as MarArB(OH)<sub>2</sub> with the same arylboronic acid. We have never been able to obtain the free arylboronic acid but only the protected variants. What had been obtained instead were identified as the deboronated products, which have characteristic <sup>19</sup>F NMR chemical shifts and an integration ratio of the different <sup>19</sup>F-signals of the Ar-F's (1:2).



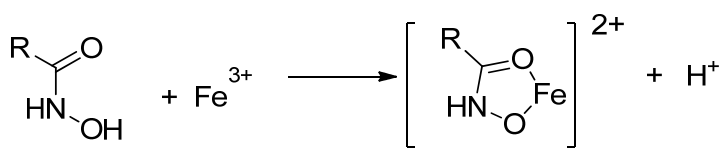
**Scheme 4.3** The proposed mechanism of the solvolysis of MarArBF<sub>3</sub> **4.15**.

### 4.3.3 The acid stability of hydroxamic acids

The <sup>18</sup>F/<sup>19</sup>F-fluoridation of arylboronates proceeds under acidic conditions (pH ≤ 1). If under such conditions, the key structure of the compound is altered to lose its function, the compound may not be a suitable substrate for this direct labeling method. The reports<sup>165-167</sup> on the acid catalyzed hydrolysis of hydroxamic acids at higher temperatures brought our attention to the acid stability of marimastat at room temperature. Since the hydroxamic acid is the key functional group that coordinates zinc(II) in the active site of MMPs, the hydrolysis of the hydroxamic acid would result in loss of its inhibitory activity. Therefore, we employed two methods to measure the stability of two different model hydroxamic acids **4.17** and **4.18** at acidities similar to those used in the fluoridation reaction. Both the ferriin test and <sup>19</sup>F NMR kinetics studies, suggest relatively stable properties of the hydroxamic acids under acidic conditions at room temperature.

*N*-Hydroxy-2-phenylacetamide **4.17** treated with the acid for different incubation periods was mixed with Fe(III) in ethanol to give an instant color change due to the

formation of the stable Fe(III) complex as shown in Scheme 4.4.<sup>172</sup> Moreover, it has been reported that Fe(III)-hydroxylamine is a good redox pair under acidic conditions that hydroxylamine reduces Fe(III) to Fe(II) and itself is oxidized to nitrous oxide,<sup>173</sup> which would not interfere with the UV absorption of the Fe(III)-hydroxamate complexes. Since an excess amount of Fe(III) was used in the experiment, only Fe(III)-**4.17** complex accounts for the UV absorption at the wavelength from 400 to 800 nm. The UV absorbance (300 nm to 800 nm) of the mixture was measured as shown in Figure 4.5, and very minor changes among different time points were observed. This suggested hydroxamic acid **4.17** was acid stable at least for a short incubation time of six hours.



Scheme 4.4 Chelation between the hydroxamic acid and Fe<sup>3+</sup>.<sup>172</sup>

In addition, a series of <sup>1</sup>H NMR spectra were recorded with both **4.17** and **4.18** in 1:1 D<sub>2</sub>O:*d*<sub>6</sub>-DMSO containing D<sub>2</sub>SO<sub>4</sub> as demonstrated in Figure 4.6 and Figure 4.7 respectively. Both compounds were consumed in this acidic solution. Hydroxamic acid **4.17** tended to fully hydrolyze with a half-life of 260 minutes to give phenylacetic acid, which was identified by analytical HPLC. However, hydroxamic acid **4.18** reached equilibrium instead, since there was nearly no change in <sup>1</sup>H NMR signals after ~ 17 hours.

As most of the <sup>18</sup>F-fluoridation reactions are carried out for one hour, any arylboronate bioconjugate would be suitable for the labeling method if a majority of the bioligand remains intact in one hour. For both cases, about 15% of the hydroxamic acids in the presence of 3.4 M of D<sup>+</sup> were consumed after one hour incubation. Furthermore, the concentration of acid (3.4 M) used for the <sup>19</sup>F NMR study is likely to be greater than that used in the <sup>18</sup>F-fluoridation reactions (< 1.5 M). Therefore, the hydrolysis of marimastat-boronate **4.14** during the radiolabeling would be less severe than that of **4.17** or **4.18** studied by NMR spectroscopy. Moreover, MarArBF<sub>3</sub> **4.15**, prepared under acidic conditions was tested for its inhibitory activity. Its IC<sub>50</sub> value of 1.88 nM, shown in 4.2.4, strongly indicates that the hydroxamic acid residue of **4.15** remained intact during the labeling process and hence marimastat-boronate **4.14** had relatively high acid stability.

#### 4.3.4 *In vitro* enzyme inhibitory activity of MarArBF<sub>3</sub> 4.15

To determine the IC<sub>50</sub> value of an enzyme inhibitor *in vitro*, the inhibitor concentration must be known. However, the concentration of MarArBF<sub>3</sub> 4.15 has been difficult to determine. This is mainly due to the difficulty in preparing a large quantity of MarArBF<sub>3</sub> 4.15 with high purity for use as a standard solution, which can be then used to construct a standard curve by plotting UV absorbance against the concentration (with a series of dilutions) at the maximum absorption wavelength. Although marimastat is a weak chromophore, its hydroxamic group is found to form a very stable hydroxamate-Fe(III) complex, which has strong UV absorption. Indeed, the formation of Fe(III)-hydroxamate complexes has been used to accurately measure the concentration of various hydroxamic acids. Since the formation of the complexes occurs upon mixing, and the Fe(III)-hydroxamate complexes have strong UV properties, this method is regarded as rapid and relatively accurate. Hence, we adopted this method to measure the concentration of the hydroxamic acid MarArBF<sub>3</sub> 4.15, involving the Fe(III)-hydroxamate complex formation, which we call here the “ferroin test”. First, a large excess of Fe(III) was used to consume all the hydroxamic acid to form only the mono-hydroxamate-Fe(III) complex. By measuring the UV-absorbance at 499 nm for Fe(III)-hydroxamate complex, a standard curve could be set up if the concentrations of the complex are known. As mentioned, it is difficult to prepare a stock solution of MarArBF<sub>3</sub> 4.15 with a known concentration. A structurally similar compound Cbz-PEG-Mar 4.16 was prepared. It was believed that, the aryl groups in both molecules play negligible roles in the formation of the Fe(III)-hydroxamate complexes and would not interfere with the UV absorption properties of the complexes at 499 nm.

The UV absorbance at 499 nm was measured right after the hydroxamate was mixed with a large excess of Fe(III) solution. It is hypothesized that all of the hydroxamate molecules present in the solution coordinate the Fe(III) cations, which means the concentration of the Fe(III)-hydroxamate complex can be calculated based on the amount of the hydroxamate added to the chelation reaction. The extinction coefficients of the Fe(III)-complexes with both 4.16 and the commercially purchased marimastat were determined via this method. It was found that the extinction coefficients of the

Fe(III)-hydroxamate complexes are very close to each other ( $1526 \text{ cm}^{-1}\text{M}^{-1}$  for Fe(III)-**4.16** v.s.  $1560 \text{ cm}^{-1}\text{M}^{-1}$  for Fe(III)-marimastat at 499 nm), which implies that the derivatization from the C-terminus of the *tert*-leucine residue contributes little to the absorption at 499 nm for the Fe(III)-complex. We thus employed the extinction coefficient of the complex Fe(III)-**4.16**, which shares more structural identities with the complex Fe(III)-MarArBF<sub>3</sub> (Fe(III)-**4.15**). Instead of directly using the extinction coefficient of the complex Fe(III)-**4.16**, a dilution calibration curve was created for the complex Fe(III)-**4.15**. The slope of this dilution calibration curve should be proportional to its concentration and the extinction coefficient, which herein is regarded the same to that of Fe(III)-**4.16**. Then the concentration of the stock solution of **4.15** was determined to be 9.07 mM.

Subsequently, marimastat and its various derivatives were tested for their enzymatic inhibitory activities. All the compounds demonstrated very potent activities in the range of 1-5 nM. This is consistent with the literature report that the derivatization from the C-terminus of *tert*-leucine would not interfere with its inhibitory potency and/or specificity.<sup>168</sup>

### **4.3.5 Cell binding assays with fluorescent marimastat-FITC**

In order to investigate the binding of marimastat to purified MMPs and to cell expressed MMPs, fluorescent marimastat-FITC **4.19** was synthesized. The renatured recombinant human MMPs, resolved by SDS-PAGE, were first incubated with marimastat-FITC **4.19** and the gel image from Alpha Image System shown in Figure 4.10A illustrated the specific binding of **4.19** to MMPs. A cell binding assay was further undertaken with the breast cancer cell line MDA-MB-231 transfected with human MMP14 or the empty vector. Cells were treated with **4.19**, counterstained with Hoechst to reveal the nucleus via DNA staining and then imaged by fluorescent microscopy. The cell assay images in Figure 4.10C further supported the synthetic **4.19** specifically bound to MMP14 outside of the cell nucleus.

### 4.3.6 *In vivo* PET imaging of MMPs in murine breast carcinomas

$^{18}\text{F}$ -Labeled MarArBF<sub>3</sub> **4.15** was prepared from marimastat-boronate **4.14** (100 nmol) and  $^{18}\text{F}$ -fluoride with carrier  $^{19}\text{F}$ -fluoride (300 ~ 400 nmol) under acidic conditions (pH < 1) for one hour, and then purified by RP-HPLC. The radiosynthesis of Mar- $^{18}\text{F}$ -ArBF<sub>3</sub> **4.15** for animal imaging work was achieved with an isolated (unoptimized) radiochemical yield of ~ 1.5%. Mar- $^{18}\text{F}$ -ArBF<sub>3</sub> **4.15** was then formulated in 1 × PBS saline and injected into female BALB/c mice with 67NR tumors. Two independent radiosyntheses gave Mar- $^{18}\text{F}$ -ArBF<sub>3</sub> **4.15** with specific activities of 0.179 Ci/μmol and 0.396 Ci/μmol at the time of packaging, values that were calculated based on tripling the specific activity of the source carrier-added  $^{18}\text{F}$ -fluoride at the BOS and then corrected for decay during the time of the synthesis.<sup>a</sup> Both values of specific activity were somewhat lower than 1 Ci/μmol, which is often regarded as a benchmark for animal imaging. However, there is no general standard for the minimal specific activity and in fact there have been several reports that provide moderate-to-good PET images<sup>61, 174, 175</sup> with specific activity values similar to those we obtained herein.

The relatively low tumor-to-background ratio in the PET images obtained, as shown in Figure 4.15, is similar as some previously reported MMP imaging probes based on MMPIs.<sup>138, 144, 158, 176</sup> In spite of that, the tumor uptake of this compound was specific as indicated by the blocking experiment, which fully blocked the tumor uptake of Mar- $^{18}\text{F}$ -ArBF<sub>3</sub> **4.15** after the pretreatment of the mice with unlabeled marimastat one hour before the injection of the radiotracer. Nevertheless, no significant improvement in image quality was obtained by increasing the specific activity of the radiotracer (from 0.179 to 0.396 Ci/μmol).

High uptake of Mar- $^{18}\text{F}$ -ArBF<sub>3</sub> in other tissues was also observed. This may be due to the fact that some normal tissues such as liver are known to express MMPs non-pathologically. Moreover, there are various MMPs in the blood. This is problematic for the broad-spectrum MMP inhibitors and could result in high background uptake compared to specific tumor uptake of the radiotracer. Hence, the low uptake of the tracer

---

<sup>a</sup> For more information about the calculation of specific activity, please refer to Chapter 1.

at the tumor position described herein most likely is due to the broad-spectrum nature of marimastat itself.

Bone and joint uptake was also observed in the images viewed at high contrast. This implied some free  $^{18}\text{F}$ -fluoride contaminated in the radiotracer, which might be either due to the *in vivo* decomposition of Mar- $^{18}\text{F}$ -ArBF<sub>3</sub> **4.15** to release  $^{18}\text{F}$ -fluoride or because of the imperfect separation of the radiotracer from  $^{18}\text{F}$ -fluoride.<sup>a</sup> The *in vivo* biodistribution/imaging work with biotin- $^{18}\text{F}$ -ArBF<sub>3</sub> from the radiolabeling of biotin-boronate **3.23** showed absolutely no bone uptake of the radioactivity,<sup>79</sup> and thus suggested the high *in vivo* stability of similar ArBF<sub>3</sub>s with the same aromatic system. On the other hand, although it is not a good idea to use the same HPLC column for both separation and analysis purposes, the analytical HPLC undertaken with the same column to check the radiochemical purity of the radiotracer, shown in Figure 4.13D and Figure 4.14B, implied there were trace amounts (< 5%) of free  $^{18}\text{F}$ -fluoride in the radiotracer. Moreover, the high radioactivity retained on the C18 column after the injection for the HPLC separation (with a high radioactivity injected) might have been the source of  $^{18}\text{F}$ -fluoride seen in the second injection on the same HPLC C18 column. Consequently, it was hard to identify the source of free  $^{18}\text{F}$ -fluoride present at the second HPLC injection.

Besides the possibility of free  $^{18}\text{F}$ -fluoride accounting for the joint uptake of the radioactivity, it is worthwhile to note that musculoskeletal toxicity is one of the major side effects of marimastat during clinical trials; it may imply that there are abundant MMPs near or at the joints that would have also bound  $^{18}\text{F}$ -labeled marimastat. Towards these ends, no further study was carried out to clarify the reasons for why radioactivity was seen in joints and bone. Moreover, in terms of the animal images, Dr. Francois Benard assisted us in rendering the images and visualizing dynamic distributions *in vivo*. Based on personal communication with him, tumor:blood ratio was approximately 1.4:1. However, since tumor specific uptake could only be observed at very high contrast, the error on the data was considered to be quite large and no further quantification in terms

---

<sup>a</sup>  $^{18}\text{F}$ -Fluoride might also come from decomposition of Mar- $^{18}\text{F}$ -ArBF<sub>3</sub> **4.15** during rotoevaporation. It was noticed that the water bath reached 50 °C during the rotoevaporation and this might promote the hydrolysis of Mar- $^{18}\text{F}$ -ArBF<sub>3</sub>.

of standard uptake values was undertaken.

### 4.3.7 Some factors related to the $^{18}\text{F}$ -fluoridation of marimastat-boronate 4.14

Mar- $^{18}\text{F}$ -ArBF<sub>3</sub> **4.15** was prepared and used to image the breast cancer in mice. Although the result of the imaging work was promising, the low radiochemical yield of the radiosynthesis raised questions about what factors influence the  $^{18}\text{F}$ -fluoridation of arylboronates including the production of the major byproduct of the  $^{18}\text{F}$ -fluoridation that had been refractory to characterization until now. In Chapter 3, several elements for the fluoridation were studied, such as the concentrations of reactants, the reaction medium, and salt effects; the reaction conditions have been at least partially optimized. Moreover, in section 4.2.6.1, it was found that CH<sub>3</sub>CN seemed a better cosolvent for the fluoridation than DMF whereas the addition of reductants did not influence the radiofluoridation of marimastat-boronate **4.14**. However, there are more factors that need considering in the radioactive reactions. As part of the collaboration with Dr. John Valliant and Dr. Karin Stephenson, a study was undertaken for two factors that might influence the incorporation of  $^{18}\text{F}$ -fluoride for Mar- $^{18}\text{F}$ -ArBF<sub>3</sub> **4.15** in order to identify the major radioactive byproduct, which elutes right after free  $^{18}\text{F}$ -fluoride in the HPLC. In addition, it was later found that reductants, at least for the levels of radioactivity used at the CPDC, were not necessary.

Different dry-down conditions for  $^{18}\text{F}$ -fluoride were tested for the labeling. We first noticed that it is critical to keep the  $^{18}\text{F}$ -fluoride solution basic for evaporation, especially when using glass containers. At lower pHs,  $^{18/19}\text{F}$ -fluoride tends to react with the borosilicate based glass during the evaporation. H $^{18/19}\text{F}$  also evaporates at elevated temperatures. Either case decreases the amount of effective  $^{18}\text{F}$ -fluoride in the dry-down container. Other than this, the quality of the “dry”  $^{18}\text{F}$ -fluoride concentrated in different containers showed no difference regarding the fluoridation of marimastat-boronate **4.14** as shown in Table 4.1.

The addition of carrier fluoride to the  $^{18}\text{F}$ -fluoride eluent from the anion exchange column prior to the solvent evaporation was first expected to suppress the loss of

$^{18}\text{F}$ -fluoride from any path, especially in the case of glass vials, which are much easier to work with due to the ease of handling. However, it was found that as long as the no-carrier-added  $^{18}\text{F}$ -fluoride solution remains basic, the removal of water from the  $^{18}\text{F}$ -fluoride solution requires no added  $^{19}\text{F}$ -fluoride. Furthermore, if carrier fluoride is added prior to the evaporation, it would be easy to obtain the specific activity of  $^{18}\text{F}$ -fluoride. However, as the sufficient resuspension of  $^{18/19}\text{F}$ -fluoride with a small volume of the aqueous solution is very hard to achieve, the stoichiometric ratio of the boronate to fluoride would be difficult to control. This may in fact influence the radiochemical yield. Nevertheless, no-carrier-added  $^{18}\text{F}$ -fluoride solution for evaporation was preferred thereafter.

A radioactive byproduct ( $t_R = 1.1$  min) eluting right after  $^{18}\text{F}$ -fluoride is often present in the radiosynthesis of  $^{18}\text{F}$ -ArBF<sub>3</sub> **4.15**. It was successfully proved to be  $^{18}\text{F}$ -BF<sub>4</sub><sup>-</sup> by the  $^{18}\text{F}$ -fluoridation of B(OCH<sub>3</sub>)<sub>3</sub>. Since  $^{19}\text{F}$ -BF<sub>4</sub><sup>-</sup> is “invisible” to the UV detection, the cold experiment with  $^{19}\text{F}$ -fluoride never suggested this valuable information. Obviously,  $^{19}\text{F}$ -BF<sub>4</sub><sup>-</sup> was not extracted into DMSO since the  $^{19}\text{F}$  NMR spectroscopy did not suggest any contamination of BF<sub>4</sub><sup>-</sup> in the DMSO extracted MarArBF<sub>3</sub> **4.15**. As this byproduct either originated from the deboronation of **4.14** during the storage as proposed in Scheme 4.2 or during the fluoridation itself, the radiochemical yield for the radiolabeling of the desired product Mar- $^{18}\text{F}$ -ArBF<sub>3</sub> **4.15** was compromised. This is the case especially for the fluoridation of marimastat-boronate **4.14** that had been stored for a longer time, and this sample always gave lower radiochemical yields to prepare Mar- $^{18}\text{F}$ -ArBF<sub>3</sub> **4.15** and correspondingly high radiochemical yields of  $^{18}\text{F}$ -BF<sub>4</sub><sup>-</sup> compared with the freshly purified boronate **4.14**. This may further suggest the deboronation of boronate **4.14** occurs upon storage, and good quality of boronates for the radiofluoridation is considerably important for high radiochemical yields. Nevertheless, the production of some  $^{18}\text{F}$ -BF<sub>4</sub><sup>-</sup> in the fluoridation of the newly purified boronate **4.14** implies that there might be some deboronation during the fluoridation, although the mechanism of the deboronation under acidic conditions might be different. This might also compromise radiochemical yields to some extent.

In conclusion, it was also found that there is no difference among the evaporation

containers made of different materials, only if the evaporation is processed under basic conditions. Carrier fluoride might not be necessarily added to  $^{18}\text{F}$ -fluoride prior to the evaporation, and it is believed that it is more reasonable to add carrier after the evaporation for better control of the radiolabeling reaction. In addition, since non-glass based containers can be directly used for the acidic fluoridation, containers, such as the polypropylene and glassy carbon vials, should be directly used for the fluoridation to maximize the specific activity by reducing the amount of carrier fluoride added to the source  $^{18}\text{F}$ -fluoride. Overall, the radiochemical yields of the fluoridation could reach 15-20% to give Mar- $^{18}\text{F}$ -ArBF<sub>3</sub> **4.15** after one hour reactions at room temperature.

## 4.4 Conclusion

The *in vivo* imaging of Mar- $^{18}\text{F}$ -ArBF<sub>3</sub> **4.15** represents a key development in PET imaging by employing the  $^{18}\text{F}$ -ArBF<sub>3</sub> technique developed in our lab. Mar- $^{18}\text{F}$ -ArBF<sub>3</sub> **4.15** was prepared via a one-step labeling reaction under acidic aqueous conditions at room temperature and isolated radiochemical yields of ~ 1.5% were obtained. The specific activities of 0.179 Ci/ $\mu\text{mol}$  and 0.396 Ci/ $\mu\text{mol}$  were achieved for the animal imaging. The *in vivo* imaging with Mar- $^{18}\text{F}$ -ArBF<sub>3</sub> **4.15** in the mice carrying breast cancer proved to be specific. This work represents the first *in vivo* PET imaging of MMPs employing marimastat and indicates that the labeling via this method can provide useful PET probes for human diagnosis, drug evaluation, and target validation.

In addition, the further study of the radiosynthesis of Mar- $^{18}\text{F}$ -ArBF<sub>3</sub> **4.15** in collaboration with Dr. John Valliant and Dr. Karin Stephenson at the CPDC has revealed several important factors to ensure the success of the radiolabeling technique. The identification of the byproduct peak as  $^{18}\text{F}$ -BF<sub>4</sub><sup>-</sup> highly suggests the importance of the quality of boronate substrates prior to use in the labeling to reduce the competition reactions for  $^{18}\text{F}$ -fluoride by liberated borates. This finding resulted in radiochemical yields of radiofluoridation that were closer to 10%. The evaporation of the  $^{18}\text{F}$ -fluoride solution can be done in different containers without carrier fluoride added, as long as the solution is basic, especially in regard to glass containers. As the efficiency of resuspending  $^{18}\text{F}$ -fluoride is always limited to some extent, reactions in non-glass based vials would be attractive alternatives, especially for reactions using high amounts of

radioactivity. Further investigation of the  $^{18}\text{F}$ -fluoridation kinetics and other factors such as the  $^{18}\text{F}$ -fluoride elution buffer, acids, solvents, and higher temperatures might be useful to drive the technique forward for higher yielding radiosyntheses.

Overall, in this chapter, we successfully radiolabeled marimastat-boronate **4.14** with  $^{18}\text{F}$ -fluoride in the presence of carrier fluoride under acidic conditions. The animal image, in spite of poor resolution, demonstrated specific tumor uptake. Further imaging work with  $^{18}\text{F}$ -ArBF<sub>3</sub> labeled biomolecules may provide more useful information to validate the method as a promising PET imaging technique.

## 4.5 Materials and methods

Commercially available chemicals were purchased from Novabiochem, Sigma-Aldrich, Acros Organics, Oakwood or Alfa Aesar. Solvents were obtained from Fisher Scientific and used without further purification unless otherwise noted. When required, solvents were dried following standard protocols.<sup>129</sup> The  $^{18}\text{F}$  Trap & Release column ( $\text{HCO}_3^-$  form, ~ 10 mg) was purchased from ORTG, Inc., or the Sep-Pak Light Accell Plus QMA cartridge ( $\text{Cl}^-$  form) 37 ~ 50  $\mu\text{m}$  was obtained from Waters.  $d_2$ -D<sub>2</sub>SO<sub>4</sub> was obtained from Sigma-Aldrich and other deuterated solvents were purchased from Cambridge Isotope Laboratories. TLC analysis was performed on aluminium-backed silica gel-60 plates from EMD Chemicals. Flash chromatography was carried out on SiliaFlash F60 (230-400 mesh) from SiliCycle. ESI-LRMS was performed on a Waters ZQ with a single quadrupole detector, attached to a Waters 2695 HPLC. ESI-HRMS were obtained on a Waters-Micromass LCT with a time-of-flight (TOF) detector. All NMR spectra were recorded on Bruker Avance instruments, with results reported as chemical shift ( $\delta$ ) in *ppm*. Unless specified,  $^1\text{H}$  NMR spectra are referenced to the trimethylsilane peak ( $\delta = 0.00$  *ppm*),  $^{13}\text{C}$  NMR spectra are referenced to the chloroform peak ( $\delta = 77.23$  *ppm*), and  $^{19}\text{F}$  NMR spectra are referenced to neat trifluoroacetic acid ( $\delta = 0.00$  *ppm*,  $-78.3$  *ppm* relative to  $\text{CFCl}_3$ ). The UV spectra reported were all obtained on a Beckman Coulter DU800 in 1 cm quartz cuvettes. All the HPLC information can be found in Appendix B.

MDA-MB-231 breast carcinoma cells were kindly provided by Dr. V. C. Jordan (Northwestern University, Chicago, IL) and the murine breast cancer cell line 67NR was

kindly provided by Dr. Fred Miller (Karmanos Cancer Institute, Detroit, MI). All the biological work described in this chapter was done in the Overall lab.

**WARNING:** All  $^{18}\text{F}$ -labeling work was done at TRIUMF or at the CPDC. Radiation protection procedures strictly followed the TRIUMF Radiation Safety Regulations. Since this work involves mainly manual handling, fairly high amounts of dosage might be applied, and special caution is required to reduce the operating time. A lead brick castle was built up to shield the radiation. All the materials that came in contact with the source water (the  $^{18}\text{O}$ -water) were collected and decayed separately from other  $^{18}\text{F}$ -contaminated stuffs including gloves, sleeves, vials, tubes, and pipette tips prior to disposal.

### 4.5.1 Synthesis

#### Benzyl 2-(2-(2-aminoethoxy)ethoxy)ethylcarbamate (4.1)

CbzOSu (3.30 g, 13.2 mmol) in 1,4-dioxane (100 mL) was dropwise added to the neat 2,2'-(ethylene-dioxy)bis(ethylamine) (10.0 mL, 68.5 mmol) over an ice-water bath.<sup>177</sup> The reaction was then incubated at rt overnight. The mixture was concentrated under vacuum and the residue mixture was resuspended in  $\text{CH}_2\text{Cl}_2$  (100 mL). The resulting  $\text{CH}_2\text{Cl}_2$  solution was washed with water ( $3 \times 50$  mL) and brine ( $1 \times 50$  mL). Dried over anhydrous  $\text{Na}_2\text{SO}_4$ , the  $\text{CH}_2\text{Cl}_2$  solution was concentrated under reduced pressure to give sticky oil. The desired product ( $R_f = 0.29$  in 0.1:1:9  $\text{NEt}_3$ :MeOH: $\text{CH}_2\text{Cl}_2$ ) was purified via flash chromatography (MeOH: $\text{CH}_2\text{Cl}_2$  5:95 then 1:9). Yield: 1.58 g, 42%.  $^1\text{H}$  NMR (400 MHz,  $\text{CD}_2\text{Cl}_2$ , rt):  $\delta$ (ppm) 1.38 (s, 2 H), 2.8 (s, 2 H), 3.36 (q,  $J = 5.25$  Hz, 2 H), 3.46 (t,  $J = 5.24$  Hz, 2 H), 3.54-3.61 (m, 6 H), 5.10 (s, 2 H), 5.86 (s, br, 1 H), 7.34 (m, 5 H);  $^{13}\text{C}$  NMR (100.6 MHz,  $\text{CD}_2\text{Cl}_2$ , rt):  $\delta$ (ppm) 41.05, 41.88, 66.41, 70.07, 70.25, 70.44, 73.59, 128.03, 128.54, 137.27, 156.54; ESI-LRMS:  $[\text{M}+\text{Na}]^+$ , 305.3 (100%).

#### *N*-Boc-*L*-tert-leucine (4.2)

*L*-tert-Leucine (1.18 g, 7.62 mmol) and NaOH (0.45 g, 11.25 mmol) were dissolved in 10 mL of water.<sup>178-180</sup> To this solution, was slowly added  $(\text{Boc})_2\text{O}$  (2.16 g, 9.90 mmol) in 10 mL of  $^t\text{BuOH}$ . The resulting mixture was then stirred at rt for 20 hr. The reaction mixture was first extracted with  $\text{Et}_2\text{O}$  ( $3 \times 50$  mL). The ether layer was further washed with saturated  $\text{NaHCO}_3$  (50 mL). The combined aqueous layer was later acidified to pH

< 1 and then extracted with EtOAc (3 × 50 mL). Washed with water (50 mL) and brine (50 mL), the EtOAc layer was dried over anhydrous Na<sub>2</sub>SO<sub>4</sub> and then concentrated under vacuum to give colorless oil, which was used without further purification. Yield: 1.90 g, 92%. <sup>1</sup>H NMR (300 MHz, CDCl<sub>3</sub>, rt): δ(ppm) 1.04 (s, 9 H), 1.47 (s, 9 H), 4.15 (d, *J* = 8.92 Hz, 1 H), 5.12 (d, *J* = 7.07 Hz, 1 H); <sup>13</sup>C NMR (75.5 MHz, CDCl<sub>3</sub>, rt): δ(ppm) 26.67, 28.46, 34.60, 61.77, 80.18, 155.79, 176.79; ESI-LRMS: [M+Na]<sup>+</sup>, 254.3(100%); [M-H]<sup>-</sup>, 230.4 (100%).

**(S)-Benzyl-2-(2-(2-(2-*N*-Boc-amino-3,3-dimethylbutanamido)ethoxy)ethylcarbamate (4.3)**

To solution of Boc-*L*-*tert*-leucine **4.2** (365 mg, 1.58 mmol) and amine **4.1** (455 mg, 1.61 mmol) in CH<sub>2</sub>Cl<sub>2</sub> (10 mL) was added with DIPEA (0.74 mL, 4.22mmol) and TBTU (621 mg, 1.93 mmol) at rt; the reaction was stirred overnight. The reaction was quenched by saturated NaHCO<sub>3</sub> (30 mL) and the aqueous layer was extracted with CH<sub>2</sub>Cl<sub>2</sub> (3 × 50 mL). The organic layers were combined and washed with H<sub>2</sub>O (1 × 50 mL), 3 N HCl (1 × 50 mL), H<sub>2</sub>O (1 × 50 mL), and brine (1 × 50 mL), and then dried over anhydrous Na<sub>2</sub>SO<sub>4</sub>. The solution was concentrated and purified by silica gel chromatography (EtOA:hexanes, 1:4 then 1:1 then 1:0) to afford sticky oil or white foam (*R<sub>f</sub>* = 0.58 in 1:9 MeOH:CH<sub>2</sub>Cl<sub>2</sub>). Yield: 780 mg, quant. This compound can also be obtained with HBTU (1.32 eq.) in a coupling reaction, which gives a 92% isolated yield. <sup>1</sup>H NMR (300 MHz, CDCl<sub>3</sub>, rt): δ(ppm) 0.96 (s, 9 H), 1.41 (s, 9 H), 3.59-3.40 (m, 12 H), 3.79 (br, d, *J* = 7.3 Hz, 1 H), 4.16 (m, 1 H), 5.10 (s, 2 H), 5.31 (m, 1 H), 5.51 (br, s, 1 H), 6.24 (br, s, 1 H), 7.34-7.29 (m, 5 H); <sup>13</sup>C NMR (75.5 MHz, CDCl<sub>3</sub>, rt): δ(ppm) 26.40, 28.17, 34.43, 38.51, 38.94, 40.65, 60.21, 62.22, 66.51, 69.48, 69.90, 70.05, 70.10, 127.91, 127.99, 128.33, 136.44, 155.63, 156.45, 170.71; ESI-HRMS calcd. for C<sub>25</sub>H<sub>41</sub>N<sub>3</sub>O<sub>7</sub>Na<sup>+</sup>: 518.2842, found 518.2843.

**(S)-Benzyl-2-(2-(2-(2-amino-3,3-dimethylbutanamido)ethoxy)ethyl)carbamate trifluoroacetate (4.4)**

TFA in CH<sub>2</sub>Cl<sub>2</sub> (10 mL, 1:1) was added to compound **4.3** (423 mg, 0.853 mmol) and the resulting mixture was stirred at rt for 2 hr. The solution was then concentrated under

vacuum and the residue was charged over a silica gel column for flash chromatography (MeOH:CH<sub>2</sub>Cl<sub>2</sub> 5:95) to afford the desired product as colorless oil ( $R_f = 0.35$  in 1:9 MeOH:CH<sub>2</sub>Cl<sub>2</sub>). Yield: 363 mg, 87%. <sup>1</sup>H NMR (400 MHz, CDCl<sub>3</sub>, rt):  $\delta(ppm)$  1.06 (s, 9 H), 3.37 (m, 4 H), 3.55 (m, 2 H), 3.57 (m, 6 H), 3.83 (s, 1 H), 5.09 (s, 2 H), 7.34 (m, 5 H); <sup>13</sup>C NMR (100.6 MHz, CDCl<sub>3</sub>, rt):  $\delta(ppm)$  26.27, 33.22, 39.46, 40.84, 62.03, 66.83, 69.52, 70.19, 128.19, 128.24, 128.64, 136.68, 156.88, 168.28; ESI-LRMS: [M+H]<sup>+</sup>, 396.3 (100%).

#### Diethyl (2*R*, 3*R*)-2-bromo-3-hydroxysuccinate (4.5)

(-)-Diethyl *D*-tartrate (8.1 mL, 47.3 mmol) was cooled over an ice-water bath and then added with 30 wt% HBr in HOAc (40 mL, 200 mmol) over a period of 1 hr.<sup>181</sup> The reaction was allowed to warm up to rt and then stirred overnight. The mixture was poured onto crushed ice (200 g) and the aqueous phase was extracted with Et<sub>2</sub>O (4 × 100 mL). The ether layer was then washed with 1 N NaOH (20 mL), H<sub>2</sub>O (3 × 100 mL), and brine (100 mL), dried over anhydrous Na<sub>2</sub>SO<sub>4</sub> and concentrated under reduced pressure to give yellow oil, which was directly used in the following step without further purification. The oil was suspended in EtOH (50 mL) and AcCl (1.5 mL, 21 mmol) was added. The resulting solution was heated to reflux for 4 hr and then the solvent was removed under vacuum. The residue was purified by silica gel chromatography (EtOAc:hexanes 1:9 then 1:4) to obtain colorless oil ( $R_f = 0.34$  in 1:3 EtOAc:hexanes). Yield: 9.0 g, 71%. <sup>1</sup>H NMR (400 MHz, CDCl<sub>3</sub>, rt):  $\delta(ppm)$  1.31 (m, 6 H), 3.53 (s, br, 1 H), 4.30 (m, 4 H), 4.68 (s, 1 H), 4.72 (d,  $J = 4.32$  Hz, 1 H); <sup>13</sup>C NMR (100.6 MHz, CDCl<sub>3</sub>, rt):  $\delta(ppm)$  14.05, 14.17, 47.80, 62.71, 62.96, 72.65, 166.77, 170.40; ESI-LRMS: [M+Na]<sup>+</sup>, 291.3 (100%), 293.3 (100%).

#### Diethyl (2*S*, 3*S*)-epoxysuccinate (4.6)

21 wt% NaOEt in EtOH (6.6 mL, 17.78 mmol) was added to diethyl (2*R*, 3*R*)-2-bromo-3-hydroxylsuccinate **4.5** (3.68 g, 13.68 mmol) in EtOH (20 mL) during 15 min over an ice-water bath.<sup>182</sup> The resulting mixture was further stirred for 1 hr and then quenched by the addition of HOAc (0.5 mL, 8.70 mmol) followed by evaporation under reduced pressure. The residue was separated via flash chromatography (EtOAc:hexanes

1:9) to obtained colorless oil ( $R_f = 0.44$  in 1:3 EtOAc:hexanes). Yield: 2.07 g, 81%.  $^1\text{H}$  NMR (400 MHz,  $\text{CDCl}_3$ , rt):  $\delta(\text{ppm})$  1.30 (m, 6 H), 3.65 (m, 2 H), 4.26 (m, 4 H);  $^{13}\text{C}$  NMR (100.6 MHz,  $\text{CDCl}_3$ , rt):  $\delta(\text{ppm})$  14.11, 52.11, 62.29, 166.86; ESI-LRMS:  $[\text{M}+\text{H}]^+$ , 189.3 (100%).

#### **Diethyl (2*S*, 3*R*)-2-hydroxyl-isobutylsuccinate (4.7)**

CuCN (467 mg, 5.21 mmol) in anhydrous  $\text{Et}_2\text{O}$  (5 mL) was cooled to  $-30\text{ }^\circ\text{C}$  and then added with 2 M  $\text{Et}_2\text{O}$  solution of iso-BuMgBr (2.5 mL, 5.09 mmol) carefully.<sup>178</sup> The mixture was incubated at  $-30\text{ }^\circ\text{C}^{\text{a}}$  for 20 min; diethyl (2*R*, 3*R*)-epoxysuccinate **4.6** (415 mg, 2.21 mmol) in  $\text{Et}_2\text{O}$  (3 mL) was dropwise added to the reaction and stirred at  $-30\text{ }^\circ\text{C}$  for an additional hour. Then the reaction was quenched by saturated  $\text{NH}_4\text{Cl}$  (10 mL) and filtered. The solid was thoroughly washed with  $\text{Et}_2\text{O}$ . The filtrate was extracted with  $\text{Et}_2\text{O}$  ( $2 \times 100$  mL). The etherate layer was washed with brine ( $2 \times 100$  mL), dried over anhydrous  $\text{Na}_2\text{SO}_4$ , concentrated, and purified with silica gel chromatography (EtOAc:hexanes 5:95 then 10:90) to afford colorless oil as the desired product ( $R_f = 0.43$  in 1:3 EtOAc:hexanes). Yield: 187 mg, 34%.  $^1\text{H}$  NMR (400 MHz,  $\text{CDCl}_3$ , rt):  $\delta(\text{ppm})$  0.95 (m, 6 H), 1.26 (td,  $J_1 = 7.18$  Hz,  $J_2 = 1.37$  Hz, 3 H), 1.32 (td,  $J_1 = 7.16$  Hz,  $J_2 = 1.40$  Hz, 3 H), 1.52 (m, 1 H), 1.68 (m, 1 H), 1.77 (m, 1 H), 2.95 (m, 1 H), 3.25 (s, br, 1 H), 4.16 (q,  $J = 7.07$  Hz, 2 H), 4.22~4.32 (m, 3 H);  $^{13}\text{C}$  NMR (100.6 MHz,  $\text{CDCl}_3$ , rt):  $\delta(\text{ppm})$  14.24, 22.49, 22.57, 25.87, 37.07, 46.69, 60.91, 61.89, 71.43, 173.20, 173.57; ESI-LRMS:  $[\text{M}+\text{Na}]^+$ , 269.3 (100%).

#### **(2*S*, 3*R*)-2-Hydroxy-3-isobutylsuccinic acid (4.8)**

Diethyl (2*S*, 3*R*)-2-hydroxyl-isobutylsuccinate **4.7** (1.13 g, 4.61 mmol) in 1,4-dioxane (10 mL) was added with 1 N NaOH (20 mL) and the reaction was stirred at rt overnight.<sup>178</sup> Then the reaction was extract with  $\text{Et}_2\text{O}$  ( $3 \times 30$  mL) and the aqueous layer was acidified with concentrated HCl to pH < 1. The aqueous layer was extracted with  $\text{CH}_2\text{Cl}_2$  ( $3 \times 50$  mL) and EtOAc ( $3 \times 50$  mL). The organic layer ( $\text{CH}_2\text{Cl}_2/\text{EtOAc}$ ) was dried over anhydrous  $\text{Na}_2\text{SO}_4$  and then concentrated under reduced pressure. The residue was purified with flash chromatography (EtOAc:hexanes 7:3 then HOAc:EtOAc:hexanes

<sup>a</sup> Aqueous  $\text{CaCl}_2$  solution with dry ice.

1:7:3) to give yellow oil ( $R_f = 0.2$  in 1:7:3 HOAc:EtOAc:hexanes;  $R_f = 0.15$  in 1:9 MeOH:CH<sub>2</sub>Cl<sub>2</sub>). Yield: 0.83 g, 95%. <sup>1</sup>H NMR (400 MHz, CDCl<sub>3</sub>, rt):  $\delta$ (ppm) 1.00 (t,  $J = 6.40$  Hz, 6 H), 1.60 (m, 1 H), 1.79 (m, 2 H), 3.15 (s, 1 H), 4.36 (s, 1 H), 9.00 (s, br, 3 H); <sup>13</sup>C NMR (100.6 MHz, CDCl<sub>3</sub>, rt):  $\delta$ (ppm) 22.16, 22.62, 25.66, 36.74, 46.25, 70.47, 178.31, 179.24; ESI-LRMS: [M-H]<sup>-</sup>, 189.4 (100%).

**(2R)-4-Methyl-2-((4S)-5-oxo-2,2-dimethyl-1,3-dioxolan-4-yl)pentanoic acid (4.9)**

2,2-Dimethoxypropane (6 mL) was added to the mixture of *p*-TsOH·H<sub>2</sub>O (50 mg, 0.26 mmol) and (2*S*, 3*R*)-2-hydroxy-3-isobutylsuccinic acid **4.8** (424 mg, 2.44 mmol) in one portion and the resulting solution was stirred at rt overnight.<sup>178</sup> Then the volatile was removed under vacuum and the residue was purified with column chromatography (MeOH:CH<sub>2</sub>Cl<sub>2</sub> 1:99) to give light yellow oil ( $R_f = 0.53$  in 1:9 MeOH:CH<sub>2</sub>Cl<sub>2</sub>). Yield: 0.39 g, 70%. <sup>1</sup>H NMR (400 MHz, CDCl<sub>3</sub>, rt):  $\delta$ (ppm) 0.95 (t,  $J = 3.0$  Hz, 6 H), 1.55 (s, 3 H), 1.61 (s, 3 H), 1.65-1.82 (m, 2 H), 3.02 (s, br, 1 H), 4.47 (d,  $J = 4.40$  Hz, 1 H); <sup>13</sup>C NMR (100.6 MHz, CDCl<sub>3</sub>, rt):  $\delta$ (ppm) 22.23, 22.63, 25.82, 26.27, 26.74, 36.59, 74.18, 111.27, 172.23; ESI-LRMS: [M+H]<sup>+</sup>, 231.2 (100%).

**Benzyl (1*S*,14*R*)-11-*tert*-butyl-14-((4*S*)-2,2-dimethyl-5-oxo-1,3-dioxolan-4-yl)-16-methyl-10,13-dioxo-3,5-dioxa-9,12-diazaheptadecylcarbamate (4.10)**

The CH<sub>2</sub>Cl<sub>2</sub> solution (10 mL) of acid **4.9** (180 mg, 0.78 mmol) and amine **4.4** (363 mg, 0.74 mmol) was cooled to 0 °C and 2,6-lutidine (0.6 mL, 5.18 mmol) and PyBop (440 mg, 0.84 mmol) were added sequentially to the solution.<sup>178</sup> The resulting solution was then stirred at rt overnight and quenched by 3 N HCl (50 mL). The aqueous phase was extracted with CH<sub>2</sub>Cl<sub>2</sub> (3 × 50 mL). The CH<sub>2</sub>Cl<sub>2</sub> layer was combined, washed with H<sub>2</sub>O (2 × 50 mL) and brine (1 × 50 mL), and dried over anhydrous Na<sub>2</sub>SO<sub>4</sub>. The solution was filtered and concentrated under vacuum, and the residue was purified via flash chromatography (MeOH:CH<sub>2</sub>Cl<sub>2</sub> 1:99 then 2:98) to obtain the desired compound as pale yellow oil ( $R_f = 0.55$  in 1:9 MeOH:CH<sub>2</sub>Cl<sub>2</sub>). Yield: 260 mg, 58%. <sup>1</sup>H NMR (400 MHz, CD<sub>2</sub>Cl<sub>2</sub>, rt):  $\delta$ (ppm) 0.91 (d,  $J = 2.40$  Hz, 3 H), 0.93 (d,  $J = 2.80$  Hz, 3 H), 0.99 (s, 9 H), 1.53 (s, 3 H), 1.59 (m, 1 H), 1.62 (s, 3 H), 1.72 (m, 1 H), 2.75 (m, 1 H), 3.38 (m, 4 H), 3.51 (m, 2 H), 3.58 (m, 6 H), 4.22 (s, br, 1 H), 4.46 (d,  $J = 6.0$  Hz, 1 H), 5.12 (s, 2 H),

7.35 (m, 5 H);  $^{13}\text{C}$  NMR (100.6 MHz,  $\text{CD}_2\text{Cl}_2$ , rt):  $\delta(\text{ppm})$  21.78, 23.00, 25.68, 25.87, 26.48, 26.70, 34.62, 36.94, 39.27, 47.49, 60.80, 69.97, 70.43, 74.76, 110.88, 128.00, 128.04, 128.53, 170.45, 172.05; ESI-LRMS:  $[\text{M}+\text{Na}]^+$ , 630.4; ESI-HRMS: calcd. for  $\text{C}_{31}\text{H}_{49}\text{N}_3\text{O}_9\text{Na}^+$ : 630.3367, found 630.3378.

**(15*S*, 18*R*, 19*S*)-Methyl 15-(*tert*-butyl)-19-hydroxy-18-isobutyl-3,14,17-trioxo-1-phenyl-2,7,10-trioxa-4,13,16-triazaicosan-20-oate (4.11)**

Compound **4.10** (260 mg, 0.428 mmol) was dissolved in MeOH (20 mL) with *p*-TsOH·H<sub>2</sub>O (32 mg, 0.168 mmol) and the solution was heated to reflux for 1 hr. The solution was then concentrated under vacuum and the resulting mixture was charged with silica gel chromatography (MeOH:CH<sub>2</sub>Cl<sub>2</sub> 2.5:97.5) to obtain colorless oil ( $R_f = 0.47$  in 1:9 MeOH: CH<sub>2</sub>Cl<sub>2</sub>). Yield: 229 mg, 92%.  $^1\text{H}$  NMR (400 MHz,  $\text{CD}_2\text{Cl}_2$ , rt):  $\delta(\text{ppm})$  0.92 (d,  $J = 6.0$  Hz, 3 H), 0.95 (d,  $J = 6.0$  Hz, 3 H), 1.00 (s, 9 H), 1.55~1.68 (m, 3 H), 2.81 (s, br, 1 H), 3.38 (m, 4 H), 3.53~3.60 (m, 9 H), 3.74 (s, 3 H), 4.17 (m, 1 H), 4.21 (s, 1 H), 5.11 (s, 2 H), 7.34 (m, 5 H);  $^{13}\text{C}$  NMR (100.6 MHz,  $\text{CD}_2\text{Cl}_2$ , rt):  $\delta(\text{ppm})$  22.39, 25.68, 26.53, 34.56, 38.69, 39.32, 41.01, 47.29, 52.34, 60.70, 66.53, 69.64, 70.06, 70.42, 71.99, 128.03, 128.08, 128.55, 156.49, 170.05, 173.36, 173.88; ESI-LRMS:  $[\text{M}+\text{Na}]^+$ , 604.5 (100%).

**(11*S*, 14*R*, 15*S*)-Methyl 1-amio-11-*tert*-butyl-15-hydroxy-14-isobutyl-10,13-dioxo-3,6-dioxa-9,12-diazahexadecan-16-oate (4.12)**

The Cbz protected amine **4.11** (228.6 mg, 0.394 mmol) in MeOH (20 mL) was added with 10% Pd/C (100 mg) and the mixture was incubated in a H<sub>2</sub> atmosphere for 1.5 hr. Then the reaction mixture was filter over Celite, and the Celite was washed with MeOH and CH<sub>2</sub>Cl<sub>2</sub> thoroughly. The filtrate was combined and concentrated under vacuum. The colorless oily residue (quant.) was used directly in the following reaction. For characterization, part of the residue was purified from silica gel flash chromatography (MeOH:CH<sub>2</sub>Cl<sub>2</sub> 5:95, then 1:9 and then MeOH:CH<sub>2</sub>Cl<sub>2</sub>:NH<sub>4</sub>OH 15:85:0.5) to obtain the desired product ( $R_f = 0.039$  in 1:9 MeOH:CH<sub>2</sub>Cl<sub>2</sub>). Yield: 170.2 mg, 97%.  $^1\text{H}$  NMR (400 MHz,  $\text{CDCl}_3$ , rt):  $\delta(\text{ppm})$  0.93 (d,  $J = 5.60$  Hz, 3 H), 0.96 (d,  $J = 6.00$  Hz, 3 H), 1.00 (s, 9 H), 1.64 (m, 3 H), 2.81 (m, 2 H), 3.34 (m, 1 H), 3.60 (m, 10 H), 3.77 (s, 3 H), 4.21 (d,  $J = 8.80$  Hz, 1 H), 4.25 (s, 1 H), 6.81 (d,  $J = 9.20$  Hz, 1 H), 7.27 (s, br, 1 H);  $^{13}\text{C}$  NMR (100.6

MHz, CDCl<sub>3</sub>, rt):  $\delta$ (ppm) 22.63, 22.66, 25.73, 26.92, 34.63, 38.97, 39.43, 47.78, 52.59, 60.74, 69.94, 70.24, 70.60, 71.61, 170.47, 173.24, 174.30; ESI-LRMS: [M+H]<sup>+</sup>, 448.4 (100%), [M+Cl]<sup>-</sup>, 482.4 (100%).

**(13*S*,16*R*,17*S*)-Methyl 13-*tert*-butyl-17-hydroxy-16-isobutyl-1,12,15-trioxo-1-(2, 4, 6-trifluoro-3-(4, 4, 5, 5-tetraphenyl-1, 3, 2-dioxaborolan-2-yl)phenyl)-5, 8-dioxa-2, 11, 14-triazaoctadecan-18-oate (4.13)**

Boronate **3.1** (217 mg, 0.393 mmol), HOBt·H<sub>2</sub>O (110 mg, 0.720 mmol) and pyridine (0.12 mL, 1.50 mmol) in DMF (10 mL) was added with EDC·HCl (104 mg, 0.540 mmol) in one portion at rt. Incubated at rt overnight, the reaction was quenched upon the addition of 3 N HCl (30 mL), and EtOAc (3 × 50 mL) was added to extract the aqueous layer. The organic layers were combined, washed with H<sub>2</sub>O (3 × 50 mL) and brine (1 × 50 mL), and then dried over anhydrous Na<sub>2</sub>SO<sub>4</sub>. The solution was filtered and concentrated under reduced pressure and then separated by flash chromatography (MeOH:CH<sub>2</sub>Cl<sub>2</sub>, gradient 0.5:99.5 to 2.5:97.5) to afford white foam as the desired product (*R<sub>f</sub>* = 0.49 in 1:9 MeOH:CH<sub>2</sub>Cl<sub>2</sub>). Yield: 202.9 mg, 53%. <sup>19</sup>F NMR (282.4 MHz, CD<sub>2</sub>Cl<sub>2</sub>, rt):  $\delta$ (ppm) -28.27 (s, 1 F), -21.87 (s, 1 F), -17.12 (s, 1 F); <sup>1</sup>H NMR (400 MHz, CD<sub>2</sub>Cl<sub>2</sub>, rt):  $\delta$ (ppm) 0.91 (d, *J* = 6.16 Hz, 2 H), 0.94 (m, 12 H), 1.58 (m, 3 H), 2.77 (td, *J*<sub>1</sub> = 7.55 Hz, *J*<sub>2</sub> = 3.16 Hz, 1 H), 3.37 (m, 2 H), 3.50 (m, 2 H), 3.58~3.70 (m, 9 H), 3.71 (s, 3 H), 4.08 (d, *J* = 9.12 Hz, 1 H), 4.17 (d, *J* = 3.16 Hz, 1 H), 6.26 (t, *J* = 4.92 Hz, 1 H), 6.52 (d, *J* = 9.04 Hz, 1 H), 6.87 (m, 2 H), 7.11 (m, 12 H), 7.23 (m, 8 H); <sup>13</sup>C NMR (100.6 MHz, CD<sub>2</sub>Cl<sub>2</sub>, rt):  $\delta$ (ppm) 22.33, 22.38, 25.70, 26.48, 34.53, 38.65, 39.28, 40.07, 47.37, 52.36, 60.78, 69.52, 69.60, 70.37, 70.47, 71.97, 96.91, 127.27, 127.44, 128.63, 142.02, 159.67, 169.96, 173.25, 173.82; ESI-LRMS: [M+Na]<sup>+</sup>, 1002.9 (100%); ESI-HRMS: calcd. for C<sub>54</sub>H<sub>61</sub>BN<sub>3</sub>O<sub>10</sub>F<sub>3</sub>Na<sup>+</sup>: 1002.4300, found: 1002.4277.

**(2*R*,3*S*)-*N*<sup>1</sup>-((*S*)-14,14-Dimethyl-1,12-dioxo-1-(2,4,6-trifluoro-3-(4,4,5,5-tetraphenyl-1,3,2-dioxaborolan-2-yl)phenyl)-5,8-dioxa-2,11-diazapentadecan-13-yl)-*N*<sup>4</sup>,3-dihydroxy-2-isobutylsuccinamide (4.14)**

Methyl ester **4.13** (76.6 mg, 0.078 mmol) and KCN (8.0 mg) were mixed in 1:1 THF:MeOH (4 mL) and added with 50% aqueous NH<sub>2</sub>OH (1.0 mL). The reaction was stirred at rt for 6.5 hr. The mixture was concentrated under reduced pressure and the

residue was charged with flash chromatography (MeOH:CH<sub>2</sub>Cl<sub>2</sub> 3:97) to give a white solid as the desired product ( $R_f = 0.32$  in 1:9 MeOH:CH<sub>2</sub>Cl<sub>2</sub>). Yield: 44.7 mg, 58%. The compound can be further purified by RP-HPLC using HPLC Program 3 with Column II ( $t_R = 12.0$  min) or analyzed by RP-HPLC using HPLC Program 1 with Column I ( $t_R = 29.4$  min) in HPLC System I. <sup>19</sup>F NMR (282.4 MHz, CD<sub>2</sub>Cl<sub>2</sub>, rt):  $\delta(ppm)$  -29.60 (s, 1 F), -23.36 (s, 1 F), -18.49 (s, 1 F); <sup>1</sup>H NMR (400 MHz, CD<sub>2</sub>Cl<sub>2</sub>, rt):  $\delta(ppm)$  0.89 (d,  $J = 6.48$  Hz, 3 H), 0.91 (d,  $J = 6.48$  Hz, 3 H), 0.94 (s, 9 H), 1.44 (m, 1 H), 1.54 (m, 1 H), 1.65 (m, 1 H), 3.19 (t,  $J = 8.06$  Hz, 1 H), 3.39 (m, 2 H), 3.53 (t,  $J = 4.88$  Hz, 2 H), 3.56~3.75 (m, 8 H), 4.13 (d,  $J = 8.96$  Hz, 1 H), 4.18 (s, br, 1 H), 6.48 (s, br, 1 H), 6.88 (td,  $J_1 = 9.16$  Hz,  $J_2 = 1.20$  Hz, 1 H), 7.00 (s, br, 1 H), 7.13 (m, 12 H), 7.24 (m, 8 H), 9.45 (s, br, 1 H); <sup>13</sup>C NMR (100.6 MHz, CD<sub>2</sub>Cl<sub>2</sub>, rt):  $\delta(ppm)$  22.12, 22.56, 25.78, 26.61, 29.79, 34.62, 39.28, 40.02, 61.26, 69.55, 70.30, 96.94, 99.11, 101.18, 101.49, 127.13, 127.28, 127.44, 127.74, 128.47, 128.61, 129.42, 137.16, 139.42, 141.92, 142.00, 143.94, 170.35, 174.50; ESI-LRMS: [M+Na]<sup>+</sup>, 1003.8 (100%), [M-H]<sup>-</sup>, 979.9; ESI-HRMS: calcd. for C<sub>53</sub>H<sub>60</sub>BN<sub>4</sub>O<sub>10</sub>F<sub>3</sub>Na<sup>+</sup>:1003.4252, found: 1003.4276.

**Potassium <sup>19</sup>F-N-marimastat-amidyl-2,4,6-trifluoro-N-(2-(2-(2-(amino)ethoxy)ethoxy)ethyl)-3-(trifluoroborate)benzamide (MarArBF<sub>3</sub>) (4.15)**

Compound **4.14** (13.6 mg, 13.9  $\mu$ mol) in MeOH (1.0 mL) was added with 4.5 M KHF<sub>2</sub> (40  $\mu$ L, 180  $\mu$ mol) and 6 M HCl (10  $\mu$ L, 60  $\mu$ mol). The resulting mixture was stirred at rt for one hour in a 1.5 mL eppendorf tube and the solvent was removed under reduced pressure. The residue was washed with Et<sub>2</sub>O (6  $\times$  1.5 mL). The pellet was then dried over vacuum overnight. The product was extracted into *d*<sub>6</sub>-DMSO (400  $\mu$ L) for characterization directly. <sup>19</sup>F NMR (282.4 MHz, *d*<sub>6</sub>-DMSO, rt):  $\delta(ppm)$  -55.13 (s, 3 F), -40.99 (s, 1 F), -27.23 (s, 1 F), -22.21 (s, 1 F); <sup>1</sup>H NMR (300 MHz, *d*<sub>6</sub>-DMSO, rt):  $\delta(ppm)$  0.78 (t,  $J = 7.23$  Hz, 6 H), 0.89 (s, 9 H), 1.40 (m, 2 H), 2.69 (m, 1 H), 3.19 (m, 2 H), 3.35~3.55 (m, 8 H), 3.70 (t,  $J = 7.64$  Hz, 1 H), 4.21 (d,  $J = 9.54$  Hz, 1 H), 5.32 (d,  $J = 7.41$  Hz, 1 H), 6.67 (t,  $J = 9.39$  Hz, 1 H), 7.48 (d,  $J = 9.54$  Hz, 1 H), 7.99 (t,  $J = 5.5.4$  Hz, 1 H), 8.90 (s, br, 1 H), 10.60 (s, br, 1 H); ESI-LRMS: [M-K]<sup>-</sup>, 673.7 (100%); ESI-HRMS: calcd. for C<sub>27</sub>H<sub>40</sub>BN<sub>4</sub>O<sub>8</sub>F<sub>6</sub><sup>-</sup>:673.2842, found: 673.2859.

**Benzyl (11-(*tert*-butyl)-14-(1-hydroxy-2-(hydroxyamino)-2-oxoethyl)-16-methyl-10,13-dioxo-3,6-dioxo-9,12-diazaheptadecyl)carbamate (Cbz-PEG-Mar) (4.16)**

50% aqueous  $\text{NH}_2\text{OH}$  (1.0 mL, 16.3 mmol) and KCN (8 mg) were added to methyl ester **4.12** (120 mg, 0.206 mmol) in THF: $\text{CH}_3\text{OH}$  (1:1, 3 mL). The resulting mixture was stirred at rt overnight. The reaction was quenched by the addition of brine ( $1 \times 30$  mL) and extracted with  $\text{CH}_2\text{Cl}_2$  ( $3 \times 50$  mL). The organic layer was washed with brine ( $1 \times 30$  mL) and dried over anhydrous  $\text{MgSO}_4$ . The solution was filtered, concentrated under reduced pressure, and then charged over silica gel chromatography ( $\text{MeOH}:\text{CH}_2\text{Cl}_2$  3:97 then 5:95) to give a pale pink solid as the desired product ( $R_f = 0.30$  in 1:9  $\text{MeOH}:\text{CH}_2\text{Cl}_2$ ). Yield: 79.6 mg, 66%.  $^1\text{H}$  NMR (400 MHz,  $\text{CDCl}_3$ , rt):  $\delta(\text{ppm})$  0.94 (m, 6 H), 0.98 (s, 9 H), 1.52 (m, 2 H), 1.77 (m, 3 H), 3.44 (m, 4 H), 3.59 (m, 8 H), 4.23 (m, 2 H), 5.14 (s, 2 H), 5.66 (s, 1 H), 6.72 (s, 1 H), 7.38 (m, 5 H), 8.08 (s, 1 H), 8.47 (s, 1 H), 9.55 (s, 1 H);  $^{13}\text{C}$  NMR (100.6 MHz,  $\text{CDCl}_3$ , rt):  $\delta(\text{ppm})$  22.31, 22.72, 25.68, 26.77, 34.67, 39.10, 39.22, 40.81, 44.98, 61.19, 66.70, 69.63, 70.12, 72.50, 128.11, 128.52, 136.59, 156.64, 168.66, 170.52, 174.73; ESI-LRMS:  $[\text{M}+\text{Na}]^+$ , 605.6 (100%); ESI-HRMS: calcd. for  $\text{C}_{28}\text{H}_{46}\text{N}_4\text{O}_9\text{Na}^+$ : 605.3162, found: 605.3157.

**Methyl 2-phenylacetate**

Phenyl acetic acid (3.0 g, 22 mmol) was suspended in thionyl chloride (15.0 mL, 206.5 mmol) for 2 min at rt in a round bottle flask connected with a condenser. Then methanol (5 mL) was added dropwise to the solution. After the addition, the reaction was heated to reflux for 4 hr. The reaction was cooled to rt and concentrated under vacuum. The residue was suspended in  $\text{CH}_2\text{Cl}_2$  (50 mL) and washed with saturated  $\text{NaHCO}_3$ . The aqueous layer was further extracted with  $\text{CH}_2\text{Cl}_2$  ( $2 \times 50$  mL). The organic layers were combined and washed with saturated  $\text{NaHCO}_3$  ( $1 \times 50$  mL),  $\text{H}_2\text{O}$  ( $2 \times 50$  mL), and brine ( $1 \times 50$  mL), and dried over anhydrous  $\text{Na}_2\text{SO}_4$ . The solution was filter and the solvent was removed in vacuum to give golden oil ( $R_f = 0.61$  in 1:1 EtOAc:hexanes), which was used without further purification. Yield: 2.66 g, 81%.  $^1\text{H}$  NMR (400 MHz,  $\text{CDCl}_3$ , rt):  $\delta(\text{ppm})$  3.70 (s, 2 H), 3.76 (s, 3 H), 7.36 (m, 5 H);  $^{13}\text{C}$  NMR (100.6 MHz,  $\text{CDCl}_3$ , rt):  $\delta(\text{ppm})$  41.64, 52.45, 127.55, 129.03, 129.69; ESI-LRMS:  $[\text{M}+\text{Na}]^+$ , 173.2 (100%).

### ***N*-Hydroxy-2-phenylacetamide (4.17)**

Methyl 2-phenylacetate (500 mg, 3.33 mmol) and KCN (8 mg) were mixed in 1:1 THF:MeOH (4 mL) and added with 50% aqueous NH<sub>2</sub>OH (1 mL).<sup>183</sup> The mixture was stirred at rt for 4 hr. The mixture was concentrated and the residue was charged with silica gel flash chromatography (MeOH:CH<sub>2</sub>Cl<sub>2</sub> 5:95) to give a pink solid (*R<sub>f</sub>* = 0.27 in 1:9 MeOH:CH<sub>2</sub>Cl<sub>2</sub>). Yield: 292 mg, 58%. <sup>1</sup>H NMR (400 MHz, *d*<sub>4</sub>-MeOD, rt): δ(*ppm*) 3.43, (s, 2 H), 7.29 (m, 5 H); <sup>13</sup>C NMR (100.6 MHz, *d*<sub>4</sub>-MeOD, rt): δ(*ppm*) 39.63, 99.38, 126.95, 128.52, 128.96; ESI-LRMS: [M+Na]<sup>+</sup>, 174.1 (100%), [M-H]<sup>-</sup>, 150.3 (100%).

### **Monomethyl succinate**

Succinic anhydride (3.0 g, 30 mmol) in MeOH (40 mL) was heated to reflux for 2 hr and then the solution was concentrated in vacuum to give colorless oil. The oil was further purified with silica gel flash chromatography (EtOAc:Hex 1:1) to give a white solid as the desired product (*R<sub>f</sub>* = 0.24 in 1:1 EtOAc:Hexanes). Yield: 3.23 g, 95%. <sup>1</sup>H NMR (400 MHz, CDCl<sub>3</sub>, rt): δ(*ppm*) 2.66 (m, 2 H), 2.75 (m, 2 H), 3.75 (s, 3 H); <sup>13</sup>C NMR (100.6 MHz, CDCl<sub>3</sub>, rt): δ(*ppm*) 29.03, 29.32, 52.39, 173.01, 178.71; ESI-LRMS: [M+Na]<sup>+</sup>, 155.1 (100%), [M-H]<sup>-</sup>, 131.2 (100%).

### **Methyl 4-((4-methoxybenzyl)amino)-4-oxobutanoate**

In CH<sub>2</sub>Cl<sub>2</sub> (20 mL) were dissolved monomethyl succinate (500 mg, 3.79 mmol), 4-methoxybenzylamine (0.59 mL, 4.50 mmol), HOBt·H<sub>2</sub>O (640 mg, 4.17 mmol), and NEt<sub>3</sub> (1.06 mL, 7.58 mmol). EDC·HCl (940 mg, 4.93 mmol) was added to the mixture in one portion to give white slurry within 10 min. THF (8 mL) was added to help dissolve the solid and the mixture was left at rt for 21 hr. The solvent was removed *in vacuo* and the residue was resuspended in EtOAc (50 mL). The EtOAc solution was washed with H<sub>2</sub>O (50 mL) and the aqueous layer was further extracted with EtOAc (2 × 50 mL). The organic layers were combined, washed with H<sub>2</sub>O (2 × 50 mL), 3 N aqueous HCl (1 × 50 mL), H<sub>2</sub>O (2 × 50 mL), and brine (1 × 50 mL), and then dried over anhydrous Na<sub>2</sub>SO<sub>4</sub>. The solution was filtered and the filtrate was concentrated for silica gel flash chromatography (MeOH:CH<sub>2</sub>Cl<sub>2</sub> 1:9) to give a white solid (*R<sub>f</sub>* = 0.51 in 1:9 MeOH:CH<sub>2</sub>Cl<sub>2</sub>). Yield: 609 mg, 90%. <sup>1</sup>H NMR (400 MHz, CD<sub>2</sub>Cl<sub>2</sub>, rt): δ(*ppm*) 2.48 (d, *J*

= 6.68 Hz, 2 H), 2.65 (t,  $J = 6.81$  Hz, 2 H), 3.66 (s, 3 H), 3.79 (s, 3 H), 4.33 (d,  $J = 5.73$  Hz, 2 H), 6.86 (d,  $J = 8.67$  Hz, 2 H), 7.20 (d,  $J = 8.67$  Hz, 2 H);  $^{13}\text{C}$  NMR (75.5 MHz,  $\text{CD}_2\text{Cl}_2$ , rt):  $\delta(\text{ppm})$  29.61, 31.23, 43.23, 51.98, 55.60, 114.26, 129.25, 131.10, 159.37, 171.25, 173.62; ESI-LRMS:  $[\text{M}+\text{Na}]^+$ , 274.3 (100%).

#### ***N*-Hydroxy-*N*'-(4-methoxybenzyl)succinamide (4.18)**

Methyl 4-((4-methoxybenzyl)amino)-4-oxobutanoate (125 mg, 0.50 mmol) and KCN (8 mg) were mixed in 1:1 THF:MeOH (7 mL) and added with 50% aqueous  $\text{NH}_2\text{OH}$  (2.5 mL). The mixture was stirred at rt for 2 hr and  $\text{CH}_2\text{Cl}_2$  (30 mL) was added to the reaction. After separation of layers, the aqueous layer was extracted with  $\text{CH}_2\text{Cl}_2$  ( $2 \times 30$  mL); the organic layers were combined and dried over anhydrous  $\text{Na}_2\text{SO}_4$ . The solution was filtered and concentrated in vacuum, and the residue was charged with silica gel flash chromatography (MeOH: $\text{CH}_2\text{Cl}_2$  1:99 then 1:9) to give a white solid as the desired product ( $R_f = 0.16$  in 1:9 MeOH: $\text{CH}_2\text{Cl}_2$ ). Yield: 28.6 mg, 23%.  $^1\text{H}$  NMR (400 MHz,  $d_6$ -DMSO, rt):  $\delta(\text{ppm})$  2.19 (t,  $J = 7.40$  Hz, 2 H), 2.34 (t,  $J = 7.40$  Hz, 2 H), 3.71 (s, 3 H), 4.16 (d,  $J = 5.60$  Hz, 2 H), 6.85 (d,  $J = 8.80$  Hz, 2 H), 7.20 (d,  $J = 8.00$  Hz, 2 H), 8.23 (s, 1 H), 8.64 (s, 1 H), 10.33 (s, 1 H);  $^{13}\text{C}$  NMR (100.6 MHz,  $d_6$ -DMSO, rt):  $\delta(\text{ppm})$  28.43, 31.16, 42.08, 55.65, 114.24, 129.11, 132.10, 158.74, 169.04, 171.52; ESI-LRMS:  $[\text{M}+\text{Na}]^+$ , 275.2 (100%).

#### **Marimastat-FITC (4.19)**

The fluorescent marimastat-FITC has been synthesized by Dr. Curtis Harwig and reported by Overall and co-workers.<sup>86</sup> Briefly, methyl ester **4.12** (21.5 mg, 0.048 mmol) was treated with fluorescein 5(6)-isothiocyanate (90%, 18.5 mg, 0.043 mmol) in anhydrous DMF (2 mL) at rt for 1.5 hours. The mixture was then concentrated for flash chromatography (HOAc:MeOH: $\text{CH}_2\text{Cl}_2$ , 0:1:9 then 1:10:89) to afford the methyl ester of the fluorescein derivative (23 mg) which was then reacted with 50% aqueous  $\text{NH}_2\text{OH}$  (100  $\mu\text{L}$ , 1.5 mmol) in 1:1 THF:MeOH (0.8 mL) in the presence of KCN (~ 1 mg). After incubation at rt for 16 hr, the reaction was concentrated in vacuum and the residue was triturated with  $\text{CH}_2\text{Cl}_2$ :MeOH (5:1,  $3 \times 5$  mL). The mixture was then filtered and the filtrate was concentrated under reduced pressure to give the desired hydroxamate **4.19**. ESI-HRMS: calcd. for  $\text{C}_{42}\text{H}_{51}\text{N}_4\text{O}_{12}\text{S}^-$ : 835.3224, found: 835.3241.

### 4.5.2 Defluoridation study of MarArBF<sub>3</sub> (4.15)

Around 130  $\mu\text{L}$  of the *d*<sub>6</sub>-DMSO solution of **4.15** was lyophilized and 300  $\mu\text{L}$  of 1  $\times$  PBS was added to the residue. Then <sup>19</sup>F NMR spectrum was recorded at different time point. The percentage of **4.15** in terms of the <sup>19</sup>F-signal was fit to the first order decay kinetics as shown in Figure 4.4.

### 4.5.3 Ferroin test

The hydroxamic acids were dissolved in EtOH to achieve a concentration around 6 mM. Then a certain amount of the solution was added to 300  $\mu\text{L}$  of FeCl<sub>3</sub> (5.0 mM) in EtOH and diluted to 600  $\mu\text{L}$  with a corresponding amount of EtOH. Then the UV absorption at 499 nm was recorded for each sample. A standard curve was then obtained to give the extinction coefficient of the complex at 499 nm.

Since the MeOD solution of **4.15** contained some free fluoride, to determine its concentration, the effect of free fluoride needs identifying. A similar ferroin test with different concentrations of free fluoride in the form of KHF<sub>2</sub> in MeOH was carried out and the result suggested that the fluoride played no role on the UV absorption. Then the concentration of **4.15** in MeOD was determined via a standard dilution curve with the extinction coefficient of Fe(III)-**4.16**.

### 4.5.4 The acid stability of hydroxamic acids studied by NMR spectroscopy

To 200  $\mu\text{L}$  of the hydroxamic acid **4.17** (43.2 mM) or **4.18** (43.2 mM) in *d*<sub>6</sub>-DMSO was added 200  $\mu\text{L}$  of D<sub>2</sub>SO<sub>4</sub> (3.4 M) in D<sub>2</sub>O. The <sup>1</sup>H NMR spectra of the resulting deuterated solution were then recorded at different time points by Bruker Avance 300 Spectrometer. The percentage of the starting material in the mixture against time was fitted exponentially.

### 4.5.5 Enzyme inhibition assays

4-Aminophenylmercuric acetate (1  $\mu\text{L}$ , 10 mM) was incubated with the recombinant human MMP2 (24.8  $\mu\text{L}$ , 0.139 mg/ mL) at 37 °C for 1 hr for activation. Then the enzyme

MMP2 in the solution was diluted with FAB solution to 0.389  $\mu\text{g/mL}$ . The rates of enzymatically cleaving 1  $\mu\text{M}$  of the fluorescent substrate (7-methoxycoumarin-4-yl)acetyl-Pro-Leu-Gly-Leu-[3-(2,4-dinitrophenyl)-L-2,3-dianopropionyl]-Ala-Arg-NH<sub>2</sub> (QF24) by 0.307  $\mu\text{g/mL}$  of the preactivated MMP2 at 37 °C in FAB solution were measured in 96-well fluorimetry plates in a Polarstar Optima (BMG Labtech GmbH) using a 320 nm excitation filter and a 405 nm emission filter in the presence of increasing concentrations of marimastat inhibitors. Curve-fitting and IC<sub>50</sub> calculations were processed via GraphPad Prism 5.0 software (GraphPad Software).

## **4.5.6 Assays for fluorescent marimastat-FITC**

### **4.5.6.1 Binding assay of marimastat-FITC with MMPs**

First, the direct binding of marimastat-FITC **4.19** to MMPs was visualized directly on the gel. Briefly, the recombinant human MMPs (MMP2, 8, 9 and 14) were expressed, purified, and then resolved nonreduced on the 10% SDS-PAGE. The SDS was removed and the enzymes were renatured in the gel, which was then incubated overnight with marimastat-FITC **4.19** at 37 °C in Tris buffer (100 mM, pH 8) containing CaCl<sub>2</sub> (30 mM). Washed with PBS, the gel was imaged with an excitation at 340 nm on an Alpha Imager System.

### **4.5.6.2 Cell assay for MMP14 by marimastat-FITC**

The breast cancer cell line MDA-MB-231 stably transfected with human MMP14 or empty vector was cultured. For MMP14 activity staining, the cells grew on glass chamber slides and were incubated with marimastat-FITC **4.19** in the culture medium for 12 hr. The cells were then washed with PBS buffer, counterstained with Hoechst<sup>a</sup> and fixed with 4% formalin. The slides were then washed with PBS, treated with ProLong Gold antifade reagent to suppress photobleaching and imaged under the Leica DMRA2 fluorescent microscope. Pictures were taken for both MMP14-transfected and vector control cells with the same exposure time.

---

<sup>a</sup> Hoechst dyes are fluorescent cell permeable nucleic acid stains.

#### 4.5.7 Radiolabeling marimastat-boronate

$^{18}\text{F}$ -Fluoride in  $\text{H}_2^{18}\text{O}$  after the cyclotron was transferred to the hotcell and trapped on the anion exchange column (239 mCi at 9:21 on Dec. 4<sup>th</sup>, 2009). The radioactivity was then released with 1 mL of  $\text{NaClO}_4$  (2 mg/mL) to give an  $^{18}\text{F}$ -fluoride solution, which was then concentrated under helium flow at 110 °C in a Pyrex V-vial. To the residue (212 mCi at 9:34 on Dec. 4<sup>th</sup>, 2009) was added 4  $\mu\text{L}$  of  $\text{H}_2\text{O}$  and 2  $\mu\text{L}$  of the radioactive solution was transferred out. 1.6  $\mu\text{L}$  of  $\text{KHF}_2$  (250 mM) and 40  $\mu\text{L}$   $\text{H}_2\text{O}$  was then added to the V-vial and the resulting mixture was then concentrated under helium flow at 110 °C. The radioactivity in the V-vial after evaporation was 108.7 mCi at 9:55 on Dec. 4<sup>th</sup>, 2009 (the specific activity = 0.136 Ci/ $\mu\text{mol}$  at 9:55). 3  $\mu\text{L}$  of the aqueous solution containing sodium ascorbate (1.0 M) and potassium iodide (197.9 mM) was added to the residue to fully resuspend the radioactivity and 2  $\mu\text{L}$  of the resulting solution was transferred to marimastat-boronate **4.14** (100 nmol) in  $\text{CH}_3\text{CN}$  (2  $\mu\text{L}$ ). Concentrated HCl (0.5  $\mu\text{L}$ ) was added to the mixture to initiate the reaction (53.4 mCi at 9:59 Dec 4<sup>th</sup>, 2009). The mixture was then incubated at rt for 88 min and quenched upon the addition of 105  $\mu\text{L}$  of 0.83% aqueous  $\text{NH}_4\text{OH}$  (30.4 mCi at 11:28 on Dec. 4<sup>th</sup>, 2009). The whole quenched mixture was then injected into the HPLC equipped with a fraction collector (0.5 mL/fraction) using HPLC Program 4 with Column I ( $t_{\text{R}}$  = 15.6 min) (HPLC System II). The fractions 29<sup>th</sup> (804  $\mu\text{Ci}$  at 11:50 on Dec. 4<sup>th</sup>, 2009) and 30<sup>th</sup> (460  $\mu\text{Ci}$  at 11:50 on Dec. 4<sup>th</sup>, 2009) containing the product were pooled and concentrated under reduced pressure over 50 °C. Then the residue was formulated with sterilized 1  $\times$  PBS buffer and delivered for animal injection (1.1 mCi at 12:05 on Dec. 4<sup>th</sup>, 2009, specific activity = 0.179 Ci/ $\mu\text{mol}$  at 12:05).

A similar procedure was carried out for the radiolabeling on Dec. 11<sup>th</sup>, 2009. More specifically, 346 mCi of  $^{18}\text{F}$ -fluoride in  $\text{H}_2^{18}\text{O}$  at 8:30 on Dec. 11<sup>th</sup>, 2009 was obtained from the target and it was concentrated under helium flow at 110 °C. Then 700 nmol of fluoride in the form of  $\text{KHF}_2$  in 120  $\mu\text{L}$  was added to the residue (291 mCi at 8:53 on Dec. 11<sup>th</sup>, 2009) and the resulting mixture was then concentrated under helium flow at 110 °C. Then 4.5  $\mu\text{L}$  of fluoride solution containing  $\text{KHF}_2$  (125 nmol), sodium ascorbate

(4.19 mmol), potassium iodide (837.5 nmol) and ammonium formate (837.5 nmol) was added to the residue and 1.5  $\mu\text{L}$  of the resulting solution (the specific activity: 0.306 Ci/ $\mu\text{mol}$  at 8:53 on Dec. 11<sup>th</sup>, 2009) was transferred to marimastat-boronate **4.14** (100 nmol) in 1.5  $\mu\text{L}$  of  $\text{CH}_3\text{CN}$ . The mixture was acidified by the addition of concentrated HCl (0.5  $\mu\text{L}$ ) to initiate the reaction (63 mCi at 9:25 on Dec. 11<sup>th</sup>, 2009). After 69 min at rt, the reaction was quenched by 105  $\mu\text{L}$  of 0.83% aqueous  $\text{NH}_4\text{OH}$  and then injected into the HPLC for separation. Fractions 31<sup>st</sup> (120  $\mu\text{Ci}$  at 10:49 on Dec. 11<sup>th</sup>, 2009), 32<sup>nd</sup> (530  $\mu\text{Ci}$  at 10:49 on Dec. 11<sup>th</sup>, 2009), 33<sup>rd</sup> (327  $\mu\text{Ci}$  at 10:49 on Dec. 11<sup>th</sup>, 2009), and 34<sup>th</sup> (141  $\mu\text{Ci}$  at 10:49 on Dec. 11<sup>th</sup>, 2009) were pooled and rotaevaporated under reduced pressure. The residue was then formulated in sterilized  $1 \times \text{PBS}$  for animal imaging (953  $\mu\text{Ci}$  at 11:10 on Dec. 11<sup>th</sup>, 2009, specific activity 0.396 Ci/ $\mu\text{mol}$  at 11:10 on Dec. 11<sup>th</sup>, 2009).

For the experiments to study the factors influencing the radiolabeling of marimastat-boronate **4.14**, similar procedures were used to operate the experiment with trivial modification. We here take reaction III in Table 4.1 as an example of the radiolabeling.  $^{18}\text{F}$ -Fluoride was trapped by a Sep-Pak Light Accell Plus QMA cartridge (Cl<sup>-</sup>, 37-55  $\mu\text{m}$ ) and eluted with 2 mg/mL  $\text{NaClO}_4$  (1 mL) to give a slightly acidic radioactive solution in a 5 mL Pyrex V-vial (pH  $\sim$  5.5, 100 mCi at 11:21, Nov. 23<sup>rd</sup>, 2010) and 0.95 M  $\text{KHCO}_3$  (14  $\mu\text{L}$ ) and 0.125 M  $\text{KHF}_2$  (4  $\mu\text{L}$ ) were added to the  $^{18}\text{F}$ -fluoride solution to give a solution of pH  $\sim$  8. The solution was added with  $\text{CH}_3\text{CN}$  (1.0 mL) and concentrated over Ar stream at 110  $^\circ\text{C}$ . Cooled to rt, the residue was added with 0.125 M  $\text{KHF}_2$  (8  $\mu\text{L}$ ) to resuspend  $^{18}\text{F}$ -fluoride. 1.25  $\mu\text{L}$  of the mixture was added to marimastat-boronate **4.14** (100 nmol) in  $\text{CH}_3\text{CN}$  (4  $\mu\text{L}$ ) and concentrated HCl (0.5  $\mu\text{L}$ ) to initiate the fluoridation. The reaction (5.63 mCi at 11:13, Nov. 23<sup>rd</sup>, 2010) was incubated at rt for 78 min and quenched with 200  $\mu\text{L}$  5%  $\text{NH}_4\text{OH}$  in 50% aqueous EtOH (the radioactivity after the reaction was quenched: 3.35 mCi at 12:31, Nov. 23<sup>rd</sup>, 2010), 10  $\mu\text{L}$  of which was injected into the UPLC using Program 6 with Column III in HPLC System III for analysis.

#### 4.5.8 MicroPET imaging

Female BALB/c mice (7 to 9 weeks old; Taconic Laboratories) were injected with  $1 \times 10^6$  viable 67NR CMV-Luciferase murine mammary cancer cells into the right fourth mammary gland (50  $\mu$ L in PBS/mouse<sup>184</sup>). The mice bearing 67NR tumors at day 26 and day 33 were injected i.p. with the radiolabeled tracer Mar-<sup>18</sup>F-ArBF<sub>3</sub> **4.15** for both the blocking and non-blocking experiments. The blocking experiment was carried out on the control 67NR tumor mice with i.p. injection of the blocking solution of 300 nmol marimastat in PBS buffer three times over one hour prior to the tracer injection. The pre-blocked and unblocked mice were then anesthetized with isoflurane and tail vein injected with 50-100  $\mu$ Ci of <sup>18</sup>F-**4.15** with decay corrected specific activities of 0.179 Ci/ $\mu$ mol and 0.396 Ci/ $\mu$ mol at the time of packaging. The mice were dynamically scanned for 80 minutes followed by a 10-minute transmission scan via a microPET Focus 120 (CTI Concorde) system. The PET imaging data were compiled with Siemens Focus 120 microPET software. PET images were generated with Amide version 0.8.19.

# Chapter 5 Radiosynthesis of an $^{18}\text{F}$ -ArBF<sub>3</sub> labeled PSMA inhibitor for prostate cancer imaging

This chapter describes our effort to label a urea-based ligand with an  $^{18}\text{F}$ -ArBF<sub>3</sub> in order to target prostate-specific membrane antigen (PSMA) in the purpose of imaging prostate cancer. Herein, the preliminary results of the radiolabeling will be presented and discussed.

## 5.1 Introduction

### 5.1.1 Prostate cancer

Prostate cancer that develops in the prostate gland in men is known worldwide as the second most common cancer and it is regarded as one of the six leading causes of cancer death in men.<sup>185</sup> It is the primary cause of death from cancer in men over the age of 70 years and it has been found that there are higher incidence rates in developed countries of Europe and North America, which might be due to the extensive utilization of the prostate-specific antigen (PSA) testing. The PSA test was approved in 1986 by the Food and Drug Administration (FDA) for detection of prostate cancer, which has assisted the diagnosis of early stage prostate cancer.<sup>186</sup> Although PSA is so far the best prostate cancer biomarker,<sup>187-189</sup> it is not entirely specific for prostate cancer because PSA levels might be also elevated in noncancerous conditions.<sup>190</sup> Moreover, the fact that individual patients display different PSA levels limits accurate detection of prostate cancer with high sensitivity, and biopsies are always involved to further confirm prostate cancer.<sup>191, 192</sup> Correspondingly, new approaches and novel biomarkers are needed to provide more precise detection/diagnosis for prostate cancer and to understand the possible cause of the diseases.

### 5.1.2 Biomarkers for prostate cancer

With renewed research efforts, many new potential biomarkers for prostate cancer ( $n \geq 91$ ) have been discovered.<sup>193</sup> An ideal disease biomarker needs to be prostate-specific, detectable in biological fluids such as serum and urine, and disease related.<sup>193</sup> However,

only a few have demonstrated potential clinical applications and been involved in the new therapeutic developments.<sup>193-199</sup> Several biomarkers for prostate cancer will be discussed below.

**Human Kallikrein 2**, a serine protease, shares 80% sequence identity with PSA. Like PSA, it has been found to be overexpressed in prostate cancer.<sup>194, 196, 198, 200</sup> In spite of the improved detection accuracy, its low presence in surrounding prostate tissue, plasma, and blood, only around 1% of that of PSA, however, makes it very challenging in terms of detection by current analytical techniques.

**Prostate cancer gene 3 (PCA3<sup>DD3</sup>)**, a prostate-specific noncoding mRNA, is found to be overexpressed 60-100 fold in more than 95% of prostate cancer/metastatic specimens over normal prostate tissues.<sup>194, 196, 199</sup> Even though the specificity and sensitivity of PCA3<sup>DD3</sup> is close to that of all serum PSA, the test's accuracy was reported to be significantly greater. Additional clinical trials are needed to provide more information for its application in the detection of prostate cancer.

**Early prostate cancer antigen (EPCA)** is a nuclear matrix protein associated with prostate cancer. It has been found with high sensitivity (94%) and specificity (92%) for prostate cancer diagnosis.<sup>194, 196, 198</sup> Further studies are required to validate its clinical application in detecting the disease.

**Prostate cancer-specific autoantibodies** are produced by the immune system when the prostate tumor associated antigens are overexpressed.<sup>194, 196, 198-200</sup>  $\alpha$ -Methyl-acyl-coenzymeA-racemase (AMACR), an enzyme involved in the oxidative metabolism, has been found at abnormally high levels in the prostate cancer tissue.<sup>199</sup> Although the concentration of AMACR is low in serum and urine, the concentration of autoantibodies against this enzyme is always increased. This difference can be used to distinguish patients with prostate cancer from healthy individuals. Thus, detection based on the prostate cancer-specific autoantibodies has demonstrated high diagnostic accuracy with higher sensitivity and improved specificity compared with PSA.<sup>201</sup> A combination of two autoantibodies against different antigens has provided a specific immunoprofile with prostate-cancer specificity and improved diagnostic performance.<sup>202</sup>

**Prostate-specific membrane antigen (PSMA)**, a protein specifically overexpressed in prostate cancer, has been regarded as a potential prostate cancer biomarker and has been extensively studied.<sup>194, 196, 198-200</sup> Although there has been no solid data to indicate the feasibility of detecting PSMA in serum for use in diagnosis, it's been used as a therapeutic target for drug development and for *noninvasive* molecular imaging applications.<sup>195, 203</sup> This is because a) the expression of PSMA occurs mainly in the prostate at all stages of the disease, b) it is overexpressed in both the androgen-insensitive and metastatic disease, c) it localizes on the cell surface instead of entering the circulation system, and d) it is involved in antibody endocytosis that is mediated by receptors.

The biomarkers introduced above have provided valuable information to detect prostate cancer, which allows patients to receive suitable treatment and therapies at early time points. Some of the biomarkers such as the tumor-associated antigens are also being targeted to control late stage and recurrent prostate cancer for drug/therapy development. More details can be found in several excellent reviews.<sup>195, 197</sup>

### **5.1.3 PSMA and molecular imaging of prostate cancer**

PSMA is a type II membrane glycoprotein containing three sub-domains: an *N*-terminal intracellular domain, a transmembrane domain, and an extracellular domain.<sup>204, 205</sup> There are two PSMA variations designated as PSMA and a spliced variant PSM', both of whose biological functions remain unclear.<sup>206, 207</sup> Although PSMA is highly expressed on the surface of all prostate tissues, PSMA has also been detected in some normal tissues such as brain, salivary gland, and renal tubules.<sup>208</sup> Elevated expression of PSMA has been observed during cancer progression and in hormone-refractory prostate cancer.<sup>209, 210</sup> Moreover, PSMA has exhibited immunoreactivity only in vascular endothelial cells, which are restricted to the cancerous region in many tumors.<sup>211</sup> The increased PSMA expression during cancer progression and its specificity for the prostate endothelial cells make it a particularly useful target for both cancer therapies and prognostic diagnosis.

Although the function of PSMA remains unknown, it has been discovered that PSMA has enzymatic activity. PSMA is now also known as folate hydrolase I and glutamate

carboxypeptidase II, which might indicate such roles during cancer progression.<sup>212</sup> Briefly, PSMA is able to cleave the glutamate residue from a peptide such as folate<sup>213, 214</sup> and *N*-acetylaspartylglutamate<sup>215</sup> with high efficiency. A study via X-ray crystallography revealed that in the external domain of PSMA there is a glutamate sensing pocket, which demonstrates a conformational change after PSMA binds to small agonists and antagonists.<sup>216</sup> By targeting its enzymatic activity, various PSMA pro-drugs have been developed and studied. Fundamentally, it is expected that the non-toxic pro-drugs would only release the active moieties at the tumor site where PSMA serves as molecular “scissors”. For example, several methotrexate-based glutamates were studied and shown to display high specificity for PSMA and stability in serum for potential cancer therapies.<sup>217</sup>

PSMA targeted therapies and diagnosis in the past were mainly focused on the antibody studies.<sup>218-220</sup> The first antibody against PSMA is ProstaScint<sup>®</sup>, an <sup>111</sup>In-labeled mouse monoantibody (mAb) that recognizes the intracellular epitope of PSMA on dead or necrotic cells, commonly present in lymph nodes.<sup>221</sup> Since it only detects dead cells, it is actually employed to provide information for the elimination of prostate cancer cells after therapy treatment as a post-therapy evaluation method. Soon, a human recombinant antibody J591 was developed by Bander and co-workers to target the extracellular domain of PSMA;<sup>218</sup> J591 has been developed for clinical use. The metal chelating agent was introduced to this antibody to deliver therapeutic radionuclides such as lutecium-177 and yttrium-90.<sup>218, 222, 223</sup> In phase I clinical studies of <sup>177</sup>Lu-J591, all locations of the metastatic disease were successfully imaged in metastatic prostate cancer patients.<sup>222</sup>

Although antibodies have proven to be useful for imaging and radioimmunotherapy for prostate cancer and other solid tumors where PSMA is overexpressed,<sup>220, 224</sup> the long circulation time required for antibodies to reach their targets can result in a prolonged whole-body radiation dose.<sup>203</sup> On the other hand, the development of inhibitors of glutamate carboxypeptidases has provided a series of drug-like candidates of low molecular weight and high potency to target PSMA. The first potent and selective synthetic PSMA inhibitor, 2-(phosphonomethyl)pentanedioic acid, now known as 2-PMPA, was developed by Guilford Pharmaceuticals in 1996.<sup>225</sup> The study on the

substrate enantiospecificity to the enzyme with 2-PMPA has disclosed that (*L*)-glutamate residue is critical for the inhibitory activity.<sup>226</sup> A further study on the substrate specificity of PSMA has revealed that the acidic residues on the substrates are more favorable for binding.<sup>227</sup> It was also found that the pharmacophore pocket of PSMA preferentially binds to glutamate or glutamate-like structures on the P1' residue while the non-pharmacophore site with an “*arginine patch*” is mainly involved in charge-to-charge interactions to recruit the negatively charged residues on the substrate (P1 residue).<sup>228-231</sup> This determines the high structure tolerance of the non-pharmacophore subpocket and the low tolerance for structural changes of the inhibitors for the pharmacophore subpocket. Based on this, a series of inhibitors, most of which contain the glutamate residue, have been developed.<sup>227, 232-236</sup> These inhibitors include phosphonamidates<sup>233-237</sup> and urea-based PSMA inhibitors<sup>238</sup> as shown in Figure 5.1.<sup>232</sup>

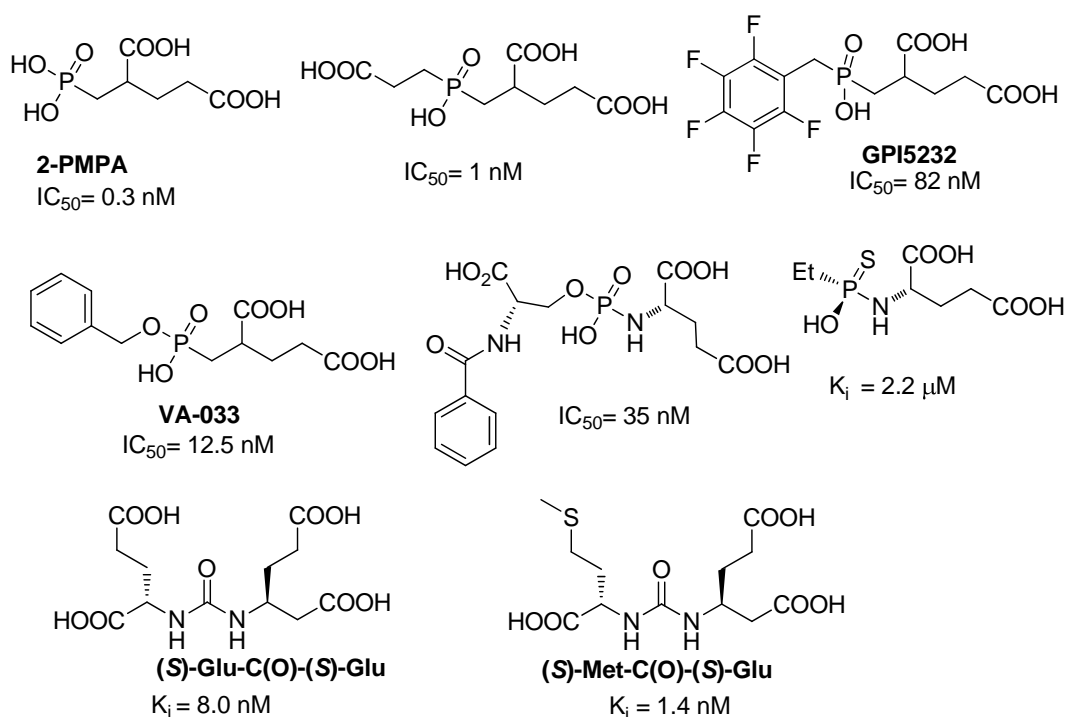


**Figure 5.1** Examples for some synthesized PSMA inhibitors.<sup>232, 234, 236</sup>

With potent inhibitory activity against PSMA, some of the inhibitors have been further developed as imaging ligands to visualize PSMA expression *in vivo* and to study their pharmacokinetics and specificity. One of the phosphonamidates, *S*-2-(((2-*S*-4-amino-4-carboxybutanamido)-*S*-2-carboxyethoxy)-hydroxyphosphorylamino)-pentadioic acid was

coupled with *N*-succinimidyl-4-<sup>18</sup>F-fluorobenzoate (<sup>18</sup>F-SFB) with a very high radiochemical yield (> 90% from <sup>18</sup>F-SFB) to give the <sup>18</sup>F-fluorobenzamido-phosphonamidate, whose structure is indicated in Figure 5.2.<sup>239</sup> The *in vivo* imaging and biodistribution study suggested that the radiolabeled phosphonamidate cleared rapidly in the mice while high tumor uptake was achieved with a tumor-to-blood ratio of 9:1 at two hours post injection. The tumor uptake was regarded as specific based on two types of experiments: 1) differential imaging of mice bearing PSMA (+) or PSMA (-) tumor models and 2) a typical blocking experiment that was undertaken with mice bearing PSMA (+) tumors. Substantially lower tumor uptake was observed in mice with PSMA (-) tumor or mice with PSMA (+) tumor treated with the blocking agent. Although high kidney uptake was observed, which was thought to be partially due to PSMA specific binding to the kidney, the low uptake in both bone and liver strongly implied high *in vivo* stability and low lipophilicity of this molecule. Therefore, these promising results would guide further development of this category of compounds for prostate cancer imaging.

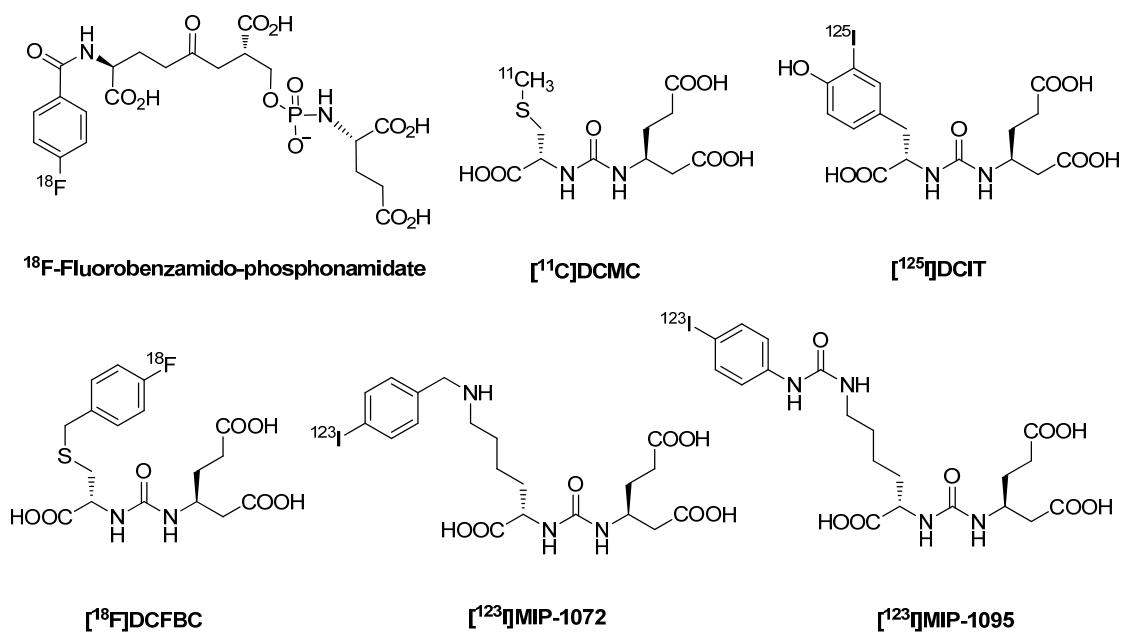


Figure 5.2 Several radiolabeled PSMA inhibitors reviewed in this chapter.

Glutamate-containing urea-based PSMA inhibitors have also been developed.<sup>238, 240</sup> Dr. Martin Pomper and co-workers in Johns Hopkins Medical Institute have published a significant amount of beautiful imaging work on this type of molecules with various radionuclides including <sup>18</sup>F, <sup>11</sup>C, <sup>125</sup>I, <sup>99m</sup>Tc, and <sup>68</sup>Ga.<sup>174, 175, 241-245</sup> The radiolabeled

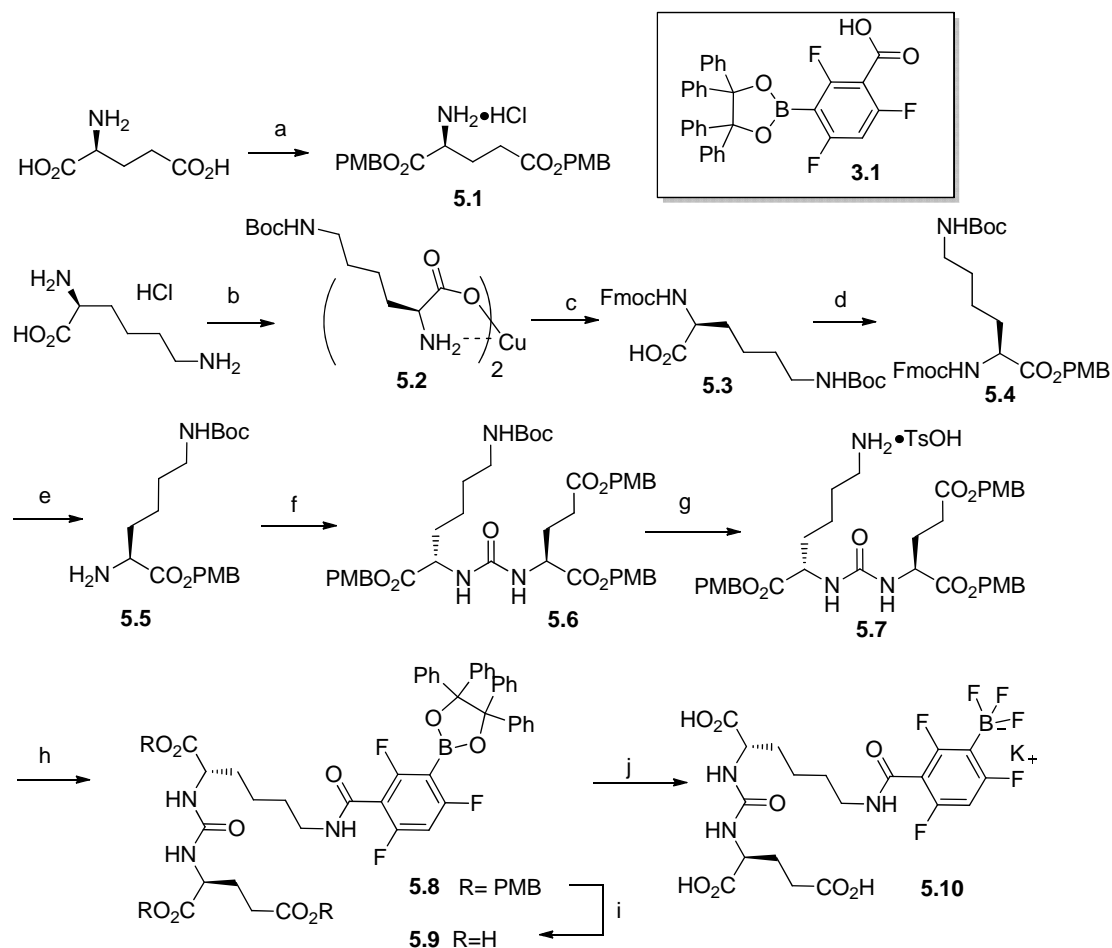
urea-based PSMA inhibitors, [ $^{11}\text{C}$ ]DCMC and [ $^{125}\text{I}$ ]DCIT, were first reported for *in vivo* imaging targeting PSMA in tumor-bearing mice.<sup>241</sup> Despite the fact that there was only mild tumor uptake of [ $^{125}\text{I}$ ]DCIT, both radiolabeled tracers showed very high PSMA specific tumor uptake. The tumor-to-muscle ratios of 10.78 for [ $^{11}\text{C}$ ]DCMC and 4.69 for [ $^{125}\text{I}$ ]DCIT in tumor-bearing mice with prostate cancer were obtained. Soon, a similar version of  $^{18}\text{F}$ -labeled urea, [ $^{18}\text{F}$ ]DCFBC, was reported to not only demonstrate high tumor uptake, but also low liver uptake.<sup>242</sup> [ $^{18}\text{F}$ ]DCFBC was therein claimed to be the first clinically useful PET imaging agent for PSMA. A glutamate-urea-lysine (Glu-C(O)-Lys) analogue was developed as a suitable scaffold for derivatization with various radionuclides.<sup>174, 175, 243-245</sup> Two of the  $^{123}\text{I}$ -labeled ureas derived from Glu-C(O)-Lys, [ $^{123}\text{I}$ ]MIP-1072 and [ $^{123}\text{I}$ ]MIP-1095, are now in preclinical evaluation for the detection and staging of prostate cancer.<sup>244, 245</sup>

#### 5.1.4 Labeling the urea-based PSMA inhibitor with an $^{18}\text{F}$ -ArBF<sub>3</sub>

The urea Glu-C(O)-Lys provides the  $\epsilon$ -amino group of the lysine residue for further derivatization of the molecule, while other known analogues all have shown very high target specificity and high affinity in promising *in vivo* imaging studies.<sup>174, 175, 243-245</sup> This molecule received our attention because the  $\epsilon$ -amino group on the lysine residue perfectly allows for conjugation to boronate **3.1**. It is expected that after the fluoridation, its ArBF<sub>3</sub> labeled version may provide improved clearance properties in addition to its inhibitory activity towards PSMA. The negatively charged ArBF<sub>3</sub> might also enhance the electrostatic interactions with the “*arginine patch*” subpocket of PSMA, which could result in enhanced inhibitory activity. In addition, labeling Glu-C(O)-Lys with an ArBF<sub>3</sub> can further enable evaluation of the potential application of ArBF<sub>3</sub>s as PET imaging agents. Therefore, in this chapter, we synthesized HO-Lys(boronate)-C(O)-Glu(OH)-OH **5.9** and its radiolabeling was studied. Further biological and animal studies are awaited to provide more information of *in vivo* properties of the  $^{18}\text{F}$ -ArBF<sub>3</sub> labeled urea.

## 5.2 Results

### 5.2.1 Synthesis



**Scheme 5.1** Synthesis of urea-borate 5.9 following the literature protocol.

(a) i. *N,N,N',N'*-Tetramethylguanidine, DMF, 0 °C, 0.5 hr, ii. ethyl acetoacetate, rt, iii. PMB-Cl, rt, 24 hr, iv. 1 N HCl, MeOH, rt, 10 min, 53% over four steps; (b) i.  $\text{CuSO}_4 \cdot 5\text{H}_2\text{O}$ ,  $\text{H}_2\text{O}$ , 80 °C, 5 min, ii.  $(\text{Boc})_2\text{O}$ , 1,4-dioxane, pH 9, rt, 48 hr, 87% over two steps; (c) i. 1.41 N EDTA (aq), rt, 3 hr, ii. Fmoc-Osu,  $\text{Na}_2\text{CO}_3$ , 0 °C to rt, overnight, 98% over two steps; (d)  $\text{Cs}_2\text{CO}_3$ , DMF, Ar, PMB-Cl, 0 °C to rt, 4 hr, 78%; (e) 20% piperidine/DMF, rt, 2 hr, 59%; (f) i. CDI, NMM,  $\text{CH}_2\text{Cl}_2$ , Ar, r.t., 1 hr, ii. 5.1, NMM,  $\text{CH}_2\text{Cl}_2$ , Ar, rt, overnight, 33%; (g)  $\text{TsOH} \cdot \text{H}_2\text{O}$ , EtOAc/THF, rota-vap, 49%; (h) 3.1, EDC-HCl,  $\text{HOBt} \cdot \text{H}_2\text{O}$ , Py,  $\text{CH}_2\text{Cl}_2$ , rt, overnight, 72%; (i) 3% anisole in TFA, 1 hr, rt, 16%.

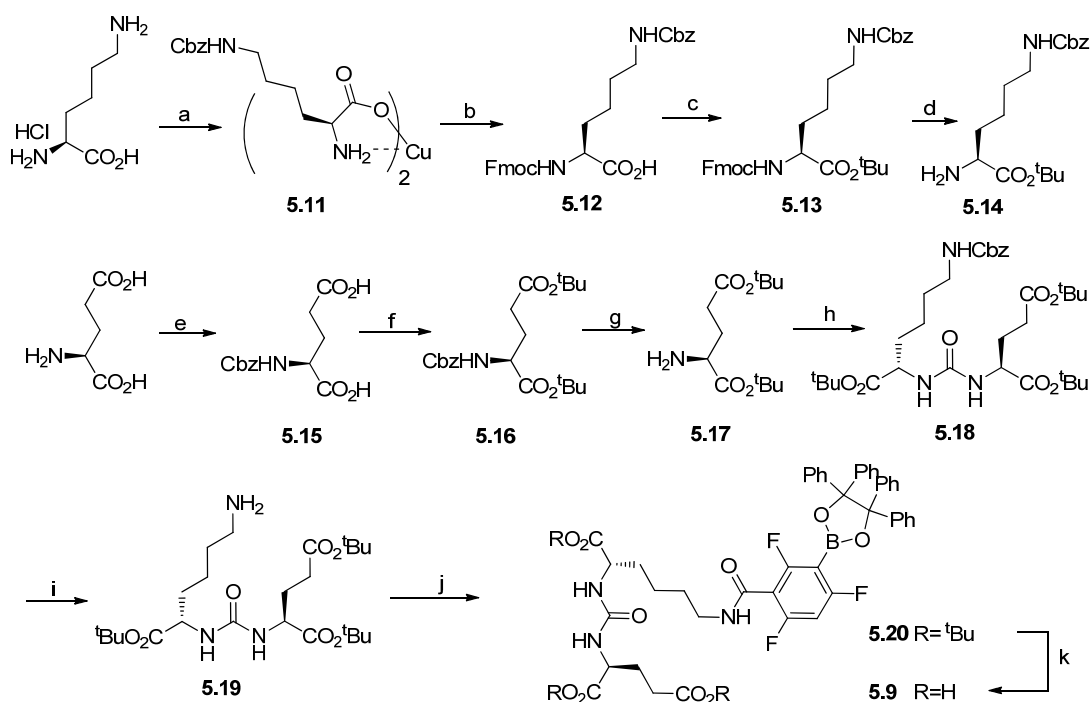
The synthesis of the urea first followed a literature protocol reported by Pomper and co-workers<sup>243</sup> with some modifications as summarized in Scheme 5.1. Briefly, (*L*)-glutamic acid was first treated with *N,N,N',N'*-tetramethylguanidine and ethyl acetoacetate to selectively block the amino group. PMB-Cl was then added to the mixture to give the *bis*-PMB ester. The *N*-protected glutamate diester was treated with HCl in MeOH for a short time (10 min) to provide the *bis*-PMB protected glutamate

HCl·H-Glu(OPMB)-OPMB **5.1**.<sup>246, 247</sup> Meanwhile, the  $\epsilon$ -amino group of (*L*)-lysine was selectively protected with a Boc group by taking advantage of copper chelation chemistry to form the stable copper(II) complex.<sup>248</sup> Then copper(II) was readily removed by EDTA to release H-Lys(Boc)-OH, which was immediately converted to Fmoc-Lys(Boc)-OH **5.3** in the presence of Fmoc-OSu under basic conditions in high yields. Following esterification with PMB-Cl and Fmoc-deprotection with piperidine, H-Lys(Boc)-OPMB **5.5** was obtained. Instead of triphosgene, carbonyldiimidazole (CDI) was used to conjugate the amino acids **5.1** and **5.5** to afford urea **5.6** in a moderate yield.<sup>249</sup> Urea **5.6** was treated with TsOH to successfully and selectively remove the Boc group on the side chain of the lysine residue to give intermediate **5.7**. EDC coupling of **5.7** and boronate **3.1** yielded **5.8** and the subsequent TFA treatment of **5.8** in the presence of anisole provided the desired product, urea-boronate **5.9**. The overall yield from (*L*)-lysine of this synthesis is 0.73% over eight steps.

The low overall yield of the synthesis in Scheme 5.1 might be attributed to low yields in two specific reactions, the deprotection of the Boc group in the presence of TsOH for **5.7** and the deprotection of the PMB groups with 3% anisole in TFA for **5.9**. Although the Boc group is more acid-labile than the PMB group, deprotection of the PMB group could not be avoided and a yield of only 33% was obtained for this reaction. In addition, severe deboronation was observed during the deprotection of **5.8**, while anisole and the byproducts further complicated the purification of the desired product **5.9**. Based on this, a more acid-labile protecting group *tert*-butyl (<sup>t</sup>Bu) was introduced to protect all the carboxylic groups and an orthogonal amine protecting group, the carbobenzyloxy (Cbz) was used instead of Boc to mask the  $\epsilon$ -amino group of lysine. This alternative synthesis is demonstrated in Scheme 5.2.

The acid-labile *bis-tert*-butyl ester **5.16** was prepared from Cbz-Glu-OH **5.15** with *tert*-butyl *N,N'*-dicyclohexylisourea, which was obtained by incubating DCC in *tert*-butanol in the presence of a catalytic amount of CuCl<sub>2</sub> for 5 days. Then, **5.16** was incubated in THF in the presence of Pd/C under the H<sub>2</sub> atmosphere to afford H-Glu(O<sup>t</sup>Bu)-O<sup>t</sup>Bu **5.17**. On the other hand, CbzCl was added to the lysine-copper(II) complex to protect the  $\epsilon$ -amino group of lysine. However, in this case EDTA was found

to be ineffective in releasing the Cbz-protected lysine from the copper. Instead, Na<sub>2</sub>S was used to destroy the complex by forming Cu<sub>2</sub>S and thereby releasing the free H-Lys(Cbz)-OH,<sup>250</sup> which was then directly reacted with Fmoc-OSu to give Fmoc-Lys(Cbz)-OH **5.12**. Following the same *tert*-butyl ester preparation from dicyclohexylisourea and a subsequent Fmoc-deprotection, lysine **5.14** was obtained and then coupled to glutamate **5.17** in the presence of CDI to form dipeptide urea **5.18**, which underwent the Pd/C catalyzed hydrogenolysis to successfully give the free amine **5.19**. Boronate **3.1** was then conjugated to urea **5.19** using EDC/HOBt as the coupling reagents to afford **5.20** in a good yield. The deprotection in TFA/CH<sub>2</sub>Cl<sub>2</sub> cleanly provided the desired product **5.9** with reasonable purity, which was further purified via RP-HPLC. The overall yield of this modified synthetic protocol for **5.9** from (*L*)-lysine is increased to 7.8% over eight steps.



**Scheme 5.2** Modified synthetic route of urea-borate **5.9**.

(a), i. NaOH, CuSO<sub>4</sub>·5H<sub>2</sub>O, H<sub>2</sub>O, 80°C to rt, ii. NaOH/NaHCO<sub>3</sub>, CbzCl, 1,4-dioxane/H<sub>2</sub>O, 0 °C to rt, overnight, 94% over two steps; (b), i. Na<sub>2</sub>S, H<sub>2</sub>O, rt, 0.5 hr, ii. NaHCO<sub>3</sub>, FmocCl, dioxane/H<sub>2</sub>O, 0 °C to rt, overnight, 38% over two steps; (c), *tert*-butyl *N,N'*-dicyclohexylisourea, CH<sub>2</sub>Cl<sub>2</sub>, reflux, overnight, 83%; (d), HNEt<sub>2</sub>, CH<sub>2</sub>Cl<sub>2</sub>, rt, 2 hr, 83%; (e), NaHCO<sub>3</sub>, CbzCl, H<sub>2</sub>O, 0 °C to rt, 26 hr, 81%; (f), *tert*-butyl *N,N'*-dicyclohexylisourea, CH<sub>2</sub>Cl<sub>2</sub>, reflux, overnight, 77%; (g), 10% Pd/C, H<sub>2</sub>, THF, rt, 24 hr, 93%; (h), i. CDI, NMM, CH<sub>2</sub>Cl<sub>2</sub>, Ar, rt, 3 hr, ii. **5.14**, NMM, CH<sub>2</sub>Cl<sub>2</sub>, rt, 24 hr, 89%; (i), 10% Pd/C, H<sub>2</sub>, THF, rt, 24 hr, 47%; (j), **3.1**, EDC·HCl, HOBt·H<sub>2</sub>O, pyridine, CH<sub>2</sub>Cl<sub>2</sub>, rt, overnight, 77%; (k), 50% TFA/CH<sub>2</sub>Cl<sub>2</sub>, rt, 3 hr, quant.

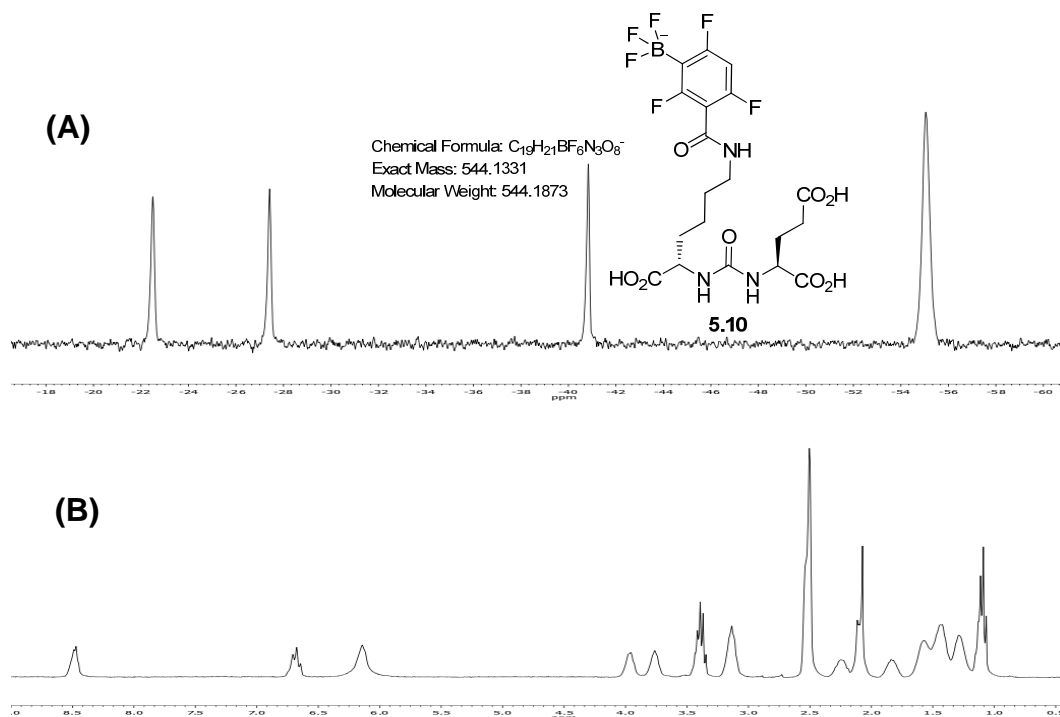


**Figure 5.3** NMR spectra of urea-ArBF<sub>3</sub> **5.10**.

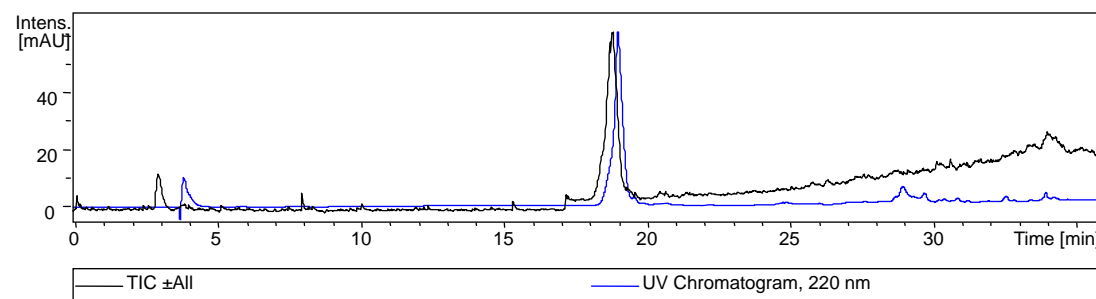
The spectrum A: <sup>19</sup>F NMR spectrum of **5.10** in *d*<sub>6</sub>-DMSO at rt; the spectrum B: <sup>1</sup>H NMR spectrum of **5.10** in *d*<sub>6</sub>-DMSO at rt.

Boronate **5.9** was then treated with a large excess of KHF<sub>2</sub> overnight to give the corresponding ArBF<sub>3</sub> **5.10**, which was used to study its HPLC chromatographic performance. Its <sup>19</sup>F NMR and <sup>1</sup>H NMR spectra are shown in Figure 5.3. From the <sup>19</sup>F NMR spectrum, the integration of the characteristic ArBF<sub>3</sub> peak at -55.0 *ppm* is perfectly three times that of each Ar-F. The <sup>1</sup>H NMR spectrum exhibits the absence of the benzopinacol group (~ 7.2 to 7.4 *ppm*) and also shows the characteristic protons of the urea compound as the two α-protons at 3.76 *ppm* and 3.98 *ppm* respectively and the *N*-protons on the urea at 6.14 *ppm*.

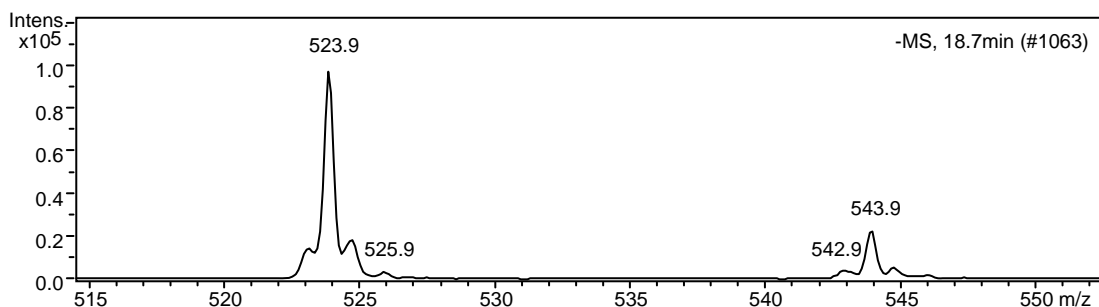
Overall, we were able to synthesize urea-boronate **5.9** via two independent routes. A better overall yield was achieved via the Cbz/<sup>t</sup>Bu protecting strategy. Urea-boronate **5.9** was successfully converted to urea-ArBF<sub>3</sub> **5.10** with relatively high purity, which can be directly used for various studies.

## 5.2.2 HPLC conditions for urea-ArBF<sub>3</sub> 5.10

### 5.2.2.1 HPLC analysis of urea-ArBF<sub>3</sub> 5.10



(A)



(B)

**Figure 5.4** The ESI-LCMS of urea-ArBF<sub>3</sub> 5.10.

(A), Both the TIC and UV-HPLC chromatograms of 5.10; (B), the ESI spectrum at 18.7 min of the TIC chromatogram of 5.10. The LC was performed via Program 16 with Column I in the ESI-LCMS system. And 5  $\mu$ L of the *d*<sub>6</sub>-DMSO stock solution of 5.10 was injected into the LCMS with the mass detector at the negative mode.

With three free carboxylic groups and an ArBF<sub>3</sub>, compound 5.10 demonstrates excellent water solubility; however, the high polarity initially complicated its purification while acids such as TFA or formic acid, which have usually been added to the mobile phase to ensure good peak shape and resolution for peptides and carboxylic acids in HPLC, are not suitable in this case as acidic conditions promote solvolytic fluoride loss.<sup>251</sup> As such has been reported<sup>164, 252</sup> and we have also learned that ArBF<sub>3</sub>s have short life times under acidic conditions, thus we tend to avoid the use of acid in the HPLC solvent system for the analysis/purification of ArBF<sub>3</sub>s. The first solvent systems we tried were CH<sub>3</sub>CN/H<sub>2</sub>O and MeOH/H<sub>2</sub>O. It was found that both 5.9 and 5.10 co-eluted at the solvent front over a C18 column in the RP-HPLC, even with 100% H<sub>2</sub>O flush. Similar results were obtained by switching the aqueous mobile phase to phosphate buffer or

ammonium formate buffer ( $\text{HCO}_2\text{NH}_4$ ). Advised by Phenomenex HPLC experts, I also tried a C4-column, a Synergi Fusion-RP C18 column and even a size exclusion Biosep-Sec2000 column. None of these solved our problem. Fortunately, when I turned to triethylammonium acetate (TEAA)/ $\text{CH}_3\text{CN}$ , which I used as the solvent system to analyze one of the oligonucleotides studied in Chapter 6, surprisingly good retention time was obtained. The buffer at pH 6 with the counter cation  $\text{HNEt}_3^+$  clearly provided good resolution. Although the lack of good chromophore on compound **5.10** resulted in poor UV signal detection, ESI-LCMS successfully identified the desired product, which eluted at 18.7 minutes with an expected mass ( $[\text{M}]^-$ : 543.9 and  $[\text{M}-\text{HF}]^-$ : 523.9) as shown in Figure 5.4.

### 5.2.2.2 The fluoridation analyzed by ESI-LCMS

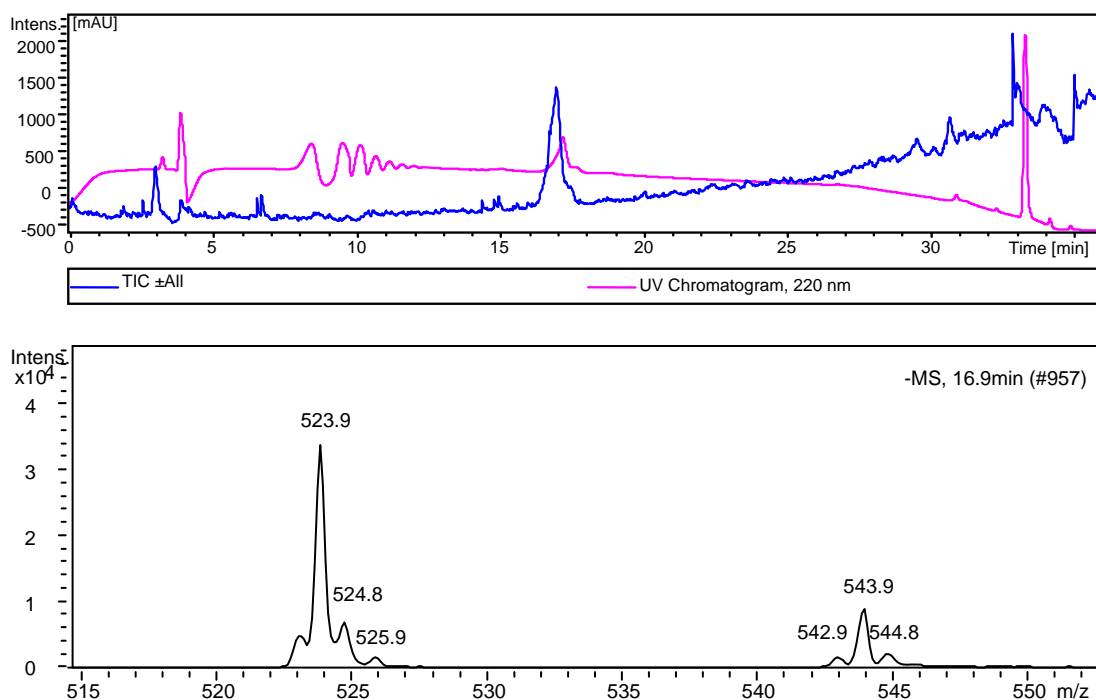


**Figure 5.5** The ESI-LCMS analysis of the fluoridation to prepare urea- $\text{ArBF}_3$  **5.10**.

The fluoridation was carried out in the presence of urea-boronate **5.9** (15.4 mM),  $\text{HCl}$  (0.97 M), and  $\text{KHF}_2$  (61.5 mM) in 6.5  $\mu\text{L}$  of 61.5% aqueous  $\text{CH}_3\text{CN}$  at rt for 84 min and quenched with 20  $\mu\text{L}$  of 5%  $\text{NH}_4\text{OH}$  in  $\text{EtOH}$ . 10  $\mu\text{L}$  of the quenched reaction was injected into the LCMS. The LC was performed via Program 16 with Column I in the ESI-LCMS system. The blue trace is the TIC for the injection at the negative mode; the purple one is the UV-HPLC chromatogram at 220 nm.

The non-radioactive fluoridation of urea-boronate **5.9** was carried out under the standard

fluoridation conditions used in this thesis. Briefly, 100 nmol of **5.9** in 4  $\mu\text{L}$   $\text{CH}_3\text{CN}$  was added with 2  $\mu\text{L}$  of 0.4 M  $\text{KHF}_2$  and 0.5  $\mu\text{L}$  of 12.6 M concentrated  $\text{HCl}$ . The reaction was incubated at room temperature and quenched with 5%  $\text{NH}_4\text{OH}$  in  $\text{EtOH}$ <sup>a</sup>. The quenched crude was then injected into ESI-LCMS for analysis. The product was detected with a retention time of 16.9 minutes as shown in Figure 5.5.

### 5.2.3 The radiosynthesis of urea-<sup>18</sup>F-ArBF<sub>3</sub> **5.10**

Since the desired urea-ArBF<sub>3</sub> **5.10** has very low UV activity, radio-HPLC was also used to study its chromatographic performance before the TEAA solvent was used. Similar results were obtained with the mobile phase of  $\text{H}_2\text{O}/\text{MeOH}$ ,  $\text{H}_2\text{O}/\text{CH}_3\text{CN}$  and aqueous  $\text{HCO}_2\text{NH}_4/\text{CH}_3\text{CN}$ . For instance, the radio-HPLC chromatogram of one <sup>18</sup>F-fluoridation of urea-boronate **5.9**, with  $\text{HCO}_2\text{NH}_4/\text{CH}_3\text{CN}$  as the mobile phase, has been shown in Figure 5.6. This disappointing result suggested that either there was no resolution between free <sup>18</sup>F-fluoride and the <sup>18</sup>F-labeled urea-ArBF<sub>3</sub> **5.10** or the reaction did not work.

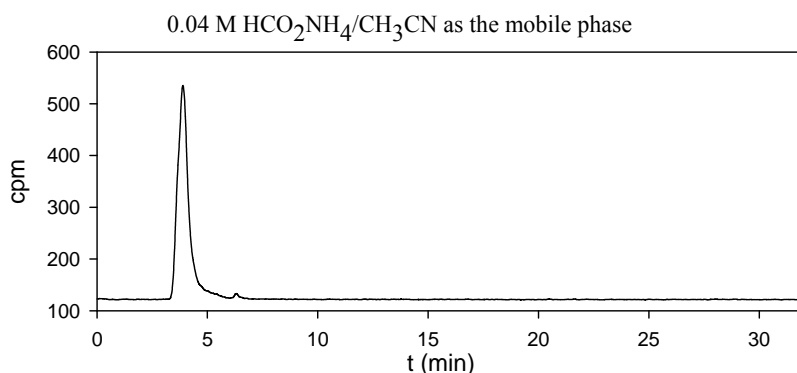


**Figure 5.6** The radio-HPLC chromatogram of the <sup>18</sup>F-fluoridation of urea-boronate **5.9** in  $\text{HCO}_2\text{NH}_4/\text{CH}_3\text{CN}$  solvent system.

The HPLC was performed via HPLC Program 7 with Column I in HPLC System IV. The radiolabeling condition: urea-boronate **5.9** (100 nmol),  $\text{HCl}$  (6.3  $\mu\text{mol}$ ), and <sup>18</sup>F-fluoride containing <sup>19</sup>F-fluoride (500 nmol) in 61.5% aqueous  $\text{CH}_3\text{CN}$  (6.5  $\mu\text{L}$ ), rt, 70 min. The reaction was quenched with 5%  $\text{NH}_4\text{OH}$  in 50% aqueous  $\text{EtOH}$  (100  $\mu\text{L}$ ). The radioactivity at the BOS: 1.35 mCi.

In contrast, using TEAA buffer instead of  $\text{H}_2\text{O}$  or  $\text{HCO}_2\text{NH}_4$  solution as the aqueous mobile phase, I obtained a radio-HPLC chromatogram with good resolution. The radiochemical yield can be calculated based on the radio-HPLC trace, since a negligible

<sup>a</sup> It was found that precipitation was caused via quenching the reaction with  $\text{NH}_4\text{OH}$  in 50% aqueous  $\text{EtOH}$ .

amount of radioactivity was retained on the column under the gradient conditions used. As shown in Figure 5.7A, the new radio-peak at 15.8 minutes produced in the reaction had a very close retention time with the ESI-LCMS chromatogram and the radiochemical yield of this labeling reaction was 20%. Moreover, same as the work in the radiolabeling of marimastat-boronate **4.14**, there was a new peak produced besides the free fluoride, which is most likely  $^{18}\text{F-BF}_4^-$  as discussed in Chapter 4.

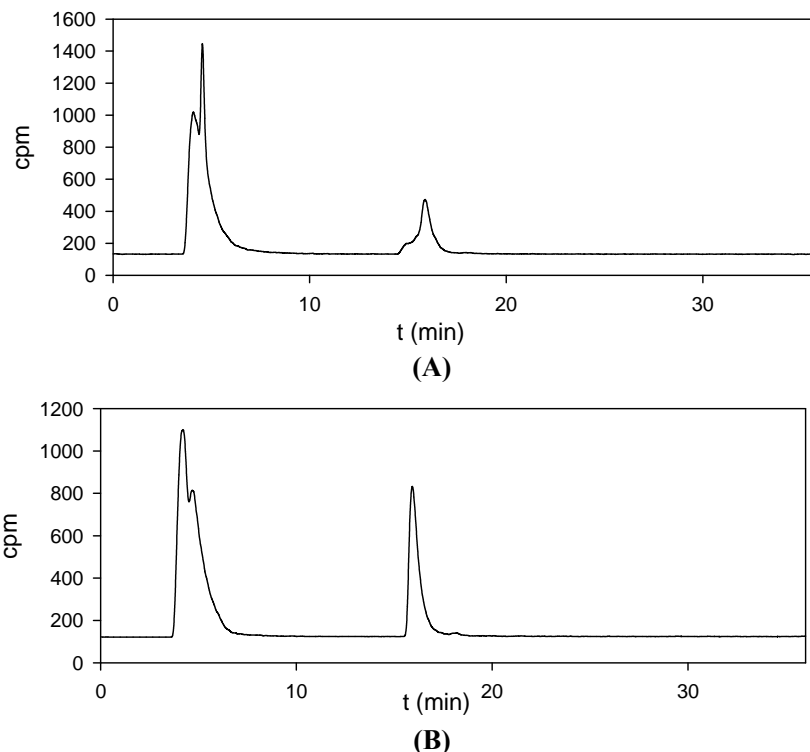


**Figure 5.7 The radio-HPLC chromatograms of the radiosynthesis of urea- $^{18}\text{F-ArBF}_3$  **5.10**.**

The HPLC was performed via HPLC Program 16 with Column I in HPLC System IV. The radiolabeling conditions for HPLC trace **A**: urea-boronate **5.9** (100 nmol), HCl (6.3  $\mu\text{mol}$ ), and  $^{18}\text{F}$ -fluoride containing  $^{19}\text{F}$ -fluoride (500 nmol) in 61.5% aqueous  $\text{CH}_3\text{CN}$  (6.5  $\mu\text{L}$ ), rt, 70 min, and quenched with 5%  $\text{NH}_4\text{OH}$  in 50% aqueous EtOH (100  $\mu\text{L}$ ), the radioactivity at the BOS: 3.26 mCi, RCY: 20%; that for HPLC trace **B**: urea-boronate **5.9** (100 nmol), HCl (6.3  $\mu\text{mol}$ ), and  $^{18}\text{F}$ -fluoride containing  $^{19}\text{F}$ -fluoride (500 nmol) in 72.7% aqueous  $\text{CH}_3\text{CN}$  (5.5  $\mu\text{L}$ ), rt, 60 min, and quenched with 2%  $\text{NEt}_3$  in 75% aqueous  $\text{CH}_3\text{CN}$  (100  $\mu\text{L}$ ), the radioactivity at the BOS: 2.69 mCi and RCY: 25%

The peak shape of the desired product at 15.8 minutes in Figure 5.7A was a bit broad, which might be due to the mobile phase, the flow rate, column temperatures or the injection conditions. Before adjusting the HPLC conditions, a different quench buffer containing triethylamine (TEA) in aqueous  $\text{CH}_3\text{CN}$  was used instead. This new quench buffer was expected to be more compatible with the HPLC solvent system. The radiolabeling reaction was undertaken in the same way, quenched with TEA solution and

injected into the HPLC. The radio-HPLC chromatogram was shown in Figure 5.7B. A similar result was obtained as that shown in Figure 5.7A, but with better product peak resolution.

## 5.3 Discussion

### 5.3.1 Synthesis

Urea-boronate **5.9** was synthesized via two similar synthetic pathways based on different protecting group strategies. The method employing the PMB-protecting groups based on a literature report<sup>243</sup> was followed with some modifications. One of the modifications during the synthesis of the urea was the use of CDI instead of triphosgene. A lower yield was obtained, which may be due to the lower reactivity of CDI in this reaction. Moreover, the deprotection of the Boc group from **5.6** by TsOH was carried out in EtOAc/THF instead of EtOAc/EtOH described in the original work. We first followed the literature conditions with EtOAc/MeOH as the reaction solvent. However, severe transesterification was observed and the separation of the desired tri-PMB ester from the Me/PMB esters was very challenging. We hence turned to EtOAc/THF as the solvent to achieve relatively clean deprotection in moderate yields. This deprotection occurred slowly at room temperature. It was found that during the rotary evaporation at 40 °C the deprotection of Boc proceeded rapidly. Consequently, the reaction was further modified by increasing the number of times ( $n \geq 3$ ) of rotary evaporation to remove the EtOAc/THF cosolvent. With eight steps from lysine, compound **5.9** was obtained in an overall yield of 0.73%.

The limiting step of the first synthesis was primarily the PMB-deprotection of **5.8**, which yielded a high amount of the deboronated product. Besides, the purification was complicated by anisole, which was present in the deprotection cocktail, and the byproducts of the deprotection reaction. We therefore turned to the *tert*-butyl protecting group. The *tert*-butyl ester is more acid-labile and the byproduct from the deprotection step is *iso*-butene, which escapes the reaction vessel as a gas. This allows a much easier purification following the deprotection reaction. Moreover, since it is more acid-labile, a lower concentration of TFA and the absence of the cation scavenger would simplify the

deprotection reaction and also minimize the extent of the deboronation. It took two more steps to introduce the *tert*-butyl groups to the glutamate, and the preparation of di-*tert*-butyl glutamate H-Glu(O<sup>t</sup>Bu)-O<sup>t</sup>Bu **5.17** was obtained in a yield of 58% over three steps. Although it took a long time to prepare *tert*-butyl dicyclohexylisourea, the esterification to prepare the *tert*-butyl esters using this method resulted in relatively high yields. At the same time, in order to selectively protect the  $\epsilon$ -amino group of lysine with the Cbz group, copper was used to block the reactivity of the  $\alpha$ -amino group by forming a stable copper complex. To our surprise, in contrast to [H-Lys(Boc)-O]<sub>2</sub>Cu(II) **5.2**, which was liberated from copper by EDTA treatment, the complex [H-Lys(Cbz)-O]<sub>2</sub>Cu(II) **5.11** showed much higher stability and use of EDTA failed to free the amino acid. Instead, Na<sub>2</sub>S was used to remove copper(II) by forming insoluble Cu<sub>2</sub>S and thereby releasing the amino acid. The filtrate from the Na<sub>2</sub>S treatment was directly used for the Fmoc-protection. Fmoc-Lys(Cbz)-OH **5.12** was obtained in a relatively low yield. A second low yielding reaction was the Pd/C catalyzed hydrogenolysis of the Cbz-protected urea **5.18**. Although TLC analysis<sup>a</sup> suggested the starting material **5.18** was 100% consumed to give the desired product, the isolated yield via flash chromatography was low. Nevertheless, *tri-tert*-butyl ester **5.20** was treated with 50% TFA in CH<sub>2</sub>Cl<sub>2</sub> for about three hours to provide the desired product in high yields and with good purity. The overall yield of the <sup>t</sup>Bu/Cbz protecting strategy was 7.8% over eight steps from lysine, which is about ten times the overall yield (0.73%) of the first synthesis from the PMB/Boc protecting method with same synthetic steps starting from lysine.

The deprotection of **5.8** and **5.20** with TFA showed very different results. The HPLC analysis of these TFA deprotections is summarized in Figure 5.8. It indicates that more impurities were present in the crude deprotection of **5.8** than that in the deprotection of **5.20**. These impurities might include the partially deprotected products such as *mono/bis*-PMB ureas and anisole used for the deprotection. Moreover, it is possible that there were some deboronated products present in the crude mixture. In contrast, the HPLC trace of the crude deprotection of **5.20** was thus much cleaner. It is much easier to isolate the desired product out from the acid treatment of **5.20** than the PMB protected

---

<sup>a</sup> The TLC plate was visualized by ninhydrin stain.

counterpart **5.8**.

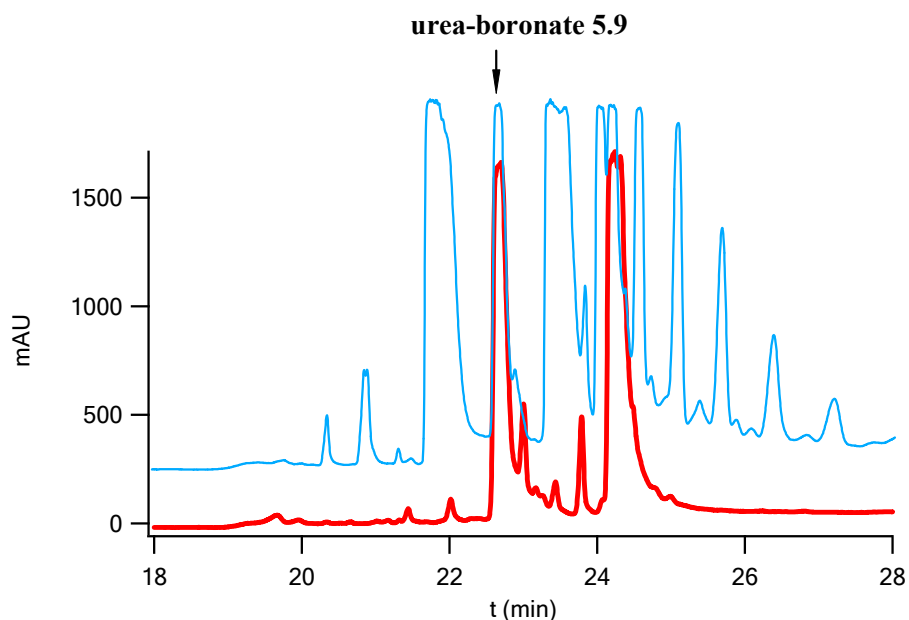


**Figure 5.8** The HPLC traces of the deprotection of **5.8** and **5.20** with TFA.

The blue trace is the deprotection of **5.8** with 3% anisole in TFA at rt for 3 hr and the red one is the deprotection of **5.20** with neat TFA at rt for 3 hr. The HPLC was performed via HPLC Program 18 with Column II in HPLC System I.

Moreover, when treating **5.20** with neat TFA, both TLC and HPLC analysis demonstrated that a very non-polar species was slowly produced in the reaction. We then purified this non-polar compound and characterized it by  $^1\text{H}$  NMR spectroscopy and ESI-mass spectrometry as shown in Figure 5.9A and Figure 5.9B. From the  $^1\text{H}$  NMR spectrum shown in Figure 5.9A, different from that of benzopinacol, there are two Ar-H's ( $\sim 7.55$  ppm) that are further shielded and thus differentiated from other Ar-H's. This suggested that the electronic and magnetic environment for these Ar-H's (at 7.55 ppm) is dramatically different from other Ar-H's. From the "Spectral Database for Organic Compounds, SDDBS"<sup>a</sup> provided by National Institute of Advanced Industrial Science and Technology (AIST), Japan, the *ortho*-Ar-H's to the carbonyl of 2,2,2-triphenylacetophenone have the similar chemical shift (7.68 ppm) with a doublet peak. Moreover, the ESI-MS spectrum in Figure 5.9B provides further information on the mass-to-charge ratio of the byproduct, which is  $[\text{M}+\text{H}]^+$  (349.3) and  $[\text{M}+\text{Na}]^+$  (371.3). All these suggest that there was a pinacol rearrangement of benzopinacol under acidic

<sup>a</sup> The link for the database is [http://riodb01.ibase.aist.go.jp/sdbs/cgi-bin/cre\\_index.cgi?lang=eng](http://riodb01.ibase.aist.go.jp/sdbs/cgi-bin/cre_index.cgi?lang=eng).

conditions to provide 2,2,2-triphenylacetophenone. In addition, the crude reaction, after the removal of TFA, was also analyzed with  $^{19}\text{F}$  NMR spectroscopy. The spectrum in Figure 5.9C for the crude reaction indicates that around 16.7% of the boronate underwent deboronation in the presence of neat TFA. This implies that high concentrated TFA facilitates the protonation of the benzopinacol group on compound **5.9** or **5.20**, as shown in Scheme 5.3. Following protonation, the benzopinacol group slowly undergoes C-O bond cleavage to provide the pinacolyl carbocation, which rapidly follows a pinacol rearrangement to release the pinacolone and the boronic acid. This free boronic acid, with several strong electron withdrawing groups on the aromatic ring, rapidly undergoes deboronation under such conditions. Nevertheless, to lower the protonation possibilities, the reaction was improved by using less concentrated TFA and none of the ketone byproduct or deboronation product was detected thereafter in RP-HPLC.

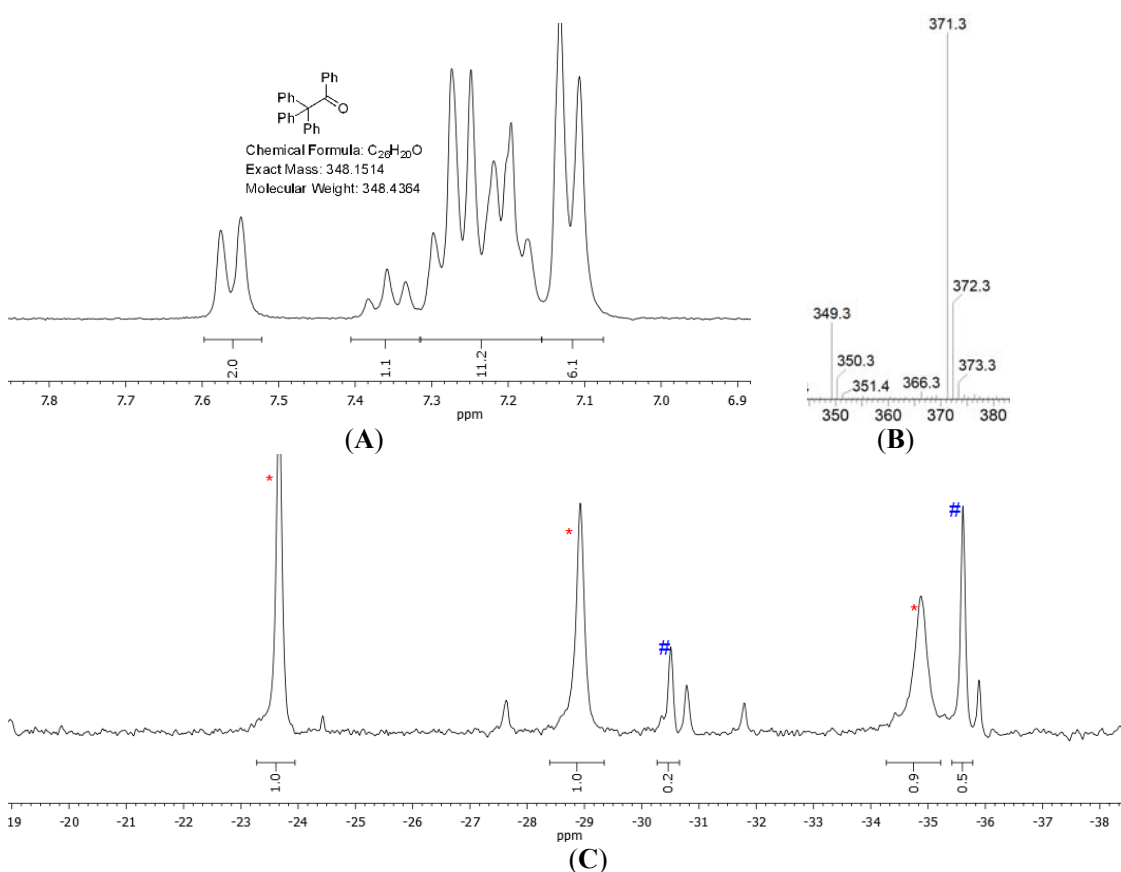
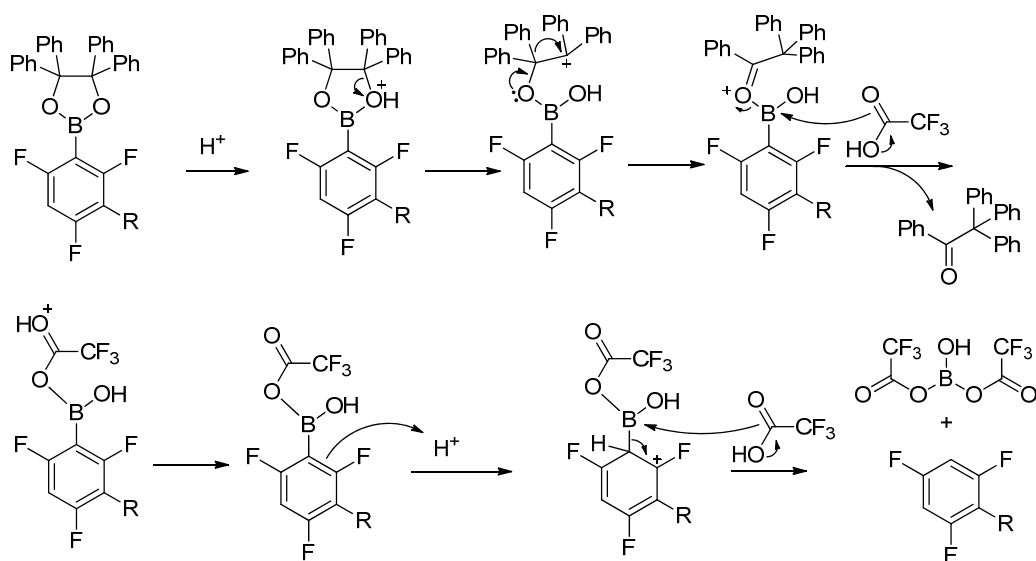


**Figure 5.9 Studies on the deprotection of **5.20** in neat TFA.**

(A),  $^1\text{H}$  NMR (300 MHz,  $d_6$ -DMSO) for the non-polar byproduct, purified via flash chromatography; (B), the ESI-LRMS of the non-polar byproduct at positive mode. The reaction condition: boronate **5.20** (40.0 mg, 0.0392 mmol), TFA (4 mL), rt, 1 hr; (C),  $^{19}\text{F}$  NMR (282.4 MHz) for the crude reaction: peaks noted with (\*) are that for the desired product **5.9**, that noted with (#) are representative for the deboronated product.



**Scheme 5.3** The proposed deboronation mechanism of the benzopinacol protected boronate in neat TFA.

Urea-boronate **5.9** was obtained with reasonable purity (without HPLC purification) and it was directly used for the fluoridation in the presence of a large amount of  $\text{KHF}_2$  overnight to achieve a 100% conversion. The benzopinacol and any other non-polar impurities were removed by  $\text{Et}_2\text{O}$  extraction. Urea- $\text{ArBF}_3$  **5.10** was then extracted from the unreacted fluoride with  $d_6$ -DMSO, in which  $^{19}\text{F}$ -fluoride was found to have a very low solubility. The NMR characterization of urea- $\text{ArBF}_3$  **5.10** displayed in Figure 5.3 confirmed its structure and purity.

### 5.3.2 The HPLC analysis of urea- $\text{ArBF}_3$ **5.10**

It took us a long time to find the right HPLC conditions to elute urea- $\text{ArBF}_3$  **5.10** with a reasonable retention time. It was found that without a suitable counteraction, the tricarboxylic groups, while fully deprotonated, showed very high polarity and would pass through the reverse-phase column rapidly with minimal retention time or no retention at all. Since acidic conditions are disfavored for the acid-labile  $\text{ArBF}_3\text{s}$ ,<sup>252</sup> three buffered aqueous solutions were tested as the aqueous mobile phase in RP-HPLC. The sodium phosphate buffer and ammonium formate buffer did not show enough counteraction capability to form the ion-pairs with the carboxylic groups of urea- $\text{ArBF}_3$  **5.10**. Because both sodium and ammonium cations are relatively polar cations, which would only form very loose ion-pairs with the carboxylic groups, the overall polarity of the compound was

not tuned sufficiently to provide more interactions with the C18-alkyl chains of the column. In contrast, TEAA provides a more hydrophobic triethylammonium cation, which likely interacts electrostatically with the carboxylic groups and the negatively charged trifluoroborate group on urea-ArBF<sub>3</sub> **5.10**. The ion pairs then have more interaction with the solid phase of the HPLC column. Consequently, ArBF<sub>3</sub> **5.10** has a longer retention time and elutes later than the solvent front when using TEAA/CH<sub>3</sub>CN as the mobile phase, compared with other solvent systems. Based on this, it would be envisioned that the more hydrophobic tertiary or quaternary amines such as tributylammonium or tetrabutylammonium be added to the aqueous mobile phase to provide even better separation/resolution of the <sup>18/19</sup>F-ArBF<sub>3</sub>s from <sup>18/19</sup>F-fluoride.

We attempted to characterize urea-ArBF<sub>3</sub> **5.10** by ESI mass spectrometry. To our surprise, the signal of the ArBF<sub>3</sub> seemed highly suppressed in the presence of trace amounts of other species such as DMSO. The suspected peak was also collected following HPLC separation and no useful information was obtained from ESI-MS. Fortunately, ESI-LCMS as an alternative provided information about the presence of urea-ArBF<sub>3</sub> **5.10** as well as its resolution under the given HPLC conditions. Based on the ESI-LCMS results shown in Figure 5.4 and Figure 5.5, the HPLC program was developed for the radio-HPLC analysis of the radiofluoridation studies.

The two minute difference between the retention times of the desired urea-ArBF<sub>3</sub> **5.10** shown in Figure 5.4 and Figure 5.5 is most likely due to the different injection sample conditions. It is known that the sample matrix would influence the retention time.<sup>253</sup> Since the NH<sub>4</sub>OH solution was used to quench the fluoridation of urea-boronate **5.9** as shown in Figure 5.5, NH<sub>4</sub>OH, fluoride, and chloride in the quenched reaction mixture might be the chemical interferences in the elution of urea-ArBF<sub>3</sub> **5.10** during HPLC isolation, and these interferences changed the sample condition dramatically to alter the retention time from that shown in Figure 5.4.

### 5.3.3 Radiosyntheses of urea-<sup>18</sup>F-ArBF<sub>3</sub> **5.10**

Before the study with ESI-LCMS, it was regarded for a long time that the low UV absorption of urea-ArBF<sub>3</sub> **5.10** was the main reason that we were unable to confirm the

success of the fluoridation of urea-boronate **5.9**. We therefore did one  $^{18}\text{F}$ -fluoridation of **5.9** in the hope that we could see the resolution of the  $^{18}\text{F}$ -radiolabeled product **5.10** from free  $^{18}\text{F}$ -fluoride via radio-HPLC with the HPLC solvents of  $\text{HCO}_2\text{NH}_4/\text{CH}_3\text{CN}$ . As shown in Figure 5.6, there was absolutely no separation between  $^{18}\text{F}$ -fluoride and the desired  $^{18}\text{F}$ - $\text{ArBF}_3$  product. Again, we were discouraged in our endeavor to obtain a cleanly separated  $^{18}\text{F}$ -labeled compound.

Based on the improvement with the new solvent system and the successful identification of urea- $\text{ArBF}_3$  **5.10** by ESI-LCMS, another  $^{18}\text{F}$ -radiolabeling experiment on urea-boronate **5.9** was successfully undertaken. As indicated in Figure 5.7, the radio-HPLC traces with the HPLC solvent system of TEAA/ $\text{CH}_3\text{CN}$  provided encouraging results for this labeling. First of all, very good resolution was obtained as urea- $^{18}\text{F}$ - $\text{ArBF}_3$  **5.10** eluted at 15.8 minutes while  $^{18}\text{F}$ -fluoride eluted at 4.2 minutes. This would allow us to efficiently purify the desired  $^{18}\text{F}$ -labeled product for eventual *in vitro* and *in vivo* studies from  $^{18}\text{F}$ -fluoride and other species. Secondly, the radiochemical yield over a one hour reaction at room temperature ranged from 20% to 25%, which seemed a bit higher than that for Mar- $^{18}\text{F}$ - $\text{ArBF}_3$  **4.15** in Chapter 4. This radiochemical yield was also comparable to that of the fluoridation of biotin-boronate **3.23**, which was mentioned in Chapter 3 to give a higher radiochemical yield than other derivatives without the piperazine linker of the same boronate **3.1**. The piperazine linker was presumed to contribute to the higher radiochemical yield for the fluoridation of biotin-boronate **3.23**. Here, for the relatively high radiochemical yield of the fluoridation of urea-boronate **5.9**, it is believed that the three carboxylic groups on the urea compound might have been involved in the fluoridation. It is proposed that the acid might first protonate the oxygen on the boronate to produce a good leaving group and upon the attacking of fluoride, one of the oxygen atoms on benzopinacol was eliminated in the form of a hydroxyl group, shown as the second step in the proposed mechanism of the fluoridation in Figure 5.10. The carboxylic groups in urea-boronate **5.9** might enable proton relay to facilitate the protonation of the oxygen atom *intra*- or *inter*-molecularly, and thus accelerate the fluoridation. This might lead to the fast fluoridation of urea-boronate **5.9**.

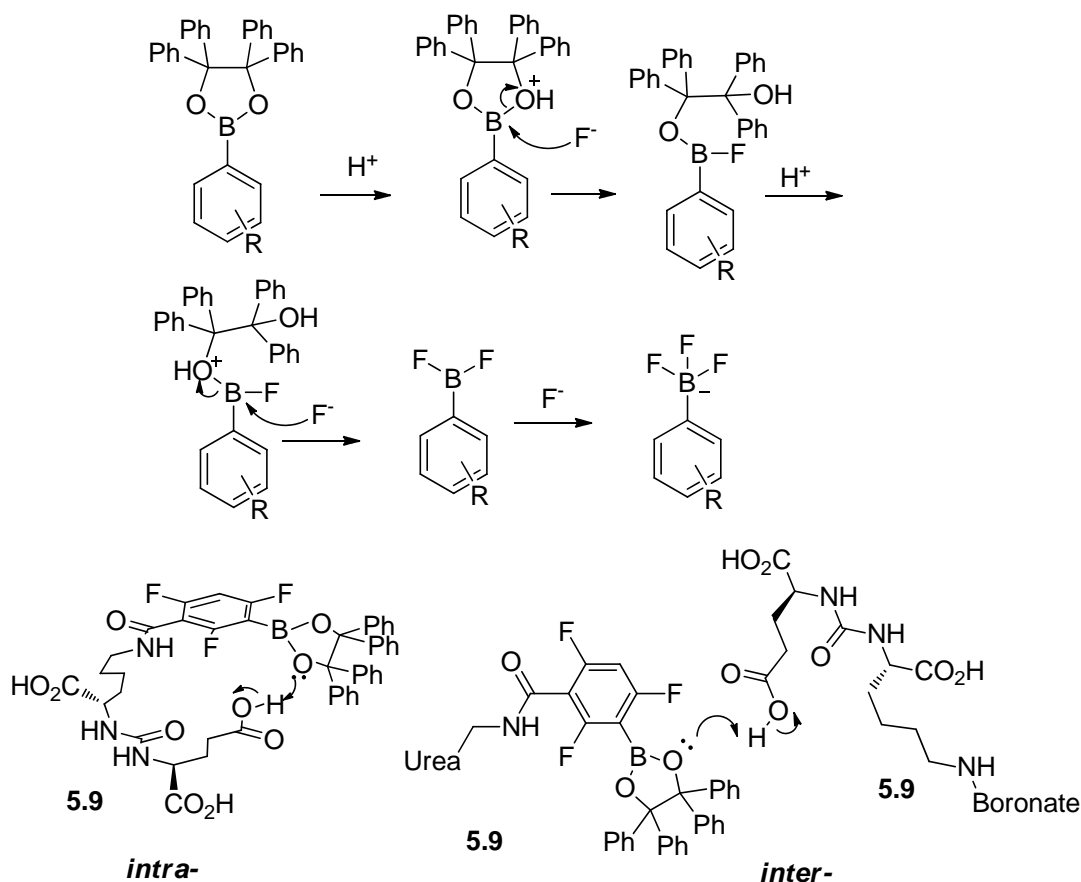


**Figure 5.10** The proposed mechanism of the fluoridation of the benzopinacol protected boronate. R is any substituent on the aromatic ring. The bottom structure is the proposed proton relay effect from the carboxylic groups of **5.9** to protonate the boronate.

On the other hand, as with the fluoridation of marimastat-boronate **4.14**, there was a second radio-peak eluting right besides  $^{18}\text{F}$ -fluoride. This implied as discussed in Chapter 4 that there might be some deboronation occurring during the storage of the boronate or in the fluoridation reaction. However, unlike marimastat-boronate **4.14**, the fluoridation of which gives a higher percentage of  $^{18}\text{F}$ - $\text{BF}_4^-$  when boronate **4.14** has been stored for a long time, all urea-boronate **5.9** tested for the  $^{18}\text{F}$ -radiolabeling has been stored for more than a year under the same conditions as the storage of **4.14** ( $-20\text{ }^\circ\text{C}$ ). Although there are three carboxylic groups on one molecule of urea-boronate **5.9**, the difference between the fluoridation of **5.9** and **4.14** suggests that urea-boronate **5.9** is relatively stable when stored properly.

One more point worth mentioning is the different peak resolution, which might be derived from different quench solutions. It is possible that the ion pair between the

triethylammonium and urea-ArBF<sub>3</sub> **5.10** was first formed during the quenching process with the TEA quench buffer prior to the HPLC injection and a sharp peak was obtained in the RP-HPLC as indicated in Figure 5.7B, while with the NH<sub>4</sub>OH/EtOH quench buffer, after injection into the HPLC, urea-ArBF<sub>3</sub> **5.10** might slowly equilibrate with the mobile phase to form the triethylammonium-ArBF<sub>3</sub> ion pair in the mobile phase and end with a broader peak as shown in Figure 5.7A.

Overall, the <sup>18</sup>F-radiolabeling of urea-boronate **5.9** was very successful. The radiochemical yields of 20-25% can be achieved within one hour incubation at room temperature under acidic conditions. It is very promising to use urea-<sup>18</sup>F-ArBF<sub>3</sub> **5.10** to image prostate cancer with suitable cancer cell lines.

## 5.4 Conclusion and future perspectives

In this chapter, boronate **3.1** was successfully conjugated to the urea-based PSMA inhibitor to give urea-boronate **5.9** via two different protecting strategies. The one with *tert*-butyl protecting group seems better regarding the overall yield of the synthesis and efficiency. Boronate **5.9** was then successfully <sup>18</sup>F-radiofluoridated with respectable radiochemical yields and nice radio-HPLC chromatograms were obtained with good resolution.

Because the structure of the urea compound is similar to others reported, derivatization via the ε-amino group should have no significance on its biological property.<sup>243</sup> Nevertheless, the lack of biological study leaves the application of this compound in doubt as for a potential prostate cancer imaging compound or not. We have already started the collaboration with Dr. Martin G. Pomper in Johns Hopkins Medical Institute and sent them the compounds for the biological testing as well as animal imaging studies. It is expected there will be some results regarding the biological properties and potential *in vivo* applications of urea-ArBF<sub>3</sub> **5.10** in the near future.

## 5.5 Materials and methods

Commercially available chemicals were purchased from Novabiochem, Sigma-Aldrich, Acros Organics or Alfa Aesar. Solvents were obtained from Fisher Scientific and used

without further purification unless otherwise noted. When required, solvents were pretreated following standard protocols.<sup>129</sup> The <sup>18</sup>F Trap & Release column (HCO<sub>3</sub><sup>-</sup> form, ~ 10 mg) was purchased from ORTG, Inc. Deuterated solvents were purchased from Cambridge Isotope Laboratories. TLC analysis was performed on aluminium-backed silica gel-60 plates from EMD Chemicals. Flash chromatography was carried out on SiliaFlash F60 (230-400 mesh) from SiliCycle. ESI-LRMS was performed on a Waters ZQ with a single quadrupole detector, attached to a Waters 2695 HPLC. ESI-HRMS were obtained on a Waters-Micromass LCT with a time-of-flight (TOF) detector. All NMR spectra were recorded on Bruker Avance instruments, with results reported as chemical shift ( $\delta$ ) in *ppm*. Unless specified, <sup>1</sup>H NMR spectra are referenced to the trimethylsilane peak ( $\delta = 0.00$  *ppm*), <sup>13</sup>C NMR spectra are referenced to the chloroform peak ( $\delta = 77.23$  *ppm*), and <sup>19</sup>F NMR spectra are referenced to neat trifluoroacetic acid ( $\delta = 0.00$  *ppm*, -78.3 *ppm* relative to CFCl<sub>3</sub>). HPLC information is attached in Appendix B.

**WARNING:** All <sup>18</sup>F-labeling work was done at TRIUMF. Radiation protection procedures strictly followed the TRIUMF Radiation Safety Regulations. Since this work involves mainly manual handling, fairly high amounts of dosage might be applied, and special caution is required to reduce the operating time. A lead brick castle was built up to shield the radiation. All the materials that came in contact with the source water (the <sup>18</sup>O-water) were collected and decayed separately from other <sup>18</sup>F-contaminated stuffs including gloves, sleeves, vials, tubes, and pipette tips prior to disposal.

#### **H-(L)-Glu(OPMB)-OPBM·HCl (5.1)**

This compound was prepared according to the literature protocol.<sup>246, 247</sup> (L)-Glutamic acid (1.47 g, 10 mmol) was suspended in DMF (10 mL) and cooled to 0 °C. *N,N,N',N'*-Tetramethylguanidine (2.5 mL, 20 mmol) was added to the DMF solution and the resulting mixture was stirred at the same temperature for 0.5 hr. Ethyl acetoacetate (1.26 mL, 10 mmol) was then added and the mixture was allowed to stir at rt till all solid disappeared. PMB-Cl (2.75 mL, 20 mmol) was added to the solution and the reaction was further stirred at rt for 24 hr. The reaction was quenched by 1 N aqueous NaHCO<sub>3</sub> (50 mL) and extracted with EtOAc (3 × 50 mL). The EtOAc layer was combined, washed with 1 N NaHCO<sub>3</sub> (1 × 50 mL) and H<sub>2</sub>O (2 × 50 mL), and dried over anhydrous Na<sub>2</sub>SO<sub>4</sub>.

The solution was filtered and concentrated in *vacuo*. The residue was added with 1 N HCl in MeOH (20 mL) and gently stirred for 10 min. MeOH was then removed under vacuum and Et<sub>2</sub>O (~ 300 mL) was added to the residue to result in precipitation. The solid was isolated and recrystallized from MeOH/Et<sub>2</sub>O to provide white flake crystals. Yield: 2.04 g, 53%. <sup>1</sup>H NMR (400 MHz, *d*<sub>4</sub>-MeOD, rt):  $\delta$ (ppm) 2.16 (m, 2 H), 2.52 (m, 2 H), 3.78 (s, 3 H), 3.79 (s, 3 H), 4.11 (t, *J* = 6.72 Hz, 1 H), 5.04 (s, 2 H), 5.18 (d, *J* = 5.56 Hz, 2 H), 6.90 (dd, *J*<sub>1</sub> = 6.76 Hz, *J*<sub>2</sub> = 1.92 Hz, 4 H), 7.27 (d, *J* = 8.64, 2 H), 7.32 (d, *J* = 8.68, 2 H); <sup>13</sup>C NMR (100.6 MHz, *d*<sub>4</sub>-MeOD, rt):  $\delta$ (ppm) 25.24, 28.90, 51.76, 54.33, 54.37, 66.15, 67.78, 113.52, 113.65, 126.87, 127.92, 129.80, 130.32, 159.90, 160.26, 168.66, 171.91; ESI-LRMS: [M+H]<sup>+</sup>, 388.2 (100%).

### **[(L)-Lys(Boc)]<sub>2</sub>Cu(II) (5.2)**

(L)-Lys-HCl (2 g, 11.0 mmol) and NaOH (0.98 g, 24.5 mmol) were dissolved in H<sub>2</sub>O (12 mL) and added with CuSO<sub>4</sub>·5H<sub>2</sub>O (1.37 g, 5.48 mmol) in H<sub>2</sub>O (6 mL).<sup>248</sup> The resulting solution was heated to 80 °C for 5 min and then cooled back to rt to adjust the pH to 9 with 2 N NaOH (~ 3 mL). (Boc)<sub>2</sub>O (4.78 g, 21.9 mmol) in 1,4-dioxane (15 mL) was dropwise added. The reaction was then stirred at rt for 48 hr. The slurry was filtered and the bluish-purple solid was washed with H<sub>2</sub>O, EtOH, and Et<sub>2</sub>O and dried over vacuum. The product was used directly without further purification in the following step. Yield: 2.65 g, 87%.

### **Fmoc-(L)-Lys(Boc)-OH (5.3)**

The copper complex **5.2** (1.1 g, 1.99 mmol) was suspended in H<sub>2</sub>O (18 mL) and 1.41 N EDTA solution (22 mL, 31.0 mmol) was added. The mixture was stirred at rt for 3 hr.<sup>248</sup> Then the solution was cooled to 0 °C and added with Na<sub>2</sub>CO<sub>3</sub> (1.20 g, 11.1 mmol) and 1,4-dioxane (10 mL). Fmoc-OSu (1.60 g, 4.74 mmol) was added to the solution in one portion and the mixture was allowed to warm up to rt and stirred overnight. The reaction was extracted with EtOAc (3 × 50 mL). The aqueous layer was acidified to pH ~ 1 with 3 N HCl and then extracted with EtOAc (3 × 50 mL). The EtOAc layers were combined, washed with H<sub>2</sub>O (3 × 50 mL) and brine (1 × 50 mL), and dried over anhydrous Na<sub>2</sub>SO<sub>4</sub>. The solution was filtered and concentrated under reduced pressure and the residue was

purified via flash chromatography (MeOH:CH<sub>2</sub>Cl<sub>2</sub> 2:98 then 3:97) to give a white solid ( $R_f = 0.26$  in 1:9 MeOH:CH<sub>2</sub>Cl<sub>2</sub>). Yield: 1.83 g, 98%. <sup>1</sup>H NMR (400 MHz, CDCl<sub>3</sub>, rt):  $\delta(ppm)$  1.47 (s, 9 H), 1.51 (m, 4 H), 1.95 (m, 2 H), 3.15 (m, 2 H), 4.24 (s, 1 H), 4.42 (m, 3 H), 7.32 (t,  $J = 7.41$  Hz, 2 H), 7.42 (t,  $J = 7.39$  Hz, 2 H), 7.62 (s, 2 H), 7.78 (d,  $J = 7.50$ , 2 H), 8.93 (s, br, 1 H); <sup>13</sup>C NMR (100.6 MHz, CDCl<sub>3</sub>, rt):  $\delta(ppm)$  28.56, 31.89, 40.21, 47.32, 53.89, 67.06, 67.26, 79.70, 81.23, 120.10, 124.99, 125.29, 127.23, 127.84, 141.45, 143.90, 144.08, 156.51; ESI-LRMS: [M+Na]<sup>+</sup>, 491.2 (100%).

#### **Fmoc-(L)-Lys(Boc)-OPMB (5.4)**

Fmoc-(L)-Lys(Boc)-OH **5.3** (2.70 g, 5.76 mmol) and Cs<sub>2</sub>CO<sub>3</sub> (2.80 g, 8.655 mmol) were suspended in DMF (40 mL) under Ar at 0 °C. PMB-Cl (1.3 mL, 9.51 mmol) was added to the mixture in one portion.<sup>243</sup> The resulting solution was allowed to warm up and stirred under Ar at rt for additional 4 hr and then quenched with 9 wt% Na<sub>2</sub>CO<sub>3</sub> solution (50 mL). The aqueous solution was extracted with EtOAc (3 × 50 mL). The organic layers were combined, washed with H<sub>2</sub>O (2 × 50 mL), 3 N HCl (1 × 50 mL), H<sub>2</sub>O (1 × 50 mL) and brine (1 × 50 mL), and dried over anhydrous Na<sub>2</sub>SO<sub>4</sub>. The solution was filtered and concentrated under vacuum; a white solid ( $R_f = 0.61$  in 1:1 EtOAc:hexanes) was isolated via a silica gel column (EtOAc:hexanes 1:3). Yield: 2.65 g, 78%. <sup>1</sup>H NMR (400 MHz, CD<sub>2</sub>Cl<sub>2</sub>, rt):  $\delta(ppm)$  1.26 (m, 2 H), 1.43 (s, 11 H), 1.71 (m, 1 H), 1.85 (m, 1 H), 3.06 (s, 2 H), 3.80 (s, 3 H), 4.24 (s, br, 1 H), 4.36-4.42 (m, 3 H), 5.12 (d,  $J = 8.40$  Hz, 2 H), 6.89 (d,  $J = 8.32$  Hz, 2 H), 7.35 (m, 4 H), 7.43 (t,  $J = 7.40$  Hz, 2 H), 7.63 (d,  $J = 7.24$  Hz, 2 H), 7.80 (d,  $J = 7.48$  Hz, 2 H); <sup>13</sup>C NMR (100.6 MHz, CD<sub>2</sub>Cl<sub>2</sub>, rt):  $\delta(ppm)$  22.34, 28.13, 29.62, 31.98, 40.01, 47.22, 55.21, 66.83, 78.79, 113.86, 119.89, 125.07, 127.02, 127.63, 130.07, 141.27, 143.92, 144.08, 155.88, 159.83, 172.24; ESI-LRMS: [M+Na]<sup>+</sup>, 611.2 (100%); [M+Cl]<sup>+</sup>, 623.3 (100%).

#### **H-(L)-Lys(Boc)-OPMB(5.5)**

20% Piperidine in DMF (6 mL) was added to Fmoc-(L)-Lys(Boc)-OPMB **5.4** (500 mg, 0.859 mmol) and the resulting solution was stirred at rt for 2 hr.<sup>243</sup> The reaction was quenched by H<sub>2</sub>O (50 mL) and extracted with CH<sub>2</sub>Cl<sub>2</sub> (3 × 50 mL). The CH<sub>2</sub>Cl<sub>2</sub> layer was combined, washed with H<sub>2</sub>O (50 mL), and dried over anhydrous Na<sub>2</sub>SO<sub>4</sub>. Then the

solution was filtered and concentrated under vacuum. The residue was purified via flash chromatography (EtOAc:hexanes 1:1 then MeOH:CH<sub>2</sub>Cl<sub>2</sub> 5:95) to give colorless oil ( $R_f$  = 0.37 in 1:9 MeOH:CH<sub>2</sub>Cl<sub>2</sub>). Yield: 182 mg, 59%. <sup>1</sup>H NMR (400 MHz, CD<sub>2</sub>Cl<sub>2</sub>, rt):  $\delta$ (ppm) 1.26-1.87 (m, 17 H), 3.06 (m, 2 H), 3.44 (s, br, 1 H), 3.82 (s, 3 H), 4.68 (m, 1 H), 5.09 (s, 2 H), 6.14 (d,  $J$  = 8.68 Hz, 2 H), 7.32 (d,  $J$  = 8.64 Hz, 2 H); <sup>13</sup>C NMR (100.6 MHz, CDCl<sub>3</sub>, rt):  $\delta$ (ppm) 22.92, 28.24, 29.90, 34.66, 40.41, 54.51, 55.34, 66.34, 113.95, 128.25, 128.53, 130.12, 136.18, 155.88; ESI-LRMS: [M+H]<sup>+</sup>, 367.5 (100%).

### PMBO-Lys(Boc)-C(O)-Glu(OPMB)-OPMB (5.6)

H-Glu(OPMB)-OPMB·HCl **5.1** (232 mg, 0.547 mmol) in CH<sub>2</sub>Cl<sub>2</sub> (10 mL) was added with NMM (60  $\mu$ L, 0.546 mmol) and CDI (89 mg, 0.549 mmol) under Ar.<sup>254</sup> The mixture was incubated at rt for 1 hr. Then the whole mixture was transferred to a round bottom flask charged with H-(L)-Lys(Boc)-OPMB **5.5** (183 mg, 0.499 mmol) and NMM (55  $\mu$ L, 0.501 mmol). The reaction was then allowed to stir at rt under Ar overnight. The solvent was removed *in vacuo* and the residue was then purified via flash chromatography (EtOAc:CH<sub>2</sub>Cl<sub>2</sub> 1:9 then 3:17) to give a white solid as the desired product ( $R_f$  = 0.37 in 1:4 EtOAc:CH<sub>2</sub>Cl<sub>2</sub>). Yield: 128 mg, 33%. <sup>1</sup>H NMR (300 MHz, CDCl<sub>3</sub>, rt):  $\delta$ (ppm) 1.27 (m, 2 H), 1.44 (s, 9 H), 1.63 (m, 1 H), 1.72 (m, 1 H), 1.96 (m, 1 H), 2.15 (m, 1 H), 2.41 (m, 2 H), 3.02 (m, 2 H), 3.81 (s, 9 H), 4.52 (m, 2 H), 4.75 (s, br, 1 H), 5.02-5.15 (m, 6 H), 5.57 (m, 2 H), 6.89 (m, 6 H), 7.26 (d,  $J$  = 8.30 Hz, 6 H); <sup>13</sup>C NMR (75.5 MHz, CDCl<sub>3</sub>, rt):  $\delta$ (ppm) 22.48, 28.13, 28.60, 29.53, 30.49, 32.53, 40.27, 52.63, 52.98, 55.42, 66.41, 67.00, 67.25, 79.21, 114.10, 127.56, 127.74, 128.10, 130.21, 130.27, 130.30, 156.35, 157.13, 159.75, 159.86, 173.00, 173.17, 173.52; ESI-LRMS: [M+Na]<sup>+</sup>, 802.5 (100%).

### PMBO-Lys-C(O)-Glu(OPMB)-OPMB·TsOH (5.7)

The compound was prepared following the literature report with some modifications.<sup>243</sup> The Boc-protected urea **5.6** (191 mg, 0.245 mmol) and TsOH·H<sub>2</sub>O (51.0 mg, .269 mmol) were mixed in EtOAc/THF<sup>a</sup> (3:1, 8 mL). The solvent was then removed under vacuum at 40 °C and CH<sub>2</sub>Cl<sub>2</sub> (5  $\times$  10 mL) was added to dissolve the residue and then removed

<sup>a</sup> EtOAc:MeOH solvent system was tried according to the literature. However, it was found severe transesterification was going on to give methyl ester (partially or fully), which caused troubles for the isolation and also for the later PMB deprotection step. This led us to turn to non MeOH system. Moreover, it has been found that the reaction can be promoted during the evaporation under vacuum.

under vacuum at 40 °C. The residue was then charged with silica gel chromatography (MeOH:CH<sub>2</sub>Cl<sub>2</sub> 2.5:97.5 then 5:95) to obtain colorless oil as the desired product (*R<sub>f</sub>* = 0.24 in 1:9 MeOH:CH<sub>2</sub>Cl<sub>2</sub>). Yield: 101.5 mg, 49%. <sup>1</sup>H NMR (400 MHz, CDCl<sub>3</sub>, rt):  $\delta$ (ppm) 1.41 (m, 2 H), 1.5-1.7 (m, 4 H), 1.82 (m, 1 H), 2.05 (m, 2 H), 2.28 (s, br, 5 H), 2.90 (m, 2 H), 3.75-3.95 (m, 9 H), 4.40 (m, 2 H), 5.01 (m, 6 H), 6.35 (dd, *J*<sub>1</sub> = 18.20 Hz, *J*<sub>2</sub> = 8.00 Hz, 2 H), 6.82 (m, 6 H), 7.08 (d, *J* = 7.60 Hz, 2 H), 7.17 (d, *J* = 8.40 Hz, 2 H), 7.21 (d, *J* = 8.40 Hz, 4 H), 7.72 (d, *J* = 8.00 Hz, 2 H); <sup>13</sup>C NMR (100.6 MHz, CDCl<sub>3</sub>, rt):  $\delta$ (ppm) 21.39, 21.72, 25.86, 26.74, 27.63, 29.28, 29.82, 30.49, 30.66, 39.59, 52.58, 53.13, 55.36, 66.27, 66.77, 67.13, 112.98, 114.06, 125.97, 126.33, 128.14, 129.27, 129.97, 130.04, 141.01, 141.21, 157.98, 159.73, 159.77, 172.85, 173.52, 174.16, 179.12; ESI-LRMS: [M+H]<sup>+</sup>, 680.7 (100%).

### **PMBO-Lys(boronate)-C(O)-Glu(OPMB)-OPMB (5.8)**

Urea-TsOH **5.7** (100 mg, 0.117 mmol) and boronate **3.1** (68.0 mg, 0.123 mmol) was mixed with HOBt·H<sub>2</sub>O (20 mg, 0.129 mmol) and pyridine (28.4  $\mu$ L, 0.351 mmol) in CH<sub>2</sub>Cl<sub>2</sub> (10 mL) at rt. EDC·HCl (26 mg, 0.135 mmol) was added to the solution in one portion and the reaction was stirred at rt overnight. The solvent was then removed and the residue was purified with column chromatography (MeOH:CH<sub>2</sub>Cl<sub>2</sub> 1:99) to afford a white solid (*R<sub>f</sub>* = 0.59 in 1:9 MeOH:CH<sub>2</sub>Cl<sub>2</sub>). Yield: 101.6 mg, 72%. <sup>19</sup>F NMR (282.4 MHz, CD<sub>2</sub>Cl<sub>2</sub>, rt):  $\delta$ (ppm) -28.03 (s, 1 F), -21.76 (s, 1 F), -17.05 (s, 1 F); <sup>1</sup>H NMR (400 MHz, CD<sub>2</sub>Cl<sub>2</sub>, rt):  $\delta$ (ppm) 1.40 (m, 2 H), 1.60 (m, 2 H), 1.69 (m, 1 H), 1.87 (m, 2 H), 2.09 (m, 1 H), 2.35 (m, 2 H), 3.39 (m, 2 H), 3.78 (s, 9 H), 4.38 (m, 2 H), 5.02 (d, *J* = 10.68 Hz, 4 H), 5.08 (d, *J* = 9.68 Hz, 2 H), 5.13 (d, *J* = 7.44 Hz, 1 H), 5.17 (d, *J* = 7.72 Hz, 1 H), 6.34 (t, *J* = 5.24 Hz, 1 H), 6.78-6.94 (m, 6 H), 7.00-7.17 (m, 12 H), 7.18-7.34 (m, 14 H), 7.51 (s, br, 2 H), 7.88 (t, *J* = 7.60 Hz, 1 H), 8.80 (s, br, 2 H); <sup>13</sup>C NMR (100.6 MHz, CD<sub>2</sub>Cl<sub>2</sub>, rt):  $\delta$ (ppm) 22.35, 27.79, 28.69, 30.31, 39.59, 55.32, 66.21, 66.80, 66.97, 96.93, 113.96, 127.26, 127.44, 128.63, 130.03, 130.07, 130.13, 142.03, 156.81, 159.64, 159.80, 159.91, 172.66, 172.71, 172.95; ESI-HRMS: calcd. for C<sub>69</sub>H<sub>65</sub>BN<sub>3</sub>O<sub>13</sub>F<sub>3</sub>Na<sup>+</sup>: 1234.4460, found: 1234.4474.

### **[(L)-Lys(Cbz)]<sub>2</sub>Cu(II) (5.11)**

(L)-Lys-HCl (2.00 g, 11.0 mmol) and NaOH (0.88 g, 22.0 mmol) in H<sub>2</sub>O (12 mL) was added with CuSO<sub>4</sub>·5H<sub>2</sub>O (1.40 g, 5.48 mmol) in H<sub>2</sub>O (6 mL).<sup>250</sup> The resulting solution was heated to 80 °C for 10 min and then cooled back to rt. The pH was adjusted to 9 with 2 N NaOH (~ 3 mL). Then NaHCO<sub>3</sub> (1.3 g, 15.5 mmol) was added to the solution and the mixture was cooled over an ice-H<sub>2</sub>O bath. Cbz-Cl (2.20 mL, 15.4 mmol) in 1,4-dioxane (20 mL) was dropwise added and the reaction was then stirred at rt overnight. The slurry was filtered and the blue solid was washed with H<sub>2</sub>O, EtOH, and Et<sub>2</sub>O and dried over vacuum. The product was used directly without further purification in the following step. Yield: 3.23 g, 94%.

### **Fmoc-(L)-Lys(Cbz)-OH (5.12)**

The copper complex **5.11** (2.00 g, 3.21 mmol) was suspended in H<sub>2</sub>O (30 mL) with Na<sub>2</sub>S (0.40 g, 5.13 mmol).<sup>250</sup> The mixture was stirred at rt for 0.5 hr and filtered over Celite and washed with H<sub>2</sub>O (30 mL). Then NaHCO<sub>3</sub> (1.20 g, 14.3 mmol) was added to the filtrate and the mixture was cooled to 0 °C. FmocCl (3.33 g, 12.9 mmol) in dioxane (10 mL) was dropwise added to the solution and the mixture was allowed to warm up to rt and stirred overnight. The reaction was then extracted with EtOAc (3 × 100 mL). The aqueous layer was acidified with 3 N HCl and then extracted with EtOAc (3 × 100 mL). The EtOAc layers were combined, washed with H<sub>2</sub>O (3 × 50 mL) and brine (1 × 50 mL), and dried over anhydrous Na<sub>2</sub>SO<sub>4</sub>. The solution was later filtered and concentrated *in vacuo* and the residue was purified via flash chromatography (EtOAc:hexanes 1:3 then 2:3) to give a white powder as the desired product (*R<sub>f</sub>* = 0.27 in 1:9 MeOH:CH<sub>2</sub>Cl<sub>2</sub>). Yield: 1.23 g, 38%. <sup>1</sup>H NMR (400 MHz, CDCl<sub>3</sub>, rt): δ(*ppm*) 1.46 (m, 2 H), 1.72 (m, 2 H), 1.81 (m, 1 H), 1.94 (m, 1 H), 3.24 (m, 2 H), 4.24 (t, *J* = 6.76 Hz, 1 H), 4.43 (m, 2 H), 5.13 (s, 2 H), 5.61 (s, br, 2 H), 7.31-7.45 (m, 9 H), 7.62 (m, 2 H), 7.79 (d, *J* = 7.44 Hz, 2 H); ESI-LRMS: [M+Na]<sup>+</sup>, 525.4 (100%).

### **Fmoc-(L)-Lys(Cbz)-O<sup>t</sup>Bu (5.13)**

DCC (12.0 g, 58.2 mmol) and CuCl<sub>2</sub> (0.20 g, 1.49 mmol) in <sup>t</sup>BuOH (50 mL) was stirred at r.t for 5 d. The solvent was then removed under vacuum and the residue containing majorly *tert*-butyl *N,N'*-dicyclohexylisourea was dried over high vacuum and used without further purification.<sup>255</sup> The isourea (1.50 g, ~ 5.35 mmol) was dissolved in CH<sub>2</sub>Cl<sub>2</sub> (10 mL) with Fmoc-(L)-Lys(Cbz)-OH **5.12** (556.6 mg, 1.108 mmol) and the solution was heated to reflux overnight. The reaction was then allowed to cool to rt and the solid was filtered off. The filtrate was further cooled at -20 °C for an additional hour and the mixture was filtered again. The filtrate was concentrated and the residue was purified via flash chromatography (EtOAc:hexanes 5:95 then 1:3) to give a white solid as the target compound (*R<sub>f</sub>* = 0.65 in 1:1 EtOAc:hexanes). Yield: 516.5 mg, 83%. <sup>1</sup>H NMR (400 MHz, CD<sub>2</sub>Cl<sub>2</sub>, rt):  $\delta$ (ppm) 1.41 (m, 2 H), 1.51 (s, 9 H), 1.56 (m, 2 H), 1.71 (m, 1 H), 1.85 (m, 1 H), 3.21 (m, 2 H), 4.27 (m, 2 H), 4.42 (m, 2 H), 5.10 (s, 2 H), 5.55 (d, *J* = 7.16 Hz, 1 H), 7.32-7.41 (m, 7 H), 7.45 (t, *J* = 7.42 Hz, 2 H), 7.67 (d, *J* = 7.40 Hz, 2 H), 7.82 (d, *J* = 7.52 Hz, 2 H); <sup>13</sup>C NMR (100.6 MHz, CD<sub>2</sub>Cl<sub>2</sub>, rt):  $\delta$ (ppm) 22.41, 27.88, 29.60, 32.36, 40.74, 47.39, 54.41, 66.43, 66.82, 81.98, 120.05, 125.23, 127.17, 127.79, 128.04, 128.54, 137.21, 141.41, 144.13, 144.24, 156.02, 156.50, 171.72; ESI-LRMS: [M+Na]<sup>+</sup>, 581.4 (100%).

### **H-(L)-Lys(Cbz)-O<sup>t</sup>Bu (5.14)**

Fmoc-(L)-Lys(Cbz)-O<sup>t</sup>Bu **5.13** (516.5 mg, 0.9245 mmol) was added with CH<sub>2</sub>Cl<sub>2</sub> (8 mL) and diethylamine (8 mL, 77.4 mmol) and the solution was stirred at rt for 2 hr. The solvent was then removed under vacuum and the residue was separated via flash chromatography (MeOH:CH<sub>2</sub>Cl<sub>2</sub> 1.5:98.5 then 3:97) to give colorless oil (*R<sub>f</sub>* = 0.42 in 1:9 MeOH:CH<sub>2</sub>Cl<sub>2</sub>). Yield: 256.7 mg, 83%. <sup>1</sup>H NMR (400 MHz, CDCl<sub>3</sub>, rt):  $\delta$ (ppm) 1.47 (s, 2 H), 1.49 (s, 9 H), 1.56 (m, 3 H), 1.65 (m, 1 H), 1.79 (m, 1 H), 3.23 (m, 4 H), 3.47 (s, br, 2 H), 5.00 (s, br, 1 H), 5.12 (s, 2 H), 7.32-7.42 (m, 5 H); <sup>13</sup>C NMR (100.6 MHz, CDCl<sub>3</sub>, rt):  $\delta$ (ppm) 22.73, 28.18, 29.68, 40.87, 54.64, 66.71, 81.94, 128.20, 128.65, 136.80, 156.58; ESI-LRMS: [M+H]<sup>+</sup>, 337.4 (100%).

### **Cbz-(L)-Glu-OH (5.15)**

(L)-Glutamic acid (3.00 g, 20.4 mmol) and NaHCO<sub>3</sub> (19.00 g, 0.2262 mol) were dissolved in H<sub>2</sub>O (120 mL) over an ice-H<sub>2</sub>O bath.<sup>256</sup> Cbz-Cl (3.50 mL, 24.52 mmol) was dropwise added to the solution and the reaction was then allowed to stir at rt for 26 hr. The mixture was extracted with Et<sub>2</sub>O (2 × 100 mL). The aqueous layer was then acidified with 3 N HCl to pH 1 and extracted with EtOAc (3 × 100 mL). The EtOAc layer was washed with 3 N HCl (1 × 50 mL) and brine (1 × 50 mL), and dried over anhydrous Na<sub>2</sub>SO<sub>4</sub>. The solution was filtered and concentrated under vacuum; the residue that was with good purity was used directly in the following synthesis. Yield: 4.65 g, 81%. <sup>1</sup>H NMR (400 MHz, *d*<sub>4</sub>-MeOD, rt): δ(ppm) 1.94 (m, 1 H), 2.19 (m, 1 H), 2.43 (t, *J* = 7.50 Hz, 2 H), 4.24 (dd, *J*<sub>1</sub> = 9.30 Hz, *J*<sub>2</sub> = 4.92 Hz, 1 H), 5.11 (s, 2 H), 7.33 (m, 5 H).

### **Cbz-Glu(O<sup>t</sup>Bu)-O<sup>t</sup>Bu (5.16)**

Cbz-Glu-OH **5.15** (800 mg, 2.84 mmol) and *tert*-butyl *N,N'*-dicyclohexylisourea<sup>a</sup> (8.80 g, 31.4 mmol) were suspended in CH<sub>2</sub>Cl<sub>2</sub> (30 mL) and heated to reflux overnight. The reaction was then cooled to rt and the solid was filtered off. The filtrate was further cooled under -20 °C for 0.5 hr and filtered again. The clear solution was then concentrated over vacuum and the residue was purified with column chromatography (EtOAc:hexanes 5:95 then 1:9) to give a white solid (*R*<sub>f</sub> = 0.50 in 1:3 EtOAc:hexanes). Yield: 855 mg, 77%. <sup>1</sup>H NMR (400 MHz, CDCl<sub>3</sub>, rt): δ(ppm) 1.35-1.60 (m, 18 H), 1.94 (m, 1 H), 2.16 (m, 1 H), 2.33 (m, 2 H), 4.29 (m, 1 H), 5.13 (s, 2 H), 5.39 (d, *J* = 7.16 Hz, 1 H), 7.35 (m, 5 H); <sup>13</sup>C NMR (100.6 MHz, CDCl<sub>3</sub>, rt): δ(ppm) 27.98, 28.07, 31.49, 53.98, 66.90, 80.67, 82.29, 128.08, 128.11, 128.49, 136.34, 155.93, 171.10, 172.07; ESI-LRMS: [M+Na]<sup>+</sup>, 416.4 (100%).

### **H-Glu(O<sup>t</sup>Bu)-O<sup>t</sup>Bu (5.17)**

Cbz-Glu(O<sup>t</sup>Bu)-O<sup>t</sup>Bu **5.17** (855 mg, 2.17 mmol) and 10% Pd/C (300 mg) in THF (30 mL) were stirred under a H<sub>2</sub> atmosphere at rt for 24 hr. Then the reaction was filtered over Celite and the Celite was washed thoroughly with THF. The filtrate was combined and concentrated over vacuum; the residue was further purified via silica gel

<sup>a</sup> The *tert*-butyldicycloisourea was prepared as described in the synthesis of **5.13**.

chromatography (MeOH:CH<sub>2</sub>Cl<sub>2</sub> 0:100 then 3:97) to give colorless oil, which solidified while standing ( $R_f = 0.50$  in 1:9 MeOH:CH<sub>2</sub>Cl<sub>2</sub>). Yield: 525 mg, 93%. <sup>1</sup>H NMR (300 MHz, CDCl<sub>3</sub>, rt):  $\delta(ppm)$  1.48 (s, 9 H), 1.51 (s, 9 H), 1.88 (m, 1 H), 2.07 (m, 1 H), 2.42 (t,  $J = 7.56$  Hz, 2 H), 2.67 (m, br, 2 H), 3.46 (m, 1 H); <sup>13</sup>C NMR (75.5 MHz, CDCl<sub>3</sub>, rt):  $\delta(ppm)$  28.46, 28.51, 29.96, 32.24, 54.56, 80.89, 82.04, 172.82; ESI-LRMS: [M+H]<sup>+</sup>, 260.5 (100%).

#### **<sup>t</sup>BuO-Lys(Cbz)-C(O)-Glu(O<sup>t</sup>Bu)-O<sup>t</sup>Bu (5.18)**

H-Glu(O<sup>t</sup>Bu)-O<sup>t</sup>Bu **5.17** (283 mg, 1.09 mmol) and NMM (150  $\mu$ L, 1.36 mmol) in CH<sub>2</sub>Cl<sub>2</sub> (5 mL) was added with CDI (177 mg, 1.09 mmol) under Ar. The resulting mixture was stirred at rt for 3 hr and then transferred to H-Lys(Cbz)-O<sup>t</sup>Bu **5.14** (282 mg, 0.838 mmol) mixed with NMM (90  $\mu$ L, 0.819 mmol). The reaction was left at rt for 24 hr and then concentrated under vacuum. The residue was charged with flash chromatography (EtOAc:CH<sub>2</sub>Cl<sub>2</sub> 5:95) to give colorless oil or sometimes a white solid as the desired product ( $R_f = 0.60$  in 1:9 MeOH:CH<sub>2</sub>Cl<sub>2</sub>). Yield: 461 mg, 89%. <sup>1</sup>H NMR (400 MHz, CDCl<sub>3</sub>, rt):  $\delta(ppm)$  1.37 (m, 2 H), 1.45 (m, 11 H), 1.47 (s, 18 H), 1.49 (m, 2 H), 1.54 (m, 1 H), 1.63 (m, 1 H), 1.76 (m, 1 H), 1.86 (m, 1 H), 2.31 (m, 2 H), 3.19 (s, br, 2 H), 4.34 (m, 2 H), 5.13 (m, 2 H), 5.37 (s, br, 2 H), 7.33-7.45 (m, 5 H); <sup>13</sup>C NMR (100.6 MHz, CDCl<sub>3</sub>, rt):  $\delta(ppm)$  22.47, 28.14, 28.21, 28.44, 29.50, 31.67, 32.68, 40.80, 53.13, 53.54, 60.54, 66.66, 80.73, 81.88, 82.38, 128.12, 128.16, 128.60, 136.87, 156.80, 157.34, 172.47, 172.62; ESI-HRMS: calcd. for C<sub>32</sub>H<sub>51</sub>N<sub>3</sub>O<sub>9</sub>Na<sup>+</sup>: 644.3523, found: 644.3514.

#### **<sup>t</sup>BuO-Lys-C(O)-Glu(O<sup>t</sup>Bu)-O<sup>t</sup>Bu (5.19)**

Cbz-urea **5.18** (90.0 mg, 0.145 mmol) and 10% Pd/C (50 mg) in THF (5 mL) were stirred at rt under a H<sub>2</sub> atmosphere for 24 hr. The mixture was then filtered over Celite and the solid was washed with THF. The filtrate was combined and concentrated over vacuum. The residue was purified with flash chromatography (MeOH:CH<sub>2</sub>Cl<sub>2</sub> 3:97 gradient to 1:9) to give white foam or sometimes colorless oil ( $R_f = 0.095$  in 1:9 MeOH:CH<sub>2</sub>Cl<sub>2</sub>). Yield: 33.0 mg, 47%. <sup>1</sup>H NMR (300 MHz, CDCl<sub>3</sub>, rt):  $\delta(ppm)$  1.46 (m, 27 H), 1.60 (m, 2 H), 1.70-1.97 (m, 5 H), 2.06 (m, 2 H), 2.36 (m, 2 H), 3.05 (m, 1 H), 3.12 (m, 1 H), 4.34 (m, 2 H), 6.11 (d,  $J = 8.16$  Hz, 1 H), 6.28 (t,  $J = 8.00$  Hz, 1 H); <sup>13</sup>C NMR (75.5 MHz, CDCl<sub>3</sub>, rt):  $\delta(ppm)$  21.94, 26.83, 28.21, 28.25, 28.42, 29.82, 31.16,

31.93, 39.58, 53.04, 53.50, 80.69, 81.69, 82.30, 157.75, 172.59, 172.75, 173.62; ESI-LRMS:  $[M+H]^+$ , 488.5 (100%).

#### **<sup>t</sup>BuO-Lys(boronate)-C(O)-Glu(O<sup>t</sup>Bu)-O<sup>t</sup>Bu (5.20)**

Urea **5.19** (168 mg, 0.344 mmol), boronate **3.1** (200 mg, 0.363 mmol), HOBt·H<sub>2</sub>O (56.0 mg, 0.366 mmol) and pyridine (84  $\mu$ L, 1.03 mmol) were dissolved in CH<sub>2</sub>Cl<sub>2</sub> (10 mL) and then added with EDC·HCl (86.0 mg, 0.449 mmol) in one portion. The resulting mixture was stirred at rt overnight and quenched by 3 N HCl (50 mL). The layers were separated and the aqueous phase was extracted with CH<sub>2</sub>Cl<sub>2</sub> (3  $\times$  50 mL). The CH<sub>2</sub>Cl<sub>2</sub> layers were combined, washed with H<sub>2</sub>O (2  $\times$  50 mL) and brine (1  $\times$  50 mL), and dried over anhydrous Na<sub>2</sub>SO<sub>4</sub>. The solution was filtered and concentrated under vacuum and the residue was isolated via flash chromatography (MeOH:CH<sub>2</sub>Cl<sub>2</sub> 1:300 gradient to 3:200) to give a white solid ( $R_f$  = 0.67 in 1:9 MeOH:CH<sub>2</sub>Cl<sub>2</sub>). Yield: 269 mg, 77%. <sup>19</sup>F NMR (400 MHz, CD<sub>2</sub>Cl<sub>2</sub>, rt):  $\delta(ppm)$  -28.56 (s, 1 F), -22.24 (s, 1 F), -17.74 (s, 1 F); <sup>1</sup>H NMR (400 MHz, CD<sub>2</sub>Cl<sub>2</sub>, rt):  $\delta(ppm)$  1.46 (s, 9 H), 1.47 (s, 9 H), 1.49 (s, 9 H), 1.53 (m, 1 H), 1.70 (m, 4 H), 1.85 (m, 2 H), 2.05 (m, 1 H), 2.30 (m, 2 H), 3.48 (m, 2 H), 4.22 (m, 1 H), 4.30 (m, 1 H), 6.49 (t,  $J$  = 5.56 Hz, 1 H), 6.87 (t,  $J$  = 8.60 Hz, 1 H), 7.06-7.20 (m, 12 H), 7.21-7.33 (m, 8 H); <sup>13</sup>C NMR (100.6 MHz, CD<sub>2</sub>Cl<sub>2</sub>, rt):  $\delta(ppm)$  22.42, 27.82, 27.89, 28.18, 28.76, 31.49, 39.77, 80.44, 81.70, 82.03, 96.88, 101.16, 101.41, 127.24, 127.42, 128.62, 142.01, 146.84, 156.95, 159.53; ESI-HRMS: calcd. for C<sub>57</sub>H<sub>65</sub>BN<sub>3</sub>O<sub>10</sub>F<sub>3</sub>Na<sup>+</sup>: 1042.4613, found: 1042.4642.

#### **HO-Lys(boronate)-C(O)-Glu(OH)-OH (urea-boronate) (5.9)**

The PMB protected boronate **5.8** (30.0 mg, 0.0248 mmol) was added with 3% anisole in TFA (5 mL) and stirred at rt for 1 hr. The solvent was then removed under vacuum and the residue was charged with toluene (2 mL). The solvent was then removed *in vacuo* and the residue was suspended in CH<sub>3</sub>CN (2 mL), which resulted in precipitation. The solid was spinned off and re-dissolved in MeOH and the solution was charged over RP-HPLC for purification (HPLC Program 18 and Column II in HPLC System I,  $t_R$  = 22.6 min) to give the pure product (analytic HPLC with Program 19/Column I/HPLC System I:  $t_R$  = 22.8 min). Yield: 3.4 mg, 16%. <sup>19</sup>F NMR (282.4 MHz, *d*<sub>4</sub>-MeOD/CDCl<sub>3</sub>,

rt):  $\delta(ppm)$  -28.26 (s, 1 F), -21.76 (s, 1 F), -16.50 (s, 1 F);  $^1H$  NMR (300 MHz,  $d_4$ -MeOD/ $CDCl_3$ , rt):  $\delta(ppm)$  0.76 (t,  $J = 7.79$  Hz, 1 H) 1.00 (m, 2 H), 1.36 (m, 3 H), 1.53 (m, 3 H), 1.77 (m, 2 H), 2.04 (m, 1 H), 2.28 (t,  $J = 7.53$  Hz, 2 H), 3.28 (m, 2 H), 4.20 (m, 2 H), 6.72 (t,  $J = 8.85$  Hz, 1 H), 6.88-7.21 (m, 20 H), 7.26 (m, 1 H); ESI-HRMS: calcd. for  $C_{45}H_{40}BN_3O_{10}F_3^-$ : 850.2759, found: 850.2772.

The same compound can be obtained from tri-*tert*-butyl ester **5.20**. Tri-*tert*-butyl ester **5.20** (30.0 mg, 0.0291 mmol) was dissolved in 50% TFA in  $CH_2Cl_2$  (16.0 mL). The resulting mixture was stirred at rt for 3 hr and then concentrated under reduced pressure. The residue was then washed with  $Et_2O$  to give a white precipitate as the desired product. Yield: 30 mg, quant<sup>a</sup>. The compound was further purified via RP-HPLC under the same conditions described above.

#### Urea-ArBF<sub>3</sub> (5.10)

Boronate **5.20** (30.0 mg, 0.029 mmol) was dissolved in 50% TFA in  $CH_2Cl_2$  (16.0 mL) and stirred at rt for 3 hr. The volatile was removed under reduced pressure and toluene (2 × 20 mL) was added to help remove the residual TFA via rota-evaporation. Then the residue was triturated with  $Et_2O$  to give a white solid. The mixture was filtered and the solid was collected, dissolved in  $CH_3CN$  (1.1 mL), and added with 0.4 M  $KHF_2$  (1.1 mL, 0.44 mmol) in a plastic falcon tube. The mixture was stirred at rt overnight and concentrated over vacuum. Toluene (3 × 3 mL) was added to azeotropically remove  $H_2O$ . Then the residue was washed with  $Et_2O$  (6 × 1 mL) to remove any non-polar species such as benzopinacol and the pellet was then dried over vacuum to remove the residual volatiles.  $d_6$ -DMSO (400  $\mu$ L) was added to extract the product for characterization.  $^{19}F$  NMR (282.4 MHz,  $d_6$ -DMSO, rt):  $\delta(ppm)$  -55.04 (s, 3 F), -40.84 (s, 1 F), -27.42 (s, 1 F), -22.50 (s, 1 F);  $^1H$  NMR (300 MHz,  $d_6$ -DMSO, rt):  $\delta(ppm)$  1.12-1.69 (m, 8 H), 1.82 (m, 1 H), 2.23 (m, 2 H), 3.14 (m, 2 H), 3.76 (m, 1 H), 3.96 (m, 1 H), 6.14 (s, br, 2 H), 6.68 (t,  $J = 9.38$  Hz, 1 H), 8.48 (m, 1 H).

<sup>a</sup> The crude product contained TFA, which could not be fully removed.

### **<sup>18</sup>F-Radiolabeling of urea-boronate 5.9**

Here is one example of the fluoridation and its HPLC trace was shown in Figure 5.7B. The <sup>18</sup>F-fluoride was trapped, released, and concentrated as described earlier. Then the radioactivity (39.4 mCi after dry down) was resuspended with 0.25 M KHF<sub>2</sub> (10 μL). The <sup>18/19</sup>F-fluoride cocktail (1 μL, containing 500 nmol <sup>19</sup>F-fluoride) was added to urea-boronate **5.9** (100 nmol) and HCl (12.6 μmol) in 4.5 μL of 88.8% aqueous CH<sub>3</sub>CN. The reaction was incubated at rt for 1 hr and quenched with 100 μL of 2% NEt<sub>3</sub> in 75% aqueous CH<sub>3</sub>CN. The quenched reaction was injected into the HPLC for analysis. The HPLC was performed via HPLC Program 16 with Column I in HPLC System IV.

## Chapter 6 Applying copper(I) catalyzed click chemistry to label oligonucleotides with $^{18}\text{F-ArBF}_3\text{s}$

The one-step labeling for  $^{18}\text{F-ArBF}_3\text{s}$  under aqueous conditions at room temperature described in earlier chapters represents the beauty of this technique for preparing  $^{18}\text{F-PET}$  imaging compounds. However, the labeling reaction, despite the advantages of proceeding in an aqueous/aqueous cosolvent system at room temperature, occurs under reasonably acidic conditions,<sup>78</sup> which limit the application of this method to acid-resistant compounds. To apply this labeling strategy as widely as possible, an indirect method is required to enable the labeling of those acid-sensitive compounds. Among the coupling methods frequently used, “click” chemistry is one that has garnered a great deal of attention over the past decade. Here in this chapter, we employed the copper(I) catalyzed “click” reaction (1,3-dipolar cycloaddition) to label oligonucleotides with  $^{18}\text{F-ArBF}_3\text{s}$  and expect it to be generally useful for the incorporation of  $^{18}\text{F-ArBF}_3\text{s}$  into acid-sensitive molecules. Similar procedure will also be used to label biomolecules such as RGD-peptides and folate with  $^{18}\text{F-ArBF}_3\text{s}$  in the following chapters.

### 6.1 Introduction

#### 6.1.1 Click chemistry

There are hundreds of reactions routinely used in synthetic labs to prepare target molecules. Usually, these reactions fall into two categories: 1) formation of C-C bonds, and 2) construction of C-X bonds where X signifies a heteroatom such as oxygen, nitrogen, and sulphur.<sup>257</sup> To prepare C-C bonds, traditionally, one might contemplate the aldol addition/condensation reactions, reactions involving organometallic compounds such as Grignard reagents and zinc or lithium reagents, the Wittig reaction, the Diels-Alder reaction, olefin metathesis, and transition-metal catalyzed cross-coupling reactions such as the Suzuki, the Stille, and the Heck reactions etc. To form C-X bonds, reactions frequently used include the nucleophilic substitution, carbonyl related reactions such as the formation of amides, oximes, and hydrazones, cycloaddition reactions such as hetero-Diels-Alder reactions involving heterodiene or dienophile and/or 1,3-dipolar

cycloaddition reactions, and reactions on multiple C-C bonds such as oxidation of olefins and electrophilic addition reactions, etc. Although there is such an enormous repertoire of reactions for conjugation, in order to match the capability of making compounds efficiently with regio- and chemoselectivity, a new term “click chemistry” was introduced to the field by Sharpless and co-workers in 2001.<sup>258</sup> According to that paper, click chemistry requires that the reaction be “*modular*”, “*wide in scope*”, “*giving very high yields*”, “*stereospecific*”, under “*simple reaction conditions*” (air and water insensitive), with “*readily available starting materials and reagents*”, the “*use of no solvent or a solvent that is benign or easily removable*” (preferable for water and low boiling point solvents), only generating “*inoffensive byproducts*” in the reaction as well as affording “*simple product isolation*”, and last but not least that the product must be physiologically stable. Among the reactions mentioned earlier, which might satisfy the requirements of click chemistry, four are frequently regarded as members of the click chemistry family.<sup>259</sup>

- A. Non-aldol type carbonyl chemistry, including the formation of oxime ethers, and hydrazones.
- B. Nucleophilic ring-opening reactions of highly strained heterocyclic electrophiles, especially three membered ring heterocycles as epoxides and aziridines.
- C. Addition reactions to carbon-carbon multiple bonds, such as the Michael addition and thiol-ene reactions.
- D. Cycloaddition reactions, e.g. (hetero-) Diels-Alder reactions and 1,3-dipolar cycloadditions.

Whereas each reaction has various advantages and drawbacks, the Huisgen 1,3-dipolar cycloaddition<sup>260</sup> has received the most attention. Ever since the Sharpless lab<sup>261</sup> and the Meldal group<sup>262</sup> each reported the copper (I) catalyzed 1,3-dipolar cycloaddition nearly simultaneously, this modified 1,3-dipolar cycloaddition has been widely explored by virtue of high regio/chemoselectivity and efficiency.

The traditional Huisgen 1,3-dipolar cycloaddition (uncatalyzed) always proceeds to give two regioisomers as shown in reaction (A) of Figure 6.1, Although a great deal of effort has been directed toward controlling the regioselectivity of the standard Huisgen

1,3-dipolar cycloaddition such as by introducing sterically bulky substituents to the substrates to force the reaction to favor certain regioisomers,<sup>263</sup> both the copper(I) and ruthenium(II) catalyzed 1,3-dipolar cycloadditions have been predominantly used to prepare regioselective products with high efficiency. The ruthenium catalyzed reactions selectively yield 1,5-disubstituted-1,2,3-triazole regioisomers with both the terminal and internal alkynes as the alkyne substrates as illustrated in Figure 6.1C.<sup>264, 265</sup> The copper(I) catalyzed alkyne-azide cycloaddition as indicated in Figure 6.1B, which regioselectively affords 1,4-disubstituted products, holds many advantageous properties, which have led to its prosperity for nearly a decade in fields of medicinal chemistry,<sup>94</sup> radiopharmaceutical chemistry,<sup>266</sup> and polymer and material science,<sup>267-269</sup> involving small molecules such as short peptides, oligonucleotides, and carbohydrates as well as large biomolecules such as proteins, virus surfaces, nucleic acids, lipids, and other macromolecules.<sup>270-272</sup>

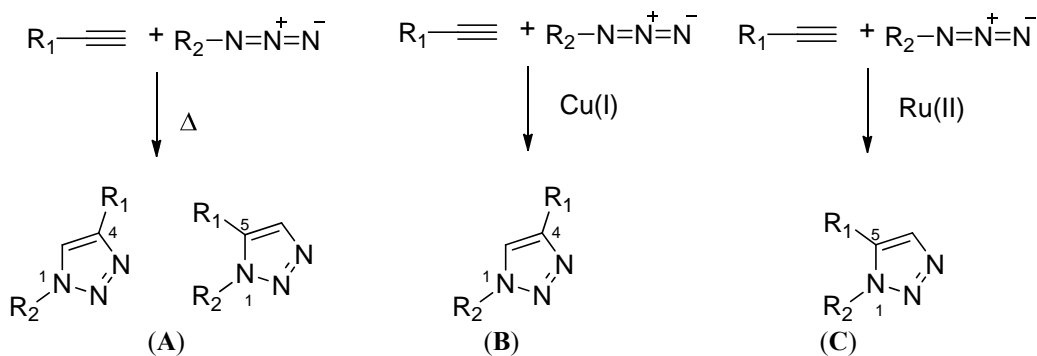


**Figure 6.1 The 1,3-dipolar cycloadditions.**

(A) The conventional Huisgen 1,3-dipolar cycloaddition at elevated temperatures. The reaction always yields both 1,4- and 1,5-disubstituted-1,2,3-triazole regioisomers with a ratio around 1:1; (B) The copper(I) catalyzed 1,3-dipolar cycloaddition. The reaction can proceed at room temperature as well as in aqueous cosolvents but yield only 1,4-disubstituted-1,2,3-triazole products regioselectively; (C) The ruthenium catalyzed 1,3-dipolar cycloaddition. The reaction yields only 1,5-disubstituted-1,2,3-triazole products regioselectively and it can also be applied to the internal alkyne species.

As shown in Figure 6.1B, with copper(I) catalysis, the reaction results in a single product, the regioselective 1,4-disubstituted-1,2,3-triazole linkage, which not only somewhat resembles a natural amide bond but is also inert to most other reaction conditions. Moreover, this reaction is very simple and robust as it is insensitive to both oxygen and water. As a matter of fact, water is one of the ideal solvents for this reaction. Furthermore, the starting materials are relatively easy to obtain. The terminal alkynes can be easily synthesized by simple methods such as elimination reactions from

1,1-dihaloalkanes, 1,2-dihaloalkanes or 1-bromoalkenes,<sup>273</sup> the Corey-Fuchs reaction,<sup>274</sup> and reaction using Ohira-Bestmann reagents<sup>275</sup> as well as derivatization with commercially available alkynes such as propargylamine. The azido compounds can be simply obtained via an azide-halide replacement or by copper(II) catalyzed diazo transfer to amines using TfN<sub>3</sub>.<sup>276</sup> There is also a wide scope of commercially available copper(I) compounds, whereas copper(I) can also be generated *in situ* via the reduction of copper(II) with ascorbate or other reducing agents. The reaction conditions are quite versatile from pH 4 to 12,<sup>261</sup> although most work has been done at neutral pH. It has also been found that increased temperatures can speed up this reaction to some point but this may also introduce competition from the conventional thermal Huisgen cycloaddition, while most examples of the copper(I) catalyzed reactions have been reported at or near room temperature. Efforts have been made to develop non-classic reaction conditions for this reaction as well; it is reported that microwave heating, continuous flow processing or different reaction media such as ionic liquids can further accelerate the copper(I) catalyzed 1,3-dipolar cycloaddition.<sup>277</sup> The reaction is very orthogonal to various functional groups yet quite specific to azido and terminal alkynyl groups.<sup>261</sup> In addition, 1,4-disubstituted-1,2,3-triazoles, which are both thermally and hydrolytically stable, have been found to have additional applications in pharmaceutical fields,<sup>94, 259</sup> and they have also been used as novel metal chelating ligands.<sup>278, 279</sup> All these features make the copper(I) catalyzed cycloadditions nearly synonymous with “click chemistry” nowadays and the “*cream of the crop*” in terms of a bio-orthogonal reaction.<sup>94, 270</sup>

In their original report, Sharpless and co-workers proposed a reaction mechanism shown in Figure 6.2.<sup>261</sup> Later the mechanism was further supported by a density functional theory computation study.<sup>280</sup> As shown in Figure 6.2, copper(I) first inserts into the terminal alkyne to form a copper-acetylide intermediate. The copper(I), bound to the intermediate, subsequently binds to the azide nitrogen proximal to the carbon. The far end nitrogen of the azide reacts with the C-2 carbon of the acetylide to form a rare copper(III) six-membered metallacycle intermediate. Then, the metallocycle intermediate rearranges to form the triazolyl-copper complex. Following protonolysis, the 1,4-disubstituted-1,2,3-triazole is released and the catalyst is regenerated.

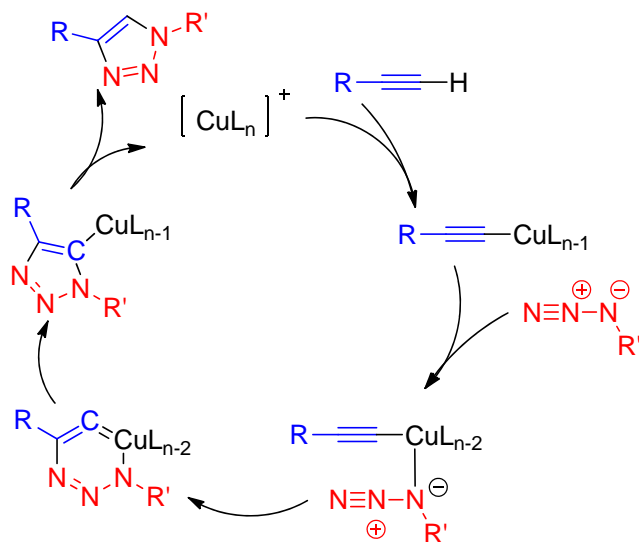
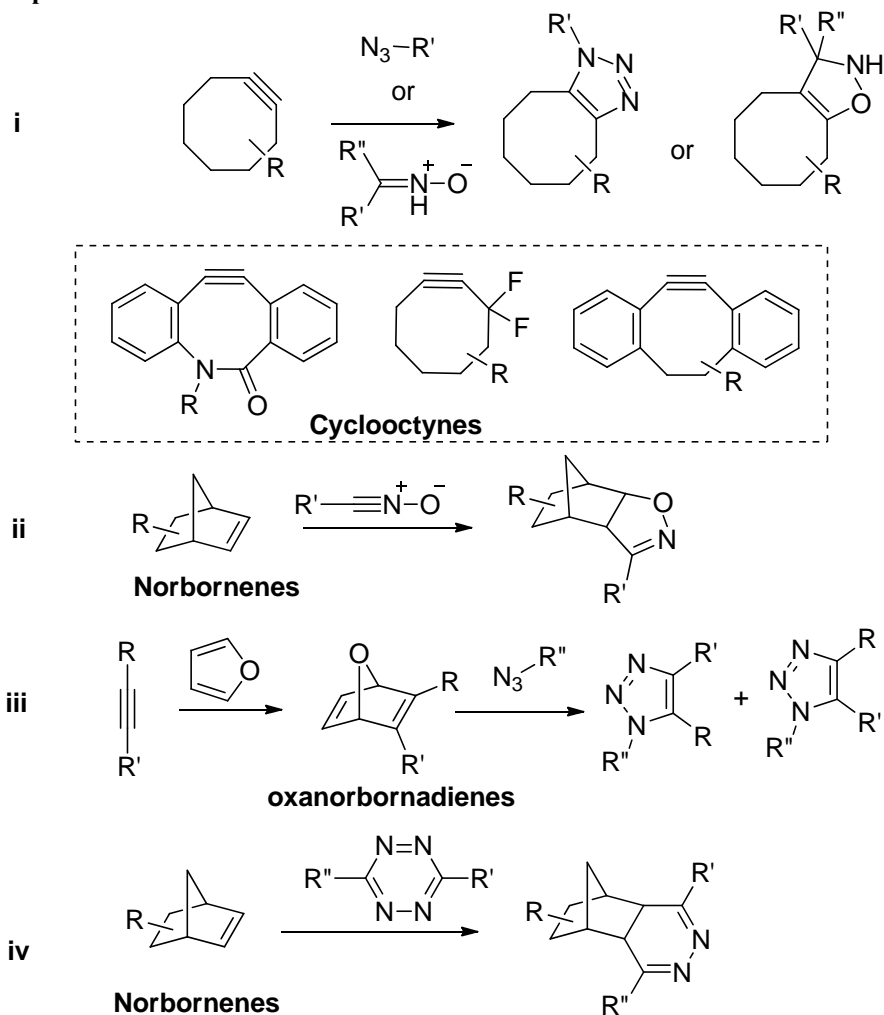


Figure 6.2 The proposed mechanism of the copper(I)-catalyzed alkyne-azide dipolar cycloaddition by Sharpless *et al.*<sup>261, 280</sup>



Scheme 6.1 Examples of some copper-free cycloaddition reactions.

Although the copper(I) catalyzed 1,3-dipolar cycloaddition proceeds with very high efficiency and regioselectivity, the toxicity of copper may limit the application of the copper(I) catalyzed dipolar cycloaddition in living systems. Efforts have been made to develop non-toxic and biocompatible copper-based catalysts as well as to explore non-copper catalyzed click reactions. From a series of screening experiments on a group of triazolole ligands, Wu and co-workers found the copper complex with a bis(*tert*-butyltriazolyl) triazolylethylene sulfonate ligand (BTTEs) can promote the cycloaddition rapidly without apparent toxicity to living cells.<sup>281</sup> On the other hand, several groups have reported the copper-free click reactions using the high ring strains as summarized in Scheme 6.1. The Bertozzi lab has pioneered various copper-free click reactions.<sup>282-284</sup> By taking advantage of the high ring strain of cyclooctynes, the activation energy barrier is lowered for the alkyne-azide [2+3] cycloaddition, and as a result the reaction can proceed rapidly in the absence of copper(I) or other metal catalysts.<sup>282</sup> Furthermore, the same group tried to perturb the electronic properties of the cyclooctyne by introducing fluorine atoms at the propargylic position<sup>283</sup> or by further increasing the ring strain through the use of dibenzo-cyclooctynes.<sup>284</sup> Both modifications dramatically accelerate the rate of the cycloaddition and can be directly applied in living systems. In 2010, a cyclooctyne-based click reaction was reported by Boons and colleagues using a nitrene dipole to enhanced rate compared to azide dipoles.<sup>285</sup> However, the preparation of these cyclooctynes poses synthetic challenges, which require multiple steps and almost always give poor overall yields. To avoid both copper(I) as the catalyst and the complicated synthesis of cyclooctynes, several groups have been making use of norbornenes, which feature high ring strain attributed to the bicyclic nature and the small ring size.<sup>286-289</sup> To these ends, Rutjens and co-workers first treated alkynes with furan via a Diels-Alder reaction to form oxanorbornadienes, which then react rapidly with organic azides, and the product then undergoes a *retro*-Diels-Alder reaction to afford the 1,2,3-triazole products.<sup>286, 287</sup> This reaction was found to be relatively slow compared with the reaction using cyclooctynes.<sup>287</sup> Another copper-free click reaction was reported to employ the 1,3-dipolar cycloaddition of nitrile oxide and norbornene.<sup>288</sup> Prior to the cycloaddition, the nitrile oxides were prepared *in situ* from the elimination of the hydroximoyl chloride under basic conditions. The reaction proceeds under neutral or

slightly basic aqueous/aqueous cosolvent conditions with a high reaction rate at room temperature. It is worth mentioning that the Diels-Alder reaction between tetrazines and norbornenes developed by the Jäschke lab was found very useful to modify DNAs post-synthetically with high efficiency at low reactant concentrations.<sup>289</sup> Despite the development of various 1,3-dipolar cycloadditions based on alkynes and azides, the copper(I) catalyzed 1,3-dipolar cycloaddition is still of major interest and has been applied for numerous objectives. In the following section, its application in radiopharmaceutical chemistry will be reviewed.

### **6.1.2 The copper(I) catalyzed 1,3-dipolar cycloaddition applied in radiopharmaceutical chemistry**

For radiochemistry, it is desirable to introduce radioisotopes in the last step of the whole synthesis. Often however, this is not readily accomplished, especially for non-metallic radioisotopes. For many radiosyntheses, sensitive functional groups are almost always protected prior to the radiolabeling step, and after the introduction of the radioisotope, further steps are employed to remove these protecting groups. Take the radiosynthesis of <sup>18</sup>F-FDG for example. No matter which method is followed, the hydroxyl groups are all protected with acetyl groups before the introduction of <sup>18</sup>F-fluorine, such that HCl treatment is needed to remove the acetyl groups to yield the desired product, <sup>18</sup>F-FDG, afterwards. In addition, most biomolecules cannot survive the harsh radiolabeling conditions such as high temperatures, non-aqueous solvents, and strongly basic/acidic conditions. Therefore, as alternatives, radioactive prosthetic precursors are usually prepared first, and then incorporated into biomolecules under more mild conditions. This generally requires a multi-step radiosynthesis, which is very time-consuming. Most importantly, due to the short half-lives of the radioisotopes, the amount of the final radiolabeled product is consequently reduced at the end of the synthesis. Hence, radiochemists have generally favored reactions between the prosthetic groups and biomolecules to be fast, robust, and both chemoselective and regioselective in order to enhance the radiochemical yields and purity of the products and to compensate for the short half-lives of the radioisotopes. With the properties mentioned earlier, click chemistry opens a door for radiopharmaceutical chemistry and speeds up the

development of new radiolabeling techniques as well as exploration of new radiolabeled compounds. In addition to the frequently used reactions including the thiol-maleimide reaction,<sup>290</sup> oxime ether formation,<sup>291, 292</sup> and thiol-haloacetamide substitution,<sup>293</sup> the radiolabeling field have benefited a lot from the copper(I) catalyzed alkyne-azide dipolar cycloaddition, which is regioselective, bioorthogonal, rapid, and high yielding.<sup>266</sup>

The first application of the copper(I) catalyzed alkyne-azide dipolar cycloaddition in radiopharmaceutical chemistry was carried out by Marik and Sutcliffe.<sup>294</sup> In this work, they prepared the  $\omega$ -<sup>18</sup>F-fluoroalkyne from the tosylate derivatized alkyne and purified it by simple co-distillation with acetonitrile. The distilled synthon was then reacted with several azidopeptides in the presence of CuSO<sub>4</sub> and sodium ascorbate to provide the desired <sup>18</sup>F-labeled peptides in about 10 minutes with good-to-excellent yields of 54-99% and excellent radiochemical purity of 81-99%. Shortly thereafter, Glaser *et al.* reported the application of click labeling reactions between 2-<sup>18</sup>F-fluoroethylazide and various terminal alkyne substrates.<sup>295</sup> 2-<sup>18</sup>F-Fluoroethylazide was also obtained via replacement of 2-azidoethyl-4-toluenesulfonate with <sup>18</sup>F-fluoride. All of the alkyne substrates tested therein gave very good yields in the presence of either copper(II)/ascorbate or copper wire in pH 6.0 phosphate buffer within 15 minutes. A one-pot two-step synthesis involving the copper(I) catalyzed 1,3-dipolar cycloaddition for <sup>18</sup>F-labeled compounds was also reported.<sup>296</sup> The <sup>18</sup>F-prosthetic alkyne was first prepared via a standard substitution reaction at 100 °C for 20 minutes, and the reaction mixture, after cooling to room temperature, was directly subjected to click reaction conditions in the presence of several organoazides and CuSO<sub>4</sub>/sodium ascorbate for 5 to 10 minutes. This one-pot two-step synthesis required no interim purification and gave an impressive overall radiochemical yield of ~ 90%. Later, a novel nonvolatile <sup>18</sup>F-azido synthon, 1-azidomethyl-4-<sup>18</sup>F-fluorobenzene, was developed for the clickable labeling strategy by the Thonon lab.<sup>297</sup> The <sup>18</sup>F-azido synthon, which was prepared from 4-formyl-*N,N',N''*-trimethyl-anilinium triflate via four steps within 75 minutes, was coupled to the model alkynyl peptide in the presence of copper(I) iodide and an organic base to give moderate-to-good chemical and radiochemical yields. The microPET imaging work of tumor expressing integrin  $\alpha_v\beta_3$  with <sup>18</sup>F-labeled RGD prepared via click chemistry was reported in the same year.<sup>298</sup> The <sup>18</sup>F-labeled RGD dimer was obtained

from the  $^{18}\text{F}$ -fluoroalkyne and the azido-peptide and purified by semi-preparative HPLC. It was found that the triazole group introduced during the click reaction has little influence on the integrin binding affinity of RGD-peptides, and the  $^{18}\text{F}$ -product shows very good tumor targeting efficacy and comparable *in vivo* stability to the  $^{18}\text{F}$ -RGD compounds obtained from other methods. The radiosynthesis itself was quite straightforward to give a decay corrected radiochemical yield of 53.8% in 110 minutes, which provides a shorter synthesis time and a higher labeling yield than that using the *N*-succinimidyl- $^{18}\text{F}$ -benzoate precursors. The copper(I) catalyzed 1,3-dipolar cycloaddition was also employed to synthesize  $^{18}\text{F}$ -labeled neurotensin (8-13) with a radiochemical yield of 66% in 20 minutes.<sup>299</sup> The  $^{18}\text{F}$ -labeled peptide A20FMDV2<sup>a</sup>, selectively binding to integrin  $\alpha_v\beta_6$ , was prepared via a similar method to image  $\alpha_v\beta_6$ -expressing tumors.<sup>300</sup> Isatin sulfonamide was also derivatized with the  $^{18}\text{F}$ -labeled triazole to study the caspase 3/7 activation and apoptosis *in vivo*.<sup>301</sup> Folic acid was labeled using the click radiosynthesis to target folate receptors overexpressed in tumors.<sup>302</sup> Furthermore, this conjugation strategy has also been applied to prepare  $^{18}\text{F}$ -labeled nanoparticles in a rapid and high efficient fashion.<sup>303</sup>

Although the method is mainly reported for  $^{18}\text{F}$ -labeled compounds, click chemistry has also been employed to prepare  $^{11}\text{C}$ -labeled compounds. In one report,  $^{11}\text{C}$ - $\text{CH}_3\text{N}_3$  was first prepared from  $^{11}\text{C}$ - $\text{CH}_3\text{I}$  and then reacted with an alkyne derivatized Tyr<sup>3</sup>-octreotate<sup>b</sup> in the presence of copper(I) with a decay corrected radiochemical yield of ~ 35% after a synthesis of 30 minutes.<sup>304</sup> A one-pot labeling approach to mix the peptide,  $\text{NaN}_3$ , copper(I), and  $^{11}\text{C}$ - $\text{CH}_3\text{I}$  was also reported in the same work and the radiochemical yield was as low as 5%.

Although the copper(I) catalyzed click coupling is always reported in high yields and with very good substrate compatibility, it has been found that the yields might depend on the size and complexity of the molecules selected for labeling.<sup>300</sup> In addition, some reports suggest there has been no loss of bioactivity due to the introduction of the triazole residue, but altered binding affinity and biodistribution of the labeled molecules via this

---

<sup>a</sup> The sequence for A20FMDV2 is NAVPNLRGDLQVLAQKVART.

<sup>b</sup> Tyr<sup>3</sup>-octreotate is a water soluble peptide used as a tumor imaging agent. It has a sequence of D-Glu-D-Tyr-[Cys-Tyr-Trp-Lys-Thr-Cys]-Thr.

method has also been observed.<sup>298</sup> Nonetheless, the method has indeed drawn a great deal of attention in the field and become more and more useful for the development of new imaging compounds.

### 6.1.3 Imaging oligonucleotides

Oligonucleotides, because of their sequence-specific interactions, can specifically recognize other oligonucleotides or part of a gene sequence. The specific recognition of oligonucleotide is the basis by which ribozymes, short interfering RNAs (siRNAs), DNA microarrays,<sup>305</sup> and antisense oligonucleotides<sup>306, 307</sup> can be explored for analysis/detection<sup>308</sup> and gene therapies.<sup>309, 310</sup> If the target gene sequence is known, a short complementary sequence of oligonucleotide can be designed and synthesized via solid phase synthesis to target a gene of interest. In addition, it has also been found that some nucleic acids can fold into complex three dimensional structures, which allow for molecular interactions with a wide range of biomolecules such as proteins. These nucleic acids are normally referred to aptamers.<sup>311-314</sup> Like various antibodies and peptides, aptamers with certain three-dimensional structures can specifically recognize and tightly bind to various molecular targets such as membrane proteins, enzymes, viruses, bacteria, and cells.<sup>315</sup> On the other hand, the recent development of *in vitro* technologies allows researchers to amplify oligonucleotides via polymerase chain reaction (PCR), and screen them for certain functions and properties by a selection method called “systematic evolution of ligands by exponential enrichment” (SELEX).<sup>315, 316</sup> In spite of various promising targeting properties and potential applications in many fields, oligonucleotides are relatively susceptible to rapid degradation *in vivo*, mainly due to cleavage by nucleases, which are very abundant in most of the tissues and organs as well as in the blood. Meanwhile, oligonucleotides usually exhibit poor cell membrane permeability because of their polyanionic nature and large molecular sizes. An extensive amount of work has been done to improve the *in vivo* stability and develop the target delivery of oligonucleotides, which includes modified nucleotides<sup>317</sup> for higher *in vivo* stability and polycationic carriers such as liposomes<sup>318</sup> for better cell uptake.

Considerable efforts have been made to apply oligonucleotides in a variety of uses. Although the gene-targeted therapies with nucleic acids might one day revolutionize

cancer treatment,<sup>309</sup> additional data are needed for their *in vivo* performance regarding target specificity, sensitivity, and drug efficacy before using the nucleic acids to treat diseases. Fortunately, with the improvement of various *in vivo* visualization technologies, direct *in vivo* evaluation is now available to characterize oligonucleotide drugs' *in vivo* stability, pharmacokinetics/dynamics, specific targeting ability, and potential therapeutic efficacy. By labeling promising oligonucleotide candidate drugs obtained from *in vitro* selections or from target design with reporting groups<sup>a</sup> such as fluorophores and/or radionuclides for *in vivo* imaging, better understanding of the oligonucleotides' *in vivo* performance can be achieved, which in turn will provide essential information for therapy and diagnosis based on the oligonucleotides.<sup>319-321</sup>

Hnatowich and colleagues used a DNA duplex with one strand of antisense phosphorothioate<sup>b</sup> DNA bearing a fluorescent emitter while the other strand carrying an effective inhibitor for antisense targeting to image tumor in mice.<sup>322</sup> Only the antisense oligonucleotide derivatized with the fluorescent emitter Cy5.5 bound to the RNA in the tumor cells and provided high fluorescent intensity, which suggested the dissociation of the duplex and the subsequent hybridization with the target mRNA both *in vitro* and *in vivo*. This work provided promising preliminary results regarding specific recognition of mRNA, and exhibited a relatively high signal-to-noise ratio. A recent report also described the imaging work using a Cy5 fluorescent labeled aptamer TD05, which was derived from cell-SELEX.<sup>323</sup> The *in vivo* imaging work targeting B-cell lymphoma showed that the aptamer could effectively recognize the tumor specifically with high sensitivity. This work represents the first reported case of aptamers screened from SELEX experiments for use in *in vivo* studies, and establishes the efficacy of the fluorescent aptamers for *in vivo* diagnosis while also providing important data to support the *in vivo* application of aptamers.

Besides these optical imaging methods, radionuclear imaging technologies can provide high sensitivity and extraordinary resolution. However, compared with other bioligands, there are far fewer reports available for radiolabeled oligonucleotides as *in vivo*

---

<sup>a</sup> Reporting groups here stand for the groups that can release any signals, which can be detected by certain instruments to record the traveling trajectory and localization of the molecules containing these groups.

<sup>b</sup> Phosphorothioate oligonucleotides are frequently used to improve the stability of oligonucleotides.

therapeutic drugs and diagnostic agents.<sup>319</sup> It is believed that the low *in vivo* stability, poor bioavailability, and “non-specific” interactions are the major factors that limit the radiopharmaceutical applications of radiolabeled oligonucleotides.<sup>319, 324</sup> Nevertheless, there has been considerable interest in radiolabeling oligonucleotides, which continues to provide promising results to recommend oligonucleotides as specific targeting drugs.

Kobori *et al.* reported a <sup>11</sup>C-labeling study on an antisense phosphorothioate oligodeoxynucleotide to target the mRNA of glial fibrillary acidic protein,<sup>325</sup> which was abnormally expressed in glioma tumors. In their work, they first annealed a 5'-aminoethyl phosphorothioate oligonucleotide to a complementary 5'-biotinylated phosphodiester oligodeoxynucleotide, which can be immobilized with BioMag Streptavidin<sup>a</sup> before labeling. The double stranded construct was then incubated with <sup>11</sup>C-ethylketene, which was prepared from <sup>11</sup>C-CO<sub>2</sub>, for 5 minutes at room temperature. When the BioMag beads carrying the complex of biotin-avidin with the double stranded oligonucleotides were incubated at the elevated temperature, the <sup>11</sup>C-labeled single stranded oligodeoxynucleotide with a specific activity of about 5 Ci/μmol was released. The tracer was then formulated and intravenously injected into rats bearing gliomas that had been implanted in the cerebrum. The rats' brains were removed 40 minutes after the injection and the autoradiographic images showed that the radioactivity in the tumor tissues was much stronger than the peripheral normal cerebral cortex.

Kobayashi and co-workers addressed the delivery issue of oligonucleotides.<sup>327</sup> They used the polycationic nature of both avidin (Av) and the generation 4 polyamidoamine dendrimer (G4) as the oligonucleotide delivery vehicle. They labeled several 20-mer multiamino-linked antisense oligonucleotides to target the *c-erbB-2* sequence with <sup>111</sup>In via a diethylenetriaminepentaacetic acid chelator. Both the <sup>111</sup>In-labeled oligonucleotides and the dendrimer G4 studied therein were biotinylated to give <sup>111</sup>In-oligo-Bt and G4-Bt respectively. Via the electrostatic interactions between the dendrimer and oligonucleotide and/or the specific binding between avidin and biotin, three vehicle pretreated <sup>111</sup>In-labeled oligonucleotides (<sup>111</sup>In-oligo/G4, <sup>111</sup>In-oligo-biotin/avidin, <sup>111</sup>In-oligo/G4-biotin/avidin) were studied for the internalization *in vitro* and *in vivo* in human ovarian

---

<sup>a</sup> BioMag Streptavidin is composed of streptavidin conjugated to 1 μm magnetic Fe<sub>3</sub>O<sub>4</sub>. The dissociation constant of biotin-streptavidin  $K_D = 10^{-15}$  M and the complex's dissociation half-life is ~ 89 days.<sup>326</sup>

cancer cells (SHIN3 cancer cells). It was found that the  $^{111}\text{In}$ -labeled oligonucleotide with these delivery vehicles could effectively enter tumor cells by non-sequence-specific targeting. It was expected that these delivery vectors could be applied to other oligonucleotides.

Several  $^{68}\text{Ga}$ -labeled 17-mer antisense oligonucleotides, from 2'-deoxyphosphodiester, 2'-deoxyphosphorothioate or 2'-*O*-methyl phosphodiester with the same sequences targeting the activated human K-ras oncogene, were evaluated for their *in vivo* biodistribution and biokinetics.<sup>328</sup> The oligonucleotides were successfully labeled via  $^{68}\text{Ga}$  chelation with 1,4,7,12-tetraazacyclododecane (DOTA), and the  $^{68}\text{Ga}$ -labeled oligonucleotides provided very high PET image quality. It also was found that the modification of the oligonucleotide backbone could influence their biokinetics.

Bertrand *et al.* reported a general method to label antisense oligonucleotides with radioactive halogens.<sup>329</sup> Briefly, *N*-(4-halogenobenzyl)-2-bromoacetamides were prepared and then incubated with 3'-phosphothioate oligonucleotides in PBS buffer (pH 8) at 120 °C for 10 minutes. The  $^{18}\text{F}$ -,  $^{76}\text{Br}$ -, and  $^{125}\text{I}$ -labeled oligonucleotides were injected into mice. However, no intact oligonucleotides were detected one hour after injection, which might be mainly due to the vulnerability of the natural backbone of the oligonucleotides against serum nucleases.

Whereas the coupling of an oligonucleotide with a radiolabeled bromoacetamide requires high temperatures e.g. 80 to 120 °C, such conditions can be quite harsh for oligonucleotides. Hence several groups have worked on a different coupling strategy involving *N*-succinimidyl-4- $^{18}\text{F}$ fluorobenzoate ( $^{18}\text{F}$ -SFB) at room temperature to the 3'- or 5'-alkylamine modified oligonucleotides. The radiosynthesis was first applied to radiolabel several G-rich oligonucleotides (GROs),<sup>330, 331</sup> including aptamer AS1411 with antiproliferative effects against cancer cell growth via binding to the nucleolin<sup>a</sup> protein.<sup>331</sup> A double-stranded siRNA was also conjugated with  $^{18}\text{F}$ -SFB.<sup>333</sup> Then the  $^{18}\text{F}$ -labeled siRNA ( $^{18}\text{F}$ -siRNA) was mixed with a liposome to form the  $^{18}\text{F}$ -siRNA/liposome complex. Both the  $^{18}\text{F}$ -siRNA and the  $^{18}\text{F}$ -siRNA/liposome complex

---

<sup>a</sup> Nucleolin is a protein playing critical role in cell proliferation, growth as well as some other functions in cells.<sup>332</sup>

were injected into mice for biodistribution studies. It was found that dramatically different biodistributions were observed. The  $^{18}\text{F}$ -siRNA cleared rapidly and was quickly excreted into urine while the  $^{18}\text{F}$ -siRNA/liposome complex accumulated in the lung. The serum stability study suggested that the  $^{18}\text{F}$ -siRNA/liposome complex had a high serum stability but  $^{18}\text{F}$ -siRNA was rapidly degraded in serum due to abundant nucleases. This work highlighted that the delivery vehicle might not only facilitate the oligonucleotide delivery to the target but also play important roles in increasing the *in vivo* stability of oligonucleotides through the formation of such liposome complexes. This clearly sheds some light on the development of siRNA drugs. In addition, all the radiolabeling work using  $^{18}\text{F}$ -SFB as the prosthetic group showed relatively clean syntheses with only some decomposition of  $^{18}\text{F}$ -SFB under the buffered conditions.<sup>330</sup>

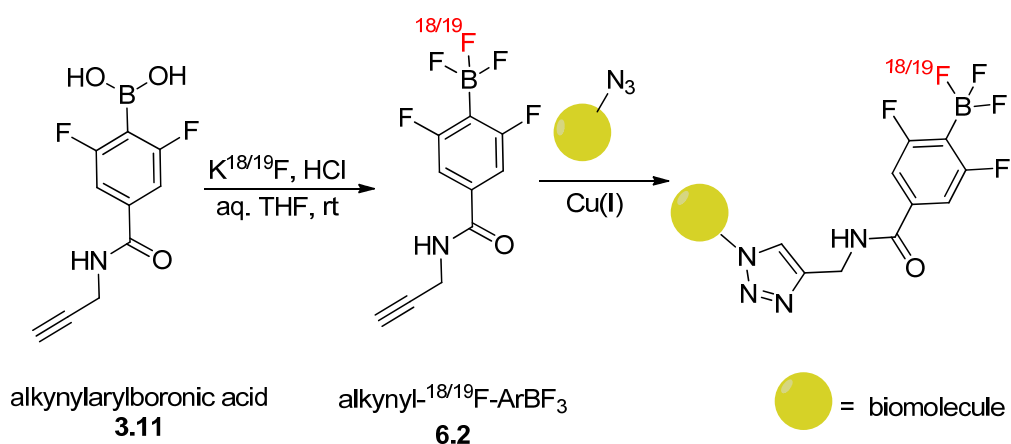
The copper(I) catalyzed azide alkyne 1,3-dipolar cycloaddition has also showed good potential for modifying oligonucleotides.<sup>272, 334</sup> A 2- $^{18}\text{F}$ -labeled pyridinyl alkyne was clicked onto an antisense oligonucleotide with an azido residue by Inkster *et al.* with a decay corrected radiochemical yield of 25% at 75 °C for 15 minutes.<sup>335</sup> Since there was an HPLC purification step for the prosthetic group 2- $^{18}\text{F}$ -labeled pyridinyl alkyne, the total radiosynthesis time was 276 minutes.

Overall, radiolabeling oligonucleotides for *in vivo* imaging is an important goal, since there are a wide variety of targets available for these biomolecules. Techniques that enable rapid and reproducible labeling of oligonucleotides could provide valuable information in terms of *in vivo* stability, biodistribution, pharmacokinetics, efficacy, and target specificity. Imaging techniques in combination with drug delivery strategies can hence highly facilitate and accelerate the investigation of oligonucleotide drugs and potential radiopharmaceuticals.

#### **6.1.4 Radiolabeling oligonucleotides with $^{18}\text{F}$ -ArBF<sub>3</sub>s via the copper(I) catalyzed 1,3-dipolar cycloaddition**

The conditions for preparing  $^{18}\text{F}$ -ArBF<sub>3</sub>s in this thesis have generally been very acidic (pH ≤ 1), and many midsize and large biomolecules are unlikely to survive at this pH; for instance, proteins become denatured,<sup>336</sup> and DNA and RNA are susceptible to

depurination.<sup>337, 338</sup> To expand and generalize the application of the labeling technique using  $^{18}\text{F}$ - $\text{ArBF}_3\text{s}$  to label acid-labile biomolecules, we pursued a one-pot two-step labeling strategy. Since copper(I) catalyzed 1,3-dipolar cycloaddition carries so many attractive advantages, especially its orthogonal property to various functional groups and mild reaction conditions,<sup>261</sup> it is proposed that the marriage between the copper(I) catalyzed 1,3-dipolar cycloaddition and the  $^{18}\text{F}$ - $\text{ArBF}_3$  labeling can be extremely useful to label acid-labile biomolecules.



**Scheme 6.2** The scheme of the one-pot two-step method to label biomolecules with an  $^{18}\text{F}$ - $\text{ArBF}_3$  via the copper(I) catalyzed alkyne-azide cycloaddition.

In 2006, Molander and Ham reported the first 1,3-dipolar cycloaddition involving organotrifluoroborates catalyzed by copper(I).<sup>339</sup> They were able to develop a facile one-pot synthesis using haloalkyltrifluoroborates as the starting materials for several organo-triazolyl-trifluoroborates. In 2009, fluoride was reported to protect boronic acid for the copper(I) catalyzed click reaction by Wang and co-workers,<sup>340</sup> where two equivalents of fluoride were added to the click reaction prior to the addition of the copper(I) catalyst and the reaction showed a very good conversion. However, only arylboronic acids with slightly electron donating substituents on the aromatic ring were studied in both reports.<sup>339, 340</sup> In our group, both Dr. Harwig<sup>a</sup> and I have tested the copper(I) catalyzed click reaction with  $\text{ArBF}_3\text{s}$  carrying electron withdrawing groups. The reactions monitored with  $^{19}\text{F}$  NMR spectroscopy showed very good conversions (data not shown) and suggested excellent stability of  $\text{ArBF}_3\text{s}$  in the presence of copper(I), which is known to insert into the C-B bond of organoboronic acids. Hence, we were

<sup>a</sup> Dr. Curtis Harwig was a post-doc in our lab from 2007-2009.

encouraged to pursue this method for a one-pot two-step labeling strategy to introduce  $\text{ArBF}_3\text{s}$  to biomolecules. Scheme 6.2 briefly illustrates the strategy with a fluoridation to provide  $^{18}\text{F}$ -alkynylaryltrifluoroborate **6.2** (alkynyl- $^{18}\text{F}$ - $\text{ArBF}_3$ ), which is subsequently subjected to a click reaction to conjugate the azide-derivatized biomolecules.

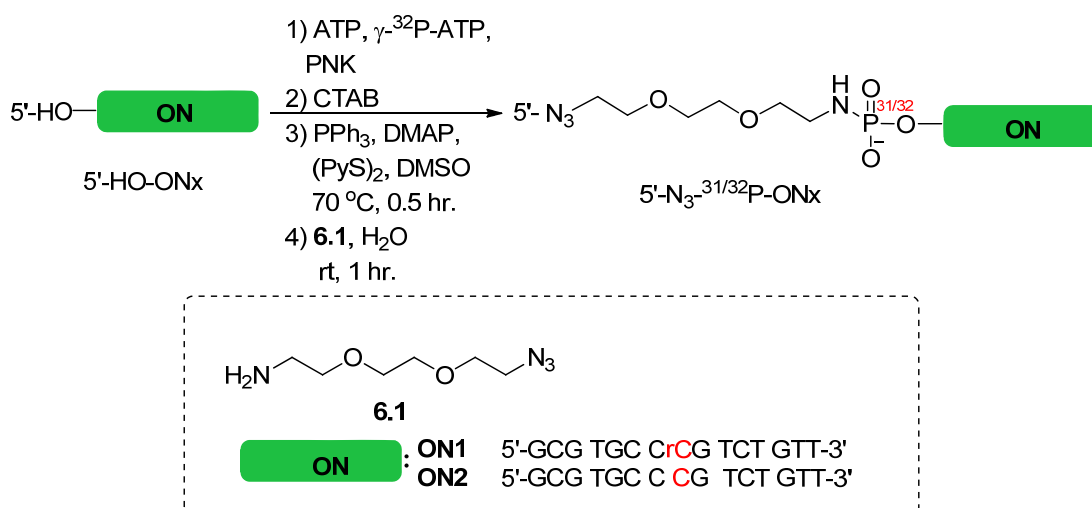
In this chapter, the one-pot two-step labeling method via the copper(I) catalyzed alkyne-azide cycloaddition will be applied to label oligonucleotides as a proof of concept that should be generalizable to labeling acid-labile molecules with  $^{18}\text{F}$ - $\text{ArBF}_3\text{s}$ . Derivatization at the 5'-terminus of oligonucleotides generally does not compromise their bioactivity including the binding affinity. It is therefore expected that this labeling method should be of general utility to label oligonucleotides generated for most purposes.

Generally, we first synthesized alkynylarylboronic acid **3.11** and labeled it with fluoride ( $^{19}\text{F}$  or  $^{18}\text{F}$ ) to obtain alkynyl $\text{ArBF}_3$  **6.2**, which was then directly added to a copper(I) catalyzed click reaction to react with the azido derivatized oligonucleotides (5'- $\text{N}_3$ -ONs). Two oligonucleotides **ON1** (5'-GCGTGCCrCGTCTGTT-3') and **ON2** (5'-GCGTGCCCGTCTGTT-3') are used in this chapter for the copper(I) catalyzed click reaction with alkynes. **ON1** has the same sequence as **ON2**, but contains a ribonucleotide cytidine (rC) at the 8<sup>th</sup> nucleotide instead of deoxyribocytosine (dC) as found in **ON2**. The oligonucleotides with 15 nucleotides, normally called 15mers, with no specific biological functions, have been used for other purposes in the Perrin lab and were chosen to study this labeling reaction. The relatively labile RNA linkage (the 2'-hydroxyl on the cytidine of **ON1**) would enable us to determine whether or not the derivatization and the click reaction would influence the integrity of oligonucleotides at least in the context of a RNA linkage. Moreover,  $^{32}\text{P}$ -labeling on the oligonucleotide is used herein to increase the detection sensitivity for the reaction on small scale. The  $^{32}\text{P}$ -labeled oligonucleotides can be further radiolabeled with an  $^{18}\text{F}$ - $\text{ArBF}_3$  to give the double isotopic labeling, which can provide distinguishable properties (different decay rates for  $^{32}\text{P}$  and  $^{18}\text{F}$ ) to understand the reaction conditions. Therefore, azido-oligonucleotides (5'- $\text{N}_3$ - $^{31/32}\text{P}$ -ONs) were prepared by a simply coupling reaction with the 5'- $^{31/32}\text{P}$ -ONs. The copper(I) catalyzed click reaction with the 5'- $^{31/32}\text{P}$ -ONs will be described herein.

## 6.2 Results

### 6.2.1 The derivatization of oligonucleotides

As shown in Scheme 6.3, commercially synthesized oligonucleotides (ONs) were directly 5'-phosphorylated in a PNK reaction with nearly quantitative conversions and the products were used directly without further purification save a simple desalting procedure for the following derivatization. The 5'-<sup>31/32</sup>P-ONs were precipitated with the phase transferring reagent cetyltrimethyl ammonium bromide (CTAB) from the aqueous medium by forming the CTA salts. The CTA salt of the 5'-<sup>31/32</sup>P-ON was activated by PPh<sub>3</sub>, DMAP, and (PyS)<sub>2</sub> in DMSO at 70 °C for 0.5 hours, and then treated with azido-PEG-amine **6.1** via a nucleophilic replacement at room temperature in the aqueous solution for one hour.<sup>341, 342</sup> Because azides can be reduced by PPh<sub>3</sub> through the Staudinger reaction,<sup>343</sup> the activating agent in the first step was thoroughly removed by the precipitation of the activated 5'-<sup>31/32</sup>P-ON with LiClO<sub>4</sub>/acetone prior to the addition of azido-PEG-amine **6.1** for the coupling reaction.



**Scheme 6.3** The scheme of the oligonucleotide derivatization.<sup>341</sup>

ONx is the oligonucleotide **ON1** or **ON2**. The sequences for the 5'-HO-ONx are shown in the scheme. (5'-HO-GCG TGC CrCG TCT GTT-3' for 5'-HO-**ON1** and 5'-HO-GCG TGC CCG TCT GTT-3' for 5'-HO-**ON2**). rC indicates a ribocytosine.

Nevertheless, the derivatization of oligonucleotides 5'-<sup>31/32</sup>P-**ON1** and 5'-<sup>31/32</sup>P-**ON2**, of the same sequence, showed different results as indicated in Figure 6.3. Following activation for bioconjugation, both oligonucleotides yielded new bands in the PAGE gel.

The coupling reaction with  $5' \text{-}^{31/32}\text{P-ON1}$  gave several additional byproducts while that with  $5' \text{-}^{31/32}\text{P-ON2}$  demonstrated a much cleaner synthesis. The major bands are indicated with A, B, C and D in the gel image presented in Figure 6.3. For the derivatization of  $5' \text{-}^{31/32}\text{P-ON2}$  in Lane 3 of Figure 6.3, two bands were separated via the 20% polyacrylamide gel electrophoresis (PAGE). One of the bands is the unreacted  $5' \text{-}^{31/32}\text{P-ON2}$  (band D) and the other, designated as the band C, is the azido-oligonucleotide product ( $5' \text{-N}_3\text{-}^{31/32}\text{P-ON2}$ ). In contrast, for the derivatization of  $5' \text{-}^{31/32}\text{P-ON1}$ , the situation is much more complicated as indicated on the gel image. There are several newly produced bands including the one representing the desired product. When compared with the derivatization of  $5' \text{-}^{31/32}\text{P-ON2}$ , Band C in Lane 2 of the  $5' \text{-}^{31/32}\text{P-ON1}$  derivatization should be the desired product ( $5' \text{-N}_3\text{-}^{31/32}\text{P-ON1}$ ), since it migrated very similarly to that of  $5' \text{-N}_3\text{-}^{31/32}\text{P-ON2}$  in the PAGE gel. A MALDI-TOF analysis of the gel-purified oligonucleotide corresponding to Band C in Lane 2 further confirmed that Band C corresponds to the desired product. In addition, the EDC/imidazole coupling method<sup>344</sup> was also attempted for the derivatization purpose, but the result was far less effective than Knorre's protocol.<sup>341</sup>

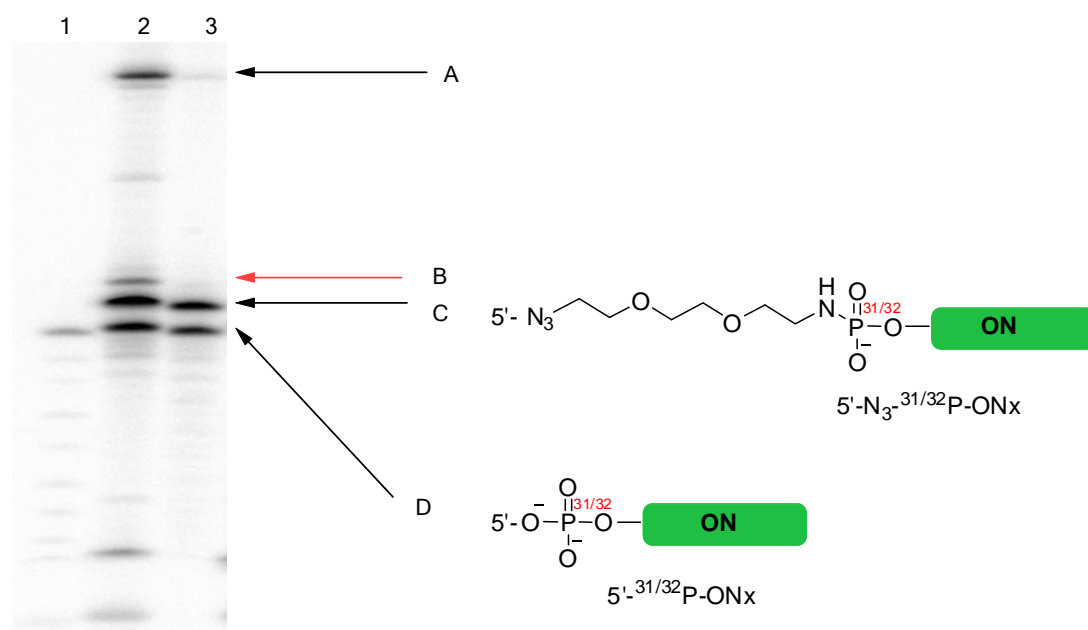
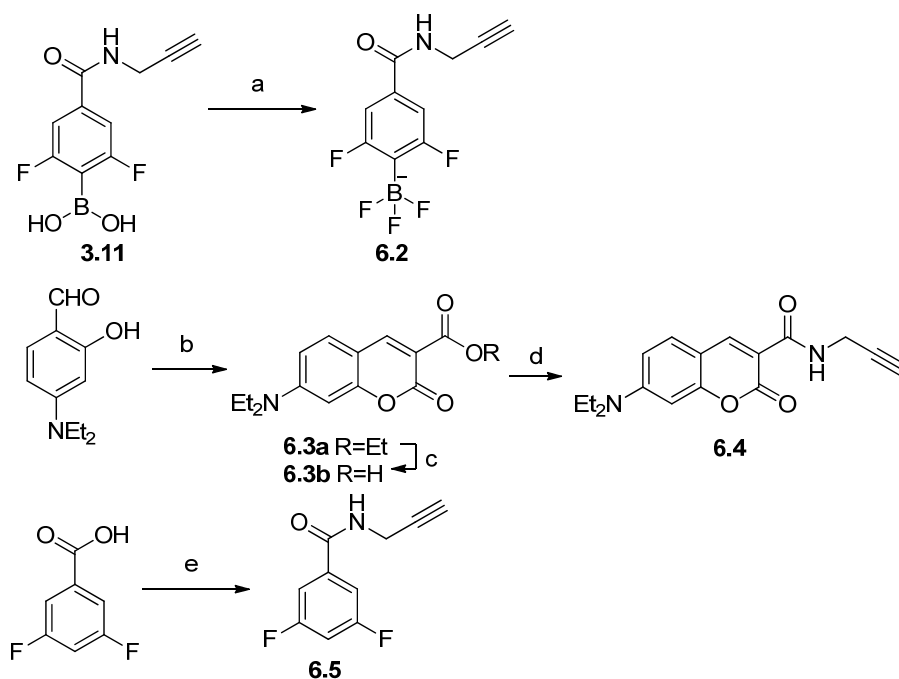


**Figure 6.3** The autoradiographic gel image of the derivatization of  $5' \text{-}^{31/32}\text{P-ON}$ . Lane 1 is  $5' \text{-}^{31/32}\text{P-ON2}$ , Lane 2 is the derivatization to prepare  $5' \text{-N}_3\text{-}^{31/32}\text{P-ON1}$  and Lane 3 is the derivatization to prepare  $5' \text{-N}_3\text{-}^{31/32}\text{P-ON2}$ . Band D is the precursor  $5' \text{-}^{31/32}\text{P-ONx}$  and Band C is the desired derivatized product  $5' \text{-N}_3\text{-}^{31/32}\text{P-ONx}$ . Bands A and B are unknown byproducts from the derivatization. Oligonucleotides were resolved in 20% PAGE (33 cm  $\times$  42 cm).

## 6.2.2 Synthesis of alkynes

While the azido-oligonucleotides were prepared successfully and purified by the PAGE, we also synthesized several alkynes with different properties to guide us in understanding the click chemistry between the oligonucleotides and alkynylArBF<sub>3</sub> **6.2**. All the terminal alkynes were synthesized from a simple coupling reaction using EDC/HOBt as indicated in Scheme 6.4. Alkynylcoumarin **6.4** was prepared to provide a highly hydrophobic and fluorescent synthon, which after the incorporation into the oligonucleotides via click chemistry, not only retards the mobility of the oligonucleotides on the PAGE gel but also gives fluorescent signals to confirm the success of the conjugation. 3,5-Difluoro-*N*-(prop-2-yn-1-yl)benzamide **6.5** was also synthesized to provide an electrophoretic standard that would represent possible deboronation products of alkynylArBF<sub>3</sub> **6.2** or alkynylarylboronic acid **3.11** during the click reaction. Alkynylarylboronic acid **3.11** was prepared as described in Chapter 3. Briefly, arylboronic acid **3.8** was first protected with 1,8-diaminonaphthalene and then coupled with propargylamine in the presence of EDC/HOBt to afford **3.10**. The protecting group on **3.10** was then removed under acidic aqueous conditions to give the desired alkynylarylboronic acid **3.11**.



**Scheme 6.4** Synthetic scheme of alkynes.

(a), KHF<sub>2</sub>, THF/H<sub>2</sub>O, rt, 5 hr, quant; (b) diethyl malonate, piperidine, EtOH, reflux, N<sub>2</sub>, 4 hr, 36%; (c), NaOH, MeOH, H<sub>2</sub>O, reflux, 1 hr, 71%; (d) propargylamine, EDC·HCl, HOBt·H<sub>2</sub>O, NEt<sub>3</sub>, CH<sub>2</sub>Cl<sub>2</sub>, rt, overnight, 94%; (e), propargylamine, EDC·HCl, HOBt·H<sub>2</sub>O, NEt<sub>3</sub>, CH<sub>2</sub>Cl<sub>2</sub>, rt, overnight, 90%.

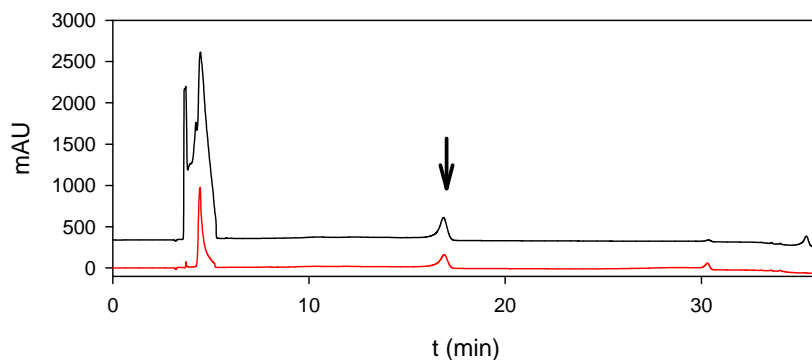


**Figure 6.4** The HPLC chromatograms at 229 nm of alkynylArBF<sub>3</sub> **6.2** (black) and the fluoridation of alkynylarylboronic acid **3.11** (red).

The black trace is the HPLC chromatogram of alkynylArBF<sub>3</sub> **6.2** in its DMSO stock solution at 229 nm; the red trace is that of the crude fluoridation of alkynylarylboronic acid **3.11** at 229 nm. The final concentrations for the fluoridation: 15.4 mM of alkynylarylboronic acid **3.11**, 0.95 M of HCl, and 76.9 mM of <sup>19</sup>F-fluoride in the form of KHF<sub>2</sub>, in 6.5 μL of 4:2.5 THF:H<sub>2</sub>O. The reaction was undertaken at rt for 32 min, and then quenched with 100 μL of 5% NH<sub>4</sub>OH/EtOH prior to the HPLC injection. The HPLC was carried out using HPLC Program 15 with Column I in HPLC System I. The peak indicated with an arrow was collected and characterized by ESI-MS ([M]<sup>-</sup>: 262.3).

AlkynylArBF<sub>3</sub> **6.2** was prepared by the fluoridation of alkynylarylboronic acid **3.11** in the presence of a large excess of fluoride under acidic conditions. A cold fluoridation reaction to prepare alkynylArBF<sub>3</sub> **6.2**, at a fluoride concentration that mimicked that used in radiolabeling conditions, was also undertaken to identify the reaction conditions prior to the <sup>18</sup>F-labeling, and the reaction analyzed by HPLC is shown in Figure 6.4. In 30 minutes, the reaction gave the desired product in a reasonable yield. Since alkynylArBF<sub>3</sub> **6.2** has a relatively low extinction coefficient and because relatively small amounts were prepared, no standard curve of the concentration-UV absorbance was obtained and the conversion of the reaction was therefore not accurately determined. The product of the crude reaction (the red HPLC trace) eluted at the same time as alkynylArBF<sub>3</sub> **6.2** (the black HPLC trace) purified previously and characterized with both <sup>19</sup>F/<sup>1</sup>H NMR spectroscopy and ESI-MS spectrometry.

Alkynyl-<sup>18</sup>F-ArBF<sub>3</sub> **6.2** was prepared under similar conditions. However, to avoid the tremendous decrease in the specific activity of <sup>18</sup>F-fluoride by the addition of carrier fluoride, a small volume of a KHF<sub>2</sub> solution (containing about 800 to 1000 nmol of <sup>19</sup>F-fluoride) was added to the “dry” <sup>18</sup>F-fluoride. Then 2 μL of the <sup>18/19</sup>F-fluoride solution containing ~ 500 nmol of <sup>19</sup>F-fluoride was added to the aqueous THF solution of boronic acid **3.11** (100 nmol) and HCl (~ 6 μmol) to afford an acidic reaction mixture.

According to the fluoridation study in Chapter 3, the reaction proceeded at room temperature for 30 minutes, and was then quenched with 5% NH<sub>4</sub>OH in 50% aqueous EtOH prior to the HPLC injection. The radio-HPLC trace shown in Figure 6.5 suggested a radiochemical yield of 34% over a 37 minute reaction. The <sup>18</sup>F-labeling reaction for alkynyl-<sup>18</sup>F-ArBF<sub>3</sub> **6.2** was repeated under the same conditions many times, and similar results were obtained.

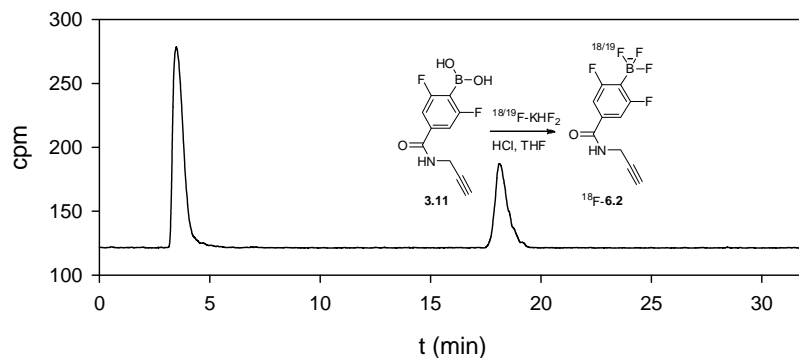


**Figure 6.5** A radio-HPLC chromatogram of the <sup>18</sup>F-fluoridation of alkynylarylboronic acid **3.11**. Reaction conditions: 15.4 mM of alkynylarylboronic acid **3.11**, 0.97 M of HCl<sup>a</sup>, <sup>18</sup>F-fluoride containing 76.9 mM of <sup>19</sup>F-fluoride (in the form of KHF<sub>2</sub>) in 6.5 μL of 4:2.5 THF:H<sub>2</sub>O was incubated at rt for 37 min. The reaction was then quenched with 5% NH<sub>4</sub>OH in 50% aq EtOH. The radioactivity at the beginning of the synthesis (BOS): 6.05 mCi. The RCY was 34% based on the radio-HPLC. The HPLC was carried out via HPLC Program 7 with Column I in HPLC System IV.

### 6.2.3 Click reactions between 5'-N<sub>3</sub>-<sup>31/32</sup>P-ONs and alkynes

Following the PAGE purification, 5'-N<sub>3</sub>-<sup>31/32</sup>P-ON1 (Band C of Lane 2 in Figure 6.3) and 5'-N<sub>3</sub>-<sup>31/32</sup>P-ON2 (Band C of Lane 3 in Figure 6.3) were coupled to specified alkynes via the copper(I) catalyzed click reaction. Based on literature reports,<sup>345, 346</sup> Cu(II)-TBTA/sodium ascorbate was used as the catalyst, which has been reported to be compatible with oligonucleotides. As shown in Figure 6.6, the 5'-N<sub>3</sub>-<sup>31/32</sup>P-ONs were stable in the presence of Cu(II)-TBTA/sodium ascorbate (data shown in Lanes 2 and 8) while the click reactions between 5'-N<sub>3</sub>-<sup>31/32</sup>P-ONs and alkynes produced new products with different mobilities as visualized by PAGE-autoradiography. The reaction between the highly hydrophobic alkynylcoumarin **6.4** and 5'-N<sub>3</sub>-<sup>31/32</sup>P-ONs gave fluorescent products (Lanes 3 and 9) with the slowest mobility during electrophoresis, while the reaction with the negatively charged alkynylArBF<sub>3</sub> **6.2** (Lanes 4, 5, 10 and 11) yielded

<sup>a</sup> The concentration of HCl in the reaction was not corrected for the consumption by neutralizing carbonate eluted from the anion exchange column over the <sup>18</sup>F-releasing process.

products migrating the fastest among products of the click reactions with the 5'-N<sub>3</sub>-<sup>31/32</sup>P-ONs. The click reactions between the oligonucleotides and alkyne **6.5**, which was prepared as the reference compound for any deboronated product in order to provide an electrophoretic reference of an oligonucleotide conjugated with a hypothetically deboronated product, gave products that exhibit intermediate electrophoretic mobility through the gel (Lanes 6 and 12). AlkynylArBF<sub>3</sub> **6.2** prepared at different times was tested as a substrate in the click reaction. The click reactions with one stock solution of alkynylArBF<sub>3</sub> **6.2** (Lanes 4 and 10), which had been stored at -20 °C for a long time, gave the same oligonucleotide products as the reactions with freshly prepared **6.2** (Lanes 5 and 11), since all the newly produced oligonucleotides had the same mobility (Lanes 4 v.s. 5 for 5'-N<sub>3</sub>-<sup>31/32</sup>P-ON1 and Lanes 10 v.s. 11 for 5'-N<sub>3</sub>-<sup>31/32</sup>P-ON2). The 5'-N<sub>3</sub>-<sup>31/32</sup>P-ONs ran the fastest in the polyacrylamide gel (Lanes 1 and 7). Although the relative mobility of the oligonucleotide products suggested the copper(I) catalyzed click reactions occurred successfully, further characterization via MALDI-TOF mass spectrometry provided no useful information for the oligonucleotide products, and this was primarily due to the low amount of oligonucleotides in the presence of high content of salts following the elution.

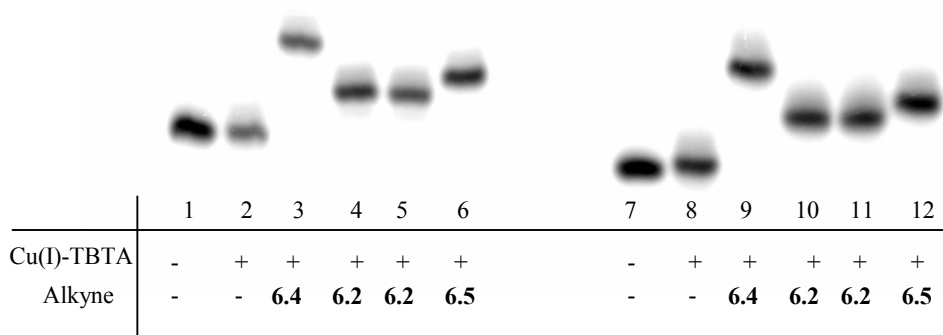


**Figure 6.6** The autoradiographic gel image of the click reactions between the gel-purified 5'-N<sub>3</sub>-<sup>31/32</sup>P-ONs and alkynes.

Lanes 1 to 6 are the click reactions with 5'-N<sub>3</sub>-<sup>31/32</sup>P-ON1, while Lanes 7 to 12 are those with 5'-N<sub>3</sub>-<sup>31/32</sup>P-ON2. The click reaction was carried out in the presence of Cu(II)-TBTA (12.5 mM) and sodium ascorbate (50 mM) in a reaction volume of 4 μL at rt for 1 hr. Lanes 1 and 7: control (the oligonucleotide); Lanes 2 and 8: background reaction (without alkyne added); Lanes 3 and 9: the click reaction with alkynylcoumarin **6.4** (7.5 mM); Lanes 4 and 10: the click reaction with alkynylArBF<sub>3</sub> **6.2** (DMSO solution stored in the freezer for more than half a year, concentration not determined, > 1 mM); Lanes 5 and 11: the click reaction with the freshly prepared alkynylArBF<sub>3</sub> **6.2** in DMSO (concentration not determined, > 1 mM); Lanes 6 and 12: click reaction with 3,6-difluorbo-*N*-(prop-2-yn-1-yl)benzamide **6.5** (7.5 mM). Oligonucleotides were resolved in 20% PAGE.

The results of the initial experiment for the click reactions with the gel-purified 5'-N<sub>3</sub>-<sup>31/32</sup>P-ONs, shown in Figure 6.6, encouraged us to further optimize the reaction at room temperature. The concentration of 5'-N<sub>3</sub>-<sup>31/32</sup>P-ON2 was then determined radiometrically via a calibration curve<sup>a</sup> generated with  $\gamma$ -<sup>32</sup>P-ATP from the same source. The first variable that was tested is the concentration of the copper(I)-TBTA catalyst. Several concentrations of the Cu(II)-TBTA solution ranging from 0.25 mM to 12.5 mM were tested in the click reaction between 5'-N<sub>3</sub>-<sup>31/32</sup>P-ON2 and alkynylArBF<sub>3</sub> **6.2** in the presence of a large amount of sodium ascorbate (50 mM) to ensure complete reduction of Cu(II) to Cu(I). The autoradiographic gel image indicated in Figure 6.7A suggested that the concentration of the copper(II)-TBTA complex is important for this reaction. The reaction was slow in the presence of low concentrations of the copper complex as shown in Lanes 5 and 6. Even for the reaction corresponding to Lane 6 where the concentration of Cu(II)-TBTA was 0.25 mM, which was still far higher than that of 5'-N<sub>3</sub>-<sup>31/32</sup>P-ON2 (0.0128 mM), the reaction seemed to proceed to ~ 13% after a 30 minute incubation at room temperature. In contrast, the reaction was more efficient at a higher concentration of Cu(II)-TBTA, and no side reaction was observed with a higher catalyst loading.

To carry out a one-pot two-step synthesis to label an oligonucleotide with an ArBF<sub>3</sub>, the labeling reaction that gives the <sup>18</sup>F-labeled ArBF<sub>3</sub> needs to be neutralized prior to the addition of the 5'-N<sub>3</sub>-<sup>31/32</sup>P-ONs and the catalyst. As a result, concentrations of reagents in the click reaction, including that of the oligonucleotide, will be reduced through dilution. Since the high concentration of catalyst did not appear to promote any other side reactions, 50 nmol of Cu(II)-TBTA was used. Correspondingly, the dilution effect and the influence of the quench buffer used for the work-up of the ArBF<sub>3</sub> labeling reaction were tested. The result, shown in Figure 6.7B, implies that the catalyst efficiency was not compromised by dilution. It also suggests that the reaction has high tolerance to pH changes, and the change in the solvent content as only low amounts of 5'-N<sub>3</sub>-<sup>31/32</sup>P-ON2 remained unreacted (Lanes 4 and 5).

---

<sup>a</sup> Ideally, the concentration can be determined from the radioactivity of the <sup>32</sup>P-labeled sample and also the known specific activity based on the carrier (ATP) added to  $\gamma$ -<sup>32</sup>P-ATP. However, only a contamination Geiger counter and a survey meter are available in the lab. Autoradiography was used to build up the radioactivity calibration curve for the concentration determination.

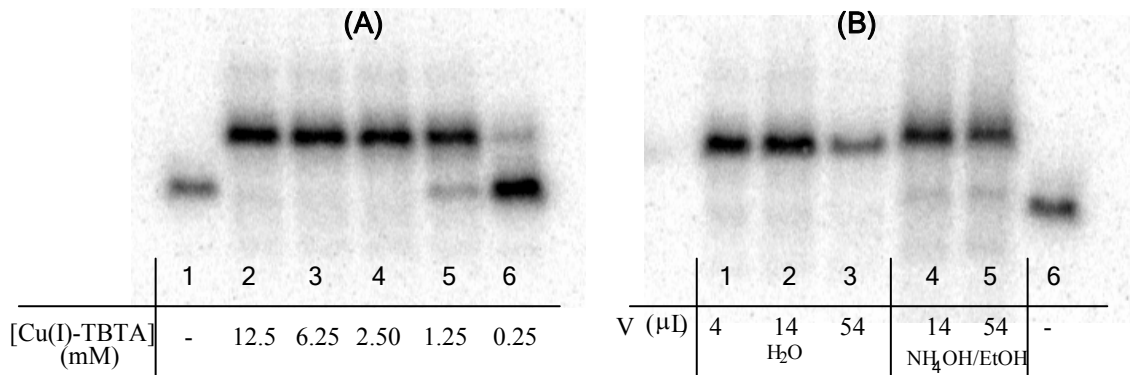


**Figure 6.7** The study of the concentrations of Cu(II)-TBTA for the click reaction between 5'-N<sub>3</sub>-<sup>31/32</sup>P-ON2 and alkyneArBF<sub>3</sub> 6.2.

(A) Test of different concentrations of Cu(II)-TBTA in the click reaction. Lane 1: control. Lanes 2 to 6: the click reaction (reaction volume: 4 μL) with 5'-N<sub>3</sub>-<sup>31/32</sup>P-ON2 (0.0128 mM) in the presence of sodium ascorbate (50 mM) and alkyneArBF<sub>3</sub> 6.2 (concentration not determined, but > 1 mM, the same amount for each reaction) with different concentrations of Cu(II)-TBTA solution at rt for 30 min. Lane 2: 12.5 mM of Cu(II)-TBTA; Lane 3: 6.25 mM of Cu(II)-TBTA; Lane 4: 2.50 mM of Cu(II)-TBTA; Lane 5: 1.25 mM of Cu(II)-TBTA (84% conversion); Lane 6: 0.25 mM of Cu(II)-TBTA (13% conversion). (B) The dilution effect on the click reaction. Lanes 1 to 5: 5'-N<sub>3</sub>-<sup>31/32</sup>P-ON2 (51.3 pmol), Cu(II)-TBTA (50 nmol), sodium ascorbate (200 nmol), rt, 38 min in different reaction volumes. Lane 1: 4 μL; Lane 2: 14 μL; Lane 3: 54 μL; Lane 4: 14 μL of 3.6% NH<sub>4</sub>OH in 68% aqueous EtOH; Lane 5: 54 μL of 4.6% NH<sub>4</sub>OH in 88% aqueous EtOH; Lane 6: control. Oligonucleotides were resolved in 20% PAGE.

Copper(I) is the actual catalyst in click reactions, and *in situ* generation of copper(I) from the reduction of copper(II) has been frequently employed with very high efficiency.<sup>272, 277</sup> Despite many reductants available for this purpose, sodium ascorbate is most commonly used on account of its availability, low cost, and high efficiency.<sup>294, 295</sup> Hence, we decided to use sodium ascorbate to generate copper(I). The concentration of sodium ascorbate is likely to be critical because sufficient reducing power is required to reduce copper(II) and to regenerate copper(I), which might be oxidized by dissolved oxygen. We then decided to keep the concentration of sodium ascorbate in the reaction at 50 mM, which is four-fold that of Cu(II)-TBTA used in a 4 μL reaction.

Using Cu(II)-TBTA (12.5 mM)/sodium ascorbate (50 mM) in a reaction of 4 μL, we studied the kinetic process of the reaction to get a better idea about the optimal reaction time. As indicated in Figure 6.8A, for 5'-N<sub>3</sub>-<sup>31/32</sup>P-ON2, the click reaction seemed to be complete within 5 minutes. This rapid conversion is very encouraging. On the other hand, the click reaction was initially considered to be quenched upon the addition of 3% LiClO<sub>4</sub>/acetone that is used to precipitate oligonucleotides while retaining the

Cu(I)-TBTA complex in solution. Nevertheless, the precipitation of oligonucleotides from LiClO<sub>4</sub>/acetone might have also promoted the reaction between the azido-species and the alkyne in the presence of copper(I) during the 15 minutes of centrifugation. To exclude this possibility, a similar kinetic study was carried out on 5'-N<sub>3</sub>-<sup>31/32</sup>P-ON2, and at various certain time points, the reaction was first quenched by aqueous EDTA (0.1 M, pH 8.4) before LiClO<sub>4</sub>/acetone precipitation to fully inhibit the catalytic activity of copper for the click reaction. A similar result shown in Figure 6.8B was obtained and thus excluded the aforementioned possibility, and it is therefore concluded that the reaction is very rapid, especially with a relatively high concentration of the catalyst and the alkyne species over the 5'-N<sub>3</sub>-<sup>31/32</sup>P-ONs. To guarantee a full conversion, we decided to incubate the click reaction between alkynyl-<sup>18</sup>F-ArBF<sub>3</sub> **6.2** and the 5'-N<sub>3</sub>-<sup>31/32</sup>P-ONs under similar conditions for 30 minutes.

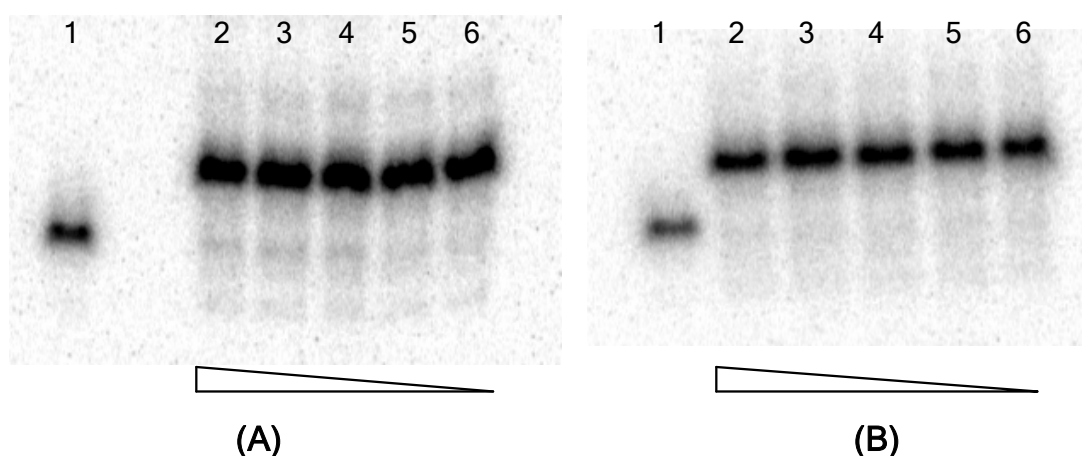


**Figure 6.8 The kinetics of the click reaction between 5'-N<sub>3</sub>-<sup>31/32</sup>P-ON2 and alkynylArBF<sub>3</sub> **6.2**.** (A): the kinetic study of the click reaction with 5'-N<sub>3</sub>-<sup>31/32</sup>P-ON2 and reactions were quenched by LiClO<sub>4</sub>/acetone; and (B): the kinetic study of the click reaction with 5'-N<sub>3</sub>-<sup>31/32</sup>P-ON2 and reactions were quenched with EDTA. The click reactions were undertaken in presence of Cu(II)-TBTA (12.5 mM), sodium ascorbate (50 mM), 5'-N<sub>3</sub>-<sup>31/32</sup>P-ON2 (0.0128 mM), and alkynylArBF<sub>3</sub> **6.2** (concentration not determined, > 1 mM) in a total volume of 4 μL and quenched at different time points. For (A) reactions directly quenched with 200 μL of 3% LiClO<sub>4</sub>/acetone: Lane 1, control; Lane 2, 65 min; Lane 3, 48 min; Lane 4, 35 min; Lane 5, 10 min; Lane 6, 5 min for (B) reactions first quenched with 1 μL of 0.1 M EDTA (pH 8.4) and then precipitated with 200 μL of 3% LiClO<sub>4</sub>/acetone: Lane 1, control; Lane 2, 27 min; Lane 3, 17 min; Lane 4, 10 min; Lane 5, 6 min; Lane 6, 2 min. Oligonucleotides were resolved in 20% PAGE.

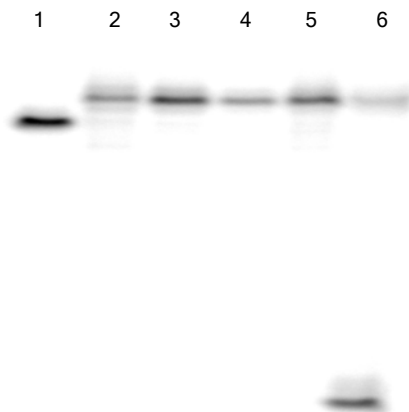


**Figure 6.9** The click reaction between 5'-N<sub>3</sub>-<sup>31/32</sup>P-ON1 and alkynylArBF<sub>3</sub> 6.2.

Lane 1, control (5'-N<sub>3</sub>-<sup>31/32</sup>P-ON1); each click reaction from Lanes 2 to 6 contains sodium ascorbate (200 nmol), Cu(II)-TBTA (50 nmol) and 5'-N<sub>3</sub>-<sup>31/32</sup>P-ON1 (concentration not determined) in different reaction volumes at rt for 56 min (35 min for Lanes 5 and 6), and the reactions were precipitated with 3% LiClO<sub>4</sub>/acetone (400 μL). Lane 2, in 33.5 μL of 4.4% NH<sub>4</sub>OH in EtOH; Lane 3, in 33.5 μL DEPC·H<sub>2</sub>O; Lane 4, in 103.5 μL of DEPC·H<sub>2</sub>O; Lane 5 and Lane 6, in 3.5 μL of DEPC·H<sub>2</sub>O; Lane 6, the click reaction after precipitation with 3% LiClO<sub>4</sub>/acetone was treated with 1.5 μL of RNase A at rt for 16 min. Oligonucleotides were resolved in 20% PAGE.

The results of the click reaction with the oligonucleotides above were obtained for reactions in small volumes (4 to 5 μL) in an aqueous DMSO/<sup>t</sup>BuOH cosolvent. Although the <sup>18</sup>F-labeling reaction for alkynyl-<sup>18</sup>F-ArBF<sub>3</sub> 6.2 would be quenched with a relatively higher volume of 5% NH<sub>4</sub>OH in 50% aqueous EtOH, the larger volume resulting thereof had minimum effects on the yield of the click reaction with 5'-N<sub>3</sub>-<sup>31/32</sup>P-ON2, as shown in Figure 6.7B. Even though the click reaction with 5'-N<sub>3</sub>-<sup>31/32</sup>P-ON2 did not appear to be influenced by NH<sub>4</sub>OH in the quench solution, it is still unknown whether the less stable ribonucleic acid linkage can survive in the presence of NH<sub>4</sub>OH or if the function of all conceivable oligonucleotides might be affected negatively by such conditions. Given such concerns, the same click reaction was undertaken between 5'-N<sub>3</sub>-<sup>31/32</sup>P-ON1 and alkynylArBF<sub>3</sub> 6.2 in the NH<sub>4</sub>OH/EtOH aqueous solution. Furthermore, the derivatized oligonucleotide from 5'-N<sub>3</sub>-<sup>31/32</sup>P-ON1 via the click reaction was treated with RNase A to determine whether or not the derivatization of the 5'-terminus would retain the property of the oligonucleotide. A very similar result, as that for 5'-N<sub>3</sub>-<sup>31/32</sup>P-ON2 shown in Figure 6.7B, was obtained for 5'-N<sub>3</sub>-<sup>31/32</sup>P-ON1. As illustrated in Figure 6.9, the click reaction between 5'-N<sub>3</sub>-<sup>31/32</sup>P-ON1 and alkynylArBF<sub>3</sub> 6.2 was not significantly influenced by the dilution with either water or 5% NH<sub>4</sub>OH in EtOH. It seemed that as

long as the reaction contains enough catalyst (the concentration of the catalyst may not be a crucial factor), the click reaction can be very robust and efficient. Moreover, the RNase A reaction with the crude click reaction mixture seemed quite efficient in cleaving the phosphodiester bond at the ribonucleotide linkage, and approximately 80% cleavage of **ON1** was achieved by RNase A. This RNase A treatment demonstrated the intactness of the oligonucleotide during the click reaction.

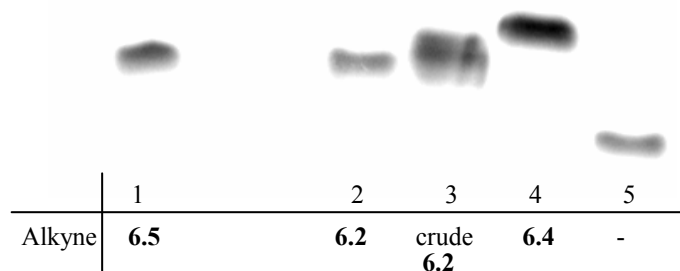


**Figure 6.10 The one-pot two-step reaction to label oligonucleotide 5'-N<sub>3</sub>-<sup>31/32</sup>P-ON1.**

Lanes 1 to 4, click reactions with 5'-N<sub>3</sub>-<sup>31/32</sup>P-ON1 (298.5 pmol for each reaction), sodium ascorbate (200 nmol), Cu(II)-TBTA (50 nmol), rt for 35 min. Lane 1, 3,5-difluoro-*N*-(prop-2-yn-1-yl)benzamide **6.5** (6 mM) in 5 μL of reaction volume; Lane 2, alkynylArBF<sub>3</sub> **6.2** (concentration not determined, > 1 mM) in 5 μL solution; Lane 3, the quenched fluoridation mixture (100 nmol of **3.11**, 200 nmol of KHF<sub>2</sub>, 3.78 μmol of HCl in 5.3 μL of 75% aqueous THF, rt, 37 min) in 20 μL of 5% NH<sub>4</sub>OH in EtOH; Lane 4, alkynylcoumarin **6.4** (6 mM) in 5 μL of reaction volume; Lane 5, control (5'-N<sub>3</sub>-<sup>31/32</sup>P-ON1). Oligonucleotides were resolved in 20% PAGE.

So far, several important factors for the click reaction between 5'-N<sub>3</sub>-<sup>31/32</sup>P-ONs and alkynylArBF<sub>3</sub> **6.2** have been investigated. Although the temperature, which is a key element for reactions, was not studied, it is believed that elevated temperatures may cause background competition of the non-copper catalyzed Huisgen reaction to give regioisomers. Given that at room temperature the click reaction was rapid, no further optimization with regard to temperatures was undertaken. On the other hand, for the transition from cold conditions to hot conditions, it is important to carry out the experiment under nonradioactive conditions in exactly the same fashion as would be followed for a radiosynthesis. Therefore, the one-pot two-step reaction was carried out starting from <sup>19</sup>F-fluoride and alkynylarylboronic acid **3.11**. Briefly, a fluoridation reaction mimicking the <sup>18</sup>F-fluoridation of **3.11** was first quenched with 5% NH<sub>4</sub>OH in EtOH, to which was added with 5'-N<sub>3</sub>-<sup>31/32</sup>P-ON1 and Cu(II)-TBTA/sodium ascorbate to initiate the click reaction as shown in Lane 3 of Figure 6.10. The reaction seemed to give a single labeled oligonucleotide species. Lanes 1, 2 and 4 are the reference reactions with

alkyne **6.5**, alkynylArBF<sub>3</sub> **6.2** and/or alkynylcoumarin **6.4**.

#### 6.2.4 The <sup>18</sup>F-labeling of oligonucleotides via click chemistry

The <sup>18</sup>F-fluoridation reaction to produce alkynyl-<sup>18</sup>F-ArBF<sub>3</sub> **6.2** was undertaken at room temperature for 37 minutes, whereupon the reaction was quenched with 5% NH<sub>4</sub>OH in 50% aqueous EtOH, as shown in Figure 6.5 in section 6.2.2. Without purifying alkynyl-<sup>18</sup>F-ArBF<sub>3</sub> **6.2** from the crude reaction, 10 μL of the quenched reaction mixture, representing one third of the total reaction, was directly added to 5'-N<sub>3</sub>-<sup>31/32</sup>P-**ON1**, followed by the addition of sodium ascorbate and Cu(II)-TBTA. Meanwhile, the click reaction between 5'-N<sub>3</sub>-<sup>31/32</sup>P-**ON1** and alkynylcoumarin **6.4** or alkyne **6.5** was also carried out at the same time to offer both electrophoretic standards and a <sup>32</sup>P-reference signal<sup>a</sup> for the ultimate visualization of the resolved polyacrylamide gel by phosphorimager autoradiography following PAGE. All click reactions were incubated at room temperature for 40 minutes. Moreover, for each click reaction, there was also a subsequent RNase A treatment for 8 minutes, for the purpose of detecting the integrity of the ribonucleotide (rC) in the middle of **ON1** after the copper catalyzed click reaction under radioactive conditions. Before being loaded on the 10% polyacrylamide gel<sup>b</sup> for electrophoresis, the oligonucleotides were precipitated with 3% LiClO<sub>4</sub> in acetone to remove the non-oligonucleotide species and most of the salts. The results were shown in Figure 6.11. Briefly, only a single band appeared for each reaction, while unfortunately there was no significant difference among bands regarding the oligonucleotide mobility. For the reactions between 5'-N<sub>3</sub>-<sup>31/32</sup>P-**ON1** and alkynyl-<sup>18</sup>F-ArBF<sub>3</sub> **6.2**, the radioactivity of the bands in Lanes 4 and 7 in Figure 6.11A appeared exalted in autoradiographic analysis 17 minutes after the gel electrophoresis, compared with other lanes. Although an equal amount of 5'-N<sub>3</sub>-<sup>31/32</sup>P-**ON1** was subjected to each click reaction, a dramatic difference of the radioactive signals registered on the phosphorimager screen, which implies that the radioactivity observed in Lanes 4 and 7 of Figure 6.11A must originate predominantly from incorporated <sup>18</sup>F-fluoride in the form of <sup>18</sup>F-ArBF<sub>3</sub>. Following storage for defined periods of time, the radioactivity due to the decay of <sup>18</sup>F-fluoride

<sup>a</sup> This <sup>32</sup>P-reference signal is based on the decay half-life of <sup>32</sup>P (14.3 days), which is much longer than that of <sup>18</sup>F-fluoride (109.8 min).

<sup>b</sup> 10% gel (20 × 20 cm) was used to minimize the gel resolution time.

decreased as shown in Figure 6.11B to D. However, it must be noticed that at later time points such as that for Figure 6.11D, the difference of the radioactivity registering on the phosphorimager screen for each band became negligible, consistent with the fact that the same amount of  $^{32}\text{P}$ -labeled oligonucleotide was present in each sample. The relative change of the radioactivity among bands, in spite of the poor resolution, suggested the introduction of  $^{18}\text{F}\text{-ArBF}_3$  into  $5'\text{-}^{31/32}\text{P}\text{-ON1}$  via the copper(I) catalyzed click reaction succeeded.

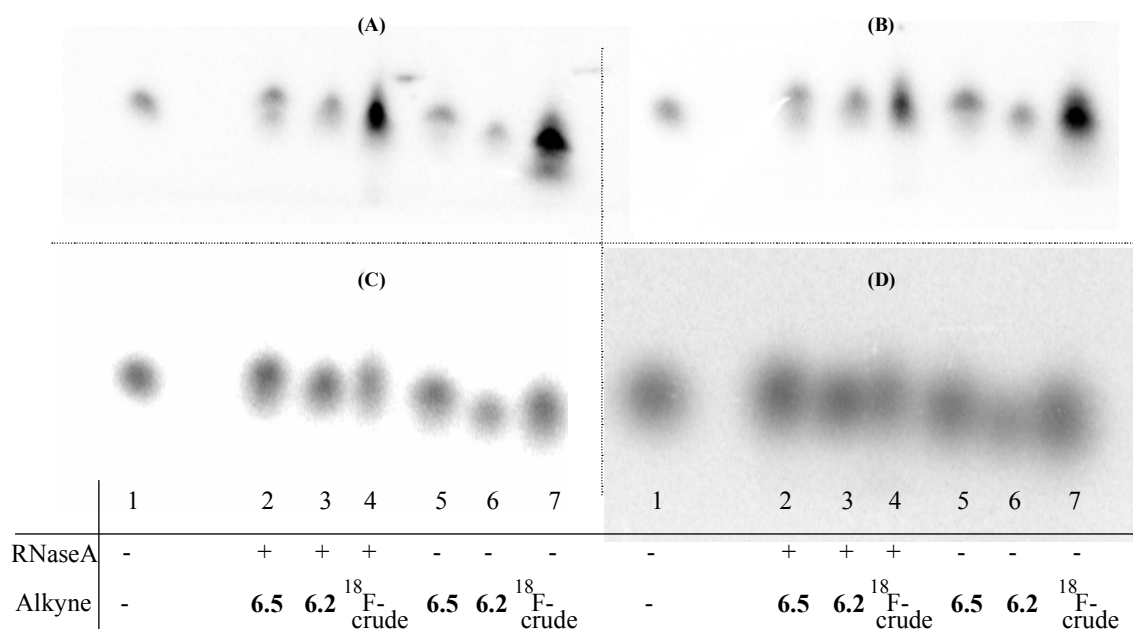


**Figure 6.11** The autoradiographic gel images of the click reactions between alkynes and  $5'\text{-N}_3\text{-}^{31/32}\text{P}\text{-ON1}$ .

The phosphorimager screen was exposed to the gel at different time points after the gel was resolved over electrophoresis (10% PAGE). (The contrast of the image was adjusted by ImageQuant 5.2.) (A) 11 min of exposure, at 17 min after the completion of the gel electrophoresis; (B) 12 min of exposure, at 194 min after the completion of the electrophoresis; (C) 5 min of exposure, at 1054 min after the completion of the electrophoresis; (D) 18 min of exposure, 3 days and 18 hours after the completion of the electrophoresis. Between exposures, the gel was stored in the fridge ( $\sim 4\text{ }^\circ\text{C}$ ) in the phosphorimager screen case. Lane 1, control ( $5'\text{-N}_3\text{-}^{31/32}\text{P}\text{-ON1}$ ) (298.5 pmol); all the other lanes refer to the click reactions as  $5'\text{-N}_3\text{-}^{31/32}\text{P}\text{-ON1}$  (60  $\mu\text{M}$ ), alkyne, sodium ascorbate (200 nmol) and Cu(II)-TBTA (50 nmol), rt, 40 min, then  $\text{LiClO}_4$ /acetone treatment. Lanes 2 and 5: alkyne **6.5** (6 mM). Lanes 3 and 6, alkynyl $\text{ArBF}_3$  **6.2** (concentration unknown, but  $> 1\text{ mM}$ ). Lanes 4 and 7, 10  $\mu\text{L}$  of the quenched  $^{18}\text{F}$ -labeling reaction indicated in Figure 6.5. For Lanes 2 to 4, the precipitated oligonucleotide from  $\text{LiClO}_4$ /acetone was further treated with RNase A (1.5  $\mu\text{L}$ ) for 8 min.

Disappointingly it seemed that the RNase A treatment was unsuccessful since no second/lower band was produced thereafter. We regarded that the negative result from the RNase A treatment in Figure 6.11 could be either due to the lack of RNase A activity under such conditions, or because of that the cleaved oligonucleotide fragments, one of which is an 8mer with 5'-<sup>18</sup>F/<sup>32</sup>P-labeled, was not resolved in a 10% polyacrylamide gel during the electrophoresis. Moreover, from the autoradiographic gel image, nearly no mobility difference of the oligonucleotides was observed. It is not clear whether that was due to the inefficient resolution among the similar sized oligonucleotides in a 10% polyacrylamide gel of smaller size used in the experiment shown in Figure 6.11.

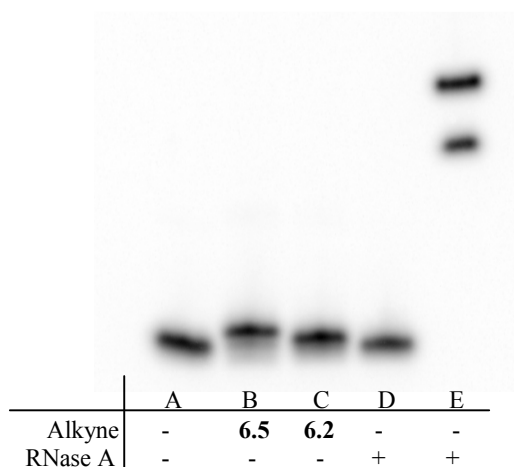


**Figure 6.12 The resolution of various oligonucleotides in 10% polyacrylamide gel.**

Lane A: control (5'-N<sub>3</sub>-<sup>31/32</sup>P-ON1), Lanes B and C: the click reaction of alkynes with 5'-N<sub>3</sub>-<sup>31/32</sup>P-ON1 (37.3 μM), alkyne, sodium ascorbate (50 mM), and Cu(II)-TBTA (12.5 mM). Lanes D and E: 5'-N<sub>3</sub>-<sup>31/32</sup>P-ON1 (149 pmol in 1 μL) treated with RNase A (1.5 μL) for 16 min. Lane B: alkyne **6.5** (7.5 mM); Lane C: alkynylArBF<sub>3</sub> **6.2** (concentration not determined, > 1 mM). All the oligonucleotide reactions were treated with LiClO<sub>4</sub>/acetone precipitation before being loaded to the gel. Lane E demonstrates that the oligonucleotide treated with RNase A was loaded after the other oligonucleotide samples (Lanes A to D) were resolved on the gel for a certain period of time (while the second indicating dye (xylene cyanol) ran through half of the gel).

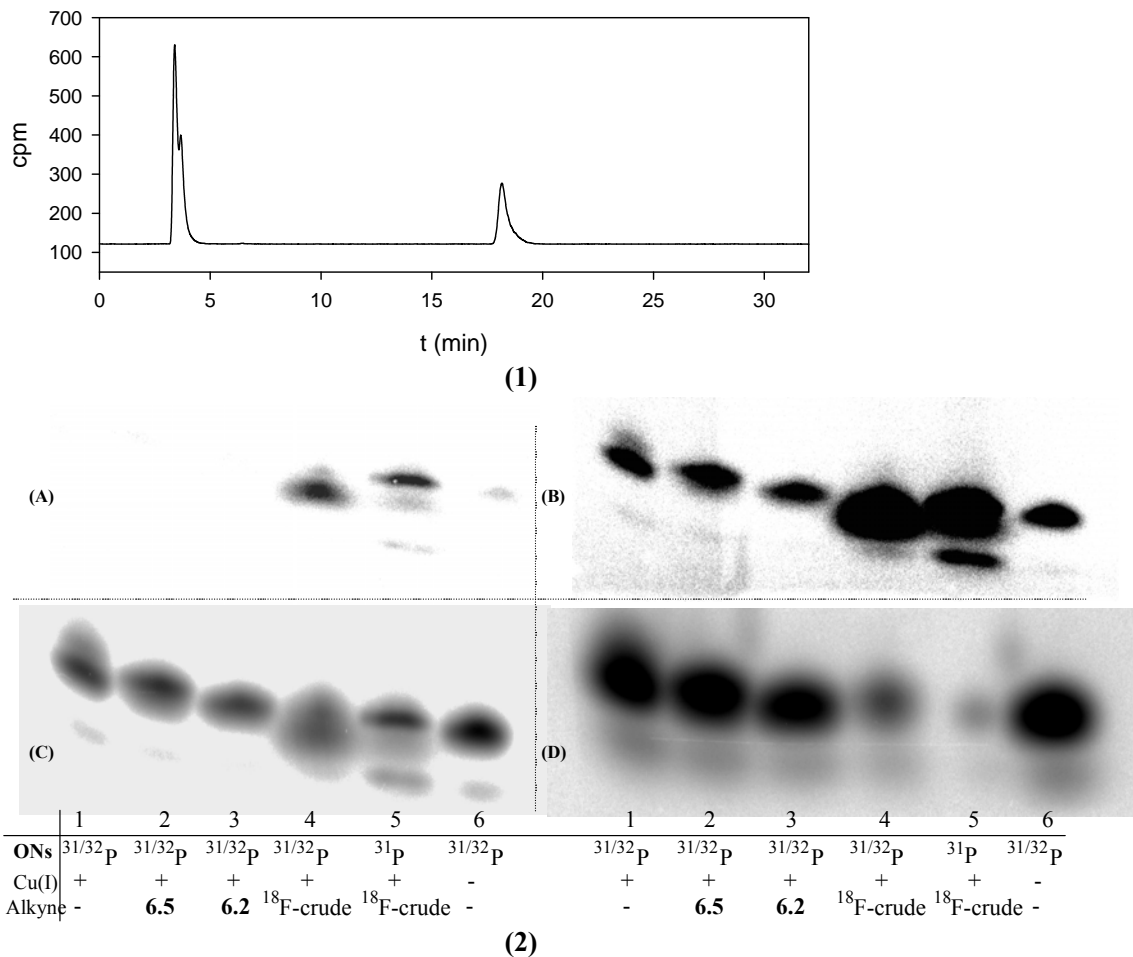


**Figure 6.13** The radio-HPLC chromatogram of the preparation of alkynyl-<sup>18</sup>F-ArBF<sub>3</sub> **6.2** and the autoradiographic gel images of click reactions with 5'-N<sub>3</sub>-<sup>31/32</sup>P-ON1.

(1): The HPLC chromatogram of the <sup>18</sup>F-fluoridation of alkynylarylboronic acid **3.11**. The reaction final concentrations: 15.4 mM of alkynylarylboronic acid **3.11**, 0.97 M of HCl, 76.9 mM of <sup>19</sup>F-fluoride in the form of KHF<sub>2</sub> in 6.5 μL of 4:2.5 THF:H<sub>2</sub>O. The reaction was incubated at rt for 35 min before being quenched with 5% NH<sub>4</sub>OH in 50% aq. EtOH. The radioactivity at the BOS: 6.26 mCi. The RCY was 29%. The HPLC was performed via Program 7 with Column I in HPLC System IV. (2): The phosphorimager screen was exposed to the gel at different periods of time after the 10% polyacrylamide gel was resolved over electrophoresis. (A) 10 min of exposure, at 20 min after the completion of gel electrophoresis; (B) 42 min of exposure, at 100 min after the completion of electrophoresis; (C) 17.5 hours of exposure, at 154 min after the completion of electrophoresis; (D) 3 days and 22 hr of exposure, 20 hours after the completion of electrophoresis. Between exposures, the gel was stored in the fridge (~ 4 °C) in the phosphorimager screen case. Lane 6, the control, 5'-N<sub>3</sub>-<sup>31/32</sup>P-ON1; all the other lanes refer to the click reactions with 5'-N<sub>3</sub>-<sup>31/32</sup>P-ON1 (149 pmol) or as noted, alkyne, sodium ascorbate (200 nmol), and Cu(II)-TBTA (50 nmol), at rt for 30 min, then LiClO<sub>4</sub> treatment before being loaded to the 10% polyacrylamide gel for electrophoresis. Lane 1, background reaction (without alkyne added), in 3 μL H<sub>2</sub>O:<sup>1</sup>BuOH (2:1); Lane 2, alkyne **6.5** (7.5 mM); Lane 3, alkynylArBF<sub>3</sub> **6.2** (concentration unknown, but > 1 mM); Lane 4, 10 μL of the quenched <sup>18</sup>F-labeling reaction, 1.17 mCi at the start of the click reaction; Lane 5, 10 μL of the quenched <sup>18</sup>F-labeling reaction, 5'-N<sub>3</sub>-<sup>31</sup>P-ON1 (1.49 nmol), 1.12 mCi at the start of the click reaction.

To clarify these puzzling problems raised in the radiolabeling experiment shown in Figure 6.11, an experiment was carried out under non-<sup>18</sup>F conditions to check the

mobility of the oligonucleotides in a 10% denaturing polyacrylamide gel (20 cm × 20 cm). 5'-N<sub>3</sub>-<sup>31/32</sup>P-**ON1** reacted with various alkynes as described previously under the click conditions. And 5'-N<sub>3</sub>-<sup>31/32</sup>P-**ON1** was directly treated with RNase A for reactions loaded in Lanes D and E. There was a time gap between the gel resolution of Lanes D and E, in which the reaction represented by Lane E was loaded to the polyacrylamide gel after that loaded to Lane D had been resolved in the PAGE for a certain time. The results are shown in Figure 6.12. For the RNase A treated sample loaded in Lane E, there are two bands of the 5'-<sup>32</sup>P-labeled oligonucleotides (the substrate or product of the RNase A reaction), which suggested RNase A partially cleaved **ON1**. However, only one of the two bands showed up in Lane D. Since the operation of the gel electrophoresis was guided by the visualization of the migration of bromophenol blue, an indicating dye, the smaller oligonucleotide produced by RNase A cleavage in Lane D must have migrated off the gel and therefore was not detected by the phosphorimager screen. On the other hand, even with a cleaner appearance of the gel image, the difference in the electrophoretic mobility of these derivatized oligonucleotides over the 10% polyacrylamide gel was small (Lanes A to D), compared with the gel images shown previously over 20% polyacrylamide gels such as in Figure 6.6.

To further verify the <sup>18</sup>F-incorporation in the oligonucleotide via the one-pot two-step coupling method, nonradioactive 5'-N<sub>3</sub>-<sup>31</sup>P-**ON1** was prepared via the same protocol,<sup>341</sup> and was tested for the <sup>18</sup>F-incorporation. In this test, the preparation of alkynyl-<sup>18</sup>F-ArBF<sub>3</sub> **6.2** was carried out under similar radiofluoridation conditions and the radio-HPLC analysis of this <sup>18</sup>F-fluoridation is shown in Figure 6.13. After the reaction was quenched with 30 μL of 5% NH<sub>4</sub>OH in 50% aqueous EtOH, 1/3 of the quenched reaction was used for the click reaction with 5'-N<sub>3</sub>-<sup>31/32</sup>P-**ON1** or 5'-N<sub>3</sub>-<sup>31</sup>P-**ON1**. At the same time, the click reaction of 5'-N<sub>3</sub>-<sup>31/32</sup>P-**ON1** was also carried out with alkyne **6.5** and alkynylArBF<sub>3</sub> **6.2**. After the reaction products were precipitated with 3% LiClO<sub>4</sub>/acetone, the oligonucleotides were resolved in 10% PAGE. As shown in the autoradiographic image (A) of Figure 6.13, the phosphorimager screen was exposed to the radioactive gel for a short time (10 min) following the completion of gel resolution. Only Lanes 4 and 5, both of which were from the <sup>18</sup>F-labeling experiments, exhibited strong radioactive signals that were registered to the phosphorimager screen. As with the

previous  $^{18}\text{F}$ -labeling experiments shown in Figure 6.11, with longer exposure time, the relatively lower radioactivity of  $^{31/32}\text{P}$  was found to be comparable to that of the  $^{18}\text{F}$ -signal as shown in images B and C of Figure 6.13. The relative intensity of the bands for  $^{18}\text{F}$ -derivatized oligonucleotides in Lanes 4 and 5 decreased due to the radioactive decay. As expected, after 20 hours (image D), there was virtually no signal in Lane 5, which was derived from the reaction between unlabeled  $5'\text{-N}_3\text{-}^{31}\text{P-ON1}$  and alkynyl- $^{18}\text{F-ArBF}_3$  **6.2**. In addition, the radioactive signal of the band in Lane 4, which still contained  $^{32}\text{P}$ -phosphorus, was much weaker than that of Lanes 1, 2, 3 and 6 after 4 days. This further suggests the strong autoradiographic density associated with Lanes 4 and 5 at the earlier time points (image A and B) were indeed primarily due to the successful incorporation of  $^{18}\text{F}$ -fluoride. Poor resolution of oligonucleotide on the PAGE gel was also observed in this experiment.

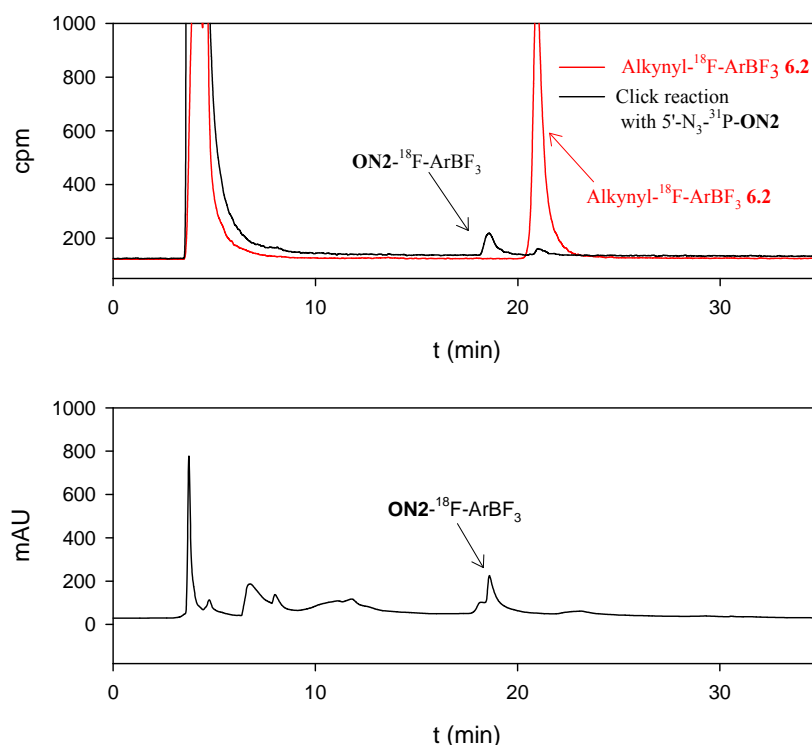


**Figure 6.14** The HPLC chromatograms of the crude click reaction with  $5'\text{-N}_3\text{-}^{31}\text{P-ON2}$ .

The top HPLC traces are the radio-HPLC traces for both the radiosynthesis of alkynyl- $^{18}\text{F-ArBF}_3$  **6.2** (red) and its click reaction with  $5'\text{-N}_3\text{-}^{31}\text{P-ON2}$  (black). The bottom trace is the HPLC at 260 nm for the click reaction between alkynyl- $^{18}\text{F-ArBF}_3$  **6.2** and  $5'\text{-N}_3\text{-}^{31}\text{P-ON2}$ . The radiosynthesis of alkynyl- $^{18}\text{F-ArBF}_3$  **6.2** (red): 15.4 mM of alkynylarylboronic acid **3.11**, 0.97 M of HCl, and 38.5 mM of KHF<sub>2</sub> in 61.5% aqueous CH<sub>3</sub>CN (6.5  $\mu\text{L}$ ) was incubated at rt for 0.5 hr (5.4 mCi at the BOS) and its RCY was 33%. The click reaction (black) with  $5'\text{-N}_3\text{-}^{31}\text{P-ON2}$ : 1/3 of the crude reaction for alkynyl- $^{18}\text{F-ArBF}_3$ , 2.627 nmol of  $5'\text{-N}_3\text{-}^{31}\text{P-ON2}$ , 33.3 mM sodium ascorbate, and 8.33 mM Cu(II)-TBTA in 30  $\mu\text{L}$  16.7% aqueous EtOH for 0.5 hr (1.9 mCi at the beginning of the click reaction). The HPLC was performed via HPLC Program 13 with Column I in HPLC System IV. The overall RCY was 1.67% (decay corrected).

The result of the dual isotope ( $^{32}\text{P}/^{18}\text{F}$ ) labeling experiments based on PAGE-autoradiographic analysis was very encouraging in qualitative terms, despite the poor resolution of the labeled oligonucleotides by PAGE. To further corroborate these encouraging results from the one-pot two-step method, a radio-HPLC analysis was developed.  $5' \text{-N}_3\text{-}^{31}\text{P}\text{-ON2}$  was prepared<sup>341</sup> and reacted with the crude fluoridation reaction for alkynyl- $^{18}\text{F}\text{-ArBF}_3$  **6.2** in the presence of Cu(II)-TBTA/sodium ascorbate. After 30 minutes, the reaction was quenched by the precipitation of the oligonucleotide from 3%  $\text{LiClO}_4$  in acetone to remove the unreacted alkynyl- $^{18}\text{F}\text{-ArBF}_3$  **6.2** and other undesired components. The oligonucleotide and other components co-precipitating were dissolved in water and injected into the C18 column (Column I) for HPLC. From the black HPLC traces shown in Figure 6.14, it was apparent that the click reaction succeeded to give the  $^{18}\text{F}\text{-ArBF}_3$  labeled oligonucleotide **ON2** (**ON2- $^{18}\text{F}\text{-ArBF}_3$** ) with a retention time of 18.4 minutes.

### 6.2.5 Specific activity

As mentioned in Chapter 1, specific activity is one of the key criteria for evaluating a radiosynthesis and also for determining *in vivo* image quality for radiotracers that are based on the receptor targeting. To refresh the reader, the specific activity is defined as the radioactivity per unit (gram or mole) of the radiolabeled compound at a given time, which means that accurate determination of the values for the radioactivity and amounts of the radiolabeled compound is important. Unfortunately, the  $\text{ArBF}_3$ s used herein are a family of compounds with poor chromophores of unknown  $\epsilon_{\text{max}}$ 's, which make it difficult to determine the concentration/amount of the radiolabeled products via UV-vis spectrometry methods. Furthermore, the bioprobes we tried to label in previous chapters also have poor UV properties. Although an indirect colorimetric method was used to determine the concentration of  $\text{MarArBF}_3$  **4.15** via the ferroin test for the inhibitory activity test, as described in Chapter 4, it was not used to determine the concentration of  $\text{Mar-}^{18}\text{F}\text{-ArBF}_3$  **4.15**. Whereas in Chapter 1 we hypothesized and mathematically derived a relationship whereby the specific activity of  $^{18}\text{F}\text{-ArBF}_3$ s must be triple that of free  $^{18}\text{F}\text{-fluoride}$ , there has been no direct experimental evidence to prove that this labeling method gives three times the specific activity of the  $^{18}\text{F}\text{-fluoride}$  used.

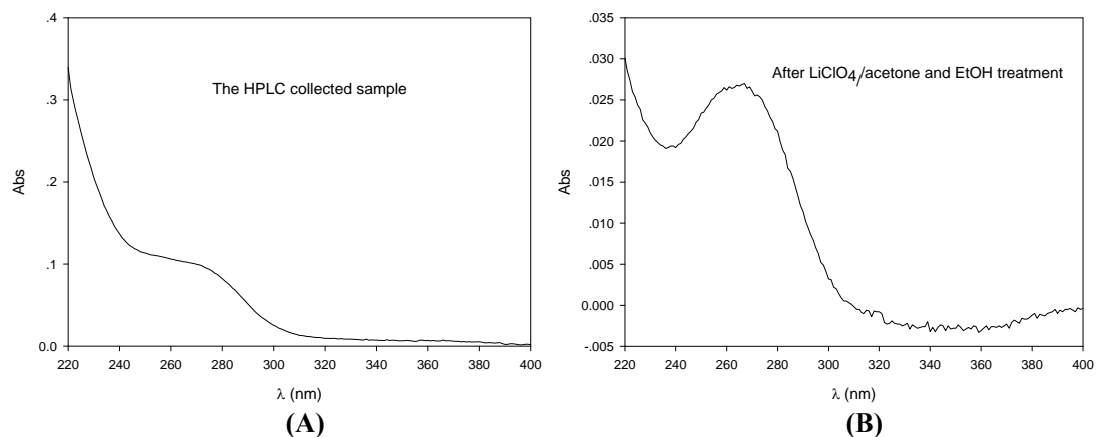


**Figure 6.15 The UV absorption spectra of the sample collected from the radio-HPLC.**

(A), The UV spectrum was for the HPLC collected sample (a total volume of 1.0755 mL collected, 16.8967  $\mu\text{Ci}^{\text{a}}$ ) without any dilution.  $A_{260\text{ nm}} = 0.1061$ ; (B), 1 mL of the HPLC collected sample after decaying for 5 days was concentrated down over vacuum, resuspended in 30  $\mu\text{L}$  of DEPC $\cdot\text{H}_2\text{O}$  and then precipitated with 1 mL of 3%  $\text{LiClO}_4/\text{acetone}$ . The precipitate was redissolved in 500  $\mu\text{L}$  of DEPC $\cdot\text{H}_2\text{O}$  and 300  $\mu\text{L}$  of the newly prepared solution was concentrated; the residue was redissolved in 30  $\mu\text{L}$  of DEPC $\cdot\text{H}_2\text{O}$  and precipitated with 1 mL of 3%  $\text{LiClO}_4/\text{acetone}$ ; the pellet was further washed with 1 mL EtOH, dried in the air for 15 min and then resuspended in 30  $\mu\text{L}$  of DEPC $\cdot\text{H}_2\text{O}$ ; 23  $\mu\text{L}$  of the fresh solution was added to 500  $\mu\text{L}$  of DEPC $\cdot\text{H}_2\text{O}$  for the UV absorption measurement,  $A_{260\text{ nm}} = 0.0262$ . The extinction coefficient (260 nm) for **ON2** is 128800  $\text{M}^{-1}\cdot\text{cm}^{-1}$ , which was provided by the Vendor based on the sum of the  $\epsilon_{\text{max}}$ 's of individual bases while the contribution of the  $\text{ArBF}_3$  was regarded to be negligible and which was directly regarded as the extinction coefficient (260 nm) of **ON2-ArBF<sub>3</sub>** or related<sup>b</sup>.

In contrast to the low UV absorption property of the  $\text{ArBF}_3\text{s}$  currently under study, oligonucleotides have excellent optical properties and can be detected at very low concentrations by using UV-vis spectrometry. Therefore, **ON2-<sup>18</sup>F-ArBF<sub>3</sub>** from the click reaction between 5'- $\text{N}_3$ -<sup>31</sup>P-**ON2** and alkynyl-<sup>18</sup>F- $\text{ArBF}_3$  **6.2** was manually collected following radio-HPLC shown in Figure 6.14. The radioactivity of the collected sample was measured and the sample was stored at 4 °C behind the shield for decay. Then the UV-absorbance of the sample was measured. Unfortunately, the acquired UV spectrum (for the HPLC collected sample) from 220 to 400 nm gave a very atypical profile as shown in Figure 6.15A, which implied that there might be interference from UV-absorbant contaminants in the HPLC solvents. The oligonucleotide solution was lyophilized, precipitated with 3%  $\text{LiClO}_4/\text{acetone}$  and ethanol, and re-dissolved in DEPC $\cdot\text{H}_2\text{O}^{\text{c}}$  before the UV-vis absorbance was re-measured. Both of the UV absorption profiles are shown in Figure 6.15. The specific activity at the time of recording the

<sup>a</sup> The radioactivity was 625178 Bq.

<sup>b</sup> It is possible that 5'-**ON2-ArBF<sub>3</sub>** would follow the  $\text{ArBF}_3$  hydrolysis to give 5'-**ON2-ArB(OH)<sub>2</sub>**, which might undergo deboronation to provide 5'-**ON2-Ar-H** or 5'-**ON2-Ar-OH**.

<sup>c</sup> DEPC $\cdot\text{H}_2\text{O}$  is  $\text{H}_2\text{O}$  treated with diethylpyrocarbonate over autoclaved conditions.

radioactivity was therefore calculated based on the concentration obtained from the UV spectrometry: 19.1 mCi/ $\mu$ mol for the HPLC collected sample and 67.9 mCi/ $\mu$ mol for the HPLC collected sample with precipitation, as summarized in Table 6.1. The specific activity of  $^{18}\text{F}$ -fluoride (10.8 mCi/ $\mu$ mol) was calculated based on the radioactivity (5.4 mCi) and the amount of carrier fluoride (500 nmol) at the beginning of the synthesis ( $t = 0$  min). It is then decay corrected to the time of recording the radioactivity of **ON2**- $^{18}\text{F}$ -ArBF<sub>3</sub> to be 4.5 mCi/ $\mu$ mol ( $t = 138$  min). When considering that three fluorine atoms are bound to one boron atom in one molecule of ArBF<sub>3</sub>, the corresponding specific activity of **ON2**- $^{18}\text{F}$ -ArBF<sub>3</sub> should be three fold that of free  $^{18}\text{F}$ -fluoride, and that is therefore calculated to be 13.6 mCi/ $\mu$ mol ( $t = 138$  min). While the UV-vis spectrum for the precipitated material is much more characteristic of a clean oligonucleotide, the overall amount of material remaining was lower clearly indicated loss following the precipitation. Unfortunately, because the sample had already decayed, there was no way to assess how much radioactivity was also lost due to the precipitation. If one assumes that no radioactivity was lost during the precipitation, then the specific activity of this sample is calculated to be much higher.

**Table 6.1 The calculation for the specific activity of **ON2**- $^{18}\text{F}$ -ArBF<sub>3</sub>.**

	t (min)	Radioactivity	$^{18}\text{F}$ -labeled material (nmol)	Specific activity
$^{18}\text{F}$ -Fluoride	0	5.4 mCi	500	10.8 mCi/ $\mu$ mol
	138	-	-	4.5 mCi/ $\mu$ mol <sup>i</sup>
<b>ON2</b> - $^{18}\text{F}$ -ArBF <sub>3</sub>	138	-	-	13.6 mCi/ $\mu$ mol <sup>ii</sup>
		16.9 $\mu$ Ci	0.886 <sup>iii</sup>	19.1 mCi/ $\mu$ mol
			0.249 <sup>iv</sup>	67.9 mCi/ $\mu$ mol

<sup>i</sup> The specific activity of  $^{18}\text{F}$ -fluoride at  $t = 138$  min was calculated from that of  $^{18}\text{F}$ -fluoride at  $t = 0$  min;

<sup>ii</sup> The specific activity of **ON2**- $^{18}\text{F}$ -ArBF<sub>3</sub> was calculated from that of  $^{18}\text{F}$ -fluoride;

<sup>iii</sup> The amount of **ON2**- $^{18}\text{F}$ -ArBF<sub>3</sub> collected from the HPLC was based on the UV absorption at 260 nm shown in Figure 6.15A;

<sup>iv</sup> The amount of **ON2**- $^{18}\text{F}$ -ArBF<sub>3</sub> collected from the HPLC was based on the UV absorption at 260 nm shown in Figure 6.15B.

## 6.3 Discussion

### 6.3.1 The derivatization of oligonucleotides

The direct conjugation of oligonucleotides with amines via Knorre's protocol has been reported with very high yields, especially for conjugation to organic amines.<sup>341, 342</sup> According to the protocol, although the activation of the phosphorylated oligonucleotides can be carried out under aqueous conditions, it is more efficient to activate the oligonucleotides in organic solvents. Since negatively charged oligonucleotides always have very poor solubility in organic solvents, even in DMSO, the phase transfer agent CTAB was used to form ion pairs between the oligonucleotides and CTA cations. The CTA salts of oligonucleotides, therefore, have good solubility in organic solvents wherein the activation reaction proceeds efficiently. To avoid the side reaction between azido-PEG-amine **6.1** and  $\text{PPh}_3$ , the activated oligonucleotides were precipitated by  $\text{LiClO}_4$  in acetone to remove CTA perchlorate and excess activating agents including  $\text{PPh}_3$ . The subsequent conjugation reaction with the amine occurred in the aqueous solution for one hour at room temperature. The gel purification was applied to purify the desired oligonucleotides  $5' \text{-N}_3\text{-}^{31/32}\text{P-ONs}$ .

Since the  $5' \text{-N}_3\text{-}^{31/32}\text{P-ONs}$  are derived from the  $5' \text{-}^{31/32}\text{P-ONs}$ , their electrophoretic mobility should be slower than that of the starting oligonucleotides as shown in the autoradiographic gel images (Figure 6.3). This can be interpreted in terms of increasing the mass-to-charge ratio, which is due to the increase of the mass and decrease of the negative charge. The electrophoretic mobility of oligonucleotides in a polyacrylamide gel is largely dependent on the oligonucleotide size. Since every phosphodiester bond represents a negative charge and the 5'-terminus of the 5'-phosphorylated oligonucleotide carries two more negative charges, any mass addition to the oligonucleotides due to the coupling at the 5'-terminus can reduce the mobility of the oligonucleotides. Therefore, the mobilities of bands A, B and C were all retarded due to the coupling reaction. Nevertheless, the autoradiographic gel image in Figure 6.3 also suggests that the reaction was accompanied by relatively significant side reactions, especially for  $5' \text{-}^{31/32}\text{P-ON1}$ . The only difference between  $5' \text{-}^{31/32}\text{P-ON1}$  and

$5'$ - $^{31/32}\text{P}$ -ON2 is that there is a ribonucleotide in the middle of the sequence of  $5'$ - $^{31/32}\text{P}$ -ON1. Therefore, the 2'-hydroxyl group most likely is involved in some reaction under the given conditions, particularly since it has been reported that the *S*-pyridylation with dipyridyldisulfide/ $\text{PPh}_3$  has been frequently used for oxygen substitution in carbohydrate chemistry.<sup>347-350</sup>

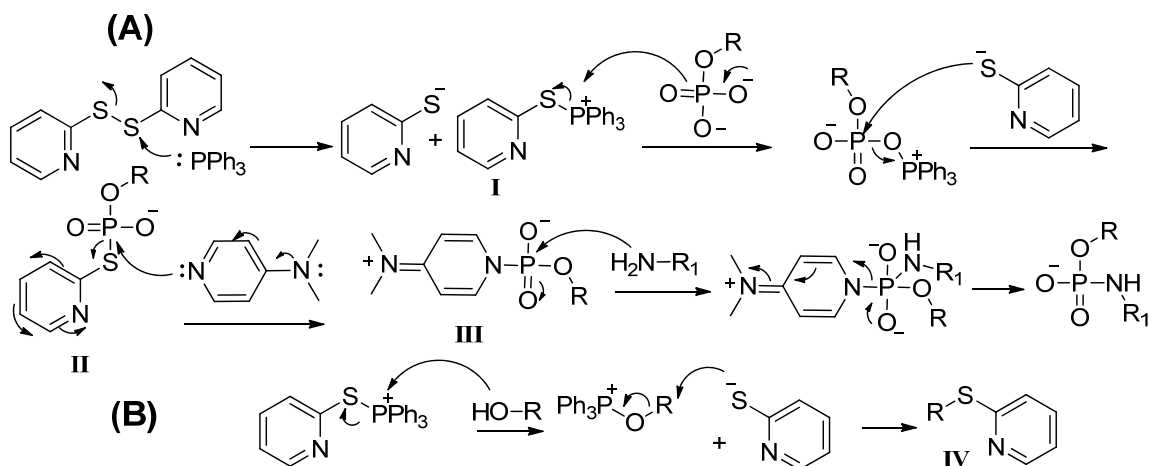


**Figure 6.16** The mechanism of the derivatization of oligonucleotides by Knorre's protocol.<sup>351</sup> (A) is the mechanism for phosphoramidate preparation via the activation of  $\text{PPh}_3$ ,  $(\text{PyS})_2$ , and DMAP. (B) is proposed for the activation of hydroxyl group under such conditions.

For the derivatization of the oligonucleotides, as indicated in Figure 6.16A, the phosphate activation starts via the production of the thiophosphonium **I** from  $(\text{PyS})_2$  and  $\text{PPh}_3$ . Intermediate **I** is nucleophilically attacked by the phosphate to give a phosphate phosphorus intermediate that is quickly attacked by the thiopyridine to give the thiophosphate intermediate **II**, which is quickly trapped by DMAP to afford the phosphoramidate active reagent **III**. After the removal of the activating agents and byproducts by  $\text{LiClO}_4/\text{acetone}$ , the active intermediate **III** is then subjected to the nucleophilic substitution by the amine acting as a nucleophile to give the desired phosphoramidate product. However, as shown in Figure 6.16B, for the case of  $5'$ - $^{31/32}\text{P}$ -ON1, the 2'-hydroxyl group of the ribonucleotide cytosine in the middle of the sequence can also be activated to form the oxophosphonium intermediate in the same fashion as with a Mitsunobu activation. And in this case, via a nucleophilic substitution, 2-pyridinylthioate generated *in situ* replaces the 2'-hydroxyl to give the 2'-*S*-pyridinyl-oligonucleotide **IV**, as well as triphenylphosphine oxide, a highly stable byproduct.<sup>351</sup> This 2'-*S*-pyridinyl-oligonucleotide **IV** might account for Band B shown in Lane 2 of

Figure 6.3, which displayed slightly slower electrophoretic mobility than the major product. An argument against this conclusion is that with the steric hindrance at the 2'-position in the middle of the oligonucleotide sequence, it could be imagined that the reaction rate would be slow and therefore only a very small amount of this product was produced in the derivatization. In any event, the above discussion remains somewhat speculative as these higher running bands were not characterized.

In the derivatization of 5'-<sup>31/32</sup>P-**ON1**, more products were produced besides those represented by bands B and C in Lane 2, as shown in Figure 6.3. Band A, with the most retained electrophoretic mobility, is most likely due to a "T-bone" structure formed between two oligonucleotides. Two possible explanations may account for the T-bone formation: a), the 2'-hydroxyl group in **ON1** nucleophilically attacked the activated phosphate of another oligonucleotide; or b), the diamine originated from azido-PEG-amine **6.1**, either produced *in situ* due to the presence of PPh<sub>3</sub> or contaminated from its preparation, nucleophilically attacked the activated oligonucleotide to form an oligonucleotide dimer. However, the near absence of Band A for 5'-N<sub>3</sub>-<sup>31/32</sup>P-**ON2** supports the assertion that 2'-hydroxyl group acted as the nucleophile to afford an oligonucleotide dimer as shown in Band A of Lane 2. On the other hand, the lower bands that appeared in Lane 2 for **ON1** may be due to the lower stability of the ribose-containing oligonucleotide because there weren't any corresponding bands for oligonucleotide **ON2**. Since these bands are not of primary interest, no further analysis was performed.

The desired 5'-N<sub>3</sub>-<sup>31/32</sup>P-ONs at Band C was purified by gel extraction. However, the loss of oligonucleotide via this method was high. Apart from the side reactions, which may have consumed the oligonucleotide instead of providing the desired 5'-N<sub>3</sub>-<sup>31/32</sup>P-ONs, normally only 6 to 10 nmol of the 5'-N<sub>3</sub>-<sup>31/32</sup>P-ONs were obtained from a reaction starting with 100 nmol of the 5'-HO-ONs.

### 6.3.2 Synthesis of alkynes

The synthesis of alkynes was mainly based on the conjugation between the carboxylic acids and propargylamine using EDC/HOBt as the coupling reagents. For the synthesis

of alkynylarylboronic acid **3.11** as shown in Scheme 3.3, the boronic acid synthon **3.8** was first protected with 1,8-diaminonaphthalene to give boronate **3.9** with high stability under basic conditions. After the introduction of the propargyl amide, the protecting group was removed in the presence of  $\text{H}_2\text{SO}_4$  to release boronic acid **3.11**. Alkynyl $\text{ArBF}_3$  **6.2** was prepared from the fluoridation of boronic acid **3.11**. A large excess of fluoride was used to fully convert alkynylarylboronic acid **3.11** to alkynyl $\text{ArBF}_3$  **6.2**. Although the reaction proceeded cleanly, initially there was no good way to purify the  $\text{ArBF}_3$  from free fluoride. Even though the chromatographic system developed by Ting *et al.*<sup>85</sup> with 5%  $\text{NH}_4\text{OH}$  in EtOH over silica column could successfully separate  $\text{ArBF}_3$ s from fluoride, the silica gel also dissolved in the elution buffer and becomes a new contaminant of the desired  $\text{ArBF}_3$ s. As a result, it would not be possible to accurately measure the amount of  $\text{ArBF}_3$ s by weighing. In addition, the  $\text{ArBF}_3$ s used in this thesis are generally poor UV chromophores. This means that UV-vis spectrometry would not be ideal to determine the concentration of  $\text{ArBF}_3$ s. We then have developed a new method to purify the  $\text{ArBF}_3$  from free fluoride and other contaminants by  $\text{Et}_2\text{O}$  wash and subsequent DMSO extraction. Although the  $^{19}\text{F}$  NMR spectrum of the sample in DMSO suggested no presence of free fluoride, complete removal of DMSO would be a challenge due to its low vapor pressure. Moreover, there is no ideal internal  $^{19}\text{F}$ -standard for the  $\text{ArBF}_3$  and therefore its concentration could only be crudely estimated by  $^{19}\text{F}$  NMR spectroscopy. For instance, tetrafluoroborate ( $\text{BF}_4^-$ ), which might be regarded suitable as the internal reference, is not exactly similar to  $\text{ArBF}_3$ s. Moreover, since normally a very small amount of alkynyl $\text{ArBF}_3$  **6.2** was prepared, we did not use  $\text{BF}_4^-$  as the internal standard for the concentration measurement of the  $\text{ArBF}_3$ s. Instead, the concentration of alkynyl $\text{ArBF}_3$  **6.2** in  $d_6$ -DMSO used in this chapter was estimated to be  $\sim 15$  mM based on  $^{19}\text{F}$  NMR spectroscopy. For the click coupling reaction with the azido-oligonucleotides, whose amount was in the nanomole or picomole range, the amount of alkynyl $\text{ArBF}_3$  **6.2** added to the reaction was always in large excess to the oligonucleotides. Therefore, no further effort was taken to determine the accurate concentration of alkynyl $\text{ArBF}_3$  **6.2**.

The  $^{18}\text{F}$ -fluoridation of alkynylarylboronic acid **3.11** was carried out under acidic conditions with radiochemical yields of 30-40% within 30 minutes. Since the reaction

requires at least 3 equivalents of fluoride, carrier  $^{19}\text{F}$ -fluoride was added to  $^{18}\text{F}$ -fluoride to facilitate the fluoridation. The addition of carrier  $^{19}\text{F}$ -fluoride no doubt decreases the specific activity. However, the specific activity of  $^{18}\text{F}$ -ArBF<sub>3</sub>s is compensated by a tripling effect. This follows the 1:3 stoichiometric ratio of the product to the boron-bound fluoride. As there should be no difference regarding chemical reactivity between  $^{18}\text{F}$ -fluoride and  $^{19}\text{F}$ -fluoride, the specific activity based on fluoride would not be changed whether or not it is bound to other molecules.

### 6.3.3 Click reactions between 5'-N<sub>3</sub>-<sup>31/32</sup>P-ONs and alkynes

Cu(II)-TBTA/sodium ascorbate were used in the study of the click reaction between the 5'-N<sub>3</sub>-<sup>31/32</sup>P-ONs and alkynes. The ligand TBTA has been reported to stabilize Cu(I),<sup>352</sup> which can be produced *in situ* by the reduction of Cu(II) with sodium ascorbate. The Cu(II)-TBTA stock solution was prepared with 1:1 Cu(II):TBTA in 4:1 <sup>t</sup>BuOH:H<sub>2</sub>O. Because of the low solubility of TBTA in the aqueous cosolvent, there was some white solid at the bottom of the stock solution and it was found that this precipitate would not influence the catalytic efficiency of Cu(II)-TBTA. For each of the click reactions, a 4:1 ratio of sodium ascorbate to Cu(II)-TBTA was added to ensure there was enough reductant in the reaction.

The click reaction was undertaken between the gel-purified 5'-N<sub>3</sub>-<sup>31/32</sup>P-ONs and various alkynes catalyzed by Cu(II)-TBTA/sodium ascorbate. The oligonucleotides were stable in the presence of Cu(II)-TBTA/sodium ascorbate as shown in Lanes 2 and 8 in Figure 6.6. Indeed as shown in Figure 6.6, the click reactions between the 5'-N<sub>3</sub>-<sup>31/32</sup>P-ONs and alkynes (**6.2**, **6.4**, and **6.5**) yielded clean bands, whose electrophoretic mobilities were all slower than the 5'-N<sub>3</sub>-<sup>31/32</sup>P-ONs. The fluorescent products from the click reaction with alkynylcoumarin **6.4** (represented by Lanes 3 and 9) moved the slowest in the polyacrylamide gel. The click reaction between the 5'-N<sub>3</sub>-<sup>31/32</sup>P-ONs and alkynylbenzamide **6.5** (Lanes 6 and 12) gave products with the second slowest electrophoretic mobility. The reaction with **6.5** provides a reference for the reaction between the 5'-N<sub>3</sub>-<sup>31/32</sup>P-ONs and the hypothetical deboronated product that might have formed *in situ* from alkynylarylboronic acid **3.11** or alkynylArBF<sub>3</sub> **6.2** during the click reaction. AlkynylArBF<sub>3</sub> **6.2** was successfully coupled onto the 5'-N<sub>3</sub>-<sup>31/32</sup>P-ONs

via the click reaction as shown in Lanes 4, 5, 10 and 11. The newly produced oligonucleotides in Lanes 4, 5, 10 and 11 moved a bit faster than those in Lanes 6 and 12, which suggested that both products  $5' \text{-}^{31/32}\text{P-ON-ArBF}_3\text{s}$  contain more negative charges than that does with **6.5**. Nonetheless, the oligonucleotide-ArBF<sub>3</sub>s ran a bit more slowly than the precursor oligonucleotides. When considering the molecular weight of alkynylArBF<sub>3</sub> **6.2** (262 g/mol), it is close to adenosine (267 g/mol). This implies that the  $5' \text{-}^{31/32}\text{P-ON-ArBF}_3\text{s}$  are close to 16mers, just as one adenosine incorporated into the  $5' \text{-N}_3\text{-}^{31/32}\text{P-ONs}$  (15mers). As a result, the electrophoretic mobility of the  $5' \text{-N}_3\text{-}^{31/32}\text{P-ON-ArBF}_3\text{s}$  resembles that of a 16mer, which moves slightly more slowly than the  $5' \text{-N}_3\text{-}^{31/32}\text{P-ONs}$  (15mers).

The investigation of different amounts of catalyst for the click reaction suggests that the reaction rate is catalyst dependent at low concentrations, while the reaction rate seemed no different at higher concentrations of copper(II)-TBTA/sodium ascorbate. As reported by Rodionov, Fokin, and Finn, the copper(I) catalyzed azide-alkyne cycloaddition reaction in the absence of ligand is 2<sup>nd</sup> order in copper(I) under catalytic conditions.<sup>353</sup> However, when a large excess of copper is used, the reaction rate has been observed independent of the copper(I) concentration.<sup>353</sup> The relatively high amount of Cu(II)-TBTA (50 nmol or 12.5 mM in 4  $\mu\text{L}$  reaction) was used for the click reactions herein to minimize the reaction time while ensuring the reaction conversion. However, when considering the possible dilution from the fluoridation mixture in the first step as well as the potential incompatibility of the quench buffer (NH<sub>4</sub>OH in EtOH) with regard to the click reaction in the second step, the dilution effect on the click reaction was tested with both DEPC·H<sub>2</sub>O and the quench buffer NH<sub>4</sub>OH/EtOH in different reaction volumes. The result suggested that in the presence of Cu(II)-TBTA (50 nmol)/sodium ascorbate (200 nmol), more than 95% of the  $5' \text{-N}_3\text{-}^{31/32}\text{P-ONs}$  were converted to the products within 40 minutes even in the reaction with 12 times dilution by NH<sub>4</sub>OH/EtOH.

In the presence of Cu(II)-TBTA (12.5 mM)/sodium ascorbate (50 mM) in a 4  $\mu\text{L}$  reaction, the click reaction for  $5' \text{-N}_3\text{-}^{31/32}\text{P-ON2}$ , as indicated in Figure 6.8A, was very fast. According to the result, the reaction was complete within 5 minutes. Since a centrifugation for 15 minutes at 13k rpm was involved to remove the catalyst and

unreacted alkynes prior to the gel electrophoresis, to exclude catalysis by heterogeneous copper(I), EDTA was added to capture copper(I/II) and thereby fully quench the click reaction involving 5'-N<sub>3</sub>-<sup>31/32</sup>P-ON2. The reaction analyzed by gel electrophoresis as shown in Figure 6.8B implies that the reaction was actually complete within 2 minutes under the given conditions. Based on this result and in order to drive the click reaction between alkynyl-<sup>18</sup>F-ArBF<sub>3</sub> and 5'-N<sub>3</sub>-<sup>31/32</sup>P-ONs to completion, a reaction time of 30 minutes was selected, which is not too long compared with the decay half-life of <sup>18</sup>F-fluorine.

The dilution effect from either DEPC·H<sub>2</sub>O or the NH<sub>4</sub>OH/EtOH quench buffer was also studied for 5'-N<sub>3</sub>-<sup>31/32</sup>P-ON1 in the same manner. The dilution effect was negligible in the presence of a high catalyst loading. More importantly, the experiment shown in Figure 6.9, is the RNase A treatment after the click reaction between alkynylArBF<sub>3</sub> 6.2 and 5'-N<sub>3</sub>-<sup>31/32</sup>P-ON1. As shown in Lane 6, a smaller oligonucleotide was produced from the treatment with RNase A. The successful cleavage of the oligonucleotide with RNase A suggests the derivatization of 5'-<sup>31/32</sup>P-ON1 via the click reaction has not changed the backbone of the oligonucleotide. Although the experiment provided no information about the integrity of the nucleobases present on the oligonucleotide, the intactness of the backbone is consistent with most of the derivatization of oligonucleotides from the 3'- or 5'-terminus.

### 6.3.4 The one-pot two-step <sup>18</sup>F-labeling of oligonucleotides

The <sup>18</sup>F-fluoridation of alkynylarylboronic acid 3.11 was carried out successfully under standard conditions with a radiochemical yield of ~ 30-40% in around 30 minutes. The reaction was quenched with 5% NH<sub>4</sub>OH in 50% aqueous EtOH. One third of the quenched reaction was then added to the oligonucleotide for the click reaction catalyzed by Cu(II)-TBTA/sodium ascorbate. The result of the click reaction was analyzed by PAGE-autoradiography. To decrease the interference of the signals from <sup>31/32</sup>P-phosphate, the oligonucleotide was labeled with <sup>32</sup>P at a low specific activity with regard to phosphate. Low specific activity in terms of <sup>32</sup>P provides for a small amount of β-decay incidents due to <sup>32</sup>P-phosphate, and thus would require longer exposure time to provide enough emission from the <sup>32</sup>P-labeled species for the phosphorimager screen to satisfy its

minimum sensitivity. If  $^{18}\text{F}$ -fluoride is incorporated into the oligonucleotide at a relatively high specific activity, then following the PAGE resolution, the radioactive signals of  $^{18}\text{F}$ -fluoride should outweigh those from  $^{32}\text{P}$ -phosphate. Following click reaction, a precipitation was undertaken to remove most of the non-oligonucleotide species. As shown in Figure 6.14, a significant amount of alkynyl- $^{18}\text{F}$ -ArBF<sub>3</sub> **6.2** could be removed by the precipitation procedure. Although  $^{18}\text{F}$ -fluoride co-precipitated with the oligonucleotide, it most likely migrated off the gel due to its small size. As shown in Figure 6.11 and Figure 6.13, at early time points, the signal registered on the phosphorimager screen was predominantly based on  $^{18}\text{F}$ -fluoride, while sufficient signal was obtained for a short time of exposure. However, at later time points, it took a longer time to accumulate enough signal, since the  $^{18}\text{F}$ -fluoride incorporated in the oligonucleotides resolved on the polyacrylamide gel had decayed during storage. Autoradiographic exposure that was initiated well after any incorporated  $^{18}\text{F}$ -fluoride had decayed ensured that only signals from  $^{32}\text{P}$ -phosphate were detected. The predominant change of the radioactivity as seen in four different exposures acquired over a period of three days highly suggested that the incorporation of the  $^{18}\text{F}$ -ArBF<sub>3</sub> was successful. However, since the gels were stored for decay at 4 °C in the fridge because of the limited equipment in the hot lab, the diffusion of the oligonucleotides on the PAGE cannot be prevented, and as a result the autoradiographic gel image at the later time points gave fuzzy bands. Fortunately, this is sufficient to represent the decay of  $^{18}\text{F}$ -fluoride. Lane 5 in Figure 6.13 also demonstrates the click reaction between 5'-N<sub>3</sub>- $^{31}\text{P}$ -**ON1** and alkynyl- $^{18}\text{F}$ -ArBF<sub>3</sub> **6.2**, which illustrates the successful incorporation of  $^{18}\text{F}$ -fluoride to the oligonucleotide by the gradual loss of radioactive signals until nearly no radioactivity was detected after 4 days.

One of the reasons that we chose to work with **ON1** is the feature of a ribonucleotide in the middle of the sequence. It was believed that the derivatization at its terminus would not affect the reactivity of the oligonucleotide at the position of the ribonucleotide. The results demonstrated in both Figure 6.9 (20% PAGE) and Figure 6.12 (10% PAGE) suggest the ribonucleotide in **ON1** remains intact through the derivatization and copper(I) catalyzed click reactions. However, it was noticed that with 10% PAGE, the RNase A cleaved product, an 8mer, moved ahead of the bromophenol blue dye. In order to achieve

the highest resolution among oligonucleotides, bromophenol blue migrated to the very bottom of the polyacrylamide gel and therefore the 8mer product likely ran off the gel as shown in Lanes 2 to 4 in Figure 6.11. Moreover, from the autoradiographic gel images of the  $^{18}\text{F}$ -labeling experiments shown in Figure 6.11 and Figure 6.13, neither of the experimental results demonstrated significant mobility difference among oligonucleotides produced from the click reactions. Even in Figure 6.12, which represents a very nice autoradiographic gel image, the difference among oligonucleotides is very small when resolved in the 10% PAGE. This might be due to 1) oligonucleotides moving faster in a 10% PAGE gel than in the 20% PAGE gel, and 2) the small size of the PAGE gel (20 cm  $\times$  20 cm) shown in Figure 6.11, Figure 6.12 and Figure 6.13, which was too short to differentiate among oligonucleotides that differ by only one base. Notably a smaller size gel was run to enable rapid resolution.

Overall, the two  $^{18}\text{F}$ -labeling experiments analyzed by PAGE-autoradiography showed the substantial radioactivity incorporation compared with the parallel click reactions undertaken with nonradioactive alkynes. The relatively rapid radioactive decay of  $^{18}\text{F}$ -containing species, either in the case of dual-isotopic labeled ( $^{18}\text{F}/^{32}\text{P}$ ) or the single-isotopic labeled ( $^{18}\text{F}$ ) oligonucleotide, suggested that the one-pot two-step reaction via copper(I) catalyzed click chemistry proceeded in a rapid fashion with very high efficiency. The lower than desired radiochemical yield is largely due to using substoichiometric amounts of oligonucleotide (*vide infra*).

Gel electrophoresis is a very efficient way to analyze reactions involving oligonucleotides and it can also be used to purify the oligonucleotides. However, the time-consuming gel purification is not practical for  $^{18}\text{F}$ -chemistry in terms of isolation of the  $^{18}\text{F}$ -labeled oligonucleotide for imaging uses. As a result, an HPLC method was also developed in order to both analyze and purify  $^{18}\text{F}$ -labeled products. We found that with the TEAA/ $\text{CH}_3\text{CN}$  solvent system, both the oligonucleotide and alkynyl- $^{18}\text{F}$ -ArBF<sub>3</sub> **6.2** can be fully resolved on a C18-column. We were able to use this HPLC system to purify 5'- $^{31}\text{P}$ -ON2- $^{18}\text{F}$ -ArBF<sub>3</sub> from the precursor alkynyl- $^{18}\text{F}$ -ArBF<sub>3</sub> **6.2**. As indicated in Figure 6.14. This further demonstrates that the incorporation of the  $^{18}\text{F}$ -ArBF<sub>3</sub> on the oligonucleotide via click chemistry was successful. It also suggests that most of the

unreacted alkynyl- $^{18}\text{F}$ -ArBF<sub>3</sub> **6.2** was washed away by 3% LiClO<sub>4</sub>/acetone but a significant amount of free  $^{18/19}\text{F}$ -fluoride co-precipitated with the oligonucleotide. Since only 2 nmol of oligonucleotide 5'-N<sub>3</sub>- $^{31}\text{P}$ -ON2 was used for the click reaction, the low radioactivity of the new peak appearing at 18.4 minutes from the HPLC is reasonable. This radio-peak was manually collected, its radioactivity was measured, and the sample was stored at 4 °C to decay. Although the ArBF<sub>3</sub> might normally hydrolyze, at least partially, under such conditions, the oligonucleotide backbone structure should not be altered. Therefore the concentration of the decayed sample, determined by UV-vis spectrometry, directly represents the concentration of the HPLC collected 5'- $^{31}\text{P}$ -ON2- $^{18}\text{F}$ -ArBF<sub>3</sub>. The concentration of the labeled oligonucleotide was calculated by dividing the value of its measured UV absorbance at 260 nm by its  $\epsilon_{\text{max}}$  and used to determine the specific activity.

### 6.3.5 Specific activity

Specific activity is one of the most important attributes for a radiotracer to provide *in vivo* images with good qualities.<sup>90, 354-356</sup> It is a very important factor that is always determined by dividing the radioactivity by the amount of the radiotracer. To determine the mass/concentration, UV absorbance has been frequently used to construct a standard curve. This requires i) a good chromophore that has a relatively high and knowable extinction coefficient to give a readable UV-absorbance; ii) the cold tracer can be prepared cleanly in a relatively large scale to provide stock solutions with precisely known concentrations; iii) in most cases, an HPLC calibration curve from the stock solution is generated to calculate the specific activity.

For the purification of organotrifluoroborates, the Molander group normally applies the hot acetone extraction with a Soxhlet extractor to extract the organotrifluoroborate, for which the fluoridation is always undertaken with a large scale of organoboronic acid (in grams).<sup>99, 104</sup> For all the arylboronic acids/esters in this thesis, we are limited to a few tens of milligrams at best, due to the difficulty in preparing a large amount of these arylboronic acids/esters with strong electron withdrawing groups. On the other hand, Ting *et al.* reported the flash chromatographic system with a silica gel column to remove free fluoride with NH<sub>4</sub>OH/EtOH as the elution solution.<sup>85</sup> However, the co-elution of

silica gel in the column poses a new contaminant, which does not allow accurate measurement of the ArBF<sub>3</sub>s by weight. Nevertheless, obtaining tens of milligrams of ArBF<sub>3</sub>s is achievable but always contaminated with free fluoride from the reaction since both fluoride and ArBF<sub>3</sub>s are insoluble in most of the organic solvents. We have found that DMSO is generally a very good solvent to dissolve ArBF<sub>3</sub>s due to their organic nature but a poor solvent for fluoride. However, to concentrate the sample in DMSO would be relatively difficult compared with other solvents due to its high boiling point. Moreover, the ArBF<sub>3</sub>s used in this thesis, if not conjugated to a good chromophore, have very low extinction coefficients. Due to these reasons, until now, there has been no successful work to determine the specific activity of an <sup>18</sup>F-ArBF<sub>3</sub> to experimentally demonstrate that the specific activity of <sup>18</sup>F-ArBF<sub>3</sub>s is three times that of <sup>18</sup>F-fluoride.

Since oligonucleotides contain multiple chromophores that allow their concentrations to be determined reasonably accurately via UV spectrophotometry even at very low concentrations, we therefore collected 5'-<sup>31</sup>P-**ON2**-<sup>18</sup>F-ArBF<sub>3</sub> via RP-HPLC and tried to determine its concentration using the UV-vis absorption spectrum. With the characteristic absorption at 260 nm of the oligonucleotides, the extinction coefficient of the oligonucleotide **ON2** (128800 M<sup>-1</sup>cm<sup>-1</sup>) as reported by the vendor was used to calculate the concentration, based on an assumption that the incorporation of the ArBF<sub>3</sub> into the oligonucleotide would not significantly change the extinction coefficient of the oligonucleotide at 260 nm.

However, as shown in Figure 6.15A, the UV profile of the collected sample was not consistent with the typical UV absorption profile for oligonucleotides. In contrast, Figure 6.15B, the UV absorption spectrum of HPLC purified oligonucleotide following precipitation, demonstrates an absorption pattern that is characteristic of oligonucleotides and this was highly suggestive of the chromophores in the otherwise ultrapure HPLC solvents (HCO<sub>2</sub>NH<sub>4</sub>/CH<sub>3</sub>CN), leading to a deviation in the UV absorption of the sample. The experimental data shown in Figure 6.15A was then fitted via deconvolution with two Gaussian functions indicated in Figure 6.17.<sup>a</sup> The red curve, representing the addition of the blue and green curves, perfectly overlaps with the experimental result and it highly

---

<sup>a</sup> Dr. Yi Cao helped with this deconvolution fitting.

suggests that the presence of salt or other contaminants perturbed the absorption of the oligonucleotides at 260 nm. Therefore, the amount of the oligonucleotide measured via Figure 6.15A might actually be less than the actual value. Consequently, the calculated specific activity would be higher.

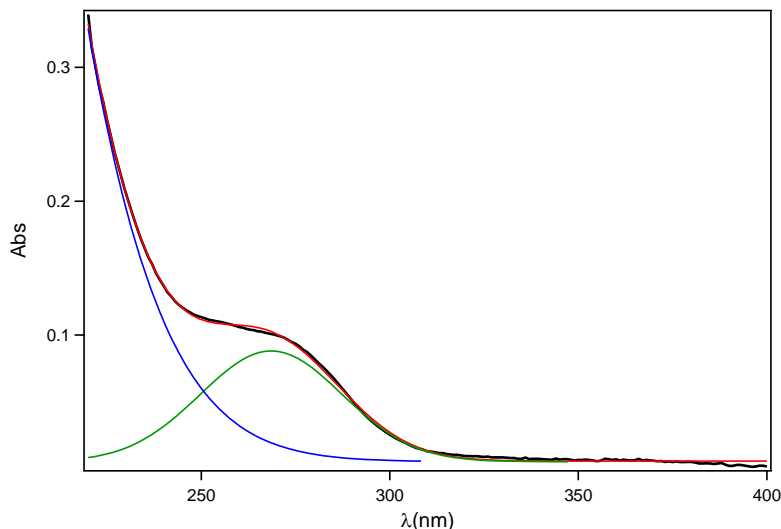


**Figure 6.17 The UV absorption of the decayed sample of the HPLC collected 5'-<sup>31</sup>P-ON2-<sup>18</sup>F-ArBF<sub>3</sub> can be corrected by deconvolution of the UV spectrum.**

The black curve: the experimental UV absorption spectrum of the HPLC collected 5'-<sup>31</sup>P-ON2-<sup>18</sup>F-ArBF<sub>3</sub> in HCO<sub>2</sub>NH<sub>4</sub>/CH<sub>3</sub>CN; the blue and green curves are the deconvolution of the experimental data via two Gaussian functions; the red curve: the sum of the blue and green curves.

For some reason, the HPLC solvents clearly interfered with the absorption of the collected sample. We then further concentrated down the sample collected following HPLC. LiClO<sub>4</sub>/acetone and ethanol were used to precipitate and wash the oligonucleotide to remove the organic contaminants. The oligonucleotide pellet was redissolved in DEPC·H<sub>2</sub>O to measure its concentration by UV spectroscopy. Based on this, the specific activity was calculated after the fact to be 67.93 μCi/nmol. This result deviated even further from the one obtained from direct measurement without the precipitation treatment. This is clearly due to the loss of oligonucleotide during the LiClO<sub>4</sub>/acetone and ethanol treatment.

In addition, the specific activity of 5'-<sup>31</sup>P-ON2-<sup>18</sup>F-ArBF<sub>3</sub> was also calculated based on that of free <sup>18</sup>F-fluoride, which was directly derived from the radioactivity measured for the reaction and the known amount of carrier <sup>19</sup>F-fluoride added. The value of 13.6 mCi/μmol for the oligonucleotide, derived from the specific activity of <sup>18</sup>F-fluoride, was

reasonably close to 19.1 mCi/ $\mu$ mol directly calculated from the radioactivity and the amount of the oligonucleotide. This should provide reasonable experimental evidence that the specific activity of  $^{18}\text{F}$ -ArBF<sub>3</sub>s is triple that of free  $^{18}\text{F}$ -fluoride.

## 6.4 Conclusion

The oligonucleotide was first derivatized by Knorre's method<sup>341</sup> and was successfully labeled with an  $^{18}\text{F}$ -ArBF<sub>3</sub> via a one-pot two-step synthesis involving copper(I) catalyzed click chemistry. The radiochemical yield for the radiolabeling of alkynylarylboronic acid **3.11** was 30-40% in 0.5 hours at room temperature and a subsequent click reaction catalyzed by Cu(I)-TBTA was undertaken to label the oligonucleotide. Sodium ascorbate exhibited a very efficient reduction capability to keep copper in its reduced form to catalyze the reaction. Both PAGE-autoradiography and radio-HPLC were used to analyze the one-pot two-step radiosynthesis. The 5'-<sup>31</sup>P-ON2- $^{18}\text{F}$ -ArBF<sub>3</sub> was successfully isolated from radio-HPLC and its specific activity was determined. Although with some deviation, the measured specific activity was relatively consistent with the calculated one based on the specific activity of  $^{18}\text{F}$ -fluoride, to which a known amount of carrier  $^{19}\text{F}$ -fluoride was added. The result follows the stoichiometric relation, governing the production of one ArBF<sub>3</sub> from three fluoride ions.

Overall, this work exhibits the beauty of the click reaction: fast, clean, and chemically specific. As for compounds that are sensitive to acidic conditions, this one-pot two-step synthetic strategy provides an alternative way to achieve the radiolabeling with an  $^{18}\text{F}$ -ArBF<sub>3</sub>s while maintaining their structure and bioactivity intact. This method will be applied in the following chapters.

## 6.5 Materials and methods

The chemicals were obtained from Oakwood Products Inc., Novabiochem, Advanced ChemTech, Sigma-Aldrich, Alfa-Aesar or Acros. Solvents were obtained from Fisher Scientific. The  $^{18}\text{F}$  Trap & Release column (HCO<sub>3</sub><sup>-</sup> form, ~ 10 mg) was purchased from ORTG, Inc. Deuterated solvents were purchased from Cambridge Isotope Laboratories. Analytical thin layer chromatography was performed on Silica Gel 60 F254 Glass TLC

plates from EMD Chemicals and SiliaFlash F60 from Silicycle was used for flash chromatography. All NMR spectra were recorded at room temperature on a Bruker Avance 300 or 400 MHz spectrometer. Chemical shifts are reported using the  $\delta$  scale in *ppm* and all coupling constants (*J*) are reported in hertz (Hz). Unless specified,  $^1\text{H}$  NMR spectra are referenced to the tetramethylsilane peak ( $\delta = 0.00$  *ppm*),  $^{13}\text{C}$  NMR spectra are referenced to the chloroform peak ( $\delta = 77.23$  *ppm*) and  $^{19}\text{F}$  NMR spectra are referenced to neat trifluoroacetic acid ( $\delta = 0.00$  *ppm*,  $-78.3$  *ppm* relative to  $\text{CFCl}_3$ ). Mass spectrometry was performed at the mass spectrometry lab of the University of British Columbia (U.B.C.) Chemistry Department. The oligonucleotides studied herein were synthesized by Integrated DNA Technologies (IDT). T4 polynucleotide kinase (T4 PNK) and the T4 PNK buffer (10 X) were purchased from New England Biolabs Inc., RNaseA from Fermentas, and  $\gamma$ - $^{32}\text{P}$ -ATP from Perkin Elmer. Sephadex G-25 desalting medium was purchased from GE Healthcare. Cetyltrimethylammonium bromide (CTAB) was recrystallized from EtOH. Nuclease free  $\text{H}_2\text{O}$  was prepared from distilled water pretreated with diethylpyrocarbonate (DEPC). All tubes and pipette tips were autoclaved for 30 min to sterilize. HPLC information is available in Appendix B.

Oligonucleotide sequences<sup>a</sup>: **ON1** is 5'-GCGTGCCrCGTCTGTT-3' and **ON2** is 5'-GCGTGCCCCGTCTGTT-3'. The extinction coefficient of oligonucleotide **ON1** is  $128,700 \text{ M}^{-1}\text{cm}^{-1}$  and that of **ON2** is  $128,800 \text{ M}^{-1}\text{cm}^{-1}$ . The oligonucleotides were directly dissolved in the nuclease free  $\text{H}_2\text{O}$  and the concentrations were determined based on the absorption at 260 nm measured by a Beckman Coulter DU 800 spectrophotometer.

Some samples were concentrated over vacuum by a LABCONCO Centrivap concentrator. An Amersham 9200 Typhoon phosphorimager was used to scan the images corresponding to  $^{32}\text{P}$ -phosphate or  $^{18}\text{F}$ -fluoride, and the images were analyzed by ImageQuant 5.2.

**WARNINGS:** Dealing with radioactive  $^{32}\text{P}$  requires certain precautions. A plexiglass shielding glass was used to reduce the radiation dose during operation and plexiglass containers were used to store the  $^{32}\text{P}$ -labeled oligonucleotides. A Ludlum Survey meter

---

<sup>a</sup> The nucleotide codes here without notification are deoxyribonucleoside. As A is deoxyadenosine, G is deoxyguanosine, T is thymidine and C is deoxycytidine. Here in the sequence, the “rC” is the ribonucleoside cytosine.

with a pancake probe was used to check the radioactivity and contamination near the work-bench. All the radioactive wastes were collected and stored to decay under shielding for at least 150 days before disposal.

All  $^{18}\text{F}$ -labeling work was done at TRIUMF lab 007. Radiation protection procedures strictly followed the TRIUMF Radiation Safety Regulations. Since this work involves mainly manual handling, fairly high amounts of dosage might be applied, and special caution is required to reduce the operating time. A lead brick castle was built up to shield the radiation. All the materials that came in contact with the source water (the  $^{18}\text{O}$ -water) were collected and decayed separately from other  $^{18}\text{F}$ -contaminated stuffs including gloves, sleeves, vials, tubes, and pipette tips prior to disposal.

### 6.5.1 The derivatization of oligonucleotides

#### 2-(2-(2-Azidoethoxy-ethoxy)ethanamine ( $\text{N}_3$ -PEG-NH $_2$ ) (6.1)

$\text{NaN}_3$  (3.44 g, 52.9 mmol) in  $\text{H}_2\text{O}$  (12.0 mL) was mixed with  $\text{CH}_2\text{Cl}_2$  (10.0 mL) in an ice-water bath.  $\text{Tf}_2\text{O}$  (1.8 mL, 10.7 mmol) in  $\text{CH}_2\text{Cl}_2$  (8.0 mL) was added dropwise to the solution for 1 hr at 0 °C.<sup>357</sup> The resulting mixture was stirred at the same temperature for an additional 4 hr, and the layers were separated. The aqueous layer was further extracted with  $\text{CH}_2\text{Cl}_2$  (40 mL). The  $\text{CH}_2\text{Cl}_2$  layers were combined, washed with aqueous saturated  $\text{Na}_2\text{CO}_3$  (30 mL) and used as is without further purification. 2,2'-(Ethylenedioxy)bis(ethylamine) (3.1 mL, 21.2 mmol) in MeOH (20 mL) was added to  $\text{K}_2\text{CO}_3$  (1.70 g, 12.3 mmol) and  $\text{CuSO}_4 \cdot 5\text{H}_2\text{O}$  (cat. 14 mg) in  $\text{H}_2\text{O}$  (4 mL). The solution was added with the  $\text{CH}_2\text{Cl}_2$  extracts of the first reaction over a period of 5 hr, and the reaction mixture was stirred at rt for 36 hr. Then the layers were separated and the organic layer was dried over anhydrous  $\text{Na}_2\text{SO}_4$ . The solution was filtered and concentrated under vacuum. The residue was purified by silica gel flash chromatography (MeOH: $\text{CH}_2\text{Cl}_2$  5:95) to afford the desired product as a light yellow oil ( $R_f = 0.24$  in 1:4 MeOH: $\text{CH}_2\text{Cl}_2$ ). Yield: 1.44 g, 78%.  $^1\text{H}$  NMR (400 MHz,  $\text{CDCl}_3$ , rt):  $\delta$ (ppm) 2.94 (s, br, 2 H), 3.41 (t,  $J = 5.00$  Hz, 2 H), 3.56 (t,  $J = 5.04$  Hz, 2 H), 3.66 (m, 6 H), 3.89 (s, br, 2 H);  $^{13}\text{C}$  NMR (100.6 MHz,  $\text{CDCl}_3$ , rt):  $\delta$ (ppm) 42.02, 51.63, 70.95, 71.17, 71.60, 72.65; ESI-LRMS:  $[\text{M}+\text{H}]^+$ , 175.4 (100%).

## 5'-Phosphorylation of oligonucleotides

General protocol:<sup>342</sup> the oligonucleotide (100 nmol) and ATP (300 nmol) were mixed in  $1 \times$  PNK buffer<sup>a</sup>. The reaction was initiated by the addition of T4 PNK (60 units) and the mixture was then incubated at 37 °C for 3 hr. The reaction was quenched by heating at 70 °C for 10 min, then cooled to rt and loaded onto a pre-packed 3 cm Sephadex G-25 spin column that was prewashed with DEPC·H<sub>2</sub>O three times. The G-25 spin column was spun for 10 min at 5000 rpm and the filtrate was collected and used in the following step without further purification.

For <sup>32</sup>P-labeling,  $\gamma$ -<sup>32</sup>P-ATP (10  $\mu$ Ci/ $\mu$ L)<sup>b</sup> was added to the reaction right before the addition of T4 PNK. The other procedure followed the general protocol. To determine the concentration of the 5'-N<sub>3</sub>-<sup>31/32</sup>P-ONs, a stock solution of the <sup>31/32</sup>P-ATP was prepared the same way for the reaction from the same source of  $\gamma$ -<sup>32</sup>P-ATP. And a series of diluted solutions were prepared. Then 0.2  $\mu$ L of each solution including the 5'-N<sub>3</sub>-<sup>31/32</sup>P-ONs was loaded to a TLC plate at different locations. The TLC plate was dried, wrapped with plastic films, and visualized with a phosphorimager screen. A standard curve was then obtained and the concentration of the 5'-N<sub>3</sub>-<sup>31/32</sup>P-ONs therefore can be calculated.

## 5'-Azido-oligonucleotide (5'-N<sub>3</sub>-P-ONs)

The derivatization was undertaken according to literature reports.<sup>341, 342</sup> A small amount (1 to 2  $\mu$ L) of 8% (w/w) CTAB aqueous solution was added to the oligonucleotide (100 nmol) aqueous solution to precipitate the oligonucleotide as CTA salt successively till no more precipitation resulted.<sup>c</sup> After the final centrifugation, the supernatant was removed. The pellet was dissolved in MeOH (100  $\mu$ L) and concentrated down over the concentrator under vacuum. The MeOH treatment was repeated two more times. Then DMSO solutions of DMAP (0.36 mg/ $\mu$ L, 40  $\mu$ L), PPh<sub>3</sub> (0.32 mg/ $\mu$ L, 20  $\mu$ L), and (PyS)<sub>2</sub> (0.26 mg/ $\mu$ L, 20  $\mu$ L) were added to the oligonucleotide pellet and the mixture was incubated at 75 °C for 0.5 hr to give a yellow solution. The activated oligonucleotide was

---

<sup>a</sup>  $1 \times$  PNK buffer is made by diluting  $10 \times$  PNK buffer 10 times with the oligonucleotide, PNK and ATP solution and a certain amount of nuclease free water.

<sup>b</sup> The amount of  $\gamma$ -<sup>32</sup>P-ATP added is based on the radioactivity preferred.

<sup>c</sup> After each addition of the CTAB solution, the mixture was thoroughly mixed with micro-pipette and spun at 13k rpm for 10 min.

then precipitated with 1 mL of 3% LiClO<sub>4</sub> in acetone, mixed well, and centrifuged at 13k rpm for 10 min. The pellet was further washed with 1 mL of 3% LiClO<sub>4</sub> in acetone three times. The supernatant was decanted off and DEPC·H<sub>2</sub>O (50 μL) was added to dissolve the pellet. N<sub>3</sub>-PEG-NH<sub>2</sub> **6.1** (50 μL) was added to the activated oligonucleotide solution and the resulting mixture was incubated at rt for 1 hr. 3% LiClO<sub>4</sub> in acetone (1 mL) was added to precipitate the oligonucleotide and the mixture was centrifuged at 13k rpm for 15 min. The supernatant was decanted and 3% LiClO<sub>4</sub> in acetone (1 mL) was added to wash the pellet for three additional times. Ethanol (1 mL) was added to the pellet to further wash the oligonucleotide. Then the pellet was dissolved in DEPC·H<sub>2</sub>O (30 μL) and then charged with 20% denatured-PAGE (33 cm × 42 cm) at 40 W. After the electrophoresis was done, the gel was visualized by UV shadowing, or a phosphorimager screen was exposed to the gel for 5 min and scanned over the Typhoon phosphorimager to help visualize the gel. The desired bands were cut off, transferred to sterilized tubes and crushed into small pieces with a tip-sealed pipette tip. Then 500 μL of elution buffer was added; the resulting mixture was mixed well and frozen in the freezer. After being completely frozen, the mixture was heated to thaw. Then the mixture was centrifuged at 13k rpm for 10 min and the supernatant was carefully collected. Elution buffer (500 μL) was again added to the gel pieces to repeat two more times the procedure described previously. The supernatant was combined and concentrated over the concentrator under vacuum. The residue was then resuspended in DEPC·H<sub>2</sub>O (100 μL) and 3% LiClO<sub>4</sub> in acetone (1 mL) was added to precipitate the oligonucleotide. The top layer was carefully removed after centrifugation at 13k rpm for 15 min. Ethanol (1 mL) was added to the residue to fully precipitate the oligonucleotide. The pellet was further washed with the 3% LiClO<sub>4</sub> in acetone three more times and then dissolved in DEPC·H<sub>2</sub>O (40 μL). The aqueous solution of the oligonucleotide was desalted through a G-25 spin column and the filtrate was collected for future use.

5'-N<sub>3</sub>-<sup>31</sup>P-**ON1**: MALDI-TOF: calcd. 4803.1, found 4805.3.

## 6.5.2 Synthesis

### (2,6-Difluoro-4-(prop-2-yn-1-ylcarbamoyl)phenyl)trifluoroborate (alkynylArBF<sub>3</sub>) (6.2)

Boronic acid **3.11** (10 mg, 0.072 mmol) in THF (2.0 mL) was added with 0.8 M KHF<sub>2</sub> (0.45 mL, 0.36 mmol) in a 1.5 mL eppendorf tube. The reaction was stirred at rt for 5 hr and concentrated under vacuum. Et<sub>2</sub>O (3 × 1 mL) was added to the residue, vortexed, and centrifuged. The supernatant was decanted and the pellet was dried under vacuum. Then *d*<sub>6</sub>-DMSO (0.5 mL) was added to the pellet to extract the product for characterization. <sup>19</sup>F NMR (282.4 MHz, *d*<sub>6</sub>-DMSO, rt): δ(*ppm*) -55.23 (s, 3 F), -24.90 (s, 2 F); <sup>1</sup>H NMR (300 MHz, *d*<sub>6</sub>-DMSO, rt): δ(*ppm*) 3.10 (t, *J* = 2.38 Hz, 1 H), 4.01 (dd, *J*<sub>1</sub> = 5.47 Hz, *J*<sub>2</sub> = 2.42 Hz, 2 H), 7.17 (d, *J* = 7.71 Hz, 2 H), 8.87 (t, *J* = 5.31 Hz, 1 H); ESI-LRMS: [M]<sup>-</sup>, 262.1 (100%).

### Ethyl 7-diethylaminocoumarin-3-carboxylate (6.3a)

Diethylamino salicylaldehyde (3.86 g, 20 mmol) and diethyl malonate (4.6 mL, 30 mmol) were dissolved in EtOH (40 mL), followed by the addition of piperidine (6 mL, 60.7 mmol).<sup>358</sup> The resulting solution was heated to reflux for 4 hr and then the reaction was concentrated under vacuum. The residue was charged with flash chromatograph (EtOAc:hexanes 1:2) to give brown oil as the desired product (*R*<sub>f</sub> = 0.27 in 1:1 EtOAc:hexanes). Yield: 2.10 g, 36%. <sup>1</sup>H NMR (300 MHz, CDCl<sub>3</sub>, rt): δ(*ppm*) 1.25 (t, *J* = 7.14 Hz, 6 H), 1.41 (t, *J* = 7.11 Hz, 3 H), 3.45 (q, *J* = 7.14 Hz, 4 H), 4.37 (q, *J* = 7.11 Hz, 2 H), 6.47 (d, *J* = 2.29 Hz, 1 H), 6.62 (dd, *J*<sub>1</sub> = 8.94 Hz, *J*<sub>2</sub> = 2.5 Hz, 1 H), 7.37 (d, *J* = 8.94 Hz, 1 H), 8.44 (s, 1 H); <sup>13</sup>C NMR (75.5 MHz, CDCl<sub>3</sub>, rt): δ(*ppm*) 12.58, 14.54, 45.25, 61.31, 96.88, 107.84, 109.14, 109.65, 131.18, 149.37, 153.01, 158.47, 158.62, 164.44; ESI-LRMS: [M+Na]<sup>+</sup>, 312.3 (100%).

### 7-Diethylaminocoumarin-3-carboxylic acid (6.3b)

Compound **6.3a** (2.10 g, 7.26 mmol) and NaOH (0.37g, 9.25 mmol) were suspended in 50% aqueous MeOH (40 mL) and heated to reflux for 1 hr.<sup>358</sup> The reaction was then cooled to rt and neutralized with 3 M HCl carefully to pH ~ 2. The orange precipitate was then filtered and washed with H<sub>2</sub>O and cold MeOH before being left over high

vacuum to afford an orange powder ( $R_f = 0.59$  in 1:9 MeOH:CH<sub>2</sub>Cl<sub>2</sub>). Yield: 1.35 g, 71%. <sup>1</sup>H NMR (300 MHz, *d*<sub>6</sub>-DMSO, rt):  $\delta$ (ppm) 1.13 (t,  $J = 6.94$  Hz, 6 H), 3.47 (q,  $J = 6.94$  Hz, 4 H), 6.56 (s, 1 H), 6.78 (d,  $J = 8.99$  Hz, 1 H), 7.62 (d,  $J = 8.99$  Hz, 1 H), 8.57 (s, 1H); <sup>13</sup>C NMR (100.6 MHz, *d*<sub>6</sub>-DMSO, rt):  $\delta$ (ppm) 12.89, 44.97, 96.50, 107.73, 107.96, 110.64, 132.42, 150.02, 153.49, 158.48, 160.12, 165.07; ESI-LRMS: [M+Na]<sup>+</sup>, 284.2 (100%).

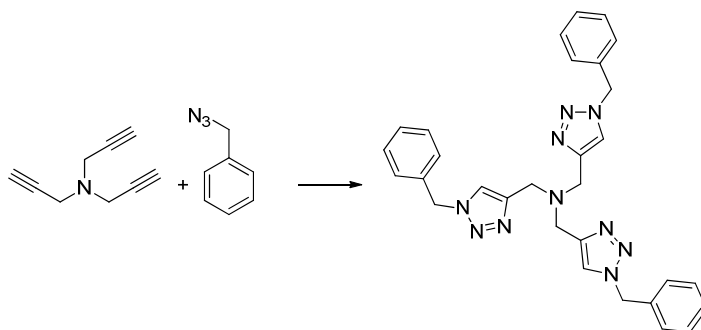
#### **7-(Diethylamino)-2-oxo-*N*-2-propyn-1-yl-2*H*-1-benzopyran-3-carboxamide (6.4)**

Diethylcoumarin **6.3b** (261 mg, 1.0 mmol), propargylamine (77  $\mu$ L, 1.2 mmol), HOBt·H<sub>2</sub>O (184 mg, 1.2 mmol) and pyridine (194  $\mu$ L, 2.4 mmol) were mixed in DMF (10 mL). Then EDC·HCl (250 mg, 1.3 mmol) was added to the DMF solution in one portion and the resulting reaction was undertaken at rt overnight. The reaction was then quenched with H<sub>2</sub>O (50 mL) and the slurry was then extracted with EtOAc (3  $\times$  50 mL). The organic layer was combined, washed with H<sub>2</sub>O (1  $\times$  50 mL) and brine (1  $\times$  50 mL), and then dried over anhydrous Na<sub>2</sub>SO<sub>4</sub>. The salt was then filtered off and the filtrate was concentrated under vacuum. The residue was loaded to a silica gel column for flash chromatography (EtOAc:hexanes 1:3) to give a yellow solid as the desired product ( $R_f = 0.26$  in 1:1 EtOAc:hexanes). Yield: 281 mg, 94%. <sup>1</sup>H NMR (400 MHz, CD<sub>2</sub>Cl<sub>2</sub>, rt):  $\delta$ (ppm) 1.24 (t,  $J = 6.96$  Hz, 6 H), 2.30 (s, 1 H), 3.47 (q,  $J = 6.91$  Hz, 4 H), 4.21 (d,  $J = 2.84$  Hz, 2 H), 6.52 (s, 1 H), 6.69 (d,  $J = 8.92$  Hz, 1 H), 7.46 (d,  $J = 7.20$  Hz, 1 H), 8.67 (s, 1 H), 8.92 (s, 1 H); <sup>13</sup>C NMR (100.6 MHz, CD<sub>2</sub>Cl<sub>2</sub>, rt):  $\delta$ (ppm) 12.29, 29.01, 45.20, 70.70, 80.31, 96.55, 108.33, 109.77, 110.18, 131.27, 148.24, 152.94, 157.92, 162.65, 162.85; ESI-HRMS: calcd. for C<sub>17</sub>H<sub>19</sub>N<sub>2</sub>O<sub>13</sub><sup>+</sup>: 299.1396, found: 299.1389.

#### **3,5-Difluoro-*N*-(prop-2-yn-1-yl)benzamide (6.5)**

3,5-Difluorobenzoic acid (630 mg, 4.0 mmol), propargylamine (256  $\mu$ L, 4.0 mmol), HOBt·H<sub>2</sub>O (700 mg, 4.5 mmol), and NEt<sub>3</sub> (1.90 mL, 13.5 mmol) were mixed in CH<sub>2</sub>Cl<sub>2</sub> (30 mL). EDC·HCl (960 mg, 5.0 mmol) was added to the mixture in one portion and the resulting mixture was stirred at rt overnight. The reaction was quenched upon the addition of 3 N HCl (50 mL). The layers were separated and the aqueous layer was extracted with CH<sub>2</sub>Cl<sub>2</sub> (3  $\times$  50 mL). The organic layers were combined, further washed

with H<sub>2</sub>O (1 × 50 mL) and brine (1 × 50 mL), and then dried over anhydrous Na<sub>2</sub>SO<sub>4</sub>. The solution was filtered, concentrated over vacuum and charged with silica gel flash chromatography (EtOAc:hexanes 1:9) to give a white solid (*R<sub>f</sub>* = 0.26 in EtOAc:hexanes). Yield: 700 mg, 90%. <sup>19</sup>F NMR (CD<sub>2</sub>Cl<sub>2</sub>, 282.4 MHz, rt): δ(*ppm*) -32.13 (s); <sup>1</sup>H NMR (300 MHz, CD<sub>2</sub>Cl<sub>2</sub>, rt): δ(*ppm*) 2.35 (t, *J* = 2.55 Hz, 1 H), 4.23 (dd, *J*<sub>2</sub> = 5.37 Hz, *J*<sub>2</sub> = 2.8 Hz, 2 H), 6.50 (s, br, 1 H), 7.01 (m, 1 H), 7.34 (m, 2 H); <sup>13</sup>C NMR (100.6 MHz, CD<sub>2</sub>Cl<sub>2</sub>, rt): δ(*ppm*) 29.89, 71.75, 79.23, 106.85, 107.10, 107.36, 110.31, 110.38, 110.49, 110.57, 137.40, 161.81, 161.93, 164.29, 164.41, 164.61; ESI-LRMS: [M+H]<sup>+</sup>: 218.3 (100%).



### Tris-(benzyltriazolylmethyl)amine (TBTA)

Tripropargylamine (354 μL, 2.50 mmol) was dissolved in acetonitrile (5 mL) and cooled over an ice-water bath.<sup>352</sup> Benzyl azide (1 mL, 8.80 mmol), 2, 6-lutidine (291 μL, 2.50 mmol), and Cu(MeCN)<sub>4</sub>PF<sub>6</sub> (55.8 mg, 0.15 mmol) were added to give a brown solution. The reaction mixture was incubated at rt for 3 days and concentrated over rota-evaporation. Then the residue was charged to silica gel flash chromatography (1:99 MeOH:CH<sub>2</sub>Cl<sub>2</sub>) to give a white solid (*R<sub>f</sub>* = 0.42 in 1:9 MeOH:CH<sub>2</sub>Cl<sub>2</sub>). Yield: 0.51 g, 38%. <sup>1</sup>H NMR (300 MHz, *d*<sub>6</sub>-DMSO, rt): δ(*ppm*) 4.29 (s, 6 H), 5.52 (s, 6 H), 7.30 (m, 15 H), 8.34 (s, 3H); ESI-MS: [M+H]<sup>+</sup> 531.5, [M+Na]<sup>+</sup> 553.5.

### Cu(II)-TBTA complex (50 mM)

The stock solution of the copper complex (50 mM) was prepared as follows: CuSO<sub>4</sub> aqueous solution (250 mM, 100 μL) was added to TBTA in <sup>t</sup>BuOH (62.5 mM, 400 μL) to result in a greenish blue solution as there was some precipitation from TBTA. The supernatant was used directly without further treatment.

### 6.5.3 Click reactions between alkynylArBF<sub>3</sub> **6.2** and 5'-N<sub>3</sub>-<sup>31/32</sup>P-ONs

General protocol: alkynylArBF<sub>3</sub> **6.2** in DMSO (1 μL, ~ 15 mM) was added to the azido-oligonucleotide (1 μL, ~ 0.15 mM), followed by the addition of 0.2 M sodium ascorbate (1 μL). 50 mM of Cu-TBTA (1 μL) solution was added to initiate the reaction. The reaction was normally incubated at rt for 0.5 hr. The reaction was quenched upon the addition of 3% LiClO<sub>4</sub> in acetone (400 μL) and followed by centrifugation at 13k rpm for 10-15 min. The pellet was redissolved in the loading buffer (5 μL) and then loaded to 20% polyacrylamide gel (31 cm × 41 cm) for resolution by electrophoresis under 40 W or 10% polyacrylamide gel (20 cm × 20 cm) under 20 W. Then the gel was visualized with the UV shadowing on the TLC plate under UV lamp at 254 nm or exposed to the phosphorimager screen for half an hour if the oligonucleotide was radioactively labeled.

### 6.5.4 The <sup>18</sup>F-radiolabeling of boronic acid **3.11**

<sup>18</sup>O-water was irradiated by proton for 5 min, transferred to the hotcell<sup>a</sup> and collected in a Pyrex glass V-vial (10 mL) with a vent outlet. The radioactivity of the collected <sup>18</sup>O-water was measured and then the solution was passed through an <sup>18</sup>F Trap & Release column. After all the solution was flushed through, the column was measured for radioactivity.<sup>b</sup> Then the radioactivity was released with NaClO<sub>4</sub> solution (1 mL, 2 mg/mL) and the eluent was collected in a Pyrex glass V-vial (5 mL). The pH of the eluent was checked by pH paper and CH<sub>3</sub>CN (1 mL) was added. Then the V-vial was heated over the oil bath at 110 °C under helium flow to concentrate the fluoride to dryness. After the evaporation was done, the V-vial was cooled to rt over He flow and then carrier fluoride solution (0.25 M) was added in the form of KHF<sub>2</sub> to resuspend <sup>18</sup>F-fluoride in the V-vial to give the <sup>18/19</sup>F cocktail. The fluoride cocktail (2 μL, 500 nmol) was transferred to alkynylarylboronic acid **3.11** (100 nmol) in THF (4 μL) mixed with concentrated HCl (0.5 μL, 12 M)<sup>c</sup>. The reaction was incubated at r.t in the hot cell for 0.5 hr and then quenched with 5% NH<sub>4</sub>OH in 50% aqueous EtOH (100 μL). 2μL of the

<sup>a</sup> The irradiation was kindly operated by either Mr. Wade English or Ms. Linda Graham.

<sup>b</sup> Most of the time, more than 95% of the radioactivity can be trapped on the <sup>18</sup>F trap & release column.

<sup>c</sup> The acid addition used to be the last to acidify the reaction. I found that it was much easier to add it prior to the addition of the radioactive fluoride. This can reduce the radiation exposure and minimize the radioactive dose during the experiment.

quenched reaction was diluted in 100  $\mu\text{L}$  of the quench buffer for the HPLC injection to analyze the  $^{18}\text{F}$ -fluoridation reaction.

### **6.5.5 Click reactions on 5'-N<sub>3</sub>-<sup>31/32</sup>P-ONs with alkynyl-<sup>18</sup>F-ArBF<sub>3</sub> 6.2**

The residue of the quenched reaction for alkynyl-<sup>18</sup>F-ArBF<sub>3</sub> **6.2** was added to the oligonucleotide 5'-N<sub>3</sub>-<sup>31/32</sup>P/<sup>31</sup>P-ON, followed by the addition of sodium ascorbate (1  $\mu\text{L}$ , 0.2 M) and Cu(II)-TBTA (1  $\mu\text{L}$ , 50 mM). The reaction was left in the hotcell at rt for 0.5 hr and then 3% LiClO<sub>4</sub> in acetone (1 mL) was added to precipitate the oligonucleotide. The pellet was settled down upon the centrifugation at 13k rpm for 10 min and the supernatant was carefully removed. The pellet was resuspended in DEPC·H<sub>2</sub>O (1  $\mu\text{L}$ ), mixed with the loading buffer (6  $\mu\text{L}$ ), and loaded to a 10% denatured polyacrylamide gel (20 cm  $\times$  20 cm) for gel electrophoresis at 10 W. Then the autoradiographic gel image was recorded on a phosphorimager screen. The phosphorimager screen was exposed with a certain amount of time (such as 10 min) in the cassette and a series of exposure was subjected at different positions of the screen to record the decay process of <sup>18</sup>F-fluorine. After 16 hr, the phosphorimager screen was exposed to the gel for 24 hr to record <sup>32</sup>P signals. The screen was scanned by Amersham 9200 Typhoon phosphorimager and the autoradiographic image was analyzed by ImageQuant 5.2.

## Chapter 7 Labeling folate with $^{18}\text{F}$ -ArBF<sub>3</sub>s

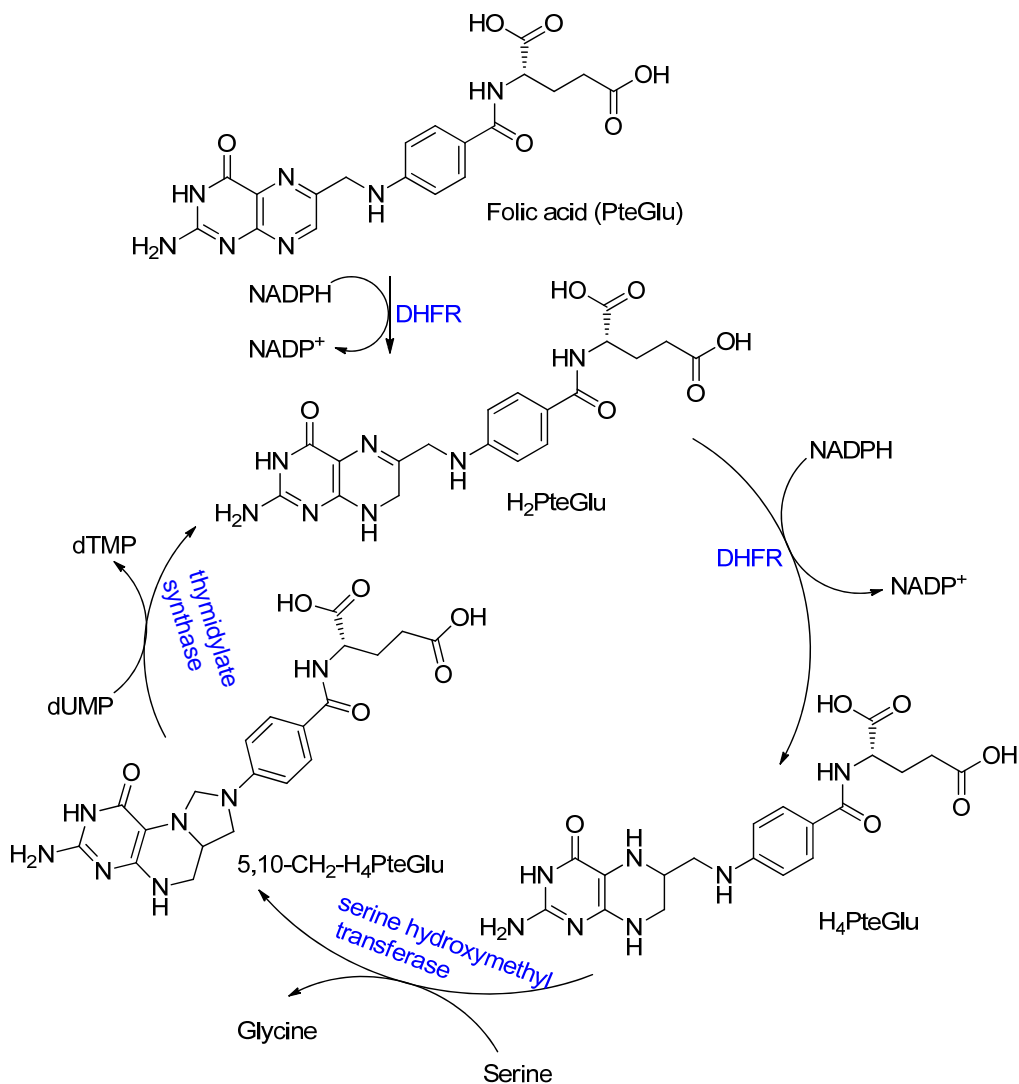
### 7.1 Introduction

#### 7.1.1 Folate and folate receptors

Folic acid, also known as vitamin B<sub>9</sub>, plays many important biological roles in living beings. Folic acid is transferred to several important folate coenzymes, which serve as donors or acceptors of one-carbon units in many bioprocesses such as nucleotide and amino acid metabolism.<sup>359</sup> For example, in the thymidylate synthesis as shown in Scheme 7.1, folic acid is first reduced by folate reductase to tetrahydrofolate (H<sub>4</sub>PteGlu), which is converted to 5,10-methylenetetrahydrofolate (5,10-CH<sub>2</sub>-H<sub>4</sub>PteGlu) by serine hydroxymethyl transferase. Then the methylene on 5,10-CH<sub>2</sub>-H<sub>4</sub>PteGlu is involved in the synthesis of thymidine monophosphate (dTMP) from deoxyuridine monophosphate (dUMP) via reductive methylation catalyzed by thymidylate synthase. The pyrazine ring of H<sub>4</sub>PteGlu also serves as the reducing reagent, which in turn recycles to H<sub>2</sub>PteGlu. Then dTMP is subsequently converted to dTTP that participates in DNA synthesis, which is required for rapid cell division. Accordingly, the biosynthesis of dTMP, mediated by thymidylate synthase, is regarded as the rate-limiting step for DNA synthesis. As tumor cells always upregulate the uptake of folate, such tumor cells can be very aggressive due to their rapid cell division and growth. Hence, the thymidylate synthase and folate reductase are always desirable targets to develop antitumor agents to shut down the biosynthesis of dTMP and eventually eliminate the tumor cells. Via the modification of folate, methotrexate<sup>360</sup> and 10-deazaaminopterin<sup>361, 362</sup> are developed to inhibit folate reductase and/or thymidylate synthase.

On the other hand, folic acid and its derivatives can be delivered to cells mainly by three different transporters.<sup>363</sup> 1), The reduced-folate carrier (RFC),<sup>364</sup> a membrane spanning protein, has high affinity for the reduced form of folic acid, i.e. H<sub>4</sub>PteGlu, and internalizes the reduced folate to cells. However, the RFC has very poor binding affinity for the oxidized form of folate, i.e. folic acid. RFC is widely expressed throughout normal tissues and performs critical roles to transport H<sub>4</sub>PteGlu to cells for the cell

division, and accounts for the daily uptake of folate in the body. 2), The proton-coupled folate transporter<sup>365-367</sup> has been identified as the major transporter of folate under lower pH environments as in the stomach and intestine. 3), Folate receptors (FRs),<sup>368</sup> which constitute a family of glycosylphosphatidylinositol anchored cell-surface glycoproteins, have affinity for folate and derivatives at nanomolar concentrations ( $K_D \sim 10^{-9}$  M).<sup>368-371</sup> The FRs transport folate into cells via receptor-mediated endocytosis.



**Scheme 7.1** The mechanism of the thymidylate synthesis.<sup>359</sup>

PteGlu: pteroyl-glutamic acid (folic acid); DHFR: dihydrofolate reductase; H<sub>2</sub>PteGlu: dihydrofolate; H<sub>4</sub>PteGlu: tetrahydrofolate; 5,10-CH<sub>2</sub>-H<sub>4</sub>PteGlu: 5,10-methylenetetrahydrofolate.

Unlike the RFC, which is present in all cells, FRs are expressed sparsely by normal cells. In healthy cells, FRs are only found to be expressed in limited tissues such as

choroid plexus, thyroid, and kidney.<sup>372</sup> However, most of the FRs expressed in these tissues are inaccessible to circulating folate conjugates, in that these FRs are localized to the “*apical surfaces of polarized epithelia cells*”.<sup>373-375</sup> It has also been discovered that folates trapped in the kidney through glomerular filtration are able to recycle back to the circulation through proximal tubule kidney cells, which express FRs on their apical membranes.<sup>376</sup> In contrast, FRs are highly expressed in some pathologic cells such as in the epithelial cancer cells of the ovary, colon, mammary gland, lung, prostate, nose, throat, and brain.<sup>372, 377-383</sup> With the assistance of abundant FRs for internalizing folic acid, malignant cells are able to aggressively import folate at low folate concentrations ( $\sim 0.2$  to  $2 \times 10^{-7}$  M)<sup>384, 385</sup> from serum and extracellular fluids. This not only allows the tumor cells to grow and the malignant tissue to expand, but also suppresses the proliferation of normal cells. Accordingly, these specific properties make FRs excellent targets for both therapeutics<sup>386</sup> and diagnostics<sup>387</sup> with folate-drug conjugates.<sup>373, 374, 388, 389</sup>

It is believed that the uptake of folate proceeds via receptor-mediated endocytosis.<sup>374, 386, 388-393</sup> Briefly, as shown in Figure 7.1, folate first binds to a FR at the surface of the cell, whereupon the cell membrane locally invaginates to wrap the FR/folate complex to form an endocytic vesicle called the endosome that moves from the cell membrane to the interior of the cell. The pH of the vesicle lumens rapidly drops to  $\sim 5$  due to proton pump activity that is located in the endosome,<sup>394</sup> which stimulates a conformational change in the FR to promote the release of the folate. Meanwhile, the endosomal compartment travels to the recycling center near the cell nucleus. The folate moves to an endosome nearer the nucleus while the free FR moves to a separate endosome to recycle back to the cell surface membrane to start another transport journey. Sometimes drugs conjugated to folate can be released by the cleavage of the linker due to either the lower pH (acid-labile linkers)<sup>394, 395</sup> or reducing power (disulfide linkers)<sup>396, 397</sup> between the extra and intracellular environments. This intricate cellular uptake cycle has been widely used to specifically deliver and release therapeutic drugs and diagnostic agents.

Folic acid can be conjugated with other functional modalities via covalent bonds without sacrificing its affinity for the FR.<sup>390-392</sup> Since FRs are almost always overexpressed on the surface of malignant cells, FRs have been widely targeted for

therapy and diagnosis based on folate conjugates with high specific binding affinity and low off-target toxicity. It has been shown that folate conjugates clear rapidly from FR negative [FR (-)] tissues with a half-life shorter than 10 minutes and the free folate is rapidly excreted from the body.<sup>387</sup>

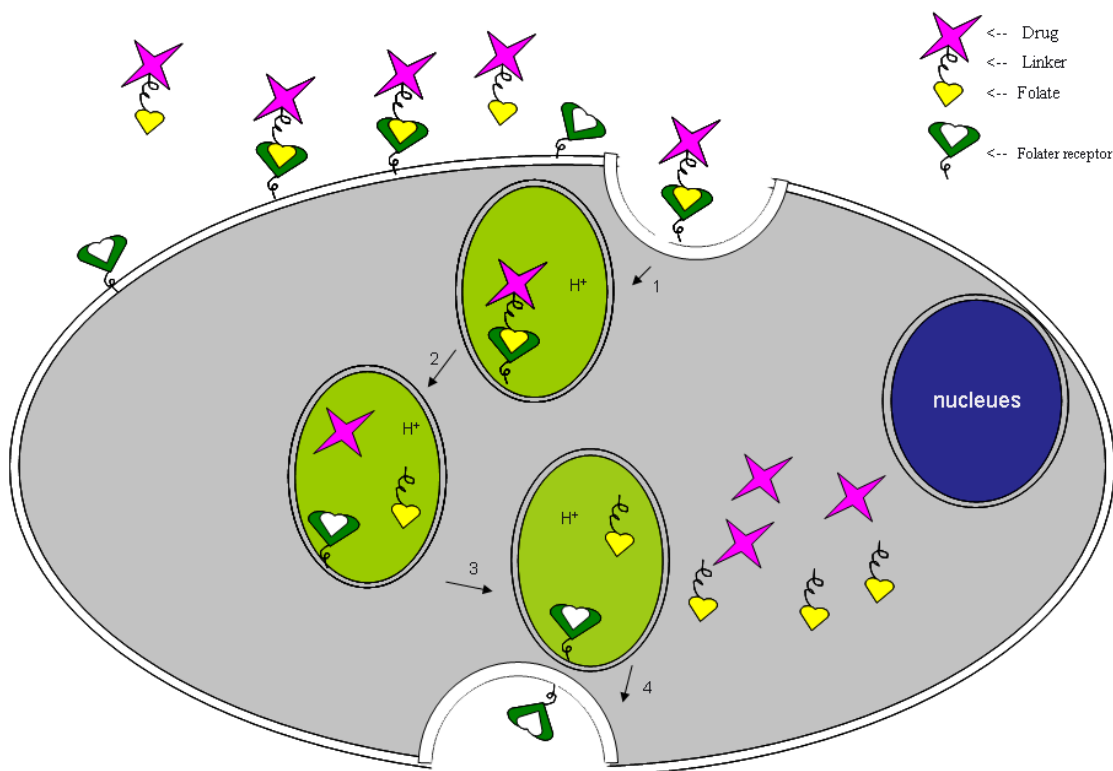


**Figure 7.1 The folate receptor-mediated endocytosis.**

The folate receptor-mediated endocytosis involves four steps.<sup>373, 374, 386, 388, 389</sup> The folate conjugates (folate conjugated to drugs via linkers) bind to folate receptors on the surface of cells and then via membrane invagination to form an endosome to pinch off the surface (step 1 shown in the figure). The endosomal compartment acidifies to not only release folate from the complex but also relieve drugs from the linker, which is acid-labile (step 2 shown in the figure). Sometimes when the linker contains disulfide bond, the disulfide bond would be reductively cleaved by the reducing power between the extra- and intracellular environment. Then the folate conjugate and released drugs may travel to the cytosol (step 3 shown in the figure) and finally most of the folate receptors recycle back to the cell surface to enter another transporting circle (step 4 shown in the figure).

The overexpression of FRs on the surface of malignant cells has aroused attention in terms of designing current therapeutic drugs. One major reason is the indiscriminate nature of many drugs such that they kill virtually all cells in the body, including malignant ones. Conjugating these drugs to folate can increase the specificity to deliver otherwise toxic drugs to target cells where FRs are always overexpressed. This strategy has been successfully used to deliver protein,<sup>391, 398, 399</sup> chemotherapeutic agents,<sup>400</sup>

immunotherapeutic antibodies,<sup>401, 402</sup> liposomes,<sup>403, 404</sup> nanoparticles,<sup>405-407</sup> and gene therapeutic drugs including DNAs,<sup>408, 409</sup> antisense oligodeoxyribonucleotides,<sup>404, 410</sup> viral/non-viral vectors,<sup>411</sup> and siRNAs<sup>412</sup> into FR overexpressing cancer cells.<sup>375, 386</sup> For instance, EC145, one of the folate-targeted *Vinca* alkaloid conjugates, shown in Figure 7.2, is currently in clinical trials and it has showed very promising cancer therapeutic efficacy.<sup>413-416</sup> This compound was designed with a hydrophilic linker containing aspartate and arginine residues to improve the water solubility of the conjugate and also with a reducible disulfide bond to release the cytotoxic drug in the cell after internalization.<sup>413</sup>

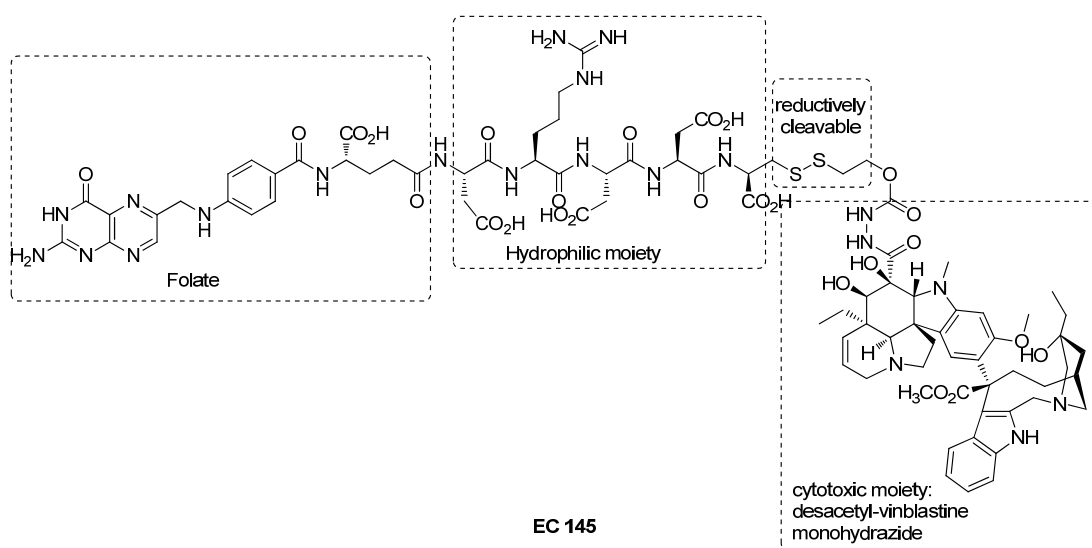


Figure 7.2 The structure of EC145.<sup>413-416</sup>

### 7.1.2 Folate and molecular imaging

Efforts have also been directed to develop imaging agents with folate for diagnosis to better understand/evaluate the antitumor agents' biodistribution, pharmacokinetics, and target specificity *in vivo*.<sup>373, 388, 389, 417</sup> The first folate conjugated imaging compound was an <sup>125</sup>I-labeled histamine derivatized folate.<sup>418</sup> It was found that the radioactive tracer was localized to FR positive [FR (+)] tumor 15 to 30 minutes after injection, while salivary glands and kidney also showed substantial uptake of the radioactivity.

Some magnetic resonance contrast agents for *in vitro* and *in vivo* imaging have also been developed. Wiener and co-workers<sup>419-421</sup> studied <sup>153</sup>Ga-folate-dendrimer for FR (+) tumors and found that the folate-conjugate accumulated with high affinity in the tumor,

while significant kidney uptake was also observed. Chen *et al.*<sup>422</sup> reported an *in vitro* and *in vivo* study on the folate-PEG-conjugated-nanoparticles of superparamagnetic iron oxide as the contrast agent. Internalization of the nanoparticles in the target FR expressing cells and good tumor uptake was also observed. These folate conjugates have demonstrated very good FR targeting properties.

In addition, a near-infrared fluorescent (NIRF) folate conjugate was developed to enhance detection of FR (+) tumors.<sup>423, 424</sup> Specific tumor uptake was similarly observed. It was found that only the FR (+) tumor had strong fluorescence uptake, which could be blocked by the pretreatment with unlabeled folate. It was also found that tumor enhancement would persist over 48 hours. Moreover, the maximum signal-to-background ratio observed at 24 hours in the FR (+) tumor was 3:1. It is therefore believed that this NIRF folate-conjugate will be useful for improved detection of FR (+) tumors.

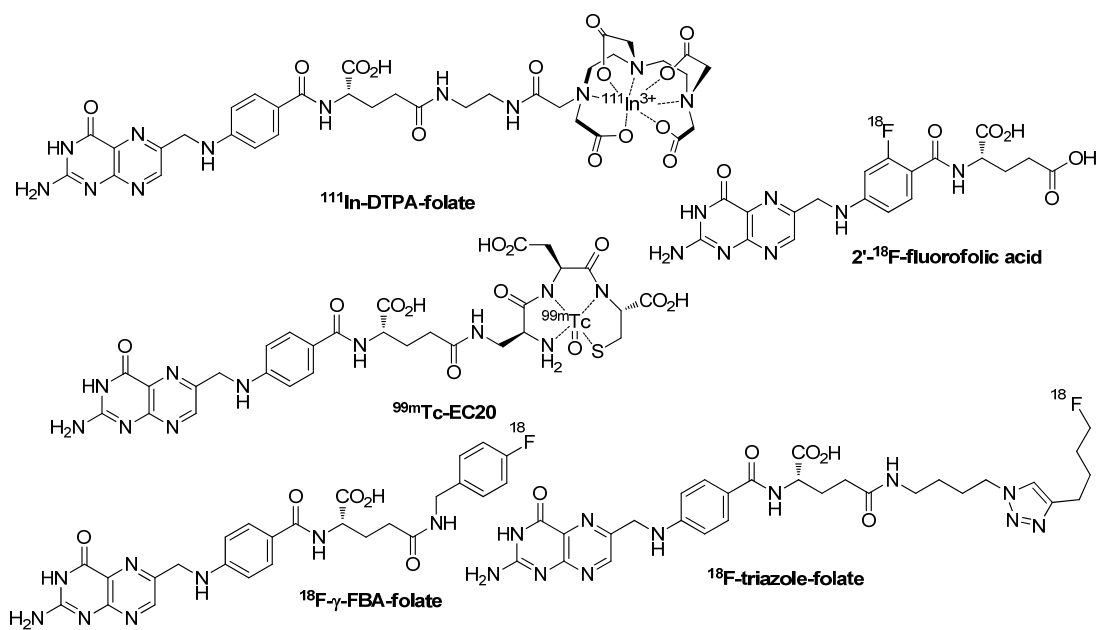


**Figure 7.3** Several radiolabeled folate conjugates.<sup>302, 387, 425-427</sup>

Labeling folate with radionuclides for SPECT and PET has received a great deal of attention and several of the radiolabeled folate conjugates are featured in Figure 7.3. A <sup>67</sup>Ga-deferoxamine-folate<sup>428, 429</sup> was prepared and its *in vivo* study showed a high tumor-to-background ratio, though it seemed part of the <sup>67</sup>Ga-labeled compound was excreted via the hepatobiliary route into intestines. To create a better radiotracer with optimal biodistribution and clearance from the body into urine, the same group

synthesized  $^{111}\text{In}$ -labeled diethylenetriamine pentaacetic acid (DTPA)-folate and the radiotracer was rapidly cleared from blood and excreted predominantly in the urine, while high and specific tumor uptake was observed.<sup>425, 430, 431</sup> Both  $^{67}\text{Ga}$ -labeled and  $^{111}\text{In}$ -labeled folates exhibited relatively high accumulation in the kidney.<sup>425, 429</sup> The high cost of  $^{111}\text{In}$  production led scientists to switch to the more easily available and low cost radiometals such as  $^{99\text{m}}\text{Tc}$  whose shorter half-life (6 hr) allows a higher injected radionuclide dose. A series of  $^{99\text{m}}\text{Tc}$ -labeled folates have been reported in the literature.<sup>278, 387, 432-435</sup> All the  $^{99\text{m}}\text{Tc}$ -labeled folates demonstrated rapid *in vivo* clearance, and specific and high tumor uptake, along with kidney uptake.<sup>278, 387, 433</sup> For example, a  $^{99\text{m}}\text{Tc}$ -tripeptide conjugated folate EC20 ( $^{99\text{m}}\text{Tc}$ -Cys-Asp-Dap-*D*-Glu-Pte)<sup>387</sup> was found to be one of the best ligands to deliver  $^{99\text{m}}\text{Tc}$  to the target. A  $^{99\text{m}}\text{Tc}$ -labeled triazole-folate derivative<sup>278</sup> via a “click-to-chelate” method was studied and interestingly it indicated that the triazole group formed via the “click reaction” is an outstanding “tripodal ligand system” for chelating  $\text{M}(\text{CO})_3\text{s}$  to provide more stable complexes, while the targeting specificity is not adversely affected.

In addition to the folate imaging agents labeled with metallic radionuclides, a few  $^{18}\text{F}$ -labeled folate compounds have been synthesized and studied. Bettio *et al.*<sup>426</sup> prepared an  $^{18}\text{F}$ - $\alpha/\gamma$ -fluorobenzylamine (FBA)-folate via a 3 step radiosynthesis with radiochemical yields ranging from 15% to 44% and a specific activity of 0.64 Ci/ $\mu\text{mol}$ . Compared to  $^{18}\text{F}$ -FDG,  $^{18}\text{F}$ - $\alpha/\gamma$ -FBA-folate showed superior tumor uptake in nude mice bearing KB-31 FR (+) tumors. As the work of Bettio *et al.* suggests the  $\gamma$ -regioisomer showed slightly better binding affinity, a two-step synthesis involving “click chemistry” was achieved for an  $^{18}\text{F}$ - $\gamma$ -conjugated folate ( $^{18}\text{F}$ -triazole-folate) with a radiochemical yield of 25-30% and a specific activity of  $4.3 \pm 1.9$  Ci/ $\mu\text{mol}$  within 90 minutes of synthesis.<sup>302</sup> This radiotracer showed very promising *in vitro* properties, and according to the *in vivo* biodistribution studies, the compound demonstrated high specificity for FRs. Both  $^{18}\text{F}$ - $\alpha/\gamma$ -FBA-folate and  $^{18}\text{F}$ - $\gamma$ -triazole-folate showed prominent kidney uptake and strong hepatobiliary excretion to the intestines.<sup>302, 426</sup> Recently, 2'- $^{18}\text{F}$ -fluorofolic acid was reported with a  $K_i$  value of 1.8 nM, which is very close to the native folic acid (1.1 nM), and it showed similar *in vivo* imaging patterns in the KB tumor xenografted nude

mice as the folate conjugates labeled with metallic radionuclides previously reported.<sup>427</sup> Additionally, only moderate hepatobiliary elimination was observed with this <sup>18</sup>F-labeled folate.

Nearly all the chemotherapeutic and imaging studies have proven that folate conjugates can specifically recognize the FRs in malignant cells *in vitro* and/or *in vivo* without significant loss of their binding affinity compared with native folic acid.<sup>374, 388, 389, 417</sup> *In vivo* studies have also suggested that folate conjugates exhibit relatively fast clearance in blood. Besides tumor uptake, there is always substantial uptake of the folate conjugates in the kidney.<sup>421, 425, 429</sup> In some studies, hepatobiliary excretion<sup>a</sup> of the folate conjugates led to strong accumulation of the folate tracers in the abdominal region.<sup>302, 388, 426</sup>

### 7.1.3 Labeling folate with ArBF<sub>3</sub>s

It is still under debate whether the  $\alpha$ - or  $\gamma$ -carboxylic acid of folic acid is more important for the receptor binding affinity. Early studies suggested that conjugation through either the  $\alpha$ - or  $\gamma$ -carboxylate with drugs made no difference in terms of their association with FR (+) cells.<sup>399, 426</sup> Leamon and co-workers<sup>399</sup> replaced the glutamic acid of folic acid with glycine and the resulting Pte-Gly showed no less binding affinity to FRs, which suggests the glutamate residue is not critical for FR recognition. Bettio *et al.*<sup>426</sup> tested the  $\alpha$ - and  $\gamma$ -regioisomers of folate-fluorobenzylamide and found IC<sub>50</sub>s of 71  $\pm$  8 and 62  $\pm$  6 nM for  $\alpha$ - and  $\gamma$ -regioisomers respectively, both of which are comparable to native folic acid's binding affinity (IC<sub>50</sub> of 41 nM). In contrast, other studies showed the free  $\alpha$ -carboxylic acid is critical for the FR binding affinity.<sup>428, 430</sup> Both the competitive binding studies of <sup>67</sup>Ga-deferoxamine-folate<sup>428</sup> and the work on <sup>111</sup>In-DTPA-folate<sup>430</sup> disclosed that only the  $\gamma$ -regioisomer of the radiotracer is recognized specifically by the FRs on KB cells. Despite some controversy,  $\gamma$ -regioselectively derivatized folate-conjugates are always prepared preferentially over  $\alpha$ -derivatized regioisomers.

There is also issue of linker arm chemistry when conjugating folate with drugs,

---

<sup>a</sup> Hepatobiliary excretion is a process of drug clearance in the liver. Briefly, drugs can be taken up to the hepatocytes from circulation by transporters and/or passive diffusion and then digested by metabolism and/or biliary excretion.<sup>436, 437</sup>

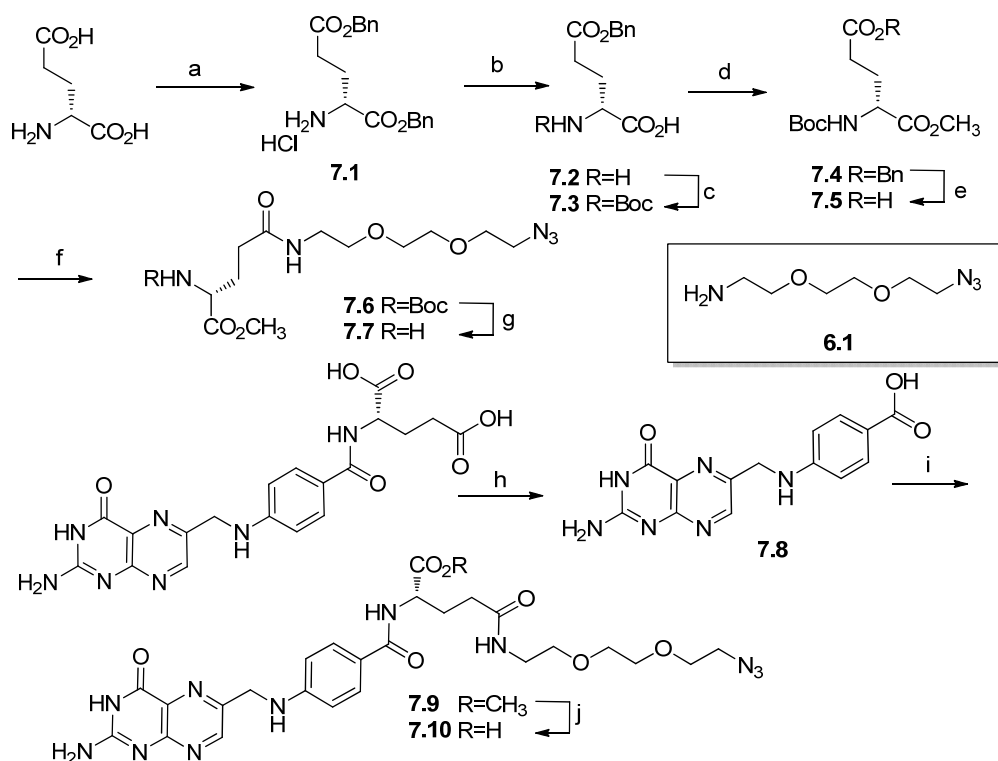
especially for larger molecules like proteins and antibodies.<sup>399</sup> Leamon and co-workers showed that when they tried to label folate with momordin, a ribosome inactivating protein, the conjugated toxin showed a low EC<sub>50</sub> to cells.<sup>399</sup> Based on the previous study, however, the folate conjugate could be internalized into cells in the same fashion as folic acid by FRs. Thus, they concluded that the close proximity of the FR and the protein might afford unknown interactions, which would prevent the FR from adopting the correct conformation that would release the folate conjugates at pH ~ 5 and cause the folate-conjugate/FR complex to recycle unproductively back to the membrane. In addition to the linker length, the hydrophilicity/lipophilicity of the linker should be considered. Reasonable hydrophilicity is very important for the circulation clearance and excretion pathways.<sup>302</sup> Hydrophilic polyethylene glycol (PEG) linkers are almost always used to link folate with other molecules to reduce the lipophilicity for favorable *in vivo* pharmacokinetic properties of the drugs.<sup>411, 438</sup>

The goal in this chapter is to label folate with an <sup>18</sup>F-ArBF<sub>3</sub> that could be used to image cancers overexpressing FRs. Since folate is an established bioligand for *in vivo* imaging, folate-<sup>18</sup>F-ArBF<sub>3</sub> can clarify various questions that remain for the labeling technique using <sup>18</sup>F-ArBF<sub>3</sub>s as PET imaging agents. Moreover, the negatively charged ArBF<sub>3</sub> can possibly improve the hydrophilicity of folate-ArBF<sub>3</sub> and therefore favor rapid excretion to avoid/decrease the hepatobiliary excretion. On the other hand, since folate is known to have low solubility under acidic aqueous conditions (pH < 3), it is therefore not practical to prepare the folate-boronate for the direct fluoridation under acidic conditions. Combining all the concerns discussed earlier, we chose to synthesize a  $\gamma$ -conjugated-azido-(PEG)<sub>2</sub>-folate (Pte-Glu[(PEG)<sub>2</sub>N<sub>3</sub>]-OH) **7.10** and then adopt a one-pot two-step labeling method as described in Chapter 6 for labeling oligonucleotides. In brief, a prosthetic group alkynyl-<sup>18</sup>F-ArBF<sub>3</sub> **6.2** was first prepared and then coupled to Pte-Glu[(PEG)<sub>2</sub>N<sub>3</sub>]-OH **7.10** via copper(I) catalyzed click chemistry to give folate-<sup>18</sup>F-ArBF<sub>3</sub> with reasonable radiochemical yields.

## 7.2 Results

### 7.2.1 Synthesis of Pte-Glu[(PEG)<sub>2</sub>N<sub>3</sub>]-OH 7.10

The two carboxylic acid groups on folic acid have very close chemical reactivity and it is thus difficult to differentiate them in most reactions. Although it has been reported in several literature reports that the derivatization on the  $\gamma$ -position of folic acid could be achieved by directly EDC or DCC coupling in the presence of the  $\alpha$ -carboxylic acid,<sup>403, 405, 439, 440</sup> the desired  $\gamma$ -derivatized product is always contaminated with the  $\alpha$ -conjugated regioisomer and/or the bis-derivatized compound.<sup>390, 441</sup> This not only decreases the yield, but also complicates the purification process. And ultimately any clearance by regulatory agencies will require pure compositions. Instead, we decided to follow one literature method<sup>302, 442</sup> with various modifications to prepare Pte-Glu[(PEG)<sub>2</sub>N<sub>3</sub>]-OH 7.10 as summarized in Scheme 7.2.



**Scheme 7.2** Synthesis of Pte-Glu[(PEG)<sub>2</sub>N<sub>3</sub>]-OH 7.10.

(a), i. *N,N,N',N'*-Tetramethylguanidine, DMF, 0 °C, 0.5 hr, ii. ethyl acetoacetate, rt, till clear, iii. BnCl, rt, 24 hr, iv. 1.25 M HCl/MeOH, 46% over four steps; (b), i. CuSO<sub>4</sub>, NaOH, EtOH, H<sub>2</sub>O, rt, 1 hr, ii. EDTA·2Na, H<sub>2</sub>O, boiled, 20 min, 43% over two steps; (c), (Boc)<sub>2</sub>O, NEt<sub>3</sub>, dioxane/H<sub>2</sub>O, 0 °C to rt, 24 hr, 94%; (d), CH<sub>3</sub>I, K<sub>2</sub>CO<sub>3</sub>, DMF, rt, 36 hr, 90%; (e), 10% Pd/C, THF, H<sub>2</sub>, rt, 24 hr, 95%; (f), **6.1**, EDC·HCl, HOBT·H<sub>2</sub>O, NEt<sub>3</sub>, CH<sub>2</sub>Cl<sub>2</sub>, rt, overnight, 92%; (g), 27% TFA/CH<sub>2</sub>Cl<sub>2</sub>, rt, 3 hr, 85%; (h), TFAA, rt, 3 days, 43%; (i), HBTU, DIPEA, DMSO, rt, 36 hr, 58%; (j), 1 N NaOH, rt, overnight, 78%.

Briefly, the carboxylic groups of glutamic acid were protected as benzyl esters via MacLaren's method.<sup>246, 247</sup> First of all, the  $\alpha$ -amino group was transiently converted to an imine with ethyl acetoacetate, whereupon the intermediate was esterified with benzyl chloride. The acid treatment successfully unmasked the amino group to provide *bis*-benzyl ester H-Glu(OBn)-OBn **7.1** in a moderate yield of 46%. Then the benzyl group on the  $\alpha$ -carboxylic group was selectively removed by saponification in the presence of copper(II) to form the copper(II) complex, which was then treated with EDTA to give the  $\gamma$ -benzyl protected glutamic acid **7.2**. Following *N*-Boc protection on the amino group, methylation of the  $\alpha$ -carboxylate and the Pd/C catalyzed hydrogenolysis of the  $\gamma$ -benzyl ester, Boc-Glu-OCH<sub>3</sub> **7.5** was obtained and coupled with azido-PEG-amine **6.1** using EDC as the dehydrating reagent to yield **7.6**. Upon TFA incubation, the Boc-protecting group of **7.6** was removed in a high yield of 85%. Compound **7.7** was then coupled to pteric acid **7.8**, which was obtained from the hydrolysis of folic acid.<sup>443</sup> Finally, the saponification of methyl ester **7.9** was undertaken to provide the desired product Pte-Glu[(PEG)<sub>2</sub>N<sub>3</sub>]-OH **7.10**, which was further purified via RP-HPLC. The overall yield of the synthesis of **7.10** was 5.6% over nine steps starting from (*L*)-glutamic acid.

It is worth commenting on the coupling reaction between H-Glu[(PEG)<sub>2</sub>N<sub>3</sub>]-OCH<sub>3</sub> **7.7** and pteric acid **7.8**. Pteric acid **7.8** was initially activated by EDC·HCl/HOBt·H<sub>2</sub>O with pyridine as the base, and the reaction resulted in many components as shown in Figure 7.4. In contrast, activation with HBTU provided much cleaner results and a higher yield. Since the EDC coupling provided many byproducts that challenged the purification, the HBTU coupling was thereafter used for this derivatization. A reevaluation of the coupling reaction with EDC/HOBt suggested that using NEt<sub>3</sub> as the base largely improved the reaction. It implied that pyridine as a weaker base used earlier might be the source of the low yielding reaction when using EDC as the dehydrating agent.

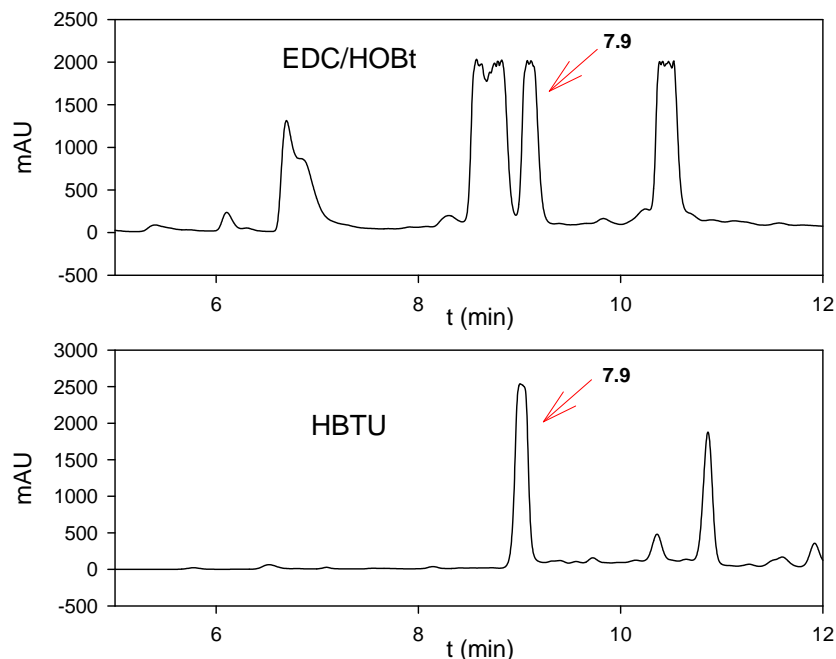


**Figure 7.4 The preparation of Pte-Glu[(PEG)<sub>2</sub>N<sub>3</sub>]-OCH<sub>3</sub> 7.9 using different coupling reagents.** The top HPLC chromatogram (at 292 nm, 5 to 12 min is shown) was for the coupling reaction using EDC/HOBt as the activating agents and the bottom one (at 292 nm, 5 to 12 min shown) was that with HBTU coupling. The HPLC was performed via HPLC Program 10 with Column I in HPLC System I. Reaction for the top HPLC trace: H-(L)-Glu[(PEG)<sub>2</sub>N<sub>3</sub>]-OCH<sub>3</sub>·TFA 7.7, pteric acid 7.8, EDC·HCl, HOBt·H<sub>2</sub>O, Py, DMSO, rt, 5 d., 31%; that for the bottom HPLC trace: H-(L)-Glu[(PEG)<sub>2</sub>N<sub>3</sub>]-OCH<sub>3</sub>·TFA 7.7, pteric acid 7.8, HBTU, DIPEA, DMSO, rt, 36 hr, 58%. The arrows in the chromatograms indicate the desired product, which was verified by ESI-LRMS.

## 7.2.2 Click reactions between Pte-Glu[(PEG)<sub>2</sub>N<sub>3</sub>]-OH 7.10 and alkynes

The click reaction involving Pte-Glu[(PEG)<sub>2</sub>N<sub>3</sub>]-OH 7.10 was first studied with the fluorescent alkyne 6.4, which had been used as a reference alkyne for the click reaction in Chapter 6. CuSO<sub>4</sub> and sodium ascorbate were used since they have been reported as the efficient combination to generate the Cu(I) catalyst used in the 1,3-dipolar cycloaddition. As shown in Figure 7.5, more than 50% of 7.10 was consumed and a new product was simultaneously produced 15 minutes after initiation of the reaction. The peak was then collected and characterized with ESI-LRMS spectrometry ([M-H]<sup>-</sup>: 894.6), which suggested that the click reaction proceeded in a rapid and efficient fashion.

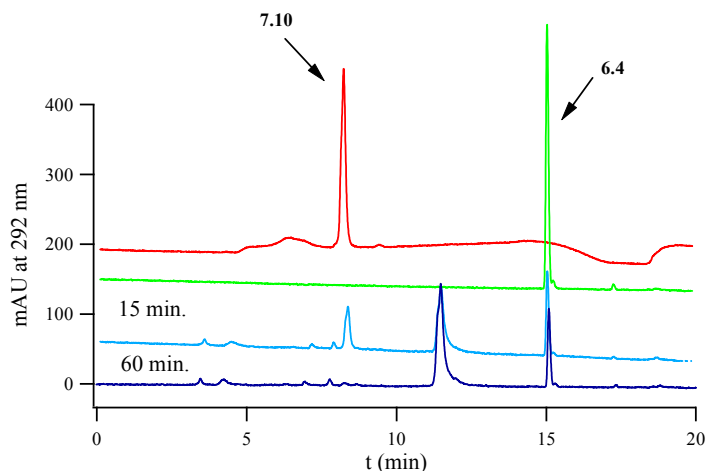


**Figure 7.5** The click reaction between **6.4** and **7.10** monitored by HPLC.

HPLC traces (UV traces at 292 nm) from the top to the bottom: the red HPLC trace was for Pte-Glu[(PEG)<sub>2</sub>N<sub>3</sub>]-OH **7.10**, and the green one was for alkyne coumarin **6.4**; both the blue one (15 min) and the purple one (60 min) were for the click reaction between **6.4** and **7.10**. The condition for the click reaction: **6.4** (442 nmol), **7.10** (308 nmol), CuSO<sub>4</sub> (50 nmol), and sodium ascorbate (400 nmol) in 1:4:5 DMSO:CH<sub>3</sub>CN:H<sub>2</sub>O (100 μL), rt. The reaction was monitored by HPLC, which was performed via Program 17 with Column I in HPLC System I.

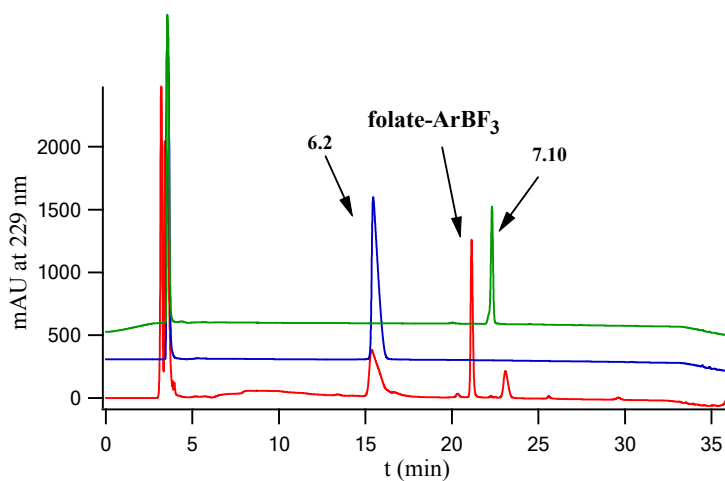


**Figure 7.6** The click reaction between **6.2** and **7.10** monitored by HPLC.

HPLC chromatograms (UV traces at 229 nm) from the top to the bottom: the green HPLC trace was for Pte-Glu[(PEG)<sub>2</sub>N<sub>3</sub>]-OH **7.10**, the blue one was for alkynylArBF<sub>3</sub> **6.2** and the red one was for the click reaction between **6.2** and **7.10**. The condition for the click reaction: **6.2** in DMSO (10 μL, concentration not determined), 10 mM of **7.10** (10 μL, 100 nmol), 0.45 M of CuSO<sub>4</sub> (2 μL, 900 nmol), and 2 M of sodium ascorbate (3 μL, 6 μmol), rt for 1 hr and 0.04 M HCO<sub>2</sub>NH<sub>4</sub> (150 μL) was added to the reaction prior to the HPLC injection. The reaction was monitored by HPLC that was performed via Program 15 with Column I in HPLC System I.

Then the click reaction between alkynylArBF<sub>3</sub> **6.2** and **7.10** was undertaken under similar conditions. However, due to the high polarity of both folic acid and alkynylArBF<sub>3</sub> **6.2**, HCO<sub>2</sub>NH<sub>4</sub>/CH<sub>3</sub>CN was found to be a suitable HPLC solvent system to analyze the

reaction. With a bit more catalyst loading in the case indicated in Figure 7.6, compound **7.10** was consumed within 39 minutes. The newly produced peak at 21.1 minutes was collected and characterized with mass spectrometry to identify the desired product ( $[M]^+$ : 859.6 and  $[M-HF]^+$ : 839.6). From the HPLC chromatogram, one can see that the product has a very close retention time to that of Pte-Glu[(PEG)<sub>2</sub>N<sub>3</sub>]-OH **7.10** yet shows very good resolution from alkynylArBF<sub>3</sub> **6.2**.

### 7.2.3 Radiolabeling folate with the <sup>18</sup>F-ArBF<sub>3</sub> via click chemistry

The initial study for the radiolabeling of folate with the <sup>18</sup>F-ArBF<sub>3</sub> was undertaken in collaboration with the CPDC in Hamilton, ON. The one-pot two-step synthesis was carried out to label folic acid with the <sup>18</sup>F-ArBF<sub>3</sub>. The radiosynthesis of alkynyl-<sup>18</sup>F-ArBF<sub>3</sub> **6.2** was undertaken with a similar protocol described in Chapter 6. Following incubation for 20-30 minutes at room temperature, the <sup>18</sup>F-fluoridation of alkynylarylboronic acid **3.11** was quenched with 5% NH<sub>4</sub>OH in 50% aqueous EtOH. Then the quenched reaction was transferred to a solution of Pte-Glu[(PEG)<sub>2</sub>N<sub>3</sub>]-OH **7.10** in DMSO, followed by addition of sodium ascorbate and CuSO<sub>4</sub> to initiate the click reaction. The click reaction was incubated at room temperature for 30 to 120 minutes prior to the HPLC analysis, the results of which are summarized in Table 7.1. One of the experiments is displayed in Figure 7.7.

**Table 7.1 A summary of the click reactions between 6.2 and 7.10 under radioactive conditions.**

#	Radioactivity (mCi) <sup>a</sup>	RCY1 (%) <sup>b</sup>	QR (μL/μL) <sup>c</sup>	7.10 (μL) <sup>d</sup>	CuSO <sub>4</sub> (μL) <sup>e</sup>	t (min) <sup>f</sup>	Conversion (%) <sup>g</sup>	Overall RCY (%) <sup>h</sup>
1	0.647	40	30/100	3	1	46	37	12
2	2.17	41	100/200	4	2	118	60	16
3	0.544	37	25/50	5	2	42	74	19
4	1.53	26	25/50	10	2	85	99	17

**NOTE:** RCY: radiochemical yield; QR: quenched reaction for alkynyl-<sup>18</sup>F-ArBF<sub>3</sub> **6.2**. <sup>a</sup> The radioactivity at the BOS of the click reaction between alkynyl-<sup>18</sup>F-ArBF<sub>3</sub> **6.2** and Pte-Glu[(PEG)<sub>2</sub>N<sub>3</sub>]-OH **7.10**; <sup>b</sup> The RCY1 is the radiochemical yield for the radiolabeling synthesis of <sup>18</sup>F-**6.2**; <sup>c</sup> the volume of the QR used for the click reaction/the total volume of the QR; <sup>d</sup> the concentration of **7.10** was 10 mM; <sup>e</sup> the concentration of CuSO<sub>4</sub> was 0.2 M; <sup>f</sup> the reaction time for the click reaction; <sup>g</sup> the yield based on the incorporation of <sup>18</sup>F-**6.2** (which eluted at 3.31 min) into the folate to give the desired product folate-<sup>18</sup>F-ArBF<sub>3</sub> via click chemistry (which eluted at 2.64 min); <sup>h</sup> the overall RCY based on folate-<sup>18</sup>F-ArBF<sub>3</sub>. The Reaction conditions: alkynylboronic acid **3.11** (100 nmol), HCl (6.3 μmol), and the <sup>18</sup>F-fluoride solution containing <sup>18</sup>F-fluoride (312.5 nmol, in the form of KHF<sub>2</sub>) in 70% aqueous THF (5.75 μL), rt, 30 min, the reaction was quenched with 5% NH<sub>4</sub>OH in 50% aqueous EtOH; then the quenched reaction from the first reaction, 10 mM Pte-Glu[(PEG)<sub>2</sub>N<sub>3</sub>]-OH **7.10** in DMSO, 0.2 M sodium ascorbate (2 μL for reaction #1, and 4 μL for other reactions), 0.2 M CuSO<sub>4</sub>, rt.

Figure 7.7 shows the HPLC traces of the one-pot two-step radiosynthesis for reaction 1, indicated in Table 7.1 under the stated conditions. The fluoridation of alkynylboronic acid **3.11** proceeded with a very high radiochemical yield (40%) in a relatively short reaction time of 30 minutes. Without purification of the  $^{18}\text{F}$ -prosthetic synthon alkynyl- $^{18}\text{F}$ -ArBF<sub>3</sub> **6.2**, the second reaction also proceeded rapidly. However, given the conditions described therein, only 37% of alkynyl- $^{18}\text{F}$ -ArBF<sub>3</sub> **6.2** produced in the first step was incorporated to give the desired radiolabeled product folate- $^{18}\text{F}$ -ArBF<sub>3</sub>.

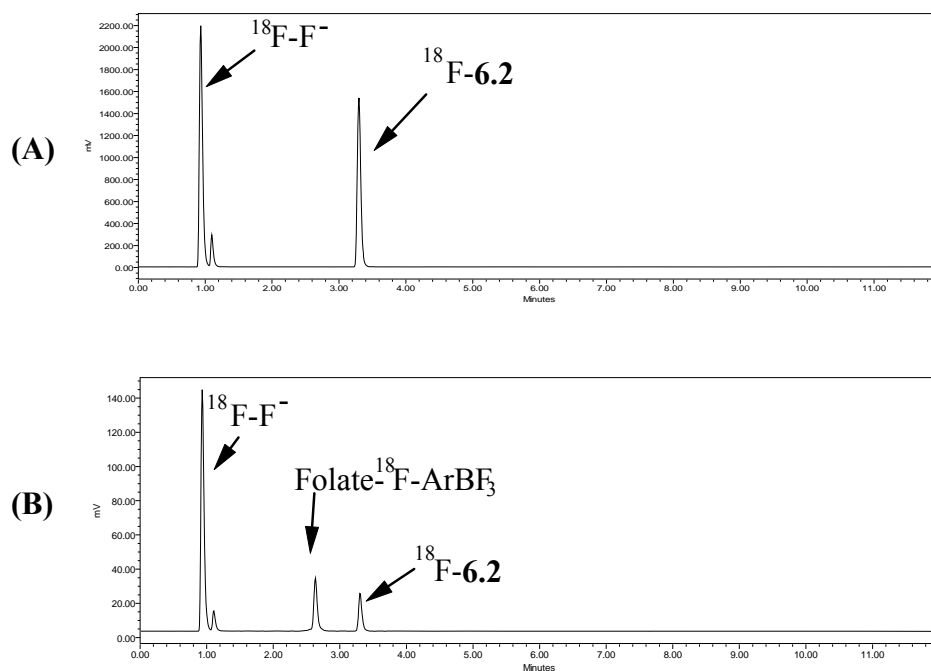


**Figure 7.7 The one-pot two-step radiolabeling of folate from alkynyl- $^{18}\text{F}$ -ArBF<sub>3</sub> **6.2** via click chemistry.**

The top UPLC trace was for the analysis of the preparation of alkynyl- $^{18}\text{F}$ -ArBF<sub>3</sub> **6.2** ( $^{18}\text{F-6.2}$ ) and the bottom trace was for the click reaction between the crude mixture of alkynyl- $^{18}\text{F}$ -ArBF<sub>3</sub> **6.2** and Pte-Glu[(PEG)<sub>2</sub>N<sub>3</sub>]-OH **7.10**. The radio-UPLC was performed via HPLC Program 6 with Column III in HPLC System III. The reaction conditions: alkynylboronic acid **3.11** (100 nmol), HCl (6.3  $\mu\text{mol}$ ), and the  $^{18}\text{F}$ -fluoride solution containing  $^{19}\text{F}$ -fluoride (312.5 nmol, in the form of KHF<sub>2</sub>), 70% aqueous THF (5.75  $\mu\text{L}$ ), rt, 30 min, the reaction was quenched with 5% NH<sub>4</sub>OH in 50% aqueous EtOH (100  $\mu\text{L}$ ), the radioactivity at the BOS: 5.54 mCi and RCY: 40%; then the quenched solution from the first reaction (30  $\mu\text{L}$ ), 10 mM Pte-Glu[(PEG)<sub>2</sub>N<sub>3</sub>]-OH **7.10** in DMSO (3  $\mu\text{L}$ ), 0.2 M sodium ascorbate (2  $\mu\text{L}$ ), 0.2 M CuSO<sub>4</sub> (1  $\mu\text{L}$ ), rt, 46 min. The radioactivity at the the beginning of the click reaction: 647  $\mu\text{Ci}$  and the overall RCY: 12%.

The relatively low conjugation yield of prosthetic synthon **6.2** to azide **7.10** shown in Figure 7.7 was further improved by adding more Pte-Glu[(PEG)<sub>2</sub>N<sub>3</sub>]-OH **7.10** as well as by using a higher catalyst loading to the reaction. As shown in Table 7.1, different amounts of **7.10** and CuSO<sub>4</sub> were applied to the click reaction. Moreover, due to the

addition of different volumes of the quenched reaction mixture of alkynyl- $^{18}\text{F}$ -ArBF<sub>3</sub> **6.2**, different final concentrations of reaction components were achieved. Unfortunately, the reaction times varied for each reaction due to the availability of the radio-UPLC. This led to uncontrolled delays in the analysis of the experiments and reflects some of the practical difficulties of doing radiochemistry. Nonetheless, improvement in the conjugation of  $^{18}\text{F}$ -ArBF<sub>3</sub> **6.2** was achieved by decreasing the amount of quench buffer added to the first reaction, and an increasing amount of the azide substrate **7.10** and CuSO<sub>4</sub>. For instance, there was a higher catalyst loading in reaction 2 than reaction 1, while slightly more dilute conditions were used in reaction 2. Nonetheless, a higher chemical conversion was achieved for reaction 2 with a longer reaction time. As expected, the increasing amount of catalyst *in situ* results in a faster reaction. Between reactions 2 and 3, higher concentrations of all reaction components in reaction 3 clearly enhanced the conversion of alkynyl- $^{18}\text{F}$ -ArBF<sub>3</sub> **6.2** even for a shorter reaction time. The reaction was then further improved by excess presence of Pte-Glu[(PEG)<sub>2</sub>N<sub>3</sub>]-OH **7.10** and nearly a full conversion was achieved.

Based on the work I did at the CPDC in ON, I then repeated the same labeling work at TRIUMF in BC. With slightly different HPLC conditions and in a different working environment, similar results have been obtained as shown in Figure 7.8 and Figure 7.9. In Figure 7.8A, the fluoridation to prepare alkynyl- $^{18}\text{F}$ -ArBF<sub>3</sub> **6.2** had a radiochemical yield of 34% following a reaction time of 37 minutes. The subsequent copper(I) catalyzed click reaction was undertaken with about 1/3 of the quenched fluoridation reaction and Pte-Glu[(PEG)<sub>2</sub>N<sub>3</sub>]-OH **7.10** at room temperature for 20 minutes. From the radio-HPLC chromatogram, only 47% of alkynyl- $^{18}\text{F}$ -ArBF<sub>3</sub> **6.2** was conjugated to folate **7.10**. Nevertheless, the HPLC chromatogram recorded under 292 nm illustrated in Figure 7.8B provided good separation between folate- $^{18}\text{F}$ -ArBF<sub>3</sub> and the unreacted **7.10**. In spite of the incomplete conversion of alkynyl- $^{18}\text{F}$ -ArBF<sub>3</sub> **6.2**, the overall radiochemical yield over two steps leading to folate- $^{18}\text{F}$ -ArBF<sub>3</sub> was 16% after a total reaction time of 57 minutes. By increasing the concentration of Pte-Glu[(PEG)<sub>2</sub>N<sub>3</sub>]-OH **7.10**, a full conversion of alkynyl- $^{18}\text{F}$ -ArBF<sub>3</sub> **6.2** to folate- $^{18}\text{F}$ -ArBF<sub>3</sub> was achieved with an overall radiochemical yield of 25% in a total synthesis of 83 minutes as shown in Figure 7.9.

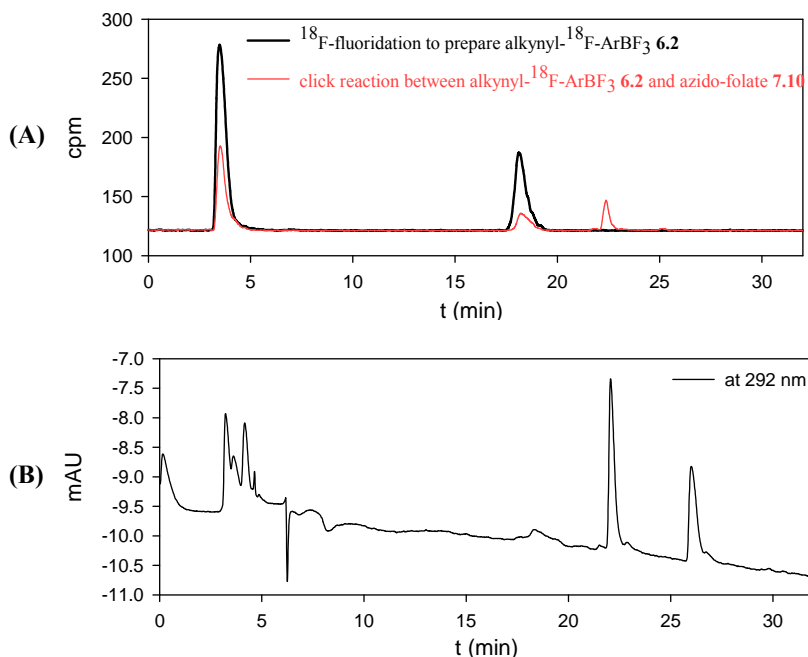


**Figure 7.8 The one-pot two-step radiosynthesis of folate- $^{18}\text{F}$ -ArBF $_3$ .**

(A) The radiolabeling chromatograms for the two steps: the black HPLC trace was for the analysis of the radiosynthesis of alkynyl- $^{18}\text{F}$ -ArBF $_3$  **6.2** and the red trace was for the click reaction of the crude mixture of  $^{18}\text{F}$ -**6.2** with Pte-Glu[(PEG) $_2$ N $_3$ ]-OH **7.10**. (B) The HPLC trace recorded at 292 nm for the click reaction between  $^{18}\text{F}$ -**6.2** and **7.10**. The HPLC was performed via HPLC Program 7 with Column I in HPLC System IV. Reaction conditions: alkynylboronic acid **3.11** (100 nmol), HCl (6.3  $\mu\text{mol}$ ) and the  $^{18}\text{F}$ -fluoride solution containing  $^{19}\text{F}$ -fluoride (500 nmol, in the form of KHF $_2$ ) in 61.5% aqueous THF (6.5  $\mu\text{L}$ ), rt, 37 min, and the reaction was quenched with 5% aqueous NH $_4$ OH in (30  $\mu\text{L}$ ), the radioactivity at the BOS: 6.05 mCi and RCY: 34%; then the quenched solution from the first reaction (8  $\mu\text{L}$ ), 10 mM Pte-Glu[(PEG) $_2$ N $_3$ ]-OH **7.10** in DMSO (2  $\mu\text{L}$ ), 0.6 M sodium ascorbate (4  $\mu\text{L}$ ), 0.2 M CuSO $_4$  (2  $\mu\text{L}$ ), rt, 20 min, the radioactivity at the beginning of the click reaction: 0.89 mCi and the overall RCY: 16% for folate- $^{18}\text{F}$ -ArBF $_3$ .

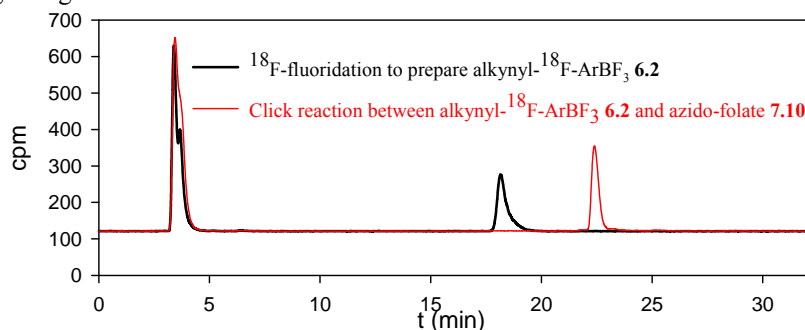


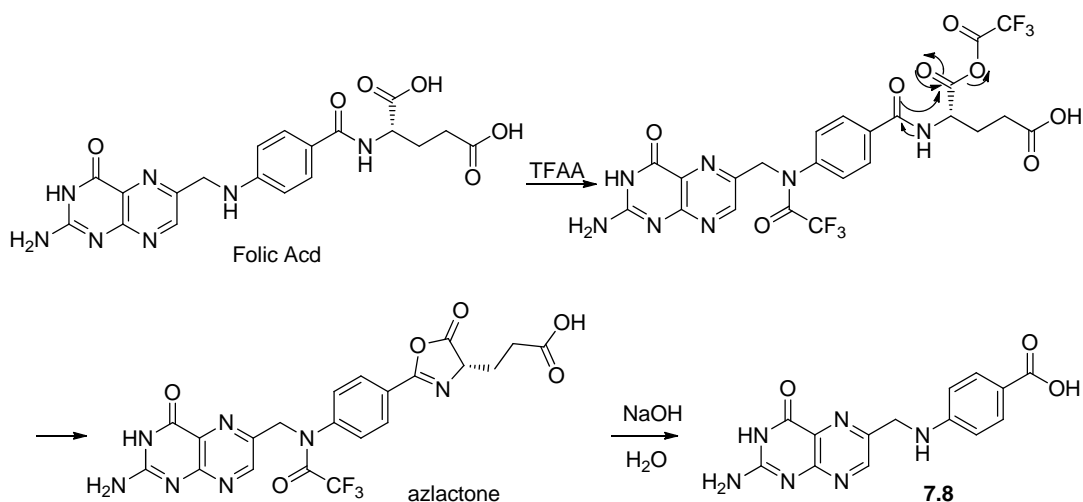
**Figure 7.9 The radio-HPLC chromatograms of the one-pot two-step radiolabeling of folate with the  $^{18}\text{F}$ -ArBF $_3$  via click chemistry.**

The black HPLC trace was for the analysis of the radiosynthesis of  $^{18}\text{F}$ -ArBF $_3$  **6.2** and the red trace was for the click reaction of the crude mixture of **6.2** with Pte-Glu[(PEG) $_2$ N $_3$ ]-OH **7.10**. The radio-HPLC was performed via HPLC Program 7 with Column I in HPLC System IV. Reaction conditions: alkynylboronic acid **3.11** (100 nmol), HCl (6.3  $\mu\text{mol}$ ), and the  $^{18}\text{F}$ -fluoride solution containing  $^{19}\text{F}$ -fluoride (500 nmol, in the form of KHF $_2$ ) in 61.5% aqueous THF (6.5  $\mu\text{L}$ ), rt, 35 min, and the reaction was quenched with 5% aqueous NH $_4$ OH in (30  $\mu\text{L}$ ), the radioactivity at the BOS: 6.26 mCi and RCY: 29%; then the quenched solution from the first reaction (10  $\mu\text{L}$ ), 10 mM Pte-Glu[(PEG) $_2$ N $_3$ ]-OH **7.10** in DMSO (5  $\mu\text{L}$ ), 0.6 M sodium ascorbate (2  $\mu\text{L}$ ), 0.2 M CuSO $_4$  (2  $\mu\text{L}$ ), rt, 48 min, the radioactivity at the beginning of the click reaction: 1.80 mCi and the overall RCY: 25%.

## 7.3 Discussion

### 7.3.1 Synthesis of Pte-Glu[(PEG)<sub>2</sub>N<sub>3</sub>]-OH 7.10

Pte-Glu[(PEG)<sub>2</sub>N<sub>3</sub>]-OH **7.10** was prepared via a modified protocol with an overall yield of 5.6%. Instead of the direct derivatization of folic acid to prepare **7.10**, conjugation between the pteronic residue and the glutamate residue was undertaken using HBTU as the dehydrating agent. This allowed us to selectively introduce an azide functionality to the  $\gamma$ -carboxylic group of glutamic acid while blocking the reactivity of the  $\alpha$ -amino group and  $\alpha$ -carboxylic group, which were protected with Boc and methyl ester respectively. TFA was used to remove the Boc-protecting group from the amino group and enable the synthesis of compound **7.7** as one of the key synthons for further elaboration by standard peptide synthesis methods.



Scheme 7.3 The proposed mechanism of the synthesis of pteronic acid **7.8**.

Pteronic acid **7.8** was prepared via hydrolysis of folic acid following two steps: the azlactone is first formed in the presence of the dehydrating agent TFAA from folic acid and then the azlactone subsequently hydrolyzes under basic conditions to give pteronic acid **7.8** as the desired product. The possible mechanism suggested in the literature<sup>443</sup> is summarized in Scheme 7.3. Briefly, folic acid reacts with TFAA to form the mixed anhydride with  $\alpha$ -carboxylic group, while the  $N^{10}$ -amino group is protected by the trifluoroacetyl at the same time. The amide-oxygen tends to attack the  $\alpha$ -carboxylic acid anhydride to form the azlactone (also called oxazolone) compound. This azlactone

rapidly hydrolyzes under basic conditions to give pteronic acid **7.8**, which might follow a fashion of saponification.

The conjugation of **7.8** to the glutamate derivative **7.7** was found to be more efficient with HBTU as the coupling reagent. However, with further optimization of the coupling reaction using EDC/HOBt as the dehydrating agents, the nature of the organic base seemed to be critical and indeed use of a stronger base,  $\text{NEt}_3$ , provided better synthesis. Following a simple saponification of **7.9**, the synthesis was complete to give the final product **7.10**, which was further purified via HPLC. The synthesis comprises nine steps with an overall yield of 5.6% starting from (*L*)-glutamic acid.

### 7.3.2 Click reactions between Pte-Glu[(PEG)<sub>2</sub>N<sub>3</sub>]-OH **7.10** and alkynes

The combination of  $\text{CuSO}_4$  and sodium ascorbate was used for the click reaction between Pte-Glu[(PEG)<sub>2</sub>N<sub>3</sub>]-OH **7.10** and alkynes in this chapter, as they are very efficient for click conjugation.<sup>295, 296, 299</sup> Since the folate compounds always have low solubility in various solvents, a DMSO stock solution (10 mM) was made, and for each click reaction, a certain amount of the stock solution was used.

To check the reactivity of Pte-Glu[(PEG)<sub>2</sub>N<sub>3</sub>]-OH **7.10** as well as to determine the conditions for the click reaction, the fluorescent alkynyl derivatized coumarin **6.4** was first used to study the click reaction with **7.10**. As shown in Figure 7.5, the reaction occurred in a rapid fashion. After 15 minutes, more than half of **7.10** was consumed with 16.7 mol% catalyst Cu(I) and the reaction was complete within one hour. A close examination of the HPLC traces suggested that only one product, eluting at 11.5 minutes, was produced. This was highly suggestive of the fact that the reaction proceeded with high regioselectivity. The product peak was then collected and characterized via ESI-LRMS to confirm it to be the desired product. Therefore we concluded that the click reaction worked quite efficiently under the conditions used. Since both DMSO and sodium ascorbate have nearly no absorption at 292 nm, they were absent in the HPLC traces shown in Figure 7.5.

Similar conditions were used for the click reaction between alkynylArBF<sub>3</sub> **6.2** and Pte-Glu[(PEG)<sub>2</sub>N<sub>3</sub>]-OH **7.10**. Unlike alkynylcoumarin **6.4**, the concentration of **6.2** was

not determined due to the relative difficulty in removing DMSO, which was used to extract **6.2** from insoluble KF and KHF<sub>2</sub>. Nevertheless, based on the <sup>19</sup>F NMR spectrum, the concentration of **6.2** was roughly determined to be around 30 mM. For the click reaction between **6.2** and **7.10**, a higher amount of CuSO<sub>4</sub>/sodium ascorbate was used. As displayed in Figure 7.6, the new peak appearing at 21.1 minutes was collected and characterized with ESI-LRMS to give a mass of 859.3 at the negative mode, which represented the desired folate-ArBF<sub>3</sub>. As pointed out earlier, since both the folate and the ArBF<sub>3</sub> are very polar, they tend to elute very fast in the RP-HPLC while acidic conditions are ill-advised due to the acid lability of ArBF<sub>3</sub>s.<sup>164, 252</sup> We finally found a reasonable solvent system (0.04 M HCO<sub>2</sub>NH<sub>4</sub>/CH<sub>3</sub>CN), the pH of which is ~ 5, to provide reasonable retention time and nice separation of folate-ArBF<sub>3</sub> from the precursors.

Overall, the click reaction between Pte-Glu[(PEG)<sub>2</sub>N<sub>3</sub>]-OCH<sub>3</sub> **7.10** and alkynes occurred rapidly and in high yields based on the HPLC chromatograms. CuSO<sub>4</sub>/sodium ascorbate have proven to be very efficient in catalyzing the 1,3-dipolar cycloaddition reaction between Pte-Glu[(PEG)<sub>2</sub>N<sub>3</sub>]-OCH<sub>3</sub> **7.10** and alkynes. Moreover, alkynylArBF<sub>3</sub> **6.2** showed reasonable reactivity in the click reaction while the C-B bond also manifested very high stability under the click reaction conditions.

### 7.3.3 Radiolabeling folate with the <sup>18</sup>F-ArBF<sub>3</sub> via click chemistry

The radiolabeling of alkynylarylboronic acid **3.11** and the subsequent click reaction with Pte-Glu[(PEG)<sub>2</sub>N<sub>3</sub>]-OCH<sub>3</sub> **7.10** have been undertaken at two research institutes: the CPDC in Hamilton, ON and TRIUMF in Vancouver, BC. The practice of the one-pot two-step radiolabeling synthesis via copper(I) catalyzed click chemistry was successful at both institutes. This demonstrates the reproducibility of this work, an important aspect to consider for time sensitive radiochemistry, wherein seemingly trivial details at different locations might determine whether or not the same work can be reproduced.

Based on the results we obtained at the CPDC, the reaction rate is both catalyst and concentration dependent as indicated in Table 7.1, which is to say that a higher catalyst loading, an excess amount of Pte-Glu[(PEG)<sub>2</sub>N<sub>3</sub>]-OCH<sub>3</sub> **7.10**, and higher concentrations

of all reagents always facilitate the reaction to give a greater conversion. This is consistent with the general principle of chemical reactions. However, the overall radiochemical yield (17%) for the 4<sup>th</sup> reaction in Table 7.1 was actually lower than that of the radiochemical yield (26%) for the first radiofluoridation of alkynylarylboronic acid **3.11**. Although no work was done to determine the loss of the radiochemical yield, it is believed that either partial defluoridation of alkynyl-<sup>18</sup>F-ArBF<sub>3</sub> **6.2** or the precipitation of the desired product folate-<sup>18</sup>F-ArBF<sub>3</sub> might account for the phenomenon.

The radiolabeling experiments regarding this method undertaken at TRIUMF provided different HPLC chromatograms from those obtained at the CPDC. This is common since different HPLC systems, columns, and gradients were used. Nevertheless, similar results were obtained. As shown in Figure 7.8A and Figure 7.9, the click reaction successfully incorporated the <sup>18</sup>F-ArBF<sub>3</sub> into the folate. Moreover, it again implies that the excess of Pte-Glu[(PEG)<sub>2</sub>N<sub>3</sub>]-OH **7.10** and a high catalyst loading with a reasonably high concentration are important considerations to achieve good yields. And, for the reaction shown in Figure 7.9, a full conversion from alkynyl-<sup>18</sup>F-ArBF<sub>3</sub> **6.2** to folate-<sup>18</sup>F-ArBF<sub>3</sub> was achieved by a click reaction of 48 minutes. Even though the overall radiochemical yield from 10% to 30% is considered somewhat modest, it is quite respectable compared with many other reported methods.

Although no solvolytic study on the folate-ArBF<sub>3</sub> derived from this click technique has been undertaken in this chapter, the same ArBF<sub>3</sub> that had been conjugated to biotin has been previously reported in our group to have a half-life of > 1000 minutes in 200 mM phosphate buffer at pH 7.4,<sup>130</sup> and the solvolytic half-life of marimastat-ArBF<sub>3</sub> **4.15**, bearing a slightly different aromatic system, was measured to be 1236 minutes in Chapter 4. It is believed that folate-ArBF<sub>3</sub> obtained in the one-pot two-step synthesis should have a similar solvolytic half-life of 1000 minutes at least.

## 7.4 Conclusion and perspectives

Pte-Glu[(PEG)<sub>2</sub>N<sub>3</sub>]-OH **7.10** was synthesized in this chapter with a reasonable overall yield. We then studied the copper(I) catalyzed click reaction between alkynylArBF<sub>3</sub> **6.2** and Pte-Glu[(PEG)<sub>2</sub>N<sub>3</sub>]-OH **7.10** non-radioactively or radioactively for the one-pot

two-step labeling strategy. The preliminary results were very encouraging. The introduction of an  $\text{ArBF}_3$  onto the folate should not significantly influence its binding affinity towards folate receptors. As the ESI-MS already suggested the successful conjugation between alkynyl $\text{ArBF}_3$  **6.2** and Pte-Glu[(PEG)<sub>2</sub>N<sub>3</sub>]-OCH<sub>3</sub> **7.10**, the future *in vitro* biological investigation of folate- $\text{ArBF}_3$  would to some point validate its potential applications to image tumors overexpressing FRs. And eventually, the animal imaging work will definitely provide enough information to clarify whether or not the  $^{18}\text{F}$ - $\text{ArBF}_3$  is a reasonable PET imaging ligand.

## 7.5 Materials and methods

Reagents and solvents were purchased from Fisher, Sigma-Aldrich, Alfa-Aesar, Novabiochem or Oakwood. All chemicals were used as supplied unless stated otherwise. The  $^{18}\text{F}$  Trap & Release column ( $\text{HCO}_3^-$  form, ~ 10 mg) was purchased from ORTG, Inc. Deuterated solvents were obtained from Cambridge Isotope Laboratories. Analytical thin layer chromatography was performed on Silica Gel 60 F<sub>254</sub> Glass TLC plates from EMD Chemicals and SiliaFlash F60 from Silicycle was used for flash chromatography. All NMR spectra were recorded at room temperature on a Bruker Avance 300 or 400 MHz spectrometer. Chemical shifts are reported using the  $\delta$  scale in *ppm* and all coupling constants (*J*) are reported in hertz (Hz). Unless specified,  $^1\text{H}$  NMR spectra are referenced to the tetramethylsilane peak ( $\delta = 0.00$  *ppm*), and  $^{13}\text{C}$  NMR spectra are referenced to the chloroform peak ( $\delta = 77.23$  *ppm*). Mass spectrometry was performed at the Mass Spectrometry lab of the UBC Chemistry Department. The HPLC information is available in Appendix B.

**WARNING:** All  $^{18}\text{F}$ -labeling work was done at TRIUMF or at the CPDC. Radiation protection procedures strictly followed the TRIUMF Radiation Safety Regulations. Since this work involves mainly manual handling, fairly high amounts of dosage might be applied, and special caution is required to reduce the operating time. A lead brick castle was built up to shield the radiation. All the materials that came in contact with the source water (the  $^{18}\text{O}$ -water) were collected and decayed separately from other  $^{18}\text{F}$ -contaminated stuffs including gloves, sleeves, vials, tubes, and pipette tips prior to disposal.

### **H-(L)-Glu(OBn)-OBn·HCl (7.1)<sup>246, 247</sup>**

(L)-H-Glu-OH (1.47 g, 10.0 mmol) was suspended in DMF (10.0 mL) over an ice-water bath. *N,N,N',N'*-Tetramethylguanidine (2.5 mL, 20 mmol) was added to the slurry and stirred at 0 °C for 0.5 hr. Ethyl acetoacetate (1.26 mL, 10.0 mmol) was added in one portion to the mixture and the ice-H<sub>2</sub>O bath was then removed. The reaction was stirred at rt till all solids dissolved. Then benzyl chloride (2.3 mL, 20 mmol) was added slowly and the resulting mixture was stirred at rt for 24 hr. The reaction was quenched by 1 N NaHCO<sub>3</sub> (50 mL) and extracted with EtOAc (3 × 50 mL). The organic layer was combined, washed with 1 N NaHCO<sub>3</sub> (1 × 50 mL), H<sub>2</sub>O (3 × 50 mL) and brine (1 × 50 mL), and then dried over anhydrous Na<sub>2</sub>SO<sub>4</sub>. The solution was filtered and the solvent was removed by evaporation. The residue was suspended in MeOH (4 mL) and added with 1.25 M HCl in MeOH (16 mL) in one portion. The mixture was gently shaken at rt for 10 min. The solvent was removed under vacuum and Et<sub>2</sub>O (300 mL) was added to the residue to result in precipitation. The solid was filtered off, washed with Et<sub>2</sub>O and then recrystallized from MeOH/Et<sub>2</sub>O to give a white powder as the desired product. Yield: 1.66 g, 46%. <sup>1</sup>H NMR (300 MHz, *d*<sub>6</sub>-MeOD, rt): δ(*ppm*) 2.21 (m, 2 H), 2.56 (m, 2 H), 4.16 (t, *J* = 6.75 Hz, 1 H), 5.12 (s, 2 H), 5.26 (s, 2 H), 7.37 (m, 10 H); ESI-LRMS: [M+H]<sup>+</sup>, 328.3(100).

### **H-(L)-Glu(OBn)-OH (7.2)**

H-(L)-Glu(OBn)-OBn·HCl **7.1** (10.0g, 27.5 mmol) was suspended in EtOH (150 mL) and CuSO<sub>4</sub>·5H<sub>2</sub>O in H<sub>2</sub>O (170 mL). The mixture was then stirred at ~ 32 °C and 1 N NaOH was added to adjust pH to ~ 8. The reaction was stirred for 1 hr and slowly turned to dark grey. Then the mixture was acidified to pH 3 with 3 N HCl carefully to result in a purplish blue slurry. The mixture was cooled down over an ice-water bath and then filtered off. The precipitate was washed with H<sub>2</sub>O, EtOH, and Et<sub>2</sub>O, and dried over high vacuum to give a blue powder (6.46 g, 12.1 mmol). The solid, without further purification, was suspended in H<sub>2</sub>O (120 mL) with EDTA·2Na (10.3 g, 27.6 mmol), and boiled for 20 min, and the reaction was filtered while hot. The filtrate was cooled to rt to give white crystals. The solid was filtered off, washed with cold H<sub>2</sub>O, EtOH, and Et<sub>2</sub>O, and dried over vacuum to give white flake crystals. Yield: 2.82 g, 43%. <sup>1</sup>H NMR (400

MHz,  $d_6$ -DMSO, rt):  $\delta(ppm)$ : 1.94 (m, 1 H), 2.11 (m, 2 H), 2.30 (m, 1 H), 4.04 (dd,  $J_1 = 8.93$  Hz,  $J_2 = 4.29$  Hz, 1 H), 4.49 (s, 2 H), 5.09 (s, 1 H), 7.30 (m, 6 H), 7.89 (s, 1 H).

### **Boc-(L)-Glu(OBn)-OH (7.3)**

H-(L)-Glu(OBn)-OH **7.2** (393.7 mg, 1.66 mmol) was dissolved in dioxane/H<sub>2</sub>O (1:1, 5 mL) and cooled to 0 °C. (Boc)<sub>2</sub>O (543 mg, 2.49 mmol) was added in one portion to the mixture followed by the slow addition of NEt<sub>3</sub> (465  $\mu$ L, 3.32 mmol). The reaction was incubated at rt for 24 hr and then acidified with 3 N HCl to pH 1. The reaction was extracted with EtOAc (3  $\times$  50 mL). The organic layers were combined, washed with brine (1  $\times$  50 mL), and dried with Na<sub>2</sub>SO<sub>4</sub>. The solution was filtered and the solvent was removed. The residue was charged to silica gel chromatography (100% EtOAc) to give colorless oil as the desired product ( $R_f = 0.25$  in 100% EtOAc). Yield: 525 mg, 94%. <sup>1</sup>H NMR (400 MHz, CDCl<sub>3</sub>, rt):  $\delta(ppm)$  1.27 (s, 9 H), 2.07 (m, 1 H), 2.29 (m, 1 H), 2.54 (m, 2 H), 4.39 (m, 1 H), 5.15 (s, 2 H), 7.37 (m, 5 H), 9.2 (s, br, 1 H); <sup>13</sup>C NMR (100.6 MHz, CDCl<sub>3</sub>, rt):  $\delta(ppm)$  28.40, 30.50, 52.93, 60.61, 66.71, 80.54, 128.36, 128.41, 128.69, 135.84, 155.79, 172.88, 176.31; ESI-LRMS: [M+Na]<sup>+</sup>, 360.4 (100%).

### **Boc-(L)-Glu(OBn)-OCH<sub>3</sub> (7.4)**

Boc-(L)-Glu(OBn)-OH **7.3** (3.61 g, 10.7 mmol) and K<sub>2</sub>CO<sub>3</sub> (18.0 g, 130 mmol) were suspended in DMF (50 mL) and cooled to 0 °C. Then CH<sub>3</sub>I (7.0 mL, 107 mmol) was added dropwise to the slurry and the resulting mixture was stirred at rt for 36 hr. The reaction was then quenched with H<sub>2</sub>O (50 mL) and the mixture was extracted with EtOAc (3  $\times$  100 mL). The EtOAc layers were combined, washed with saturated NaHCO<sub>3</sub> (1  $\times$  50 mL), H<sub>2</sub>O (3  $\times$  50 mL) and brine (1  $\times$  50 mL), and dried over anhydrous Na<sub>2</sub>SO<sub>4</sub>. The drying agent was filtered off and the solvent was removed under vacuum. The residue was purified with flash chromatography (EtOAc:hexanes 1:4) to afford the desired product ( $R_f = 0.19$  in 1:4 EtOAc:hexanes). Yield: 3.37 g, 90%. <sup>1</sup>H NMR (300 MHz, CDCl<sub>3</sub>, rt):  $\delta(ppm)$  1.46 (s, 9 H), 2.03 (m, 1 H), 2.25 (m, 1 H), 2.50 (m, 2 H), 3.75 (s, 3 H), 4.39 (m, 1 H), 5.14 (s, 2 H), 7.38 (m, 5 H); <sup>13</sup>C NMR (75.5 MHz, CDCl<sub>3</sub>, rt):  $\delta(ppm)$  27.92, 28.44, 30.42, 52.57, 52.97, 66.66, 80.22, 128.42, 128.73, 135.92, 172.66, 172.84; ESI-LRMS: [M+Na]<sup>+</sup>, 374.4 (100%).

### **Boc-(L)-Glu-OCH<sub>3</sub> (7.5)**

Boc-(L)-Glu(OBn)-OCH<sub>3</sub> **7.4** (3.37 g, 9.59 mmol) and 10% Pd/C (1.5 g) was mixed in THF (30 mL) under a H<sub>2</sub> atmosphere at rt for 24 hr. Then the mixture was filtered over Celite and the Celite was washed with THF. The THF solution was concentrated over vacuum and the residue was charged to silica gel chromatography (EtOAc:hexanes 1:3 to 1:1) to give the desired product as colorless oil (*R<sub>f</sub>* = 0.10 in 1:1 EtOAc:hexanes). Yield: 2.38 g, 95%. <sup>1</sup>H NMR (400 MHz, CDCl<sub>3</sub>, rt): δ(*ppm*) 1.45 (s, 9 H), 1.97 (m, 1 H), 2.20 (m, 1 H), 2.48 (m, 2 H), 3.76 (s, 3 H), 4.38 (m, 1 H), 5.27 (d, *J* = 7.60 Hz, 1 H), 10.34 (s, br, 1 H); <sup>13</sup>C NMR (100.6 MHz, CDCl<sub>3</sub>, rt): δ(*ppm*) 27.71, 28.38, 30.16, 52.58, 52.89, 60.60, 80.35, 155.65, 172.86, 177.95; ESI-HRMS: calcd. for C<sub>11</sub>H<sub>19</sub>NO<sub>6</sub>Na<sup>+</sup>: 284.1110, found 284.1116.

### **Boc-(L)-Glu[(PEG)<sub>2</sub>N<sub>3</sub>]-OCH<sub>3</sub> (7.6)**

Boc-(L)-Glu-OCH<sub>3</sub> **7.5** (262 mg, 1.0 mmol), N<sub>3</sub>-PEG-NH<sub>2</sub> **6.1** (192 mg, 1.1 mmol) and HOBt·H<sub>2</sub>O (160 mg, 1.05 mmol) in CH<sub>2</sub>Cl<sub>2</sub> (10.0 mL) was added with NEt<sub>3</sub> (419 μL, 3.0 mmol) and EDC·HCl (210 mg, 1.1 mmol). The mixture was then stirred at rt overnight and quenched by 3 N HCl (30 mL). The layers were separated and the aqueous layer was further extracted with CH<sub>2</sub>Cl<sub>2</sub> (3 × 50 mL). The CH<sub>2</sub>Cl<sub>2</sub> layers were combined, washed with H<sub>2</sub>O (1 × 50 mL) and brine (1 × 50 mL), and dried over anhydrous Na<sub>2</sub>SO<sub>4</sub>. The sodium salt was filtered off and the solution was concentrated over vacuum. The resulting residue was charged with column chromatography (MeOH:CH<sub>2</sub>Cl<sub>2</sub> 1:99) to afford colorless oil as the desired product (*R<sub>f</sub>* = 0.62 in 1:9 MeOH:CH<sub>2</sub>Cl<sub>2</sub>). Yield: 382 mg, 92%. <sup>1</sup>H NMR (400 MHz, CDCl<sub>3</sub>, rt): δ(*ppm*) 1.44 (s, 9 H), 1.96 (m, 1 H), 2.18 (m, 1 H), 2.26 (m, 2 H), 3.39 (t, *J* = 4.80 Hz, 2 H), 3.46 (m, 2 H), 3.56 (t, *J* = 4.98 Hz, 2 H), 3.64 (m, 4 H), 3.69 (t, *J* = 4.96 Hz, 2 H), 3.74 (s, 3 H), 4.29 (s, br, 1 H), 5.33 (s, br, 1 H), 6.27 (s, br, 1 H); <sup>13</sup>C NMR (100.6 MHz, CDCl<sub>3</sub>, rt): δ(*ppm*) 28.44, 28.76, 32.54, 39.43, 50.77, 52.48, 53.22, 69.94, 70.24, 70.37, 70.67, 80.12, 172.04, 172.91; ESI-HRMS: calcd. for C<sub>17</sub>H<sub>31</sub>N<sub>5</sub>O<sub>7</sub>Na<sup>+</sup>: 440.2121, found 440.2126.

### **H-(L)-Glu[(PEG)<sub>2</sub>N<sub>3</sub>]-OCH<sub>3</sub>·TFA (7.7)**

Boc-(L)-Glu[(PEG)<sub>2</sub>N<sub>3</sub>]-OCH<sub>3</sub> **7.6** (348 mg, 0.91 mmol) in CH<sub>2</sub>Cl<sub>2</sub> (11 mL) was added with TFA (4 mL) and the mixture was stirred at rt for 3 hr. The solvent was removed and the residue was directly charged with silica gel flash chromatography (MeOH:CH<sub>2</sub>Cl<sub>2</sub> 5:95 to 1:9) to give colorless oil (*R<sub>f</sub>* = 0.18 in 1:9 MeOH:CH<sub>2</sub>Cl<sub>2</sub>). Yield: 295 mg, 85%. <sup>1</sup>H NMR (400 MHz, CDCl<sub>3</sub>, rt): δ(*ppm*) 2.25 (m, 1 H), 2.32 (m, 1 H), 2.50 (t, *J* = 6.34 Hz, 2 H), 3.40 (m, 4 H), 3.55 (t, *J* = 5.02 Hz, 2 H), 3.65 (m, 6 H), 3.8 (s, 3 H), 4.15 (m, 1 H), 7.01 (s, 1 H), 8.66 (s, br, 2 H); <sup>13</sup>C NMR (100.6 MHz, CDCl<sub>3</sub>, rt): δ(*ppm*) 25.96, 31.91, 39.60, 50.76, 52.74, 53.45, 69.48, 70.07, 70.24, 70.55, 169.78, 172.66. ESI-LRMS: [M+H]<sup>+</sup>, 318 (100%).

### **Pteric acid (7.8)**

Folic acid (2.00 g, 4.55 mmol) in neat TFAA (40 mL) was stirred at rt for 3 days. The solvent was then removed.<sup>443</sup> NaOH (8.0 g, 0.20 mol) in H<sub>2</sub>O (40 mL) was added to the residue and the resulting slurry was stirred at rt for 2 hr. Then the solution was acidified with concentrated HCl to pH ~ 1 and filtered<sup>a</sup>. The solid was thoroughly washed with H<sub>2</sub>O, MeOH, and Et<sub>2</sub>O, and dried over vacuum to give a brown powder as the desired product. Yield: 607 mg, 43%. <sup>1</sup>H NMR (400 MHz, *d*<sub>6</sub>-DMSO, rt): δ(*ppm*) 4.52 (s, 2 H), 6.64 (d, *J* = 8.68 Hz, 2 H), 7.65 (d, *J* = 8.64 Hz, 2 H), 8.69 (s, 1 H). ESI-LRMS: [M+H]<sup>+</sup>, 357.2 (100%).

### **Pte-Glu[(PEG)<sub>2</sub>N<sub>3</sub>]-OCH<sub>3</sub> (7.9)**

Pteric acid (620 mg, 2.00 mmol) **7.8**, H-(L)-Glu[(PEG)<sub>2</sub>N<sub>3</sub>]-OCH<sub>3</sub>·TFA **7.7** (990 mg, 2.37 mmol), and DIPEA (2.5 mL, 7.11 mL) were mixed in DMSO. HBTU<sup>b</sup> was added to the mixture in one portion and the resulting mixture was stirred at rt for 36 hr. The solvent was then removed under vacuum and the residue was added with H<sub>2</sub>O (50 mL) and stirred at rt for 0.5 hr. The mixture was filtered off. The solid was washed with H<sub>2</sub>O, MeOH, EtOAc, and Et<sub>2</sub>O, and then dried over high vacuum to afford a dark brown solid.

<sup>a</sup> The filtration for folate related compounds takes very long time. If possible, the author suggests the readers to use centrifugation to spin down everything instead. Unfortunately, high volume centrifugation is not available in this lab.

<sup>b</sup> The coupling reaction with pteric acid can be achieved with EDC·HCl and HOBt·H<sub>2</sub>O as the coupling reagents. However, the conversion is much lower and the purity of the product is much lower too.

Yield: 846 mg, 58%. The product was used in the next step without further purification. For characterization, ~ 20 mg of the product was dissolved in DMSO (2 mL) and then purified by semi-preparative HPLC to collect the desired product at 9.86 min (Program 9 with Column II in HPLC System I) (analytical HPLC Program 10 with Column I in HPLC System I,  $t_R = 9.1$  min).  $^1\text{H}$  NMR (400 MHz,  $d_6$ -DMSO, rt):  $\delta(\text{ppm})$  1.91 (m, 1 H), 2.04 (m, 1 H), 2.19 (m, 2 H), 2.53 (s, 1 H), 3.17 (m, 2 H), 3.37 (m, 4 H), 3.49 (m, 2 H), 3.52 (m, 2 H), 3.57 (t,  $J = 4.88$  Hz, 2 H), 3.60 (s, 3 H), 4.31 (m, 1 H), 4.53 (s, 2 H), 6.64 (d,  $J = 8.56$  Hz, 2 H), 7.64 (d,  $J = 8.52$  Hz, 2 H), 7.75 (s, br, 2 H), 7.88 (t,  $J = 5.46$  Hz, 1 H), 8.32 (d,  $J = 7.12$  Hz, 1 H), 8.71 (s, 1 H);  $^{13}\text{C}$  NMR (100.6 MHz,  $d_6$ -DMSO, rt):  $\delta(\text{ppm})$  26.96, 32.29, 39.13, 41.03, 46.40, 50.57, 52.31, 52.91, 69.70, 69.83, 70.16, 70.18, 111.84, 121.76, 128.64, 129.62, 148.76, 150.94, 151.34, 153.72, 160.62, 166.91, 172.12, 173.45. ESI-HRMS: calcd. for  $\text{C}_{26}\text{H}_{34}\text{N}_{11}\text{O}_7^+$ : 612.2643, found: 612.2637.

#### **Pte-Glu[(PEG)<sub>2</sub>N<sub>3</sub>]-OH (7.10)**

Pte-Glu[(PEG)<sub>2</sub>N<sub>3</sub>]-OCH<sub>3</sub> **7.9** (non-purified) (100 mg, 0.164 mmol) was suspended in 1 N NaOH (10 mL) and incubated at rt overnight. The mixture was acidified with 3 N HCl to pH ~ 2 and filtered off. The solid was then washed with H<sub>2</sub>O, MeOH, and Et<sub>2</sub>O, and then dried over vacuum to give a brown solid. Yield: 76.0 mg, 78%. 40 mg of the product was dissolved in DMSO (3 mL) and subjected to HPLC purification to give the pure product as a yellow solid (15.8 mg). The semi-preparative HPLC was performed via Program 9 with Column II in HPLC System I,  $t_R = 8.7$  min, and the analytical one was done via HPLC Program 17 with Column I in HPLC System I,  $t_R = 8.2$  min.  $^1\text{H}$  NMR (400 MHz,  $d_6$ -DMSO, rt):  $\delta(\text{ppm})$  1.88 (m, 1 H), 2.02 (m, 1 H), 2.17 (t,  $J = 6.98$  Hz, 2 H), 3.17 (q,  $J = 5.67$  Hz, 2 H), 3.37 (m, 4 H), 3.45-3.54 (m, 4 H), 3.57 (t,  $J = 4.88$  Hz, 2 H), 4.26 (m, 1 H), 4.51 (s, 2 H), 6.63 (d,  $J = 8.56$  Hz, 2 H), 7.52 (s, br, 1 H), 7.64 (d,  $J = 8.56$  Hz, 2 H), 7.86 (t,  $J = 5.56$  Hz, 1 H), 8.16 (d,  $J = 7.48$  Hz, 1 H), 8.67 (s, 1 H);  $^{13}\text{C}$  NMR (100.6 MHz,  $d_6$ -DMSO, rt):  $\delta(\text{ppm})$  27.12, 32.53, 39.11, 41.03, 46.45, 50.56, 52.81, 69.69, 69.83, 70.17, 111.81, 122.02, 128.59, 129.56, 148.86, 150.47, 151.27, 153.89, 160.90, 166.84, 172.28, 174.43; ESI-HRMS: calcd. for  $\text{C}_{25}\text{H}_{32}\text{N}_{11}\text{O}_7^+$ : 598.2486, found: 598.2467.

### One-pot two-step radiolabeling of folate with an $^{18}\text{F}$ -ArBF<sub>3</sub>

$^{18}\text{F}$ -Fluoride was prepared as described in previous chapters.  $^{18}\text{F}$ -Fluoride was trapped on the anion exchange column ( $\text{HCO}_3^-$  form) and released with  $\text{NaClO}_4$  (2 mg/mL, 1 mL).  $\text{CH}_3\text{CN}$  was added to azeotropically remove  $\text{H}_2\text{O}$  at 110 °C under He stream till no residual liquid was observed.  $^{19}\text{F}$ -KHF<sub>2</sub> (6  $\mu\text{L}$ , 0.125 M) was added to resuspend the radioactivity.

The  $^{18/19}\text{F}$ -fluoride cocktail (2  $\mu\text{L}$ , 500 nmol of  $^{19}\text{F}$ -fluoride, 6.26 mCi at the BOS) was added to alkynylarylboronic acid **3.11** (100 nmol) and HCl (6.25  $\mu\text{mol}$ ) in 88.9% aqueous THF (4.5  $\mu\text{L}$ ) and the mixture was incubated at rt for 35 min. The reaction was quenched with 5%  $\text{NH}_4\text{OH}$  (30  $\mu\text{L}$ ) and 2  $\mu\text{L}$  of the quenched mixture was added to 5%  $\text{NH}_4\text{OH}$  (100  $\mu\text{L}$ ) for HPLC analysis. The quenched reaction (10  $\mu\text{L}$ ) was added to the Pte-Glu[(PEG)<sub>2</sub>N<sub>3</sub>]-OH **7.10** (50 nmol, 5  $\mu\text{L}$ ), followed by the addition of 0.6 M sodium ascorbate (2  $\mu\text{L}$ ) and 0.2 M  $\text{CuSO}_4$  (2  $\mu\text{L}$ ). The copper catalyzed reaction was then left still for 48 min. 10  $\mu\text{L}$  of which was then added to 5%  $\text{NH}_4\text{OH}$  (100  $\mu\text{L}$ ) for HPLC analysis. The radio-HPLC traces were shown in Figure 7.9. The radioactivity at the BOS of the first step: 6.26 mCi, and that at the BOS of the second reaction: 1.80 mCi. The HPLC was performed via HPLC Program 7 with Column I in HPLC System IV.

# Chapter 8 Preparation of $^{18}\text{F}$ -ArBF<sub>3</sub> labeled RGD-peptides for cancer imaging

In this chapter, the cyclic peptides containing the Arg-Gly-Asp (RGD) sequence will be labeled with ArBF<sub>3</sub>S via two labeling methods described in earlier chapters.

## 8.1 Introduction

### 8.1.1 Integrin $\alpha_v\beta_3$ and RGD

Integrins, a class of surface receptors, are the major receptors, by which cells attach themselves to the extracellular matrices, and some of them are involved in cell-cell adhesion events.<sup>444</sup> They have been found to participate in various biological processes including embryonic development, cell activity mediation, regulation of the balance between cell proliferation and cell death, and cancer development.<sup>444, 445</sup> Thus, the specific and selective recognition of certain integrins is of great pharmaceutical significance.

Whereas integrins always consist of one  $\alpha$  subunit and one  $\beta$  subunit, fifteen different  $\alpha$  subunits and eight different  $\beta$  subunits have been found.<sup>444, 446</sup> The vitronectin receptor,  $\alpha_v\beta_3$  integrin, binds to many different ligands and is involved in a variety of cell-adhesion processes.<sup>446</sup> Unlike the integrins in charge of cell adhesion in tissues, those responsible for cell migration are always overexpressed in tumor cells.<sup>446</sup> Particularly,  $\alpha_v\beta_3$  is highly expressed in many tumor cells during the tumor development including metastasis, angiogenesis and/or neovascularization.<sup>446</sup>

The extracellular matrix proteins that bind to the  $\alpha_v\beta_3$  receptor have been studied for their sequences, and it has been found that one of the most recognized motifs contains the amino acid sequence: Arg-Gly-Asp (RGD).<sup>446, 447</sup> Based on this discovery, different  $\alpha_v\beta_3$  antagonists have been developed to inhibit the  $\alpha_v\beta_3$  receptor and suppress/delay the tumor development.<sup>448, 449</sup>

### 8.1.2 $\alpha_v\beta_3$ Antagonists based on RGD sequences

Since  $\alpha_v\beta_3$  has been found to be overexpressed in several pathological processes, it has become an excellent target for anti-tumor therapy and drug development.<sup>444-446, 448-451</sup> The identification of the structural adhesion site carrying the RGD sequence was a milestone for understanding cell-cell and cell-matrix interactions,<sup>452-457</sup> and this has paved the way for the development of a wide range of RGD-based ligands. To better understand the interaction between the substrate and the receptor, conformational restraints are always introduced to the ligand, and cyclization of the substrate is one of the most common techniques to restrict the freedom of the conformational movements.<sup>458</sup> Similarly, to achieve the effective conformation of the ligands to fit into the receptor, both the linear and cyclic peptides containing the RGD sequence were prepared and investigated.

The very first synthetic peptide bearing the RGD sequence was reported by Aumailley *et al.*<sup>447</sup> In that work, a series of cyclic pentapeptides containing the RGD sequence were synthesized and studied for their inhibitory capacity for cell adhesion on the natural extracellular adhesion proteins vitronectin and laminin fragment P1 for the  $\alpha_v\beta_3$  receptor and fibrinogen for the  $\alpha_{II}\beta_3$  receptor. The cyclic peptide *c*(RGDfV) was discovered to possess extremely potent inhibitory activity of 0.1-4.0  $\mu$ M for the  $\alpha_v\beta_3$  receptor. Based on the 2D NMR spectroscopy study and molecular dynamics simulation, it was found that the peptide adopts an “all-*trans* conformation” with a  $\beta$ II' turn and a  $\gamma$  turn while the *D*-phenylalanine occupies the (i+1) position of the  $\beta$ II' turn.<sup>447</sup> Compared with the linear pentapeptide GRGDS or the cyclic hexapeptide *c*(RGDfVA), the cyclic pentapeptide *c*(RGDfV) exhibits much higher activity and specificity for certain adhesion proteins.<sup>447</sup> This is interpreted that the constraint of the cyclopentapeptide favours the ligand with the optimal conformation to bind to the recognition site of the  $\alpha_v\beta_3$  receptor.<sup>446</sup> A more systematic investigation using the cyclopentapeptides *cyclo*(Arg-Gly-Asp-Xxx-Yyy) has disclosed that *D*-amino acids with hydrophobic side chains, or a *D*-serine at position 4 is critical for binding affinity, while the amino acid at position 5 appears to play no role in activity.<sup>446, 459</sup> Due to this discovery, lysine or glutamic acid is frequently introduced at position 5 to allow efficient conjugation of the peptide to various moieties.

The *N*-methylated analogues of *c*(RGDfV) were prepared and studied for their activity

and selectivity targeting integrin  $\alpha_v\beta_3$ .<sup>460</sup> This modification has provided a new  $\alpha_v\beta_3$  antagonist *c*(RGDf-N(Me)-V) with an extremely enhanced binding affinity (0.58 nM) against  $\alpha_v\beta_3$  receptor compared with that of *c*(RGDfV) (0.21  $\mu$ M).<sup>460</sup> This peptide, also called Cilengitide (EMD 121974, Merck KGaA, Darmstadt, Germany), has showed potentially very high activity towards various malignant diseases and low toxicities to healthy cells, and is currently being investigated under clinical studies against advanced diseases.<sup>461-468</sup>

Besides their high potency and selective inhibition to tumor metastasis and angiogenesis etc, RGD-peptides were also found to initiate cell death via activating caspase-3, a cysteine-aspartic protease.<sup>469</sup> It is indicated that the RGD motif binds to pro-caspase-3, and thereby induces conformational changes to allow caspase-3 to follow auto-processing and ultimately promotes apoptosis. Based on this study, the RGD sequence was successfully installed on various delivery vehicles to activate the intracellular caspases to induce apoptosis *in vivo*.<sup>470, 471</sup> Bernard *et al.*<sup>470</sup> prepared an RGD-conjugated somatostatin peptide [RGD-Lys(<sup>111</sup>In-DTPA)-Tyr<sup>3</sup>-Octreotate] targeting the subtype-2 cell surface receptor to achieve enhanced tumoricidal effects. Recently, Yang *et al.* coupled an RGD motif to a <sup>99m</sup>Tc- $\alpha$ -melanocyte stimulating the hormone hybrid peptide to target the melanocortin-1 (MC1) receptor.<sup>471</sup> It was found that the clearance of the conjugate was rapid, while high tumor uptake, improved melanoma retention, and remarkable clonogenic cytotoxic effects of the conjugate were achieved. The uptake was found to be mainly MC1 receptor-mediated.

### 8.1.3 RGD-containing peptides as drug delivery vehicles

Since RGD has such high specific affinity to integrin  $\alpha_v\beta_3$ , RGD-containing peptides have been proposed as drug vehicles to deliver therapeutic drugs, which generally have very high therapeutic activity but poor targeting capability. To visualize the binding events of RGD-peptides to the tumor and tumor endothelial cells *in vivo*, Sabine *et al.* synthesized a fluorescent peptide RGD-4C-FITC with the sequence of CDCRGDCFC and used the fluorescence-activated cell-sorting (FACS) analysis in combination with an isopentane freezing method to study the binding of the peptide *in vivo*.<sup>472</sup> They found that strong fluorescent signals were achieved with both endothelial cells and tumor cells in

human breast cancer xenografts in nude mice, while there was no uptake of the fluorescent peptide in non-tumorous cells. This work suggested specific binding of the RGD-peptide to the tumor/tumor endothelial cells.

The peptide RGD-4C and a reference linear peptide with a sequence of CNGRC were each conjugated to the anticancer drug doxorubicin (dox).<sup>451</sup> RGD-4C-dox demonstrated much higher activity in inhibiting both the primary tumor growth and metastasis than did CNGRC-dox. This work suggested that RGD is a very effective drug delivery agent to target tumor vasculature. RGD-4C was also incorporated to the *N*-terminus of interleukin 24, a novel tumor suppressor and apoptosis inducing cytokine.<sup>473</sup> The conjugate was found to specifically bind to MCF-7 cancer cells and induce cancer cell death. This work supported the strategy of coupling the anticancer cytokines with the RGD-containing peptides for tumor targeting therapies.

Ghandehari and colleagues reported that a copolymer-drug conjugate containing the RGD sequence targeted prostate cancer and the conjugate showed superior *in vitro* and *in vivo* activity.<sup>474</sup> Briefly, with the water soluble *N*-(2-hydroxypropyl)methacrylamide (HPMA) copolymers containing side chains with *c*(RGDfK) units at the terminals, the HPMA copolymer-*c*(RGDfK)-aminohexylgeldanamycin conjugates were prepared. The water soluble copolymer highly improved the drug's water solubility and safety, and exhibited enhanced permeability and retention in solid tumors. The *c*(RGDfK) moieties increased the accumulation of the copolymer in various solid tumors including prostate, lung, and breast tumors. The *c*(RGDfK) conjugates also demonstrated significantly enhanced inhibition to tumor progression and displayed optimal advantages in suppression of the endothelial cell migration. These results imply that the application of combining RGD-containing peptides and water soluble copolymers improves the delivery of chemotherapeutic drugs to solid tumors.

In 2011, the *C*-terminal fragment of the NC-1 domain of collagen XVIII, endostatin, which inhibits angiogenesis to suppress the tumor growth in several clinic models, was modified with both RGD and the Fc fragment of IgG4 via molecular biology techniques with a single point mutation at position 125 (P125A).<sup>475</sup> The derivatized proteins exhibited stronger inhibitory effects on the endothelial cell migration and growth than

that of the original yeast-derived P125A-endostatin. Both the RGD/Fc fused P125A-endostatin proteins succeeded in inhibiting the ovarian tumor proliferation while the introduction of IgG4-Fc extended the half-life of P125A-endostatin in the blood. Compared with the humanized monoclonal anti-VEGF antibody Bevacizumab<sup>476</sup> that inhibits the vascular endothelial growth factor A, the RGD-modified proteins displayed less toxicity.

The cyclic peptide *c*(RGDfK) was successfully conjugated to Alexa Fluor-488 to give a water soluble fluorescent peptide *c*(RGDfK)-488.<sup>477</sup> This peptide showed very high binding affinity to  $\alpha_v\beta_3$  integrin, which is overexpressed in human umbilical vascular endothelial cells (HUVEC). This peptide also displayed very high cell uptake at 37 °C. Although no solid data were obtained to support the integrin-mediated endocytosis, this work has raised the interest for the “*intracellular delivery of ligand associated drugs in antiangiogenic applications*”.

Ligands with multivalent RGD residues have also been applied to achieve improved targeting properties. The antitumor agent paclitaxel (PTX) was conjugated to the dimeric RGD-peptides via the malonate<sup>478</sup> or succinate<sup>479</sup> linkers, while the 4<sup>th</sup> amino acid in the cyclic pentapeptides was *D*-tyrosine<sup>478</sup> or *D*-phenylalanine<sup>479</sup> respectively. Both studies suggested very high *in vitro* inhibition potency against HUVEC cell proliferation. However, the E-*c*(RGDyK)<sub>2</sub>-malonate-PTX demonstrated enhanced *in vivo* tumor growth inhibition,<sup>478</sup> while there was not any antitumor efficacy reported for the E-*c*(RGDfK)<sub>2</sub>-succinate-PTX.<sup>479</sup> As pointed out by Chen and co-workers,<sup>478</sup> the lipophilicity and fast clearance due to small molecular weights might account for the absolute low tumor uptake value. Hence, improvement of the water solubility of the divalent RGD-drug conjugates might help to achieve better pharmacological properties.<sup>478</sup>

#### **8.1.4 RGD-peptides in molecular imaging**

The cyclopentapeptides with the RGD sequence discussed above have not only entered therapeutic development for antitumor/antiangiogenic drugs as well as apoptosis inducers, but they have also been applied as drug vehicles to transport potent drugs in order to treat

advanced diseases. Since they are such excellent ligands for integrins, especially integrin  $\alpha_v\beta_3$  that is frequently overexpressed during tumor-cell progression, peptides with the RGD sequence have turned out to be ideal ligands for molecular imaging to assist diagnosis, gauge the stage of cancers/tumor, and evaluate therapies and drugs. Accordingly, a great deal of beautiful imaging work has been reported recently by labeling RGD-peptides with a variety of radionuclides,<sup>480-482</sup> fluorescent probes,<sup>483, 484</sup> and contrast agents to locate the *in vivo* distribution of the  $\alpha_v\beta_3$  receptor.<sup>485</sup> Shortly after the discovery of the  $\alpha_v\beta_3$  antagonists, such as the cyclopentapeptide *c*(RGDfV) and its analogues,<sup>446, 459</sup> the diagnostic field began to apply these peptides to target integrin  $\alpha_v\beta_3$ , and a large amount of work has resulted in very promising noninvasive imaging ligands. Herein, we will mainly focus on the radiolabeling aspect.

Goligorsky and co-workers<sup>486</sup> reported the radiosynthesis of a linear peptide with a sequence of **GRGDSPC** labeled by <sup>99m</sup>Tc to study its renal uptake in rats with ischemic acute renal failure, during which the expression of integrin receptors has been found on the apical cell membrane to cause tubular obstruction.<sup>487</sup> The <sup>99m</sup>Tc-labeled RGD-containing peptide demonstrated significantly enhanced accumulation in the malfunctioned kidney within a short period of time but less specifically and selectively compared with the cyclic RGD-peptide studied earlier by the same group.<sup>488</sup> Using the same complexation strategy between cysteine and <sup>99m</sup>Tc, a synthetic linear decapeptide designated  $\alpha$ P2 with two RGD sequences<sup>a</sup> was radiolabeled with <sup>99m</sup>Tc to visualize the malignant melanoma *in vivo*.<sup>489</sup> With rapid clearance to the kidney and bladder, the labeled peptide successfully localized to the metastatic melanoma lesion albeit with a poor tumor-to-nontumor ratio of 2.9. To improve tumor uptake and the stability of the <sup>99m</sup>Tc-RGD complexes, different chelators have been introduced to the peptides.<sup>490</sup> For example, Edwards *et al.* adopted a diamine-dioxime chelator on the RGD-4C-derivatized peptide to give <sup>99m</sup>Tc-NC100692, which showed rapid *in vivo* clearance and elevated affinity to the vitronectin receptors  $\alpha_v\beta_3$  and  $\alpha_v\beta_5$ . Successful detection of breast cancer by this radiotracer has been achieved with very promising results and this ligand is currently under clinical evaluations.<sup>491, 492</sup> Another study, using 3,5-Me<sub>2</sub>-pz(CH<sub>2</sub>)<sub>2</sub>N-((CH<sub>2</sub>)<sub>3</sub>COOH)(CH<sub>2</sub>)<sub>2</sub>NH<sub>2</sub> on *c*(RGDyK) peptide to chelate with <sup>99m</sup>Tc, also showed very

---

<sup>a</sup> The sequence for this decapeptide designated  $\alpha$ P2 is **RGDSRCGDSY**.

fast *in vivo* clearance from the blood and high *in vivo* stability against dissociation and metabolism, but only with a moderate tumor-to-blood/muscle ratio.<sup>493</sup> Moreover, 6-hydrazinonicotinic acid (HYNIC) installed on peptides with monomeric<sup>494</sup> or multimeric<sup>495-498</sup> RGD sequences and coligands have been used to form the <sup>99m</sup>Tc-complexes with highly improved properties such as the *in vivo* stability and favourable pharmacokinetics. With the case of multimeric RGD complexes, elevated integrin-mediated tumor uptake was also observed.

Other radiometals such as <sup>64</sup>Cu, <sup>68</sup>Ga, and <sup>111</sup>In have also been used to radiolabel RGD-containing peptides.<sup>499-503</sup> Similar *in vitro* and *in vivo* results were obtained regarding the difference among radionuclides. On the other hand, it has also been shown that cyclic peptides with the RGD sequence demonstrate higher tumor uptake than the linear counterparts, while multimerization of the *c*(RGDxY) units provide even more enhanced receptor avidity and affinity.<sup>497, 499-502</sup>

Haubner and colleagues reported the radiolabeling of RGD-peptides with <sup>125</sup>I-iodine on *c*(RGDfY) and *c*(RGDyV).<sup>504</sup> The <sup>125</sup>I-labeled peptides specifically accumulated at the tumor location, showed very rapid blood clearance, demonstrated primarily hepatobiliary excretion and exhibited relatively high *in vivo* stability against deiodination. To increase the hydrophilicity, a glycosyl moiety was introduced to *c*(RGDyK), and the peptide was labeled with <sup>125</sup>I-iodine.<sup>505</sup> The <sup>125</sup>I-labeled peptide was injected into nude mice bearing xenotransplanted melanomas and/or mice with osteosarcomas for imaging studies. The newly developed <sup>125</sup>I-peptide showed specific binding and good tumor-to-organ ratios. In addition, liver uptake was significantly reduced.

Following the similar principle to decrease the lipophilicity, the Haubner laboratory then prepared the <sup>18</sup>F-labeled galacto-*c*(RGDfK) by coupling 4-nitrophenyl 2-[<sup>18</sup>F]fluoropropionate to galacto-*c*(RGDfK).<sup>506, 507</sup> In spite of the tedious radiosynthesis, a radiochemical yield of 29%, in a total preparation time of 200 minutes including the HPLC purification, was obtained. Although uptake in the liver, colon, and kidney was comparable to the tumor, a high tumor-to-blood ratio (27.5) was achieved. Furthermore, <sup>18</sup>F-galacto-*c*(RGDfK) demonstrated rapid excretion, good metabolic stability, specific integrin-mediated tumor uptake, and low estimated radiation dose, which allows this

radiotracer to be evaluated in human studies.

Hatano and co-workers reported a one-step electrophilic radiofluoridation to prepare  $^{18}\text{F}$ -*c*(RGDfMeV) with  $^{18}\text{F}$ -acetylhypofluoride ( $\text{AcO}^{18}\text{F}$ ).<sup>508</sup> Although regioisomers were obtained during the radiosynthesis, all the  $^{18}\text{F}$ -*c*(RGDfMeV) peptides showed high and specific affinity for the integrin. High tumor-to-blood/muscle ratios were obtained, while there was very high uptake of the radioactivity in the liver and kidney, and some in the bone. Chen *et al.* also reported their  $^{18}\text{F}$ -labeled RGD with  $^{18}\text{F}$ -SFB to image brain tumor angiogenesis with an orthotopic U251T brain tumor model.<sup>509</sup> A high tumor-to-brain ratio was obtained with high receptor specificity for this radiotracer. Recently, *O*-(2-(2-[ $^{18}\text{F}$ ]fluoroethoxy)-ethyl)-*N*-methylhydroxyl amine<sup>510</sup> and/or 4-[ $^{18}\text{F}$ ]fluorobenzaldehyde<sup>511</sup> was regioselectively introduced to the RGD-4C-derivatized analogues via either the Michael addition or oxime formation. Promising biodistribution and tumor uptake were reported.

Dimeric RGD-peptides have also been labeled with  $^{18}\text{F}$ -fluoride. Chen and colleagues reported their effort to image tumors by the RGD dimeric peptides containing either a PEG linker<sup>512, 513</sup> or a galacto-linker.<sup>513</sup> The dimeric tracers exhibited very high and specific receptor binding affinity, good to excellent pharmacokinetic properties, and good *in vivo* metabolic stability, which makes them very useful radiotracers for diagnosis.

Taken together, the examples discussed above demonstrate that integrin  $\alpha_v\beta_3$  is an excellent and validated target for RGD-containing peptides, especially the RGD-containing cyclic pentapeptides as very robust bio-probes for diagnostic imaging. However, the RGD substrates studied so far are rather lipophilic, which leads to high liver uptake and hepatobiliary excretion. The modification of the peptides by introducing hydrophilic groups such as galactose or PEG linkers would help to decrease the hydrophobicity of the ligands and hence the ligands may have more favourable properties in the circulation/excretion. Preparing peptides containing multimeric RGD residues is another strategy frequently used to improve the target specificity/affinity.

### 8.1.5 Labeling RGD-containing peptides with ArBF<sub>3</sub>s

As an ArBF<sub>3</sub> carries a negative charge, labeling RGD-containing peptides with <sup>18</sup>F-ArBF<sub>3</sub>s can greatly increase the hydrophilicity of the peptides; favourable *in vivo* clearance should be achieved by this labeling approach. Moreover, since RGD has been established as a powerful ligand targeting integrin α<sub>v</sub>β<sub>3</sub>, introducing ArBF<sub>3</sub>s on RGD-containing peptides may help to validate the hypothesis of applying <sup>18</sup>F-ArBF<sub>3</sub>s as PET imaging agents, which is the goal of this thesis. Hence, in this chapter, the linear peptide **RGDfK** and its analogues were synthesized via the solid phase peptide synthesis and the cyclopentapeptides were obtained via macrolactamization under high dilution conditions. The *c*(RGDfK) was successfully coupled to boronate **3.1**. A piperazine linker was also introduced into the RGD-boronate to investigate the linker effect on the <sup>18</sup>F-fluoridation. Meanwhile, *c*[RGDfK(N<sub>3</sub>)] **8.4** was prepared to apply the one-pot two-step strategy to introduce the <sup>18</sup>F-ArBF<sub>3</sub> onto the peptide via copper(I) catalyzed click chemistry as studied in Chapter 6. Overall, three ArBF<sub>3</sub> labeled RGD-containing peptides (RGD-ArBF<sub>3</sub>s) have been prepared and we expect to have a direct comparison of the two <sup>18</sup>F-labeling methods in this chapter.

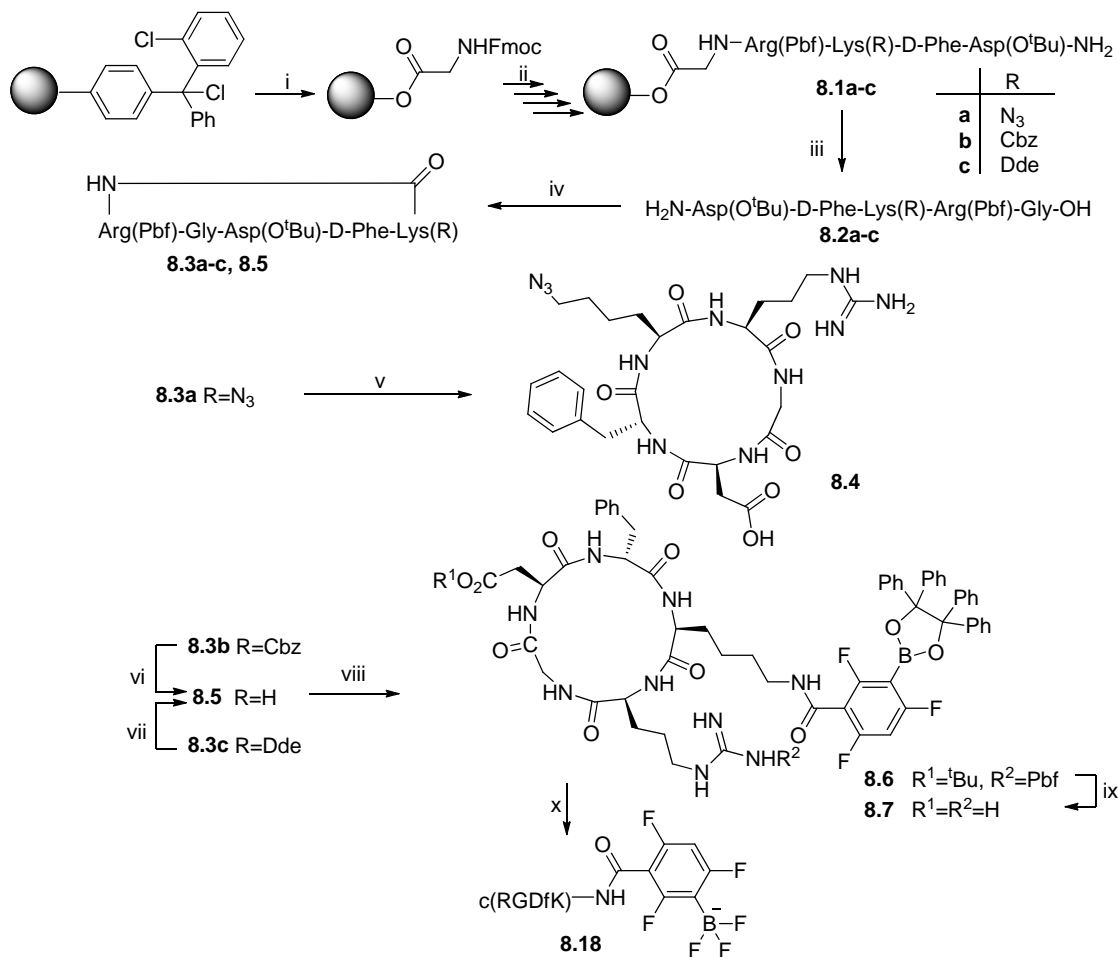
## 8.2 Results

Although multimeric cyclic RGD-peptides have been shown to be promising tumor targeting substrates with elevated affinities and specificities,<sup>449, 481, 482, 500, 512-515</sup> the monomeric cyclic pentapeptides containing the RGD sequence have demonstrated high specificity and affinity towards integrin α<sub>v</sub>β<sub>3</sub>, and a great deal of excellent work has already shown their applications in therapeutics, drug delivery, and molecular imaging.<sup>446, 449, 460, 485</sup> To simplify the synthesis as well as to focus on the purpose of verifying <sup>18</sup>F-ArBF<sub>3</sub>s as suitable PET imaging agents, monomeric cyclic RGD-peptides have been prepared and their fluoridation to afford RGD-<sup>18</sup>F-ArBF<sub>3</sub>s is described herein.

### 8.2.1 Preparation of the RGD-containing peptides

The cyclic pentapeptides with the RGD sequence were synthesized via the Fmoc solid phase peptide synthesis on the 2-chlorotrityl resin<sup>516</sup> following a reported protocol<sup>459</sup> with some modifications as shown in Scheme 8.1. Briefly, Fmoc-Gly-OH was first

attached to the resin to avoid racemization during the cyclization later on, and 20% piperidine in DMF was used to remove the Fmoc protecting group. HBTU was used as the coupling reagent to extend the peptide in the presence of DIPEA. The peptide was cleaved from the 2-chlorotrityl resin with 20% HFIP in CH<sub>2</sub>Cl<sub>2</sub>. The cyclization of the linear peptide was achieved using HBTU as the activating agent under high dilution conditions in CH<sub>3</sub>CN. The deprotection of the acid-labile protecting groups on the side chains of the cyclic peptides was carried out with 5% H<sub>2</sub>O in TFA at room temperature.



**Scheme 8.1 Synthetic scheme of the cyclic RGD pentapeptides.**

(i), Fmoc-Gly-OH, CH<sub>2</sub>Cl<sub>2</sub>, Ar, rt, 1.5 hr; (ii), a. 20% piperidine/DMF, rt, 3 × 5 min, then Fmoc-Arg(Pbf)-OH, HBTU, DIPEA, DMF, rt, 2 hr, b. 20% piperidine/DMF, rt, 3 × 5 min, then Fmoc-Lys(R)-OH, HBTU, DIPEA, DMF, rt, 2 hr, c. 20% piperidine/DMF, rt, 3 × 5 min, then Fmoc-D-Phe-OH, HBTU, DIPEA, DMF, rt, 2 hr, d. 20% piperidine/DMF, rt, 3 × 5 min, then Fmoc-Asp(O<sup>t</sup>Bu)-OH, HBTU, DIPEA, DMF, rt, 2 hr, e. 20% piperidine/DMF, rt, 3 × 5 min; (iii), 1:4 HFIP:CH<sub>2</sub>Cl<sub>2</sub>, rt, 20 min; (iv), HBTU, DIPEA, CH<sub>3</sub>CN, rt, 24 hr, 76% for **8.3a**, 95% for **8.3b**, 94% for **8.3c**; (v), 5% H<sub>2</sub>O in TFA, rt, 3 hr, 90%; (vi), Pd/C, DMA/H<sub>2</sub>O, rt, 16 hr, 62%; (vii), 2% NH<sub>2</sub>NH<sub>2</sub>·H<sub>2</sub>O in THF, rt, 20 min, 87%; (viii), EDC·HCl, HOBt·H<sub>2</sub>O, DMF, Py, rt, 36 hr; (ix), 5% H<sub>2</sub>O in TFA, rt, 3 hr, 40% over two steps (step viii and ix); (x), KHF<sub>2</sub>, HCl, CH<sub>3</sub>CN, rt, 1 hr.

DPPA,<sup>286, 447</sup> TBTU,<sup>517</sup> PyBOP,<sup>477</sup> and HBTU<sup>518</sup> have been reported to be suitable for the head-to-tail cyclization of similar pentapeptides. We then tested the cyclization of the azido-peptide **8.2a** with PyBOP and HBTU<sup>a</sup> in DMF or CH<sub>3</sub>CN. Based on the macrolactamization of amatoxin reported by Dr. David Dietrich in his thesis,<sup>519</sup> three equivalents of the coupling reagent/base (DIPEA) were used for the cyclization. As shown in Figure 8.1, the macrolactamization in the presence of the coupling reagents worked very well after 24 hours under high dilution conditions, and nearly a full conversion of the starting peptide was observed. The two solvents tested, DMF and CH<sub>3</sub>CN, demonstrated almost no difference in regard to the conversion of the peptide. From the HPLC traces obtained, the synthesis with HBTU appeared cleaner than that with PyBOP, and we then decided to use HBTU in all our macrolactamizations. Since CH<sub>3</sub>CN has a much lower boiling point than DMF but behaved as efficiently as DMF, CH<sub>3</sub>CN was chosen as the solvent for the high dilution reactions.

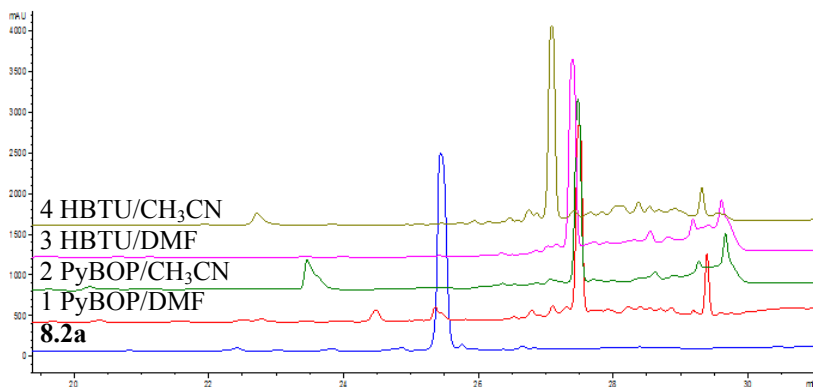


**Figure 8.1** The macrolactamization of H<sub>2</sub>N-Asp(O<sup>t</sup>Bu)-D-Phe-Lys(N<sub>3</sub>)-Arg(Pbf)-Gly-OH (**8.2a**). The cyclization was carried out for each reaction: **8.2a** (1 mM), the coupling reagent (3 mM) and DIPEA (3 mM) in the tested solvent (DMF/CH<sub>3</sub>CN) at rt for 24 hr. The HPLC was performed via HPLC Program 1 with Column I in HPLC System I. Part (19 to 32 min) of the HPLC chromatograms (at 229 nm) are shown in this figure. The reaction for chromatogram 1: PyBOP/DMF; that for trace 2: PyBOP/CH<sub>3</sub>CN; that for trace 3: HBTU/DMF; that for trace 4: HBTU/CH<sub>3</sub>CN. The blue trace was that for the precursor **8.2a**.

Two methods, based on different protecting groups on the ε-amino group of lysine, were applied to prepare peptide **8.5**, as indicated in Scheme 8.1. Both Cbz<sup>477</sup> and Dde<sup>520</sup> groups have been reported to protect the ε-amino group of lysine for the peptide synthesis, and they can be removed to free the amino group for the derivatization of the peptides. The Cbz-protected peptide **8.3b** was first prepared. However, it was soon

<sup>a</sup> These coupling reagents were available in the lab that time.

realized that the hydrogenolysis to deblock this protecting group required a high catalyst loading in the presence of 1.5% HOAc in dimethylacetamide at room temperature for six hours, while the hydrazine treatment took less than 0.5 hours to unmask the Dde-protected peptide **8.3c**. Moreover, in several cases, the Pd/C catalyst was not fully removed via filtration over Celite, and this trivial amount of the Pd/C residue forced the deboronation of boronate **3.1** or **8.6** in the subsequent coupling reaction. In contrast, peptide **8.5** was obtained cleanly via the deprotection of the Dde group with  $\text{NH}_2\text{NH}_2$  from **8.3c** since other reagents and byproducts in the mixture could be easily removed by the  $\text{Et}_2\text{O}$  wash.

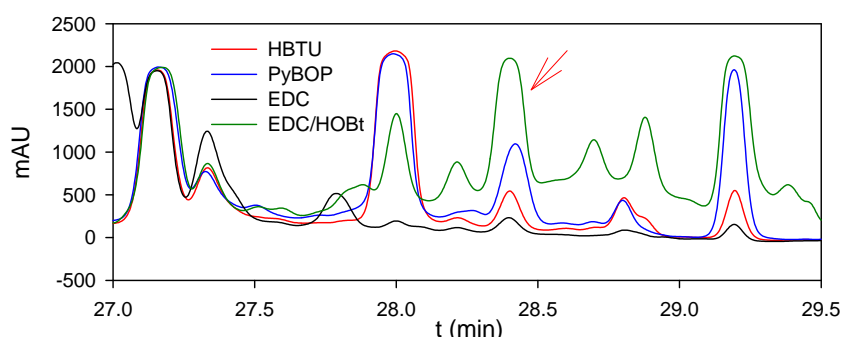
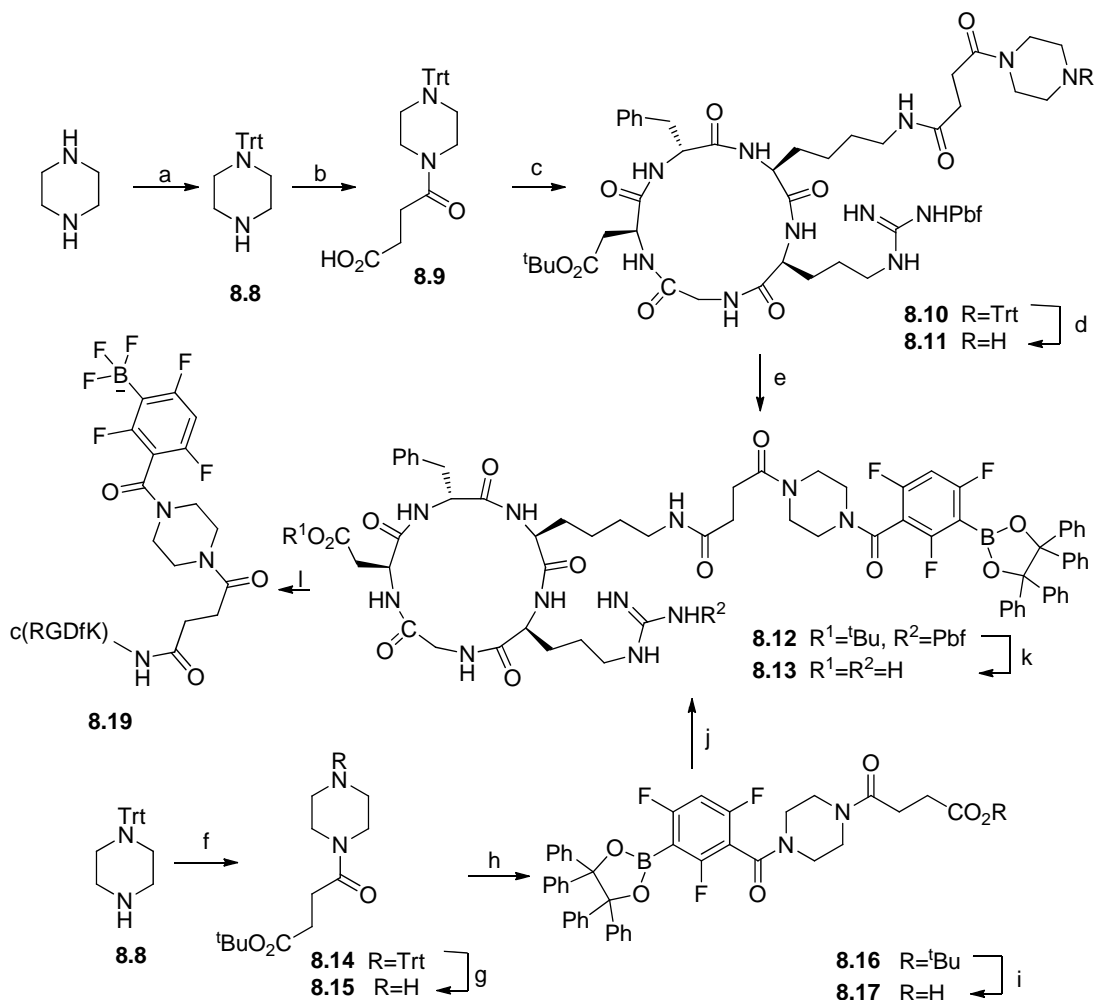


**Figure 8.2** The test of different coupling reagents to conjugate boronate **3.1** to peptide **8.5**.

The four HPLC chromatograms at 229 nm for four different coupling conditions and only the region from 27.0 to 29.5 min is shown. The coupling reaction: peptide **8.5** (10 mM), boronate **3.1** (20 mM), pyridine (40 mM), and coupling reagent (22 mM) as noted in the HPLC profile in DMF. That with EDC/HOBt as shown in the green trace was in the presence of HOBt (21 mM). The chromatograms were for the reaction solutions incubated at rt for around 50 hr. The peak noted by the red arrow at 28.4 min is the desired product, which was confirmed by ESI-LRMS. The HPLC was performed via HPLC Program 1 with Column I in HPLC System I.

To introduce boronate **3.1** onto peptide **8.5**, we tested several coupling reagents. Based on the previous experience to work with this boronate, a relatively weak base such as pyridine was used to keep the reaction slightly basic. To ensure that the reaction was homogeneous, DMF was chosen as the reaction solvent because it is a frequently used solvent for coupling reactions besides  $\text{CH}_2\text{Cl}_2$  and THF. The reactions were monitored by HPLC every two hours. Figure 8.2 demonstrates the portion of the HPLC chromatograms from 27.0 to 29.5 minutes for a better comparison among the different reactions that had been incubated for 50 hours. From the HPLC traces, every reaction was complicated, since there were many components present. However, only the reaction with EDC/HOBt as the coupling combination successfully produced predominant amounts of the desired product with a retention time of 28.4 minutes, which was collected and confirmed by

ESI-MS. Subsequently, EDC/HOBt were used for all the coupling reactions involving boronate **3.1**.

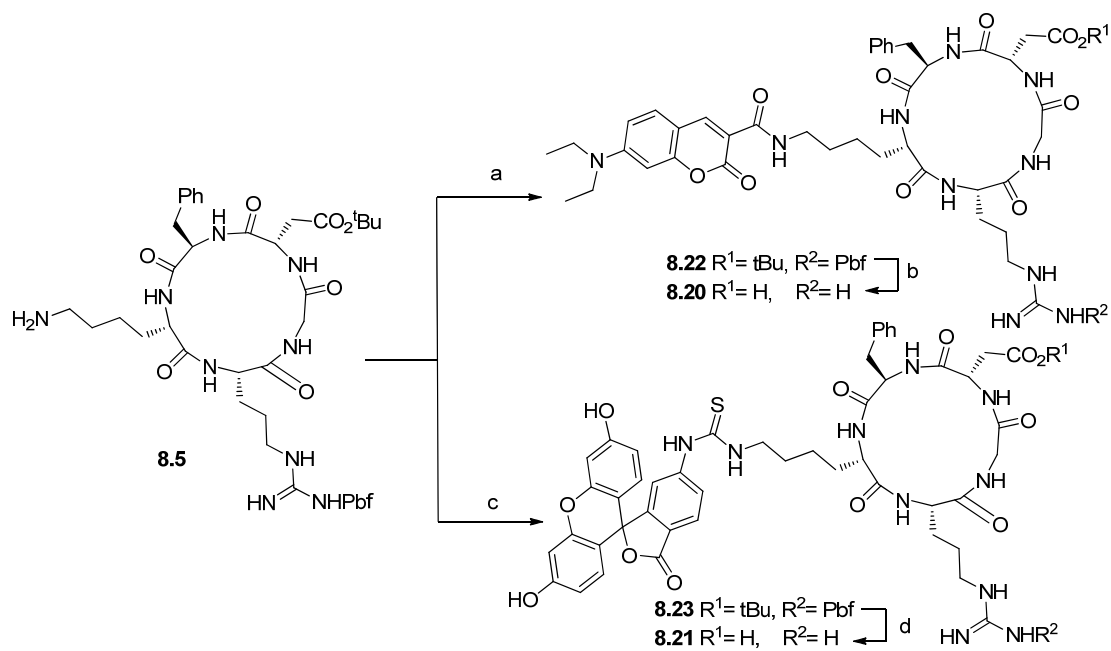


**Scheme 8.2** Synthesis of *cyclo*[Arg-Gly-Asp-D-Phe-Lys(suc-piperazinyl-boronate)] **8.13** and the corresponding RGD-ArBF<sub>3</sub> **8.19**.

(a), Trt-Cl, CH<sub>2</sub>Cl<sub>2</sub>, 0 °C then rt, 0.5 hr, 64%; (b), succinic anhydride, NEt<sub>3</sub>, CH<sub>2</sub>Cl<sub>2</sub>, rt, 1.5 hr, 64%; (c), **8.5**, DIPEA, HBTU, DMF, rt, overnight; (d), HFIP, CF<sub>3</sub>CH<sub>2</sub>OH, rt, 2 hr, 78% over two steps (c and d); (e), EDC·HCl, HOBt·H<sub>2</sub>O, pyridine, DMF, rt, 36 hr; (f), mono-*tert*-butyl succinate, NEt<sub>3</sub>, HBTU, CH<sub>2</sub>Cl<sub>2</sub>, rt, 2.5 hr, 98%; (g), HFIP, CF<sub>3</sub>CH<sub>2</sub>OH, 40 °C, 4 hr, 96%; (h), **3.1**, EDC·HCl, HOBt·H<sub>2</sub>O, pyridine, CH<sub>2</sub>Cl<sub>2</sub>, rt, overnight, 83%; (i), TFA, CH<sub>2</sub>Cl<sub>2</sub>, rt, 3 hr, 88%; (j), **8.5**, EDC·HCl, HOBt·H<sub>2</sub>O, pyridine, DMF, rt, 36 hr, 77%; (k), 5% H<sub>2</sub>O in TFA, rt, 1.5 hr, 47%; (l), KHF<sub>2</sub>, HCl, CH<sub>3</sub>CN, rt, 1 hr.

On the other hand, RGD-boronate **8.13** containing a succinimidyl-piperazine linker between *c*(RGDfK) and the boronate was prepared via two synthetic approaches as shown in Scheme 8.2; one route coupled boronate **3.1** to the piperazine derivatized peptide **8.11** at the last second step (the top synthetic route) whereas the other first coupled **8.5** to boronate derivative **8.17** (the bottom synthetic route). Whereas both methods succeeded to provide the desired product, the second method seems more

effective since the best way to pre-purify the peptide involved MeOH/Et<sub>2</sub>O precipitation. More steps involving the precipitation might have led to the co-precipitation of unknown impurities, which would complicate the overall synthesis and/or the final purification. Hence for later preparations, the second synthetic route was followed.



**Scheme 8.3 Synthesis of the fluorescent RGD-peptides 8.20 and 8.21.**

(a), **6.3b**, HBTU, DIPEA, DMF, rt, 23 hr, 12%; (b), 4.8% H<sub>2</sub>O in TFA, rt, 1 hr, quant.; (c), FITC, DIPEA, DMF, rt, 3 hr, 35%; (d), 4.8% H<sub>2</sub>O in TFA, rt, 1.5 hr, 91%.

Two fluorescent RGD derivatives were also prepared for use in studying the *in vitro* cell binding. As shown in Scheme 8.3, 7-diethylaminocoumarin-3-carboxylic acid **6.3b** was coupled to peptide **8.5** with HBTU/DIPEA to give the coumarin labeled peptide **8.22**, while peptide **8.5** nucleophilically attacked fluorescein isothiocyanate (FITC) to provide the FITC derivatized peptide **8.23**. Followed by deprotection, *c*[RGDfK(coumarin)] **8.20** and *c*[RGDfK(FITC)] **8.21** were obtained with relatively high purities.

The final step for the overall syntheses is to remove all the acid-labile protecting groups. Catalytic amounts of H<sub>2</sub>O appeared important to drive the reactions forward and it generally took two to three hours for the reactions to accomplish with quantitative conversions. Then RGD-boronates **8.7** and **8.13** were subjected to the fluoridation to prepare the corresponding RGD-ArBF<sub>3</sub>s **8.18** and **8.19** for HPLC method development.

Overall, *c*[RGDfK(N<sub>3</sub>)] and two boronates containing the *c*(RGDfK) unit have been

prepared in this chapter to study the labeling of the RGD-containing peptides with ArBF<sub>3</sub>s using two different methods. Two fluorescent c(RGDfK) derivatives were also acquired to study the *in vitro* binding affinity to integrin  $\alpha_v\beta_3$ .

## 8.2.2 The one-step fluoridation of RGD-boronates

### 8.2.2.1 The HPLC conditions for RGD-ArBF<sub>3</sub>s

The fluoridation of RGD-boronates **8.7** and **8.13** was undertaken under the similar conditions described in the previous chapters. As noted in previous chapters, the HCO<sub>2</sub>NH<sub>4</sub>/CH<sub>3</sub>CN solvent system was found to be quite suitable for the HPLC analysis of the corresponding ArBF<sub>3</sub>s. The cold standards of the RGD-ArBF<sub>3</sub>s were analyzed via RP-HPLC as shown in Figure 8.3. The peptides, with slightly different linkers, showed very close retention times. The RGD-ArBF<sub>3</sub>s were identified by ESI-LCMS with the desired masses of [M]<sup>-</sup>: 828.1 and [M-HF]<sup>-</sup>: 808.3 for RGD-ArBF<sub>3</sub> **8.18** (*t<sub>R</sub>* = 16.8 min), and [M]<sup>-</sup>: 996.3 and [M-HF]<sup>-</sup>: 976.5 for RGD-ArBF<sub>3</sub> **8.19** (*t<sub>R</sub>* = 16.2 min).<sup>a</sup>

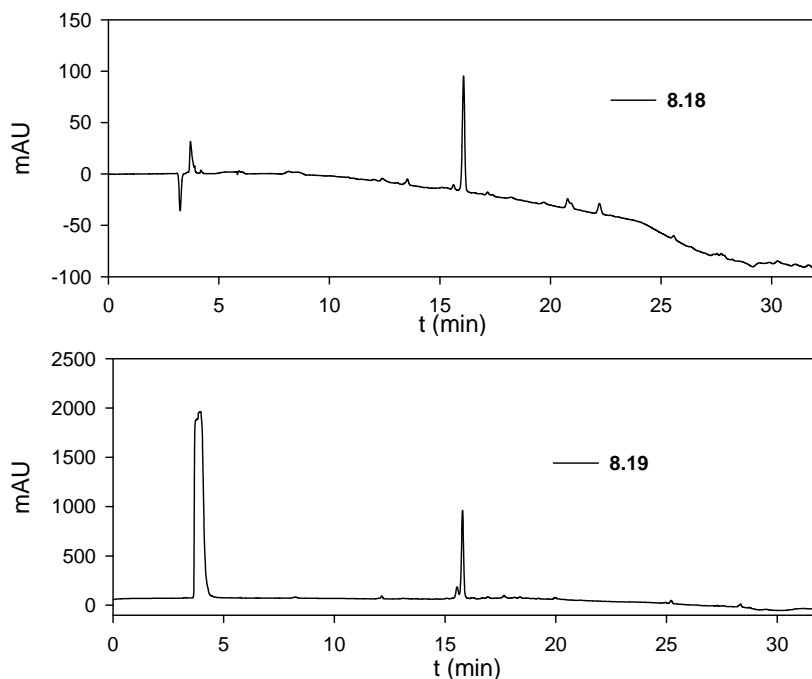


**Figure 8.3** The HPLC traces of the RGD-ArBF<sub>3</sub>s.

The RP-HPLC was performed via HPLC Program 8 with Column I in HPLC System I and the UV traces at 229 nm were indicated here. The top HPLC chromatogram is for RGD-ArBF<sub>3</sub> **8.18**; the bottom HPLC chromatogram is for RGD-ArBF<sub>3</sub> **8.19**.

<sup>a</sup> The ESI-LCMS chromatograms are in Appendix C.

### 8.2.2.2 The one-step radiolabeling of RGD-boronates

The radiofluoridation of RGD-boronates **8.7** and **8.13** was carried out under carrier-added conditions. Similarly, CH<sub>3</sub>CN was used as the aqueous cosolvent while HCl was used to acidify the system with 5 equivalents of carrier fluoride added to drive the fluoridation forward. Each reaction was undertaken at room temperature for one hour and then quenched with 5% NH<sub>4</sub>OH in 50% aqueous EtOH prior to the HPLC injection for analysis. The fluoridation was very reproducible, and an average radiochemical yield of 10-15% was achieved from reactions with radioactivity of 1-5 mCi as shown in Figure 8.4. Peptide **8.13** containing the piperazine linker gave slightly better incorporation of <sup>18/19</sup>F-fluoride in the one hour reaction than **8.7**.

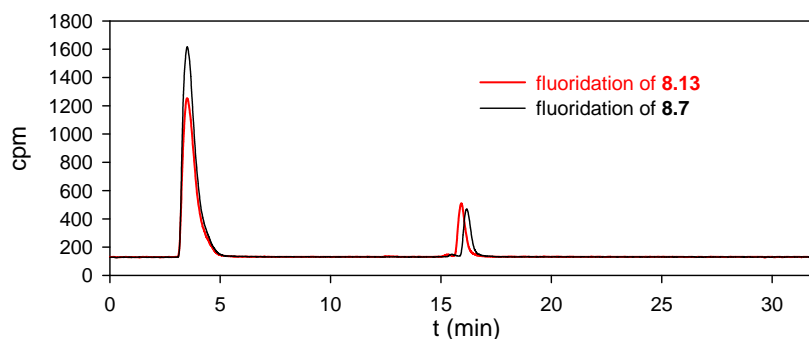


**Figure 8.4** The radio-HPLC traces of the one-step <sup>18</sup>F-fluoridation of RGD-boronates **8.7** and **8.13**. The black HPLC trace represented the <sup>18</sup>F-fluoridation of RGD-boronate **8.7** and the red one indicated the <sup>18</sup>F-fluoridation of RGD-boronate **8.13**. The HPLC was performed via Program 8 with Column 1 in HPLC System IV. The reaction condition for the fluoridation of **8.7**: **8.7** (100 nmol), CH<sub>3</sub>CN (4 μL), concentrated HCl (1 μL), and <sup>18</sup>F-fluoride containing <sup>19</sup>F-fluoride (500 nmol, 1 μL), rt, 1 hr, the radioactivity at the BOS: 1.86 mCi and RCY: 12%; that for the fluoridation of **8.13**: **8.13** (100 nmol), CH<sub>3</sub>CN (4 μL), concentrated HCl (1 μL), and <sup>18</sup>F-fluoride containing <sup>19</sup>F-fluoride (500 nmol, 1 μL), rt, 1 hr, the radioactivity at the BOS: 1.46 mCi and RCY: 16%.

### 8.2.3 One-pot two-step syntheses of RGD-ArBF<sub>3</sub>s via click chemistry

It has been demonstrated in Chapter 6 and Chapter 7 that the radiofluoridation of alkynylboronic acid **3.11** could reach a radiochemical yield of more than 30% within 0.5 hours at room temperature and the subsequent copper(I) catalyzed click reaction was very efficient to incorporate the <sup>18</sup>F-ArBF<sub>3</sub> into the molecule of interest. To compare this one-pot two-step radiolabeling strategy for the incorporation of an ArBF<sub>3</sub> with the one-step labeling method, *c*[RGDfK(N<sub>3</sub>)] **8.4** was prepared and its conjugation to ArBF<sub>3</sub> via the copper(I) catalyzed click reaction was studied.

### 8.2.3.1 The one-pot two-step synthesis via click chemistry to prepare an RGD-ArBF<sub>3</sub>

AlkynylArBF<sub>3</sub> **6.2** was obtained as described in Chapter 6. The click reaction was undertaken under similar conditions. CuSO<sub>4</sub>/sodium ascorbate was used as the catalyst. The click reaction was incubated at room temperature for 0.5 hours and then injected into the HPLC. The HPLC chromatogram (red HPLC trace) in Figure 8.5 showed good resolution among the reactants and product. The massive peak (3 to 10 min) of the red HPLC trace probably contained DMSO and sodium ascorbate, the amount of which in the reaction was very high to cause overloading on the column. Although the accurate concentration of **6.2** in its DMSO stock solution was not determined, the HPLC trace indicates that 10  $\mu$ L of the stock solution of **6.2** seemed a large excess compared with the peptide charged in the click reaction.

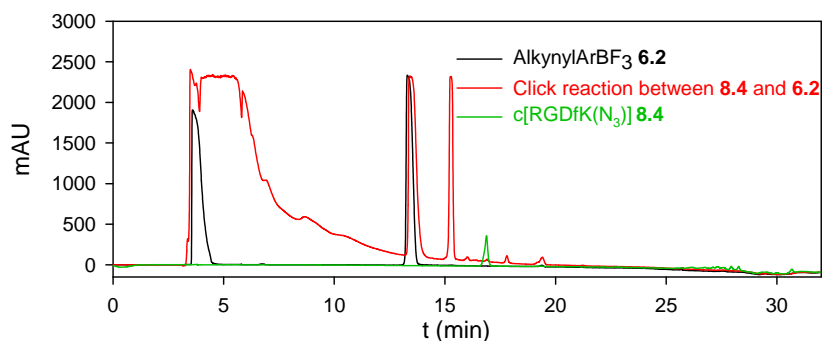


**Figure 8.5** The HPLC chromatogram of the click reaction between **8.4** and **6.2**.

The RP-HPLC was performed via HPLC Program 8 with Column I in HPLC System I and the HPLC traces recorded at 229 nm were indicated here. The black trace is that of alkynylArBF<sub>3</sub> **6.2** and the peak at 13.4 min represents **6.2**; the green HPLC chromatogram is for c[RGDfK(N<sub>3</sub>)] **8.4** and the peak at 16.8 min is **8.4**; the red HPLC trace is for the crude click reaction between **8.4** and **6.2** and the newly produced peak at 15.3 min is the desired product of the click reaction. The condition for the click reaction: **8.4** (100 nmol), CH<sub>3</sub>CN (10  $\mu$ L), **6.2** in *d*<sub>6</sub>-DMSO (concentration not determined, > 30 mM based on <sup>19</sup>F NMR, 10  $\mu$ L), 0.60 M sodium ascorbate (5  $\mu$ L), and 0.998 M CuSO<sub>4</sub> (5  $\mu$ L), rt, 0.5 hr. The reaction was diluted with 80  $\mu$ L of 0.04 M HCO<sub>2</sub>NH<sub>4</sub> aqueous solution prior to the HPLC injection.

An ESI-LCMS was carried out to analyze the reaction, as shown in Figure 8.6. The HPLC chromatogram demonstrated similar resolution pattern as shown in Figure 8.5. With a smaller amount of the stock solution of **6.2**, the click reaction was incubated at room temperature for 0.5 hours and then injected into the ESI-LCMS. AlkynylArBF<sub>3</sub> **6.2** was detected at about 15.1 minutes, while the peak at 16.4 minutes provided the mass-to-charge ratio (*m/z*) (891.1 for [M]<sup>-</sup> and 871.3 for [M-HF]<sup>-</sup> at the negative mode)

of the desired product. This suggested that the reaction worked successfully. With slightly different HPLC systems, the small difference of retention times is reasonable due to the different loop length and pressure applied to the system.

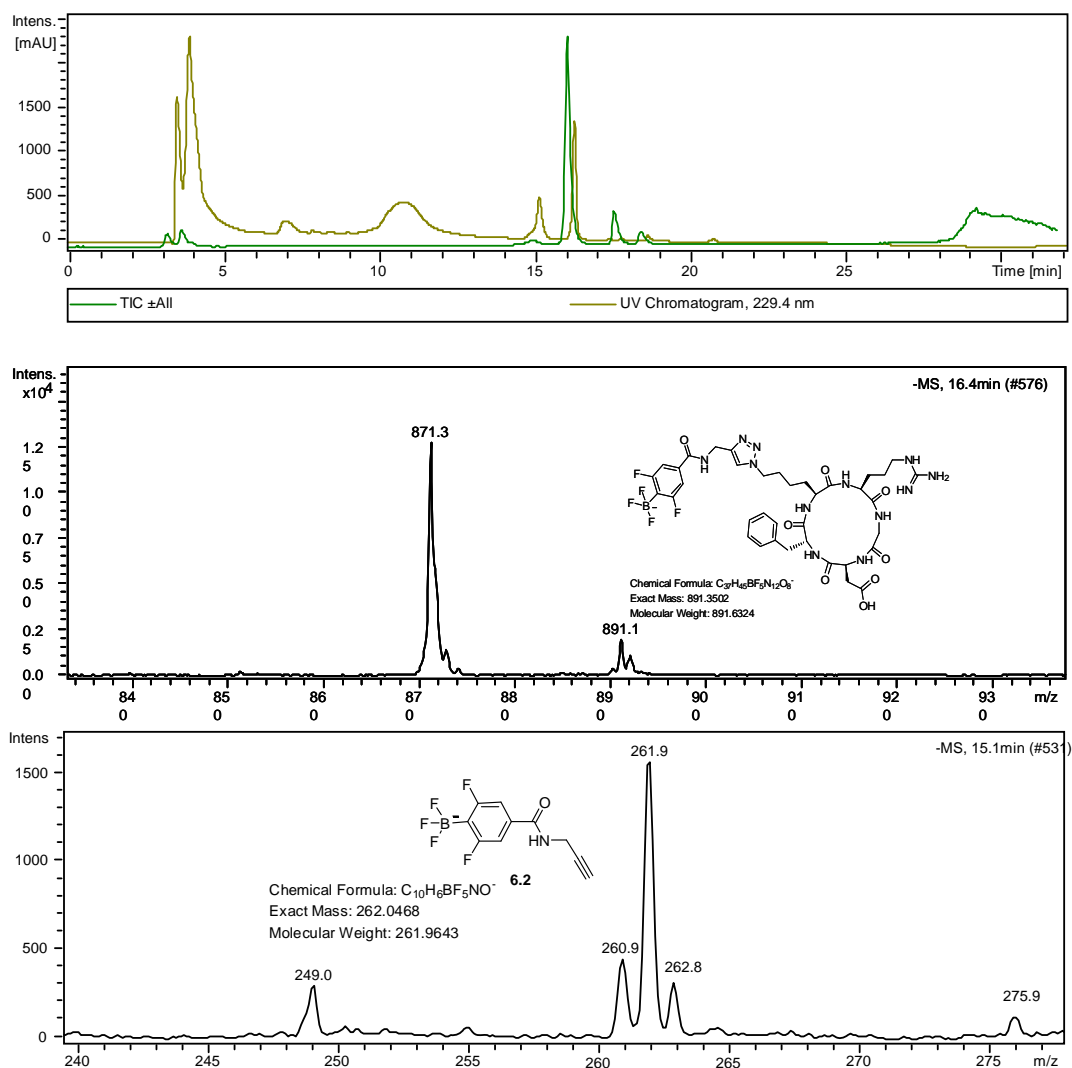


**Figure 8.6** The LCMS chromatograms and ESI-spectra of the click reaction between **6.2** and **8.4**.

The LCMS was performed via HPLC Program 8 with Column I in ESI-LCMS and the HPLC traces recorded at 229 nm were indicated here. The first ESI-spectrum is for the peak detected at 16.4 min. The second ESI-spectrum is for the peak at 15.1 min. Both of the structures corresponding to the  $m/z$  are shown in the ESI-spectra. The conditions for the click reaction: **8.4** (100 nmol), CH<sub>3</sub>CN (10  $\mu$ L), **6.2** in *d*<sub>6</sub>-DMSO (concentration not determined, > 30 mM based on <sup>19</sup>F NMR, 5  $\mu$ L), 0.60 M sodium ascorbate (5  $\mu$ L), and 0.998 M CuSO<sub>4</sub> (5  $\mu$ L), rt, 0.5 hr. The reaction was diluted with 79  $\mu$ L of 0.04 M HCO<sub>2</sub>NH<sub>4</sub> aqueous solution prior to the LCMS injection.

### 8.2.3.2 The one-pot two-step <sup>18</sup>F-labeling to prepare an RGD-ArBF<sub>3</sub>

Under the same reaction conditions as described above, the one-pot two-step radiosynthesis to label the RGD-peptide with an ArBF<sub>3</sub> was undertaken through the click

reaction with the prosthetic group alkyne- $^{18}\text{F}$ -ArBF<sub>3</sub> **6.2**. Alkyne- $^{18}\text{F}$ -ArBF<sub>3</sub> **6.2** was prepared the same way as described in the previous chapters, and a radiochemical yield of 36% was obtained for the reaction whose HPLC is shown in Figure 8.7. Similarly, the reaction was quenched with 5% NH<sub>4</sub>OH/EtOH, and the quenched reaction was added to the mixture of *c*[RGDfK(N<sub>3</sub>)] **8.4** and sodium ascorbate in aqueous CH<sub>3</sub>CN. CuSO<sub>4</sub> was added to initiate the click reaction. After 0.5 hours, the reaction was analyzed by HPLC. The conjugation of the ArBF<sub>3</sub> was highly dependent on the amounts of *c*[RGDfK(N<sub>3</sub>)] **8.4** and the catalyst, same as that described in Chapter 7. As shown in Figure 8.7, alkyne- $^{18}\text{F}$ -ArBF<sub>3</sub> **6.2** from the first step was almost all consumed to give the newly produced radioactive product at ~ 15.6 minutes. The overall radiochemical yield was 29% in 58 minutes.

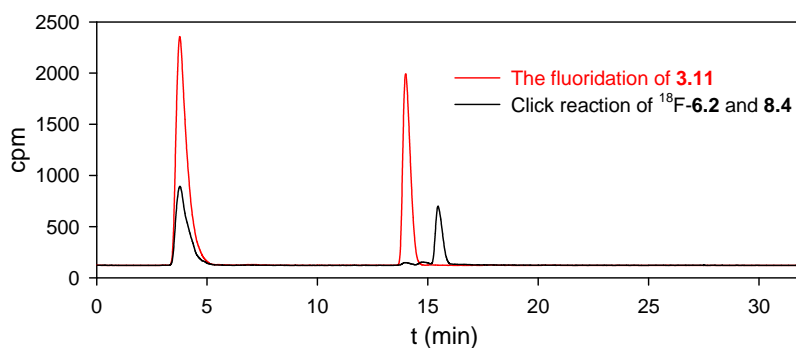


**Figure 8.7** The radio-HPLC traces of the one-pot two-step labeling reaction to prepare RGD- $^{18}\text{F}$ -ArBF<sub>3</sub>.

The red trace was for the crude fluoridation reaction of **3.11** to prepare alkyne- $^{18}\text{F}$ -ArBF<sub>3</sub> **6.2** and the black trace was for the click reaction between the crude  $^{18}\text{F}$ -**6.2** and *c*[RGDfK(N<sub>3</sub>)] **8.4**. The HPLC was performed via Program 8 with Column I in HPLC System IV. The reaction condition for the fluoridation of **3.11**: **3.11** (100 nmol), THF (4  $\mu\text{L}$ ), concentrated HCl (0.5  $\mu\text{L}$ ),  $^{18}\text{F}$ -solution containing  $^{19}\text{F}$ -fluoride (500 nmol, 2  $\mu\text{L}$ ), rt, 30 min, the radioactivity at the BOS: 6.05 mCi and RCY: 36%; the click reaction between the crude **6.2** and **8.4**: the quenched reaction of  $^{18}\text{F}$ -**6.2** (30  $\mu\text{L}$  out of 36  $\mu\text{L}$  was used in this reaction), **8.4** (100 nmol), 0.6 M sodium ascorbate (6  $\mu\text{L}$ ), 0.25 M CuSO<sub>4</sub> (6  $\mu\text{L}$ ), rt, 28 min, the radioactivity at the BOS: 3.58 mCi. RCY over two steps: 29%.

## 8.3 Discussion

### 8.3.1 Synthesis

The preparation of the RGD-containing peptides is summarized in Scheme 8.1 and Scheme 8.2. Briefly, the core structure of the peptides was prepared via the Fmoc solid phase peptide synthesis starting with the 2-chlorotrityl chloride resin. To avoid racemization during the macrolactamization, glycine was first introduced to the resin and

the resin loading with glycine was determined to be from 0.3 to 0.6 mmol/g. Then, the other amino acids were introduced to the resin in the order of arginine, *D*-phenylalanine, lysine or derivatives, and aspartic acid as their Fmoc-protected counterparts with side chains protected with orthogonal protecting groups. The Fmoc protecting group was removed rapidly and efficiently by the treatment with 20% piperidine in DMF and HBTU/DIPEA was used to extend the peptide. When the linear sequence was constructed, the linear peptides were cleaved from the 2-chlorotrityl resin with HFIP, which is not strong enough of an acid to influence the other acid-labile protecting groups such as *tert*-butyl and Pbf groups. The Et<sub>2</sub>O wash very effectively removed most of the non-polar impurities from the peptides.

To prepare the cyclopentapeptides, the macrolactamization of the linear peptide H<sub>2</sub>N-Asp(O<sup>t</sup>Bu)-*D*-Phe-Lys(N<sub>3</sub>)-Arg(Pbf)-Gly-OH **8.2a** was studied with PyBOP or HBTU as the dehydrating agent in DMF or CH<sub>3</sub>CN. The results did not exhibit significant difference between the coupling reagents/solvents. Based on the HPLC analysis of the coupling reactions shown in Figure 8.1, we decided to work with HBTU in CH<sub>3</sub>CN since HBTU is much cheaper and the use of CH<sub>3</sub>CN as the reaction solvent simplifies the work-up. As a result, cyclopentapeptides **8.3a**, **8.3b** and **8.3c** were obtained with moderate-to-high yields (75-95%).

To conjugate the cyclopentapeptides with other molecules of interest, peptide **8.5** was prepared from either **8.3b** or **8.3c**. Although both methods successfully gave the desired product with relatively high yields, the faster and more efficient protocol involving NH<sub>2</sub>NH<sub>2</sub> to remove the Dde protecting group was favoured. Moreover, it was also found that if there was any residual Pd/C in the peptide **8.5** from the deprotection of the Cbz group of **8.3b** after the work-up, the following coupling reaction with boronate **3.1** always failed and gave the oxidatively deboronated product<sup>a</sup> instead. It is believed that trace amounts of Pd can possibly act as a catalyst that inserts into the C-B bond. When air or water is present, deboronation may occur under such conditions. As a result, the preparation of peptide **8.5** from peptide **8.3c** was then followed more closely. The cyclopentapeptide **8.5** was directly coupled to the boronates to give boronates **8.6** and

---

<sup>a</sup> The oxidatively deboronated product was verified by ESI-LRMS: [M+Na]<sup>+</sup>: 934.8.

**8.12.** For peptide **8.12**, a piperazine linker was used to connect the RGD and the boronate residue, and it was expected that the piperazine linker might enhance the fluoridation, based on the fluoridation studies on several similar boronate derivatives in Chapter 3. The succinimide linker was used to connect the amino group on the lysine side chain and the piperazine. The detailed synthesis of **8.12** is summarized in Scheme 8.2. To achieve peptide **8.12**, two coupling strategies were used: one was focused on the final conjugation of boronate **3.1** with the piperazine-bearing peptide **8.11**, while the other involved coupling the piperazinyl derivatized boronate **8.17** and the cyclopentapeptide **8.5**. Although both synthetic routes worked as planned, the latter synthetic pathway with one more step, as shown in Scheme 8.2, had a bit higher overall yield of 34% to give the fully protected RGD-boronate **8.12**. One more advantage for the second synthesis is that most of the intermediates can be purified via flash chromatography, which at least ensures the final coupling reaction experiences fewer side reactions. The fluorescent peptides *c*[RGDfK(coumarin)] **8.20** and *c*[RGDfK(FITC)] **8.21** were also synthesized for use in *in vitro* cell binding studies. Since only a small amount is needed for such studies, the reactions were carried out successfully on a small scale. Finally, all the protected RGD-peptides were treated with 5% H<sub>2</sub>O in TFA to remove the *tert*-butyl and Pbf groups to free the side chains of the glutamate and arginine residues in high yields. The peptides **8.4**, **8.7** and **8.13** were further purified via semi-preparative RP-HPLC.

### **8.3.2 The fluoridation to prepare RGD-ArBF<sub>3</sub>s**

Two methods were used to label the RGD-containing peptides with ArBF<sub>3</sub>s in this chapter. The one-step fluoridation was undertaken with RGD-boronates **8.7** and **8.13** under acidic conditions. The one-pot two-step labeling method based on copper(I) catalyzed azide-alkyne cycloaddition was also investigated.

#### **8.3.2.1 The one-step fluoridation of RGD-boronates**

Both RGD-boronates **8.7** and **8.13** were initially studied for their fluoridation under cold conditions. The reactions occurred in a similar manner as described in the previous chapters. However, unlike some of the compounds studied earlier, which provide clear LRMS or HRMS traces, the corresponding ArBF<sub>3</sub>s **8.18** and **8.19** collected from the

HPLC separation tended not to fly, or for reasons that are unclear, the signals were suppressed by the presence of unknown species in the ESI-MS instrument. Instead, ESI-LCMS was used to directly detect the mass of the product during purification. The results suggested that both the fluoridation reaction and HPLC separation were very successful to afford the desired products. Moreover, it may be worthwhile to mention that since there is a free carboxylic group present in the molecule, the  $\text{ArBF}_3$  tested gave both the desired anion with only one negative charge and also the doubly charged anion. Meanwhile, we also observed relatively strong mass signals of the  $[\text{M-HF}]^-$  species for every  $\text{ArBF}_3$  tested in this chapter.

Following the same labeling and HPLC separation conditions, RGD-boronates **8.7** and **8.13** were  $^{18}\text{F}$ -radiolabeled as previously described. Carrier  $^{19}\text{F}$ -fluoride was added to the  $^{18}\text{F}$ -fluoride to push the fluoridation reaction forward. For both peptides, the radiochemical yields of approximately 10-15% were achieved. The fluoridation of **8.13**, which contains the piperazine linker, exhibited a slightly higher conversion than that of **8.7** with the same portion of  $^{18/19}\text{F}$ -fluoride cocktail. This tiny difference on the radiochemical yield may or may not be due to the structural modification from the linker since operating error cannot be excluded. Furthermore, the succinimide linker in **8.13** might also play some role during the fluoridation. Further systematic study on the fluoridation might be needed to confirm the influence of the structure modification.

### **8.3.2.2 The one-pot two-step labeling of an RGD-peptide with the $\text{ArBF}_3$**

The one-pot two-step labeling method via click chemistry was also applied to prepare the RGD- $\text{ArBF}_3$ . The nonradioactive click reaction between **6.2** and **8.4** catalyzed by  $\text{CuSO}_4$ /sodium ascorbate was analyzed by ESI-LCMS and the mass of the product was detected at a retention time of approximately 16 minutes. Based on these results, the radiolabeling using this method was undertaken. One such  $^{18}\text{F}$ -radiosynthesis is shown in Figure 8.7. The radiochemical yield of the fluoridation of alkynylarylboronic acid **3.11** was 36% after 30 minutes. The subsequent click reaction with  $c[\text{RGDfK}(\text{N}_3)]$  **8.4**, catalyzed with sodium ascorbate/ $\text{CuSO}_4$  was incubated at room temperature for another 30 minutes and then injected into the HPLC for analysis. From Figure 8.7, most of the radioactive product from the first step was consumed to give a new  $^{18}\text{F}$ -labeled species. It

was also noticed that a fast click reaction relies significantly on the catalyst loading as well as the amount of the reactant besides the  $^{18}\text{F}$ -prosthetic synthon **6.2** in Chapter 7, in which the folate was radiolabeled with the  $^{18}\text{F}$ -ArBF<sub>3</sub> by the same one-pot two-step labeling method. With the amounts of CuSO<sub>4</sub> and sodium ascorbate used in the experiment shown in Figure 8.7, the reaction was complete within 30 minutes. A few experiments ( $n \geq 4$ ) thus far have indicated that the click reaction for labeling the peptide with the  $^{18}\text{F}$ -ArBF<sub>3</sub> using alkynyl- $^{18}\text{F}$ -ArBF<sub>3</sub> **6.2** as the  $^{18}\text{F}$ -prosthetic group is highly efficient.

When comparing the radiolabeling of the two methods to label the peptides containing the RGD sequences, the one-pot two-step labeling strategy involving click chemistry, resulted in a higher radiochemical yield, which was almost double that of the one-step labeling, with a totally reaction time of one hour. This difference is only due to the  $^{18}\text{F}$ -fluoridation of the boronates. This implies that more effort will be required to improve the fluoridation of the benzopinacol protected boronate while synthetic strategies may need to be developed for non-protected-boronate-biomolecular conjugates to ensure faster/higher yielding fluoridations.

None of the RGD-ArBF<sub>3</sub>s has yet been tested for their stability under physiological conditions. This is majorly due to the fact that no large scale preparation of the RGD-ArBF<sub>3</sub>s was obtained. However, based on previous experience, the ArBF<sub>3</sub> should have solvolytic half-lives of ~ 1000 to 1200 minutes. If this assumption is correct, they are ready for animal imaging studies since it is about 10 times the half-life of  $^{18}\text{F}$ -fluoride (109.8 minutes).

The specific activity in both reactions was limited by the addition of carrier fluoride. It is expected that high specific activities can be achieved by working with higher levels of radioactivity as we reported for marimastat-ArBF<sub>3</sub>. Given that the reaction is manually performed, the radiation safety might become a substantial concern, especially if we need high levels of radioactivity. The execution of the  $^{18}\text{F}$ -fluoridation with microfluidic reactors or some automatic controlled systems may resolve this problem.

## 8.4 Conclusion and future perspectives

Overall, several linear RGD-containing peptides have been synthesized via the Fmoc solid phase peptide synthesis. The cyclopentapeptides were obtained from the linear peptides via the macrolactamization using HBTU/DIPEA as the coupling reagent/base. The  $\epsilon$ -amino group on the side chain of lysine was used to derivatize the peptide with either boronate or fluorophores. The products were then treated with TFA to remove all the acid-labile protecting groups to provide peptides **8.4**, **8.7**, **8.13**, **8.20** and **8.21**. RGD-boronates **8.7** and **8.13** were  $^{18}\text{F}$ -radiofluoridated in the presence of carrier  $^{19}\text{F}$ -fluoride at room temperature for one hour in reasonable radiochemical yields (10-15%). It was found that the piperazine linker on boronate **8.13** might have slightly enhancing effects for the fluoridation but not dramatically. In addition, the one-pot two-step labeling strategy based on copper(I) catalyzed click chemistry has also been practiced to label the cyclopentapeptide with the  $^{18}\text{F}$ - $\text{ArBF}_3$  and a much higher yield was obtained than the one-step labeling protocols of either **8.7** or **8.13**. The specific activity could be calculated based on carrier  $^{19}\text{F}$ -fluoride added to  $^{18}\text{F}$ -fluoride. For the calculation for the specific activity of the  $^{18}\text{F}$ - $\text{ArBF}_3$ s prepared, it is believed to be triple that of the free fluoride as discussed in Chapter 1.

However, none of the biological properties of these peptides have been studied yet. The fluorescent peptides **8.20** and **8.21** were synthesized for this purpose. In the near future, when suitable cell lines are ready, the binding affinity will be tested for all these cyclopentapeptides. Eventually, the animal imaging studies for the  $^{18}\text{F}$ - $\text{ArBF}_3$  radiolabeled cyclopentapeptides with suitable tumor models will hopefully validate the hypothesis of “*applying  $\text{ArBF}_3$ s as PET imaging agents*”.

## 8.5 Methods and materials

Reagents and solvents were purchased from Fisher, Sigma-Aldrich, Alfa-Aesar, Novabiochem or Oakwood. All chemicals were used as supplied unless stated otherwise. The  $^{18}\text{F}$  Trap & Release column ( $\text{HCO}_3^-$  form,  $\sim 10$  mg) was purchased from ORTG, Inc. Deuterated solvents were obtained from Cambridge Isotope Laboratories. Analytical thin layer chromatography was undertaken on Silica Gel 60 F254 Glass TLC plates from

EMD Chemicals and SiliaFlash F60 from Silicycle was used for flash chromatography. All NMR spectra were recorded at room temperature on a Bruker Avance 300 or 400 MHz spectrometer. Chemical shifts are reported using the  $\delta$  scale in *ppm* and all coupling constants (*J*) are reported in hertz (Hz). Unless specified,  $^1\text{H}$  NMR spectra are referenced to the tetramethylsilane peak ( $\delta = 0.00$  *ppm*),  $^{13}\text{C}$  NMR spectra are referenced to the chloroform peak ( $\delta = 77.23$  *ppm*), and  $^{19}\text{F}$  NMR spectra are referenced to NEAT trifluoroacetic acid ( $\delta = 0.00$  *ppm*,  $-78.3$  *ppm* relative to  $\text{CFCl}_3$ ). Mass spectrometry was performed at the Mass Spectrometry lab of the University of British Columbia (U.B.C.) Chemistry Department. The radiolabeling experiments were performed at TRIUMF, Vancouver, BC, Canada. The HPLC information is attached in Appendix B.

**WARNING:** All  $^{18}\text{F}$ -labeling work was done at TRIUMF. Radiation protection procedures strictly followed the TRIUMF Radiation Safety Regulations. Since this work involves mainly manual handling, fairly high amounts of dosage might be applied, and special caution is required to reduce the operating time. A lead brick castle was built up to shield the radiation. All the materials that came in contact with the source water (the  $^{18}\text{O}$ -water) were collected and decayed separately from other  $^{18}\text{F}$ -contaminated stuffs including gloves, sleeves, vials, tubes, and pipette tips prior to disposal.

## 8.5.1 Synthesis

### Fmoc-*D*-Phe-OH

*D*-Phe-OH (2.36 g, 14.3 mmol) in 9%  $\text{Na}_2\text{CO}_3$  solution (30 mL) was slowly added with Fmoc-OSu (5.00 g, 15.0 mmol) in 1,4-dioxane (40 mL) at rt for 0.5 hr. The mixture was stirred at rt overnight and extracted with EtOAc ( $3 \times 50$  mL). The organic layers were combined, washed with  $\text{H}_2\text{O}$  ( $1 \times 50$  mL) and brine ( $1 \times 50$  mL), and then dried over anhydrous  $\text{Na}_2\text{SO}_4$ . The solution was filtered and concentrated under reduced pressure. The residue was recrystallized with toluene/hexanes to give a white solid as the desired product, which was used directly without further purification. Yield: 4.54 g, 82%.  $^1\text{H}$  NMR (400 MHz,  $\text{CDCl}_3$ , rt):  $\delta$ (*ppm*) 3.04 (m, 1 H), 3.19 (m, 1 H), 4.14 (t,  $J = 6.80$  Hz, 1 H), 4.26 (m, 1 H), 4.38 (m, 1 H), 4.58 (d,  $J = 5.20$  Hz, 1 H), 5.37 (d,  $J = 7.60$  Hz, 1 H), 7.15 (d,  $J = 6.40$  Hz, 2 H), 7.26 (m, 5 H), 7.37 (d,  $J = 7.40$  Hz, 2 H), 7.49 (t,  $J = 6.15$  Hz,

2 H), 7.73 (d,  $J = 7.20$  Hz, 2 H);  $^{13}\text{C}$  NMR (100.6 MHz,  $\text{CDCl}_3$ , rt):  $\delta(\text{ppm})$  37.88, 47.21, 55.37, 67.20, 120.10, 125.16, 125.25, 127.19, 127.85, 128.75, 129.49, 136.15, 141.41, 143.81, 143.91, 156.15; ESI-LRMS:  $[\text{M}+\text{Na}]^+$ : 410.2 (100%),  $[\text{2M}-1]^-$ : 773.4 (100%).

### **Fmoc-(L)-Lys-OH·xTFA/HOAc**

Fmoc-(L)-Lys(Boc)-OH **5.3** (2.00 g, 4.27 mmol) in 50% TFA in  $\text{CH}_2\text{Cl}_2$  (60 mL) was stirred at rt for 2 hr and the solvent was removed under reduced pressure. The residue was loaded to a silica gel packed column for flash chromatography (MeOH: $\text{CH}_2\text{Cl}_2$  5:95 then 1:9 then HOAc:MeOH: $\text{CH}_2\text{Cl}_2$  1:1:9) to give pale yellow oil, which soon solidified upon stand to give a white powder as the desired product ( $R_f = 0.02$  in 1:9 MeOH: $\text{CH}_2\text{Cl}_2$ ). Yield: 2.26 g.<sup>a</sup>  $^1\text{H}$  NMR (400 MHz,  $d_6$ -DMSO, rt):  $\delta(\text{ppm})$  1.13-1.79 (m, 6 H), 2.76 (m, 2 H), 3.21 (m, 1 H), 4.24 (m, 1 H), 7.34 (td,  $J_1 = 7.40$  Hz,  $J_2 = 1.04$  Hz, 2 H), 7.41 (td,  $J_1 = 7.40$  Hz,  $J_2 = 0.72$  Hz, 2 H), 7.84 (d,  $J = 7.40$  Hz, 2 H), 7.89 (d,  $J = 4.08$  Hz, 2 H); ESI-LRMS:  $[\text{M}+\text{H}]^+$ : 369.4 (100%).

### **Fmoc-(L)-Lys(N<sub>3</sub>)-OH**

$\text{NaN}_3$  (1.46 g, 22.5 mmol) was suspended in  $\text{H}_2\text{O}$  (4.0 mL) and  $\text{CH}_2\text{Cl}_2$  (6.0 mL) over an ice- $\text{H}_2\text{O}$  bath.  $\text{Tf}_2\text{O}$  (0.76 mL, 4.49 mmol) was slowly added to the mixture for 0.5 hr at 0 °C. The reaction was then stirred at 0 °C for 5 hr and extracted with  $\text{CH}_2\text{Cl}_2$  ( $2 \times 20$  mL). The  $\text{CH}_2\text{Cl}_2$  layers were combined, washed with saturated  $\text{Na}_2\text{CO}_3$  ( $1 \times 20$  mL), and directly used without further purification. The  $\text{CH}_2\text{Cl}_2$  solution was then dropwise added to the mixture of  $\text{K}_2\text{CO}_3$  (1.12 g, 7.9 mmol),  $\text{CuSO}_4 \cdot 5\text{H}_2\text{O}$  (5.0 mg, cat.), and Fmoc-Lys-OH·xTFA/HOAc (1.30 g, 2.60 mmol) in 54% aqueous MeOH (6.5 mL) and the resulting mixture was stirred at rt overnight. The reaction was quenched by the addition of 2.5 N HCl (30 mL) and extracted with  $\text{CH}_2\text{Cl}_2$  ( $3 \times 50$  mL). The  $\text{CH}_2\text{Cl}_2$  layers were combined, washed with brine ( $1 \times 50$  mL), and dried over anhydrous  $\text{Na}_2\text{SO}_4$ . The solution was filtered and concentrated under vacuum to give sticky oil, which was directly charged over flash chromatography (MeOH:  $\text{CH}_2\text{Cl}_2$  0.5:99.5 then 1:99) to afford yellowish oil as the desired product ( $R_f = 0.37$  in 1:9 MeOH: $\text{CH}_2\text{Cl}_2$ ). Yield: 1.21 g, 99%.  $^1\text{H}$  NMR (400 MHz,  $\text{CD}_2\text{Cl}_2$ , rt):  $\delta(\text{ppm})$  1.20-1.90 (m, 6 H), 3.31 (t,  $J = 5.40$  Hz,

<sup>a</sup> The yield was not determined since the compound may contain unknown amount of TFA or HOAc. And it was assumed to be quantitatively converted.

2 H), 4.27 (m, 1 H), 4.39-4.56 (m, 3 H), 5.39 (m, 1 H), 7.35 (t,  $J = 7.40$  Hz, 2 H), 7.44 (t,  $J = 7.40$  Hz, 2 H), 7.64 (d,  $J = 5.60$  Hz, 2 H), 7.81 (d,  $J = 7.60$  Hz, 2 H), 10.40 (s, br, 1 H);  $^{13}\text{C}$  NMR (100.6 MHz,  $\text{CD}_2\text{Cl}_2$ , rt):  $\delta(\text{ppm})$  22.65, 28.43, 31.78, 47.29, 51.26, 53.74, 67.11, 120.07, 125.13, 127.18, 127.83, 141.42, 143.92, 156.33, 176.89; ESI-LRMS:  $[\text{M}+\text{Na}]^+$ , 417.3 (100%).

### Dde-OH

5,5-Dimethyl-1,3-cyclohexanedione (5.00 g, 35.7 mmol), DMAP (4.80 g, 39.2 mmol), and EDC·HCl (7.50 g, 39.2 mmol) were dissolved in DMF (75.0 mL).<sup>521</sup> HOAc (2.25 mL, 39.3 mmol) was slowly added to the solution. The resulting mixture was stirred at rt overnight and then concentrated under reduced pressure. The residue was resuspended in EtOAc (200 mL), washed with 1 N HCl ( $2 \times 50$  mL),  $\text{H}_2\text{O}$  ( $2 \times 50$  mL) and brine ( $1 \times 50$  mL), and dried with anhydrous  $\text{Na}_2\text{SO}_4$ . The solution was filtered and concentrated *in vacuo*. The residue was loaded to a silica gel column for flash chromatography (EtOAc:hexanes 1:19 to 1:9) to give yellowish oil ( $R_f = 0.36$  in 1:3 EtOAc:hexanes) which solidified upon cooling. Yield: 5.34 g, 82%.  $^1\text{H}$  NMR (300 MHz,  $\text{CDCl}_3$ , rt):  $\delta(\text{ppm})$  1.07 (t,  $J = 2.66$  Hz, 6 H), 2.34 (d,  $J = 5.03$  Hz, 2 H), 2.52 (d,  $J = 4.67$  Hz, 2 H), 2.59 (d,  $J = 3.38$  Hz, 3 H);  $^{13}\text{C}$  NMR (75.5 MHz,  $\text{CDCl}_3$ , rt):  $\delta(\text{ppm})$  28.32, 28.66, 30.77, 47.01, 52.58, 112.48, 195.28, 198.01, 202.55; ESI-LRMS:  $[\text{M}-\text{H}]^-$  181.3 (100%).

### Fmoc-(L)-Lys(Dde)-OH

Fmoc-(L)-Lys-OH·xTFA/HOAc (2.26 g, 4.27 mmol) and Dde-OH (2.0 g, 10.98 mmol) in EtOH (50 mL) was heated to reflux for 48 hr and the solvent was removed under reduced pressure.<sup>522, 523</sup> The residue was charged with flash chromatography (MeOH: $\text{CH}_2\text{Cl}_2$  1:99 to 3:97) to give a white solid as the desired product ( $R_f = 0.26$  in 1:9 MeOH: $\text{CH}_2\text{Cl}_2$ ). Yield: 1.28 g, 56%.  $^1\text{H}$  NMR (400 MHz,  $\text{CDCl}_3$ , rt):  $\delta(\text{ppm})$  1.05 (s, 6 H), 1.56 (m, 2 H), 1.68-1.94 (m, 3 H), 2.02 (m, 1 H), 2.40 (s, 4 H), 2.59 (s, 3 H), 3.46 (m, 2 H), 3.24 (m, 3 H), 4.41 (d,  $J = 7.09$  Hz, 2 H), 4.50 (m, 1 H), 5.80 (d,  $J = 8.29$  Hz, 1 H), 7.33 (td,  $J_1 = 7.46$  Hz,  $J_2 = 1.14$  Hz, 2 H), 7.42 (t,  $J = 7.34$  Hz, 2 H), 7.63 (t,  $J = 8.65$  Hz, 2 H), 7.79 (d,  $J = 7.44$  Hz, 2 H);  $^{13}\text{C}$  NMR (100.6 MHz,  $\text{CDCl}_3$ , rt):  $\delta(\text{ppm})$  22.60, 28.36, 30.49, 32.08, 43.87, 47.37, 51.98, 53.58, 67.32, 120.22, 125.34, 127.29, 127.96, 141.51, 143.92, 156.38, 174.57, 198.37; ESI-HRMS: calcd. for  $\text{C}_{31}\text{H}_{35}\text{N}_2\text{O}_6^-$ : 531.2495, found

531.2505.

From the same reaction, a byproduct Fmoc-Lys(Dde)-OEt<sup>a</sup> was also obtained (0.74 g, 31%). This compound was dissolved in 1 M CaCl<sub>2</sub> in 7:3 <sup>1</sup>PrOH:H<sub>2</sub>O (100.0 mL) and added with 0.88 M aqueous NaOH (15.0 mL) dropwise.<sup>524, 525</sup> The reaction was stirred at rt for 3 hr and extracted with EtOAc (50 mL). The EtOAc layer was discarded; the aqueous layer was acidified with 3 N HCl to pH ~ 1 and extracted with EtOAc (3 × 50 mL). The EtOAc layers were combined, washed with H<sub>2</sub>O (3 × 50 mL) and brine (1 × 50 mL), and dried over anhydrous Na<sub>2</sub>SO<sub>4</sub>. The salt was filtered off and the solvent was removed under reduced pressure. The residue was loaded to a silica gel column for flash chromatography (MeOH:CH<sub>2</sub>Cl<sub>2</sub> 3:97) to give the desired product. Yield: 498.4 mg, 71%.

#### **H-Asp(O<sup>t</sup>Bu)-D-Phe-Lys(R)-Arg(Pbf)-Gly-OH (8.2a-c)**

The linear peptides **8.2a-c** were prepared following the standard Fmoc solid phase peptide synthesis with 2-chlorotrityl chloride resin.<sup>459, 516</sup> Briefly, Fmoc-Gly-OH (1.00 g, 3.38 mmol) and DIPEA (2.35 mL, 13.52 mmol) were suspended in anhydrous CH<sub>2</sub>Cl<sub>2</sub> (20 mL) in a flame-dried round bottom flask under an Ar atmosphere. DMF (6 mL) was added to assist to dissolve the amino acid prior to the addition of the 2-Cl-trityl chloride resin (2.00 g, 2.60 mmol). The mixture was stirred at rt for 90 min and the solution was filtered off. The capping solution (MeOH:DIPEA:CH<sub>2</sub>Cl<sub>2</sub> 2:1:17, 3 × 20 mL) was mixed thoroughly with the resin and slowly filtered off by gravity. Then the resin was washed with CH<sub>2</sub>Cl<sub>2</sub> (3 × 20 mL), DMF (3 × 20 mL) and CH<sub>2</sub>Cl<sub>2</sub> (6 × 20 mL), and dried thoroughly over high vacuum. The Fmoc-Gly-attached resin was directly used without further treatment. The resin loading of the Fmoc-Gly-resin was tested based on the DBU/DMF/CH<sub>3</sub>CN method and the reported extinction coefficient (7624 M<sup>-1</sup>·cm<sup>-1</sup>) for 9-methylene-9H-fluorene at 304 nm was used.<sup>526</sup> Then the resin was swollen in DMF (1.5 volumes of the resin) for 30 min prior to the synthesis in a spin column (5 mL or 10 mL) sealed with a plastic pipette tip. The DMF was filtered and Fmoc was removed with

<sup>a</sup> Characterization for Fmoc-Lys(Dde)-OEt: <sup>1</sup>H (300 MHz, CDCl<sub>3</sub>, rt): δ(ppm) 1.04 (s, 6 H), 1.31 (t, *J*= 7.10 Hz, 3 H), 1.50 (m, 2 H), 1.74 (m, 2 H), 1.93 (m, 1 H), 2.37 (s, 4 H), 2.58 (s, 3 H), 3.41 (m, 2 H), 4.25 (m, 3 H), 4.43 (m, 3 H), 5.43 (d, *J*= 8.19 Hz, 1 H), 7.34 (t, *J*= 7.10 Hz, 2 H), 7.43 (t, *J*= 7.38 Hz, 2 H), 7.63 (d, *J*= 6.96 Hz, 2 H), 7.79 (d, *J*= 7.47, 2 H); ESI-LRMS: [M+H]<sup>+</sup>, 561.5 (100%).

20% piperidine/DMF (1.5 volumes of the resin) 3 times with each time for 5 min. Then the resin was thoroughly washed with DMF ( $3 \times 10$  mL),  $\text{CH}_2\text{Cl}_2$  ( $3 \times 10$  mL), and DMF ( $3 \times 10$  mL). Fmoc-Arg(Pbf)-OH (4 equivalents) and HBTU (4 equivalents) in DMF (1.5 volumes of the resin) was added to the resin followed by the addition of DIPEA (8 equivalents). The spin column was capped and shaken at rt for 2 hr. Then the solution was directly filtered through the spin column and the resin was washed with DMF ( $3 \times 10$  mL),  $\text{CH}_2\text{Cl}_2$  ( $3 \times 10$  mL), and DMF ( $3 \times 10$  mL) before the next cycle of the addition of the next amino acid (Fmoc-Lys(R)-OH, Fmoc-*D*-Phe-OH, and the last Fmoc-Asp(O<sup>t</sup>Bu)-OH). After the fifth amino acid (Fmoc-Asp(O<sup>t</sup>Bu)-OH) was attached, the Fmoc group was removed following the same procedure and the resin was thoroughly washed with DMF ( $3 \times 10$  mL),  $\text{CH}_2\text{Cl}_2$  ( $3 \times 10$  mL), DMF ( $3 \times 10$  mL), and  $\text{CH}_2\text{Cl}_2$  ( $5 \times 10$  mL), and dried over vacuum to remove the residual solvent. Then the resin was transferred to a round bottom flask and treated with 20% HFIP/ $\text{CH}_2\text{Cl}_2$  (10 volumes of the resin). The mixture was incubated at rt for 20 min and then filtered off. The filtrate was concentrated under reduced pressure and the residue was triturated with MeOH/Et<sub>2</sub>O to give a whitish solid. The peptides were directly used for cyclization without further purification. Peptides **8.2a-c** were analyzed with RP-HPLC via HPLC Program 1 with Column I in HPLC System I and characterized with ESI mass spectrometry.

H-Asp(O<sup>t</sup>Bu)-*D*-Phe-Lys(N<sub>3</sub>)-Arg(Pbf)-Gly-OH **8.2a**  $t_R = 25.4$  min; ESI-HRMS: calcd. for  $\text{C}_{44}\text{H}_{66}\text{N}_{11}\text{O}_{11}\text{S}^+$ : 956.4664, found: 956.4639;

H-Asp(O<sup>t</sup>Bu)-*D*-Phe-Lys(Cbz)-Arg(Pbf)-Gly-OH **8.2b**  $t_R = 25.8$  min; ESI-HRMS: calcd. for  $\text{C}_{52}\text{H}_{73}\text{N}_9\text{O}_{13}\text{NaS}^+$ : 1086.4946, found: 1086.4930;

H-Asp(O<sup>t</sup>Bu)-*D*-Phe-Lys(Dde)-Arg(Pbf)-Gly-OH **8.2c**  $t_R = 25.2$  min; ESI-HRMS: calcd. for  $\text{C}_{54}\text{H}_{80}\text{N}_9\text{O}_{13}\text{S}^+$ : 1094.5596, found: 1094.5588.

### ***Cyclo*[Arg(Pbf)-Gly-Asp(O<sup>t</sup>Bu)-*D*-Phe-Lys(N<sub>3</sub>)] (8.3a)**

The linear peptide H-Asp(O<sup>t</sup>Bu)-*D*-Phe-Lys(N<sub>3</sub>)-Arg(Pbf)-Gly-OH **8.2a** (100 mg, 0.105 mmol) and DIPEA (54.7  $\mu\text{L}$ , 0.314 mmol) in  $\text{CH}_3\text{CN}$  (105 mL) was added with HBTU (119 mg, 0.314 mmol). The resulting mixture was stirred at rt for 24 hr and concentrated under reduced pressure. Then the residue was suspended in EtOAc (100 mL)

and H<sub>2</sub>O (100 mL) was added to wash the EtOAc layer. The aqueous layer was further extracted with EtOAc (2 × 100 mL). The organic layers were combined, washed with brine (2 × 100 mL), and dried over anhydrous Na<sub>2</sub>SO<sub>4</sub>. The solution was filtered and concentrated to give colorless oil. The residue was then dissolved in minimum MeOH (~ 5 mL) and Et<sub>2</sub>O (300 mL) was added to precipitate the peptide. The solid was filtered off, washed thoroughly with Et<sub>2</sub>O, dried over high vacuum, and used directly without further purification. Yield: 74.5 mg, 76%. The quality of the peptide was determined by RP-HPLC with HPLC Program 1 and Column I in HPLC System I, t<sub>R</sub> = 26.2 min. <sup>1</sup>H NMR (400 MHz, *d*<sub>4</sub>-MeOD, rt): δ(*ppm*) 1.06 (m, 2 H), 1.45 (m, 20 H), 1.68 (m, 2 H), 1.84 (m, 1 H), 2.09 (s, 3 H), 2.51 (m, 4 H), 2.57 (s, 3 H), 2.75 (m, 1 H), 2.98 (m, 1 H), 3.02 (s, 3 H), 3.20 (m, 4 H), 3.99 (m, 1 H), 4.23 (m, 2 H), 4.55 (m, 1 H), 4.75 (m, 1 H), 7.21-7.32 (m, 5 H), 7.90 (m, 1 H), 8.21 (m, 1 H), 8.42 (m, 1 H); ESI-HRMS: calcd. for C<sub>44</sub>H<sub>64</sub>N<sub>11</sub>O<sub>10</sub>S<sup>+</sup>: 938.4558, found: 938.4542.

### ***Cyclo*[Arg(Pbf)-Gly-Asp(O<sup>t</sup>Bu)-D-Phe-Lys(Cbz)] (8.3b)**

The linear peptide H-Asp(O<sup>t</sup>Bu)-D-Phe-Lys(Cbz)-Arg(Pbf)-Gly-OH **8.2b** (50.0 mg, 0.0470 mmol) and DIPEA (25 μL, 0.141 mmol) in CH<sub>3</sub>CN (50 mL) was added with HBTU (53.5 mg, 0.141 mmol). The resulting mixture was stirred at rt for 24 hr and then concentrated under reduced pressure. The residue was suspended in EtOAc (50 mL) and H<sub>2</sub>O (50 mL) was added to wash the EtOAc layer. The aqueous layer was further extracted with EtOAc (2 × 50 mL). The organic layers were combined, washed with brine (2 × 50 mL), and dried over anhydrous Na<sub>2</sub>SO<sub>4</sub>. The solution was filtered and concentrated to give pale yellow oil. The residue was then dissolved in minimum MeOH (~ 2 mL) and Et<sub>2</sub>O (100 mL) was added to triturate the peptide. The solid was filtered off, washed thoroughly with Et<sub>2</sub>O, dried over vacuum, and used directly without further purification. Yield: 46.8 mg, 95%. The quality of the peptide was determined by RP-HPLC with HPLC Program 1 and Column I in HPLC System I, t<sub>R</sub> = 26.4 min. ESI-HRMS: calcd. for C<sub>52</sub>H<sub>71</sub>N<sub>9</sub>O<sub>12</sub>NaS<sup>+</sup>: 1068.4841, found: 1068.4821.

### ***Cyclo*[Arg(Pbf)-Gly-Asp(O<sup>t</sup>Bu)-D-Phe-Lys(Dde)] (8.3c)**

The linear peptide H-Asp(O<sup>t</sup>Bu)-D-Phe-Lys(Dde)-Arg(Pbf)-Gly-OH **8.2c** (200 mg, 0.182 mmol) and DIPEA (96  $\mu$ L, 0.549 mmol) in CH<sub>3</sub>CN (200 mL) was added with HBTU (208 mg, 0.182 mmol). The resulting mixture was stirred at rt for 24 hr and then concentrated under reduced pressure. The residue was suspended in EtOAc (100 mL) and H<sub>2</sub>O (100 mL) was added to wash the EtOAc layer. The aqueous layer was further extracted with EtOAc (2  $\times$  100 mL). The organic layers were combined, washed with brine (2  $\times$  100 mL), and dried over anhydrous Na<sub>2</sub>SO<sub>4</sub>. The solution was filtered and concentrated to give colorless oil. The residue was then dissolved in minimum MeOH (~ 5 mL) and Et<sub>2</sub>O (300 mL) was added to precipitate the peptide. The solid was filtered off, washed thoroughly with Et<sub>2</sub>O, dried over vacuum, and used directly without further purification. Yield: 184.3 mg, 94%. The quality of the peptide was determined by RP-HPLC with HPLC Program 1 and Column I in HPLC System I,  $t_R$  = 26.0 min. ESI-HRMS: calcd. for C<sub>54</sub>H<sub>77</sub>N<sub>9</sub>O<sub>12</sub>NaS<sup>+</sup>: 1098.5310, found: 1098.5328.

### ***Cyclo*[Arg-Gly-Asp-D-Phe-Lys(N<sub>3</sub>)] (*c*[RGDfK(N<sub>3</sub>))](8.4)**

The protected peptide **8.3a** *cyclo*[Arg(Pbf)-Gly-Asp-D-Phe-Lys(N<sub>3</sub>)] (74.5 mg, 0.0794 mmol) was dissolved in TFA:H<sub>2</sub>O (20:1, 42 mL) and the reaction was stirred at rt for 3 hr. Then the solution was concentrated under reduced pressure and toluene (3  $\times$  20 mL) was added to the residue to azeotropically remove the residual TFA and H<sub>2</sub>O. The residue was redissolved in minimum MeOH (~ 2 mL) and triturated with Et<sub>2</sub>O (~ 30 mL) to result in a white solid. The mixture was filtered. The solid was washed with Et<sub>2</sub>O thoroughly and dried over vacuum. Yield: 45.0 mg, 90%. The crude peptide was further purified via semi-preparative HPLC via HPLC Program 9 with Column II in HPLC System I,  $t_R$  = 10.9 min or analyzed via HPLC Program 1 with Column I in HPLC System I,  $t_R$  = 15.1 min. <sup>1</sup>H NMR (400 MHz, *d*<sub>6</sub>-DMSO, rt):  $\delta$  (ppm) 1.06 (m, 2 H), 1.27-1.53 (m, 6 H), 1.54 (m, 1 H), 1.71 (m, 1 H), 2.36 (dd,  $J_1$  = 16.24 Hz,  $J_2$  = 5.60 Hz, 1 H), 2.69 (dd,  $J_1$  = 16.26 Hz,  $J_2$  = 8.70 Hz, 1 H), 2.79 (m, 1 H), 2.91 (m, 1 H), 3.06 (m, 2 H), 3.22 (m, 3 H), 3.93 (m, 1 H), 4.03 (dd,  $J_1$  = 14.18 Hz,  $J_2$  = 7.82 Hz, 1 H), 4.13 (dd,  $J_1$  = 14.14 Hz,  $J_2$  = 7.22 Hz, 1 H), 4.43 (dd,  $J_1$  = 14.16 Hz,  $J_2$  = 7.24 Hz, 1 H), 4.62 (m, 1 H), 6.87 (s, br, 2 H), 7.10-7.29 (m, 7 H), 7.57 (t,  $J$  = 5.48 Hz, 1 H), 7.69 (d,  $J$  = 3.92 Hz, 1 H), 8.00-8.16 (m, 3

H), 8.40 (m, 1 H);  $^{13}\text{C}$  NMR (100.6 MHz,  $d_6$ -DMSO, rt):  $\delta$  (ppm) 23.29, 25.81, 28.18, 28.97, 31.38, 35.66, 37.87, 43.81, 49.48, 51.00, 52.51, 54.92, 126.87, 128.71, 129.70, 137.89, 157.25, 170.11, 170.57, 171.18, 171.70, 172.26, 172.61; ESI-HRMS: calcd. for  $\text{C}_{27}\text{H}_{40}\text{N}_{11}\text{O}_7^+$ : 630.3122, found: 630.3119.

### ***Cyclo*[Arg(Pbf)-Gly-Asp(O<sup>t</sup>Bu)-D-Phe-Lys] (8.5)**

The peptide *cyclo*[Arg(Pbf)-Gly-Asp(O<sup>t</sup>Bu)-D-Phe-Lys(Dde)] **8.3c** (106 mg, 0.099 mmol) in THF (10 mL) was added with  $\text{NH}_2\text{NH}_2\cdot\text{H}_2\text{O}$  (0.4 mL). The resulting mixture was stirred at rt for 20 min and the solution was concentrated under reduced pressure. The residue was dissolved in minimum MeOH (~ 1.5 mL) and  $\text{Et}_2\text{O}$  (40 mL) was added to precipitate the peptide. The peptide was filtered off, washed with  $\text{Et}_2\text{O}$ , dried over high vacuum, and then used directly for the following step without further purification. Yield: 78.4 mg, 87%. The quality of the peptide was determined by RP-HPLC with HPLC Program 1 and Column I in HPLC System I,  $t_{\text{R}} = 22.3$  min. ESI-HRMS: calcd. for  $\text{C}_{44}\text{H}_{66}\text{N}_9\text{O}_{10}\text{S}^+$ : 912.4653, found: 912.4633.

The same peptide can also be obtained from the hydrogenolysis of the Cbz protected peptide **8.3b**. Briefly, 10% Pd/C (100 mg), **8.3b** (100 mg, 0.0956 mmol), and HOAc (6  $\mu\text{L}$ , 0.105 mmol) in dimethyl acetamide (2.0 mL) was stirred at rt under a  $\text{H}_2$  atmosphere for 16 hr. Then the mixture was filtered over Celite and concentrated under reduced pressure. The residue was dissolved in minimum MeOH (~ 2 mL) and  $\text{Et}_2\text{O}$  (~ 50 mL) was added to triturate the peptide. The mixture was then filtered to give a whitish solid as the desired product. Yield: 53.9 mg, 62%.

### ***Cyclo*[Arg(Pbf)-Gly-Asp(O<sup>t</sup>Bu)-D-Phe-Lys(boronate)] (8.6)**

Peptide *cyclo*[Arg(Pbf)-Gly-Asp(O<sup>t</sup>Bu)-D-Phe-Lys] **8.5** (10.0 mg, 0.0110 mmol), boronate ester **3.1** (18.0 mg, 0.0327 mmol), HOBt $\cdot\text{H}_2\text{O}$  (5.0 mg, 0.0327 mmol), and pyridine (6.0  $\mu\text{L}$ , 0.0726 mmol) in DMF (1.0 mL) was added with EDC $\cdot\text{HCl}$  (8.0 mg, 0.0396 mmol). The reaction was stirred at rt for 36 hr and the DMF was removed under vacuum. The residue was washed with  $\text{Et}_2\text{O}$  to give sticky oil, which was used directly in the following step. For characterization, the peptide was purified by RP-HPLC with HPLC program 11 and column II in HPLC System I,  $t_{\text{R}} = 13.8$  min or analyzed by

RP-HPLC with HPLC Program 12 and column I in HPLC System I,  $t_R = 23.9$  min.  $^{19}\text{F}$  NMR (282.4 MHz,  $d_6$ -DMSO, rt):  $\delta(\text{ppm})$  -28.07 (s, 1 F), -23.09 (s, 1 F), -18.16 (s, 1 F);  $^1\text{H}$  NMR (400 MHz,  $d_6$ -DMSO, rt):  $\delta(\text{ppm})$  1.07 (m, 2 H), 1.23 (m, 1 H), 1.24-1.50 (m, 1 H), 1.26-1.49 (m, 18 H), 1.50-1.70 (m, 2 H), 1.98 (s, 3 H), 2.32 (s, 1 H), 2.40 (s, 2 H), 2.45 (s, 3 H), 2.61 (t,  $J = 7.80$  Hz, 1 H), 2.63 (m, 1 H), 2.80 (m, 1 H), 2.90 (m, 1 H), 2.94 (s, 2 H), 3.00 (m, 2 H), 3.16 (m, 4 H), 3.92 (m, 2 H), 4.03 (dd,  $J_1 = 14.92$  Hz,  $J_2 = 7.48$  Hz, 1 H), 4.13 (q,  $J = 7.43$  Hz, 1 H), 4.45 (q,  $J = 7.20$  Hz, 1 H), 4.61 (q,  $J = 7.69$  Hz, 1 H), 5.76 (s, 1 H), 7.13 (m, 20 H), 7.23 (m, 2 H), 7.40 (t,  $J = 9.38$  Hz, 1 H), 7.51 (d,  $J = 8.16$  Hz, 1 H), 8.00 (m, 2 H), 8.10 (d,  $J = 7.36$  Hz, 1 H), 8.44 (m, 1 H), 8.74 (t,  $J = 5.60$  Hz, 1 H); ESI-HRMS: calcd. for  $\text{C}_{77}\text{H}_{86}\text{BN}_9\text{O}_{13}\text{F}_3\text{S}^+$ : 1444.6111, found: 1444.6085.

### ***Cyclo*[Arg-Gly-Asp-*D*-Phe-Lys(boronate)] (8.7)**

TFA (2.4 mL) was added to the crude of *cyclo*[Arg(Pbf)-Gly-Asp(O<sup>t</sup>Bu)-*D*-Phe-Lys(boronate)] **8.6** in 6.7% H<sub>2</sub>O in CH<sub>3</sub>CN (0.75 mL) and the resulting reaction was incubated at rt for 3 hr. Then the reaction was concentrated under reduced pressure and toluene (3 × 10 mL) was added to help remove TFA/H<sub>2</sub>O. The residue was then dissolved in minimum MeOH and Et<sub>2</sub>O was added to give a white solid as the desired product (HPLC Program 12 with Column I in HPLC System I,  $t_R = 18.5$  min). Yield: 6.1 mg, 40% over two steps. The crude compound was purified via semi-preparative HPLC via HPLC Program 14 with Column II in HPLC System I,  $t_R = 10.1$  min.  $^{19}\text{F}$  NMR (282.4 MHz,  $d_6$ -DMSO, rt):  $\delta(\text{ppm})$  -28.12 (s, 1 F), -23.14 (s, 1 F), -18.03 (s, 1 F); ESI-HRMS: calcd. for  $\text{C}_{60}\text{H}_{62}\text{BN}_9\text{O}_{10}\text{F}_3^+$ : 1136.4665, found: 1136.4648.

### ***N*-Tritylpiperazine (8.8)**

Trityl chloride (2.0 g, 7.0 mmol) was added in one portion to piperazine (3.0 g, 34.8 mmol) in CH<sub>2</sub>Cl<sub>2</sub> (20.0 mL) at 0 °C.<sup>527</sup> Then the ice-water bath was removed and the reaction was stirred at rt for 0.5 hr. The reaction was then quenched by the addition of H<sub>2</sub>O (50 mL) and extracted with CH<sub>2</sub>Cl<sub>2</sub> (3 × 50 mL). The CH<sub>2</sub>Cl<sub>2</sub> layers were combined, washed with H<sub>2</sub>O (2 × 50 mL) and brine (1 × 50 mL), and dried over anhydrous Na<sub>2</sub>SO<sub>4</sub>. The solution was then filtered and concentrated under reduced pressure. The residue was treated with flash chromatography (MeOH: CH<sub>2</sub>Cl<sub>2</sub> 3:97) to afford a white solid as the desired product ( $R_f = 0.53$  in 1:9 MeOH: CH<sub>2</sub>Cl<sub>2</sub>). Yield: 1.48 g, 64%.  $^1\text{H}$  NMR (300

MHz, CD<sub>2</sub>Cl<sub>2</sub>, rt):  $\delta$ (ppm) 2.15 (s, 2 H), 2.99 (s, 6 H), 7.18 (m, 3 H), 7.29 (d,  $J$  = 7.73 Hz, 6 H), 7.48 (s, 6 H); <sup>13</sup>C NMR (100.6 MHz, CD<sub>2</sub>Cl<sub>2</sub>, rt):  $\delta$ (ppm) 46.82, 49.87, 77.45, 126.07, 127.55, 129.55.

#### **4-Oxo-4-(4-tritylpiperazin-1-yl)butanoic acid (8.9)**

NEt<sub>3</sub> (0.28 mL, 2.0 mmol) was added to the CH<sub>2</sub>Cl<sub>2</sub> solution (10.0 mL) of *N*-tritylpiperazine (215.0 mg, 0.655 mmol) and succinic anhydride (70.0 mg, 0.700 mmol). The mixture was stirred at rt for 1.5 hr and then poured to 10% aqueous citric acid solution (50 mL). The aqueous slurry was extracted with CH<sub>2</sub>Cl<sub>2</sub> (2 × 50 mL). The organic layers were combined, washed with H<sub>2</sub>O (1 × 50 mL) and brine (1 × 50 mL), and dried over anhydrous Na<sub>2</sub>SO<sub>4</sub>. The salt was then removed by filtration and the filtrate was concentrated under vacuum. Then the oily residue was purified via silica gel flash chromatography (MeOH:CH<sub>2</sub>Cl<sub>2</sub> 3:97) to give a white solid as the pure product ( $R_f$  = 0.32 in 1:9 MeOH:CH<sub>2</sub>Cl<sub>2</sub>). Yield: 179.3 mg, 64%. <sup>1</sup>H NMR (400 MHz, CDCl<sub>3</sub>, rt):  $\delta$ (ppm) 2.31 (s, br, 4 H), 2.58 (m, 2 H), 2.63 (m, 2 H), 3.61 (m, 4 H), 3.75 (s, br, 2 H), 7.18 (t,  $J$  = 7.24 Hz, 3 H), 7.28 (t,  $J$  = 7.02 Hz, 6 H), 7.47 (d,  $J$  = 5.92 Hz, 6 H); <sup>13</sup>C NMR (75.5 MHz, CDCl<sub>3</sub>, rt):  $\delta$ (ppm) 28.14, 29.89, 42.73, 46.17, 47.80, 48.28, 126.53, 127.90, 129.37, 170.76, 175.69; ESI-HRMS: calcd. for C<sub>27</sub>H<sub>27</sub>N<sub>2</sub>O<sub>3</sub><sup>-</sup>: 427.2022, found: 427.2017.

#### **Cyclo[Arg(Pbf)-Gly-Asp(O<sup>t</sup>Bu)-D-Phe-Lys(suc-piperazinyl-Trt)] (8.10)**

DIPEA (18.0  $\mu$ L, 0.10 mmol) was added to *cyclo*[Arg(Pbf)-Gly-Asp(O<sup>t</sup>Bu)-D-Phe-Lys] **8.5** (10.0 mg, 11.0  $\mu$ mol) and tritylpiperazinylsuccinic acid **8.9** (20.0 mg, 46.7  $\mu$ mol) in CH<sub>3</sub>CN/DMF (1:1, 2.0 mL). After the solution got clear, HBTU (19.0 mg, 50  $\mu$ mol) was added in one portion and the reaction was left at rt overnight. Then the solvent was removed under reduced pressure and Et<sub>2</sub>O (10 mL) was added to the residue to afford sticky oil. The Et<sub>2</sub>O was carefully decanted and the residue was further washed with Et<sub>2</sub>O (2 × 10 mL). The oil was dried *in vacuo* to remove the residual volatile and used directly in the following step without further purification. ESI-LRMS: [M+Na]<sup>+</sup>: 1345.1 (100%).

### ***Cyclo*[Arg(Pbf)-Gly-Asp(O<sup>t</sup>Bu)-D-Phe-Lys(suc-piperazine)] (8.11)**

HFIP (100  $\mu$ L, 0.95 mmol) was added to peptide **8.10** (quantitatively from previous step,  $\sim$  11.0  $\mu$ mol) in trifluoroethanol (1.0 mL). The reaction was undertaken at rt for 2 hr and then concentrated under vacuum. The residue was then redissolved in a minimum amount of MeOH ( $\sim$  0.2 mL) and Et<sub>2</sub>O (10 mL) was added to precipitate the peptide. The solid was then filtered off and washed with Et<sub>2</sub>O to give the desired product. Yield: 9.2 mg, 78% over two steps. The quality of the peptide was determined by RP-HPLC with HPLC Program 1 and Column I in HPLC System I,  $t_R$  = 22.0 min. ESI-HRMS: calcd. for C<sub>52</sub>H<sub>78</sub>N<sub>11</sub>O<sub>12</sub>S<sup>+</sup>: 1080.5552, found: 1080.5559.

### **Mono-*tert*-butyl succinate**

Succinic anhydride (3.0 g, 30.0 mmol), *N*-hydroxyl succinimide (1.0 g, 8.7 mmol), DMAP (0.35 g, 2.9 mmol), and NEt<sub>3</sub> (1.25 mL, 9.0 mmol) were dissolved in <sup>t</sup>BuOH (5.0 mL) and toluene (50.0 mL).<sup>528, 529</sup> The solution was heated to reflux for 24 hr. After being cooled to rt, the reaction was diluted with EtOAc (50 mL) and washed with 10% aqueous citric acid solution (50 mL). The layers were separated and the aqueous layer was further extracted with EtOAc (2  $\times$  50 mL). The combined organic layers were washed with 10% aqueous citric acid (2  $\times$  50 mL) and brine (1  $\times$  50 mL), and dried over anhydrous Na<sub>2</sub>SO<sub>4</sub>. The solution was then filtered and concentrated under reduced pressure. The residue was purified by flash chromatography (1:3 EtOAc: hexanes, visualized on TLC by *p*-anisaldehyde stain) to give a white solid as the product ( $R_f$  = 0.16 in 1:1 EtOAc:hexanes). Yield: 2.45 g, 47%. <sup>1</sup>H NMR (300 MHz, CDCl<sub>3</sub>, rt):  $\delta$ (*ppm*) 1.46 (d,  $J$  = 1.69 Hz, 9 H), 2.54 (m, 2 H), 2.64 (m, 2 H); <sup>13</sup>C NMR (75.5 MHz, CDCl<sub>3</sub>, rt):  $\delta$ (*ppm*) 28.16, 29.33, 30.23, 81.16, 171.54, 178.81; ESI-LRMS: [M+Na]<sup>+</sup>, 197.1 (100%).

### ***Tert*-butyl 4-oxo-4-(4-tritylpiperazin-1-yl)butanoate (8.14)**

HBTU (493 mg, 1.30 mmol) was added to tritylpiperazine **8.8** (330 mg, 1.00 mmol), *tert*-butyl succinate (200 mg, 1.15 mmol), and NEt<sub>3</sub> (0.42 mL, 3.0 mmol) in CH<sub>2</sub>Cl<sub>2</sub> (10.0 mL). The reaction was undertaken at rt for 2.5 hr. The reaction mixture was then poured to 10% aqueous citric acid solution (30 mL) and extracted with CH<sub>2</sub>Cl<sub>2</sub> (3  $\times$  50 mL). The organic layers were combined and washed with H<sub>2</sub>O (1  $\times$  50 mL), saturated

NaHCO<sub>3</sub> (1 × 50 mL), H<sub>2</sub>O (1 × 50 mL), and brine (1 × 50 mL). Dried over anhydrous Na<sub>2</sub>SO<sub>4</sub>, the CH<sub>2</sub>Cl<sub>2</sub> solution was concentrated under vacuum. The residue was charged with silica gel flash chromatography (EtOAc:hexanes 1:9 then 1:6) to give a white solid as the desired product (*R<sub>f</sub>* = 0.51 in 1:1 EtOAc:hexanes). Yield: 473.8 mg, 98%. <sup>1</sup>H NMR (400 MHz, CD<sub>2</sub>Cl<sub>2</sub>, rt): δ(*ppm*) 1.40 (s, 9 H), 2.28 (s, br, 2 H), 2.45 (s, 4 H), 3.61 (m, 2 H), 3.72 (s, br, 2 H), 7.21 (m, 3 H), 7.31 (m, 6 H), 7.51 (m, 6 H); <sup>13</sup>C NMR (100.6 MHz, CD<sub>2</sub>Cl<sub>2</sub>, rt): δ(*ppm*) 27.90, 30.50, 42.15, 45.81, 47.98, 48.40, 77.15, 80.07, 126.35, 127.75, 129.40, 169.77, 172.25.

#### ***Tert*-butyl 4-oxo-4-(piperazin-1-yl)butanoate (8.15)**

*Tert*-butyl ester **8.14** (110.0 mg, 0.227 mmol) and HFIP (1.2 mL, 11.4 mmol) were dissolved in trifluoroethanol (5.0 mL) and stirred at 40 °C for 4 hr. The reaction was concentrated *in vacuo* to give oily residue. The residue was then loaded to a silica gel column for separation (MeOH:CH<sub>2</sub>Cl<sub>2</sub> 3:97 then 1:9) and colorless oil was obtained as the desired product (*R<sub>f</sub>* = 0.13 in 1:9 MeOH:CH<sub>2</sub>Cl<sub>2</sub>). Yield: 52.9 mg, 96%. <sup>1</sup>H NMR (400 MHz, CDCl<sub>3</sub>, rt): δ(*ppm*) 1.46 (d, *J* = 1.35 Hz, 9 H), 2.58 (d, *J* = 1.11 Hz, 4 H), 2.90 (d, *J* = 15.88 Hz, 4 H), 3.17 (s, br, 2 H), 3.52 (s, 2 H), 3.63 (s, 2 H); <sup>13</sup>C NMR (100.6 MHz, CDCl<sub>3</sub>, rt): δ(*ppm*) 28.32, 28.52, 30.85, 42.78, 45.18, 45.91, 46.27, 80.89, 170.34, 172.79; ESI-LRMS: [M+Na]<sup>+</sup>, 265.1.

#### ***Tert*-butyl 4-oxo-4-(4-(2,4,6-trifluoro-3-(4,4,5,5-tetraphenyl-1,3,2-dioxaborolan-2-yl)benzoyl)piperazin-1-yl)butanoate (8.16)**

*Tert*-butyl ester **8.15** (91.1 mg, 0.376 mmol), boronate **3.1** (238.0 mg, 0.432 mmol), HOBt·H<sub>2</sub>O (73.0 mg, 0.475 mmol), and pyridine (0.14 mL, 1.79 mmol) was dissolved in CH<sub>2</sub>Cl<sub>2</sub> (15 mL) and added with EDC·HCl (125.0 mg, 0.648 mmol) in one portion. The resulting mixture was reacted at rt overnight and then quenched by the addition of 10% aqueous citric acid solution (50 mL). The product was extracted into CH<sub>2</sub>Cl<sub>2</sub> (3 × 50 mL). The organic layers were combined, washed with H<sub>2</sub>O (1 × 50 mL) and brine (1 × 50 mL), and dried over anhydrous Na<sub>2</sub>SO<sub>4</sub>. The solution was filtered and the solvent was removed under vacuum. The residue was isolated via silica gel flash chromatography (MeOH:CH<sub>2</sub>Cl<sub>2</sub> 0:100 to 1:99) to afford a white solid as the desired product (*R<sub>f</sub>* = 0.63 in 1:9 MeOH:CH<sub>2</sub>Cl<sub>2</sub>). Yield: 241.0 mg, 83%. <sup>19</sup>F NMR (282.4 MHz, CD<sub>2</sub>Cl<sub>2</sub>, rt): δ(*ppm*)

-28.75 (s, 1 F), -22.36 (s, 1 F), -17.25 (s, 1 F);  $^1\text{H}$  NMR (400 MHz,  $\text{CD}_2\text{Cl}_2$ , rt):  $\delta(\text{ppm})$  1.45 (s, 9 H), 2.58 (m, 4 H), 3.41-3.85 (m, 8 H), 6.91 (t,  $J = 8.80$  Hz, 1 H), 7.13 (m, 12 H), 7.21 (m, 4 H), 7.26 (t,  $J = 3.54$  Hz, 4 H);  $^{13}\text{C}$  NMR (100.6 MHz,  $\text{CD}_2\text{Cl}_2$ , rt):  $\delta(\text{ppm})$  27.93, 28.00, 30.45, 42.06, 46.80, 80.31, 96.98, 101.26, 127.26, 127.32, 127.45, 128.62, 128.65, 141.82, 142.17, 170.18, 172.12; ESI-HRMS: calcd. for  $\text{C}_{45}\text{H}_{43}\text{BN}_2\text{O}_6\text{F}_3^+$ : 775.3166, found: 775.3174.

**4-Oxo-4-(4-(2,4,6-trifluoro-3-(4,4,5,5-tetraphenyl-1,3,2-dioxaborolan-2-yl)benzoyl) piperazin-1-yl)butanoic acid (8.17)**

TFA (5.0 mL) was added to *tert*-butyl ester **8.16** (77.3 mg, 0.0998 mmol) in  $\text{CH}_2\text{Cl}_2$  (10.0 mL) and the mixture was stirred at rt for 3 hr. The mixture was then concentrated under vacuum and the residue was purified via silica gel flash chromatography (MeOH: $\text{CH}_2\text{Cl}_2$  1:200 to 1:99) to afford white foam as the desired product ( $R_f = 0.32$  in 1:9 MeOH: $\text{CH}_2\text{Cl}_2$ ). Yield: 62.9 mg, 88%.  $^{19}\text{F}$  NMR (282.4 MHz,  $\text{CD}_2\text{Cl}_2$ , rt):  $\delta(\text{ppm})$  -28.84 (s, 1 F), -22.47 (s, 1 F), -16.99 (s, 1 F);  $^1\text{H}$  NMR (400 MHz,  $\text{CD}_2\text{Cl}_2$ , rt):  $\delta(\text{ppm})$  2.70 (m, 4 H), 3.41-3.89 (m, 8 H), 6.75 (s, br, 1 H), 6.91 (t,  $J = 8.91$  Hz, 1 H), 7.08-7.27 (m, 20 H);  $^{13}\text{C}$  NMR (100.6 MHz,  $\text{CD}_2\text{Cl}_2$ , rt):  $\delta(\text{ppm})$  28.07, 29.45, 41.61, 42.00, 42.21, 45.18, 45.71, 97.00, 101.33, 127.28, 127.33, 127.45, 128.62, 128.64, 141.74, 141.82, 142.13, 159.71, 171.03, 175.67; ESI-HRMS: calcd. for  $\text{C}_{41}\text{H}_{34}\text{BN}_2\text{O}_6\text{F}_3\text{Na}^+$ : 741.2360, found: 741.2346.

**Cyclo[Arg(pbf)-Gly-Asp(O<sup>t</sup>Bu)-D-Phe-Lys(suc-piperazinyl-boronate)] (8.12)**

EDC·HCl (16.0 mg, 57.5  $\mu\text{mol}$ ) was added to the DMF solution (1.5 mL) of peptide **8.17** (27.7 mg, 38.6  $\mu\text{mol}$ ), *cyclo*[Arg(Pbf)-Gly-Asp(O<sup>t</sup>Bu)-D-Phe-Lys] **8.5** (23.0 mg, 25.5  $\mu\text{mol}$ ), HOBt·H<sub>2</sub>O (7.0 mg, 57.5  $\mu\text{mol}$ ), and pyridine (24.0  $\mu\text{L}$ , 0.27 mmol). The DMF solution was stirred at rt for 36 hr. The reaction mixture was then poured to 10% aqueous citric acid (20 mL) and extracted with EtOAc (3  $\times$  30 mL). The EtOAc layers were combined, washed with H<sub>2</sub>O (1  $\times$  30 mL) and brine (1  $\times$  30 mL), and dried over anhydrous  $\text{Na}_2\text{SO}_4$ . The solution was filtered and concentrated under reduced pressure, and the residue was dissolved in minimum MeOH (~ 1 mL). Et<sub>2</sub>O (20 mL) was added to the methanolic solution to precipitate the peptide. The mixture was filtered and the pellet

was washed with Et<sub>2</sub>O thoroughly to give a whitish solid, which was directly used in the following step without further purification. Yield: 31.7 mg, 77%. The quality of the peptide was determined by RP-HPLC with HPLC Program 1 and Column I in HPLC System I, t<sub>R</sub> = 28.2 min. ESI-HRMS: calcd. for C<sub>85</sub>H<sub>98</sub>BN<sub>11</sub>O<sub>15</sub>F<sub>3</sub>S<sup>+</sup>: 1612.7010, found: 1612.6984.

The desired compound can also be obtained by the coupling of peptide **8.11** (9.2 mg, 8.5 μmol) and boronate **3.1** (15.0 mg, 25.5 μmol) in DMF (1.0 mL) in the presence of EDC·HCl (6.0 mg, 31.3 μmol), HOBt·H<sub>2</sub>O (5.0 mg, 32.6 μmol), and pyridine (8.0 μL, 99.0 μmol) for 36 hr. The reaction was then concentrated *in vacuo* and Et<sub>2</sub>O (3 × 10 mL) to give colorless oily residue, which was directly used in the following step without further purification.

#### ***Cyclo*[Arg-Gly-Asp-D-Phe-Lys(suc-piperazinyl-boronate)] (8.13)**

The protected peptide **8.12** (31.7 mg, 0.0197 mmol) was dissolved in TFA (12 mL) and H<sub>2</sub>O (0.58 mL). The reaction was incubated at rt for 1.5 hr and the solvent was removed under vacuum. The residue was then dissolved in minimum MeOH (~ 2 mL) and Et<sub>2</sub>O (30 mL) was added to crystallize the peptide. The mixture was filtered and the pellet was thoroughly washed with Et<sub>2</sub>O to give a whitish powder as the crude product. Yield: 21.1 mg, 82%. The product was analyzed by RP-HPLC via HPLC Program 1 and Column I in HPLC System I, t<sub>R</sub> = 26.2 min. The crude peptide (~ 10 mg) was dissolved in CH<sub>3</sub>CN containing 10% H<sub>2</sub>O (2 mL) and purified by semi-preparative HPLC via HPLC Program 14 and Column II in HPLC System I (t<sub>R</sub> = 9.7 min) to give a white solid. Yield: 4.0 mg, 47%. <sup>19</sup>F NMR (282.4 MHz, MeOD, rt): δ(*ppm*) -29.73 (s, 1 F), -23.76 (s, 1 F), -17.35 (s, 1 F); <sup>1</sup>H NMR (400 MHz, MeOD, rt): δ(*ppm*) 1.04 (m, 2 H), 1.31 (s, 1 H), 1.40-1.47 (m, 3 H), 1.54 (m, 2 H), 1.67 (m, 2H), 1.87 (m, 1 H), 2.34 (s, 2 H), 2.46-2.62 (m, 3 H), 2.64-2.90 (m, 3 H), 2.99 (m, 2 H), 3.03-3.19 (m, 3 H), 3.49 (m, 2 H), 3.55 (m, 1 H), 3.58-3.69 (m, 3 H), 3.72 (m, 2 H), 3.81 (m, 1 H), 3.89 (m, 1 H), 3.94 (m, 1 H), 4.26 (m, 2 H), 4.55 (m, 1 H), 4.76 (m, 1 H), 7.10 (m, 11 H), 7.14-7.31 (m, 15 H), 7.86 (m, 1 H), 8.23 (m, 1 H), 8.43 (m, 1 H). ESI-HRMS: calcd. for C<sub>68</sub>H<sub>74</sub>BN<sub>11</sub>O<sub>12</sub>F<sub>3</sub><sup>+</sup>: 1304.5564, found: 1304.5536.

### ***Cyclo*[Arg-Gly-Asp-*D*-Phe-Lys(suc-piperazinyl-ArBF<sub>3</sub>)] (8.19)**

The crude peptide **8.13** (~ 8 mg, 4.96 μmol) was dissolved in MeOH (1 mL) and was added with 4 M KHF<sub>2</sub> (200 μL, 0.80 mmol) in a 15 mL Falcon tube. The reaction was then stirred at rt overnight and the solvent was removed under vacuum. Et<sub>2</sub>O (10 mL) was added to the residue and the mixture was centrifuged after being thoroughly mixed. The Et<sub>2</sub>O layer was discarded. The Et<sub>2</sub>O wash was then repeated two more times. The residue was then dried over vacuum to remove the residual Et<sub>2</sub>O for 5 hr. Then *d*<sub>6</sub>-DMSO (~ 400 μL) was added to extract the product from the crude. <sup>19</sup>F NMR (282.4 MHz, *d*<sub>6</sub>-DMSO, rt): δ(*ppm*) -21.13 (s, 1 F), -27.30 (s, 1 F), -40.54 (s, 1 F), -54.91 (s, 3 F).<sup>a</sup> ESI-LRMS: [M]<sup>-</sup>, 996.4 (100%).

### ***Cyclo*[Arg(Pbf)-Gly-Asp(O<sup>t</sup>Bu)-*D*-Phe-Lys(coumarin)] (8.22)**

7-Diethylaminocoumarin-3-carboxylic acid **6.3b** (4.0 mg, 16.0 μmol), peptide **8.7** (10.0 mg, 11.0 μmol), and DIPEA (9.0 μL, 51.0 μmol) in DMF (1.0 mL) was added with HBTU (7.0 mg, 18.0 μmol). The resulting mixture was incubated at rt for 23 hr and then concentrated under reduced pressure. The residue was resuspended in MeOH (~ 1 mL) and Et<sub>2</sub>O (20 mL) was added to precipitate the peptide. The solid was settled down by centrifugation and washed with Et<sub>2</sub>O (2 × 5 mL). 20 mg of the crude product was obtained. The pellet was then dissolved in THF (~ 0.5 mL) and was purified via the preparative TLC (MeOH:CH<sub>2</sub>Cl<sub>2</sub> 7.5:92.5) to give the desired product. Yield: 1.5 mg, 12%. ESI-HRMS: calcd. for C<sub>58</sub>H<sub>79</sub>N<sub>10</sub>O<sub>13</sub>S<sup>+</sup>: 1155.5549, found: 1155.5569.

### ***Cyclo*[Arg-Gly-Asp-*D*-Phe-Lys(coumarin)] (8.20)**

The fully protected coumarin derivatized peptide **8.22** (2.0 mg, 1.7 μmol) was treated with TFA (100 μL) and H<sub>2</sub>O (5 μL) for 1 hr. The acid was removed under vacuum. The residue was then washed with Et<sub>2</sub>O (3 × 5 mL) and dried over vacuum to give the crude product. ESI-HRMS: calcd. for C<sub>41</sub>H<sub>55</sub>N<sub>10</sub>O<sub>10</sub><sup>+</sup>: 847.4103, found: 847.4092.

<sup>a</sup> The <sup>1</sup>H NMR was attempted, however, due to the low concentration of the materials, the <sup>1</sup>H NMR was with very poor quality and therefore not reported herein.

### ***Cyclo*[Arg(Pbf)-Gly-Asp(O<sup>t</sup>Bu)-D-Phe-Lys(FITC)] (8.23)**

Peptide *cyclo*[Arg(Pbf)-Gly-Asp(O<sup>t</sup>Bu)-D-Phe-Lys] **8.5** (17.0 mg, 18.6 μmol) and fluorescein isothiocyanate (FITC) (9.0 mg, 24.4 μmol) in DMF (1.0 mL) was added with DIPEA (13.2 μL, 75.8 μmol). The reaction was stirred at rt for 3 hr and then poured to H<sub>2</sub>O (10 mL). EtOAc (3 × 10 mL) was added to extract the aqueous mixture, washed with 3 N HCl (10 mL), H<sub>2</sub>O (30 mL), and brine (30 mL), and dried over anhydrous Na<sub>2</sub>SO<sub>4</sub>. The solution was filtered and concentrated under reduced pressure. The residue was dissolved in minimum MeOH (~ 0.5 mL) and Et<sub>2</sub>O (5 mL) was added to precipitate the peptide. The mixture was transferred to a 2 mL plastic eppendorf tube and centrifuged at 13k rpm for 10 min. The pellet was dissolved in THF and loaded to the preparative TLC plate and resolved with 12.5% MeOH in CH<sub>2</sub>Cl<sub>2</sub> to give the desired product. Yield: 8.4 mg, 35%. ESI-HRMS: calcd. for C<sub>65</sub>H<sub>76</sub>N<sub>10</sub>O<sub>15</sub>NaS<sub>2</sub><sup>+</sup>: 1323.4831, found: 1323.4846.

### ***Cyclo*[Arg-Gly-Asp-D-Phe-Lys(FITC)] (8.21)**

Peptide *cyclo*[Arg(Pbf)-Gly-Asp(O<sup>t</sup>Bu)-D-Phe-Lys(FITC)] **8.23** (8.4 mg, 6.45 μmol) in a 1.5 mL eppendorf tube was added with TFA:H<sub>2</sub>O (20:1, 210 μL) and the mixture was shaken at rt for 1.5 hr. Then the acid was removed under reduced pressure and the residue was precipitated with MeOH/Et<sub>2</sub>O to give a yellow solid as the desired product. Yield: 5.8 mg, 91%. ESI-HRMS: calcd. for C<sub>48</sub>H<sub>53</sub>N<sub>10</sub>O<sub>12</sub>S<sup>+</sup>: 993.3565, found: 993.3578.

## **8.5.2 The fluoridation of RGD-peptides**

### **The fluoridation of *cyclo*[Arg-Gly-Asp-D-Phe-Lys(boronate)] **8.7****

Peptide **8.7** (100 nmol) was suspended in CH<sub>3</sub>CN (4 μL). Then 0.4 M KHF<sub>2</sub> (2 μL, 800 nmol) and concentrated HCl (0.5 μL, ~ 6.3 μmol) were added to initiate the reaction. The mixture was incubated at rt for 2 hr and then quenched with 5% NH<sub>4</sub>OH in 50% aqueous EtOH (79 μL). The quenched reaction was injected into the LCMS. The LC was performed via HPLC Program 8 with column I in ESI-LCMS. ESI-LRMS: [M]: 828.1, [M-HF]: 808.3; t<sub>R</sub> (based on TIC<sup>a</sup>) = 16.8 min.

<sup>a</sup> TIC is the total ion current chromatography.

### The fluoridation of *cyclo*[Arg-Gly-Asp-D-Phe-Lys(suc-piperazinyl-boronate)] **8.13**

Peptide **8.13** (100 nmol) was suspended in CH<sub>3</sub>CN (4 μL). Then 0.4 M KHF<sub>2</sub> (2 μL, 800 nmol) and concentrated HCl (0.5 μL, ~ 6.3 μmol) were added to initiate the reaction. The mixture was incubated at rt for 1.5 hr and quenched with 5% NH<sub>4</sub>OH in 50% aqueous EtOH (79 μL). The quenched reaction was injected into the LCMS. The LC was performed via HPLC Program 8 with column I in ESI-LCMS. ESI-LRMS: [M]<sup>-</sup>: 996.3, [M-HF]<sup>-</sup>: 976.3; t<sub>R</sub> (based on TIC) = 16.2 min.<sup>a</sup>

### The click reaction between **6.2** and **8.4** under cold conditions

*c*[RGDfK(N<sub>3</sub>)] **8.4** in CH<sub>3</sub>CN (4 μL) was added with the *d*<sub>6</sub>-DMSO stock solution of **6.2** (10 μL, concentration unknown, > 30 mM based on <sup>19</sup>F NMR). Then 0.6 M sodium ascorbate (5 μL, 3 μmol) and 1.0 M CuSO<sub>4</sub> (5 μL) were added to initiate the reaction. The reaction was left at rt for 30 min and diluted with 0.04 M HCO<sub>2</sub>NH<sub>4</sub> (79 μL) prior to the injection of HPLC. The HPLC trace for the crude solution was shown in Figure 8.5. The HPLC was performed via HPLC Program 8 with column I in HPLC System I. t<sub>R</sub> = 15.4 min. Similar reaction was carried out except the amount of the **6.2** stock solution was 5 μL instead of 10 μL. The reaction was also quenched with 0.04 M HCO<sub>2</sub>NH<sub>4</sub> (79 μL) and the quenched reaction was analyzed with ESI-LCMS with HPLC Program 8 and Column I in ESI-LCMS. ESI-LCMS: [M]<sup>-</sup>: 891.3, [M-HF]<sup>-</sup>: 871.3; t<sub>R</sub> (based on TIC) = 15.8 min as shown in Figure 8.6.

### 8.5.3 Preparation of the <sup>18</sup>F-ArBF<sub>3</sub> labeled RGD-peptides

The <sup>18</sup>F-fluoride was prepared as described in the previous chapters. The <sup>18</sup>F-fluoride was trapped on the anion-exchange column (HCO<sub>3</sub><sup>-</sup> form) and released with NaClO<sub>4</sub> (2 mg/mL, 1 mL). CH<sub>3</sub>CN (1 mL) was added to azeotropically remove H<sub>2</sub>O at 110 °C under He stream till no residual liquid was observed. The <sup>19</sup>F-fluoride solution (0.25 M or 0.125 M KHF<sub>2</sub>)<sup>b</sup> was added to resuspend the radioactivity. The specific activity (mCi/μmol) of fluoride was calculated via the radioactivity (mCi) divided by [0.5 or 0.25 (M) times volume (μL) of the <sup>18/19</sup>F-cocktail added to each reaction].

<sup>a</sup> The ESI-LCMS traces for both of the fluoridations of **8.7** and **8.13** can be found in Appendix C.

<sup>b</sup> 6 to 20 μL was added to achieve different specific activities.

### One-step radiolabeling of peptide **8.7**

1  $\mu\text{L}$  of [ $^{18/19}\text{F}$ ]-fluoride (500 nmol  $^{19}\text{F}$ -fluoride, 3.73 mCi/ $\mu\text{mol}$  at the BOS) was transferred to the labeling reaction in a PCR tube containing *c*[RGDfK(boronate)] **8.7** (100 nmol) and HCl (12.6  $\mu\text{mol}$ ) in 80% aqueous  $\text{CH}_3\text{CN}$  (5  $\mu\text{L}$ ). The reaction was incubated at rt for 1 hr and quenched with 100  $\mu\text{L}$  of 5%  $\text{NH}_4\text{OH}$  in 50% aqueous EtOH. The quenched reaction was injected into the HPLC for analysis and the radio-HPLC trace was shown in Figure 8.4. The radioactivity at the BOS: 1.86 mCi. The HPLC was performed via HPLC Program 8 with Column I in HPLC System IV.

### One-step radiolabeling of peptide **8.13**

[ $^{18/19}\text{F}$ ]-Fluoride cocktail (1  $\mu\text{L}$ , 500 nmol, 2.92 mCi/ $\mu\text{mol}$  at the BOS) was added to 80% aqueous  $\text{CH}_3\text{CN}$  (5  $\mu\text{L}$ ) solution containing *c*[RGDfK(suc-piperazinyl-boronate)] **8.13** (100 nmol) and HCl (12.6  $\mu\text{mol}$ ) in a PCR tube. The reaction was stored at rt for 1 hr and then quenched with 100  $\mu\text{L}$  of 5%  $\text{NH}_4\text{OH}$  in 50% aqueous EtOH. The quenched reaction was injected into the HPLC for analysis and the radio-HPLC trace was shown in Figure 8.4. The radioactivity at the BOS: 1.46 mCi. The HPLC was performed via HPLC Program 8 with Column I in HPLC System IV.

### One-pot two-step radiolabeling the cyclopentapeptide **8.4** with the $\text{ArBF}_3$

$^{18/19}\text{F}$ -Fluoride cocktail (2  $\mu\text{L}$ , 500 nmol, 12.1 mCi/ $\mu\text{mol}$  at the BOS) was added to alkynylarylboronic acid **3.11** (100 nmol) and HCl (6.3  $\mu\text{mol}$ ) in 88.9% aqueous THF (4.5  $\mu\text{L}$ ), and the mixture was incubated at rt for 32 min. The reaction was quenched with 5%  $\text{NH}_4\text{OH}$  in 50% aqueous EtOH (30  $\mu\text{L}$ ) and 2  $\mu\text{L}$  of the quenched mixture was added to 5%  $\text{NH}_4\text{OH}$  in 50% aqueous EtOH (100  $\mu\text{L}$ ) for the HPLC injection. The quenched reaction (30  $\mu\text{L}$ ) was added to cyclopentapeptide **8.4** (100 nmol), followed by the addition of 0.6 M sodium ascorbate (6  $\mu\text{L}$ ) and 0.25 M  $\text{CuSO}_4$  (6  $\mu\text{L}$ ). The copper catalyzed reaction was then left still for 32 min. 5  $\mu\text{L}$  of the reaction was then added to 5%  $\text{NH}_4\text{OH}$  in 50% aqueous EtOH (100  $\mu\text{L}$ ) for the HPLC injection. The radio-HPLC traces were shown in Figure 8.7. The radioactivity at the BOS of the first step: 6.05 mCi, that at the BOS of the second reaction: 3.58 mCi. The HPLC was performed via HPLC

Program 8 with Column I in HPLC System IV.

## Chapter 9 Discussion and conclusion

### 9.1 Discussion

In the previous chapters, two labeling methods have been applied to label biomolecules with  $^{18}\text{F}$ -ArBF<sub>3</sub>s. Based on the results presented herein, several important aspects of radiofluoridation are discussed and some related perspectives are included.

#### 9.1.1 Defluoridation and fluoridation: rapid preparation and slow decomposition of $^{18}\text{F}$ -ArBF<sub>3</sub>s

##### 9.1.1.1 The stability of ArBF<sub>3</sub>s

In Chapter 2, a defluoridation study was carried out with a series of HetArBF<sub>3</sub>s. It was found that most of the *N*-HetArBF<sub>3</sub>s studied therein have high or very high solvolytic stability under physiological conditions. Among the HetArBF<sub>3</sub>s, the pyridazinylArBF<sub>3</sub>s exhibit extraordinarily long half-lives, even at elevated temperatures. Since no intermediate has ever been observed as monitored by the  $^{19}\text{F}$  NMR spectroscopy method and because the reaction was not dramatically influenced by pH changes, a solvolytic mechanism, which involves only one slow step governing the loss of the first fluoride and fast subsequent steps, has been proposed. An energy diagram for the slow step was also proposed, as shown in Figure 2.2, where it was believed that the inductive effect of the electron withdrawing groups (EWGs) can help stabilize the negative charge on the boron atom both in the ground state and the transition state. Similar to the previous systematic study of the hydrolytic stability of ArBF<sub>3</sub>s,<sup>85</sup> the HetArBF<sub>3</sub>s comprising more electron-deficient heteroaromatic rings always are even more hydrolytically stable. Accordingly, the pyridazinylArBF<sub>3</sub>s as well as the pyridinylArBF<sub>3</sub>s are shown to be with very promising stability as potential PET imaging agents.

Moreover, understanding the molecular components that contribute to the hydrolytic stability of ArBF<sub>3</sub>s could inform the design of appropriate boronates for PET imaging purposes. Subsequently, one would have to establish proper methods for the bioconjugation. For example, *N*-methyl pyridiniumtrifluoroborate **TFB-2.5** has a

hydrolytic half-life of about 103 hours in the phosphate buffer at pH ~ 7. The *N*-methyl could likely be replaced by other alkyl residues with different functional groups for bioconjugation, such as propargyl or maleimidyl groups. Since the replacement of the methyl group with other alkyl groups would not perturb the electron properties of the pyridinyl system, it is probable that the long half-life of the pyridiniumtrifluoroborate could be maintained by such modifications. Although none of the HetArBF<sub>3</sub>s have been investigated further as *in vivo* stable PET imaging agents in this thesis, they represent the next generation synthons for the purpose of PET imaging, for which they might prove to be excellent <sup>18</sup>F-PET imaging agents. This study may guide the development of other HetArBF<sub>3</sub>s for PET imaging. Because the ArBF<sub>3</sub> from the derivative of boronate **3.1** had been shown to be stable *in vivo* in the context of a biotinylated derivative,<sup>79</sup> we continued our studies with this compound for labeling other important biomolecules in Chapters 4-8. Our rationale for continuing with this compound, which might not be as hydrolytically stable as some of the HetArBF<sub>3</sub>s, reflected a need to demonstrate *in vivo* stability and *in vivo* targeting to funding agencies.

#### 9.1.1.2 The fluoridation to prepare ArBF<sub>3</sub>s

Besides the high solvolytic stability of ArBF<sub>3</sub>s, a rapid <sup>18</sup>F-fluoridation of the corresponding arylboronic acid/ester is extremely important for a high yielding radiosynthesis. To determine the optimal fluoridation conditions, a variety of boronate esters were prepared and studied for their fluoridations in Chapter 3. By studying the fluoridation of the fluorescent BODIPY-boronate ester **3.6**, a convenient screening method was adopted to provide the optimal reaction conditions. These results were further tested by the fluoridations of some other boronates, analyzed by <sup>19</sup>F NMR spectroscopy or radio-HPLC. Based on the <sup>19</sup>F NMR study and the radio-HPLC analysis, boronates with different protecting groups demonstrated distinct fluoridation rates. More specifically, free boronic acids such as **3.8** and **3.11** were converted to the corresponding <sup>18/19</sup>F-ArBF<sub>3</sub>s with the fastest rate, while the acid-sensitive protecting groups such as 1,8-diaminonaphthalene and its derivative DiDiAN on the boronic acids would facilitate the fluoridation. Benzopinacol protected boronate esters such as **3.7** and **3.19** showed slower fluoridation rates, which might be ascribed to the bulky nature that affords high

steric hindrance likely to block the fluoride to attack the boron. Moreover, the introduction of a piperazine linker between the arylboronate and conjugated biomolecules seemed to enhance the fluoridation, although the basis for this enhancement remains a bit unclear. Under the same conditions, the benzopinacol protected boronate **3.19** and the 1,8-diaminonaphthalene protected boronate **3.20**, both of which contained the piperazine linker, showed very small differences in radiochemical yields after one hour reactions. Moreover, in Chapter 8, RGD-boronates **8.7** and **8.13** were prepared to study the linker effect of the piperazine. The radiofluoridation suggested that the piperazine containing RGD-boronate **8.13** had a slightly faster fluoridation rate than RGD-boronate **8.7**. It is still unclear how the piperazine linker would influence the fluoridation of boronates with the bulky protecting group. A more systematic study would help to elucidate this.

### 9.1.2 One-step labeling or one-pot two-step labeling to prepare $^{18}\text{F}$ -ArBF<sub>3</sub>s?

**Table 9.1** A summary of the radiosyntheses of several bioligands in this dissertation.

	Bioconjugated boronates or the azide substrate for the radiolabeling	RCY <sup>a</sup>	Specific activity (Ci/μmol) <sup>b</sup>
<b>One-step labeling</b>	Marimastat-boronate ( <b>4.14</b> )	1.5% <sup>c</sup>	0.396 <sup>d</sup>
	Urea-boronate ( <b>5.9</b> )	25%	$1.11 \times 10^{-2}$
	c[RGDfK(boronate)] ( <b>8.7</b> )	12%	$7.64 \times 10^{-3}$
	c[RGDfK(suc-piperazinyl-boronate)] ( <b>8.13</b> )	16%	$6.00 \times 10^{-3}$
	Alkynylarylboronic acid ( <b>3.11</b> )	44%	$6.83 \times 10^{-2}$
<b>One-pot two-step labeling</b>	Folate-azide ( <b>7.10</b> )	25%	$2.22 \times 10^{-2}$
	c[RGDfK(N <sub>3</sub> )] ( <b>8.4</b> )	29%	$2.52 \times 10^{-2}$

<sup>a</sup> The best RCY achieved for the bioligand reported in this dissertation, and the RCY was based on the radioHPLC trace except for marimastat-boronate **4.14**; <sup>b</sup> specific activity at the end of synthesis except for **4.14**; <sup>c</sup> the isolated RCY of the radiolabeling for the imaging experiment; <sup>d</sup> at the end of packaging;

Through this dissertation, majorly two labeling strategies were applied to label biomolecules with  $^{18}\text{F}$ -ArBF<sub>3</sub>s. The one-step labeling method has been applied to label MMP inhibitor marimastat (Chapter 4), the urea-based PSMA inhibitor (Chapter 5), and the integrin targeting RGD-containing cyclopeptides (Chapter 8). The isolated radiochemical yield in the one hour fluoridation varies from 2% to 25% as shown in Table 9.1, yet these yields are largely unoptimized. Since these compounds were derived from boronate **3.1**, it is therefore regarded that some functional groups of the bioligands

might also play some roles in the fluoridation to afford different radiochemical yields. For instance, the radiofluoridation of urea-boronate **5.9** could achieve a radiochemical yield of 25% and it was therein proposed that the participation of the carboxylic groups might facilitate the protonation of the leaving group and hence accelerates the fluoridation.

On the other hand, a one-pot two-step labeling method was developed in Chapter 6 and used to label oligonucleotides (Chapter 6), folate (Chapter 7), and the RGD-containing peptide (Chapter 8) based on the copper(I) catalyzed alkyne-azide cycloaddition. A relatively fast fluoridation was carried out with alkynylarylboronic acid **3.11** to provide alkynyl- $^{18}\text{F}$ -ArBF<sub>3</sub> **6.2** in radiochemical yields of 30-40% within half an hour, and without purification, the azido-residue was added into the previous reaction for bioconjugation catalyzed by CuSO<sub>4</sub>/sodium ascorbate for another half an hour. The overall radiochemical yields of folate (~ 25%) and RGD (~ 29%) were comparable to or slightly better than those in the single step labeling. Moreover, although the radiolabeling experiment of the oligonucleotides was undertaken in the presence of a very small amount of azido-oligonucleotides, the reaction was very rapid and efficient. Even though this method was mainly developed to accommodate acid-sensitive biomolecules such as oligonucleotides, the high radiochemical yield suggests that this method is also suitable for acid-resistant molecules, particularly if there is more synthetic difficulty in introducing the boronate into a molecule otherwise considered for a one-step aqueous fluoridation.

The one-pot two-step labeling method is complementary to the one-step fluoridation to prepare the  $^{18}\text{F}$ -ArBF<sub>3</sub> labeled molecules. For either method, suitable synthetic strategies would be needed to install the substrates with either a boronate or an azide. The choice as to which one will be used will depend on the nature of the ligands to be labeled as well as the available chemistry to prepare the bioconjugates. Generally, a total reaction time of one hour for both methods was always employed and the overall radiochemical yields can be achieved from 20-30%, which is very promising to provide sufficient radioactivity for *in vivo* imaging work.

### 9.1.3 Specific activity of $^{18}\text{F-ArBF}_3\text{s}$

As defined in Chapter 1, specific activity is the radioactivity per unit of the radiolabeled compound.<sup>16, 88</sup> Also mentioned therein is that the actual specific activity of  $^{18}\text{F}$ -fluoride ( $\sim 5\text{-}14\text{ Ci}/\mu\text{mol}$ )<sup>16, 17, 52</sup> from cyclotrons is far less than the theoretical value ( $\sim 1710\text{ Ci}/\mu\text{mol}$ ). This implies that the no-carrier-added  $^{18}\text{F}$ -fluoride is far from “carrier-free” and there is always  $^{19}\text{F}$ -fluoride present in the cyclotron during the production/elution of  $^{18}\text{F}$ -fluoride. In Chapter 1, the relationship of the specific activity of the  $^{18}\text{F-ArBF}_3$  and that of  $^{18}\text{F}$ -fluoride was mathematically deduced to be a ratio of 1:3. Furthermore, although with some deviations, this tripling effect of the specific activity was supported in Chapter 6, in which the  $^{18/19}\text{F-ArBF}_3$  labeled oligonucleotide was purified via HPLC and its specific activity was measured.

However, for the formation of  $^{18}\text{F-ArBF}_3\text{s}$ , several steps are involved as noted in the introduction section of Chapter 3. It appears that the increase of both the concentration of the acid, which acts as a catalyst, and fluoride will dramatically enhance the fluoridation rate. However, if a high amount of a boronic acid/ester is used in the presence of very limited amounts of fluoride, the fluoride will be rapidly consumed in the first step to yield a monofluorodialkoxyborate or related species yet the formation of the desired product  $\text{ArBF}_3$  will be limited. Therefore, while a perfect 1:3 ratio of boronic acid/ester to fluoride is not necessary, a relatively low concentration of fluoride solution with respect to the boronate is not favored for this reaction.<sup>a</sup> As a result, 3 to 4 equivalents of fluoride with respect to the boronic acid/ester must be present for effective fluoridations. As mentioned in several of our publications, the specific activity can be compensated by working either with a high level of radioactivity, e.g.  $> 0.5\text{ Ci}$ , or in low reaction volumes ( $0.1\text{ to }20\ \mu\text{L}$ ) through the use of microreactors. Given the limits of working with  $\sim 50\text{ mCi}$  imposed by safety regulations at TRIUMF, carrier fluoride was added in most cases. Nevertheless, specific activities of  $\sim 0.5\text{ Ci}/\mu\text{mol}$  were still achievable and these values are still useful based on previous reports, albeit somewhat lower than what might be realized in production facilities that work with  $5\text{ Ci}$ .

---

<sup>a</sup> The attempt for the no-carrier-added  $^{18}\text{F}$ -fluoridation of boronic acid **3.11** failed to give any  $^{18}\text{F}$ -labeled species.

Furthermore, the decay of  $^{18}\text{F}$ -fluoride during the radiosynthesis would further decrease the specific activity, the basis of which has also been discussed in Chapter 1. As in every radiofluoridation, a reaction time window is chosen to be one hour to allow sufficient incorporation of  $^{18}\text{F}$ -fluoride. However, the specific activity drops 31.5% for this one hour reaction. A radiosynthesis with a shorter reaction time is thus desired. As investigated in Chapter 3, the fluoridation of BODIPY-boronate **3.6** in aqueous NMP at  $50\text{ }^{\circ}\text{C}$  might provide a way for a faster fluoridation at the elevated temperature.

It was mentioned above that if a high amount of radioactivity e.g.  $> 1\text{ Ci}$  can be used to prepare  $^{18}\text{F}$ -ArBF<sub>3</sub>S, the specific activity would not be significantly sacrificed by the addition of carrier  $^{19}\text{F}$ -fluoride. However, since we have never been able to obtain such a high level of radioactivity, this must be confirmed in future studies. It is therefore necessary to develop an automatic radiosynthetic system for the fluoridation of arylboronic acids/esters with high levels of radioactivity. Moreover, considering there is always  $^{19}\text{F}$ -fluoride present in the  $^{18}\text{F}$ -fluoride solution from the target, which means that at a high radioactivity, there should be a sufficient amount of  $^{19}\text{F}$ -fluoride available in the no-carrier-added  $^{18}\text{F}$ -fluoride solution to drive the reaction forward to a considerable and useful yield. It is hence possible to carry out a no-carrier-added fluoridation of arylboronates at high radioactivity. For example, if the actual specific activity of  $^{18}\text{F}$ -fluoride from the cyclotron is  $5\text{ Ci}/\mu\text{mol}$ , with radioactivity of  $2\text{ Ci}$ , there is  $400\text{ nmol}$  of  $^{19}\text{F}$ -fluoride present in the no-carrier-added  $^{18}\text{F}$ -fluoride solution and it would be enough for the fluoridation of arylboronates for  $^{18}\text{F}$ -ArBF<sub>3</sub>S under the reaction scales studied in this dissertation. An automatic radiosynthesis is therefore extremely significant for the no-carrier-added experiment under high levels of radioactivity.

It is widely appreciated that the receptor binding based imaging probes with low specific activity need to compete for receptors with the non-radioactive compounds. Especially when the receptor is limited, the specific uptake of the radiotracers would be blocked by the unlabeled ligands. However, the specific activities reported in some successful imaging work have ranged from  $0.2$  to  $10\text{ Ci}/\mu\text{mol}$ .<sup>56, 76, 174, 509</sup> Low specific activities have been reported for successful human imaging. Wild *et al.* recently published their work to image somatostatin (sst) receptor using the SPECT radionuclide

labeled peptides,  $^{111}\text{In}$ -DTPA octreotide <sup>a</sup> and  $^{111}\text{In}$ -DOTA-BASS, <sup>b</sup> for SPECT imaging.<sup>530</sup> They injected about 5 mCi of the  $^{111}\text{In}$ -labeled somatostatin analogues (with a specific activity of 0.32 Ci/ $\mu\text{mol}$  for  $^{111}\text{In}$ -DOTA-BASS and 0.70 Ci/ $\mu\text{mol}$  for  $^{111}\text{In}$ -DTPA-octreotide) in patients with neuroendocrine tumors. Both radiolabeled peptides showed high tumor-to-background ratios in patients, while  $^{111}\text{In}$ -DOTA-BASS showed superior tumor uptake to  $^{111}\text{In}$ -DTPA-octreotide. This work suggests that the specific activity is not the only factor determining the image quality. Accordingly, we believe that the specific activity of  $^{18}\text{F}$ -ArBF<sub>3</sub>s can be achieved to be 0.3 Ci/ $\mu\text{mol}$  easily, especially taking the triplet specific activity from that of  $^{18}\text{F}$ -fluoride into account. We are very optimistic to expect that the  $^{18}\text{F}$ -ArBF<sub>3</sub> labeled RGD-peptides, folate and PSMA inhibitor would provide beautiful animal images through the carrier-added radiosyntheses.

## 9.2 Perspectives

In the Discussion section, some of the perspectives have been addressed. And for those not fit in, I would like to put some more thoughts in this individual “Perspectives” section. I hope this can provide more directions for the future development of this technique.

### 9.2.1 Are $^{18}\text{F}$ -alkyltrifluoroborates suitable for PET imaging?

In addition to ArBF<sub>3</sub>s and HetArBF<sub>3</sub>s, there is another category of organotrifluoroborates: alkyltrifluoroborates. Alkyltrifluoroborates have received increasing attention in the transition-metal catalyzed cross-coupling reactions for the sp<sup>2</sup>-sp<sup>3</sup> C-C bond formation.<sup>121, 122, 531-539</sup> Compared to ArBF<sub>3</sub>s and HetArBF<sub>3</sub>s, alkyltrifluoroborates may add less mass to the molecules of interest. Moreover, it is possible that alkyltrifluoroborates would have higher hydrophilicity than the aryl counterparts. The inductive effect and even steric influence might contribute more strongly to the solvolytic stability of the alkyltrifluoroborates. Therefore, it is necessary to investigate whether or not they can be used for PET imaging applications. A more

---

<sup>a</sup> Octreotide is an sst agonist with a sequence of *D*-Phe-c(Cys-Tyr-*D*-Trp-Lys-Thr-Cys)-Thr(ol).

<sup>b</sup> BASS is an sst antagonist with a sequence of *p*-NO<sub>2</sub>-Phe-c(*D*-Cys-Tyr-*D*-Trp-Lys-thr-Cys)-*D*-Tyr-NH<sub>2</sub>.

systematic study on this is required.

## 9.2.2 Developing new protecting groups to facilitate the fluoridation of boronates

Although free arylboronic acids would be the best candidates for the fluoridation, however, arylboronic acids with poor electron density, which can provide more hydrolytically stable  $\text{ArBF}_3\text{s}$ , display relatively low stability and are prone to deboronation during bioconjugation and/or storage. The boronic acids protected with acid-sensitive protecting groups can be the alternatives for higher stability under normal conditions and with comparable fluoridation process to prepare  $\text{ArBF}_3\text{s}$ , as suggested in Chapter 3. However, there might also be synthetic challenges to prepare these boronates. For example, the fluoridation of the DiDiAN protected boronate **3.16** has a comparable fluoridation rate to that of the free boronic acid **3.11**. Although the preparation of DiDiAN protected boronate esters from DiDiAN $\cdot$ 2HCl **3.14** is generally simple and rapid, the yield of this synthesis is always low (< 40%). Moreover, the subsequent derivatization on the DiDiAN protected boronate esters often results in poor yields and difficult isolation, compared with the 1,8-diaminonaphthalene protected counterparts. Due to these reasons, the DiDiAN protecting procedure was not fully investigated in this thesis. However, its great performance in the fluoridation suggests it is worthy of further development. More understanding of this protecting group would be definitely helpful to apply it in this whole boron based technique.

1,8-Diaminonaphthalene protected boronate esters have been used in this thesis mainly as intermediates for the corresponding boronic acids. 1,8-Diaminonaphthalene protected boronate esters also displayed rapid fluoridation based on the  $^{19}\text{F}$  NMR studies in Chapter 3 to suggest their potential for use in the  $^{18}\text{F}$ -fluoridation. In addition, the 1,8-diaminonaphthalene protected boronates are known to have high stability under various conditions. Since this protecting group is acid-sensitive, the derivatization with 1,8-diaminonaphthalene protected boronates needs to avoid acid treatment along the synthesis. Thorough investigation on this protecting group in the radiolabeling will provide more information.

In addition to the acid-sensitive protecting groups discussed above, some other protecting groups with different properties are also worthy of investigation. The photocleavable protecting groups, such as the protecting group containing the *ortho*-nitrobenzyl group, is of interest to provide an alternative way to free the boronic acid, without any other treatment but light. However, the stability of the C-B bond under photochemistry conditions may also need consideration. Furthermore, if after the fluoridation, both the protecting group and unreacted boronate substrates can be easily removed by simple filtration or extraction, the reaction purification would be much simpler. Hence, biotin chemistry or resin based protecting groups might satisfy the requirement for easier purification of  $^{18}\text{F}$ -ArBF<sub>3</sub>S from nonradioactive materials.

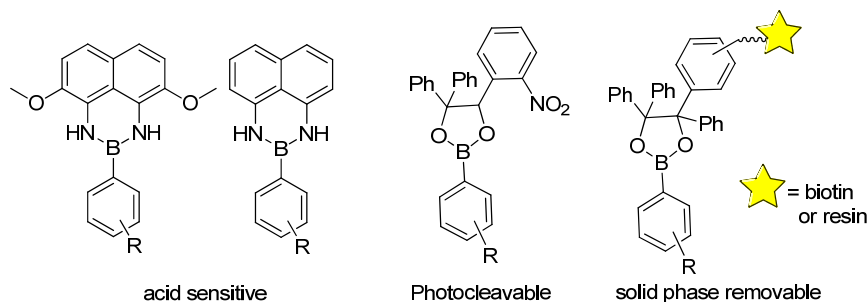


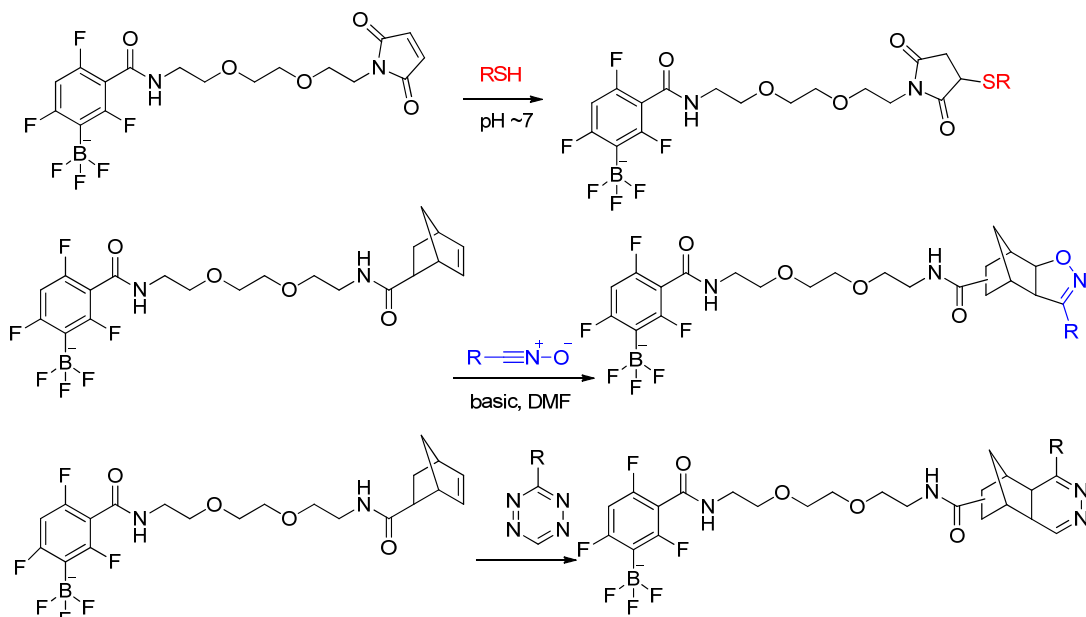
**Figure 9.1** The structures of possible pursued protecting groups for boronic acids.

No matter which protecting group shown in Figure 9.1 is used, there are several basic rules for choosing a boron protecting group to develop the boronates as suitable precursors to ArBF<sub>3</sub>S: a) the protected boronate esters are stable enough to undergo various or certain derivatization; b) it must be easy to remove the protecting group and release the free boronic acid under orthogonal and mild conditions; c) The protecting groups are acid-sensitive enough for the protected boronate esters to undergo rapid fluoridations, or under certain conditions, such as light, the protecting groups are able to be removed to reveal the boronic acids, which can undergo fast fluoridations; and d) if possible, it must be easy to remove any unreacted boronate esters and the free protecting group released from the labeling reaction.

### 9.2.3 Alternative one-pot two-step strategies

The one-pot two-step strategy based on the copper(I) catalyzed 1,3-dipolar cycloaddition developed in this thesis to label acid-sensitive biomolecules with

$^{18}\text{F}$ - $\text{ArBF}_3\text{s}$  proceeded with high efficiency and good radiochemical yields. The potential copper contamination in the  $^{18}\text{F}$ - $\text{ArBF}_3\text{s}$  from the click reaction may address the limitation of this technique. Therefore, more biocompatible labeling techniques should also be explored as alternatives for different substrates. Thiol-ene reactions, especially the thiol-maleimide chemistry frequently used to label biomolecules such as affibodies and proteins,<sup>540-544</sup> and the norbornene chemistry, including 1,3-dipolar cycloadditions with nitrile oxides<sup>288</sup> and the Diels-Alder reactions with tetrazines,<sup>289, 545</sup> may be also worth exploring as shown in Scheme 9.1. The preliminary results (rapid and high-yielding in non-radioactive experiments) with the thiol-maleimide reaction (within 30 minutes) and the dipolar cycloaddition between the norbornene and nitrile oxides (within 10 minutes) were very encouraging. Overall, whichever method is chosen might depend on the chemistry of the ligands chosen. However, the production of a diverse chemical toolkit for the one-pot two-step radiosyntheses of the  $^{18}\text{F}$ - $\text{ArBF}_3$  labeled molecules can provide more options for different ligands.



Scheme 9.1 Potential one-pot two-step labeling alternatives to label molecules with  $\text{ArBF}_3\text{s}$ .

#### 9.2.4 Where is $^{19}\text{F}$ -fluoride in the irradiated $^{18}\text{OH}_2$ from?

Mentioned both in Chapter 1 and the previous section in this chapter, the actual specific activity of no-carrier-added  $^{18}\text{F}$ -fluoride ( $5 \sim 14 \text{ Ci}/\mu\text{mol}$ ) is far less than the theoretical value ( $\sim 1710 \text{ Ci}/\mu\text{mol}$ ) and it varies to some extent from one cyclotron site to another

yet rarely surpasses a value of 40 Ci/ $\mu\text{mol}$ . It therefore would be worthwhile to study the source of  $^{19}\text{F}$ -fluoride in the target. This would a) guide possible modifications in the target to achieve a higher specific activity of  $^{18}\text{F}$ -fluoride by suppressing the presence of  $^{19}\text{F}$ -fluoride, and b) be possible to predict the amount of  $^{19}\text{F}$ -fluoride present in  $^{18}\text{F}$ -fluoride with a certain radioactivity and thus provide more information for the possibility of a successful no-carrier-added radiosynthesis of  $^{18}\text{F}$ -ArBF<sub>3</sub>S.

By removing Teflon tubings, valves, and fittings to avoid the radiolysis of Teflon to release  $^{19}\text{F}$ -fluoride, the residual  $^{19}\text{F}$ -fluoride present in  $^{18}\text{F}$ -fluoride was found to be significantly reduced and the specific activity was correspondingly increased to more than 100 Ci/ $\mu\text{mol}$ , which is still far less than the theoretical value ( $\sim 1710$  Ci/ $\mu\text{mol}$ ).<sup>52, 91</sup> Berridge and co-workers therein claimed that the synthetic reagents, which they used to prepare  $^{18}\text{F}$ -fluorobenzaldehyde as a way to measure the specific activity of  $^{18}\text{F}$ -fluoride, accounted for the residual carrier fluoride.<sup>91</sup> This later hypothesis was so bereft of proof that their study raised more questions than they answered. In fact, in their earlier work to synthesize  $^{18}\text{F}$ -fluorocarazolol mentioned therein, the synthesis with either non-irradiated  $^{18}\text{OH}_2$  passed through the target/delivery system or irradiated  $^{16}\text{OH}_2$  provided “*negligible mass compared to a normal radiolabeling experiment with irradiated  $^{18}\text{OH}_2$* ”.<sup>91</sup> The contradictory fact and conclusion shed light on other possibilities. Whether or not there is  $^{19}\text{F}$ -fluoride co-produced in the nuclear reaction for  $^{18}\text{F}$ -fluoride needs to be investigated. The fact that there seems to be a consistent value that rarely surpasses 40 Ci/ $\mu\text{mol}$  irrespective of what synthon is labeled and in what context leaves us to wonder whether  $^{19}\text{F}$ -fluoride may be produced as a consequence of the nuclear reaction. More work is expected to clear all the possibilities.

### 9.3 Conclusion

In a radiosynthesis, a route with fewer steps involving the radionuclide is always favored, which is due to the short half-lives of the radionuclides and concerns about radiation safety. As both of the methods investigated in this thesis require no protecting groups on the biomolecule residues and the reactions are undertaken in aqueous solutions, the  $^{18}\text{F}$ -labeling strategy based on  $^{18}\text{F}$ -ArBF<sub>3</sub>S therefore provides an alternative to the

traditional  $^{18}\text{F}$ -labeling methods. In this thesis, we have successfully radiolabeled several biomolecules with  $^{18}\text{F}$ -ArBF<sub>3</sub>S, including MMP inhibitor marimastat, PSMA inhibitor Glu-C(O)-Lys, folate, RGD-peptides, and oligonucleotides. The radiochemical yields varied from 2% to 30% for radiosyntheses within 60 minutes. We expect that with further optimization, the radiolabeling can be further improved. In addition, biological test and animal imaging work will finally provide more significant information about whether this technique can be used as a practical labeling method, complementary to the traditional labeling techniques.

# Bibliography

1. Herschman, H. R., *Science* **2003**, *302*, 605-608.
2. Tsien, R. Y., *Nat. Rev. Mol. Cell Biol.* **2003**, Ss16-Ss21.
3. Doubrovin, M.; Serganova, I.; Mayer-Kuckuk, P.; Ponomarev, V.; Blasberg, R. G., *Bioconjugate Chem.* **2004**, *15*, 1376-1388.
4. Willmann, J. K.; van Bruggen, N.; Dinkelborg, L. M.; Gambhir, S. S., *Nat. Rev. Drug Discovery* **2008**, *7*, 591-607.
5. Czernin, J.; Weber, W. A.; Herschman, H. R., *Annu. Rev. Med.* **2006**, *57*, 99-118.
6. Mather, S., *Bioconjugate Chem.* **2009**, *20*, 631-643.
7. Leblond, F.; Davis, S. C.; Valdes, P. A.; Pogue, B. W., *J. Photochem. Photobiol. B, Biol.* **2010**, *98*, 77-94.
8. Prescher, J. A.; Contag, C. H., *Curr. Opin. Chem. Biol.* **2010**, *14*, 80-89.
9. Roach, M.; Alberini, J. L.; Pecking, A. P.; Testori, A.; Verrecchia, F.; Soteldo, J.; Ganswindt, U.; Joyal, J. L.; Babich, J. W.; Witte, R. S.; Unger, E.; Gottlieb, R., *J. Surg. Oncol.* **2010**, *103*, 587-601.
10. Dobrucki, L. W.; Sinusas, A. J., *Curr. Opin. Biotechnol.* **2007**, *18*, 90-96.
11. Neves, A. A.; Brindle, K. M., *Biochim. Biophys. Acta, Rev. Cancer*; **2006**, *1766*, 242-261.
12. Hentschel, B.; Oehler, W.; Strauß, D.; Ulrich, A.; Malich, A.; Hentschel, B., *Strahlenther. Onkol.* **2011**, *187*, 183-190.
13. Mariani, G.; Bruselli, L.; Kuwert, T.; Kim, E. E.; Flotats, A.; Israel, O.; Dondi, M.; Watanabe, N., *Eur. J. Nucl. Med. Mol. Imag.* **2010**, *37*, 1959-1985.
14. Czernin, J.; Allen-Auerbach, M.; Schelbert, H. R., *J. Nucl. Med.* **2007**, *48*, 78s-88s.
15. Bonne, O.; Krausz, Y.; Lerer, B., *Gen. Hosp. Psychiatry* **1992**, *14*, 296-306.
16. Ametamey, S. M.; Honer, M.; Schubiger, P. A., *Chem. Rev.* **2008**, *108*, 1501-1516.
17. Le Bars, D., *J. Fluorine Chem.* **2006**, *127*, 1488-1493.
18. Budinger, T. F.; Brennan, K. M.; Moses, W. W.; Derenzo, S. E., *Nucl. Med. Biol.* **1996**, *23*, 659-667.
19. Saha, G. B., Performance Characteristics of PET Scanners. In *Basics of PET Imaging: Physics, Chemistry, and Regulations*, Springer: New York, 2010; pp 97-113.
20. Vallabhajosula, S., *Semin. Nucl. Med.* **2007**, *37*, 400-419.
21. Delacroix, D.; Guerre, J. P.; Leblanc, P.; Hickman, C., *Radionuclide and Radiation Protection Data Handbook 2002*. Nuclear Technology Publishing: **2002**.
22. Schlyer, D. J., *Ann. Acad. Med. Singap.* **2004**, *33*, 146-154.
23. Tu, Z.; Mach, R. H., *Curr. Top. Med. Chem.* **2010**, *10*, 1060-1095.
24. Toyohara, J.; Sakata, M.; Wu, J.; Ishikawa, M.; Oda, K.; Ishii, K.; Iyo, M.; Hashimoto, K.; Ishiwata, K., *Ann. Nucl. Med.* **2009**, *23*, 301-309.
25. Ishiwata, K.; Tsukada, H.; Kubota, K.; Nariai, T.; Harada, N.; Kawamura, K.; Kimura, Y.; Oda, K.; Iwata, R.; Ishii, K., *Nucl. Med. Biol.* **2005**, *32*, 253-262.

26. Anderson, C. J.; Ferdani, R., *Cancer Biother. Radiopharm.* **2009**, *24*, 379-393.
27. Smith, S. V., *Expert Opinion on Drug Discovery* **2007**, *2*, 659-672.
28. Smith, S. V., *J. Inorg. Biochem.* **2004**, *98*, 1874-1901.
29. Cutler, P. D.; Schwarz, S. W.; Anderson, C. J.; Connett, J. M.; Welch, M. J.; Philpott, G. W.; Siegel, B. A., *J. Nucl. Med.* **1995**, *36*, 2363-2371.
30. Fani, M.; Andre, J. P.; Maecke, H. R., *Contrast Media Mol. Imaging* **2008**, *3*, 53-63.
31. Varagnolo, L.; Stokkel, M. P. M.; Mazzi, U.; Pauwels, E. K. J., *Nucl. Med. Biol.* **2000**, *27*, 103-112.
32. Helus, F.; Maierborst, W.; Sahn, U.; Wiebe, L. I., *Radiochem. Radioa. Lett.* **1979**, *38*, 395-410.
33. Snell, A. H. Proceedings of the American Physical Society, *Minutes of the Pasadena Meeting*, Pasadena, December 18 and 19, 1936; Phys. Rev.: Pasadena, *Phys. Rev.*: **1937**, *51*, pp 142-150.
34. Nickles, R. J.; Hichwa, R. D.; Daube, M. E.; Hutchins, G. D.; Congdon, D. D., *Int. J. Appl. Radiat. Isot.* **1983**, *34*, 625-629.
35. Ruth, T. J.; Wolf, A. P., *Radiochimica Acta* **1979**, *26*, 21-24.
36. Kilbourn, M. R.; Hood, J. T.; Welch, M. J., *Int. J. Appl. Radiat. Isot.* **1984**, *35*, 599-602.
37. Ido, T.; Wan, C. N.; Fowler, J. S.; Wolf, A. P., *J. Org. Chem.* **1977**, *42*, 2341-2342.
38. Fowler, J. S.; MacGregor, R. R.; Wolf, A. P.; Farrell, A. A.; Karlstrom, K. I.; Ruth, T. J., *J. Nucl. Med.* **1981**, *22*, 376-380.
39. Bida, G. T.; Satyamurthy, N.; Barrio, J. R., *J. Nucl. Med.* **1984**, *25*, 1327-1334.
40. Korytnyk, W.; Valentekovic-Horvat, S., *Tetrahedron Lett.* **1980**, *21*, 1493-1496.
41. Shiue, C. Y.; To, K. C.; Wolf, A. P., *J. Labelled. Comp. Rad.* **1983**, *20*, 157-162.
42. Sood, S.; Firnau, G.; Garnett, E. S., *Int. J. Appl. Radiat. Isot.* **1983**, *34*, 743-745.
43. Firnau, G.; Chirakal, R.; Sood, S.; Garnett, E. S., *J. Labelled. Comp. Rad.* **1981**, *18*, 7-8.
44. Firnau, G.; Chirakal, R.; Sood, S.; Garnett, S., *Can. J. Chem./Rev. Can. Chim.* **1980**, *58*, 1449-1450.
45. Shiue, C. Y.; Salvadori, P. A.; Wolf, A. P.; Fowler, J. S.; Macgregor, R. R., *J. Nucl. Med.* **1982**, *23*, 899-903.
46. Ehrenkauf, R. E.; Potocki, J. F.; Jewett, D. M., *J. Nucl. Med.* **1984**, *25*, 333-337.
47. Bishop, A.; Satyamurthy, N.; Bida, G.; Barrio, J. R., *Nucl. Med. Biol.* **1996**, *23*, 559-565.
48. Lerman, O.; Tor, Y.; Hebel, D.; Rozen, S., *J. Org. Chem.* **1984**, *49*, 806-813.
49. Hess, E.; Sichler, S.; Kluge, A.; Coenen, H. H., *Appl. Radiat. Isot.* **2002**, *57*, 185-191.
50. Dolle, F.; Demphel, S.; Hinnen, F.; Fournier, D.; Vaufrey, F.; Crouzel, C., *J. Labelled. Comp. Rad.* **1998**, *41*, 105-114.
51. Hamacher, K.; Coenen, H. H.; Stocklin, G., *J. Nucl. Med.* **1986**, *27*, 235-238.
52. Fuchtnner, F.; Preusche, S.; Mading, P.; Zessin, J.; Steinbach, J., *Nuklearmed. Nucl. Med.* **2008**, *47*, 116-119.
53. Schirmacher, R.; Wangler, C.; Schirmacher, E., *Mini Rev. Org. Chem.* **2007**, *4*, 317-329.
54. Alauddin, M. M.; Fissekis, J. D.; Conti, P. S., *J. Labelled. Comp. Rad.* **2003**, *46*, 805-814.

55. Fookes, C. J. R.; Pham, T. Q.; Mattner, F.; Loc'h, C.; Liu, X.; Berghofer, P.; Shepherd, R.; Gregoire, M. C.; Katsifis, A.; Greguric, I., *J. Med. Chem.* **2008**, *51*, 3700-3712.
56. Gill, H. S.; Tinianow, J. N.; Ogasawara, A.; Flores, J. E.; Vanderbilt, A. N.; Raab, H.; Scheer, J. M.; Vandlen, R.; Williains, S. P.; Marik, J., *J. Med. Chem.* **2009**, *52*, 5816-5825.
57. Sachin, K.; Kim, E. M.; Cheong, S. J.; Jeong, H. J.; Lim, S. T.; Sohn, M. H.; Kim, D. W., *Bioconjugate Chem.* **2010**, *21*, 2282-2288.
58. Gao, M. Z.; Wang, M.; Miller, K. D.; Sledge, G. W.; Hutchins, G. D.; Zheng, Q. H., *Bioorg. Med. Chem. Lett.* **2006**, *16*, 5767-5772.
59. Viel, T.; Kuhnast, B.; Hinnen, F.; Boisgard, R.; Tavitian, B.; Dolle, F., *J. Labelled. Comp. Rad.* **2007**, *50*, 1159-1168.
60. Kapur, S.; Jones, C.; DaSilva, J.; Wilson, A.; Houle, S., *Nucl. Med. Commun.* **1997**, *18*, 395-399.
61. Flavell, R. R.; Kothari, P.; Bar-Dagan, M.; Synan, M.; Vallabhajosula, S.; Friedman, J. M.; Muir, T. W.; Ceccarini, G., *J. Am. Chem. Soc.* **2008**, *130*, 9106-9112.
62. Schottelius, M.; Berger, S.; Poethko, T.; Schwaiger, M.; Wester, H. J., *Bioconjugate Chem.* **2008**, *19*, 1256-1268.
63. Pike, V. W.; Aigbirhio, F. I., *J. Chem. Soc. Chem. Commun.* **1995**, 2215-2216.
64. Chun, J.; Lu, S.; Lee, Y. S.; Pike, V. W., *J. Labelled. Comp. Rad.* **2009**, *52*, S159-S159.
65. Chun, J. H.; Lu, S. Y.; Lee, Y. S.; Pike, V. W., *J. Org. Chem.* **2010**, *75*, 3332-3338.
66. Studenov, A. R.; Adam, M. J.; Wilson, J. S.; Ruth, T. J., *J. Labelled. Comp. Rad.* **2005**, *48*, 497-500.
67. McBride, W. J.; Sharkey, R. M.; Karacay, H.; D'Souza, C. A.; Rossi, E. A.; Laverman, P.; Chang, C. H.; Boerman, O. C.; Goldenberg, D. M., *J. Nucl. Med.* **2009**, *50*, 991-998.
68. McBride, W. J.; D'Souza, C. A.; Sharkey, R. M.; Karacay, H.; Rossi, E. A.; Chang, C. H.; Goldenberg, D. M., *Bioconjugate Chem.* **2010**, *21*, 1331-1340.
69. Laverman, P.; McBride, W. J.; Sharkey, R. M.; Eek, A.; Joosten, L.; Oyen, W. J. G.; Goldenberg, D. M.; Boerman, O. C., *J. Nucl. Med.* **2010**, *51*, 454-461.
70. D'Souza, C. A.; McBride, W. J.; Sharkey, R. M.; Todaro, L. J.; Goldenberg, D. M., *Bioconjugate Chem.* **2011**, *22*, 1793-1803.
71. Schirmacher, R.; Bradtmoller, G.; Schirmacher, E.; Thews, O.; Tillmanns, J.; Siessmeier, T.; Buchholz, H. G.; Bartenstein, P.; Waengler, B.; Niemeyer, C. M.; Jurkschat, K., *Angew. Chem. Int. Ed.* **2006**, *45*, 6047-6050.
72. Hoehne, A.; Mu, L.; Honer, M.; Schubiger, P. A.; Ametamey, S. M.; Graham, K.; Stellfeld, T.; Borkowski, S.; Berndorff, D.; Klar, U.; Voigtmann, U.; Cyr, J. E.; Friebe, M.; Dinkelborg, L.; Srinivasan, A., *Bioconjugate Chem.* **2008**, *19*, 1871-1879.
73. Mu, L. J.; Hohne, A.; Schubiger, R. A.; Ametamey, S. M.; Graham, K.; Cyr, J. E.; Dinkelborg, L.; Stellfeld, T.; Srinivasan, A.; Voigtmann, U.; Klar, U., *Angew. Chem. Int. Ed.* **2008**, *47*, 4922-4925.
74. Iovkova, L.; Konning, D.; Wangler, B.; Schirmacher, R.; Schoof, S.; Arndt, H. D.; Jurkschat, K., *Eur. J. Inorg. Chem.* **2011**, 2238-2246.
75. Kostikov, A. P.; Iovkova, L.; Chin, J.; Schirmacher, E.; Wangler, B.; Wangler, C.; Jurkschat, K.; Cosa, G.; Schirmacher, R., *J. Fluorine Chem.* **2011**, *132*, 27-34.
76. Wangler, C.; Waser, B.; Alke, A.; Iovkova, L.; Buchholz, H. G.; Niedermoser, S.; Jurkschat, K.; Fottner, C.; Bartenstein, P.; Schirmacher, R.; Reubi, J. C.; Weste, H. J.; Wangler, B., *Bioconjugate Chem.*

**2010**, *21*, 2289-2296.

77. Iovkova, L.; Wangler, B.; Schirmmayer, E.; Schirmmayer, R.; Quandt, G.; Boening, G.; Schurmann, M.; Jurkschat, K., *Chem. Eur. J.* **2009**, *15*, 2140-2147.
78. Ting, R.; Adam, M. J.; Ruth, T. J.; Perrin, D. M., *J. Am. Chem. Soc.* **2005**, *127*, 13094-13095.
79. Ting, R.; Harwig, C.; auf dem Keller, U.; McCormick, S.; Austin, P.; Overall, C. M.; Adam, M. J.; Ruth, T. J.; Perrin, D. M., *J. Am. Chem. Soc.* **2008**, *130*, 12045-12055.
80. Ting, R.; Lo, J.; Adam, M. J.; Ruth, T. J.; Perrin, D. M., *J. Fluorine Chem.* **2008**, *129*, 349-358.
81. Ting, R.; Aguilera, T. A.; Crisp, J. L.; Hall, D. J.; Eckelman, W. C.; Vera, D. R.; Tsien, R. Y., *Bioconjugate Chem.* **2010**, *21*, 1811-1819.
82. Jauregui-Osoro, M.; Sunassee, K.; Weeks, A. J.; Berry, D. J.; Paul, R. L.; Cleij, M.; Banga, J.; O'Doherty, M. J.; Marsden, P. K.; Clarke, S. E. M.; Ballinger, J. R.; Szanda, I.; Cheng, S. Y.; Blower, P. J., *Eur. J. Nucl. Med. Mol. Imag.* **2010**, *37*, 2108-2116.
83. Crouch, R. D., *Tetrahedron* **2004**, *60*, 5833-5871.
84. Rosenthal, M. S.; Bosch, A. L.; Nickles, R. J.; Gatley, S. J., *Int. J. Appl. Radiat. Isot.* **1985**, *36*, 318-319.
85. Ting, R.; Harwig, C. W.; Lo, J.; Li, Y.; Adam, M. J.; Ruth, T. J.; Perrin, D. M., *J. Org. Chem.* **2008**, *73*, 4662-4670.
86. Keller, U. A. D.; Bellac, C. L.; Li, Y.; Lou, Y. M.; Lange, P. F.; Ting, R.; Harwig, C.; Kappelhoff, R.; Dedhar, S.; Adam, M. J.; Ruth, T. J.; Benard, F.; Perrin, D. M.; Overall, C. M., *Cancer Res.* **2010**, *70*, 7562-7569.
87. Weeks, A. J.; Jauregui-Osoro, M.; Cleij, M.; Blower, J. E.; Ballinger, J. R.; Blower, P. J., *Nucl. Med. Commun.* **2011**, *32*, 98-105.
88. Phelps, M. E., *PET: Molecular Imaging and Its Biological Applications*. Springer-Verlag: New York, **2004**, p 160.
89. Sadzot, B.; Price, J. C.; Mayberg, H. S.; Douglass, K. H.; Dannals, R. F.; Lever, J. R.; Ravert, H. T.; Wilson, A. A.; Wagner, H. N.; Feldman, M. A.; Frost, J. J., *J. Cereb. Blood Flow Metab.* **1991**, *11*, 204-219.
90. Hume, S. P.; Gunn, R. N.; Jones, T., *Eur. J. Nucl. Med.* **1998**, *25*, 173-176.
91. Berridge, M. S.; Apana, S. M.; Hersh, J. M., *J. Labelled. Comp. Rad.* **2009**, *52*, 543-548.
92. Carey, F. A.; Sunderberg, R. J., *Advanced Organic Chemistry, Part A: Structure and Mechanisms*. 4<sup>th</sup> ed.; Springer: New York, **2000**, pp 569-570.
93. Stefani, H. A.; Cella, R.; Vieira, A. S., *Tetrahedron* **2007**, *63*, 3623-3658.
94. Darses, S.; Genet, J. P., *Chem. Rev.* **2008**, *108*, 288-325.
95. Wright, S. W.; Hageman, D. L.; McClure, L. D., *J. Org. Chem.* **1994**, *59*, 6095-6097.
96. Batey, R. A.; Quach, T. D., *Tetrahedron Lett.* **2001**, *42*, 9099-9103.
97. Cella, R.; Cunha, R. L. O. R.; Reis, A. E. S.; Pimenta, D. C.; Klitzke, C. F.; Stefani, H. A., *J. Org. Chem.* **2006**, *71*, 244-250.
98. Barder, T. E.; Buchwald, S. L., *Org. Lett.* **2004**, *6*, 2649-2652.
99. Molander, G. A.; Bernardi, C. R., *J. Org. Chem.* **2002**, *67*, 8424-8429.
100. Molander, G. A.; Biolatto, B., *Org. Lett.* **2002**, *4*, 1867-1870.

101. Molander, G. A.; Rivero, M. R., *Org. Lett.* **2002**, *4*, 107-109.
102. Molander, G. A.; Biolatto, B., *J. Org. Chem.* **2003**, *68*, 4302-4314.
103. Molander, G. A.; Fumagalli, T., *J. Org. Chem.* **2006**, *71*, 5743-5747.
104. Molander, G. A.; Beaumard, F., *Org. Lett.* **2010**, *12*, 4022-4025.
105. Molander, G. A.; Canturk, B.; Kennedy, L. E., *J. Org. Chem.* **2009**, *74*, 973-980.
106. Molander, G. A.; Jean-Gerard, L., *J. Org. Chem.* **2009**, *74*, 1297-1303.
107. Quach, T. D.; Batey, R. A., *Org. Lett.* **2003**, *5*, 1381-1384.
108. Marzi, E.; Bigi, A.; Schlosser, M., *Eur. J. Org. Chem.* **2001**, *2001*, 1371-1376.
109. Maki, T.; Ishihara, K.; Yamamoto, H., *Org. Lett.* **2005**, *7*, 5043-5046.
110. Coburn, M. D.; Buntain, G. A.; Harris, B. W.; Hiskey, M. A.; Lee, K. Y.; Ott, D. G., *J. Heterocycl. Chem.* **1991**, *28*, 2049-2050.
111. Chavez, D. E.; Hiskey, M. A., *J. Heterocycl. Chem.* **1998**, *35*, 1329-1332.
112. Helm, M. D.; Plant, A.; Harrity, J. P. A., *Org. Bioimol. Chem.* **2006**, *4*, 4278-4280.
113. Abu Ali, H.; El Aziz Al Quntar, A.; Goldberg, I.; Srebnik, M., *Organometallics* **2002**, *21*, 4533-4539.
114. Le Bars, D.; Lemaire, C.; Ginovart, N.; Plenevaux, A.; Aerts, J.; Brihaye, C.; Hassoun, W.; Leviel, V.; Mekhsian, P.; Weissmann, D.; Pujol, J. F.; Luxen, A.; Comar, D., *Nucl. Med. Biol.* **1998**, *25*, 343-350.
115. Karramkam, M.; Hinnen, F.; Vaufrey, F.; Dolle, F., *J. Labelled. Comp. Rad.* **2003**, *46*, 979-992.
116. Ponde, D. E.; Dence, C. S.; Schuster, D. P.; Welch, M. J., *Nucl. Med. Biol.* **2004**, *31*, 133-138.
117. Glaser, M.; Arstad, E.; Luthra, S. K.; Robins, E. G., *J. Labelled. Comp. Rad.* **2009**, *52*, 327-330.
118. Lee, S. J.; Oh, S. J.; Chi, D. Y.; Kil, H. S.; Kim, E. N.; Ryu, J. S.; Moon, D. H., *Eur. J. Nucl. Med. Mol. Imag.* **2007**, *34*, 1406-1409.
119. Zhu, L.; Liu, Y. J.; Plossl, K.; Lieberman, B.; Liu, J. Y.; Kung, H. F., *Nucl. Med. Biol.* **2010**, *37*, 133-141.
120. Liu, Y. J.; Zhu, L.; Plossl, K.; Choi, S. R.; Qiao, H. W.; Sun, X. T.; Li, S.; Zha, Z. H.; Kung, H. F., *Nucl. Med. Biol.* **2010**, *37*, 917-925.
121. Molander, G. A.; Canturk, B., *Org. Lett.* **2008**, *10*, 2135-2138.
122. Molander, G. A.; Ham, J., *Org. Lett.* **2006**, *8*, 2031-2034.
123. Matsumoto, T.; Urano, Y.; Shoda, T.; Kojima, H.; Nagano, T., *Org. Lett.* **2007**, *9*, 3375-3377.
124. Kuhnert, N.; Burzlaff, N.; Patel, C.; Lopez-Periago, A., *Org. Bioimol. Chem.* **2005**, *3*, 1911-1921.
125. Kischer, O.; Kern, W., *J. Prakt. Chem.* **1916**, *94*, 15.
126. Noguchi, H.; Hojo, K.; Suginome, M., *J. Am. Chem. Soc.* **2007**, *129*, 758-759.
127. Noguchi, H.; Shioda, T.; Chou, C. M.; Suginome, M., *Org. Lett.* **2008**, *10*, 377-380.
128. Iwadate, N.; Suginome, M., *Org. Lett.* **2009**, *11*, 1899-1902.
129. Perrin, D. D.; Armarego, W. L. F., *Purification of Laboratory Chemicals*. 3rd ed.; Pergamon Press: **1988**.
130. Harwig, C. W.; Ting, R.; Adam, M. J.; Ruth, T. J.; Perrin, D. M., *Tetrahedron Lett.* **2008**, *49*,

3152-3156.

131. Antoni, P.; Hed, Y.; Nordberg, A.; Nystrom, D.; von Holst, H.; Hult, A.; Malkoch, M., *Angew. Chem. Int. Ed.* **2009**, *48*, 2126-2130.
132. Gill, S. E.; Parks, W. C., *Int. J. Biochem. Cell Biol.* **2008**, *40*, 1334-1347.
133. Murphy, G.; Nagase, H., *Mol. Aspects Med.* **2008**, *29*, 290-308.
134. Sternlicht, M. D.; Werb, Z., *Annu. Rev. Cell Dev. Biol.* **2001**, *17*, 463-516.
135. Overall, C. M., *Mol. Biotechnol.* **2002**, *22*, 51-86.
136. Galis, Z. S.; Khatri, J. J., *Circ. Res.* **2002**, *90*, 251-262.
137. Page-McCaw, A.; Ewald, A. J.; Werb, Z., *Nat. Rev. Mol. Cell Biol.* **2007**, *8*, 221-233.
138. Van de Wiele, C.; Oltenfreiter, R., *Cancer Biother. Radiopharm.* **2006**, *21*, 409-417.
139. Ennis, B. W.; Matrisian, L. M., *J. Neurooncol.* **1994**, *18*, 105-109.
140. Sato, H.; Takino, T.; Okada, Y.; Cao, J.; Shinagawa, A.; Yamamoto, E.; Seiki, M., *Nature* **1994**, *370*, 61-65.
141. Brew, K.; Dinakarpanian, D.; Nagase, H., *Biochim. Biophys. Acta. Protein. Struct. Mol. Enzymol.* **2000**, *1477*, 267-283.
142. Woessner, J. F., *Mol. Biotechnol.* **2002**, *22*, 33-49.
143. Brew, K.; Nagase, H., *Biochim. Biophys. Acta, Mol. Cell Res.* **2010**, *1803*, 55-71.
144. Wagner, S.; Breyholz, H. J.; Faust, A.; Holtke, C.; Levkau, B.; Schober, O.; Schafers, M.; Kopka, K., *Curr. Med. Chem.* **2006**, *13*, 2819-2838.
145. Thomas, A. L.; Steward, W. P., *Expert Opin. Inv. Drug.* **2000**, *9*, 2913-2922.
146. Goffin, J. R.; Anderson, I. C.; Supko, J. G.; Eder, J. P.; Shapiro, G. I.; Lynch, T. J.; Shipp, M.; Johnson, B. E.; Skarin, A. T., *Clin. Cancer Res.* **2005**, *11*, 3417-3424.
147. Skipper, J. B.; McNally, L. R.; Rosenthal, E. L.; Wang, W. Q.; Buchsbaum, D. J., *ORL-J. Otorhinolaryngol. Relat. Spec.* **2009**, *71*, 1-5.
148. Bissett, D.; O'Byrne, K. J.; von Pawel, J.; Gatzemeier, U.; Price, A.; Nicolson, M.; Mercier, R.; Mazabel, E.; Penning, C.; Zhang, M. H.; Collier, M. A.; Shepherd, F. A., *J. Clin. Oncol.* **2005**, *23*, 842-849.
149. Cianfrocca, M.; Cooley, T. P.; Lee, J. Y.; Rudek, M. A.; Scadden, D. T.; Ratner, L.; Pluda, J. M.; Figg, W. D.; Krown, S. E.; Dezube, B. J., *J. Clin. Oncol.* **2002**, *20*, 153-159.
150. Cianfrocca, M.; Cooley, T. P.; Lee, J.; Scadden, D. T.; Ratner, L.; Dezube, B. J., *J. Acquir. Immune Defic. Syndr.* **2000**, *23*, A33-A33.
151. Bremer, C.; Bredow, S.; Mahmood, U.; Weissleder, R.; Tung, C. H., *Radiology* **2001**, *221*, 523-529.
152. Pham, W.; Choi, Y. D.; Weissleder, R.; Tung, C. H., *Bioconjugate Chem.* **2004**, *15*, 1403-1407.
153. McIntyre, J. O.; Fingleton, B.; Wells, K. S.; Piston, D. W.; Lynch, C. C.; Gautam, S.; Matrisian, L. M., *Biochem. J.* **2004**, *377*, 617-628.
154. Su, H. L.; Spinale, F. G.; Dobrucki, L. W.; Song, J.; Hua, J.; Sweterlitsch, S.; Dione, D. P.; Cavaliere, P.; Chow, C.; Bourke, B. N.; Hu, X. Y.; Azure, M.; Yalamanchili, P.; Liu, R.; Cheesman, E. H.; Robinson, S.; Edwards, S.; Sinusas, A. J., *Circulation* **2005**, *112*, 3157-3167.
155. Fei, X. S.; Zheng, Q. H.; Hutchins, G. D.; Liu, X.; Stone, K. L.; Carlson, K. A.; Mock, B. H.; Winkle,

- W. L.; Glick-Wilson, B. E.; Miller, K. D.; Fife, R. S.; Sledge, G. W.; Sun, H. B.; Carr, R. E., *J. Labelled. Comp. Rad.* **2002**, *45*, 449-470.
156. Fei, X. S.; Zheng, Q. H.; Liu, X.; Wang, J. Q.; Stone, K. L.; Miller, K. D.; Sledge, G. W.; Hutchins, G. D., *J. Labelled. Comp. Rad.* **2003**, *46*, 343-351.
157. Zheng, Q. H.; Fei, X. S.; Liu, X.; Wang, J. Q.; Sun, H. B.; Mock, B. H.; Stone, K. L.; Martinez, T. D.; Miller, K. D.; Sledge, G. W.; Hutchins, G. D., *Nucl. Med. Biol.* **2002**, *29*, 761-770.
158. Zheng, Q. H.; Fei, X. S.; Liu, X.; Wang, J. Q.; Stone, K. L.; Martinez, T. D.; Gay, D. J.; Baity, W. L.; Miller, K. D.; Sledge, G. W.; Hutchins, G. D., *Nucl. Med. Biol.* **2004**, *31*, 77-85.
159. Zheng, Q. H.; Fei, X. S.; DeGrado, T. R.; Wang, J. Q.; Stone, K. L.; Martinez, T. D.; Gay, D. J.; Baity, W. L.; Mock, B. H.; Glick-Wilson, B. E.; Sullivan, M. L.; Miller, K. D.; Sledge, G. W.; Hutchins, G. D., *Nucl. Med. Biol.* **2003**, *30*, 753-760.
160. Kuhnast, B.; Bodenstern, C.; Wester, H. E.; Weber, W., *J. Labelled. Comp. Rad.* **2003**, *46*, 539-553.
161. Furumoto, S.; Iwata, R.; Ido, T., *J. Labelled. Comp. Rad.* **2002**, *45*, 975-986.
162. Furumoto, S.; Takashima, K.; Kubota, K.; Ido, T.; Iwata, R.; Fukuda, H., *Nucl. Med. Biol.* **2003**, *30*, 119-125.
163. Kwon, Y., Handbook of Essential Pharmacokinetics, Pharmacodynamics and Drug Metabolism for Industrial Scientists. In 1<sup>st</sup> ed.; Springer: 2001; p 46.
164. Molander, G. A.; Cavalcanti, L. N.; Canturk, B.; Pan, P. S.; Kennedy, L. E., *J. Org. Chem.* **2009**, *74*, 7364-7369.
165. Mane, B. S.; Jagdale, M. H., *React. Kinet. Catal. Lett.* **1977**, *6*, 417-424.
166. Ghosh, K. K.; Ghosh, S., *J. Org. Chem.* **1994**, *59*, 1369-1374.
167. Ghosh, K. K.; Patle, S. K.; Sharma, P.; Rajput, S. K., *Bull. Chem. Soc. Jpn.* **2003**, *76*, 283-290.
168. Saghatelian, A.; Jessani, N.; Joseph, A.; Humphrey, M.; Cravatt, B. F., *Proc. Natl. Acad. Sci. U. S. A.* **2004**, *101*, 10000-10005.
169. Antonis, A., *J. Lipid Res.* **1960**, *1*, 485-486.
170. Brammar, W. J.; Clarke, P. H., *J. Gen. Microbiol.* **1964**, *37*, 307-319.
171. Fournand, D.; Pirat, J. L.; Bigey, F.; Arnaud, A.; Galzy, P., *Anal. Chim. Acta* **1997**, *353*, 359-366.
172. Notari, R. E.; Munson, J. W., *J. Pharm. Sci.* **1969**, *58*, 1060-1064.
173. Rao, G. G.; Somidevamma, G., *Fresenius Z. Anal. Chem.* **1959**, *165*, 432-436.
174. Chen, Y.; Foss, C. A.; Byun, Y.; Nimmagadda, S.; Pullambhatla, M.; Fox, J. J.; Castanares, M.; Lupold, S. E.; Babich, J. W.; Mease, R. C.; Pomper, M. G., *J. Med. Chem.* **2008**, *51*, 7933-7943.
175. Banerjee, S. R.; Pullambhatla, M.; Byun, Y.; Nimmagadda, S.; Green, G.; Fox, J. J.; Horti, A.; Mease, R. C.; Pomper, M. G., *J. Med. Chem.* **2010**, *53*, 5333-5341.
176. Scherer, R. L.; McIntyre, J. O.; Matrisian, L. M., *Cancer Metastasis Rev.* **2008**, *27*, 679-690.
177. Pastorin, G.; Wu, W.; Wieckowski, S.; Briand, J. P.; Kostarelos, K.; Prato, M.; Bianco, A., *Chem. Comm.* **2006**, 1182-1184.
178. Jenssen, K.; Sewald, K.; Sewald, N., *Bioconjugate Chem.* **2004**, *15*, 594-600.
179. Chinigo, G. M.; Paige, M.; Grindrod, S.; Hamel, E.; Dakshanamurthy, S.; Chruszcz, M.; Minor, W.; Brown, M. L., *J. Med. Chem.* **2008**, *51*, 4620-4631.

180. Vernall, A. J.; Ballet, S.; Abell, A. D., *Tetrahedron* **2008**, *64*, 3980-3997.
181. Chehade, K. A. H.; Baruch, A.; Verhelst, S. H. L.; Bogyo, M., *Synthesis-Stuttgart* **2005**, 240-244.
182. Saito, S.; Komada, K.; Moriwake, T., *Organic Synthesis, Vol 73* **1996**, *73*, 184-200.
183. Ho, C. Y.; Strobel, E. D. Preparation of Hydroxamic Acids From Esters in Solution and on the Solid Phase. US 7091378B2, 2006.
184. Lou, Y. M.; Preobrazhenska, O.; Keller, U. A. D.; Sutcliffe, M.; Barclay, L.; McDonald, P. C.; Roskelley, C.; Overall, C. M.; Dedhar, S., *Clin. Exp. Metastasis* **2009**, *26*, 898-899.
185. Jemal, A.; Bray, F.; Center, M. M.; Ferlay, J.; Ward, E.; Forman, D., *CA. Cancer J. Clin.* **2011**, *61*, 69-90.
186. Ung, J. O.; Richie, J. P.; Chen, M. H.; Renshaw, A. A.; D'Amico, A. V., *Urology* **2002**, *60*, 458-463.
187. Diamandis, E. P., *Trends Endocrinol. Metab.* **1998**, *9*, 310-316.
188. Polascik, T. J.; Oesterling, J. E.; Partin, A. W., *J. Urol.* **1999**, *162*, 293-306.
189. Clements, R., *Eur. Radiol.* **1999**, *9*, 529-535.
190. Klein, L. T.; Lowe, F. C., *Urol. Clin. North Am.* **1997**, *24*, 293-297.
191. Thompson, I. M.; Ankerst, D. P.; Chi, C.; Lucia, M. S.; Goodman, P. J.; Crowley, J. J.; Parnes, H. L.; Coltman, C. A., *J. Am. Med. Assoc.* **2005**, *294*, 66-70.
192. Stamey, T. A., *BJU Int.* **2004**, *94*, 963-964.
193. Tricoli, J. V.; Schoenfeldt, M.; Conley, B. A., *Clin. Cancer Res.* **2004**, *10*, 3943-3953.
194. Nogueira, L.; Corradi, R.; Eastham, J. A., *BJU Int.* **2010**, *105*, 166-169.
195. Li, Y.; Cozzi, P. J.; Russell, P. J., *Med. Res. Rev.* **2010**, *30*, 67-101.
196. You, J. J.; Cozzi, P.; Walsh, B.; Willcox, M.; Kearsley, J.; Russell, P.; Li, Y., *Crit. Rev. Oncol. Hematol.* **2010**, *73*, 10-22.
197. Detchokul, S.; Frauman, A. G., *Br. J. Clin. Pharmacol.* **2011**, *71*, 157-174.
198. Bensalah, K.; Lotan, Y.; Karam, J. A.; Shariat, S. F., *Prostate Cancer Prostatic Dis.* **2008**, *11*, 112-120.
199. Sardana, G.; Dowell, B.; Diamandis, E. P., *Clin. Chem.* **2008**, *54*, 1951-1960.
200. Bjartell, A.; Montironi, R.; Berney, D. M.; Egevad, L., *Acta Oncol.* **2011**, *50*, 76-84.
201. Sreekumar, A.; Laxman, B.; Rhodes, D. R.; Bhagavathula, S.; Harwood, J.; Giacherio, D.; Ghosh, D.; Sanda, M. G.; Rubin, M. A.; Chinnaiyan, A. M., *J. Natl. Cancer Inst.* **2004**, *96*, 834-843.
202. Minelli, A.; Ronquist, G.; Carlsson, L.; Mearini, E.; Nilsson, O.; Larsson, A., *Anticancer Res.* **2005**, *25*, 4399-4402.
203. Wang, X.; Yin, L.; Rao, P.; Stein, R.; Harsch, K. M.; Lee, Z.; Heston, W. D. W., *J. Cell. Biochem.* **2007**, *102*, 571-579.
204. Fair, W. R.; Israeli, R. S.; Heston, W. D. W., *Prostate* **1997**, *32*, 140-148.
205. Ghosh, A.; Heston, W. D. W., *J. Cell. Biochem.* **2004**, *91*, 528-539.
206. Su, S. L.; Huang, I. P.; Fair, W. R.; Powell, C. T.; Heston, W. D. W., *Cancer Res.* **1995**, *55*, 1441-1443.

207. Grauer, L. S.; Lawler, K. D.; Marignac, J. L.; Kumar, A.; Goel, A. S.; Wolfert, R. L., *Cancer Res.* **1998**, *58*, 4787-4789.
208. Israeli, R. S.; Powell, C. T.; Corr, J. G.; Fair, W. R.; Heston, W. D. W., *Cancer Res.* **1994**, *54*, 1807-1811.
209. Wright, G. L.; Grob, B. M.; Haley, C.; Grossman, K.; Newhall, K.; Petrylak, D.; Troyer, J.; Konchuba, A.; Schellhammer, P. F.; Moriarty, R., *Urology* **1996**, *48*, 326-334.
210. Kawakami, M.; Nakayama, J., *Cancer Res.* **1997**, *57*, 2321-2324.
211. Liu, H.; Moy, P.; Kim, S.; Xia, Y.; Rajasekaran, A.; Navarro, V.; Knudsen, B.; Bander, N. H., *Cancer Res.* **1997**, *57*, 3629-3634.
212. Chang, S. S.; Gaudin, P. B.; Reuter, V. E.; Heston, W. D. W., *Urology* **2000**, *55*, 622-629.
213. Pinto, J. T.; Suffoletto, B. P.; Berzin, T. M.; Qiao, C. H.; Lin, S. L.; Tong, W. P.; May, F.; Mukherjee, B.; Heston, W. D. W., *Clin. Cancer Res.* **1996**, *2*, 1445-1451.
214. Halsted, C. H.; Ling, E. H.; Luthi-Carter, R.; Villanueva, J. A.; Gardner, J. M.; Coyle, J. T., *J. Biol. Chem.* **1998**, *273*, 20417-20424.
215. Carter, R. E.; Feldman, A. R.; Coyle, J. T., *Proc. Natl. Acad. Sci. U. S. A.* **1996**, *93*, 749-753.
216. Davis, M. I.; Bennett, M. J.; Thomas, L. M.; Bjorkman, P. J., *Proc. Natl. Acad. Sci. U. S. A.* **2005**, *102*, 5981-5986.
217. Mhaka, A.; Gady, A. M.; Rosen, D. M.; Lo, K. M.; Gillies, S. D.; Denmeade, S. R., *Canc. Biol. Ther.* **2004**, *3*, 548-555.
218. Bander, N. H.; Trabulsi, E. J.; Kostakoglu, L.; Yao, D.; Vallabhajosula, S.; Smith-Jones, P.; Joyce, M. A.; Milowsky, M.; Nanus, D. M.; Goldsmith, S. J., *J. Urol.* **2003**, *170*, 1717-1721.
219. Vallabhajosula, S.; Smith-Jones, P. M.; Navarro, V.; Goldsmith, S. J.; Bander, N. H., *Prostate* **2004**, *58*, 145-155.
220. Bander, N. H., *Nat. Clin. Pract. Urol.* **2006**, *3*, 216-225.
221. Horoszewicz, J. S.; Kawinski, E.; Murphy, G. P., *Anticancer Res.* **1987**, *7*, 927-936.
222. Bander, N. H.; Milowsky, M. I.; Nanus, D. M.; Kostakoglu, L.; Vallabhajosula, S.; Goldsmith, S. J., *J. Clin. Oncol.* **2005**, *23*, 4591-4601.
223. Milowsky, M. I.; Nanus, D. M.; Kostakoglu, L.; Vallabhajosula, S.; Goldsmith, S. J.; Bander, N. H., *J. Clin. Oncol.* **2004**, *22*, 2522-2531.
224. Milowsky, M. I.; Nanus, D. M.; Kostakoglu, L.; Sheehan, C. E.; Vallabhajosula, S.; Goldsmith, S. J.; Ross, J. S.; Bander, N. H., *J. Clin. Oncol.* **2007**, *25*, 540-547.
225. Jackson, P. F.; Cole, D. C.; Slusher, B. S.; Stetz, S. L.; Ross, L. E.; Donzanti, B. A.; Trainor, D. A., *J. Med. Chem.* **1996**, *39*, 619-622.
226. Vitharana, D.; France, J. E.; Scarpetti, D.; Bonneville, G. W.; Majer, P.; Tsukamoto, T., *Tetrahedron Asymmetry* **2002**, *13*, 1609-1614.
227. Barinka, C.; Rinnova, M.; Sacha, P.; Rojas, C.; Majer, P.; Slusher, B. S.; Konvalinka, J., *J. Neurochem.* **2002**, *80*, 477-487.
228. Mesters, J. R.; Barinka, C.; Li, W. X.; Tsukamoto, T.; Majer, P.; Slusher, B. S.; Konvalinka, J.; Hilgenfeld, R., *EMBO J.* **2006**, *25*, 1375-1384.
229. Barinka, C.; Rovenska, M.; Mlcochova, P.; Hlouchova, K.; Plechanovova, A.; Majer, P.; Tsukamoto, T.; Slusher, B. S.; Konvalinka, J.; Lubkowski, J., *J. Med. Chem.* **2007**, *50*, 3267-3273.

230. Barinka, C.; Starkova, J.; Konvalinka, J.; Lubkowski, J., *Acta Crystallogr. Sect. F Struct. Biol. Cryst. Commun.* **2007**, *63*, 150-153.
231. Barinka, C.; Hlouchova, K.; Rovenska, M.; Majer, P.; Dauter, M.; Hin, N.; Ko, Y. S.; Tsukamoto, T.; Slusher, B. S.; Konvalinka, J.; Lubkowski, J., *J. Mol. Biol.* **2008**, *376*, 1438-1450.
232. Zhou, J.; Neale, J. H.; Pomper, M. G.; Kozikowski, A. P., *Nat. Rev. Drug Discovery* **2005**, *4*, 1015-1026.
233. Lu, H. Y.; Hu, Y.; Choy, C. J.; Mallari, J. P.; Villanueva, A. F.; Arrozal, A. F.; Berkman, C. E., *Tetrahedron Lett.* **2001**, *42*, 4313-4316.
234. Mallari, J. P.; Choy, C. J.; Hu, Y.; Martinez, A. R.; Hosaka, M.; Toriyabe, Y.; Maung, J.; Blecha, J. E.; Pavkovic, S. F.; Berkman, C. E., *Biorg. Med. Chem.* **2004**, *12*, 6011-6020.
235. Maung, J.; Mallari, J. P.; Girtsman, T. A.; Wu, L. Y.; Rowley, J. A.; Santiago, N. M.; Brunelle, A. N.; Berkman, C. E., *Biorg. Med. Chem.* **2004**, *12*, 4969-4979.
236. Wu, L. Y.; Anderson, M. O.; Toriyabe, Y.; Maung, J.; Campbell, T. Y.; Tajon, C.; Kazak, M.; Moser, J.; Berkman, C. E., *Biorg. Med. Chem.* **2007**, *15*, 7434-7443.
237. Ding, P.; Helquist, P.; Miller, M. J., *Biorg. Med. Chem.* **2008**, *16*, 1648-1657.
238. Barinka, C.; Byun, Y.; Dusich, C. L.; Banerjee, S. R.; Chen, Y.; Castanares, M.; Kozikowski, A. P.; Mease, R. C.; Lubkowski, J.; Pomper, M. G., *J. Med. Chem.* **2008**, *51*, 7737-7743.
239. Lapi, S. E.; Wahnische, H.; Pham, D.; Wu, L. Y.; Nedrow-Byers, J. R.; Liu, T. C.; Vejdani, K.; VanBrocklin, H. F.; Berkman, C. E.; Jones, E. F., *J. Nucl. Med.* **2009**, *50*, 2042-2048.
240. Kozikowski, A. P.; Nan, F.; Conti, P.; Zhang, J. H.; Ramadan, E.; Bzdega, T.; Wroblewska, B.; Neale, J. H.; Pshenichkin, S.; Wroblewski, J. T., *J. Med. Chem.* **2001**, *44*, 298-301.
241. Foss, C. A.; Mease, R. C.; Fan, H.; Wang, Y.; Ravert, H. T.; Dannals, R. F.; Olszewski, R. T.; Heston, W. D.; Kozikowski, A. P.; Pomper, M. G., *Clin. Cancer Res.* **2005**, *11*, 4022-4028.
242. Mease, R. C.; Dusich, C. L.; Foss, C. A.; Ravert, H. T.; Dannals, R. F.; Seidel, J.; Prideaux, A.; Fox, J. J.; Sgouros, G.; Kozikowski, A. P.; Pomper, M. G., *Clin. Cancer Res.* **2008**, *14*, 3036-3043.
243. Banerjee, S. R.; Foss, C. A.; Castanares, M.; Mease, R. C.; Byun, Y.; Fox, J. J.; Hilton, J.; Lupold, S. E.; Kozikowski, A. P.; Pomper, M. G., *J. Med. Chem.* **2008**, *51*, 4504-4517.
244. Hillier, S. M.; Maresca, K. P.; Femia, F. J.; Marquis, J. C.; Foss, C. A.; Nguyen, N.; Zimmerman, C. N.; Barrett, J. A.; Eckelman, W. C.; Pomper, M. G.; Joyal, J. L.; Babich, J. W., *Cancer Res.* **2009**, *69*, 6932-6940.
245. Hillier, S. M.; Kern, A. M.; Maresca, K. P.; Marquis, J. C.; Eckelman, W. C.; Joyal, J. L.; Babich, J. W., *J. Nucl. Med.* **2011**, *52*, 1087-1093.
246. MacLaren, J. A., *Aust. J. Chem.* **1972**, *25*, 1293-1299.
247. MacLaren, J. A., *Aust. J. Chem.* **1978**, *31*, 1865-1868.
248. Liu, M.; Zeng, Y.; Yang, P.; Li, Y.; Luo, D.; Su, S., *Jinxi Huagong Zhongjianti* **2009**, *39*, 26-29.
249. Staab, H. A., *Angew. Chem. Int. Ed. Int. Engl.* **1962**, *1*, 351-367.
250. Nowshuddin, S.; Reddy, A. R., *Tetrahedron Lett.* **2006**, *47*, 5159-5161.
251. Buslig, B. S.; Wilson, C. W.; Shaw, P. E., *J. Agric. Food. Chem.* **1982**, *30*, 342-345.
252. Chambers, R. D.; Clark, H. C.; Willis, C. J., *J. Am. Chem. Soc.* **1960**, *82*, 5298-5301.
253. Snyder, L. R.; Kirkland, J. J.; Dolan, J. W., *Introduction to Modern Liquid Chromatography*. 3<sup>rd</sup> ed.;

John Wiley and Sons: **2010**.

254. Batey, R. A.; Santhakumar, V.; Yoshina-Ishii, C.; Taylor, S. D., *Tetrahedron Lett.* **1998**, *39*, 6267-6270.
255. Schultz, M.; Kunz, H., *Tetrahedron Asymmetry* **1993**, *4*, 1205-1220.
256. Leblanc, A.; Gravel, C.; Labelle, J.; Keillor, J. W., *Biochemistry (Mosc)*. **2001**, *40*, 8335-8342.
257. Carey, F. A.; Sunderberg, R. J., *Advanced Organic Chemistry, Part B: Reactions and Synthesis*. 4<sup>th</sup> ed.; Kluwer Academic/Plenum Publishers: New York, **2001**.
258. Kolb, H. C.; Finn, M. G.; Sharpless, K. B., *Angew. Chem. Int. Ed.* **2001**, *40*, 2004-2021.
259. Kolb, H. C.; Sharpless, K. B., *Drug Discov. Today* **2003**, *8*, 1128-1137.
260. Huisgen, R.; Szeimies, G.; Mobius, L., *Chem. Ber. Recl.* **1967**, *100*, 2494-2507.
261. Rostovtsev, V. V.; Green, L. G.; Fokin, V. V.; Sharpless, K. B., *Angew. Chem. Int. Ed.* **2002**, *41*, 2596-2599.
262. Tornøe, C. W.; Christensen, C.; Meldal, M., *J. Org. Chem.* **2002**, *67*, 3057-3064.
263. Hlasta, D. J.; Ackerman, J. H., *J. Org. Chem.* **1994**, *59*, 6184-6189.
264. Zhang, L.; Chen, X. G.; Xue, P.; Sun, H. H. Y.; Williams, I. D.; Sharpless, K. B.; Fokin, V. V.; Jia, G. C., *J. Am. Chem. Soc.* **2005**, *127*, 15998-15999.
265. Boren, B. C.; Narayan, S.; Rasmussen, L. K.; Zhang, L.; Zhao, H. T.; Lin, Z. Y.; Jia, G. C.; Fokin, V. V., *J. Am. Chem. Soc.* **2008**, *130*, 8923-8930.
266. Wangler, C.; Schirrmacher, R.; Bartenstein, P.; Wangler, B., *Curr. Med. Chem.* **2010**, *17*, 1092-1116.
267. Diaz, D. D.; Rajagopal, K.; Strable, E.; Schneider, J.; Finn, M. G., *J. Am. Chem. Soc.* **2006**, *128*, 6056-6057.
268. Binder, W. H.; Sachsenhofer, R., *Macromol. Rapid Commun.* **2008**, *29*, 952-981.
269. Lau, Y. H.; Rutledge, P. J.; Watkinson, M.; Todd, M. H., *Chem. Soc. Rev.* **2011**, *40*, 2848-2866.
270. Moses, J. E.; Moorhouse, A. D., *Chem. Soc. Rev.* **2007**, *36*, 1249-1262.
271. Best, M. D., *Biochemistry (Mosc)*. **2009**, *48*, 6571-6584.
272. Amblard, F.; Cho, J. H.; Schinazi, R. F., *Chem. Rev.* **2009**, *109*, 4207-4220.
273. Okutani, M.; Mori, Y., *J. Org. Chem.* **2009**, *74*, 442-444.
274. Corey, E. J.; Fuchs, P. L., *Tetrahedron Lett.* **1972**, 3769-3772.
275. Roth, G. J.; Liepold, B.; Muller, S. G.; Bestmann, H. J., *Synthesis-Stuttgart* **2004**, 59-62.
276. Cavender, C. J.; Shiner, V. J., *J. Org. Chem.* **1972**, *37*, 3567-3569.
277. Kappe, C. O.; Van der Eycken, E., *Chem. Soc. Rev.* **2010**, *39*, 1280-1290.
278. Mindt, T. L.; Muller, C.; Melis, M.; de Jong, M.; Schibli, R., *Bioconjugate Chem.* **2008**, *19*, 1689-1695.
279. Kim, E. M.; Joung, M. H.; Lee, C. M.; Jeong, H. J.; Lim, S. T.; Sohn, M. H.; Kim, D. W., *Bioorg. Med. Chem. Lett.* **2010**, *20*, 4240-4243.
280. Himo, F.; Lovell, T.; Hilgraf, R.; Rostovtsev, V. V.; Noodleman, L.; Sharpless, K. B.; Fokin, V. V., *J. Am. Chem. Soc.* **2005**, *127*, 210-216.

281. del Amo, D. S.; Wang, W.; Jiang, H.; Besanceney, C.; Yan, A. C.; Levy, M.; Liu, Y.; Marlow, F. L.; Wu, P., *J. Am. Chem. Soc.* **2010**, *132*, 16893-16899.
282. Agard, N. J.; Prescher, J. A.; Bertozzi, C. R., *J. Am. Chem. Soc.* **2004**, *126*, 15046-15047.
283. Codelli, J. A.; Baskin, J. M.; Agard, N. J.; Berozzi, C. R., *J. Am. Chem. Soc.* **2008**, *130*, 11486-11493.
284. Jewett, J. C.; Sletten, E. M.; Bertozzi, C. R., *J. Am. Chem. Soc.* **2010**, *132*, 3688-3690.
285. Ning, X. H.; Temming, R. P.; Dommerholt, J.; Guo, J.; Ania, D. B.; Debets, M. F.; Wolfert, M. A.; Boons, G. J.; van Delft, F. L., *Angew. Chem. Int. Ed.* **2010**, *49*, 3065-3068.
286. Van Berkel, S. S.; Dirks, A. J.; Meeuwissen, S. A.; Pingen, D. L. L.; Boerman, O. C.; Laverman, P.; van Delft, F. L.; Cornelissen, J. J. L. M.; Rutjes, F. P. J. T., *ChemBioChem* **2008**, *9*, 1805-1815.
287. Van Berkel, S. S.; Dirks, A. T. J.; Debets, M. F.; van Delft, F. L.; Cornelissen, J. J. L. M.; Nolte, R. J. M.; Rutjes, F. P. J. T., *ChemBioChem* **2007**, *8*, 1504-1508.
288. Gutsmedl, K.; Wirges, C. T.; Ehmke, V.; Carell, T., *Org. Lett.* **2009**, *11*, 2405-2408.
289. Schoch, J.; Wiessler, M.; Jaschke, A., *J. Am. Chem. Soc.* **2010**, *132*, 8846-8847.
290. de Bruin, B.; Kuhnast, B.; Hinnen, F.; Yaouancq, L.; Amessou, M.; Johannes, L.; Samson, A.; Boisgard, R.; Tavitian, B.; Dolle, F., *Bioconjugate Chem.* **2005**, *16*, 406-420.
291. Poethko, T.; Schottelius, M.; Thumshirn, G.; Herz, M.; Haubner, R.; Henriksen, G.; Kessler, H.; Schwaiger, M.; Wester, H. J., *Radiochimica Acta* **2004**, *92*, 317-327.
292. Poethko, T.; Schottelius, M.; Thumshirn, G.; Hersel, U.; Herz, M.; Henriksen, G.; Kessler, H.; Schwaiger, M.; Wester, H. J., *J. Nucl. Med.* **2004**, *45*, 892-902.
293. Koslowsky, I.; Shahhosseini, S.; Wilson, J.; Mercer, J., *J. Labelled. Comp. Rad.* **2008**, *51*, 352-356.
294. Marik, J.; Sutcliffe, J. L., *Tetrahedron Lett.* **2006**, *47*, 6681-6684.
295. Glaser, M.; Arstad, E., *Bioconjugate Chem.* **2007**, *18*, 989-993.
296. Sirion, U.; Kim, H. J.; Lee, J. H.; Seo, J. W.; Lee, B. S.; Lee, S. J.; Oh, S. J.; Chi, D. Y., *Tetrahedron Lett.* **2007**, *48*, 3953-3957.
297. Thonon, D.; Kech, C.; Paris, J.; Lemaire, C.; Luxen, A., *Bioconjugate Chem.* **2009**, *20*, 817-823.
298. Li, Z. B.; Wu, Z.; Chen, K.; Chin, F. T.; Chen, X., *Bioconjugate Chem.* **2007**, *18*, 1987-1994.
299. Ramenda, T.; Bergmann, R.; Wuest, F., *Lett. Drug Des. Discovery* **2007**, *4*, 279-285.
300. Hausner, S. H.; Marik, J.; Gagnon, M. K. J.; Sutcliffe, J. L., *J. Med. Chem.* **2008**, *51*, 5901-5904.
301. Smith, G.; Glaser, M.; Perumal, M.; Nguyen, Q. D.; Shan, B.; Arstad, E.; Aboagye, E. O., *J. Med. Chem.* **2008**, *51*, 8057-8067.
302. Ross, T. L.; Honer, M.; Lam, P. Y. H.; Mindt, T. L.; Groehn, V.; Schibli, R.; Schubiger, P. A.; Ametamey, S. M., *Bioconjugate Chem.* **2008**, *19*, 2462-2470.
303. Devaraj, N. K.; Kelihier, E. J.; Thurber, G. M.; Nahrendorf, M.; Weissleder, R., *Bioconjugate Chem.* **2009**, *20*, 397-401.
304. Schirmacher, R.; Lakhri, Y.; Jolly, D.; Goodstein, J.; Lucas, P.; Schirmacher, E., *Tetrahedron Lett.* **2008**, *49*, 4824-4827.
305. Miller, M. B.; Tang, Y. W., *Clin. Microbiol. Rev.* **2009**, *22*, 611-633.
306. Crooke, S. T., *Biochim. Biophys. Acta:Gene Struct. Expr.* **1999**, *1489*, 31-44.

307. Vidal, L.; Blagden, S.; Attard, G.; de Bono, J., *Eur. J. Cancer* **2005**, *41*, 2812-2818.
308. Burgess, J. K., *Clin. Exp. Pharmacol. Physiol.* **2001**, *28*, 321-328.
309. Opalinska, J. B.; Gewirtz, A. M., *Nat. Rev. Drug Discovery* **2002**, *1*, 503-514.
310. Herweijer, H.; Wolff, J. A., *Gene Ther.* **2003**, *10*, 453-458.
311. Ellington, A. D.; Szostak, J. W., *Nature* **1990**, *346*, 818-822.
312. Tuerk, C.; Gold, L., *Science* **1990**, *249*, 505-510.
313. Bunka, D. H. J.; Stockley, P. G., *Nat. Rev. Microbiol.* **2006**, *4*, 588-596.
314. Stoltenburg, R.; Reinemann, C.; Strehlitz, B., *Biomol. Eng* **2007**, *24*, 381-403.
315. Famulok, M.; Hartig, J. S.; Mayer, G., *Chem. Rev.* **2007**, *107*, 3715-3743.
316. Keefe, A. D.; Pai, S.; Ellington, A., *Nat. Rev. Drug Discovery* **2010**, *9*, 537-550.
317. Keefe, A. D.; Cload, S. T., *Curr. Opin. Chem. Biol.* **2008**, *12*, 448-456.
318. Jaaskelainen, I.; Monkkonen, J.; Urtti, A., *BBA-Biomembranes* **1994**, *1195*, 115-123.
319. Younes, C. K.; Boisgard, R.; Tavitian, B., *Curr. Pharm. Des.* **2002**, *8*, 1451-1466.
320. Lewis, M. R.; Jia, F., *J. Cell. Biochem.* **2003**, *90*, 464-472.
321. Duatti, A., *Curr. Drug Targets* **2004**, *5*, 753-760.
322. Liu, X.; Wang, Y.; Nakamura, K.; Liu, G.; Dou, S.; Kubo, A.; Rusckowski, M.; Hnatowich, D. J., *Bioconjugate Chem.* **2007**, *18*, 1905-1911.
323. Shi, H.; Tang, Z. W.; Kim, Y.; Nie, H. L.; Huang, Y. F.; He, X. X.; Deng, K.; Wang, K. M.; Tan, W. H., *Chem. Asian J.* **2010**, *5*, 2209-2213.
324. Stein, C. A.; Cheng, Y. C., *Science* **1993**, *261*, 1004-1012.
325. Kobori, N.; Imahori, Y.; Mineura, K.; Ueda, S.; Fujii, R., *Neuroreport* **1999**, *10*, 2971-2974.
326. Green, N. M., *Methods Enzymol.* **1990**, *184*, 51-67.
327. Sato, N.; Kobayashi, H.; Saga, T.; Nakamoto, Y.; Ishimori, T.; Togashi, K.; Fujibayashi, Y.; Konishi, J.; Brechbiel, M. W., *Clin. Cancer Res.* **2001**, *7*, 3606-3612.
328. Roivainen, A.; Tolvanen, T.; Salomaki, S.; Lendvai, G.; Velikyan, I.; Numminen, P.; Valila, M.; Sipila, H.; Bergstrom, M.; Harkonen, P.; Lonnberg, H.; Langstrom, B., *J. Nucl. Med.* **2004**, *45*, 347-355.
329. Kuhnast, B.; Dolle, F.; Terrazzino, S.; Rousseau, B.; Loc'h, C.; Vaufrey, F.; Hinnen, F.; Doignon, I.; Pillon, F.; David, C.; Crouzel, C.; Tavitian, B., *Bioconjugate Chem.* **2000**, *11*, 627-636.
330. Li, J. L.; Trent, J. O.; Bates, P. J.; Ng, C. K., *J. Labelled. Comp. Rad.* **2006**, *49*, 1213-1221.
331. Li, J. L.; Trent, J. O.; Bates, P. J.; Ng, C. K., *J. Labelled. Comp. Rad.* **2007**, *50*, 1255-1259.
332. Srivastava, M.; Pollard, H. B., *FASEB J.* **1999**, *13*, 1911-1922.
333. Hatanaka, K.; Asai, T.; Koide, H.; Kenjo, E.; Tsuzuku, T.; Harada, N.; Tsukada, H.; Oku, N., *Bioconjugate Chem.* **2010**, *21*, 756-763.
334. Gramlich, P. M. E.; Wirges, C. T.; Manetto, A.; Carell, T., *Angew. Chem. Int. Ed.* **2008**, *47*, 8350-8358.
335. Inkster, J. A. H.; Adam, M. J.; Storr, T.; Ruth, T. J., *Nucleos. Nucleot. Nucl* **2009**, *28*, 1131-1143.

336. Yang, A. S.; Honig, B., *J. Mol. Biol.* **1993**, *231*, 459-474.
337. Miano, M. L.; Ferrini, U., *Biochim. Biophys. Acta* **1969**, *174*, 749-751.
338. Hakala, H.; Oivanen, M.; Saloniemi, E.; Gouzaev, A.; Lonnberg, H., *J. Phys. Org. Chem.* **1992**, *5*, 824-828.
339. Molander, G. A.; Ham, J., *Org. Lett.* **2006**, *8*, 2767-2770.
340. Jin, S.; Choudhary, G.; Cheng, Y. F.; Dai, C. F.; Li, M. Y.; Wang, B. H., *Chem. Comm.* **2009**, 5251-5253.
341. Knorre, D. G.; Alekseyev, P. V.; Gerassimova, Y. V.; Silnikov, V. N.; Maksakova, G. A.; Godovikova, T. S., *Nucleos. Nucleot. Nucl* **1998**, *17*, 397-410.
342. Grimm, G. N.; Boutorine, A. S.; Helene, C., *Nucleos. Nucleot. Nucl* **2000**, *19*, 1943-1965.
343. Gololobov, Y. G.; Zhmurova, I. N.; Kasukhin, L. F., *Tetrahedron* **1981**, *37*, 437-472.
344. Chu, B. C. F.; Wahl, G. M.; Orgel, L. E., *Nucleic Acids Res.* **1983**, *11*, 6513-6529.
345. Weller, R. L.; Rajsiki, S. R., *Org. Lett.* **2005**, *7*, 2141-2144.
346. Seela, F.; Ingale, S. A., *J. Org. Chem.* **2010**, *75*, 284-295.
347. Descotes, G.; Mentech, J., *Carbohydr. Res.* **1986**, *149*, 455-457.
348. Stewart, A. O.; Williams, R. M., *J. Am. Chem. Soc.* **1985**, *107*, 4289-4296.
349. Williams, R. M.; Stewart, A. O., *Abstr. Pap. Am. Chem. Soc.* **1984**, *187*, 24-Carb.
350. Williams, R. M.; Stewart, A. O., *Tetrahedron Lett.* **1983**, *24*, 2715-2718.
351. Mukaiyama, T., *Phosphorus, Sulfur Silicon Relat. Elem.* **1976**, *1*, 371-387.
352. Chan, T. R.; Hilgraf, R.; Sharpless, K. B.; Fokin, V. V., *Org. Lett.* **2004**, *6*, 2853-2855.
353. Rodionov, V. O.; Fokin, V. V.; Finn, M. G., *Angew. Chem. Int. Ed.* **2005**, *44*, 2210-2215.
354. Alexoff, D. L.; Vaska, P.; Marsteller, D.; Gerasimov, T.; Li, J.; Logan, J.; Fowler, J. S.; Taintor, N. B.; Thanos, P. K.; Volkow, N. D., *J. Nucl. Med.* **2003**, *44*, 815-822.
355. Thanos, P. K.; Taintor, N. B.; Alexoff, D.; Vaska, P.; Logan, J.; Grandy, D. K.; Fang, Y. A.; Lee, J. H.; Fowler, J. S.; Volkow, N. D., *J. Nucl. Med.* **2002**, *43*, 1570-1577.
356. Weissleder, R.; Ross, B. D.; Rehemtulla, A.; Gambhir, S. S., *Molecular Imaging: principles and practice*. People's Medical Publishing House-USA: **2010**.
357. Natarajan, A.; Du, W. J.; Xiong, C. Y.; DeNardo, G. L.; DeNardo, S. J.; Gervay-Hague, J., *Chem. Comm.* **2007**, 695-697.
358. Berthelot, T.; Talbot, J. C.; Lain, G.; Deleris, G.; Latxague, L., *J. Pept. Sci.* **2005**, *11*, 153-160.
359. Shane, B.; Stokstad, E. L. R., *Annu. Rev. Nutr.* **1985**, *5*, 115-141.
360. Mauritz, R.; Bekkenk, M. W.; Rots, M. G.; Pieters, R.; Mini, E.; van Zantwijk, C. H.; Veerman, A. J. P.; Peters, G. J.; Jansen, G., *Clin. Cancer Res.* **1998**, *4*, 2399-2410.
361. Matherly, L. H.; Angeles, S. M.; McGuire, J. J., *Biochem. Pharmacol.* **1993**, *46*, 2185-2195.
362. Li, W. W.; Tong, W. P.; Bertino, J. R., *Clin. Cancer Res.* **1995**, *1*, 631-636.
363. Antony, A. C., *Blood* **1992**, *79*, 2807-2820.

364. Matherly, L. H.; Hou, Z. J.; Deng, Y. J., *Cancer Metastasis Rev.* **2007**, *26*, 111-128.
365. Qiu, A. D.; Jansen, M.; Sakaris, A.; Min, S. H.; Chattopadhyay, S.; Tsai, E.; Sandoval, C.; Zhao, R. B.; Akabas, M. H.; Goldman, I. D., *Cell* **2006**, *127*, 917-928.
366. Zhao, R. B.; Min, S. H.; Wang, Y. H.; Campanella, E.; Low, P. S.; Goldman, I. D., *J. Biol. Chem.* **2009**, *284*, 4267-4274.
367. Yuasa, H.; Inoue, K.; Hayashi, Y., *J. Pharm. Sci.* **2009**, *98*, 1608-1616.
368. Kamen, B. A.; Capdevila, A., *Proc. Natl. Acad. Sci. U. S. A.* **1986**, *83*, 5983-5987.
369. McHugh, M.; Cheng, Y. C., *J. Biol. Chem.* **1979**, *254*, 1312-1318.
370. Antony, A. C.; Utley, C. S.; Marcell, P. D.; Kolhouse, J. F., *J. Biol. Chem.* **1982**, *257*, 81-89.
371. Antony, A. C., *Annu. Rev. Nutr.* **1996**, *16*, 501-521.
372. Parker, N.; Turk, M. J.; Westrick, E.; Lewis, J. D.; Low, P. S.; Leamon, C. P., *Anal. Biochem.* **2005**, *338*, 284-293.
373. Leamon, C. P.; Low, P. S., *Drug Discov. Today* **2001**, *6*, 44-51.
374. Hilgenbrink, A. R.; Low, P. S., *J. Pharm. Sci.* **2005**, *94*, 2135-2146.
375. Salazar, M. D.; Ratnam, M., *Cancer Metastasis Rev.* **2007**, *26*, 141-152.
376. Birn, H.; Nielsen, S.; Christensen, E. I., *Am. J. Physiol. Renal. Physiol.* **1997**, *272*, F70-F78.
377. Mattes, M. J.; Major, P. P.; Goldenberg, D. M.; Dion, A. S.; Hutter, R. V. P.; Klein, K. M., *Cancer Res.* **1990**, *50*, S880-S884.
378. Holm, J.; Hansen, S. I.; Hoier-Madsen, M.; Bostad, L., *Biochem. J.* **1991**, *280*, 267-271.
379. Weitman, S. D.; Lark, R. H.; Coney, L. R.; Fort, D. W.; Frasca, V.; Zurawski, V. R.; Kamen, B. A., *Cancer Res.* **1992**, *52*, 3396-3401.
380. Ross, J. F.; Chaudhuri, P. K.; Ratnam, M., *Cancer* **1994**, *73*, 2432-2443.
381. Weitman, S. D.; Frazier, K. M.; Kamen, B. A., *J. Neurooncol.* **1994**, *21*, 107-112.
382. Toffoli, G.; Cernigoi, C.; Russo, A.; Gallo, A.; Bagnoli, M.; Boiocchi, M., *Int. J. Cancer* **1997**, *74*, 193-198.
383. Garin-Chesa, P.; Campbell, I.; Saigo, P. E.; Lewis, J. L.; Old, L. J.; Rettig, W. J., *Am. J. Pathol.* **1993**, *142*, 557-567.
384. Netteland, B.; Bakke, O. M., *Clin. Chem.* **1977**, *23*, 1505-1506.
385. Lawrence, V. A., *Acta Haematol.* **1983**, *69*, 289-293.
386. Xia, W.; Low, P. S., *J. Med. Chem.* **2010**, *53*, 6811-6824.
387. Leamon, C. P.; Parker, M. A.; Vlahov, I. R.; Xu, L. C.; Reddy, J. A.; Vetzal, M.; Douglas, N., *Bioconjugate Chem.* **2002**, *13*, 1200-1210.
388. Reddy, J. A.; Allagadda, V. M.; Leamon, C. P., *Curr. Pharm. Biotechnol.* **2005**, *6*, 131-150.
389. Low, P. S.; Kularatne, S. A., *Curr. Opin. Chem. Biol.* **2009**, *13*, 256-262.
390. Leamon, C. P.; Low, P. S., *Proc. Natl. Acad. Sci. U. S. A.* **1991**, *88*, 5572-5576.
391. Leamon, C. P.; Low, P. S., *Biochem. J.* **1993**, *291*, 855-860.

392. Turek, J. J.; Leamon, C. P.; Low, P. S., *J. Cell Sci.* **1993**, *106*, 423-430.
393. Paulos, C. M.; Reddy, J. A.; Leamon, C. P.; Turk, M. J.; Low, P. S., *Mol. Pharmacol.* **2004**, *66*, 1406-1414.
394. Lee, R. J.; Wang, S.; Low, P. S., *Biochim. Biophys. Acta, Mol. Cell Res.* **1996**, *1312*, 237-242.
395. Yang, J.; Chen, H. T.; Vlahov, I. R.; Cheng, J. X.; Low, P. S., *J. Pharmacol. Exp. Ther.* **2007**, *321*, 462-468.
396. Ladino, C. A.; Chari, R. V. J.; Bourret, L. A.; Kedersha, N. L.; Goldmacher, V. S., *Int. J. Cancer* **1997**, *73*, 859-864.
397. Yang, J.; Chen, H.; Vlahov, I. R.; Cheng, J. X.; Low, P. S., *Proc. Natl. Acad. Sci. U. S. A.* **2006**, *103*, 13872-13877.
398. Leamon, C. P.; Low, P. S., *J. Biol. Chem.* **1992**, *267*, 24966-24971.
399. Leamon, C. P.; DePrince, R. B.; Hendren, R. W., *J. Drug Target.* **1999**, *7*, 157-169.
400. Leamon, C. P.; Reddy, J. A., *Adv. Drug Del. Rev.* **2004**, *56*, 1127-1141.
401. Lu, Y. J.; Low, P. S., *Cancer Immunol. Immunother.* **2002**, *51*, 153-162.
402. Lu, Y. J.; Segal, E.; Leamon, C. P.; Low, P. S., *Adv. Drug Del. Rev.* **2004**, *56*, 1161-1176.
403. Lee, R. J.; Low, P. S., *J. Biol. Chem.* **1994**, *269*, 3198-3204.
404. Wang, S.; Lee, R. J.; Cauchon, G.; Gorenstein, D. G.; Low, P. S., *Proc. Natl. Acad. Sci. U. S. A.* **1995**, *92*, 3318-3322.
405. Dixit, V.; Van den Bossche, J.; Sherman, D. M.; Thompson, D. H.; Andres, R. P., *Bioconjugate Chem.* **2006**, *17*, 603-609.
406. Yang, S. J.; Lin, F. H.; Tsai, K. C.; Wei, M. F.; Tsai, H. M.; Wong, J. M.; Shieh, M. J., *Bioconjugate Chem.* **2010**, *21*, 679-689.
407. Yang, S. J.; Chen, J. W.; Lin, F. H.; Young, T. H.; Lou, P. J.; Shieh, M. J., *Biomed. Eng. App. Basis Commun.* **2010**, *22*, 9-17.
408. Mislick, K. A.; Baldeschwieler, J. D.; Kayyem, J. F.; Meade, T. J., *Bioconjugate Chem.* **1995**, *6*, 512-515.
409. Lee, R. J.; Guo, W., *Abstr. Pap. Am. Chem. Soc.* **1999**, *217*, U557-U557.
410. Citro, G.; Szczylik, C.; Ginobbi, P.; Zupi, G.; Calabretta, B., *Br. J. Cancer* **1994**, *69*, 463-467.
411. Oh, I. K.; Mok, H.; Park, T. G., *Bioconjugate Chem.* **2006**, *17*, 721-727.
412. Thomas, M.; Kularatne, S. A.; Qi, L.; Kleindl, P.; Leamon, C. P.; Hansen, M. J.; Low, P. S., *Ann. N.Y. Acad. Sci.* **2009**, *1175*, 32-9.
413. Vlahov, I. R.; Santhapuram, H. K. R.; Kleindl, P. J.; Howard, S. J.; Stanford, K. M.; Leamon, C. P., *Bioorg. Med. Chem. Lett.* **2006**, *16*, 5093-5096.
414. Reddy, J. A.; Dorton, R.; Westrick, E.; Dawson, A.; Smith, T.; Xu, L. C.; Vetzal, M.; Kleindl, P.; Vlahov, I. R.; Leamon, C. P., *Cancer Res.* **2007**, *67*, 4434-4442.
415. Leamon, C. P.; Reddy, J. A.; Vlahov, I. R.; Westrick, E.; Parker, N.; Nicoson, J. S.; Vetzal, M., *Int. J. Cancer* **2007**, *121*, 1585-1592.
416. Li, J.; Sausville, E. A.; Klein, P. J.; Morgenstern, D.; Leamon, C. P.; Messmann, R. A.; LoRusso, P., *J. Clin. Pharmacol.* **2009**, *49*, 1467-1476.

417. Ke, C. Y.; Mathias, C. J.; Green, M. A., *Adv. Drug Del. Rev.* **2004**, *56*, 1143-1160.
418. Antich, P.; Kulkarni, P. V.; Constantinescu, A.; Prior, J.; Nguyen, T.; Anderson, J.; Weitman, S.; Kamen, B.; Parkey, R. W., *J. Nucl. Med.* **1994**, *35*, P222-P222.
419. Konda, S. D.; Wang, S.; Brechbiel, M.; Wiener, E. C., *Invest. Radiol.* **2002**, *37*, 199-204.
420. Aref, M.; Brechbiel, M.; Wiener, E. C., *Invest. Radiol.* **2002**, *37*, 178-192.
421. Wiener, E. C.; Konda, S. D.; Wang, S.; Brechbiel, M., *Acad. Radiol.* **2002**, *9*, S316-S319.
422. Chen, T. J.; Cheng, T. H.; Hung, Y. C.; Lin, K. T.; Liu, G. C.; Wang, Y. M., *J. Biomed. Mater. Res. A.* **2008**, *87A*, 165-175.
423. Tung, C. H.; Lin, Y. H.; Moon, W. K.; Weissleder, R., *ChemBioChem* **2002**, *3*, 784-786.
424. Moon, W. K.; Lin, Y. H.; O'Loughlin, T.; Tang, Y.; Kim, D. E.; Weissleder, R.; Tung, C. H., *Bioconjugate Chem.* **2003**, *14*, 539-545.
425. Mathias, C. J.; Wang, S.; Waters, D. J.; Turek, J. J.; Low, P. S.; Green, M. A., *J. Nucl. Med.* **1998**, *39*, 1579-1585.
426. Bettio, A.; Honer, M.; Muller, C.; Bruhlmeier, M.; Muller, U.; Schibli, R.; Groehn, V.; Schubiger, A. P.; Ametamey, S. M., *J. Nucl. Med.* **2006**, *47*, 1153-1160.
427. Ross, T. L.; Honer, M.; Muller, C.; Groehn, V.; Schibli, R.; Ametamey, S. M., *J. Nucl. Med.* **2010**, *51*, 1756-1762.
428. Wang, S.; Lee, R. J.; Mathias, C. J.; Green, M. A.; Low, P. S., *Bioconjugate Chem.* **1996**, *7*, 56-62.
429. Mathias, C. J.; Wang, S.; Lee, R. J.; Waters, D. J.; Low, P. S.; Green, M. A., *J. Nucl. Med.* **1996**, *37*, 1003-1008.
430. Wang, S.; Luo, J.; Lantrip, D. A.; Waters, D. J.; Mathias, C. J.; Green, M. A.; Fuchs, P. L.; Low, P. S., *Bioconjugate Chem.* **1997**, *8*, 673-679.
431. Mathias, C. J.; Wang, S.; Waters, D. J.; Turek, J. J.; Low, P. S.; Green, M. A., *J. Nucl. Med.* **1997**, *38*, 500-500.
432. Ligan, S.; Yang, D. J.; Higuchi, T.; Zareneyrizi, F.; Bayhan, H.; Yu, D. F.; Kim, E. E.; Podoloff, D. A., *Cancer Biother. Radiopharm.* **1998**, *13*, 427-435.
433. Guo, W. J.; Hinkle, G. H.; Lee, R. J., *J. Nucl. Med.* **1999**, *40*, 1563-1569.
434. Mathias, C. J.; Hubers, D.; Low, P. S.; Green, M. A., *Bioconjugate Chem.* **2000**, *11*, 253-257.
435. Trump, D. P.; Mathias, C. J.; Yang, Z. F.; Low, P. S.; Marmion, M. E.; Green, M. A., *J. Nucl. Med.* **2000**, *41*, 228p-228p.
436. Shitara, Y.; Sato, H.; Sugiyama, Y., *Annu. Rev. Pharmacol. Toxicol.* **2005**, *45*, 689-723.
437. Hacker, M. P.; Messer, W. S.; Bachmann, K. A., *Pharmacology: Principles and Practice.* Elsevier/Academic Press: Boston, **2009**, p 188.
438. Klibanov, A. L.; Maruyama, K.; Torchilin, V. P.; Huang, L., *FEBS Lett.* **1990**, *268*, 235-237.
439. Schneider, R. L.; Schmitt, F.; Frochot, C.; Fort, Y.; Lourette, N.; Guillemin, F.; Muller, J. F.; Barberi-Heyob, M., *Biorg. Med. Chem.* **2005**, *13*, 2799-2808.
440. Mohapatra, S.; Mallick, S. K.; Maiti, T. K.; Ghosh, S. K.; Pramanik, P., *Nanotechnology* **2007**, *18*.
441. Nomura, M.; Shuto, S.; Matsuda, A., *J. Org. Chem.* **2000**, *65*, 5016-5021.

442. Muller, C.; Dumas, C.; Hoffmann, U.; Schubiger, P. A.; Schibli, R., *J. Organomet. Chem.* **2004**, *689*, 4712-4721.
443. Luo, J.; Smith, M. D.; Lantrip, D. A.; Wang, S.; Fuchs, P. L., *J. Am. Chem. Soc.* **1997**, *119*, 10004-10013.
444. Hynes, R. O., *Cell* **1992**, *69*, 11-25.
445. Felding-Habermann, B.; Mueller, B. M.; Romerdahl, C. A.; Cheresh, D. A., *J. Clin. Invest.* **1992**, *89*, 2018-2022.
446. Haubner, R.; Finsinger, D.; Kessler, H., *Angew. Chem. Int. Ed. Engl.* **1997**, *36*, 1375-1389.
447. Aumailley, M.; Gurrath, M.; Muller, G.; Calvete, J.; Timpl, R.; Kessler, H., *FEBS Lett.* **1991**, *291*, 50-54.
448. Brooks, P. C.; Montgomery, A. M. P.; Rosenfeld, M.; Reisfeld, R. A.; Hu, T. H.; Klier, G.; Cheresh, D. A., *Cell* **1994**, *79*, 1157-1164.
449. Auzzas, L.; Zanardi, F.; Battistini, L.; Burreddu, P.; Carta, P.; Rassu, G.; Curti, C.; Casiraghi, G., *Curr. Med. Chem.* **2010**, *17*, 1255-1299.
450. Felding-Habermann, B.; Fransvea, E.; O'Toole, T. E.; Manzuk, L.; Faha, B.; Hensler, M., *Clin. Exp. Metastasis* **2002**, *19*, 427-436.
451. Arap, W.; Pasqualini, R.; Ruoslahti, E., *Science* **1998**, *279*, 377-380.
452. Pierschbacher, M. D.; Ruoslahti, E., *Nature* **1984**, *309*, 30-33.
453. Pierschbacher, M. D.; Ruoslahti, E., *Proc. Natl. Acad. Sci. USA Biol. Sci.* **1984**, *81*, 5985-5988.
454. Ruoslahti, E.; Pierschbacher, M. D., *Science* **1987**, *238*, 491-497.
455. Albelda, S. M.; Buck, C. A., *FASEB J.* **1990**, *4*, 2868-2880.
456. Humphries, M. J., *J. Cell Sci.* **1990**, *97*, 585-592.
457. Ruoslahti, E., *J. Clin. Invest.* **1991**, *87*, 1-5.
458. Kessler, H., *Angew. Chem. Int. Ed. Engl.* **1982**, *21*, 512-523.
459. Haubner, R.; Gratias, R.; Diefenbach, B.; Goodman, S. L.; Jonczyk, A.; Kessler, H., *J. Am. Chem. Soc.* **1996**, *118*, 7461-7472.
460. Dechantsreiter, M. A.; Planker, E.; Matha, B.; Lohof, E.; Holzemann, G.; Jonczyk, A.; Goodman, S. L.; Kessler, H., *J. Med. Chem.* **1999**, *42*, 3033-3040.
461. Taga, T.; Suzuki, A.; Gonzalez-Gomez, I.; Gilles, F. H.; Stins, M.; Shimada, H.; Barsky, L.; Weinberg, K. I.; Laug, W. E., *Int. J. Cancer* **2002**, *98*, 690-697.
462. Raguse, J. D.; Gath, H. J.; Bier, J.; Riess, H.; Oettle, H., *Oral Oncol.* **2004**, *40*, 228-230.
463. Belvisi, L.; Riccioni, T.; Marcellini, M.; Vesce, L.; Chiarucci, I.; Efrati, D.; Potenza, D.; Scolastico, C.; Manzoni, L.; Lombardo, K.; Stasi, M. A.; Orlandi, A.; Ciucci, A.; Nico, B.; Ribatti, D.; Giannini, G.; Presta, M.; Carminati, P.; Pisano, C., *Mol. Cancer Ther.* **2005**, *4*, 1670-1680.
464. Beekman, K. W.; Colevas, A. D.; Cooney, K.; DiPaola, R.; Dunn, R. L.; Gross, M.; Keller, E. T.; Pienta, K. J.; Ryan, C. J.; Smith, D.; Hussain, M., *Clin. Genitourin. Canc.* **2006**, *4*, 299-302.
465. Mas-Moruno, C.; Rechenmacher, F.; Kessler, H., *Anti. Canc. Agents Med. Chem.* **2010**, *10*, 753-768.
466. Reardon, D. A.; Nabors, L. B.; Stupp, R.; Mikkelsen, T., *Expert Opin. Inv. Drug.* **2008**, *17*, 1225-1235.

467. Reardon, D. A.; Neyns, B.; Weller, M.; Tonn, J. C.; Nabors, L. B.; Stupp, R., *Future Oncol.* **2011**, *7*, 339-354.
468. Nabors, L. B.; Mikkelsen, T.; Rosenfeld, S. S.; Hochberg, F.; Akella, N. S.; Fisher, J. D.; Cloud, G. A.; Zhang, Y.; Carson, K.; Wittmer, S. M.; Colevas, A. D.; Grossman, S. A., *J. Clin. Oncol.* **2007**, *25*, 1651-1657.
469. Buckley, C. D.; Pilling, D.; Henriquez, N. V.; Parsonage, G.; Threlfall, K.; Scheel-Toellner, D.; Simmons, D. L.; Albar, A. N.; Lord, J. M.; Salmon, M., *Nature* **1999**, *397*, 534-539.
470. Bernard, B.; Capello, A.; van Hagen, M.; Breeman, W.; Srinivasan, A.; Schmidt, M.; Erion, J.; van Gameren, A.; Krenning, E.; de Jong, M., *Cancer Biother. Radiopharm.* **2004**, *19*, 173-180.
471. Yang, J. Q.; Guo, H. X.; Gallazzi, F.; Berwick, M.; Padilla, R. S.; Miao, Y. B., *Bioconjugate Chem.* **2009**, *20*, 1634-1642.
472. Zitzmann, S.; Ehemann, V.; Schwab, M., *Cancer Res.* **2002**, *62*, 5139-5143.
473. Xiao, B.; Li, W.; Yang, J.; Guo, G.; Mao, X. H.; Zou, Q. M., *Mol. Biotechnol.* **2009**, *41*, 138-144.
474. Greish, K.; Ray, A.; Bauer, H.; Larson, N.; Malugin, A.; Pike, D.; Haider, M.; Ghandehari, H., *J. Controlled Release* **2011**, *151*, 263-270.
475. Jing, Y. W.; Lu, H. R.; Wu, K. L.; Subramanian, I. V.; Ramakrishnan, S., *Int. J. Cancer* **2011**, *129*, 751-761.
476. Eremina, V.; Jefferson, J. A.; Kowalewska, J.; Hochster, H.; Haas, M.; Weisstuch, J.; Richardson, C.; Kopp, J. B.; Kabir, M. G.; Backx, P. H.; Gerber, H. P.; Ferrara, N.; Barisoni, L.; Alpers, C. E.; Quaggin, S. E., *N. Engl. J. Med.* **2008**, *358*, 1129-1136.
477. Cressman, S.; Sun, Y.; Maxwell, E. J.; Fang, N.; Chen, D. D. Y.; Cullis, P. R., *Int. J. Pept. Res. Ther.* **2009**, *15*, 49-59.
478. Cao, Q. Z.; Li, Z. B.; Chen, K.; Wu, Z. H.; He, L. N.; Neamati, N.; Chen, X. Y., *Eur. J. Nucl. Med. Mol. Imag.* **2008**, *35*, 1489-1498.
479. Ryppa, C.; Mann-Steinberg, H.; Biniössek, M. L.; Satchi-Fainaro, R.; Kratz, F., *Int. J. Pharm.* **2009**, *368*, 89-97.
480. Haubner, R., *Eur. J. Nucl. Med. Mol. Imag.* **2006**, *33*, S54-S63.
481. Liu, S., *Mol. Pharm.* **2006**, *3*, 472-487.
482. Liu, S., *Bioconjugate Chem.* **2009**, *20*, 2199-2213.
483. Cheng, Z.; Wu, Y.; Xiong, Z. M.; Gambhir, S. S.; Chen, X. Y., *Bioconjugate Chem.* **2005**, *16*, 1433-1441.
484. Ye, Y. P.; Bloch, S.; Xu, B. G.; Achilefu, S., *J. Med. Chem.* **2006**, *49*, 2268-2275.
485. Schottelius, M.; Laufer, B.; Kessler, H.; Wester, H. J., *Acc. Chem. Res.* **2009**, *42*, 969-980.
486. Noiri, E.; Goligorsky, M. S.; Wang, G. J.; Wang, J.; Cabahug, C. J.; Sharma, S.; Rhodes, B. A.; Som, P., *J. Am. Soc. Nephrol.* **1996**, *7*, 2682-2688.
487. Goligorsky, M. S.; Dibona, G. F., *Proc. Natl. Acad. Sci. U. S. A.* **1993**, *90*, 5700-5704.
488. Noiri, E.; Gailit, J.; Sheth, D.; Magazine, H.; Gurrath, M.; Muller, G.; Kessler, H.; Goligorsky, M. S., *Kidney Int.* **1994**, *46*, 1050-1058.
489. Sivolapenko, G. B.; Skarlos, D.; Pectasides, D.; Stathopoulou, E.; Milonakis, A.; Sirmalis, G.; Stuttle, A.; Courtenay-Luck, N. S.; Konstantinides, K.; Epenetos, A. A., *Eur. J. Nucl. Med.* **1998**, *25*, 1383-1389.

490. Haubner, R.; Bruchertseifer, F.; Bock, M.; Kessler, H.; Schwaiger, M.; Wester, H., *Nuklearmed. Nucl. Med.* **2004**, *43*, 26-32.
491. Bach-Gansmo, T.; Danielsson, R.; Saracco, A.; Wilczek, B.; Bogsrud, T. V.; Fangberget, A.; Tangerud, A.; Tobin, D., *J. Nucl. Med.* **2006**, *47*, 1434-1439.
492. Edwards, D.; Jones, P.; Haramis, H.; Battle, M.; Lear, R.; Barnett, D. J.; Edwards, C.; Crawford, H.; Black, A.; Godden, V., *Nucl. Med. Biol.* **2008**, *35*, 365-375.
493. Alves, S.; Correia, J. D. G.; Gano, L.; Rold, T. L.; Prasanphanich, A.; Haubner, R.; Rupprich, M.; Alberto, R.; Decristoforo, C.; Santos, I.; Smith, C. J., *Bioconjugate Chem.* **2007**, *18*, 530-537.
494. Decristoforo, C.; Faintuch-Linkowski, B.; Rey, A.; von Guggenberg, E.; Rupprich, M.; Hernandez-Gonzales, I.; Rodrigo, T.; Haubner, R., *Nucl. Med. Biol.* **2006**, *33*, 945-952.
495. Liu, S.; Hsieh, W. Y.; Kim, Y. S.; Mohammed, S. I., *Bioconjugate Chem.* **2005**, *16*, 1580-1588.
496. Wang, J. J.; Kim, Y. S.; Liu, S., *Bioconjugate Chem.* **2008**, *19*, 634-642.
497. Liu, S.; Hsieh, W. Y.; Jiang, Y.; Kim, Y. S.; Sreerama, S. G.; Chen, X. Y.; Jia, B.; Wang, F., *Bioconjugate Chem.* **2007**, *18*, 438-446.
498. Shi, J. Y.; Wang, L. J.; Kim, Y. S.; Zhai, S. Z.; Liu, Z. F.; Chen, X. Y.; Liu, S., *J. Med. Chem.* **2008**, *51*, 7980-7990.
499. Wu, Y.; Zhang, X. Z.; Xiong, Z. M.; Cheng, Z.; Fisher, D. R.; Liu, S.; Gambhir, S. S.; Chen, X. Y., *J. Nucl. Med.* **2005**, *46*, 1707-1718.
500. Li, Z. B.; Cai, W. B.; Cao, Q. Z.; Chen, K.; Wu, Z. H.; He, L. N.; Chen, X. Y., *J. Nucl. Med.* **2007**, *48*, 1162-1171.
501. Li, Z. B.; Chen, K.; Chen, X., *Eur. J. Nucl. Med. Mol. Imag.* **2008**, *35*, 1100-1108.
502. Dijkgraaf, I.; Rijnders, A. Y.; Soede, A.; Dechesne, A. C.; van Esse, G. W.; Brouwer, A. J.; Corstens, F. H. M.; Boerman, O. C.; Rijkers, D. T. S.; Liskamp, R. M. J., *Org. Bioimol. Chem.* **2007**, *5*, 935-944.
503. Decristoforo, C.; Gonzalez, I. H.; Carlsen, J.; Rupprich, M.; Huisman, M.; Virgolini, I.; Wester, H. J.; Haubner, R., *Eur. J. Nucl. Med. Mol. Imag.* **2008**, *35*, 1507-1515.
504. Haubner, R.; Wester, H. J.; Reuning, U.; Senekowitsch-Schmidtke, R.; Diefenbach, B.; Kessler, H.; Stocklin, G.; Schwaiger, M., *J. Nucl. Med.* **1999**, *40*, 1061-1071.
505. Haubner, R.; Wester, H. J.; Burkhart, F.; Senekowitsch-Schmidtke, R.; Weber, W.; Goodman, S. L.; Kessler, H.; Schwaiger, M., *J. Nucl. Med.* **2001**, *42*, 326-336.
506. Haubner, R.; Wester, H. J.; Weber, W. A.; Mang, C.; Ziegler, S. I.; Goodman, S. L.; Senekowitsch-Schmidtke, R.; Kessler, H.; Schwaiger, M., *Cancer Res.* **2001**, *61*, 1781-1785.
507. Haubner, R.; Kuhnast, B.; Mang, C.; Weber, W. A.; Kessler, H.; Wester, H. J.; Schwaiger, M., *Bioconjugate Chem.* **2004**, *15*, 61-69.
508. Ogawa, M.; Hatano, K.; Oishi, S.; Kawasumi, Y.; Fujii, N.; Kawaguchi, M.; Doi, R.; Imamura, M.; Yamamoto, M.; Ajito, K.; Mukai, T.; Saji, H.; Ito, K., *Nucl. Med. Biol.* **2003**, *30*, 1-9.
509. Chen, X. Y.; Park, R.; Shahinian, A. H.; Tohme, M.; Khankaldyyan, V.; Bozorgzadeh, M. H.; Bading, J. R.; Moats, R.; Laug, W. E.; Conti, P. S., *Nucl. Med. Biol.* **2004**, *31*, 179-189.
510. Olberg, D. E.; Cuthbertson, A.; Solbakken, M.; Arukwe, J. M.; Qu, H.; Kristian, A.; Bruheim, S.; Hjelstuen, O. K., *Bioconjugate Chem.* **2010**, *21*, 2297-2304.
511. Battle, M. R.; Goggi, J. L.; Allen, L.; Barnett, J.; Morrison, M. S., *J. Nucl. Med.* **2011**, *52*, 424-430.
512. Liu, Z. F.; Liu, S. L.; Wang, F.; Liu, S.; Chen, X. Y., *Eur. J. Nucl. Med. Mol. Imag.* **2009**, *36*,

1296-1307.

513. Liu, S. L.; Liu, Z. F.; Chen, K.; Yan, Y. J.; Watzlowik, P.; Wester, H. J.; Chin, F. T.; Chen, X. Y., *Mol. Imag. Biol.* **2010**, *12*, 530-538.
514. Thumshirn, G.; Hersel, U.; Goodman, S. L.; Kessler, H., *Chem. Eur. J.* **2003**, *9*, 2717-2725.
515. Thumshirn, G.; Hersel, U.; Poethko, T.; Rau, F.; Haubner, R.; Schwaiger, M.; Wester, H. J.; Kessler, H., *Peptide Revolution: Genomics, Proteomics & Therapeutics* **2004**, 693-694.
516. Fields, G. B.; Noble, R. L., *Int. J. Pept. Protein Res.* **1990**, *35*, 161-214.
517. Cini, N.; Trabocchi, A.; Menchi, G.; Bottoncetti, A.; Raspanti, S.; Pupi, A.; Guarna, A., *Biorg. Med. Chem.* **2009**, *17*, 1542-1549.
518. Chen, X. Y.; Park, R.; Shahinian, A. H.; Bading, J. R.; Conti, P. S., *Nucl. Med. Biol.* **2004**, *31*, 11-19.
519. Dietrich, D. J. SYNTHESIS AND EVALUATION OF PROBES OF RNA POLYMERASE II: ADAPTATION OF THE BICYCLIC SCAFFOLD OF THE OCTAPEPTIDE AMANITIN. the University of British Columbia, Vancouver, 2010.
520. McCusker, C. F.; Kocienski, P. J.; Boyle, F. T.; Schatzlein, A. G., *Bioorg. Med. Chem. Lett.* **2002**, *12*, 547-549.
521. Demmer, O.; Dijkgraaf, I.; Schottelius, M.; Wester, H. J.; Kessler, H., *Org. Lett.* **2008**, *10*, 2015-2018.
522. Chhabra, S. R.; Parekh, H.; Khan, A. N.; Bycroft, B. W.; Kellam, B., *Tetrahedron Lett.* **2001**, *42*, 2189-2192.
523. Portal, C.; Launay, D.; Merritt, A.; Bradley, M., *J. Comb. Chem.* **2005**, *7*, 554-560.
524. Pascal, R.; Sola, R., *Tetrahedron Lett.* **1998**, *39*, 5031-5034.
525. Granier, S.; Jean-Alphonse, F.; Demene, H.; Guillon, G.; Pascal, R.; Mendre, C., *Bioorg. Med. Chem. Lett.* **2006**, *16*, 521-524.
526. Gude, M.; Ryf, J.; White, P. D., *Lett. Pept. Sci.* **2002**, *9*, 203-206.
527. Li, Y. F.; Morcos, P. A., *Bioconjugate Chem.* **2008**, *19*, 1464-1470.
528. Srinivasan, R.; Uttamchandani, M.; Yao, S. Q., *Org. Lett.* **2006**, *8*, 713-716.
529. Liu, F.; Zha, H. Y.; Yao, Z. J., *J. Org. Chem.* **2003**, *68*, 6679-6684.
530. Wild, D.; Fani, M.; Behe, M.; Brink, I.; Rivier, J. E. F.; Reubi, J. C.; Maecke, H. R.; Weber, W. A., *J. Nucl. Med.* **2011**, *52*, 1-6.
531. Doucet, H., *Eur. J. Org. Chem.* **2008**, 2013-2030.
532. Dreher, S. D.; Dormer, P. G.; Sandrock, D. L.; Molander, G. A., *J. Am. Chem. Soc.* **2008**, *130*, 9257-9259.
533. Dreher, S. D.; Lim, S. E.; Sandrock, D. L.; Molander, G. A., *J. Org. Chem.* **2009**, *74*, 3626-3631.
534. Hasnik, Z.; Pohl, R.; Hocek, M., *Synthesis-Stuttgart* **2009**, 1309-1317.
535. Kim, B. J.; Matteson, D. S., *Angew. Chem. Int. Ed.* **2004**, *43*, 3056-3058.
536. Molander, G. A.; Ham, J.; Seapy, D. G., *Tetrahedron* **2007**, *63*, 768-775.
537. Molander, G. A.; Ito, T., *Org. Lett.* **2001**, *3*, 393-396.
538. Molander, G. A.; Yun, C. S.; Ribagorda, M.; Biolatto, B., *J. Org. Chem.* **2003**, *68*, 5534-5539.

539. Stefani, H. A.; Vieira, A. S.; Ferreira, F. P.; Guarezemini, A. S., *Aust. J. Chem.* **2009**, *62*, 909-916.
540. Wangler, C.; Maschauer, S.; Prante, O.; Schafer, M.; Schirrmacher, R.; Bartenstein, P.; Eisenhut, M.; Wangler, B., *ChemBioChem* **2010**, *11*, 2168-2181.
541. Bhojani, M. S.; Ranga, R.; Luker, G. D.; Rehemtulla, A.; Ross, B. D.; Van Dort, M. E., *Plos One* **2011**, *6*, e22418.
542. Bauwens, M.; De Saint-Hubert, M.; Devos, E.; Deckers, N.; Reutelingsperger, C.; Mortelmans, L.; Himmelreich, U.; Mottaghy, F. M.; Verbruggen, A., *Nucl. Med. Biol.* **2011**, *38*, 381-392.
543. Cheng, Z.; De Jesus, O. P.; Kramer, D. J.; De, A.; Webster, J. M.; Gheysens, O.; Levi, J.; Namavari, M.; Wang, S.; Park, J. M.; Zhang, R.; Liu, H. G.; Lee, B.; Syud, F. A.; Gambhir, S. S., *Mol. Imag. Biol.* **2010**, *12*, 316-324.
544. Kramer-Marek, G.; Kiesewetter, D. O.; Martiniova, L.; Jagoda, E.; Lee, S. B.; Capala, J., *Eur. J. Nucl. Med. Mol. Imag.* **2008**, *35*, 1008-1018.
545. Devaraj, N. K.; Weissleder, R.; Hilderbrand, S. A., *Bioconjugate Chem.* **2008**, *19*, 2297-2299.

## Appendices

### Appendix A. Preparation of various solutions

**Nuclease free water (DEPC·H<sub>2</sub>O):** 10  $\mu$ L of DEPC was added to 100 mL distilled H<sub>2</sub>O, and the solution was autoclaved for 30 min and then used without further treatment.

**3% LiClO<sub>4</sub> in acetone:** 3 g of LiClO<sub>4</sub> in 100 mL acetone.

**G-25 desalting mixture:** 15 g of Sephadex G-25 in 300 mL of distilled water was autoclaved for 30 min and cooled to room temperature. The mixture was added with 60 mg of NaN<sub>3</sub> and stored in the fridge for future use.

**20% Gel solution:** 500 mL of 40% acrylamide and bisacrylamide (29:1, w/w) solution, 90 mL H<sub>2</sub>O, 100 mL 10  $\times$  TBE buffer and 420 g urea.

**Urea dilution solution:** 590 mL H<sub>2</sub>O, 100 mL 10  $\times$  TBE buffer and 420 g urea.

**20% PAGE gel:** 60 mL of 20% gel solution was added with 60  $\mu$ L of TMEDA and 600  $\mu$ L of 10% APS (33 cm  $\times$  42 cm).

**10% PAGE gel:** 30 mL of 20% 29:1 gel solution and 30 mL of urea dilution solution was added with 60  $\mu$ L of TMEDA and 600  $\mu$ L of 10% APS (20 cm  $\times$  20 cm).

**Loading buffer:** 3 mL of 0.5 M EDTA, 15 mg of xylene cyanol, and 15 mg of bromophenol blue in 27 mL of formamide.

**Gel elution buffer:** 50 mM NaCl, 1 mM EDTA, 10 mM Tris-HCl, pH 7.5.

**FAB solution:** 100 mM Tris-HCl, 100 mM NaCl, 10 mM CaCl<sub>2</sub>, 0.05% Brij 35, pH 7.5.

**1  $\times$  PBS buffer:** 0.8 g of NaCl, 20 mg of KCl, 144 mg of Na<sub>2</sub>HPO<sub>4</sub> and 24 mg of KH<sub>2</sub>PO<sub>4</sub> in 100 mL H<sub>2</sub>O, pH 7.4.

**5% NH<sub>4</sub>OH in (50% aqueous) EtOH:** 5 mL of concentrated NH<sub>4</sub>OH aqueous solution in 95 mL of (50% aqueous) EtOH.

**2% NEt<sub>3</sub> in 75% aqueous CH<sub>3</sub>CN:** 200  $\mu$ L of NEt<sub>3</sub> in 9.8 mL of 75% aqueous CH<sub>3</sub>CN.

## **Appendix B. HPLC information**

### **Appendix B.1. HPLC systems**

**HPLC System I:** Agilent 1100 series HPLC system equipped with an auto-injector, a fraction collector and a diode array detector.

**HPLC System II:** Waters 600 controller in combination with a Waters 2487 dual wavelength absorbance detector and a NaI detector.

**HPLC System III:** Waters Acquity UPLC system comprised of a Waters Acquity Binary Solvent Manager, a Waters Acquity Sample Manager, a Waters Acquity Column Manager and a Waters Acquity Photodiode Array Detector, connected to a Bioscan Flow Count radiodetector.

**HPLC System IV:** Agilent 1200 series HPLC system equipped with an auto-injector, a diode array detector and a Raytest's Gabi Star scintillation detector equipped with a Gabi Star Gamma flow monitor and a Gabi Star flow cell with variable volume.

**ESI-LCMS:** Agilent 1100 series HPLC equipped with an auto-injector, diode array detector and Bruker Esquire mass spectrometer which is equipped with both electrospray (ESI) and atmospheric pressure chemical ionization (APCI) ion source.

### **Appendix B.2. HPLC C18 columns**

**Column I:** Phenomenex Jupiter 10u C18 300A 4.6 × 250 mm column

**Column II:** Agilent Eclipse XDB-C18 5 μm 9.4 × 250 mm column

**Column III:** Waters Acquity BEH C18, 2.1 × 100 mm, 1.7 μm HPLC column

**Column IV:** Agilent Eclipse XDB-C18 5 μm 4.6 × 150 mm column

### **Appendix B.3. HPLC programs**

**HPLC Program 1:** Gradient (solvent A: 0.1% TFA in water, solvent B: 0.05% TFA in CH<sub>3</sub>CN) 0 to 2 min: 10% B, 2 to 20 min: 10% to 50% B, 20 to 25 min: 50% to 100% B, 25 to 28 min: 100% B, 28 to 30 min: 100% to 10% B, 30 to 32 min: 10% B; flow rate: 1 mL/min, column temperature: 50 °C.

**HPLC Program 2:** Gradient (solvent A: water; solvent B: MeOH) 0 to 2 min: 0% B; 2

to 3 min: 0% to 10% B; 3 to 10 min: 10% to 50% B; 10 to 20 min: 50% to 100% B; 20 to 22 min: 100% B; 22 to 25 min: 100% to 0% B; 25 to 32 min: 0% B; flow rate: 1 mL/min column temperature: 17-19 °C.

**HPLC Program 3:** Gradient (solvent A: 0.1% TFA in water, solvent B: 0.05% TFA in CH<sub>3</sub>CN) 0 to 2 min: 10% B, 2 to 5 min: 10% to 50% B, 5 to 8 min: 50% to 100% B, 8 to 11 min: 100% B, 11 to 15 min: 100% to 10% B; flow rate: 3 mL/min, column temperature: 50 °C.

**HPLC Program 4:** Gradient (solvent A: water, solvent B: MeOH) 0 to 2 min: 0% B, 2 to 3 min: 0% to 10% B, 3 to 10 min: 10% to 50% B, 10 to 20 min: 50% to 100% B, 20 to 40 min: 100% B, 40 to 45 min: 100% to 0% B; flow rate: 1 mL/min, column temperature: 17–19 °C.

**HPLC Program 5:** Gradient (solvent A: 0.4% HCO<sub>2</sub>NH<sub>4</sub>, solvent B: CH<sub>3</sub>CN) 0 to 15 min: 5% to 95% B, 15 to 0 min: 95% to 5% B; flow rate: 1.0 mL/min, column temperature: 35 °C.

**HPLC Program 6:** Gradient (solvent A: 0.4% HCO<sub>2</sub>NH<sub>4</sub>, solvent B: CH<sub>3</sub>CN) 0 to 10 min: 5% A to 95% A; flow rate: 0.25 mL/min, column temperature: 35 °C.

**HPLC Program 7:** Gradient (solvent A: 0.04 M HCO<sub>2</sub>NH<sub>4</sub>, solvent B: CH<sub>3</sub>CN) 0 to 5 min: 0% to 5% B, 5 to 15 min: 5% to 10% B, 15 to 28 min: 10% to 30% B, 28 to 30 min: 30% to 95% B, 30 to 32 min: 95% B; flow rate: 1 mL/min, column temperature: rt.

**HPLC Program 8:** Gradient (solvent A: 0.04 M HCO<sub>2</sub>NH<sub>4</sub>, solvent B: CH<sub>3</sub>CN) 0 to 5 min: 0% to 5% B, 5 to 10 min: 5% to 20% B, 10 to 20 min: 20% to 50% B, 20 to 25 min: 50% to 100% B, 25 to 28 min: 100% to 95% B, 28 to 30 min: 95% to 5% B, 30 to 32 min: 5% B; flow rate: 1 mL/min, column temperature: rt.

**HPLC Program 9:** Gradient (solvent A: 0.1% TFA in water, solvent B: 0.05% TFA in CH<sub>3</sub>CN) 0 to 1 min: 5% to 10% B, 1 to 10 min: 10% to 50% B, 10 to 13 min: 50% to 100% B, 13 to 14 min: 100% B; flow rate: 3 mL/min, column temperature: 50 °C.

**HPLC Program 10:** Gradient (solvent A: 0.1% TFA in water, solvent B: 0.05% TFA in CH<sub>3</sub>CN) 0 to 1 min, 20% B, 1 to 10 min: 10% to 50% B, 10 to 15 min: 50% to 100% B,

15 to 20 min: 100% B, 20 to 22 min: 100% to 50% B, 22 to 25 min: 50% to 10% B; flow rate: 1 mL/min, column temperature: 50 °C.

**HPLC Program 11:** Gradient (solvent A: 0.1% TFA in water, solvent B: 0.05% TFA in CH<sub>3</sub>CN) 0 to 1 min: 20% B to 30% B, 1 to 3 min: 30% to 50% B, 3 to 10 min: 50% to 100% B, 10 to 13 min: 100% B, 13 to 15 min: 100% to 10% B; flow rate: 3 mL/min, column temperature: 50 °C.

**HPLC Program 12:** Gradient (solvent A: 0.1% TFA in water, solvent B: 0.05% TFA in CH<sub>3</sub>CN) 0 to 2 min: 20% B, 2 to 10 min: 20% to 50% B, 10 to 25 min: 50% to 100% B, 25 to 28 min: 100% B, 28 to 30 min: 100% to 10% B, 30 to 32 min: 10% B; flow rate: 1 mL/min, column temperature: 50 °C.

**HPLC Program 13:** Gradient (solvent A: 0.03 M TEAA (pH 6.0) in water, solvent B: CH<sub>3</sub>CN) 0 to 2 min: 0% B, 2 to 12 min: 0% to 10% B, 12 to 22 min: 10% to 30% B, 22 to 32 min: 30% to 60% B, 32 to 35 min: 60% to 5% B, 35 to 36 min: 5% B; flow rate: 1 mL/min, column temperature: rt.

**HPLC Program 14:** Gradient (solvent A: 0.1% TFA in water, solvent B: 0.05% TFA in CH<sub>3</sub>CN) 0 to 1 min: 20% B to 30% B, 1 to 3 min: 30% to 50% B, 3 to 10 min: 50% to 100% B, 10 to 13 min: 100% B, 13 to 15 min: 100% to 50% B, 15 to 16 min: 50% to 20% B; flow rate: 3 mL/min, column temperature: 50 °C.

**HPLC Program 15:** Gradient (solvent A: 0.04 M HCO<sub>2</sub>NH<sub>4</sub>, solvent B: CH<sub>3</sub>CN) 0 to 5 min: 0% to 5% B, 5 to 15 min: 5% to 10% B, 15 to 28 min: 10% to 30% B, 28 to 32 min: 30% to 95% B, 32 to 36 min: 95% B; flow rate: 1 mL/min, column temperature: rt.

**HPLC Program 16:** Gradient (solvent A: 0.03 M TEAA (pH 6.0) in water, solvent B: CH<sub>3</sub>CN) 0 to 2 min: 0% B, 2 to 12 min: 0% to 10% B, 12 to 22 min: 10% to 20% B, 22 to 27 min: 30% to 60% B, 27 to 30 min: 60% to 100% B, 30 to 32 min: 100% B, 32 to 36 min: 100% to 5% B; flow rate: 1 mL/min, column temperature: rt.

**HPLC Program 17:** Gradient (solvent A: 0.1% TFA in water, solvent B: 0.05% TFA in CH<sub>3</sub>CN) 0 to 1 min: 10% B, 1 to 10 min: 10% to 50% B, 10 to 13 min: 50% to 100% B, 13 to 14 min: 100% B, 14 to 16 min: 100% to 50% B, 16 to 18 min: 50% to 10% B, 18 to

20 min: 10% B; flow rate: 1 mL/min, column temperature: 50 °C.

**HPLC Program 18:** Gradient (solvent A: 0.1% TFA in water, solvent B: 0.05% TFA in CH<sub>3</sub>CN) 0 to 15 min: 25% B, 15 to 20 min: 25% to 100% B, 20 to 25 min: 100% B, 25 to 30 min: 100% to 25% B; flow rate: 3 mL/min, column temperature: 50 °C.

**HPLC Program 19:** Gradient (solvent A: 0.1% TFA in water, solvent B: 0.05% TFA in CH<sub>3</sub>CN) 0 to 15 min, 25% B, 15 to 20 min: 25% to 100% B, 20 to 25 min: 100% B, 25 to 30 min: 100% to 25% B; flow rate: 1 mL/min, column temperature: 50 °C.

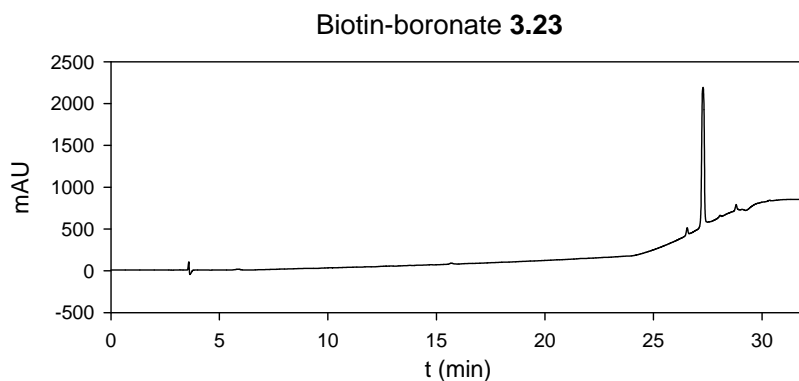
## Appendix C. HPLC chromatograms

The HPLC analysis has been performed in several HPLC systems with different columns. Here the HPLC chromatograms of several compounds synthesized in this thesis are reported. All of the traces were recorded at 229 nm, or otherwise noted. All the programs and retention times are also indicated next to the chromatograms.

### Biotin-boronate (3.23)

HPLC Program 1 with Column I in HPLC System I.

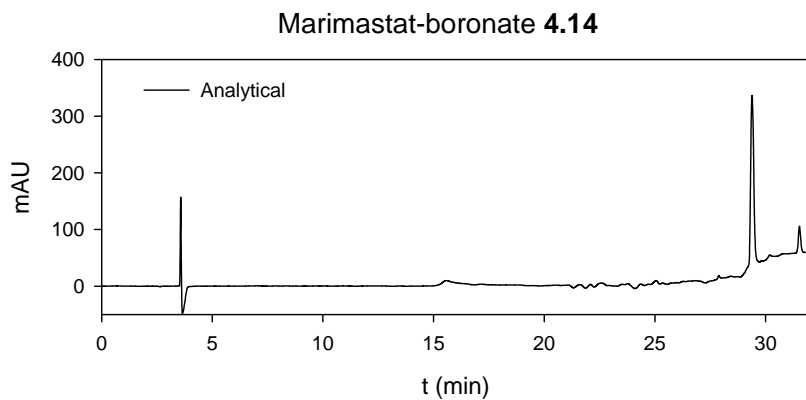
$t_R = 27.3$  min.



### Marimastat-boronate (4.14)

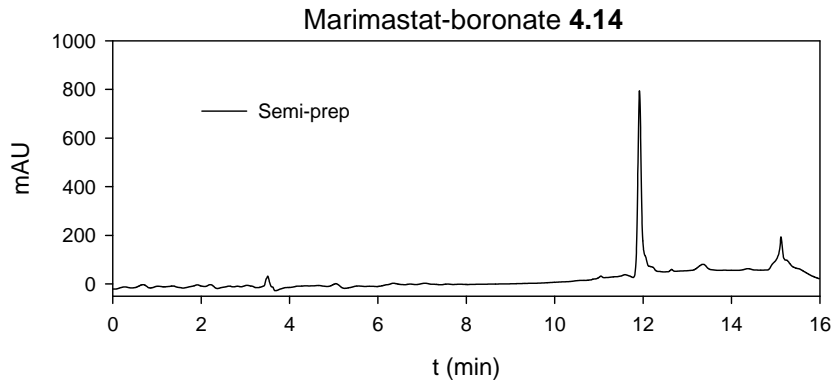
HPLC Program 1 with Column I in HPLC System I

$t_R = 29.4$  min.



HPLC Program 3 with Column II in HPLC System I

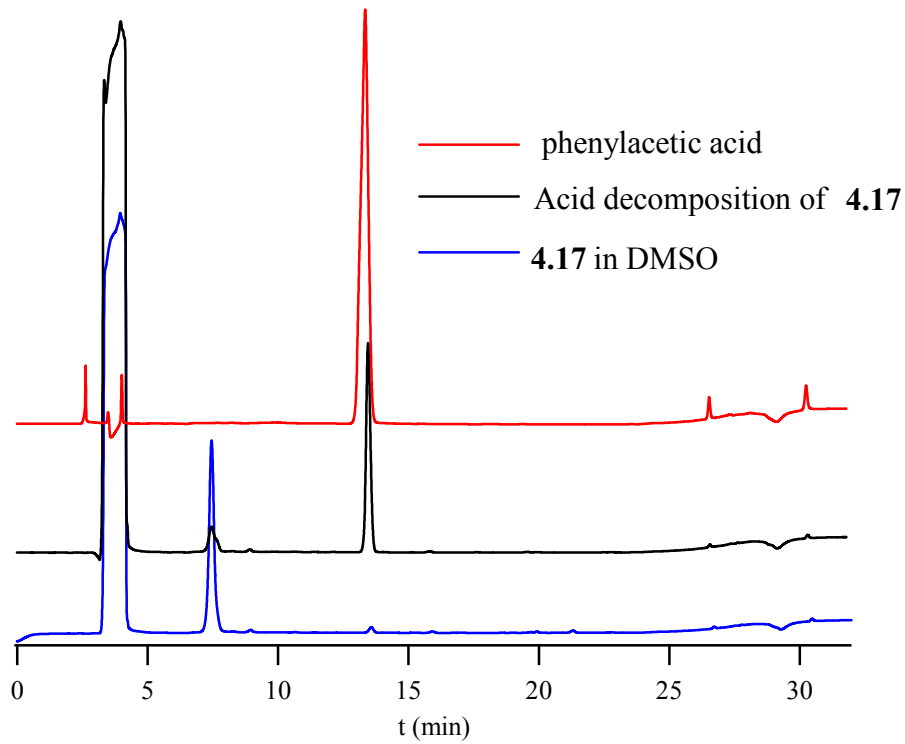
$t_R = 12.0$  min.



**The acid stability of 4.17 analyzed by HPLC**

HPLC Program 1 with Column I in HPLC System I

$t_R$  (phenylacetic acid) = 13.5 min.

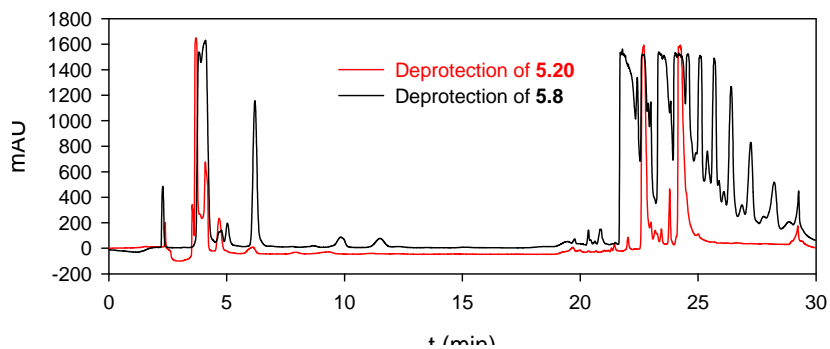


## Urea-boronate (5.9)

HPLC Program 18 with Column II in HPLC System I

$t_R = 22.6$  min.

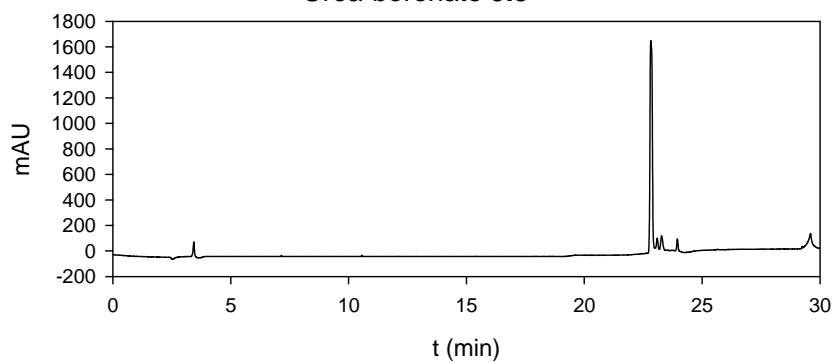
### Preparation of urea-boronate 5.9



HPLC Program 19 with Column I in HPLC System I

$t_R = 22.8$  min.

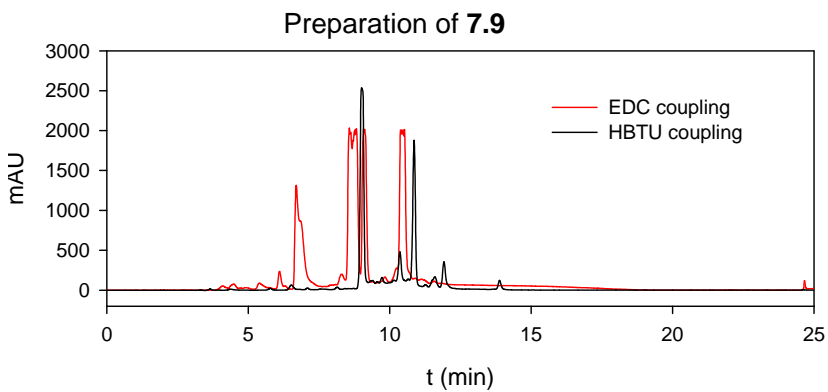
### Urea-boronate 5.9



### Pte-Glu[(PEG)<sub>2</sub>N<sub>3</sub>]-OCH<sub>3</sub> (7.9)

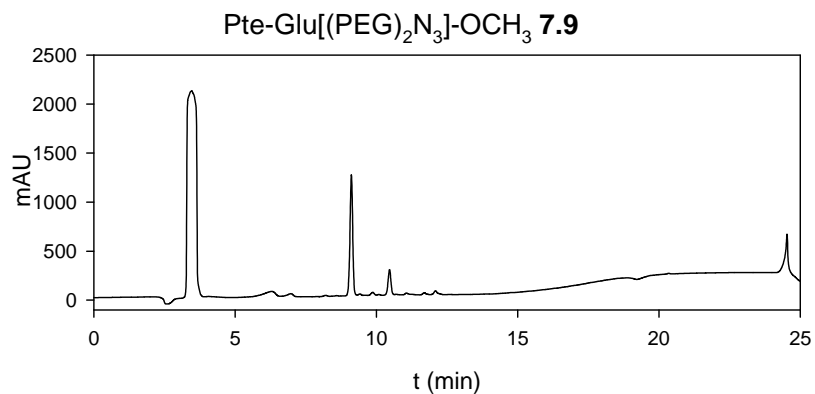
IHPLC chromatograms recorded at 292 nm.

Program 10 with Column I in HPLC System



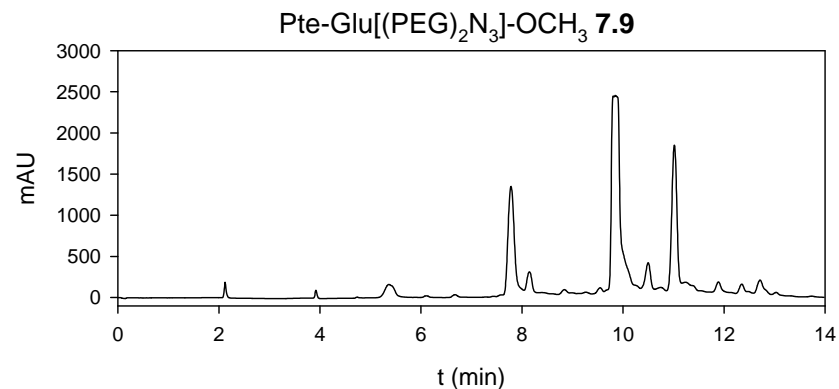
HPLC Program 10 with Column I in HPLC System I

$t_R = 9.1$  min.



HPLC Program 9 with Column II in HPLC System I

$t_R = 9.9$  min.

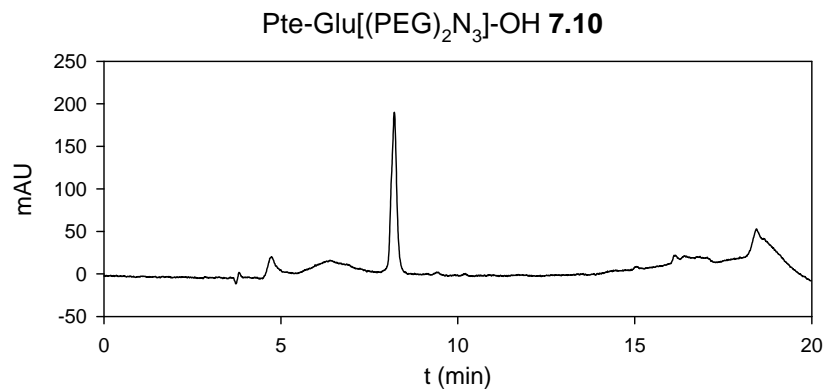


**Pte-Glu[(PEG)<sub>2</sub>N<sub>3</sub>]-OH (7.10)**

HPLC chromatograms recorded at 292 nm.

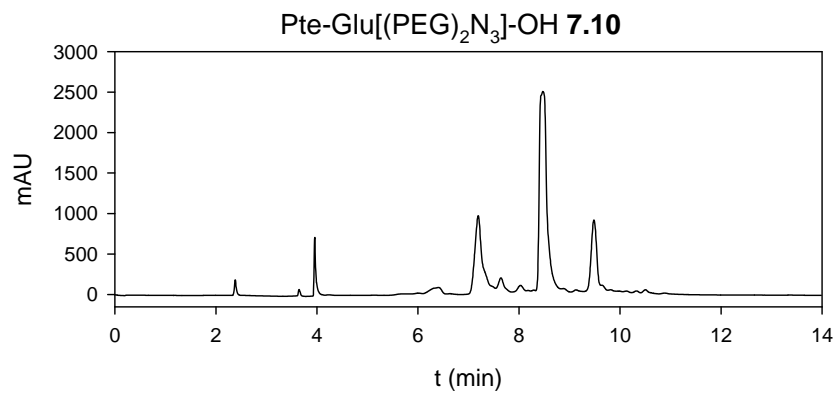
HPLC Program 17 with Column I in HPLC System I

$t_R = 8.2$  min (292 nm).



HPLC Program 9 with Column II in HPLC System I

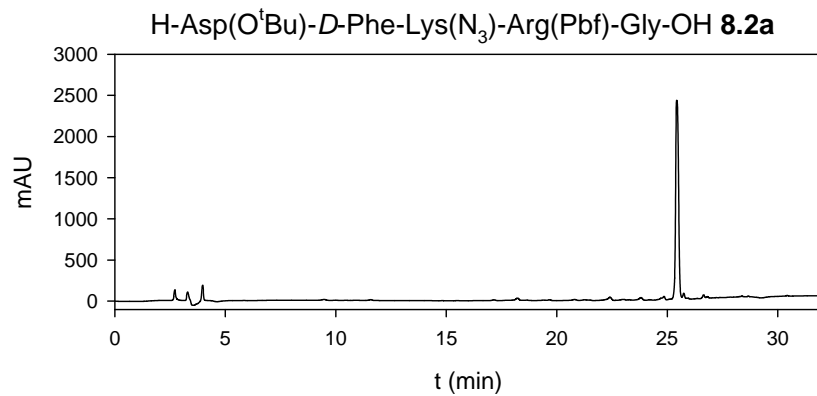
$t_R = 8.7$  min.



**H-Asp(O<sup>t</sup>Bu)-D-Phe-Lys(N<sub>3</sub>)-Arg(Pbf)-Gly-OH (8.2a)**

HPLC Program 1 with Column I in HPLC System I

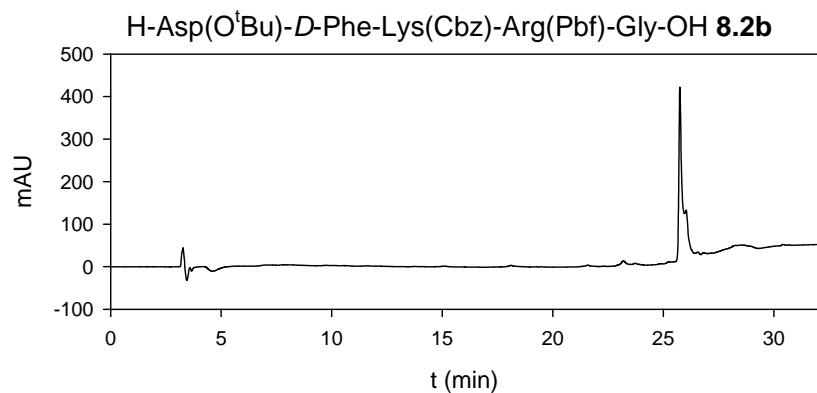
$t_R = 25.4$  min.



**H-Asp(O<sup>t</sup>Bu)-D-Phe-Lys(Cbz)-Arg(Pbf)-Gly-OH (8.2b)**

HPLC Program 1 with Column I in HPLC System I

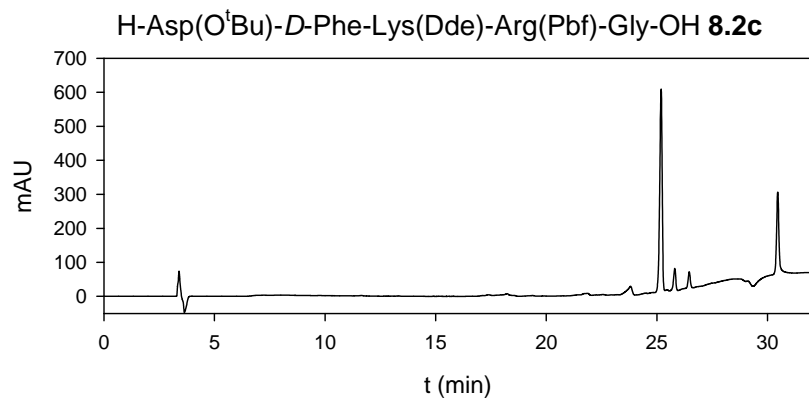
$t_R = 25.8$  min.



**H-Asp(O<sup>t</sup>Bu)-D-Phe-Lys(Dde)-Arg(Pbf)-Gly-OH (8.2c)**

HPLC Program 1 with Column I in HPLC System I

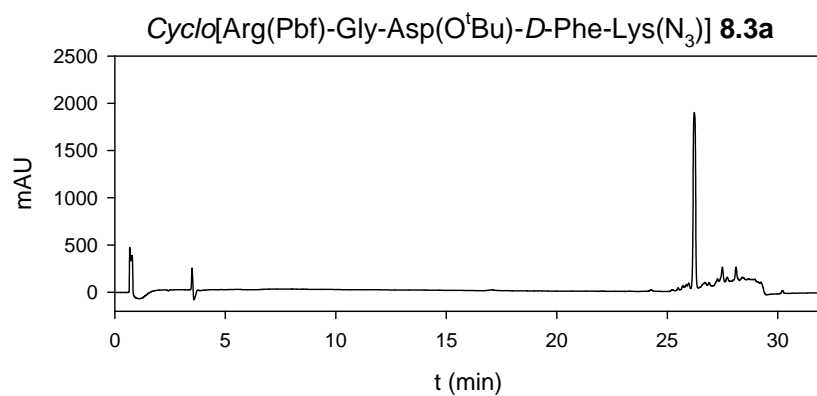
$t_R = 25.2$  min.



**Cyclo[Arg(Pbf)-Gly-Asp(O<sup>t</sup>Bu)-D-Phe-Lys(N<sub>3</sub>)] (8.3a)**

HPLC Program 1 with Column I in HPLC System I

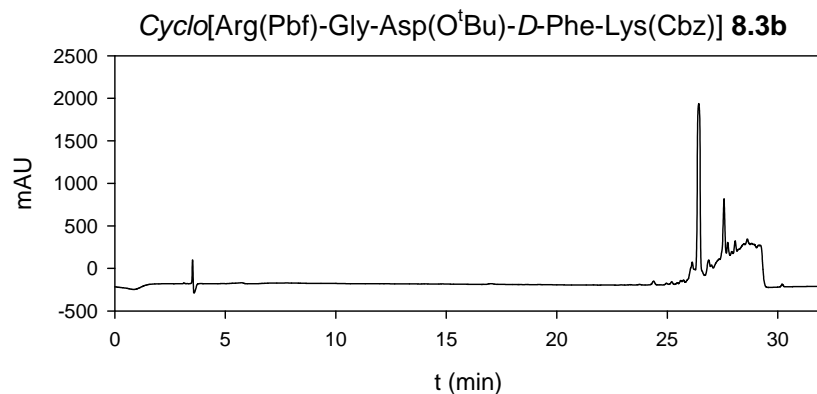
$t_R = 26.2$  min.



**Cyclo[Arg(Pbf)-Gly-Asp(O<sup>t</sup>Bu)-D-Phe-Lys(Cbz)] (8.3b)**

HPLC Program 1 with Column I in HPLC System I

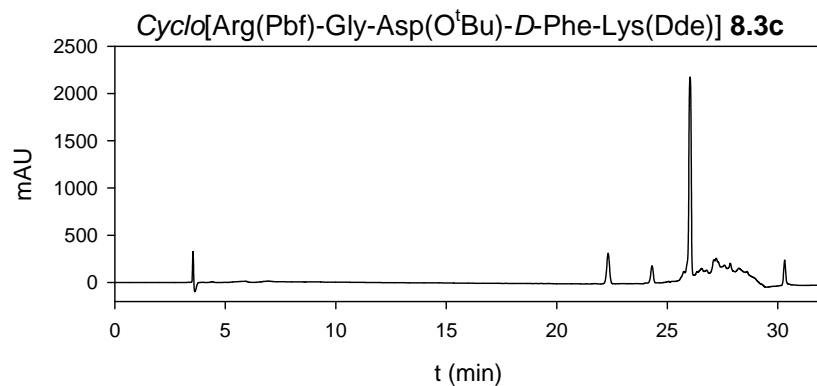
$t_R = 26.4$  min.



***Cyclo[Arg(Pbf)-Gly-Asp(O<sup>t</sup>Bu)-D-Phe-Lys(Dde)] (8.3c)***

HPLC Program 1 with Column I in HPLC System I

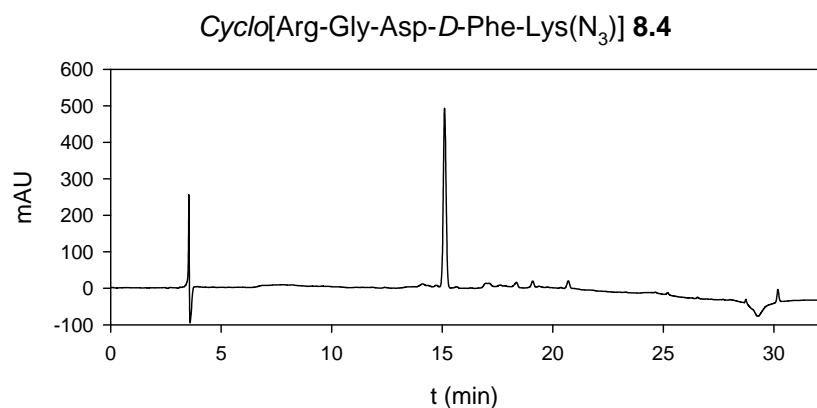
$t_R = 26.0$  min.



***Cyclo[Arg-Gly-Asp-D-Phe-Lys(N<sub>3</sub>)] (8.4)***

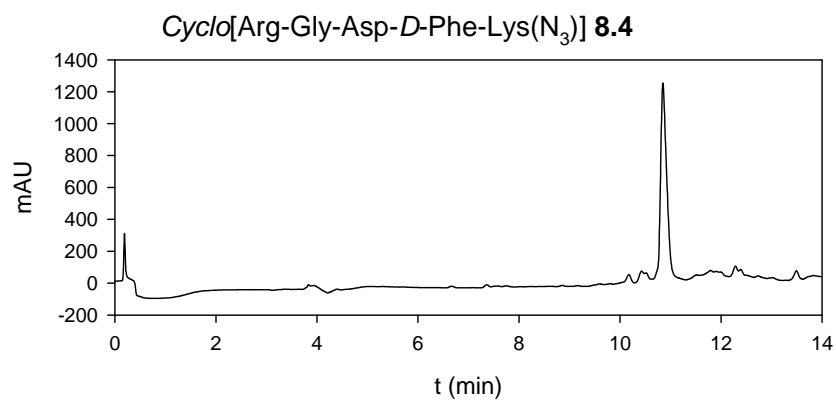
HPLC Program 1 with Column I in HPLC System I

$t_R = 15.1$  min.



HPLC Program 9 with Column II in HPLC System I

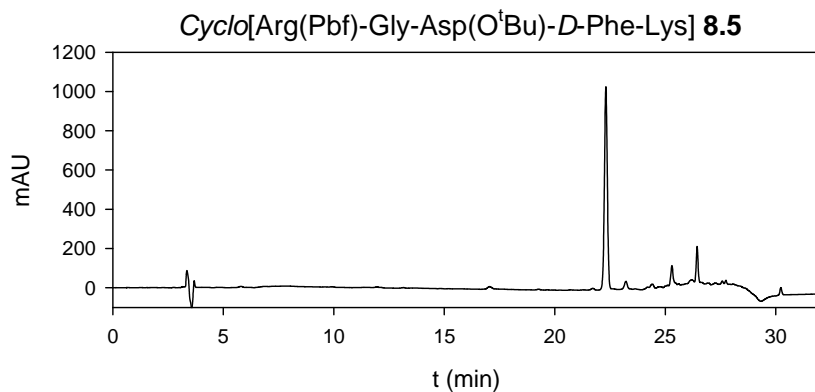
$t_R = 10.9$  min.



***Cyclo[Arg(Pbf)-Gly-Asp(O<sup>t</sup>Bu)-D-Phe-Lys]* (8.5)**

HPLC Program 1 with Column I in HPLC System I

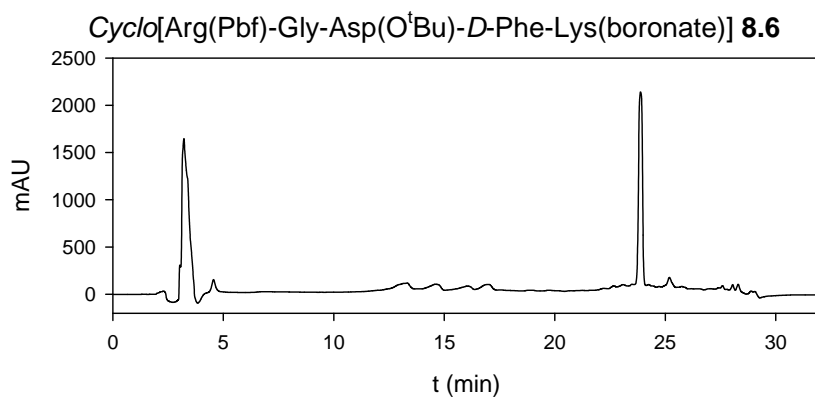
$t_R = 22.3$  min.



***Cyclo[Arg(Pbf)-Gly-Asp(O<sup>t</sup>Bu)-D-Phe-Lys(boronate)]* (8.6)**

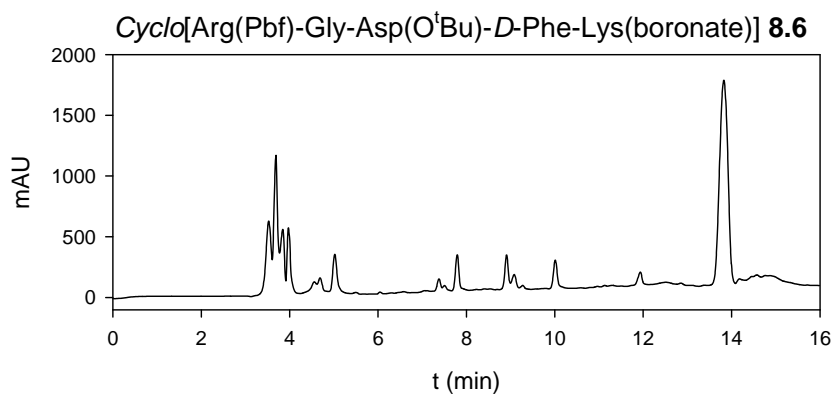
HPLC Program 12 with Column I in HPLC System I

$t_R = 23.9$  min.



HPLC Program 11 with Column II in HPLC System I

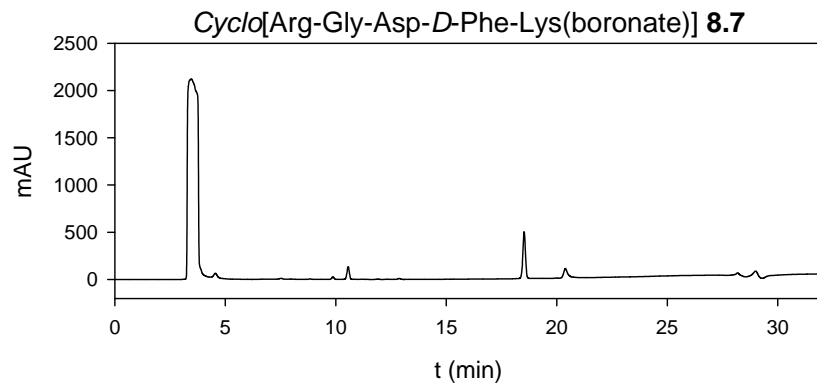
$t_R = 13.8$  min.



***Cyclo[Arg-Gly-Asp-D-Phe-Lys(boronate)] (8.7)***

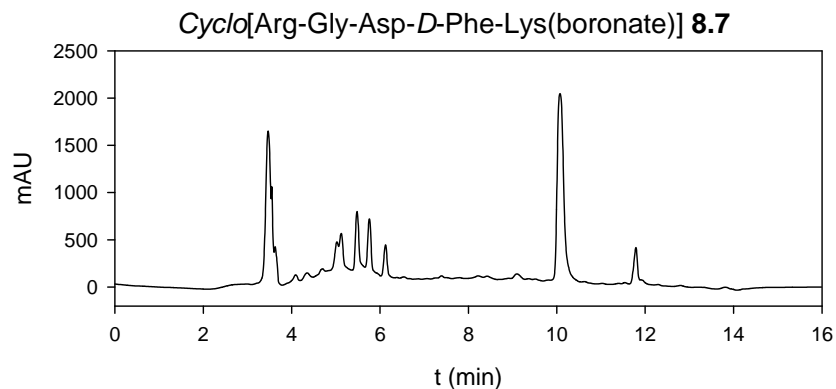
HPLC Program 12 with Column I in HPLC System I

$t_R = 18.5$  min.



HPLC Program 14 with Column II in HPLC System I

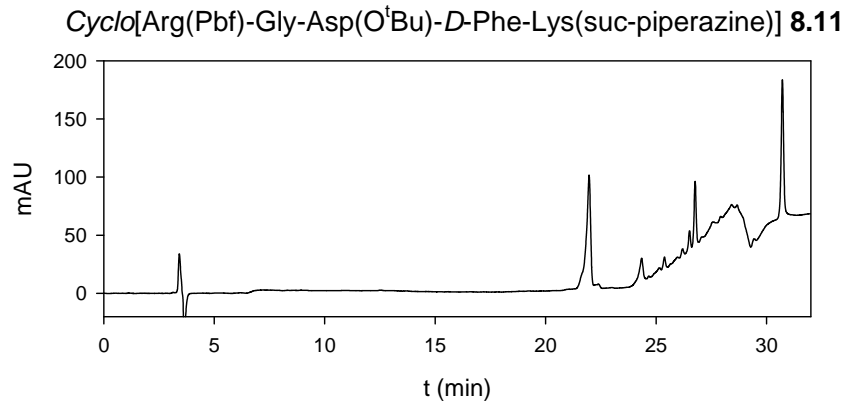
$t_R = 10.1$  min.



***Cyclo[Arg(Pbf)-Gly-Asp(O<sup>t</sup>Bu)-D-Phe-Lys(suc-piperazine)] (8.11)***

HPLC Program 1 with Column I in HPLC System I

$t_R = 22.0$  min.

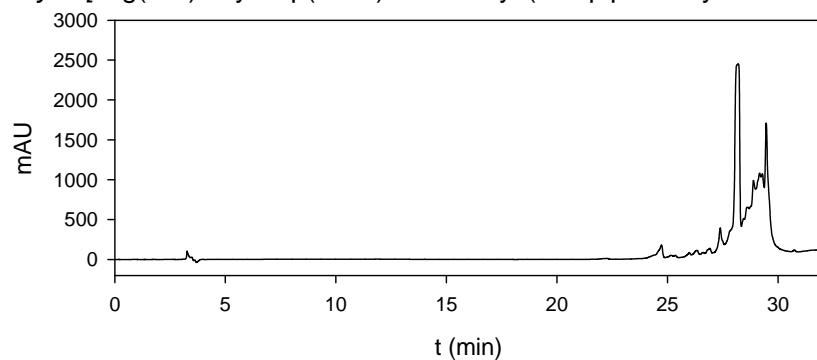


***Cyclo[Arg(Pbf)-Gly-Asp(O<sup>t</sup>Bu)-D-Phe-Lys(suc-piperazinyl-boronate)] (8.12)***

HPLC Program 1 with Column I in HPLC System I

$t_R = 28.2$  min.

***Cyclo[Arg(Pbf)-Gly-Asp(O<sup>t</sup>Bu)-D-Phe-Lys(suc-piperazinyl-boronate)] 8.12***

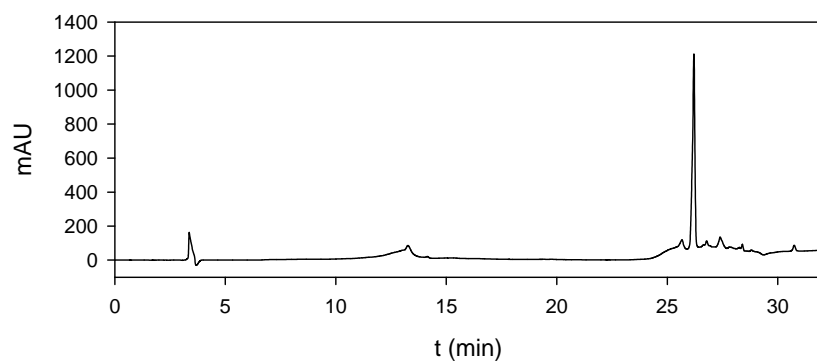


***Cyclo[Arg-Gly-Asp-D-Phe-Lys(suc-piperazinyl-boronate)] (8.13)***

HPLC Program 1 with Column I in HPLC System I

$t_R = 26.2$  min.

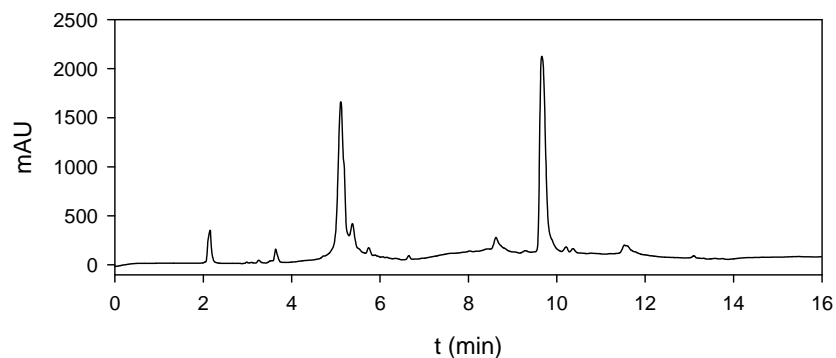
***Cyclo[Arg-Gly-Asp-D-Phe-Lys(suc-piperazinyl-boronate)] 8.13***



HPLC Program 14 with Column II in HPLC System I

$t_R = 9.7$  min.

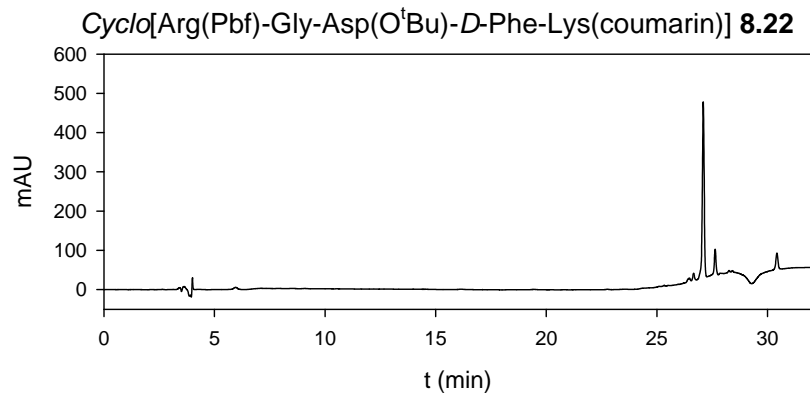
***Cyclo[Arg-Gly-Asp-D-Phe-Lys(suc-piperazinyl-boronate)] 8.13***



***Cyclo[Arg(Pbf)-Gly-Asp(O<sup>t</sup>Bu)-D-Phe-Lys(coumarin)] (8.22)***

HPLC Program 1 with Column I in HPLC System I

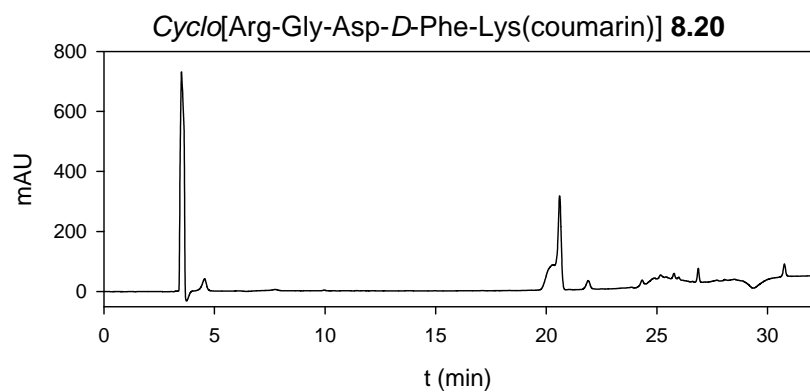
$t_R = 27.1$  min.



***Cyclo[Arg-Gly-Asp-D-Phe-Lys(coumarin)] (8.20)***

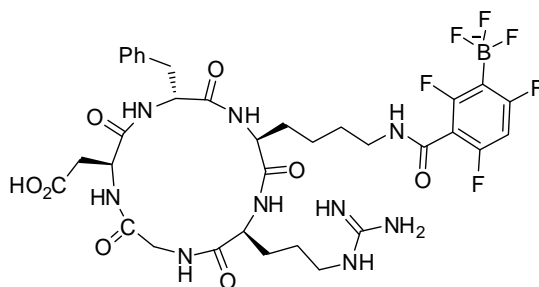
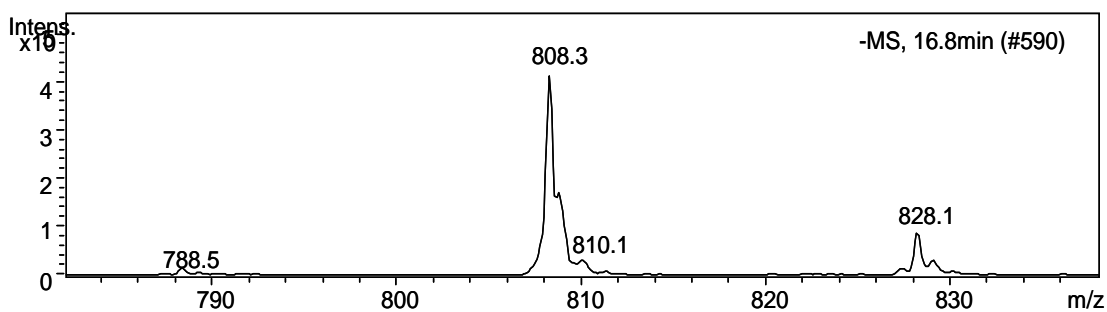
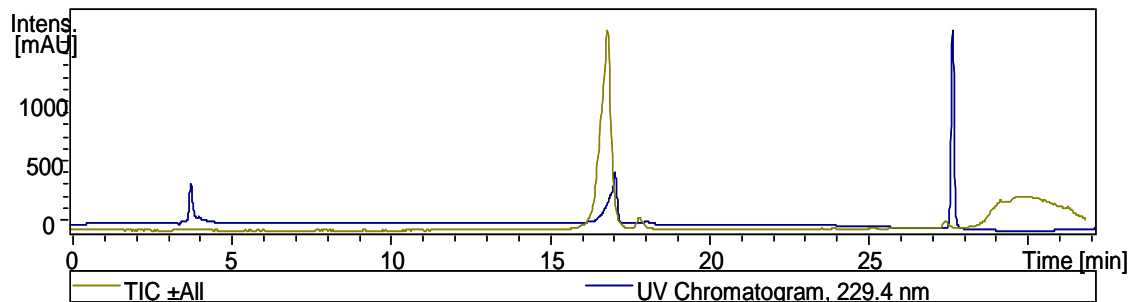
HPLC Program 1 with Column I in HPLC System I

$t_R = 20.7$  min.



# LCMS for RGD-ArBF<sub>3</sub> **8.18**

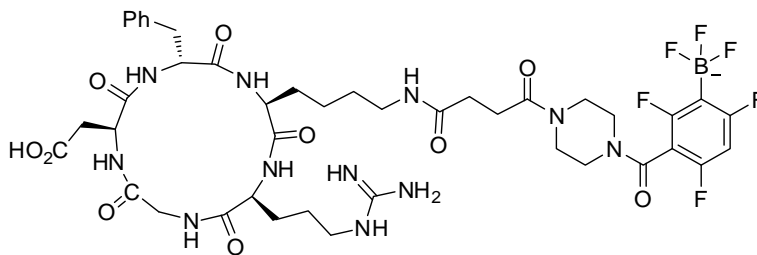
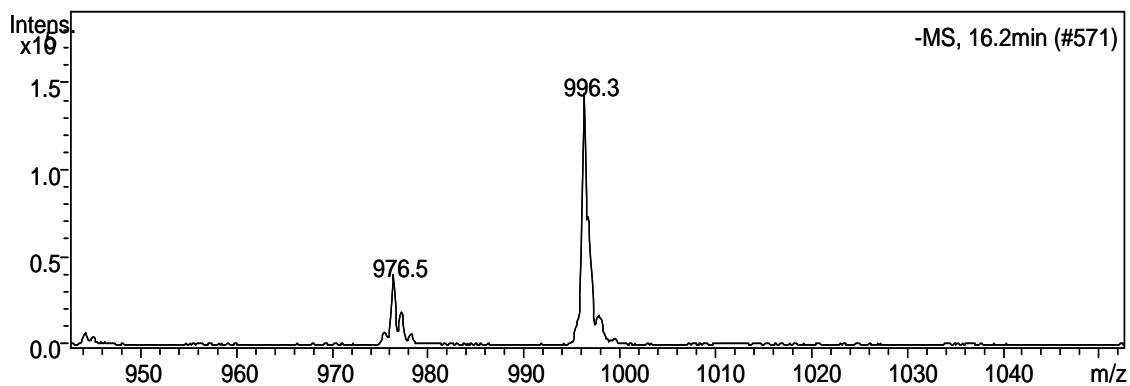
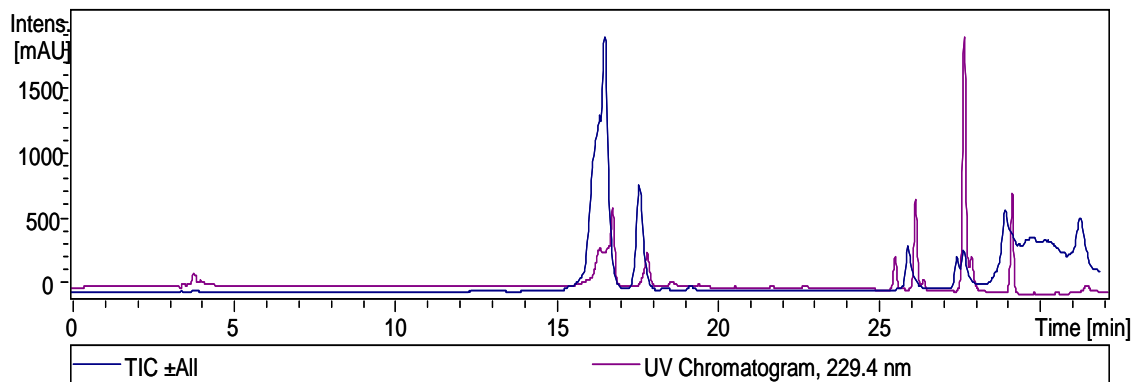
HPLC Program 8 with Column I in ESI-LCMS



Chemical Formula: C<sub>34</sub>H<sub>41</sub>BF<sub>6</sub>N<sub>9</sub>O<sub>8</sub><sup>-</sup> **8.18**  
Exact Mass: 828.3081  
Molecular Weight: 828.5468

# LCMS for RGD-ArBF<sub>3</sub> **8.19**

HPLC Program 8 with Column I in ESI-LCMS

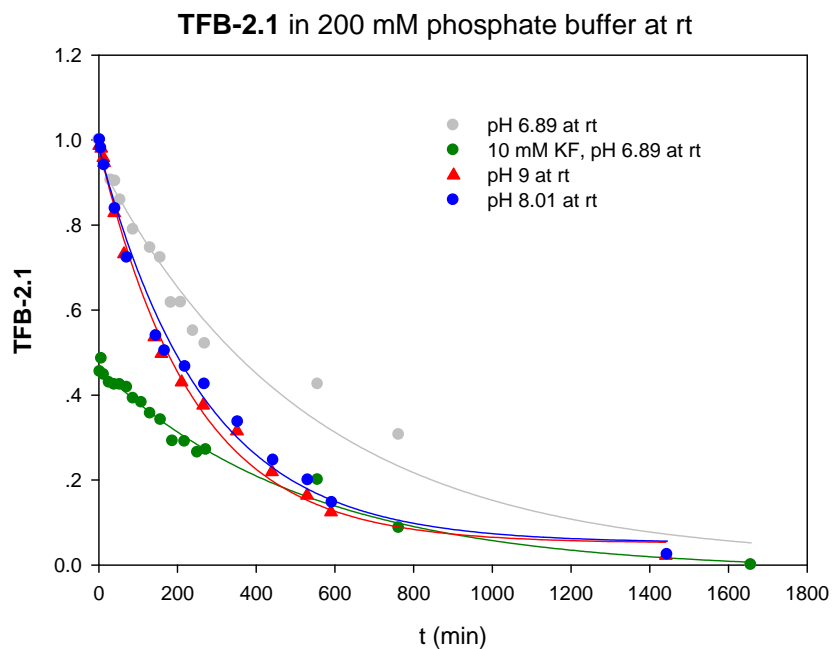


Chemical Formula:  
 $C_{42}H_{53}BF_6N_{11}O_{10}^-$   
Exact Mass: 996.3980  
Molecular Weight: 996.7399

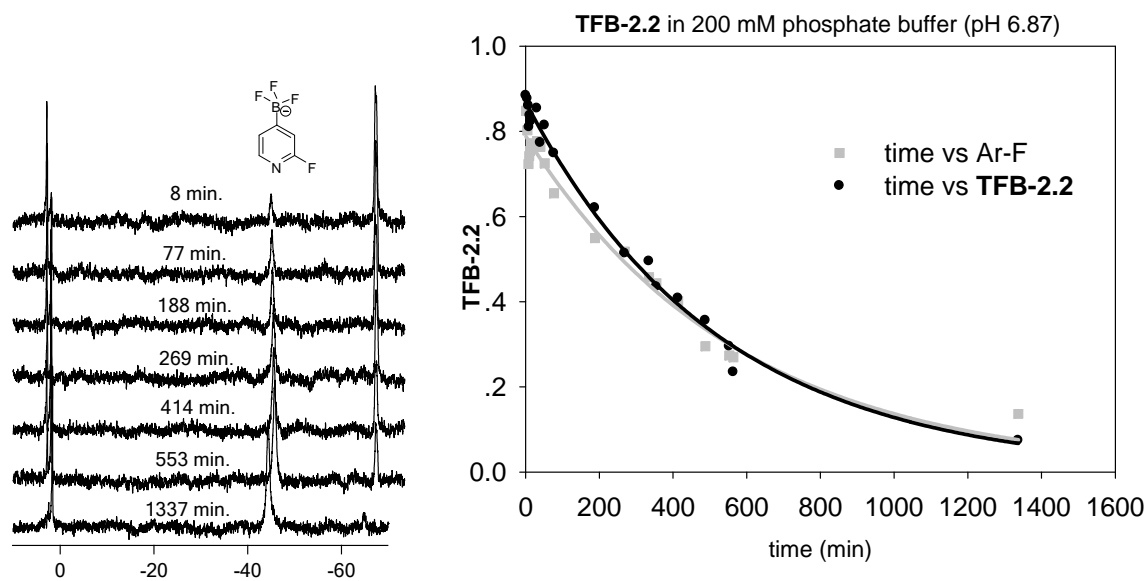
**8.19**

## Appendix D. The kinetic study on the solvolysis of *N*-HetArBF<sub>3</sub>s by <sup>19</sup>F NMR spectroscopy

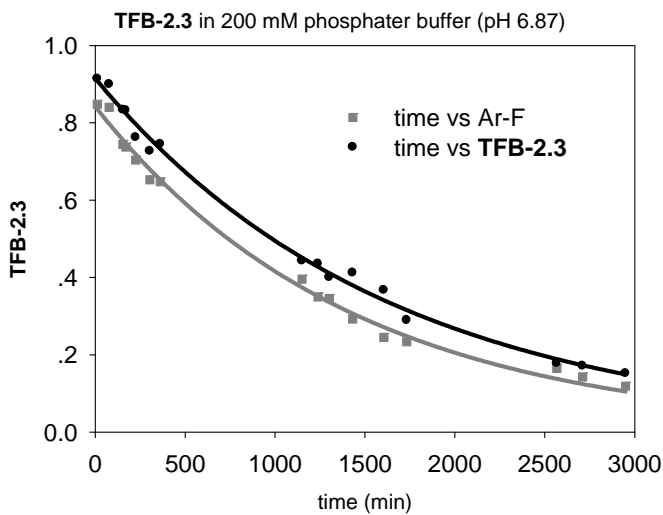
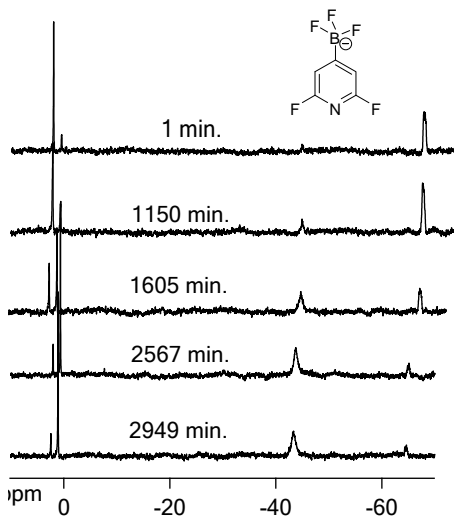
Hydrolysis of TFB-2.1 in 200 mM phosphate buffer (different pHs) at rt.



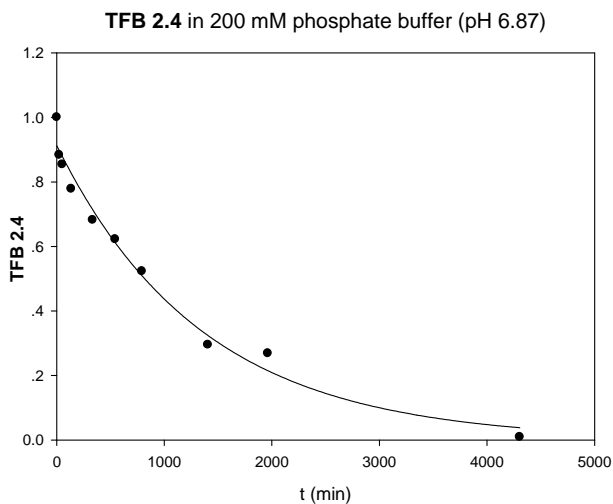
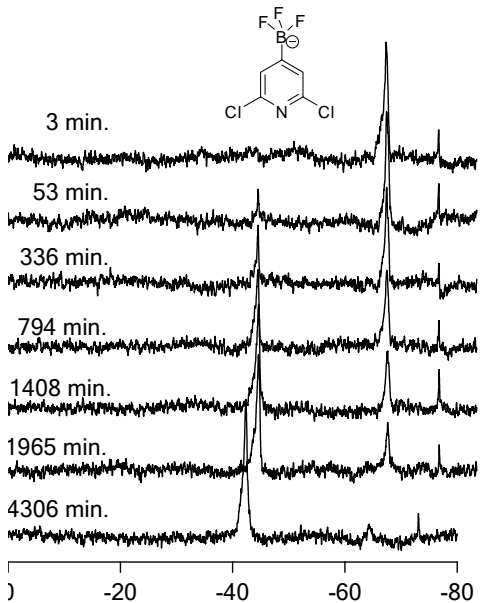
Hydrolysis of TFB-2.2 in 200 mM phosphate buffer (pH 6.87) at rt.



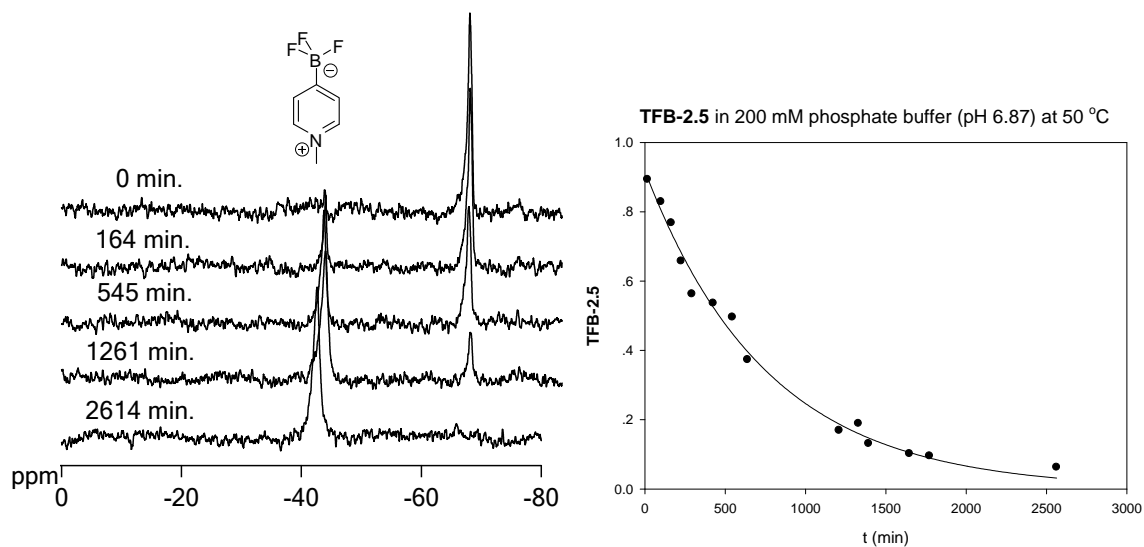
Hydrolysis of **TFB-2.3** in 200 mM phosphate buffer (pH 6.87) at rt.



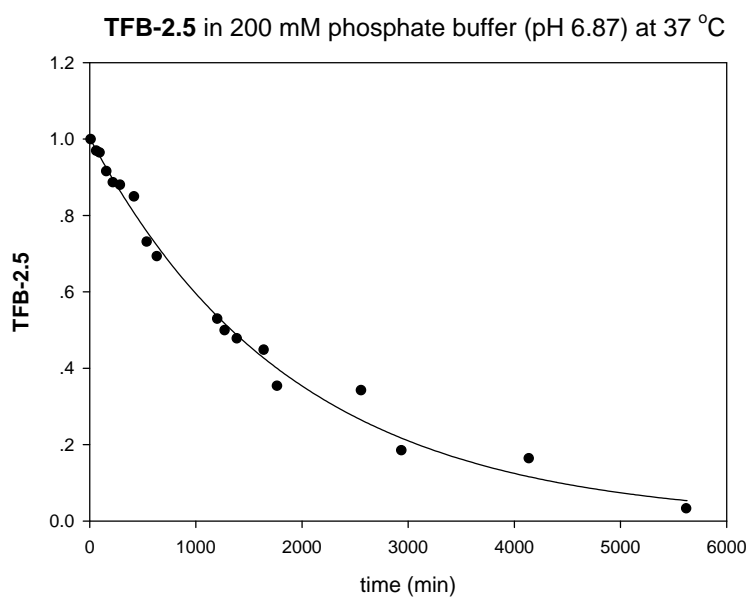
Hydrolysis of **TFB-2.4** in 200 mM phosphate buffer (pH 6.87) at rt.



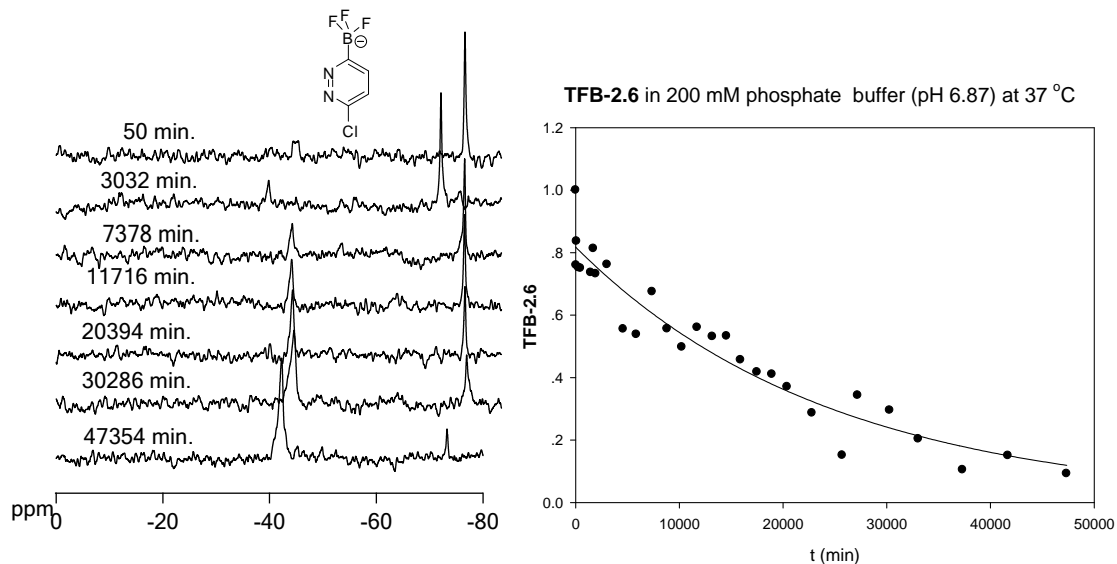
Hydrolysis of **TFB-2.5** in 200 mM phosphate buffer (pH 6.87) at 50 °C



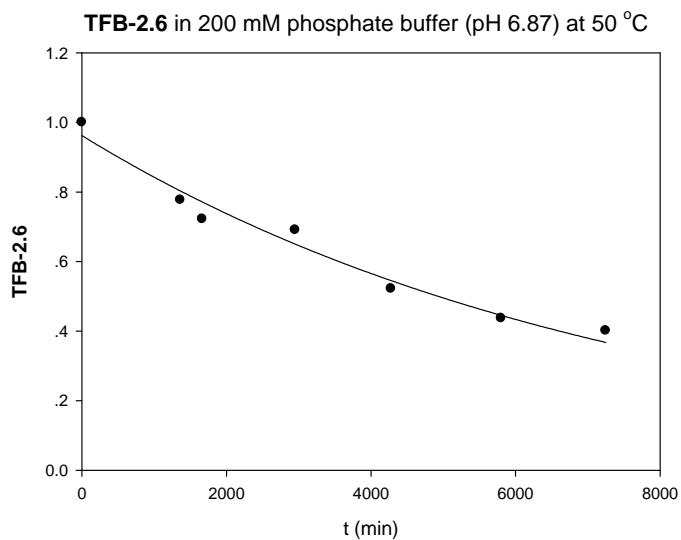
Hydrolysis of **TFB-2.5** in 200 mM phosphate buffer (pH 6.87) at 37 °C



Hydrolysis of **TFB-2.6** in 200 mM phosphate buffer (pH 6.87) at 37 °C.

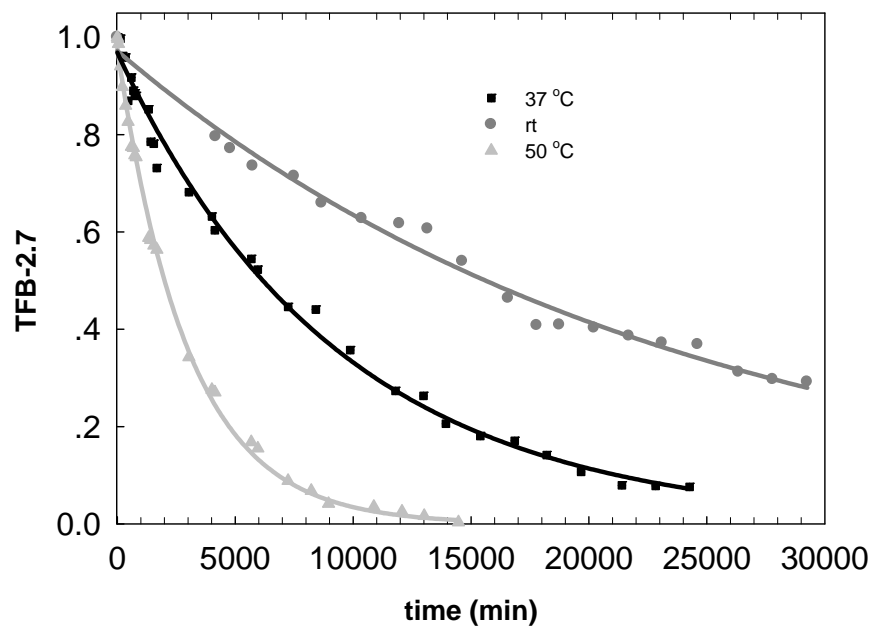


Hydrolysis of **TFB-2.6** in 200 mM phosphate buffer (pH 6.87) at 50 °C.



Hydrolysis of **TFB-2.7** in 200 mM phosphate buffer (pH 6.87) at different temperatures.

**TFB-2.7** in 200 mM phosphate buffer (pH 6.87) at various temperatures

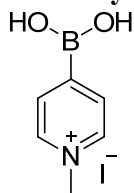


## Appendix E. NMR spectra

The NMR spectra reported here are for most of the compounds synthesized in this thesis. For the cleanliness of the spectra, only integration was indicated for  $^1\text{H}$  NMR spectra, peak picking for  $^{13}\text{C}$  NMR spectra and both the integration and peak picking for  $^{19}\text{F}$  NMR spectra. Both the structures and parameters for the NMR spectra are listed above the spectra. The spectra reported herein are based on individual chapters.

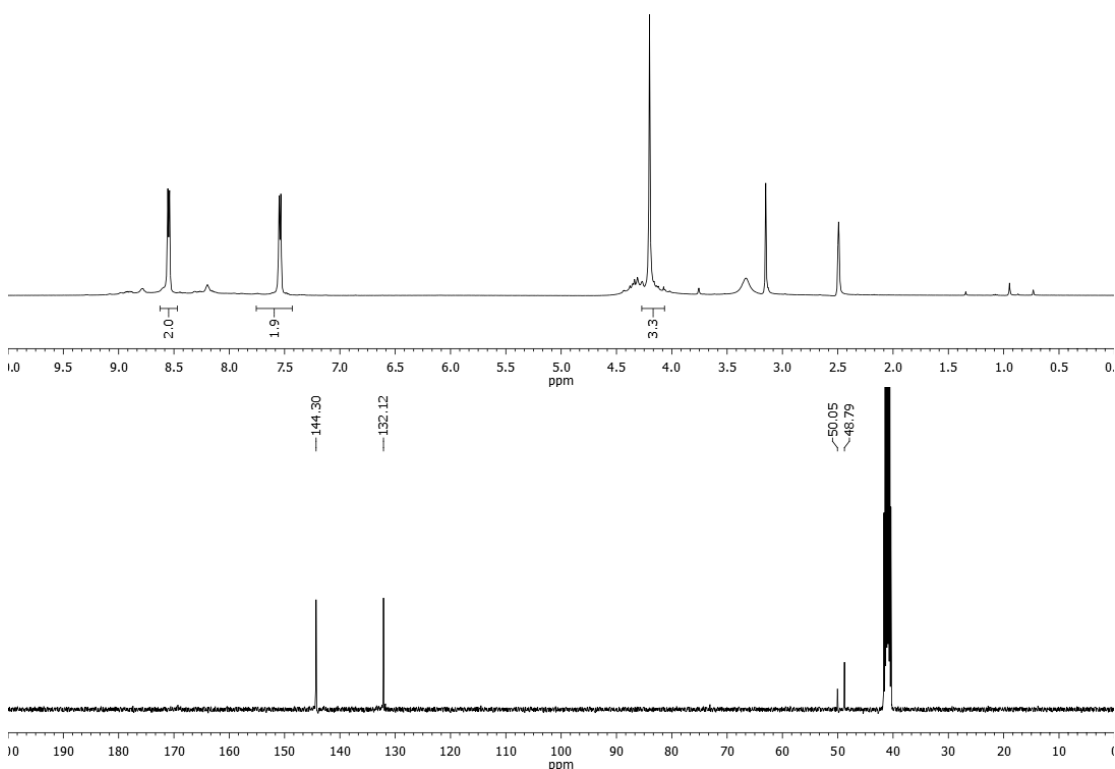
### Appendix E.1. NMR spectra for Chapter 2

#### *N*-Methyl-4-pyridineboronic acid iodide (2.5)

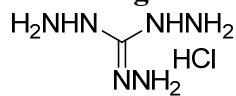


**2.5**

$^1\text{H}$  NMR 400 MHz,  $^{13}\text{C}$  NMR 100.6 MHz,  $d_6$ -DMSO



### Triaminoguanidine monohydrochloride (2.7a)



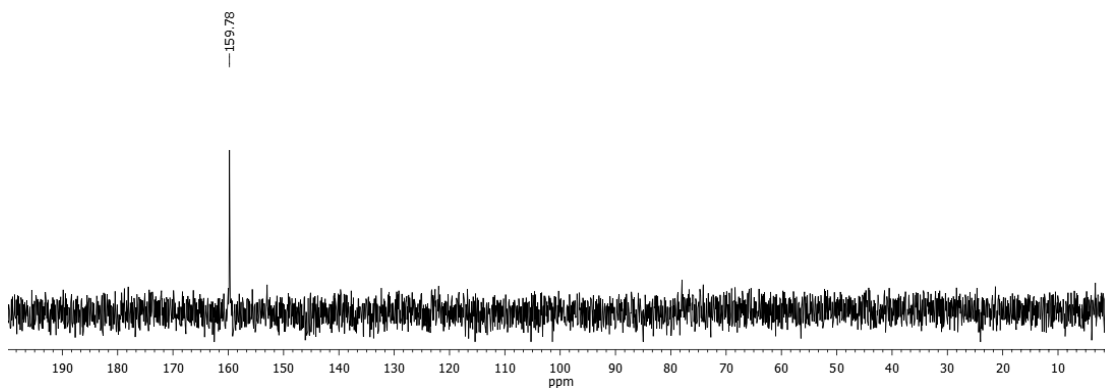
Chemical Formula:  $\text{CH}_9\text{ClN}_6$

Exact Mass: 140.0577

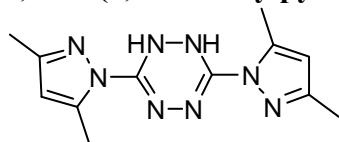
Molecular Weight: 140.5754

**2.7a**

$^{13}\text{C}$  NMR 75.5 MHz,  $\text{D}_2\text{O}$



### 3,6-Bis(3,5-dimethylpyrazol-1-yl)-1,2-dihydro-1,2,4,5-tetrazine (2.7b)



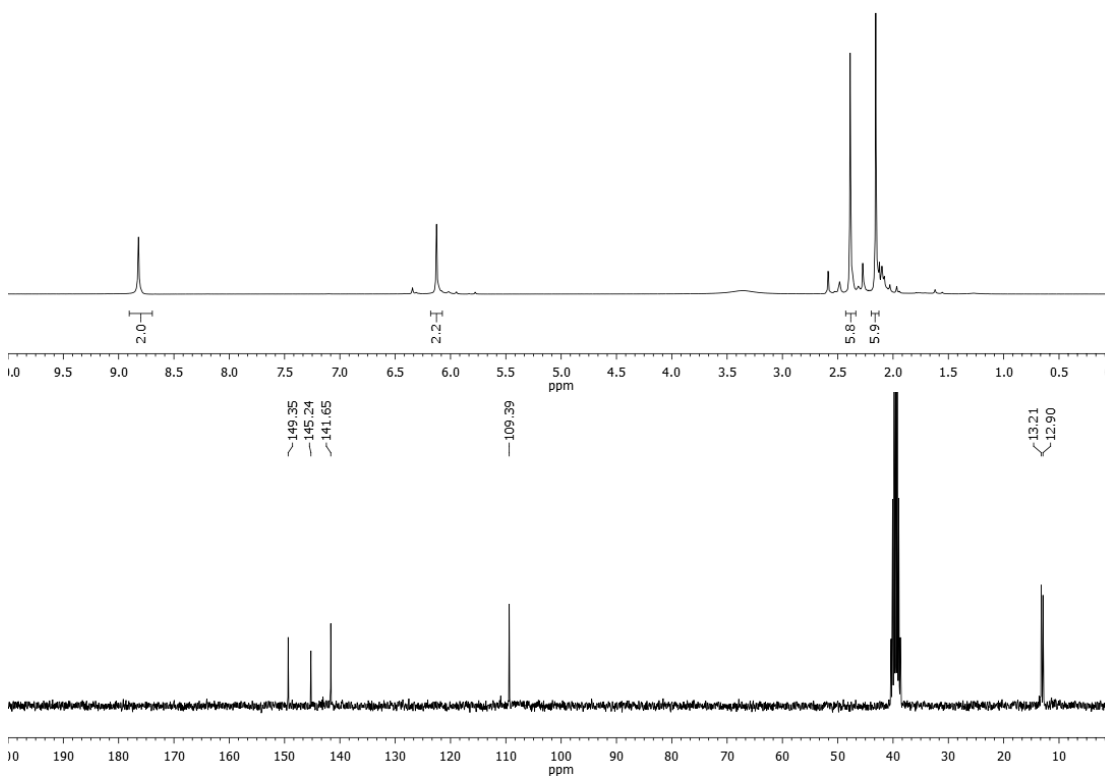
Chemical Formula:  $\text{C}_{12}\text{H}_{16}\text{N}_8$

Exact Mass: 272.1498

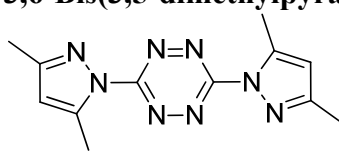
Molecular Weight: 272.3090

**2.7b**

$^1\text{H}$  NMR 300 MHz,  $^{13}\text{C}$  NMR 75.5 MHz,  $d_6$ -DMSO.



### 3,6-Bis(3,5-dimethylpyrazol-1-yl)-1,2,4,5-tetrazine (2.7c)



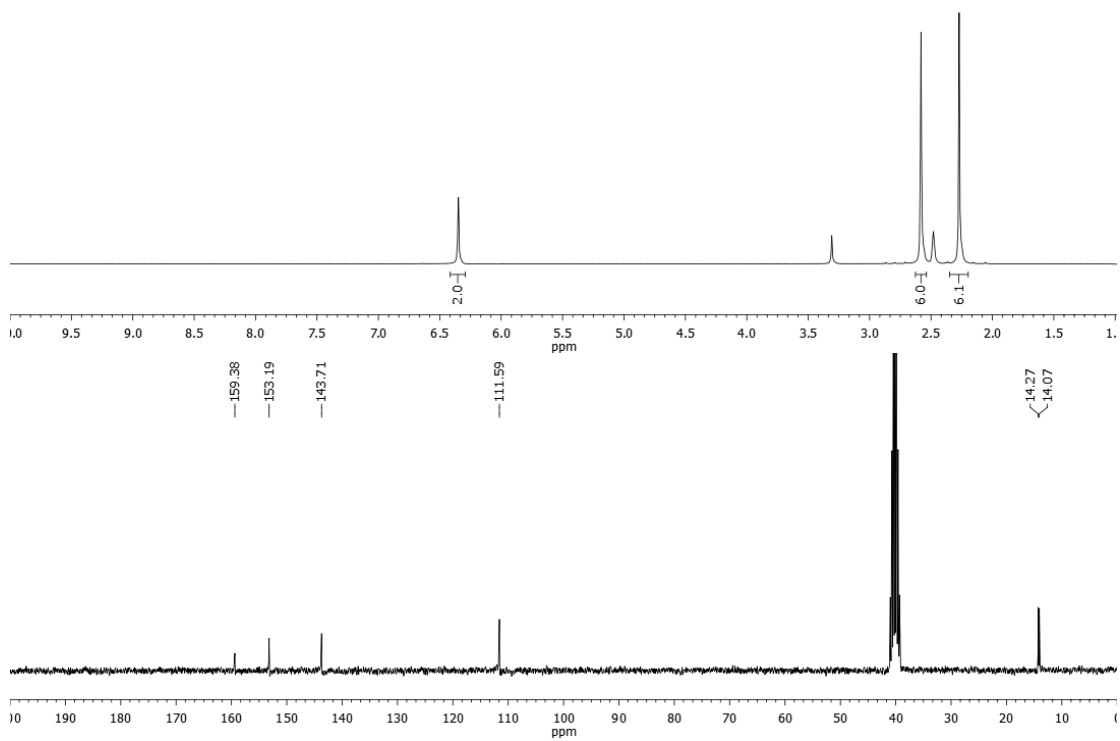
Chemical Formula: C<sub>12</sub>H<sub>14</sub>N<sub>8</sub>

Exact Mass: 270.1341

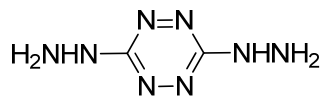
Molecular Weight: 270.2932

**2.7c**

<sup>1</sup>H NMR 300 MHz, <sup>13</sup>C NMR 75.5 MHz, *d*<sub>6</sub>-DMSO



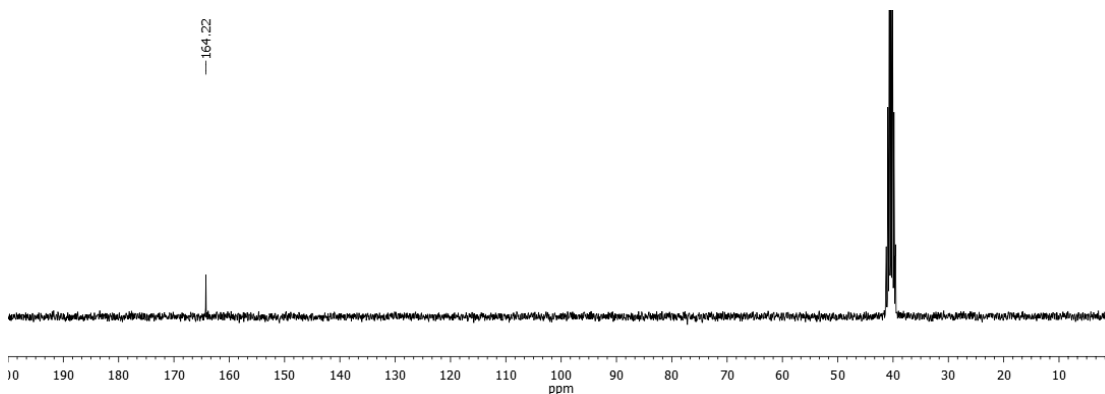
### 3,6-Dihydrazino-1,2,4,5-tetrazine (2.7d)



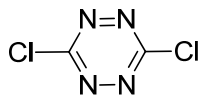
Chemical Formula: C<sub>2</sub>H<sub>6</sub>N<sub>8</sub>  
Exact Mass: 142.0715  
Molecular Weight: 142.1226

**2.7d**

<sup>13</sup>C NMR 75.5 MHz, *d*<sub>6</sub>-DMSO



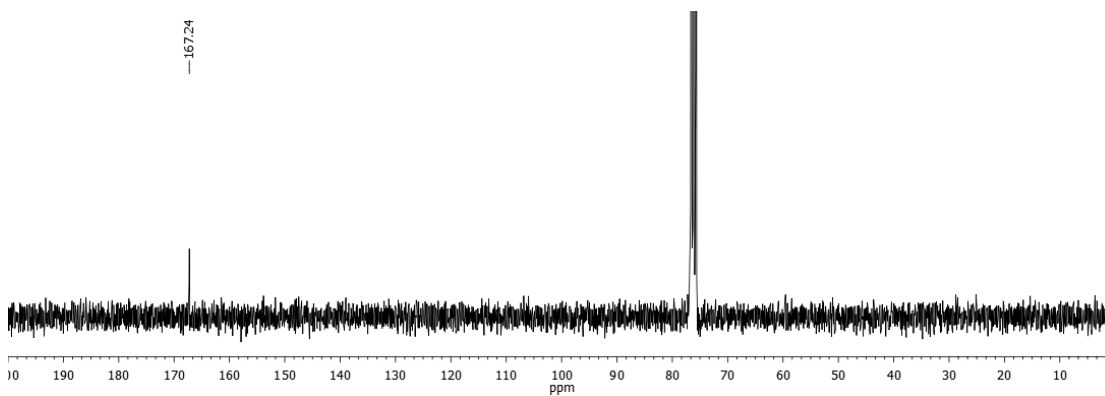
### 3,6-Dichloro-1,2,4,5-tetrazine (2.7e)



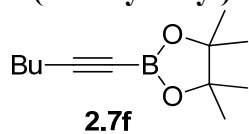
Chemical Formula: C<sub>2</sub>Cl<sub>2</sub>N<sub>4</sub>  
Exact Mass: 149.9500  
Molecular Weight: 150.9542

**2.7e**

<sup>13</sup>C NMR 75.5 MHz, CDCl<sub>3</sub>



**2-(1-Hexyn-1-yl)-4,4,5,5,-tetramethyl-1,3,2-dioxaborolane (2.7f)**

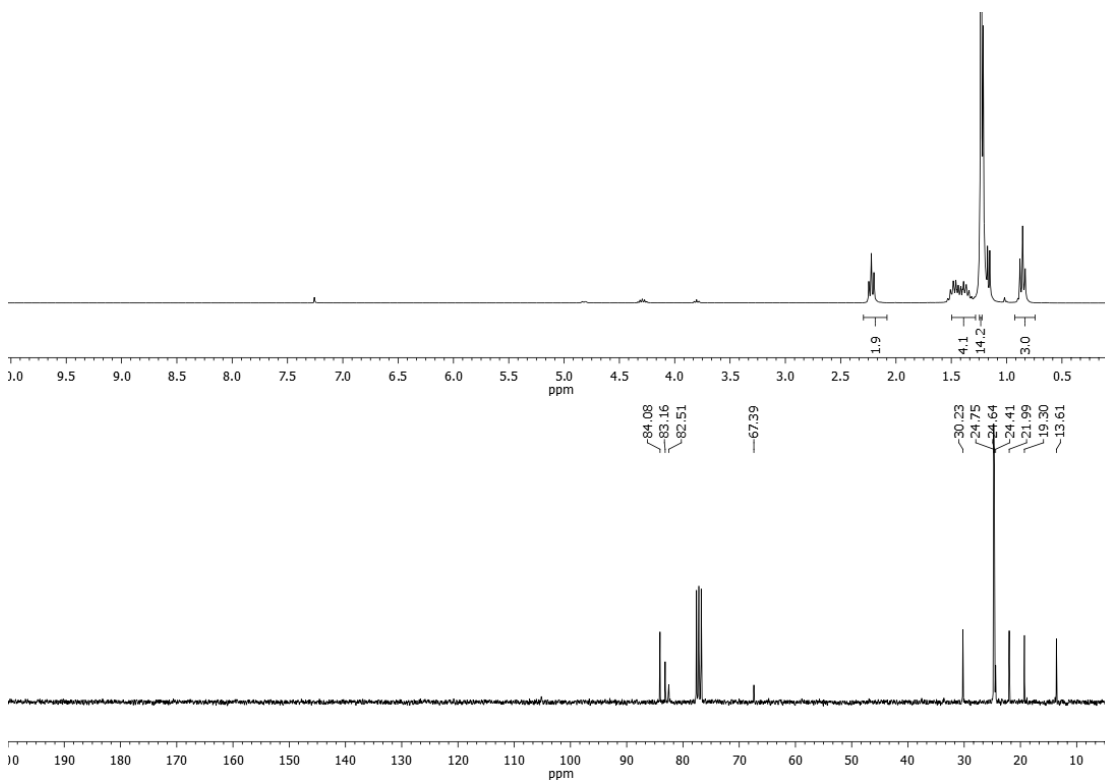


Chemical Formula: C<sub>12</sub>H<sub>21</sub>BO<sub>2</sub>

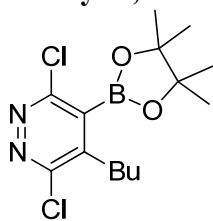
Exact Mass: 208.1635

Molecular Weight: 208.1049

<sup>1</sup>H NMR 300 MHz, <sup>13</sup>C NMR 75.5 MHz, CDCl<sub>3</sub>



### 4-Butyl-3,6-dichloro-5-(4,4,5,5-tetramethyl-1,3,2-dioxaborolan-2-yl)pyridazine (2.7)



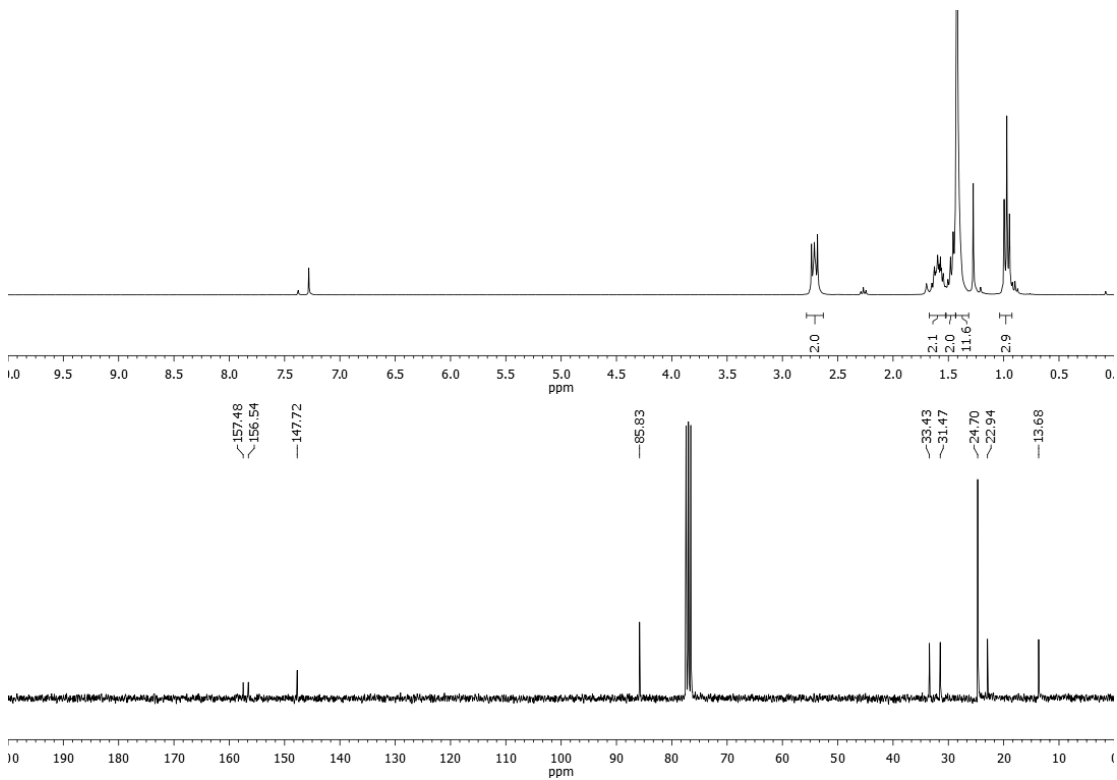
Chemical Formula:  $C_{14}H_{21}BCl_2N_2O_2$

Exact Mass: 330.1073

Molecular Weight: 331.0457

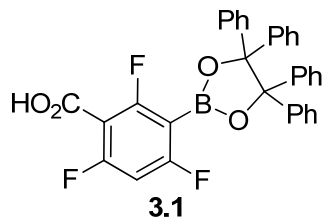
**2.7**

$^1H$  NMR 300 MHz,  $^{13}C$  NMR 75.5 MHz,  $CDCl_3$



## Appendix E.2. NMR spectra for Chapter 3

### 2,4,6-Trifluoro-3-(4,4,5,5-tetraphenyl-1,3,2-dioxaborolan-2-yl)benzoic acid (3.1)

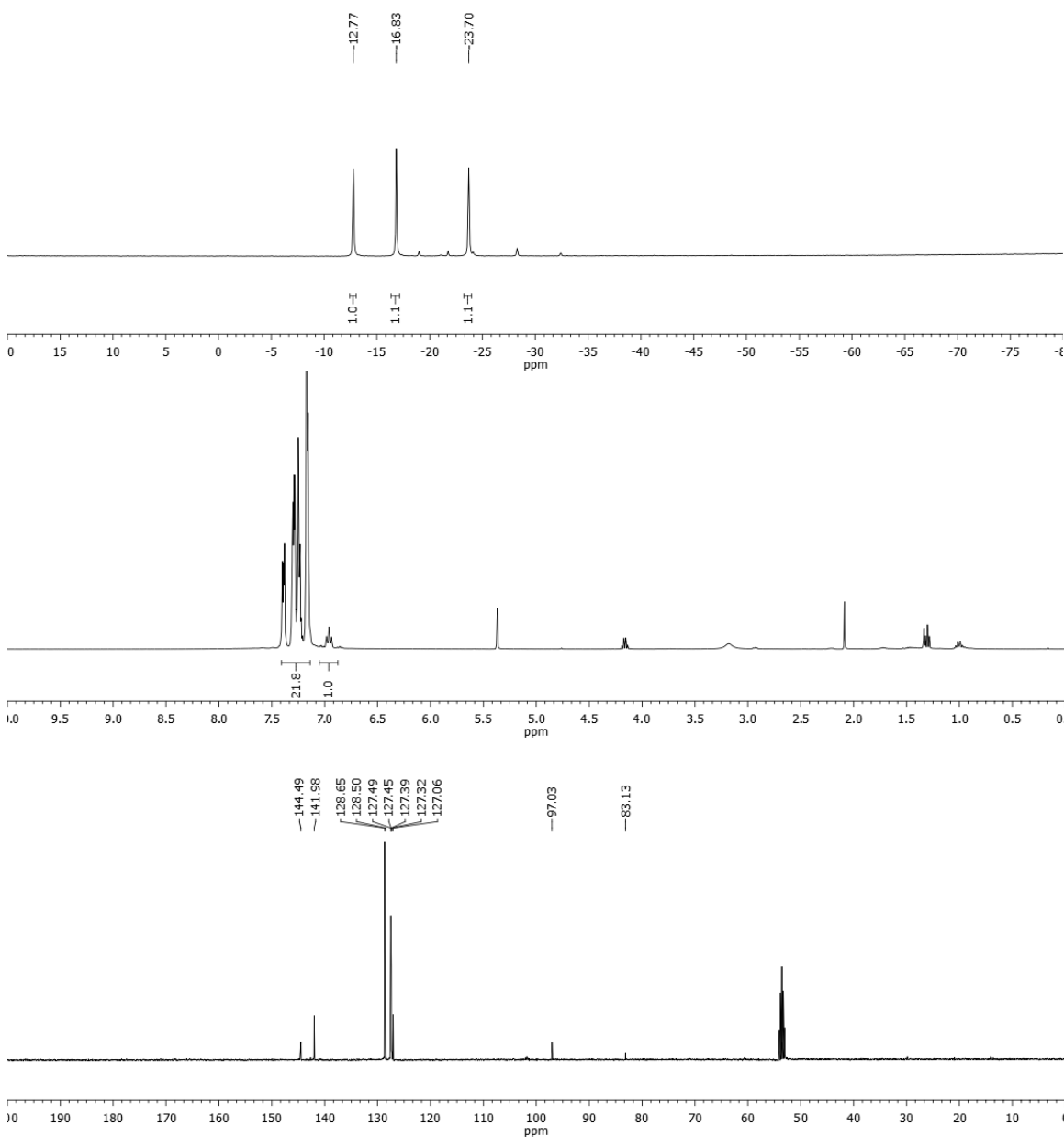


Chemical Formula:  $C_{33}H_{22}BF_3O_4$

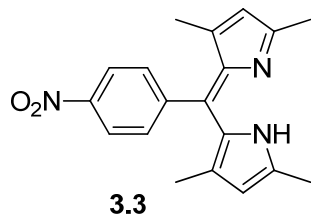
Exact Mass: 550.1563

Molecular Weight: 550.3316

$^{19}F$  NMR 282.4 MHz,  $^1H$  NMR 400 MHz,  $^{13}C$  NMR 100.6 MHz,  $CD_2Cl_2$



**(Z)-2-((3,5-Dimethyl-2H-pyrrol-2-ylidene)(4-nitrophenyl)methyl)-3,5-dimethyl-1H-pyrrole (3.3)**

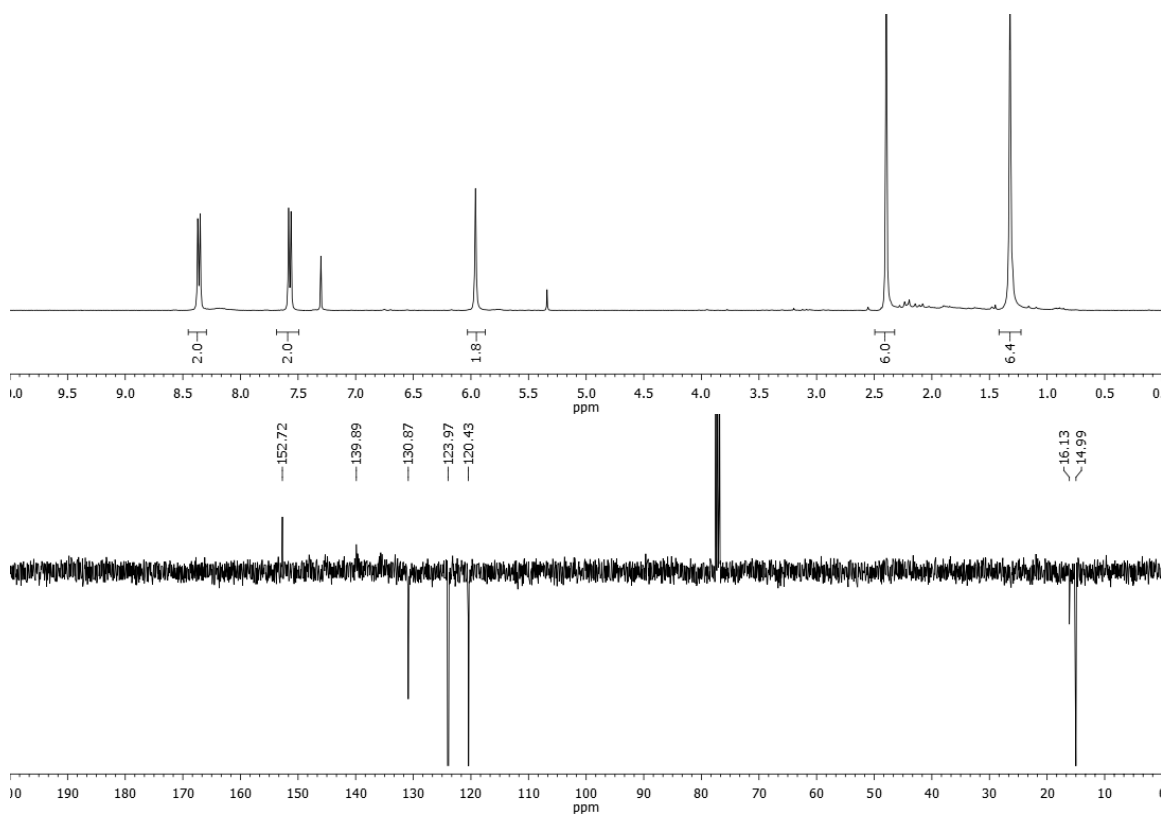


Chemical Formula: C<sub>19</sub>H<sub>19</sub>N<sub>3</sub>O<sub>2</sub>

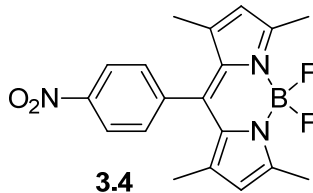
Exact Mass: 321.1477

Molecular Weight: 321.3731

<sup>1</sup>H NMR 400 MHz, <sup>13</sup>C NMR 100.6 MHz, CDCl<sub>3</sub>



### BODIPY-NO<sub>2</sub> (3.4)

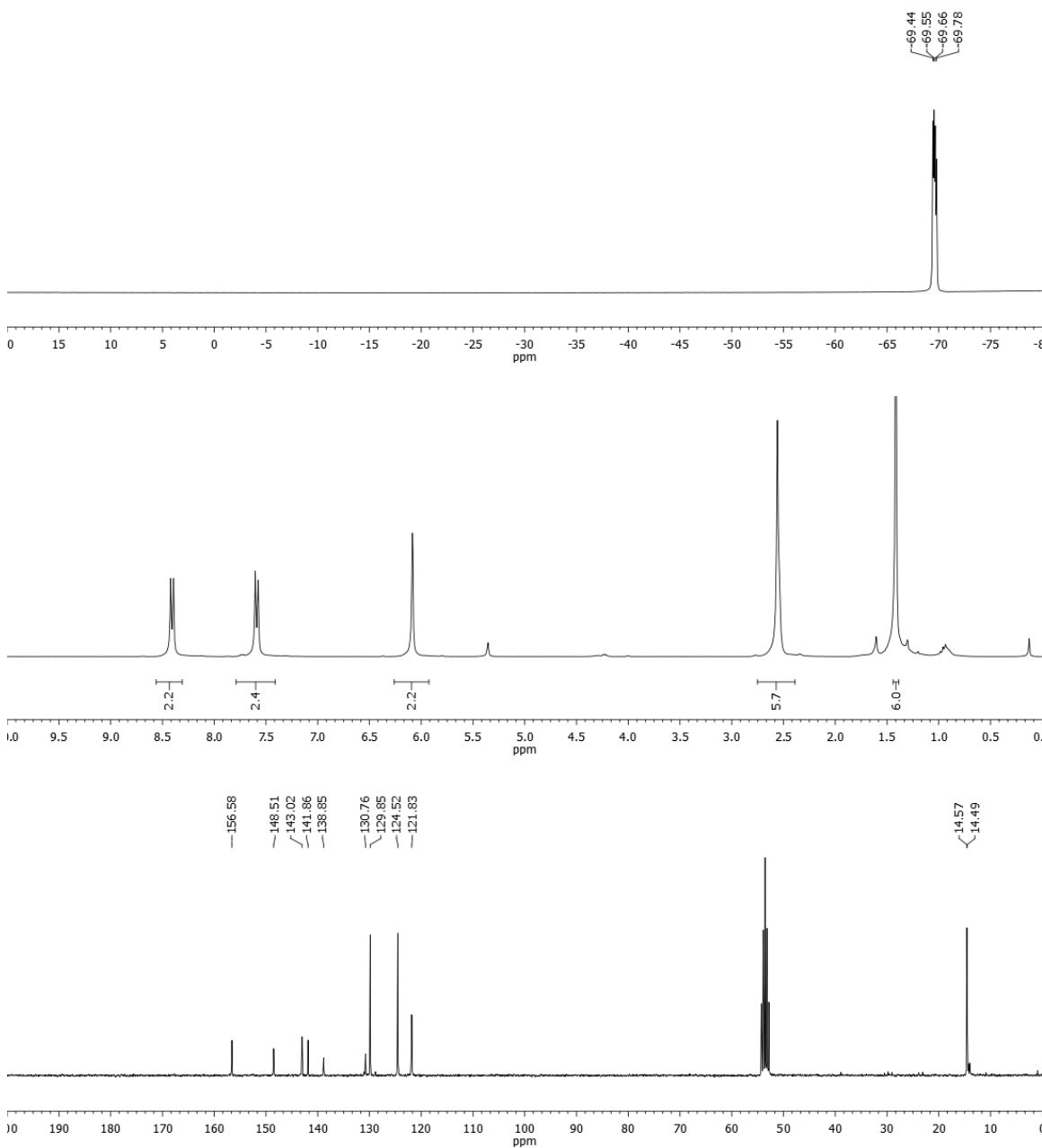


Chemical Formula: C<sub>19</sub>H<sub>18</sub>BF<sub>2</sub>N<sub>3</sub>O<sub>2</sub>

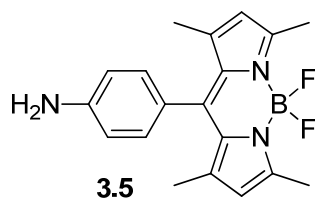
Exact Mass: 369.1460

Molecular Weight: 369.1729

<sup>19</sup>F NMR 282.4 MHz, <sup>1</sup>H NMR 300 MHz, <sup>13</sup>C NMR 75.5 MHz, CD<sub>2</sub>Cl<sub>2</sub>



### BODIPY-NH<sub>2</sub> (3.5)

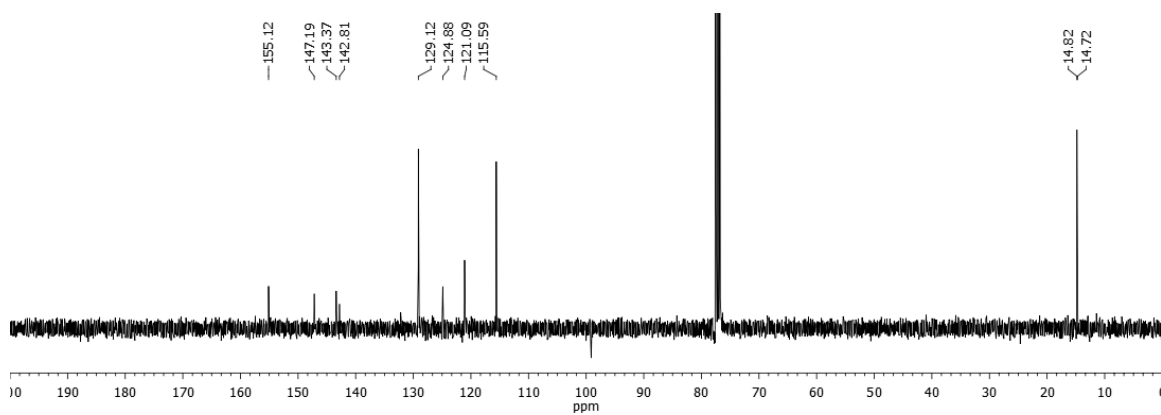
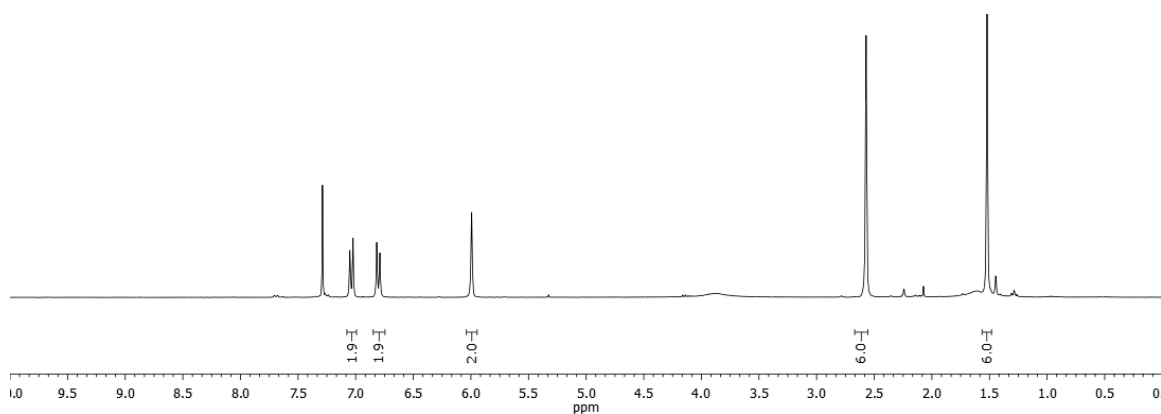
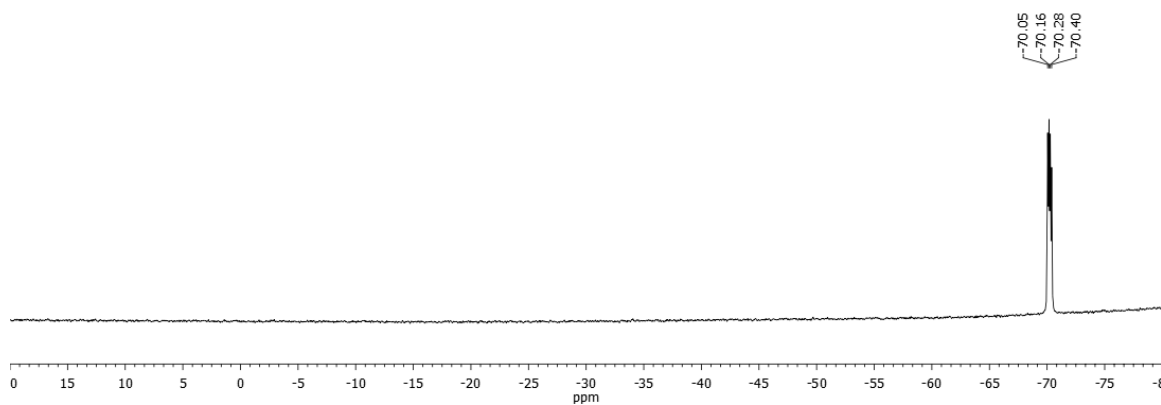


Chemical Formula: C<sub>19</sub>H<sub>20</sub>BF<sub>2</sub>N<sub>3</sub>

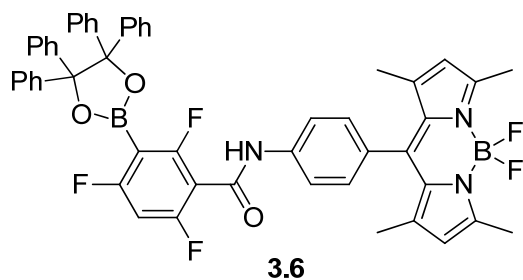
Exact Mass: 339.1718

Molecular Weight: 339.1900

<sup>19</sup>F NMR 282.4 MHz, <sup>1</sup>H NMR 300 MHz, <sup>13</sup>C NMR 100.6 MHz, CDCl<sub>3</sub>



### BODIPY-boronate (3.6)

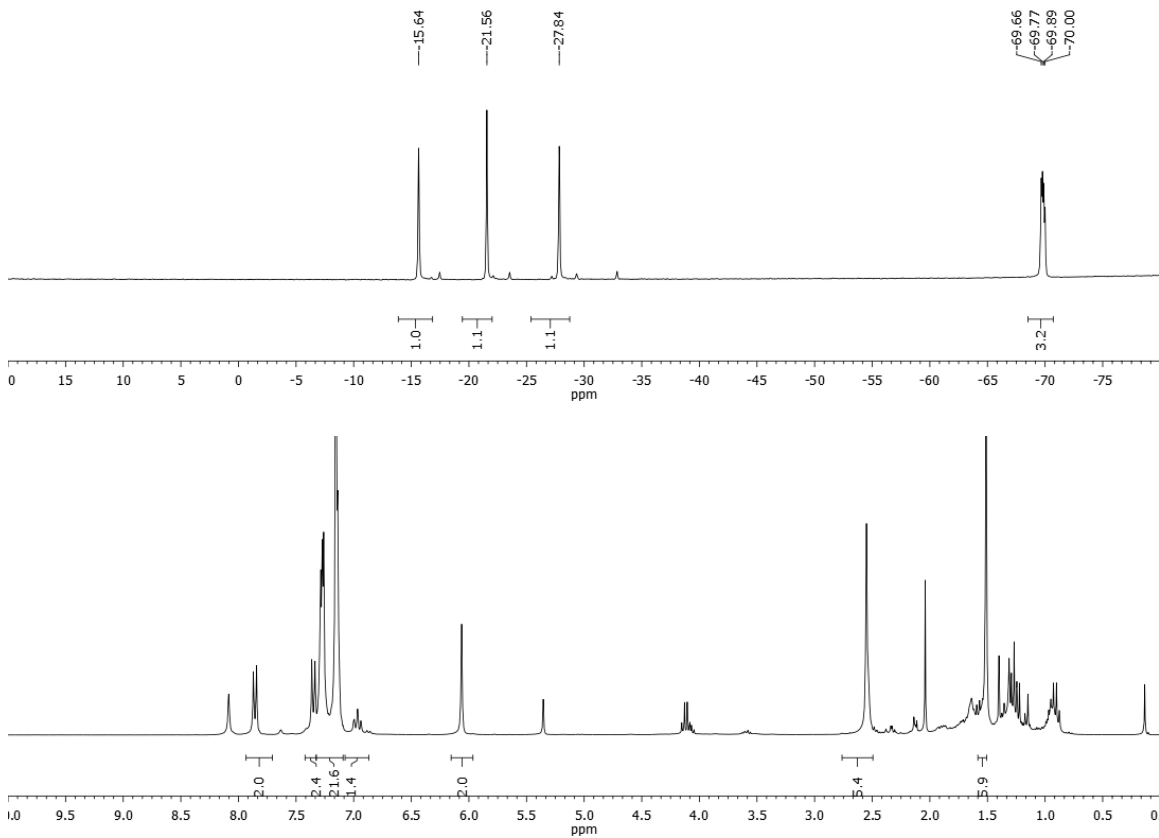


Chemical Formula:  $C_{52}H_{40}B_2F_5N_3O_3$

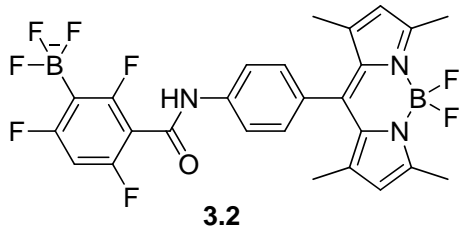
Exact Mass: 871.3176

Molecular Weight: 871.5063

$^{19}F$  NMR 282.4 MHz,  $^1H$  NMR 300 MHz,  $CD_2Cl_2$



### BODIPY-ArBF3 (3.2)

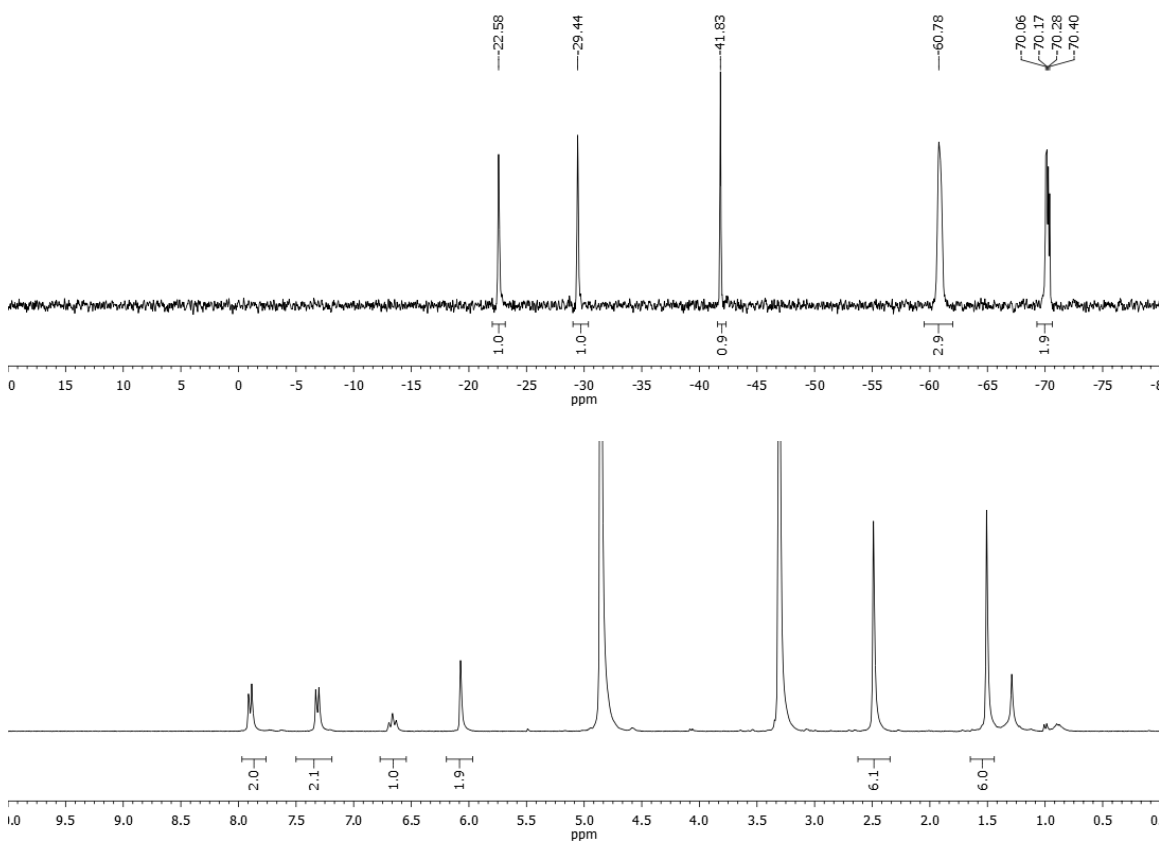


Chemical Formula:  $C_{26}H_{20}B_2F_8N_3O^-$

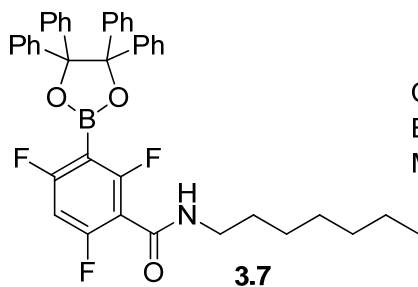
Exact Mass: 564.1670

Molecular Weight: 564.0663

$^{19}F$  NMR 282.4 MHz,  $^1H$  NMR 300 MHz,  $^{13}C$  NMR 100.6 MHz,  $d_4$ -MeOD



**2,4,6-Trifluoro-N-heptyl-3-(4,4,5,5-tetraphenyl-1,3,2-dioxaborolan-2-yl) benzamide (3.7)**

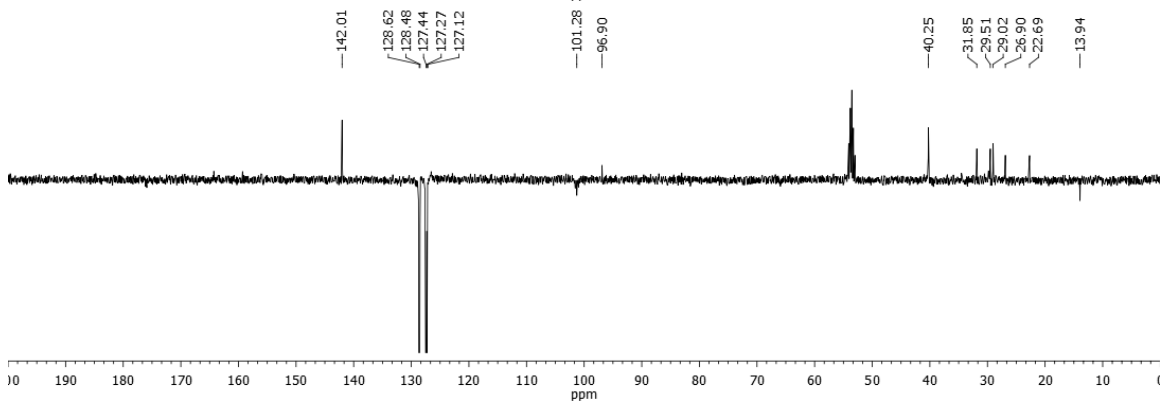
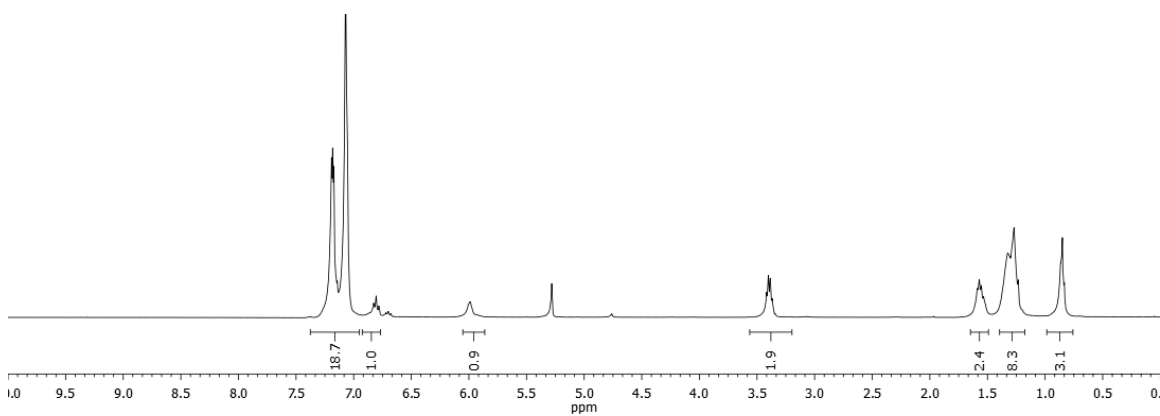
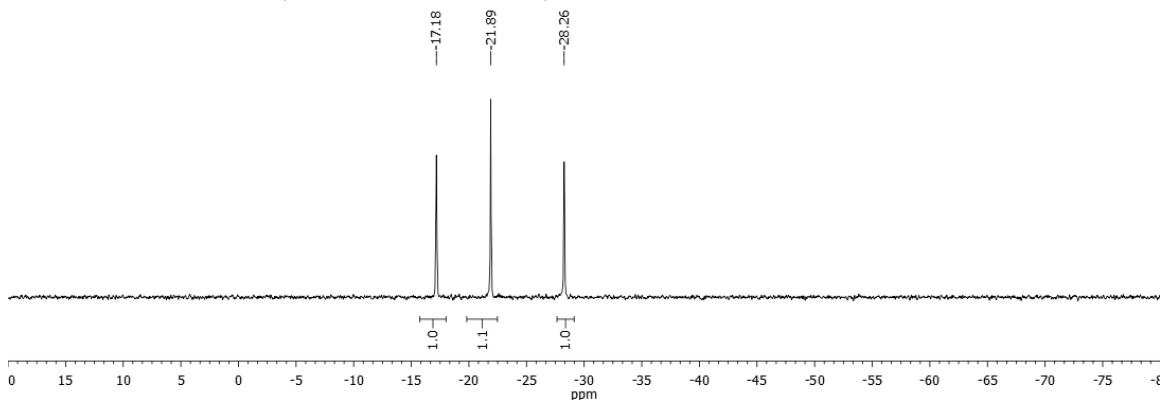


Chemical Formula:  $C_{40}H_{37}BF_3NO_3$

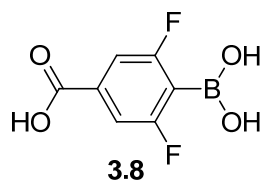
Exact Mass: 647.2819

Molecular Weight: 647.5329

$^{19}F$  NMR 282.4 MHz,  $^1H$  NMR 400 MHz,  $^{13}C$  NMR 100.6 MHz  $CD_2Cl_2$



### 4-Borono-3,5-difluorobenzoic acid (3.8)

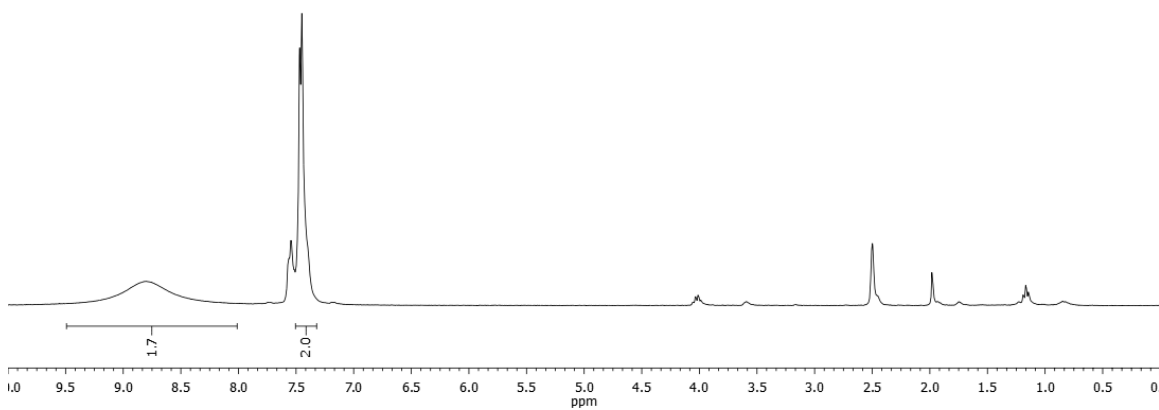
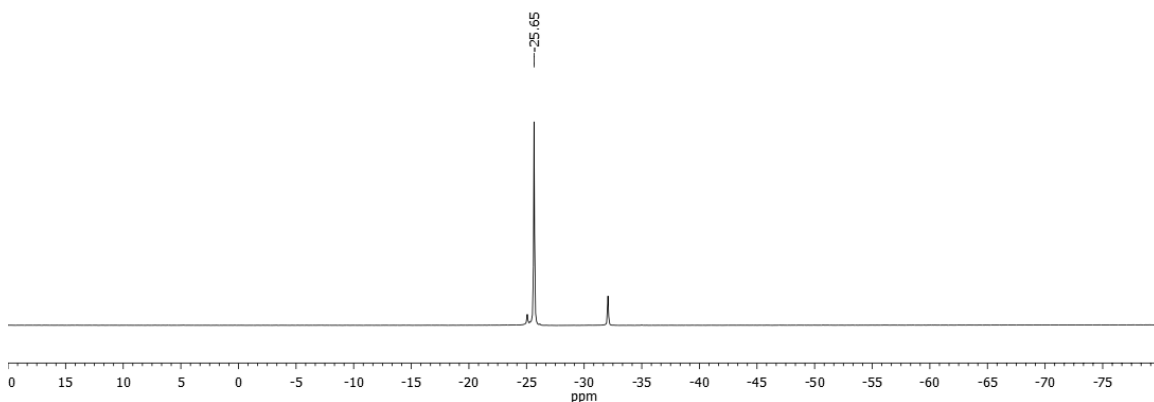


Chemical Formula: C<sub>7</sub>H<sub>5</sub>BF<sub>2</sub>O<sub>4</sub>

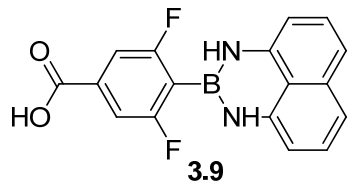
Exact Mass: 202.0249

Molecular Weight: 201.9200

<sup>19</sup>F NMR 282.4 MHz, <sup>1</sup>H NMR 300 MHz, *d*<sub>6</sub>-DMSO



### 3,5-Difluoro-4-(*1H*-naphtho[1,8-de]-1,3,2-diazaborinyl)benzoic acid (3.9)

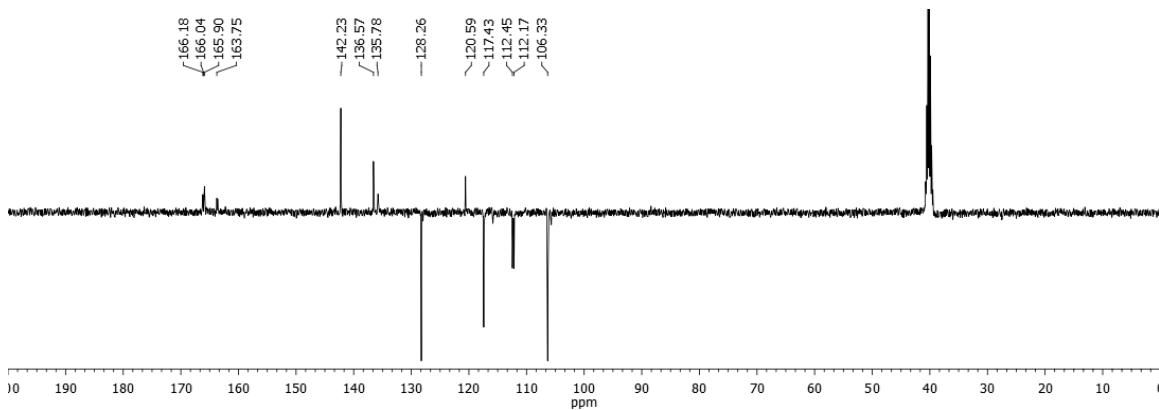
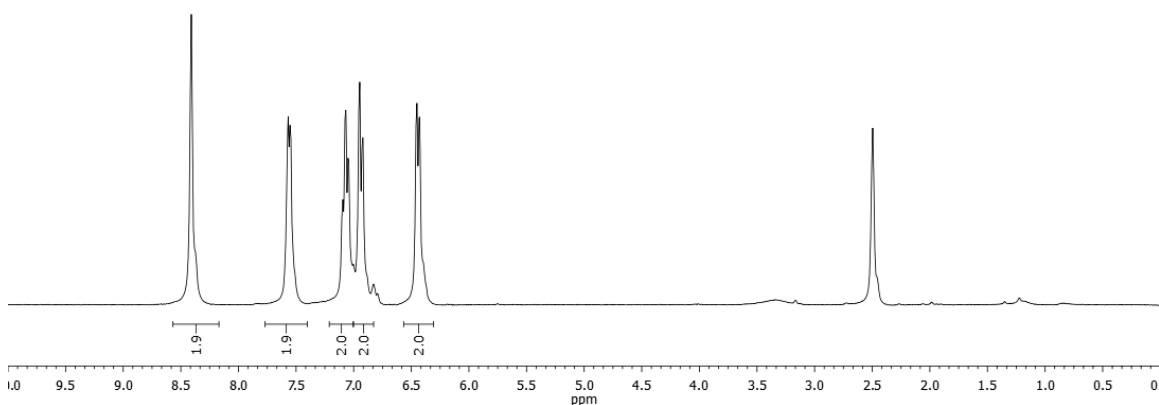
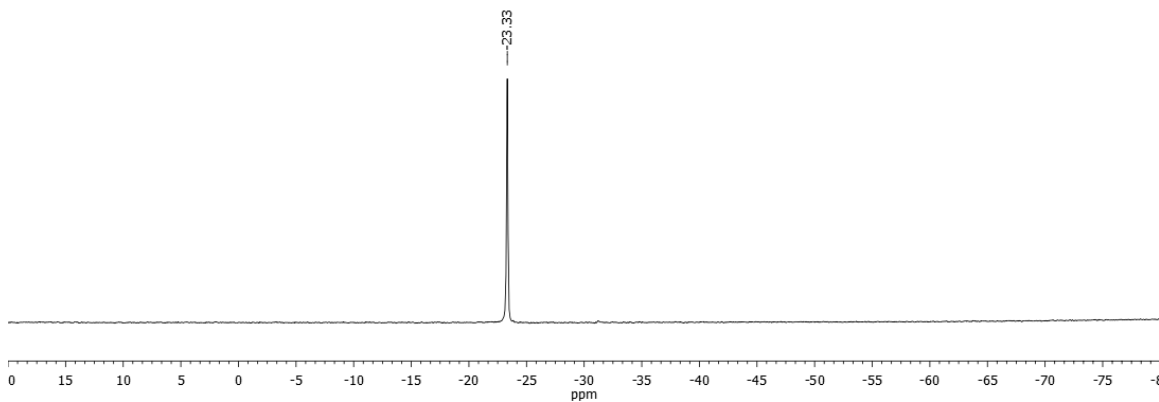


Chemical Formula: C<sub>17</sub>H<sub>11</sub>BF<sub>2</sub>N<sub>2</sub>O<sub>2</sub>

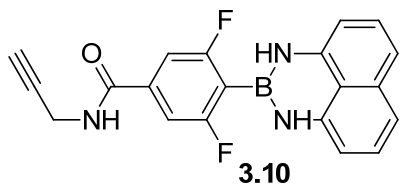
Exact Mass: 324.0882

Molecular Weight: 324.0892

<sup>19</sup>F NMR 282.4 MHz, <sup>1</sup>H NMR 300 MHz, <sup>13</sup>C NMR 100.6 MHz, *d*<sub>6</sub>-DMSO



**3,5-Difluoro-4-(1*H*-naphtho[1,8-*de*][1,3,2]diazaborinin-2(3*H*)-yl)-*N*-(prop-2-yn-1-yl) benzamide (3.10)**

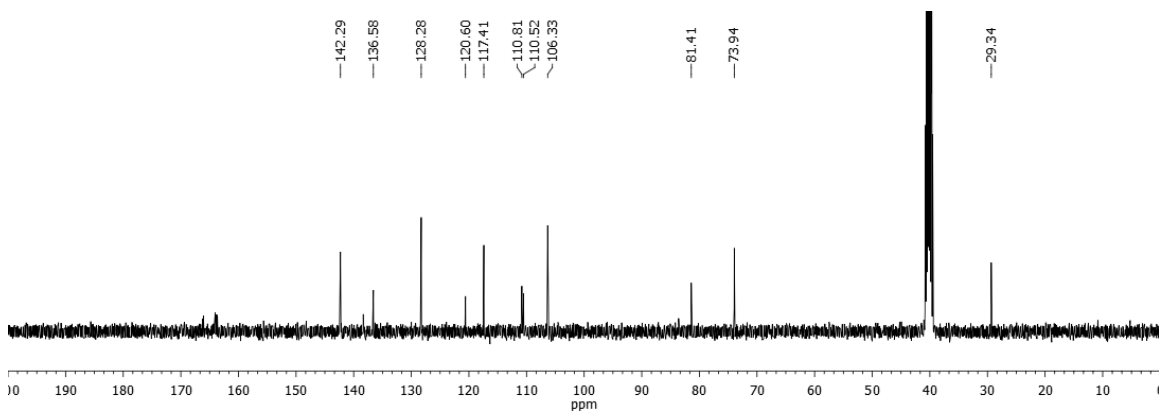
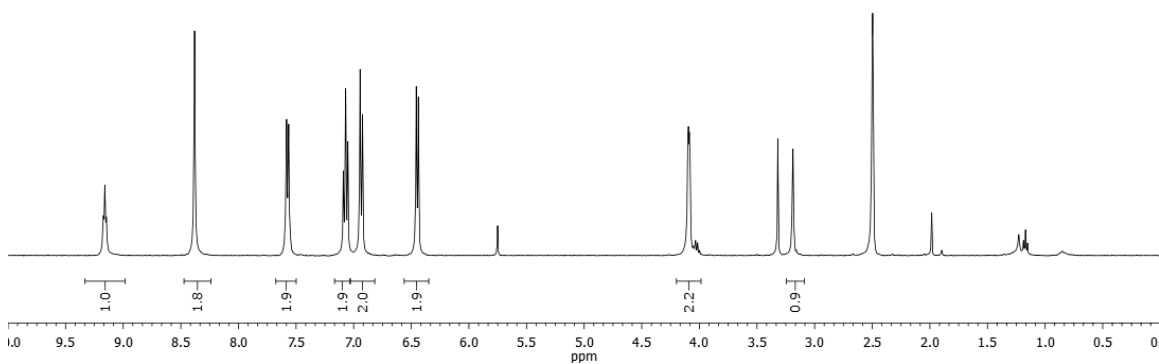
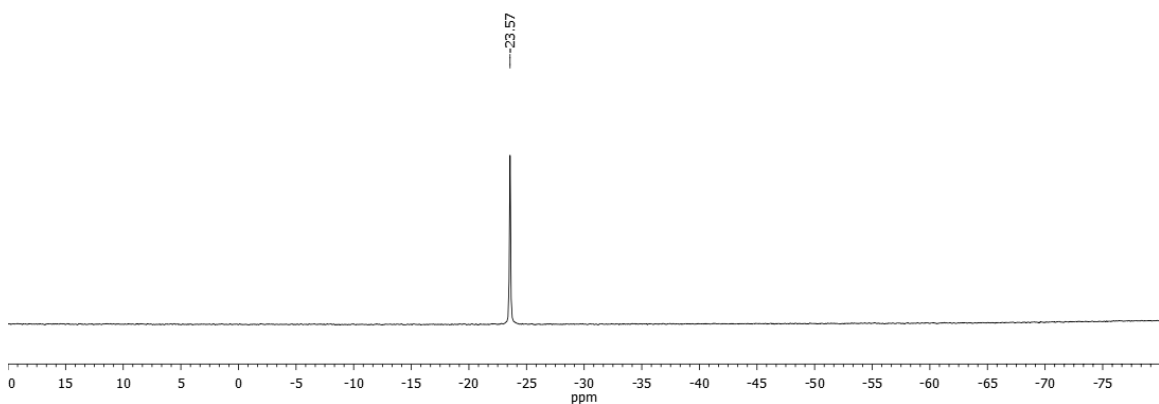


Chemical Formula: C<sub>20</sub>H<sub>14</sub>BF<sub>2</sub>N<sub>3</sub>O

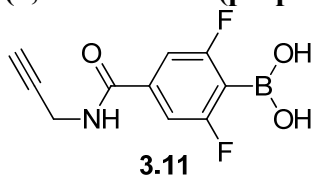
Exact Mass: 361.1198

Molecular Weight: 361.1525

<sup>19</sup>F NMR 282.4 MHz, <sup>1</sup>H NMR 400 MHz, <sup>13</sup>C NMR 100.6 MHz, *d*<sub>6</sub>-DMSO



**(2,6-Difluoro-4-(prop-2-yn-1-ylcarbamoyl)phenyl)boronic acid (3.11)**

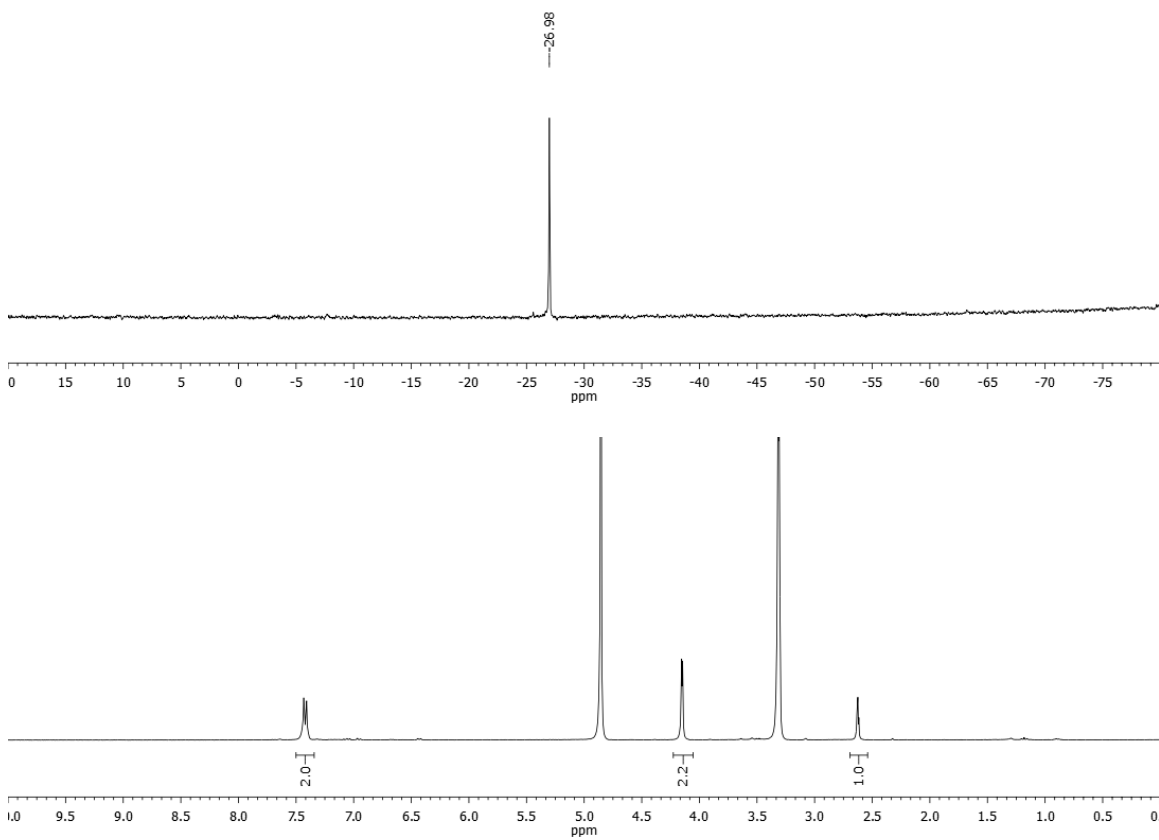


Chemical Formula:  $C_{10}H_8BF_2NO_3$

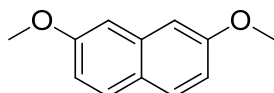
Exact Mass: 239.0565

Molecular Weight: 238.9832

$^{19}F$  NMR 282.4 MHz,  $^1H$  NMR 300 MHz,  $d_6$ -MeOD



## 2,7-Dimethoxynaphthalene (3.12)



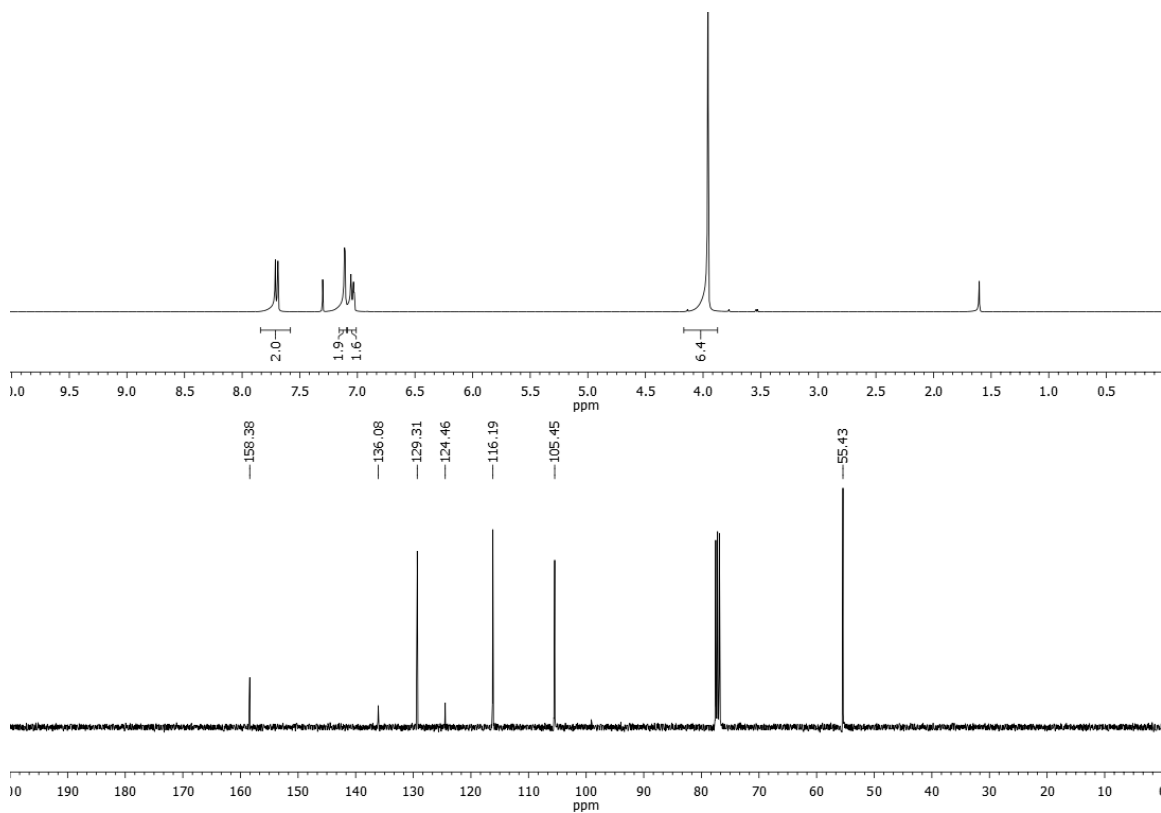
3.12

Chemical Formula: C<sub>12</sub>H<sub>12</sub>O<sub>2</sub>

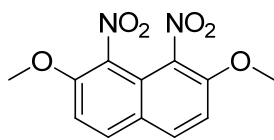
Exact Mass: 188.0837

Molecular Weight: 188.2225

<sup>1</sup>H NMR 400 MHz, <sup>13</sup>C NMR 100.6 MHz, CDCl<sub>3</sub>



### 1,8-Dinitro-2,7-dimethoxynaphthalene(3.13)



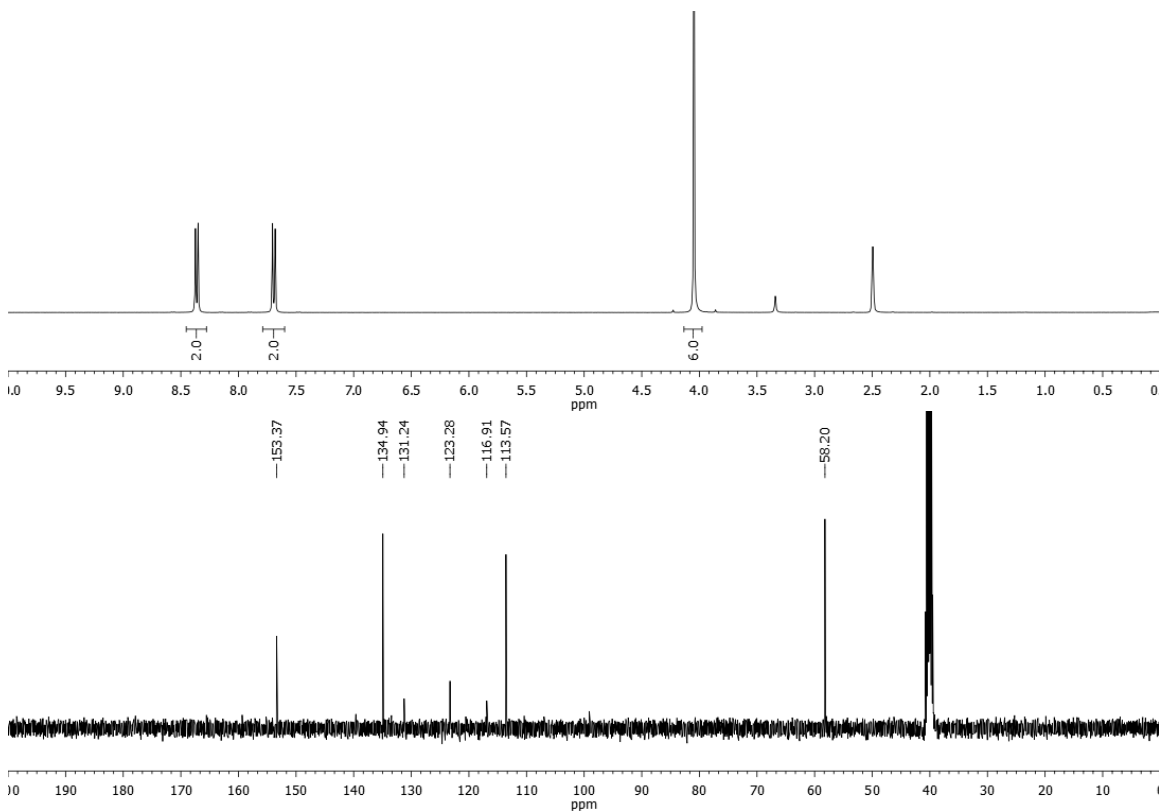
**3.13**

Chemical Formula: C<sub>12</sub>H<sub>10</sub>N<sub>2</sub>O<sub>6</sub>

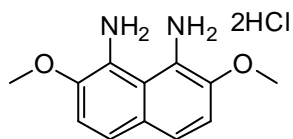
Exact Mass: 278.0539

Molecular Weight: 278.2176

<sup>1</sup>H NMR 400 MHz, <sup>13</sup>C NMR 100.6 MHz, *d*<sub>6</sub>-DMSO



### 1,8-Diamino-2,7-dimethoxynaphthalene dihydrochloride (DiDiAN·2HCl) (3.14)



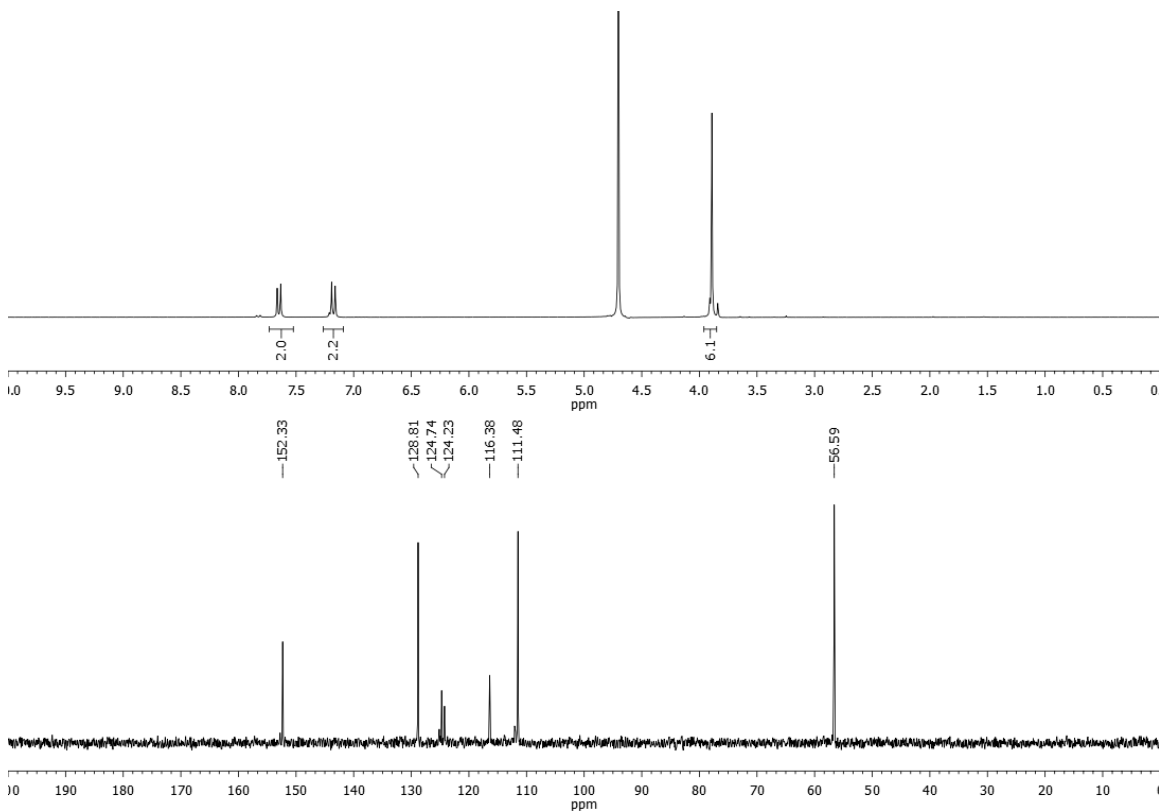
Chemical Formula:  $C_{12}H_{14}N_2O_2$

Exact Mass: 218.1055

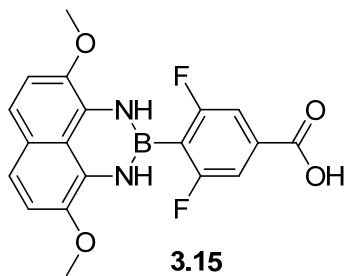
Molecular Weight: 218.2518

3.14

$^1H$  NMR 300 MHz,  $^{13}C$  NMR 75.5 MHz,  $D_2O$



**4-(4,9-dimethoxy-1*H*-naphtho[1,8-*de*][1,3,2]diazaborinin-2(3*H*)-yl)-3,5-difluorobenzoic acid (3.15)**



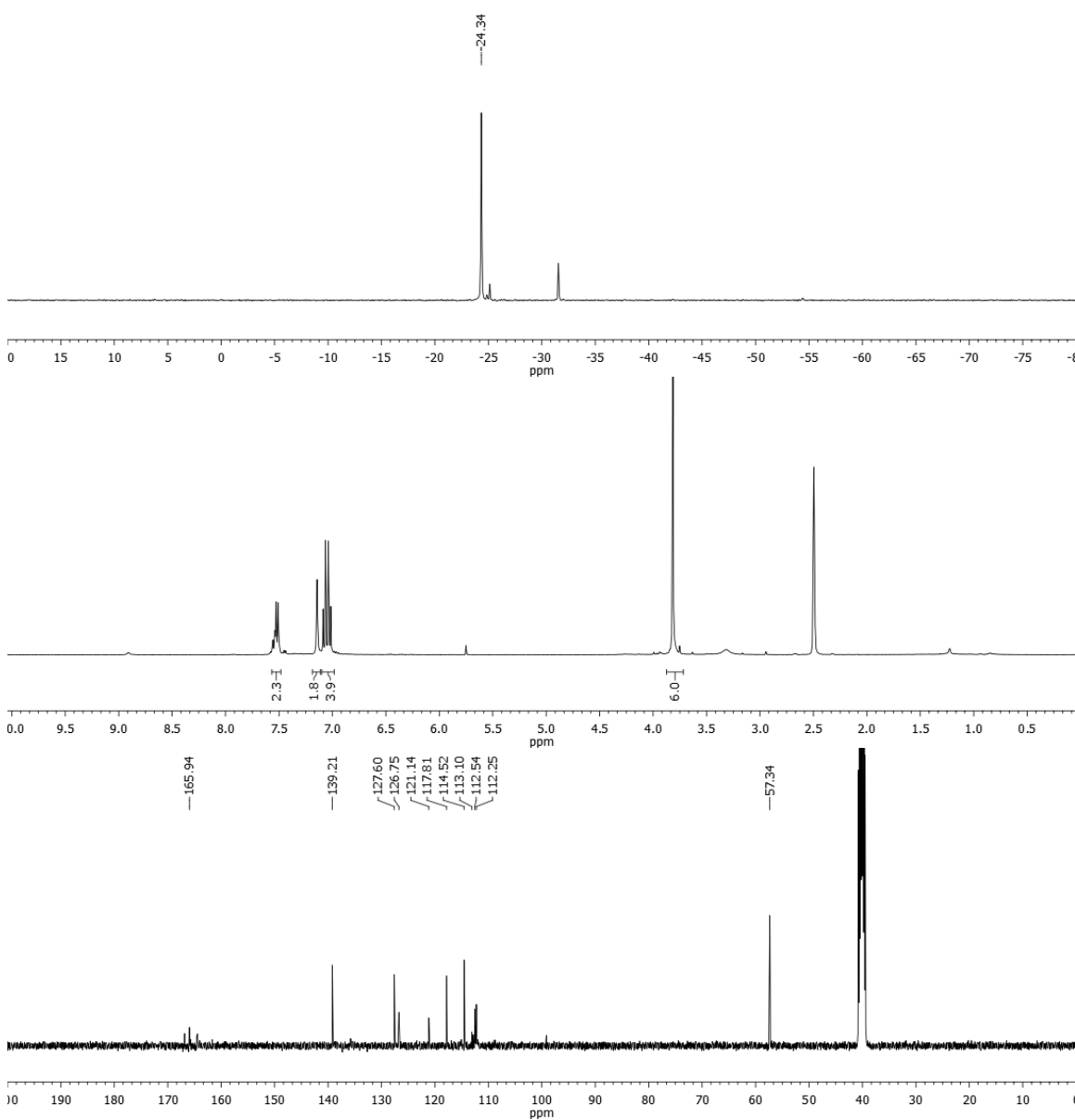
Chemical Formula: C<sub>19</sub>H<sub>15</sub>BF<sub>2</sub>N<sub>2</sub>O<sub>4</sub>

Exact Mass: 384.1093

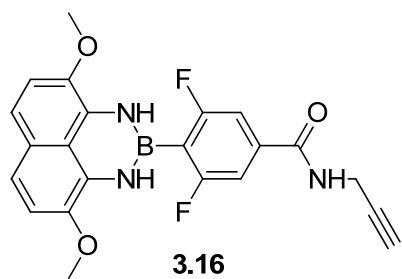
Molecular Weight: 384.1412

**3.15**

<sup>19</sup>F NMR 282.4 MHz, <sup>1</sup>H NMR 400 MHz, <sup>13</sup>C NMR 100.6 MHz, *d*<sub>6</sub>-DMSO

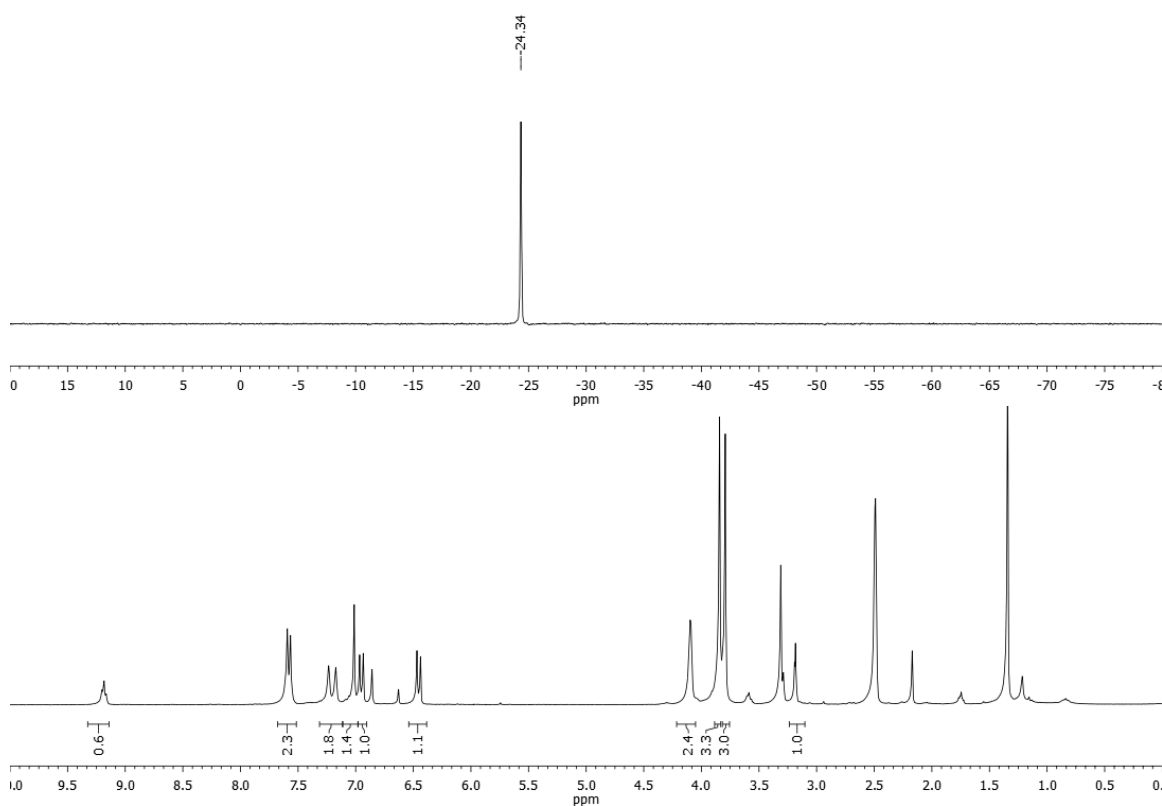


**4-(4,9-dimethoxy-1*H*-naphtho[1,8-*de*][1,3,2]diazaborinin-2(3*H*)-yl)-3,5-difluoro-*N*-(prop-2-yn-1-yl)benzamide (3.16)**

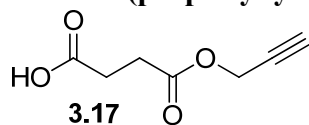


Chemical Formula: C<sub>22</sub>H<sub>18</sub>BF<sub>2</sub>N<sub>3</sub>O<sub>3</sub>  
Exact Mass: 421.1409  
Molecular Weight: 421.2044

<sup>19</sup>F NMR 282.4 MHz, <sup>1</sup>H NMR 300 MHz, *d*<sub>6</sub>-DMSO



### 4-Oxo-4-(prop-2-ynoxy)butanoic acid (3.17)

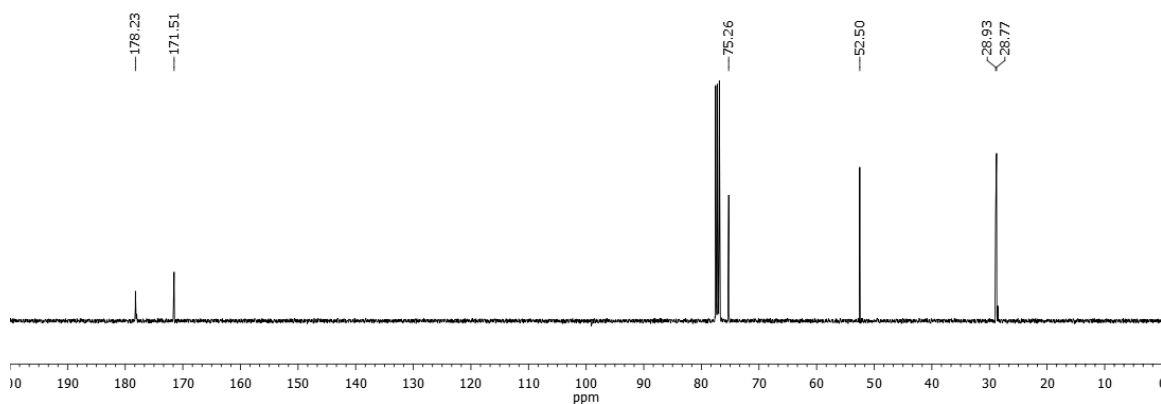
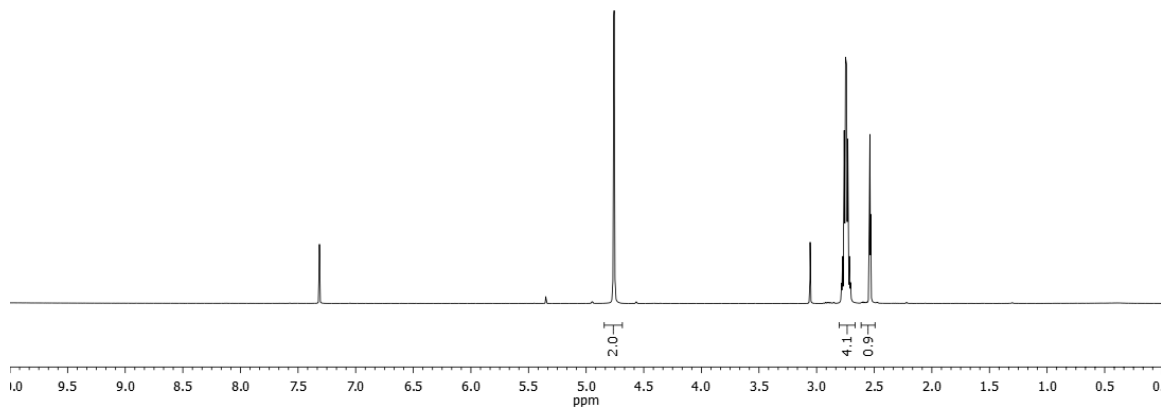


Chemical Formula: C<sub>7</sub>H<sub>8</sub>O<sub>4</sub>

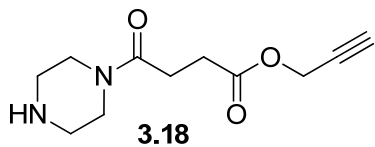
Exact Mass: 156.0423

Molecular Weight: 156.1360

<sup>1</sup>H NMR 400 MHz, <sup>13</sup>C NMR 100.6 MHz, CDCl<sub>3</sub>



**Prop-2-yn-1-yl 4-oxo-4-(piperazin-1-yl)butanoate (3.18)**

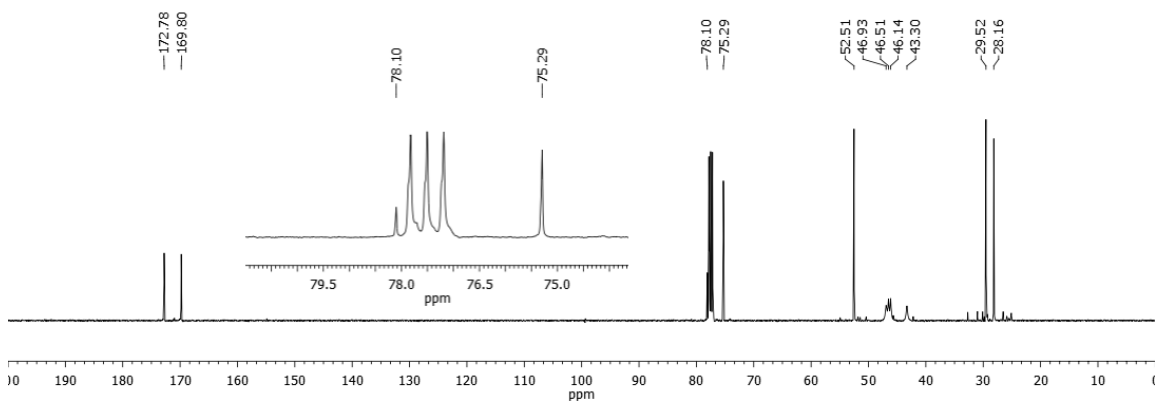
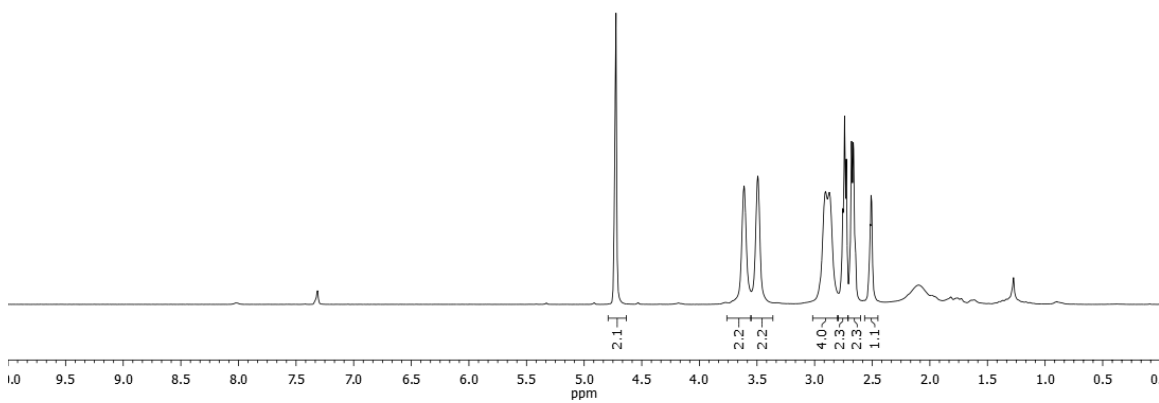


Chemical Formula: C<sub>11</sub>H<sub>16</sub>N<sub>2</sub>O<sub>3</sub>

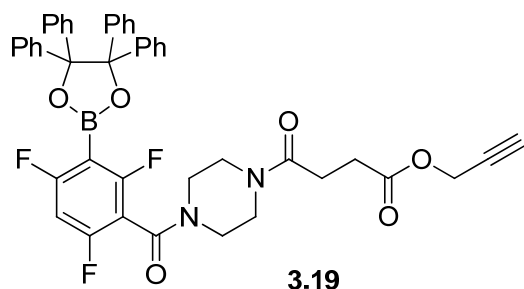
Exact Mass: 224.1161

Molecular Weight: 224.2563

<sup>1</sup>H NMR 400 MHz, <sup>13</sup>C NMR 100.6 MHz, CDCl<sub>3</sub>



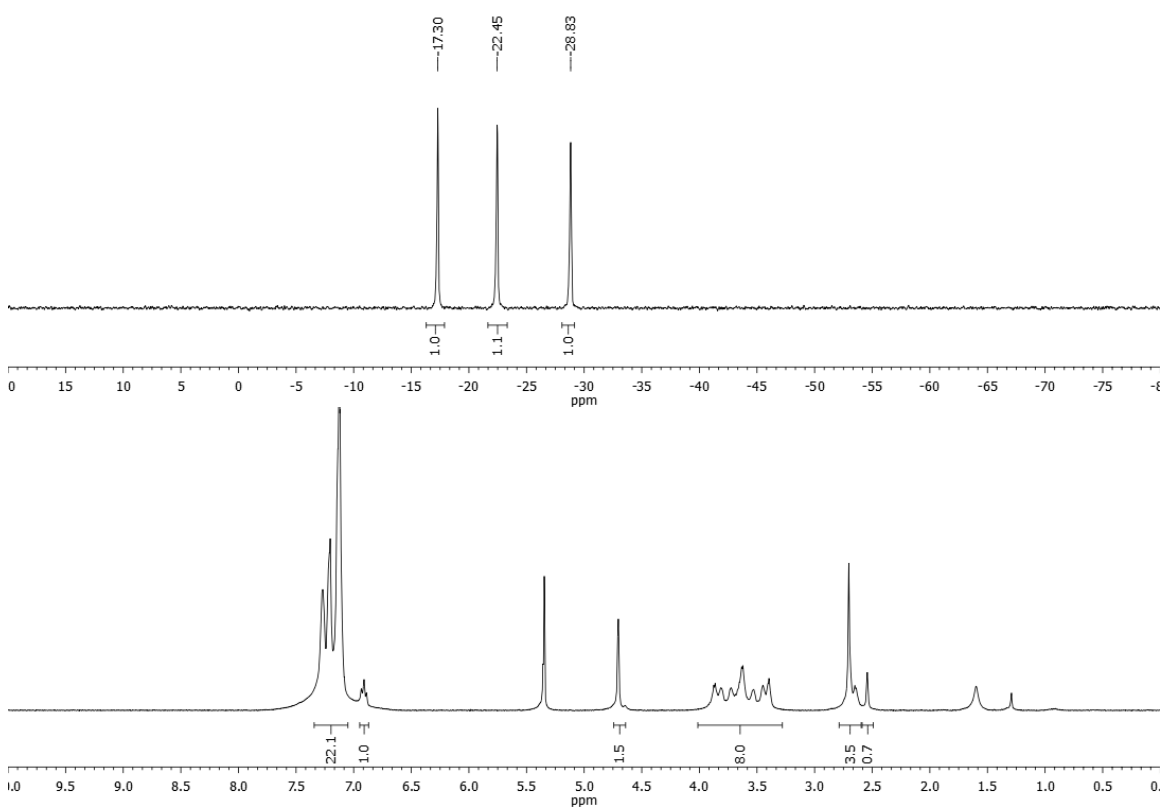
**Prop-2-yn-1-yl 4-oxo-4-(4-(2, 4, 6-trifluoro-3-(4, 4, 5, 5-tetraphenyl-1, 3, 2-dioxaborolan-2-yl)benzoyl)piperazin-1-yl)butanoate (3.19)**



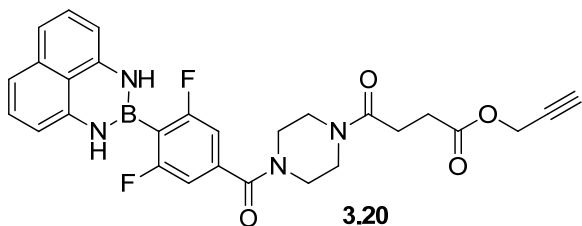
Chemical Formula: C<sub>44</sub>H<sub>36</sub>BF<sub>3</sub>N<sub>2</sub>O<sub>6</sub>  
Exact Mass: 756.2619  
Molecular Weight: 756.5726

**3.19**

<sup>19</sup>F NMR 282.4 MHz, <sup>1</sup>H NMR 400 MHz, CD<sub>2</sub>Cl<sub>2</sub>



**Prop-2-yn-1-yl 4-(4-(3,5-difluoro-4-(1*H*-naphtho[1,8-de][1,3,2]diazaborinin-2(3*H*)-yl)benzoyl)piperazin-1-yl)-4-oxobutanoate (3.20)**

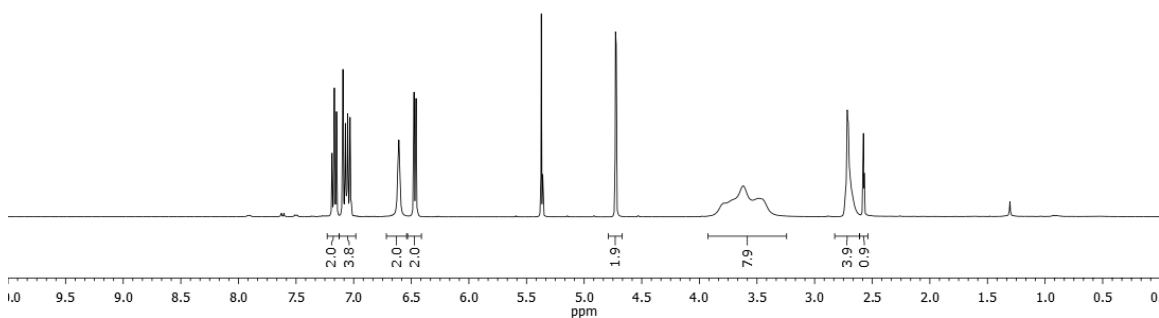
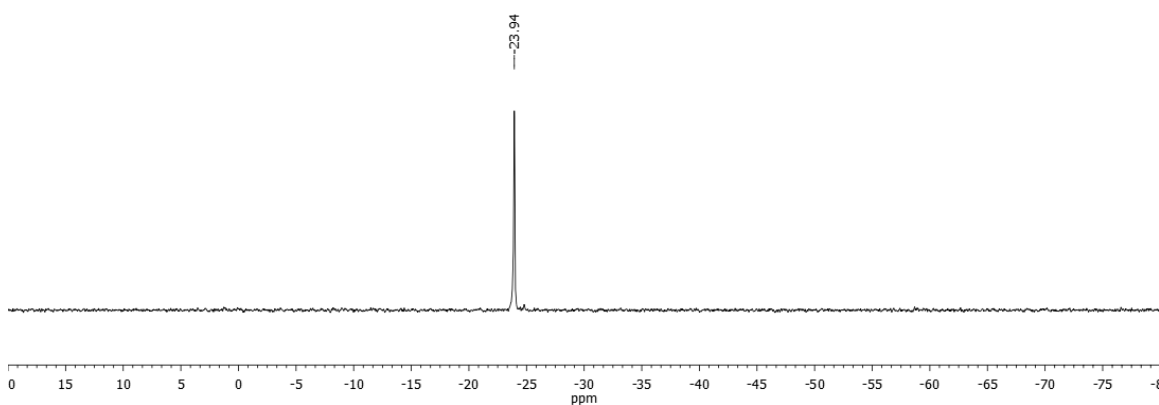


Chemical Formula:  $C_{28}H_{25}BF_2N_4O_4$

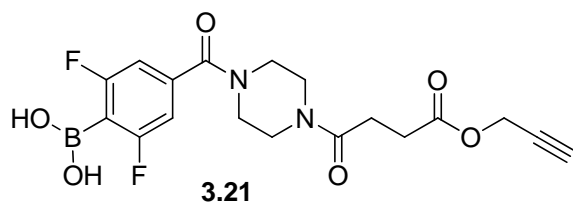
Exact Mass: 530.1937

Molecular Weight: 530.3303

$^{19}F$  NMR 282.4 MHz,  $^1H$  NMR 400 MHz,  $CD_2Cl_2$



**(2,6-Difluoro-4-(4-(4-oxo-4-(prop-2-yn-1-yloxy)butanoyl)piperazine-1-carbonyl)phenyl)boronic acid (3.21)**

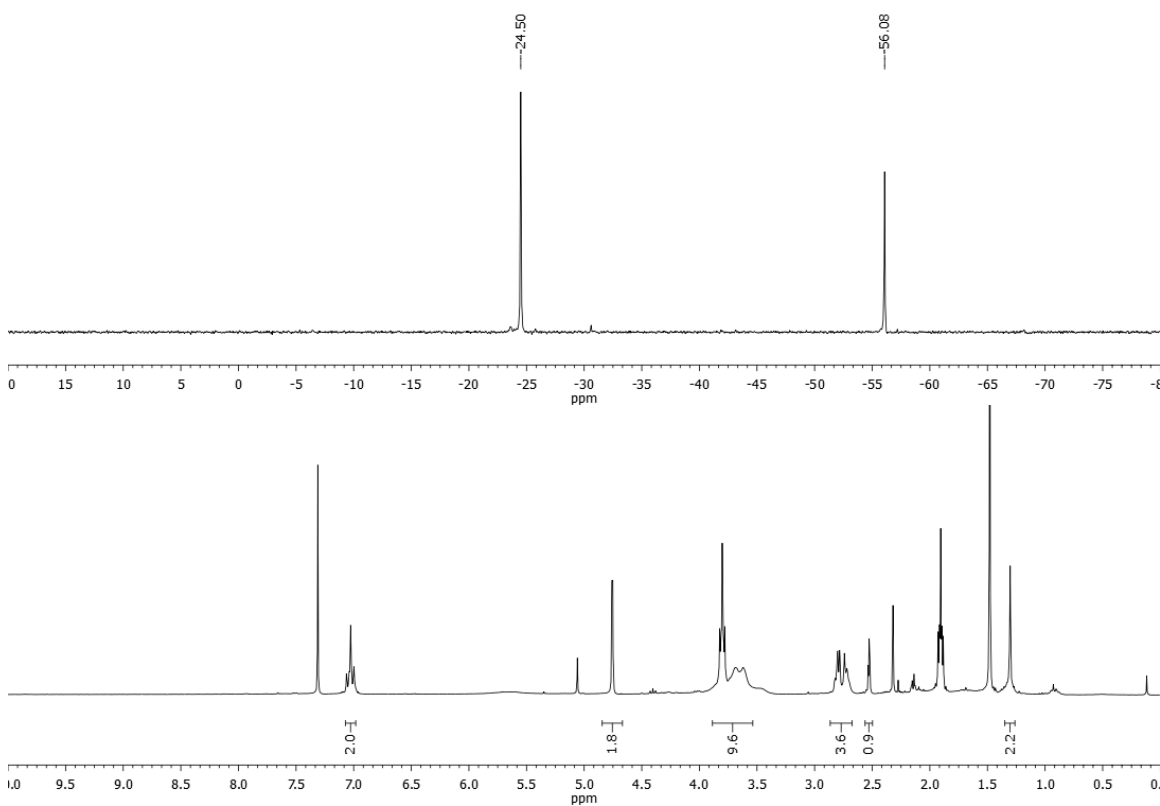


Chemical Formula: C<sub>18</sub>H<sub>19</sub>BF<sub>2</sub>N<sub>2</sub>O<sub>6</sub>

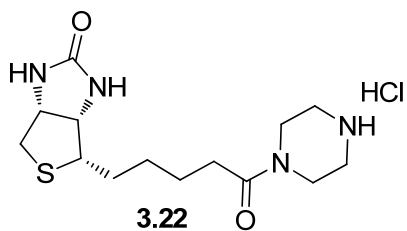
Exact Mass: 408.1304

Molecular Weight: 408.1611

<sup>19</sup>F NMR 282.4 MHz, <sup>1</sup>H NMR 300 MHz, CDCl<sub>3</sub>



### Piperidinyl-biotin·HCl (3.22)

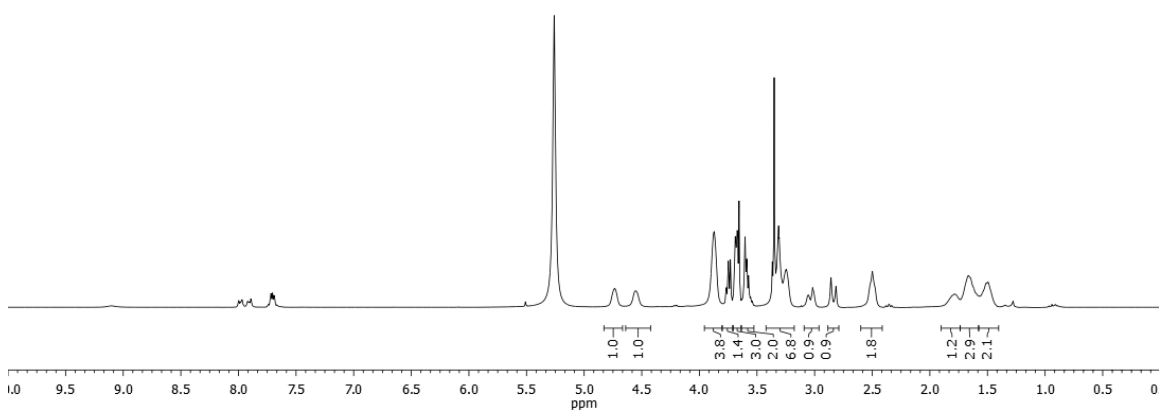


Chemical Formula: C<sub>14</sub>H<sub>25</sub>ClN<sub>4</sub>O<sub>2</sub>S

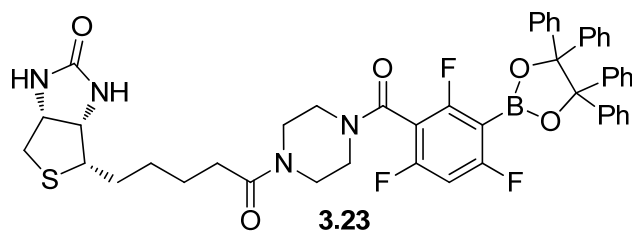
Exact Mass: 348.1387

Molecular Weight: 348.8919

<sup>1</sup>H NMR 300 MHz, CDCl<sub>3</sub>



### Biotin-boronate (3.23)

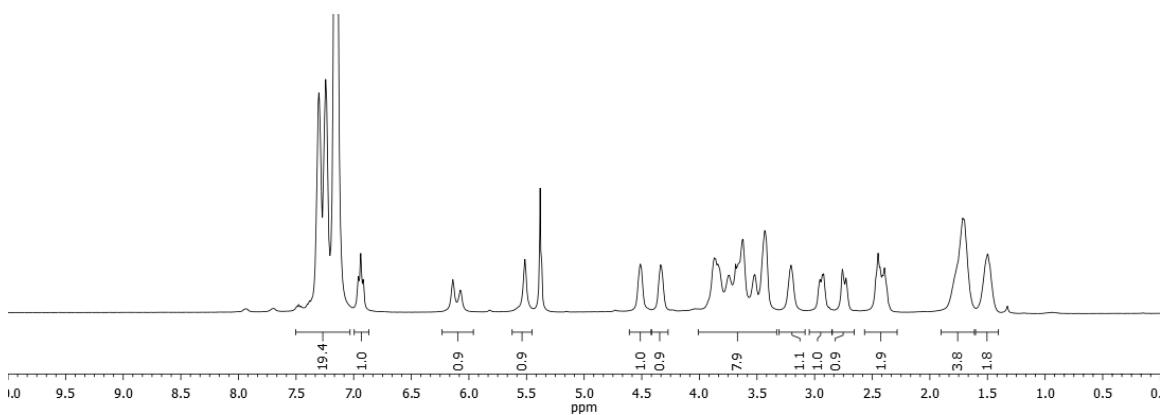
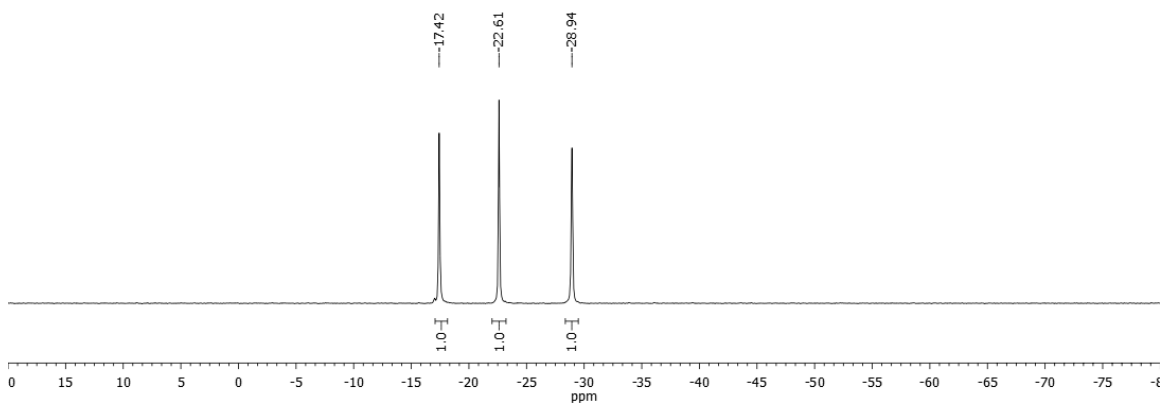


Chemical Formula: C<sub>47</sub>H<sub>44</sub>BF<sub>3</sub>N<sub>4</sub>O<sub>5</sub>S

Exact Mass: 844.3078

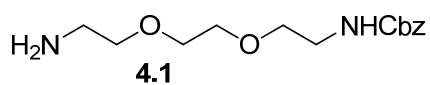
Molecular Weight: 844.7473

<sup>19</sup>F NMR 282.4 MHz, <sup>1</sup>H NMR 300 MHz, CD<sub>2</sub>Cl<sub>2</sub>



### Appendix E.3. NMR spectra for Chapter 4

#### Benzyl 2-(2-(2-aminoethoxy)ethoxy)ethylcarbamate (4.1)

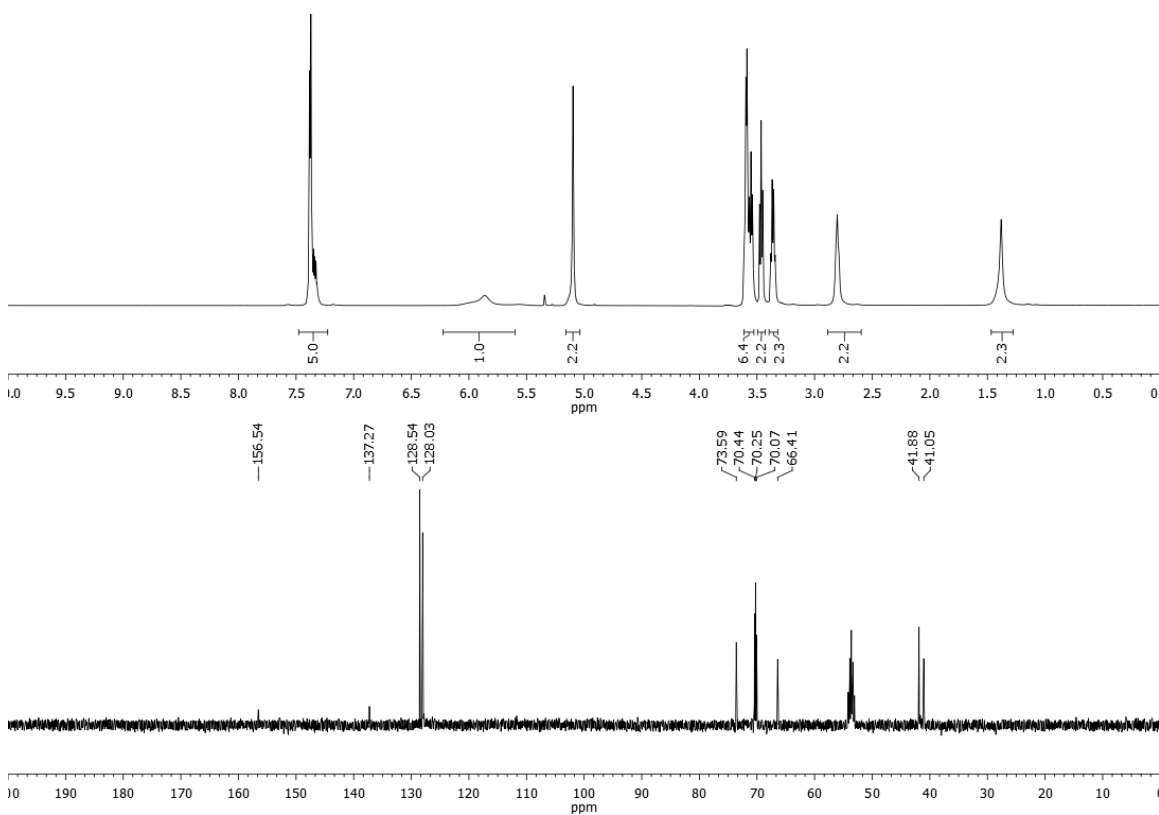


Chemical Formula: C<sub>14</sub>H<sub>22</sub>N<sub>2</sub>O<sub>4</sub>

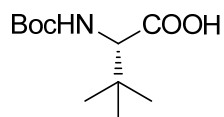
Exact Mass: 282.1580

Molecular Weight: 282.3355

<sup>1</sup>H NMR 400 MHz, <sup>13</sup>C NMR 100.6 MHz, CD<sub>2</sub>Cl<sub>2</sub>



### *N*-Boc-*L*-*tert*-Leucine (4.2)



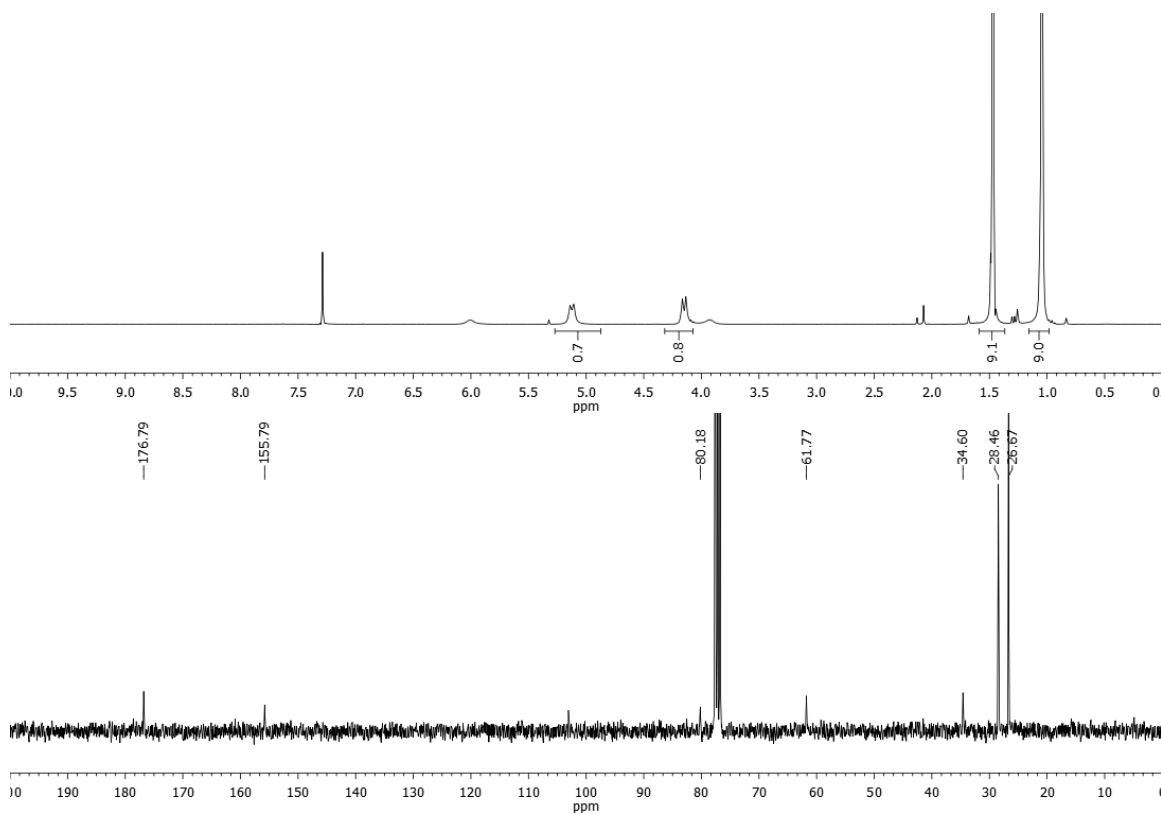
**4.2**

Chemical Formula: C<sub>11</sub>H<sub>21</sub>NO<sub>4</sub>

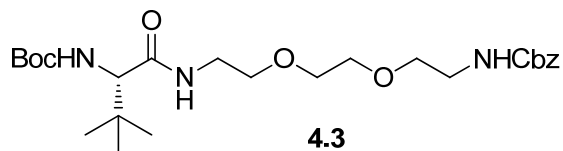
Exact Mass: 231.1471

Molecular Weight: 231.2887

<sup>1</sup>H NMR 300 MHz, <sup>13</sup>C NMR 75.5 MHz, CDCl<sub>3</sub>

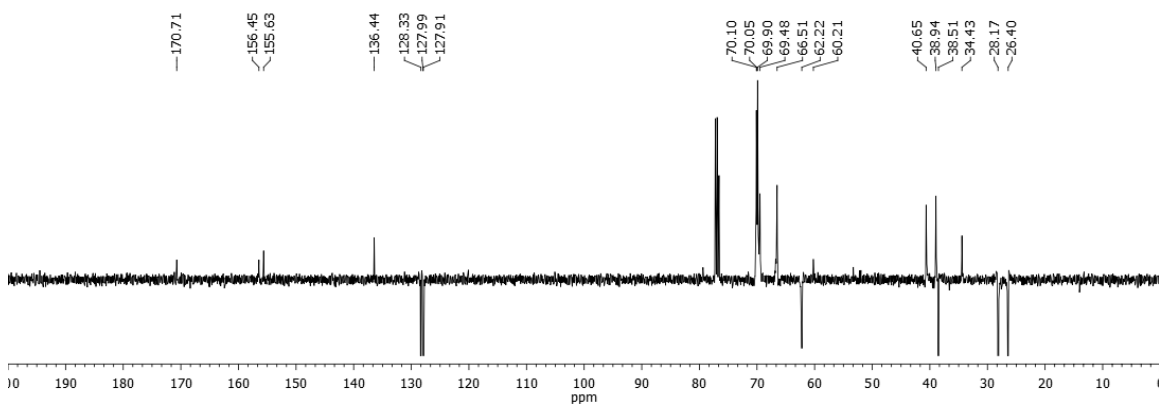
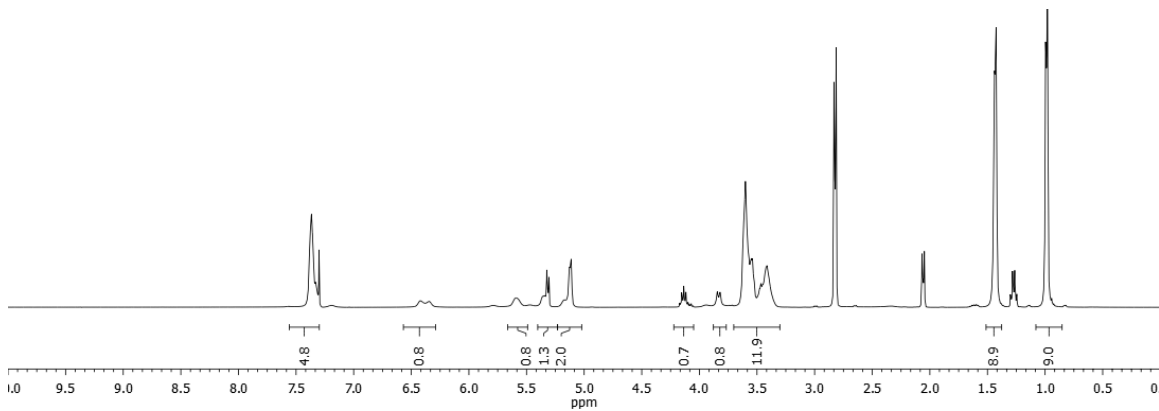


**(S)-Benzyl-2-(2-(2-(2-N-Boc-amino-3,3-dimethylbutanamido)ethoxy)ethylcarbamate (4.3)**

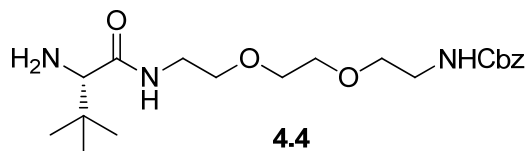


Chemical Formula: C<sub>25</sub>H<sub>41</sub>N<sub>3</sub>O<sub>7</sub>  
Exact Mass: 495.2945  
Molecular Weight: 495.6089

<sup>1</sup>H NMR 400 MHz, <sup>13</sup>C NMR 100.6 MHz, CDCl<sub>3</sub>



**(S)-Benzyl-2-(2-(2-(2-amino-3,3-dimethylbutanamido)ethoxy)ethyl)carbamate trifluoroacetate (4.4)**

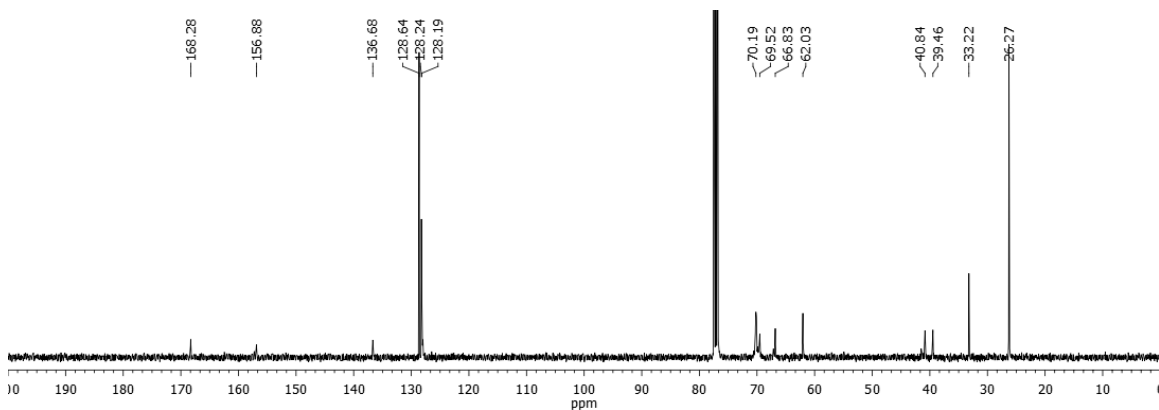
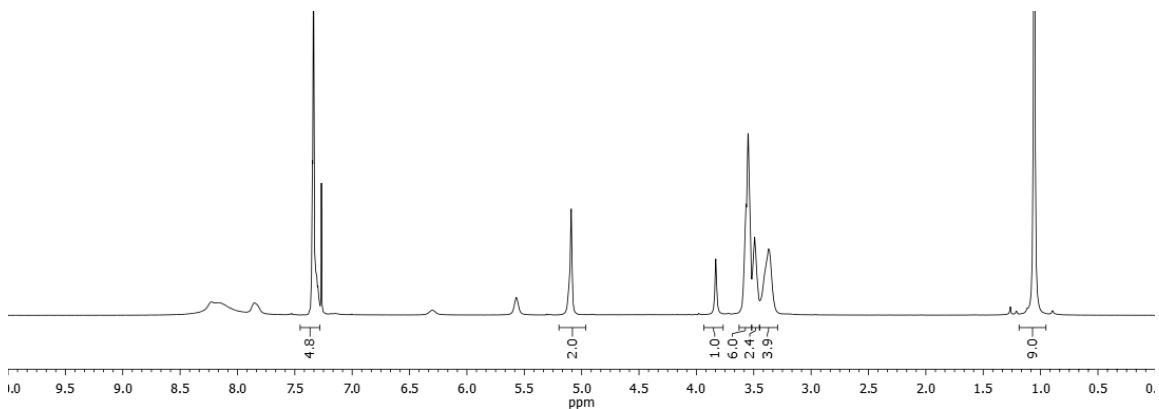


Chemical Formula: C<sub>20</sub>H<sub>33</sub>N<sub>3</sub>O<sub>5</sub>

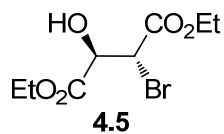
Exact Mass: 395.2420

Molecular Weight: 395.4931

<sup>19</sup>F NMR 282.4 MHz, <sup>1</sup>H NMR 400 MHz, <sup>13</sup>C NMR 100.6 MHz, CDCl<sub>3</sub>



### Diethyl (2*R*, 3*R*)-2-bromo-3-hydroxysuccinate (4.5)

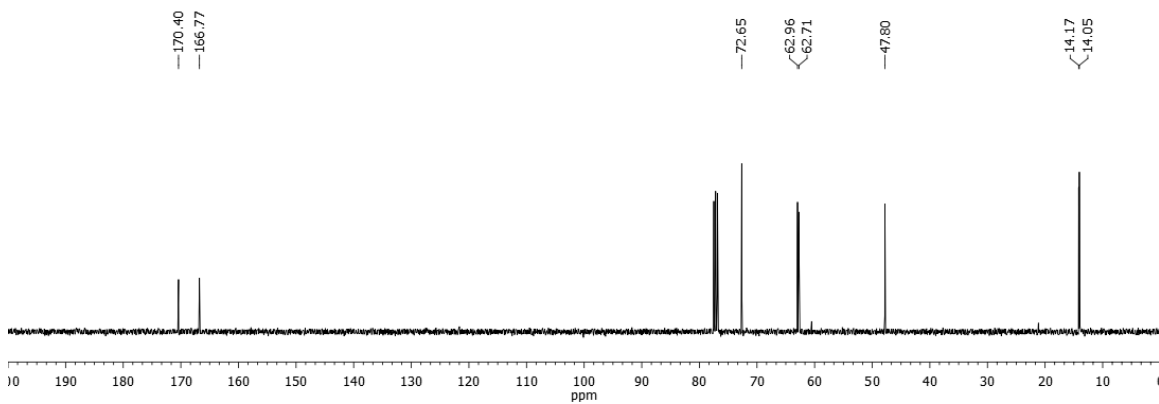
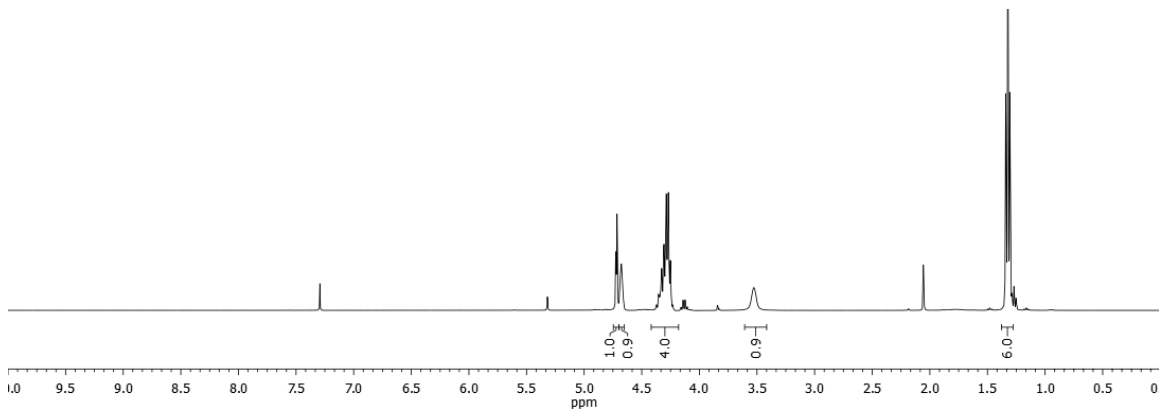


Chemical Formula: C<sub>8</sub>H<sub>13</sub>BrO<sub>5</sub>

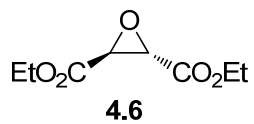
Exact Mass: 267.9946

Molecular Weight: 269.0898

<sup>1</sup>H NMR 400 MHz, <sup>13</sup>C NMR 100.6 MHz, CDCl<sub>3</sub>

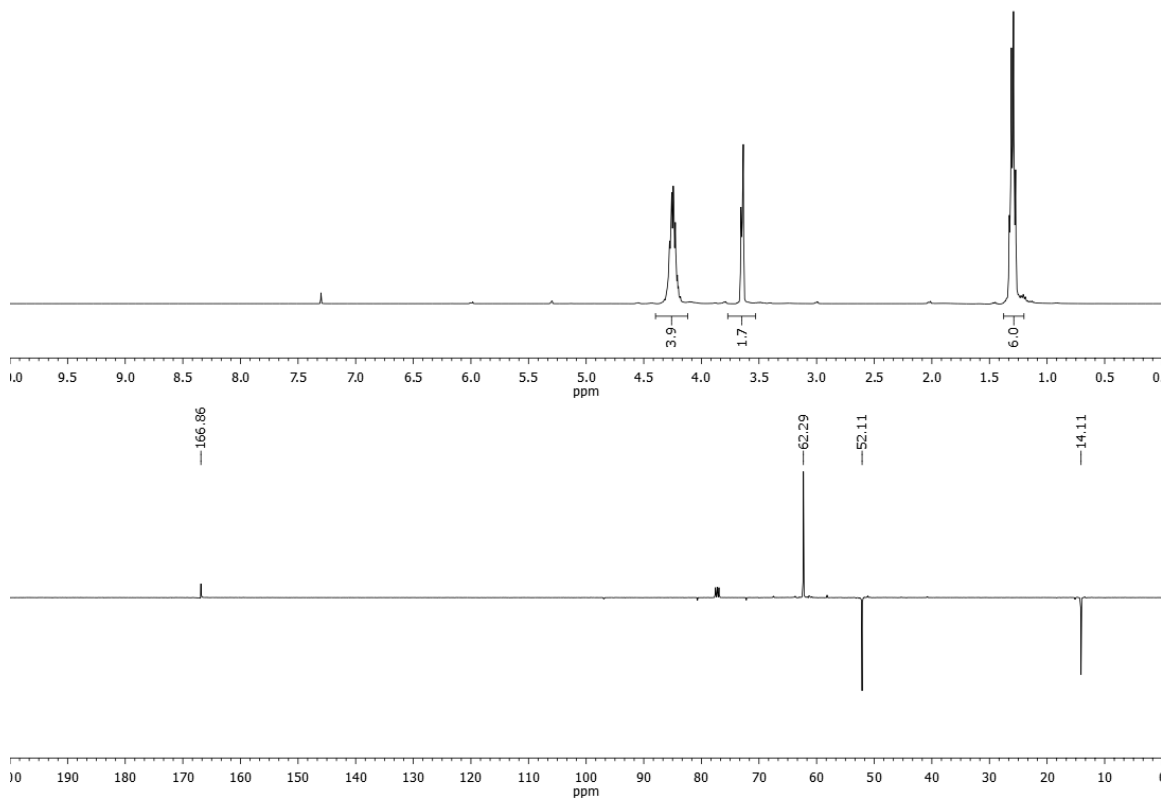


### Diethyl (2*S*, 3*S*)-epoxysuccinate (4.6)

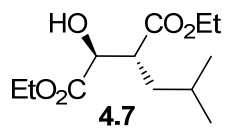


Chemical Formula: C<sub>8</sub>H<sub>12</sub>O<sub>5</sub>  
Exact Mass: 188.0685  
Molecular Weight: 188.1779

<sup>1</sup>H NMR 400 MHz, <sup>13</sup>C NMR 100.6 MHz, CDCl<sub>3</sub>



### Diethyl (2*S*, 3*R*)-2-hydroxy-isobutylsuccinate (4.7)

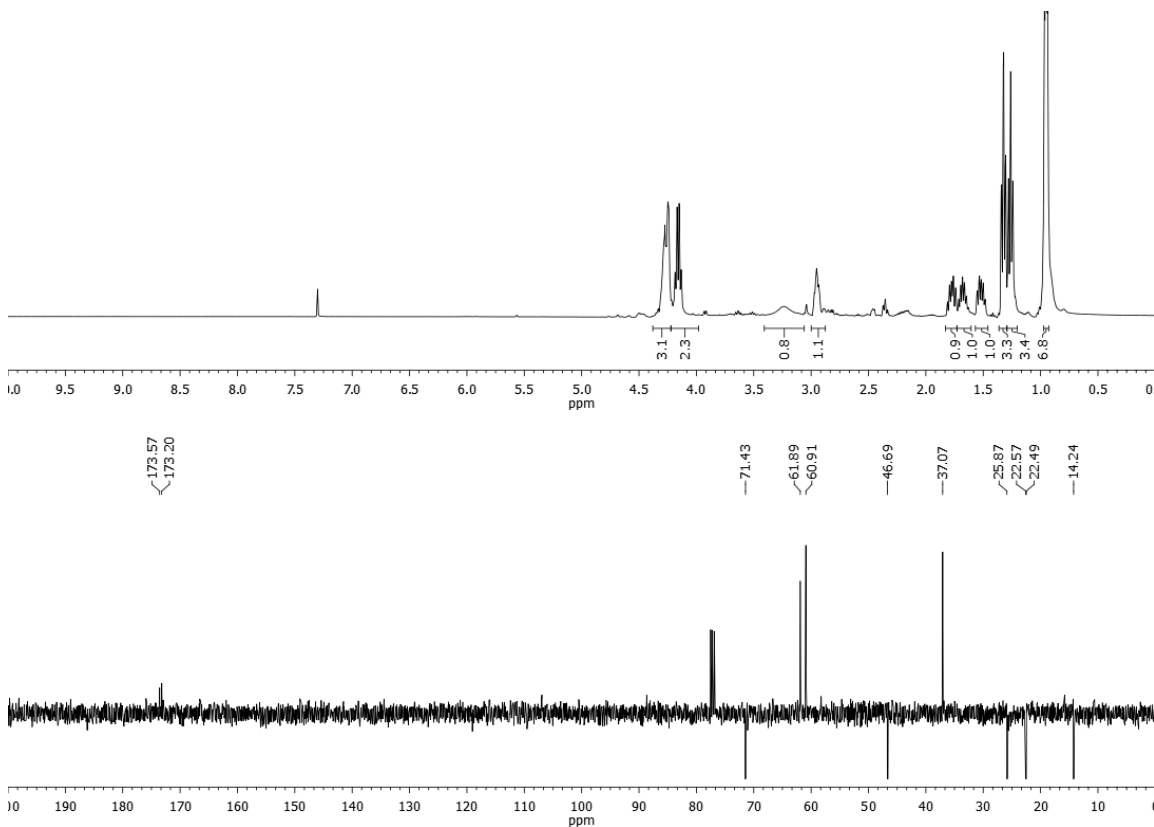


Chemical Formula: C<sub>12</sub>H<sub>22</sub>O<sub>5</sub>

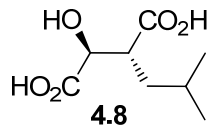
Exact Mass: 246.1467

Molecular Weight: 246.3001

<sup>1</sup>H NMR 400 MHz, <sup>13</sup>C NMR 100.6 MHz, CDCl<sub>3</sub>



**(2*S*, 3*R*)-2-Hydroxy-3-isobutylsuccinic acid (4.8)**

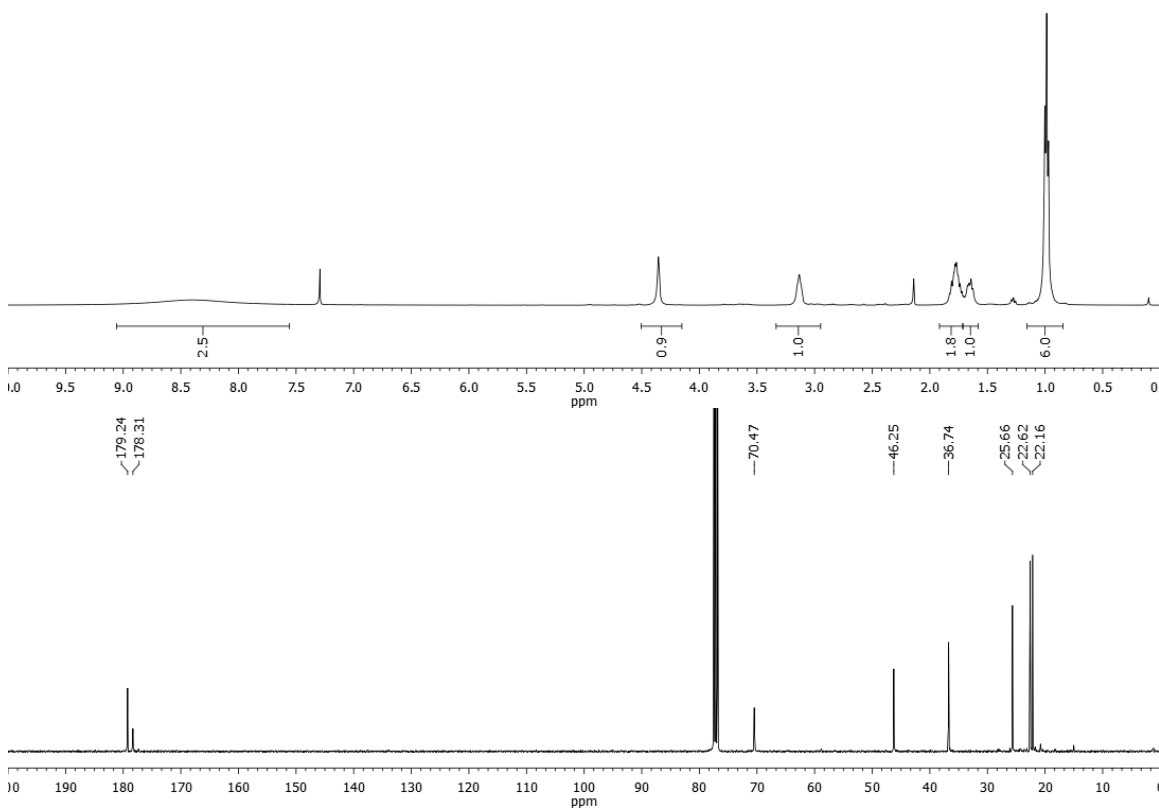


Chemical Formula: C<sub>8</sub>H<sub>14</sub>O<sub>5</sub>

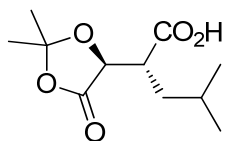
Exact Mass: 190.0841

Molecular Weight: 190.1938

<sup>1</sup>H NMR 400 MHz, <sup>13</sup>C NMR 100.6 MHz, CDCl<sub>3</sub>



**(2R)-4-Methyl-2-((4S)-5-oxo-2,2-dimethyl-1,3-dioxolan-4-yl)pentanoic acid (4.9)**



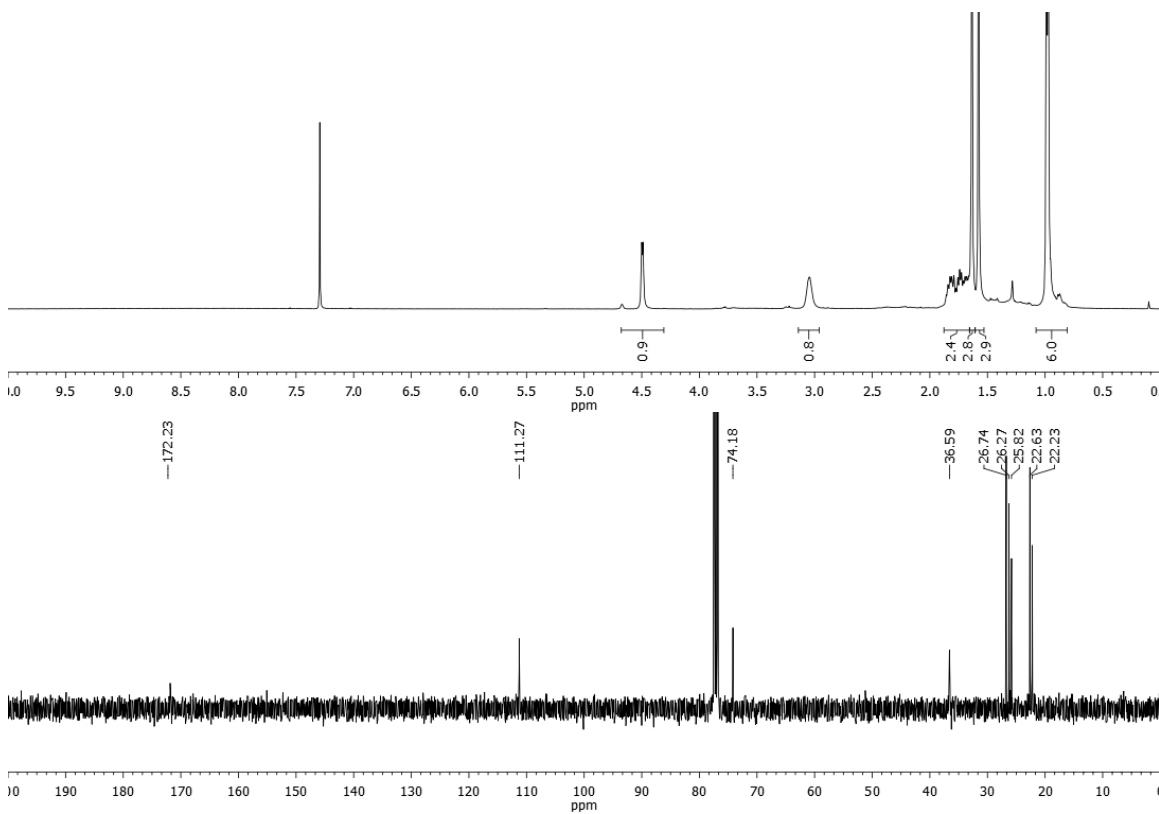
Chemical Formula: C<sub>11</sub>H<sub>18</sub>O<sub>5</sub>

Exact Mass: 230.1154

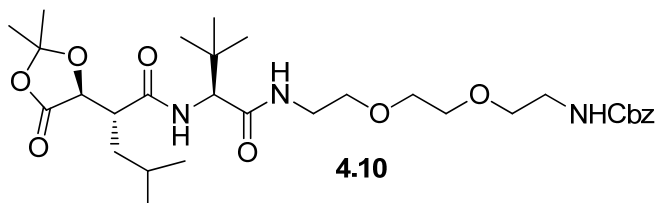
Molecular Weight: 230.2576

**4.9**

<sup>1</sup>H NMR 400 MHz, <sup>13</sup>C NMR 100.6 MHz, CDCl<sub>3</sub>

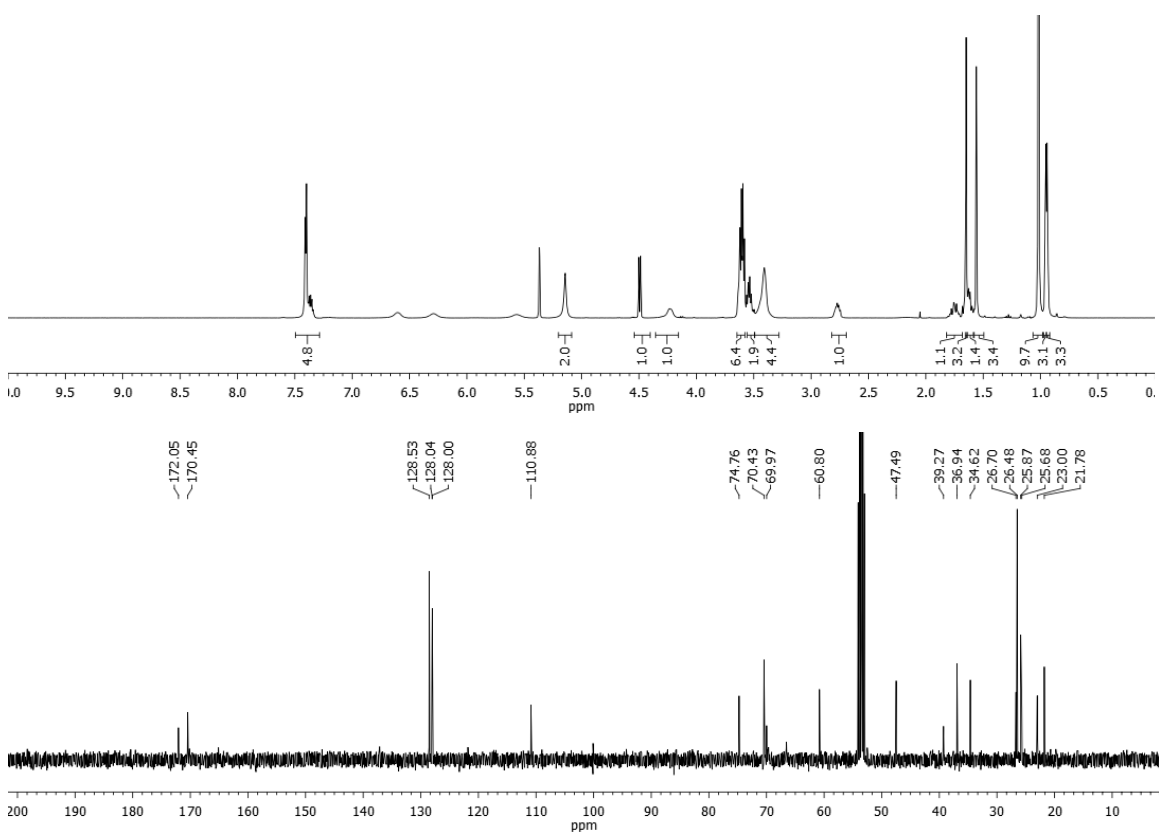


**Benzyl (1*S*,14*R*)-11-*tert*-butyl-14-((4*S*)-2,2-dimethyl-5-oxo-1,3-dioxolan-4-yl)-16-methyl-10,13-dioxo-3,5-dioxo-9,12-diazaheptadecylcarbamate (4.10)**

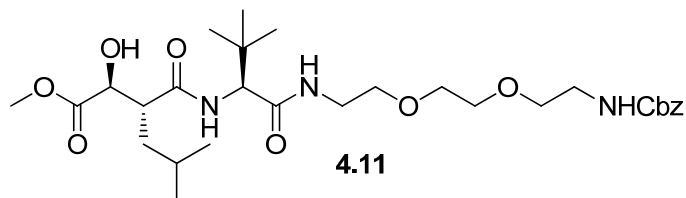


Chemical Formula: C<sub>31</sub>H<sub>49</sub>N<sub>3</sub>O<sub>9</sub>  
Exact Mass: 607.3469  
Molecular Weight: 607.7355

<sup>1</sup>H NMR 400 MHz, <sup>13</sup>C NMR 100.6 MHz, CD<sub>2</sub>Cl<sub>2</sub>

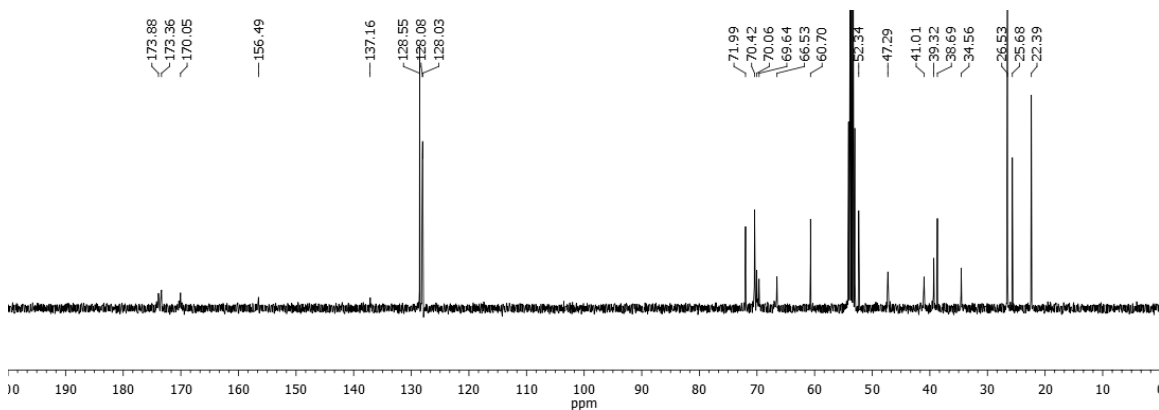
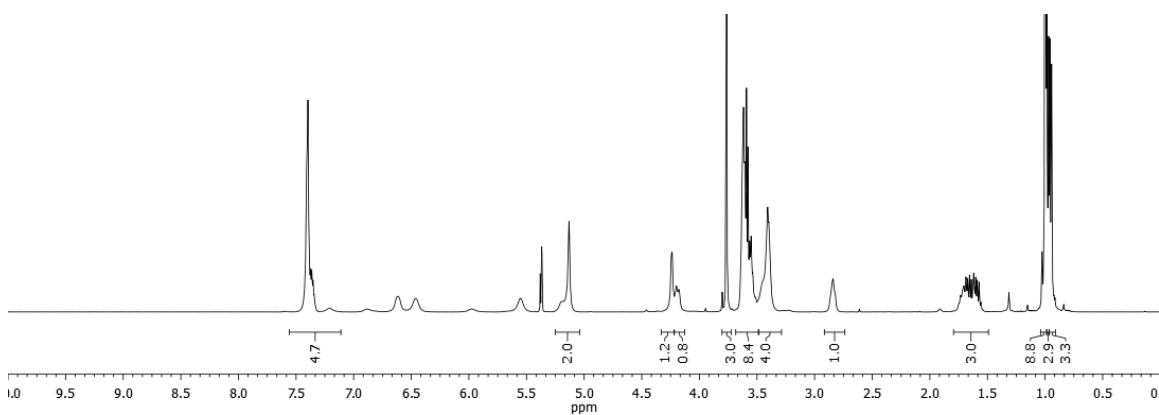


**(15*S*,18*R*,19*S*)-Methyl 15-(*tert*-butyl)-19-hydroxy-18-isobutyl-3,14,17-trioxo-1-phenyl-2,7,10-trioxa-4,13,16-triazaicosan-20-oate (4.11)**

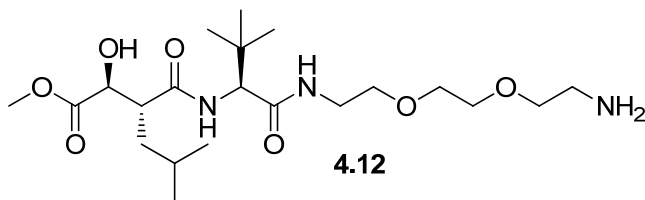


Chemical Formula: C<sub>29</sub>H<sub>47</sub>N<sub>3</sub>O<sub>9</sub>  
Exact Mass: 581.3312  
Molecular Weight: 581.6982

<sup>1</sup>H NMR 400 MHz, <sup>13</sup>C NMR 100.6 MHz, CD<sub>2</sub>Cl<sub>2</sub>



**(11S, 14R, 15S)-Methyl 1-amio-11-*tert*-butyl-15-hydroxy-14-isobutyl-10,13-dioxo-3,6-dioxa-9,12-diazahexadecan-16-oate (4.12)**

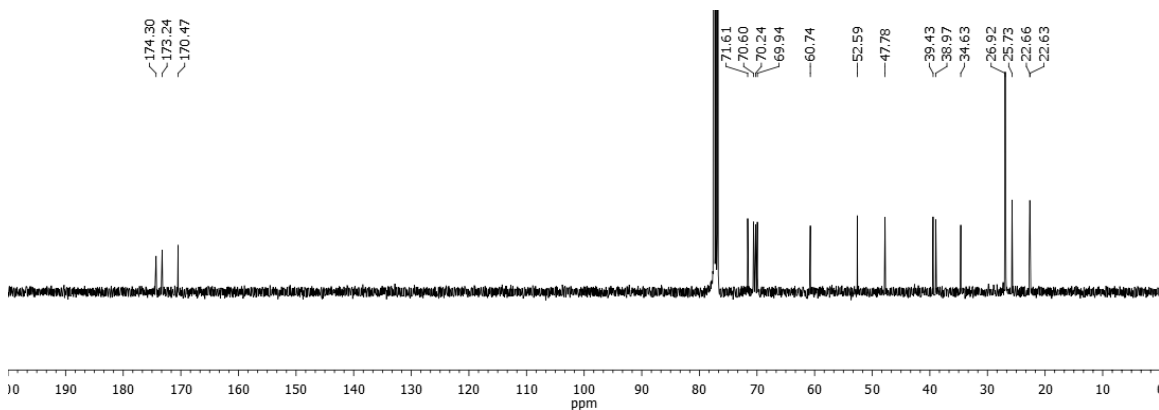
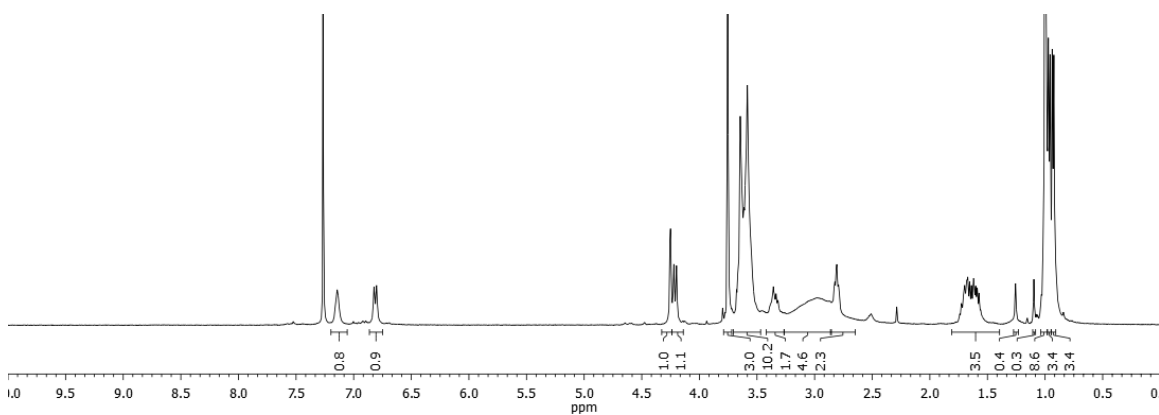


Chemical Formula: C<sub>21</sub>H<sub>41</sub>N<sub>3</sub>O<sub>7</sub>

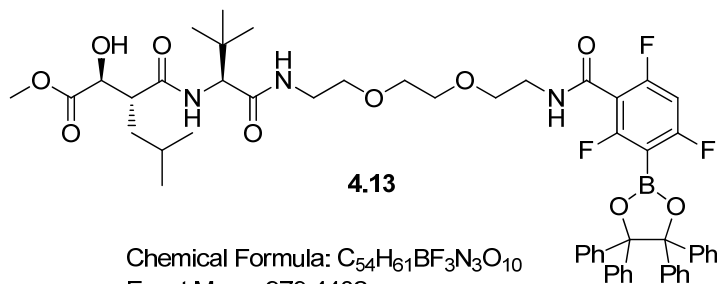
Exact Mass: 447.2945

Molecular Weight: 447.5661

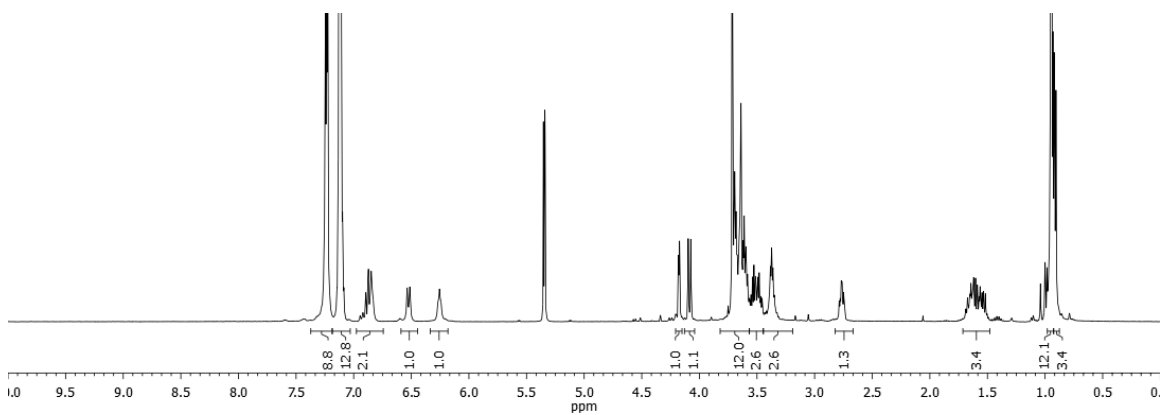
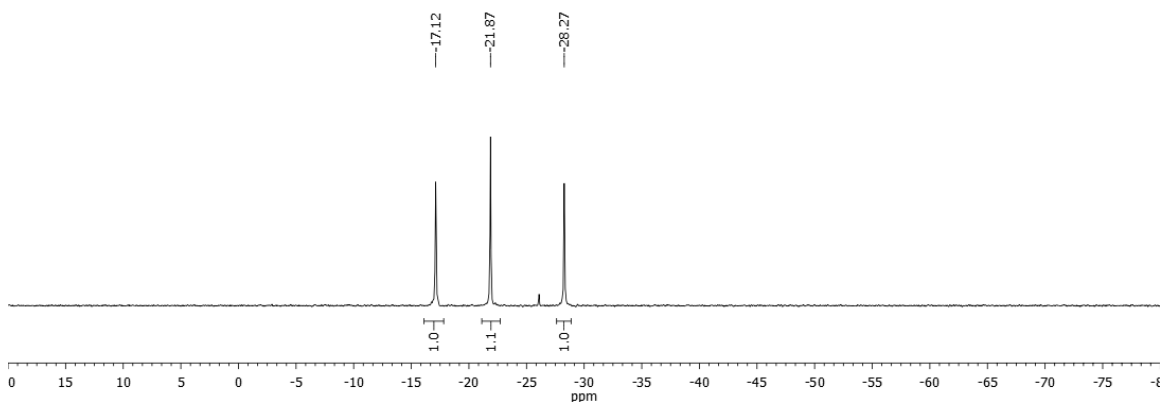
<sup>1</sup>H NMR 400 MHz, <sup>13</sup>C NMR 100.6 MHz, CDCl<sub>3</sub>

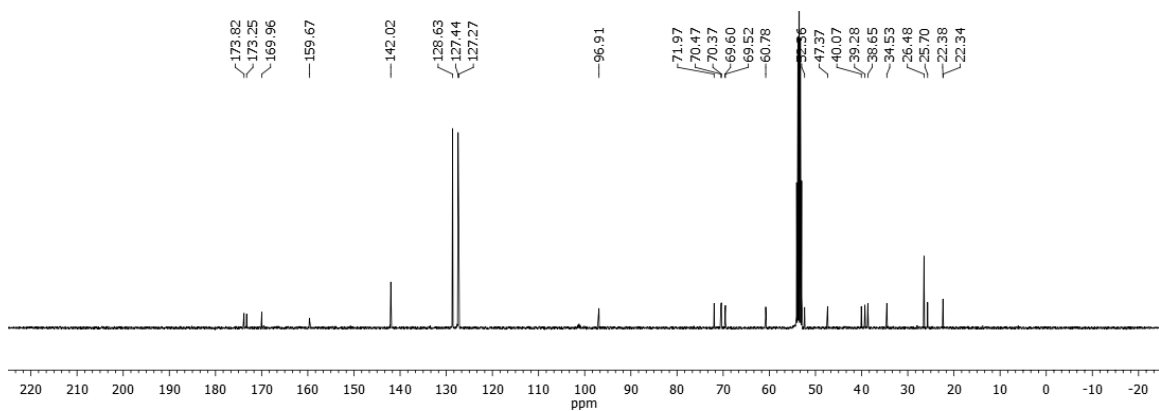


**(13*S*,16*R*,17*S*)-Methyl 13-*tert*-butyl-17-hydroxy-16-isobutyl-1,12,15-trioxo-1-(2,4,6-trifluoro-3-(4,4,5,5-tetraphenyl-1,3,2-dioxaborolan-2-yl)phenyl)-5,8-dioxo-2,11,14-triazaoctadecan-18-oate (4.13)**

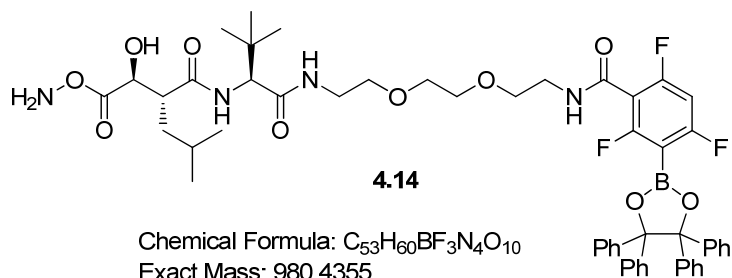


$^{19}F$  NMR 282.4 MHz,  $^1H$  NMR 400 MHz,  $^{13}C$  NMR 100.6 MHz,  $CD_2Cl_2$





**(2*R*,3*S*)-*N*<sup>1</sup>-((*S*)-14,14-Dimethyl-1,12-dioxo-1-(2,4,6-trifluoro-3-(4,4,5,5-tetraphenyl-1,3,2-dioxaborolan-2-yl)phenyl)-5,8-dioxa-2,11-diazapentadecan-13-yl)-*N*<sup>4</sup>,3-dihydroxy-2-isobutylsuccinamide (4.14)**



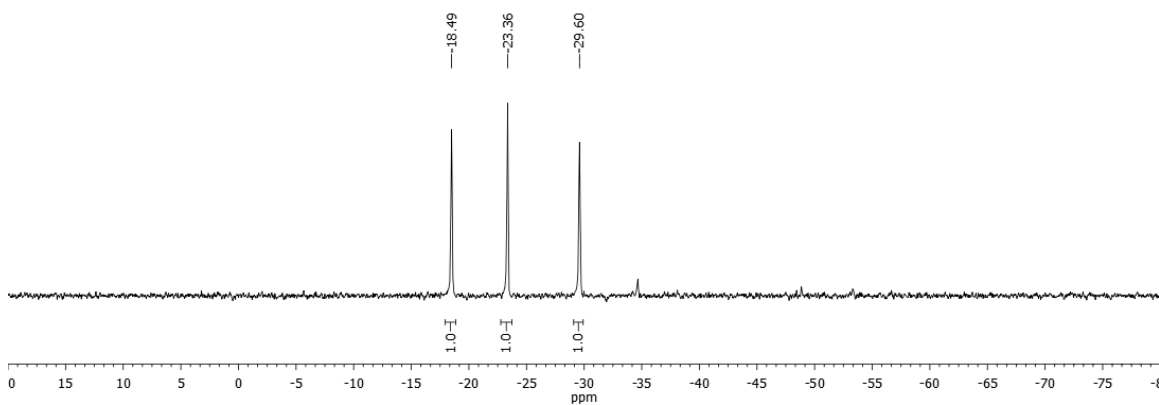
**4.14**

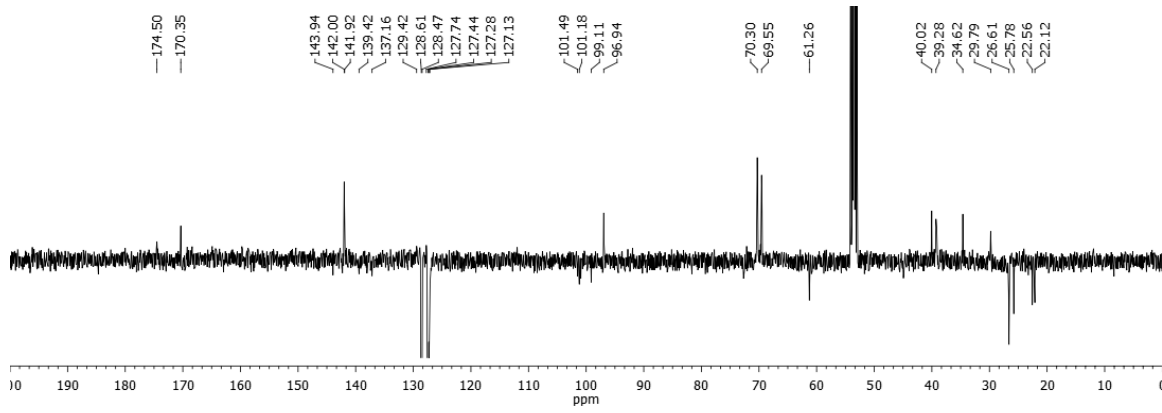
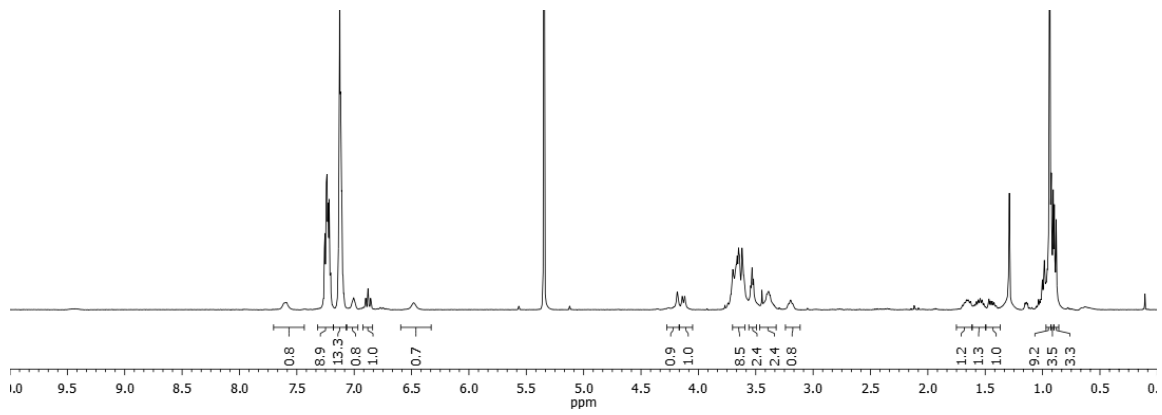
Chemical Formula: C<sub>53</sub>H<sub>60</sub>BF<sub>3</sub>N<sub>4</sub>O<sub>10</sub>

Exact Mass: 980.4355

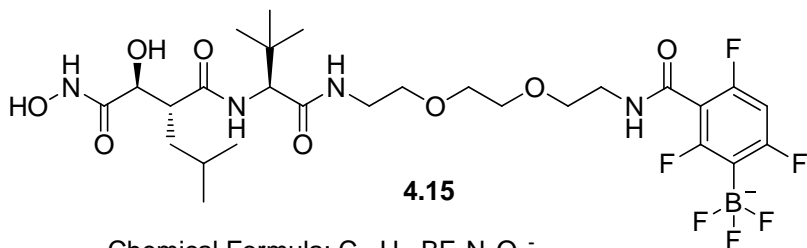
Molecular Weight: 980.8705

<sup>19</sup>F NMR 282.4 MHz, <sup>1</sup>H NMR 400 MHz, <sup>13</sup>C NMR 100.6 MHz, CD<sub>2</sub>Cl<sub>2</sub>





**Potassium <sup>19</sup>F-N-marimastat-amidyl-2,4,6-trifluoro-N-(2-(2-(2-(amino)ethoxy)ethoxy)ethyl)-3-(trifluoroborate)benzamide (MarArBF<sub>3</sub>) (4.15)**

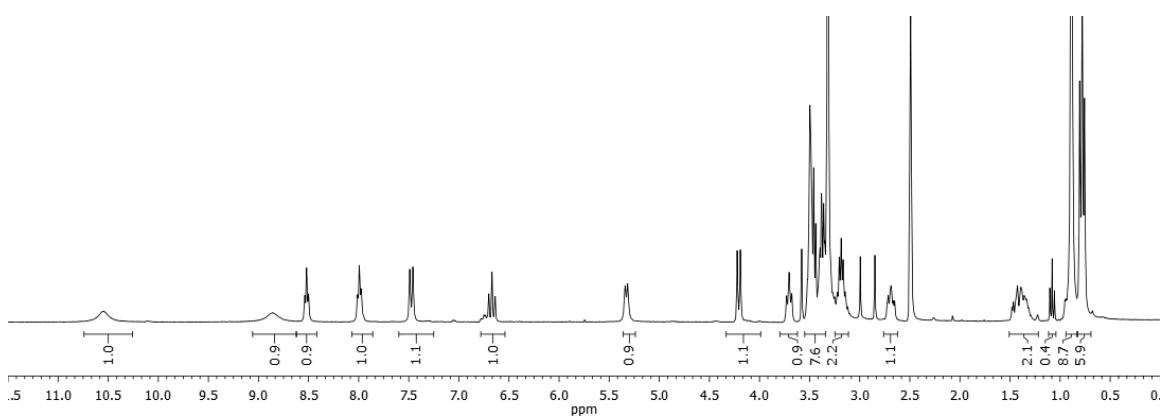
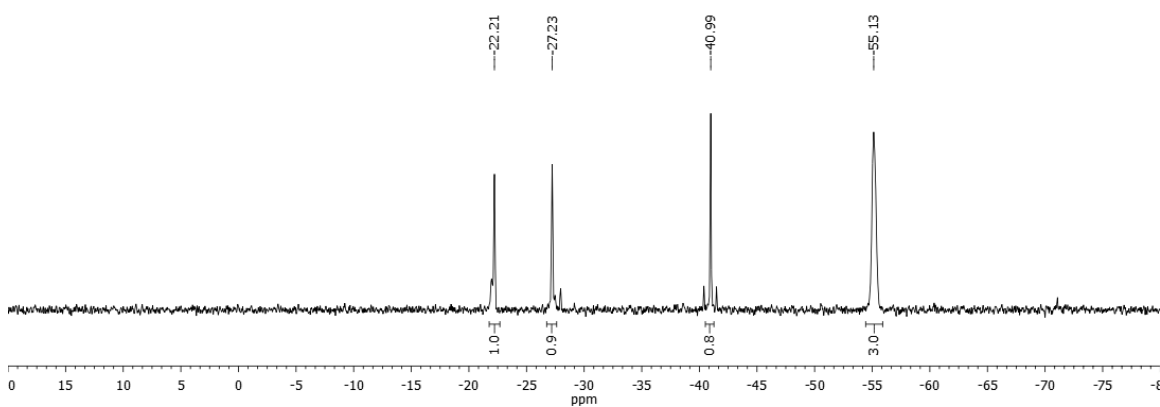


Chemical Formula: C<sub>27</sub>H<sub>40</sub>BF<sub>6</sub>N<sub>4</sub>O<sub>8</sub><sup>-</sup>

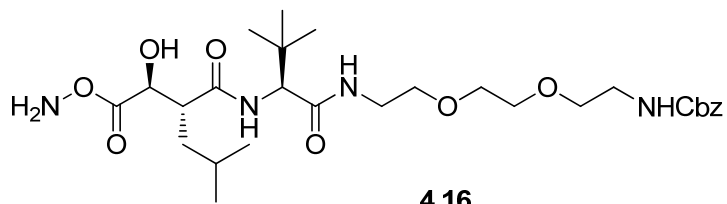
Exact Mass: 673.2849

Molecular Weight: 673.4305

<sup>19</sup>F NMR 282.4 MHz, <sup>1</sup>H NMR 300 MHz, d<sub>6</sub>-DMSO

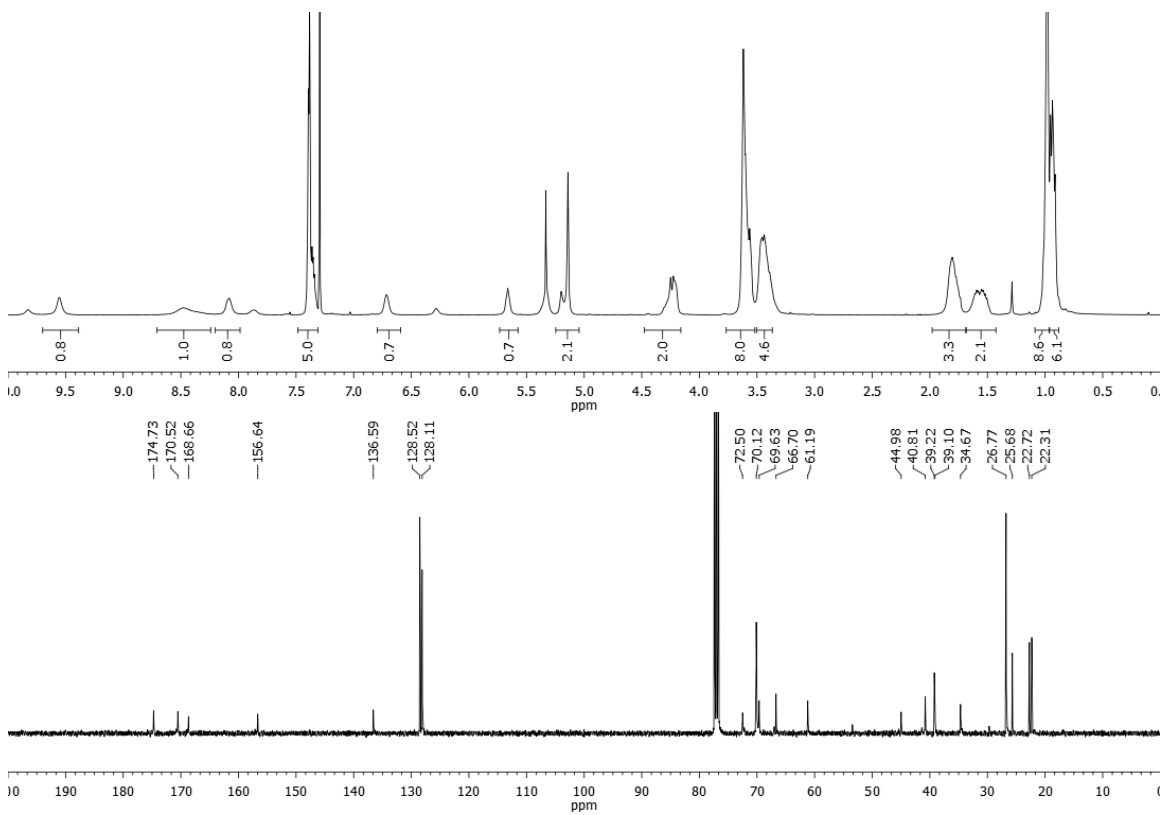


**Benzyl (11-(*tert*-butyl)-14-(1-hydroxy-2-(hydroxyamino)-2-oxoethyl)-16-methyl-10,13-dioxo-3,6-dioxo-9,12-diazaheptadecyl)carbamate (4.16)**

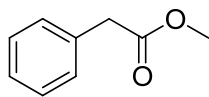


Chemical Formula: C<sub>28</sub>H<sub>46</sub>N<sub>4</sub>O<sub>9</sub>  
 Exact Mass: 582.3265  
 Molecular Weight: 582.6862

<sup>1</sup>H NMR 400 MHz, <sup>13</sup>C NMR 100.6 MHz, CDCl<sub>3</sub>



## Methyl 2-phenylacetate

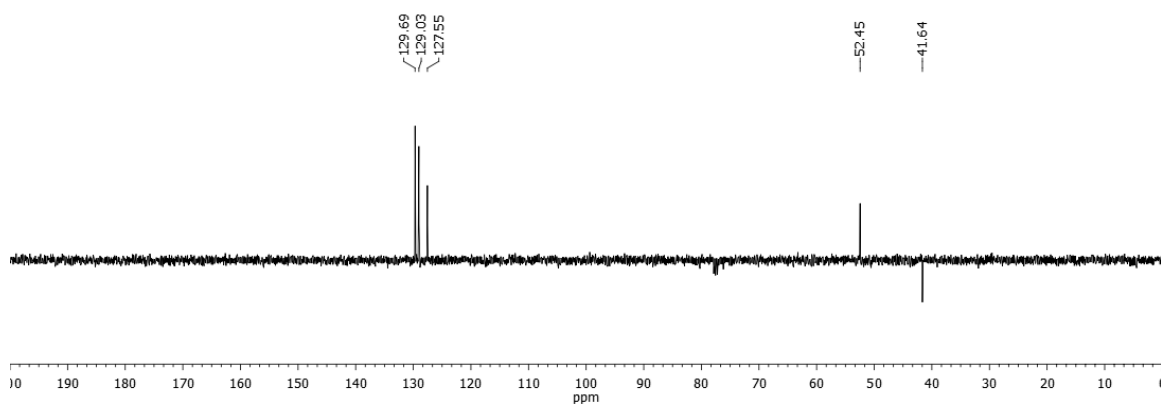
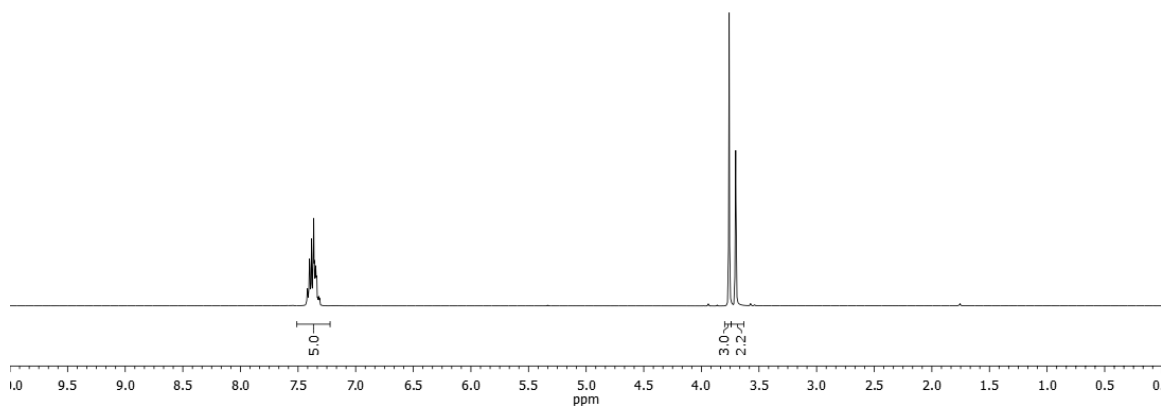


Chemical Formula: C<sub>9</sub>H<sub>10</sub>O<sub>2</sub>

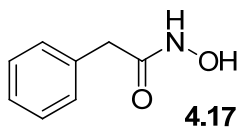
Exact Mass: 150.0681

Molecular Weight: 150.1745

<sup>1</sup>H NMR 400 MHz, <sup>13</sup>C NMR 100.6 MHz, CDCl<sub>3</sub>



### ***N*-Hydroxy-2-phenylacetamide (4.17)**

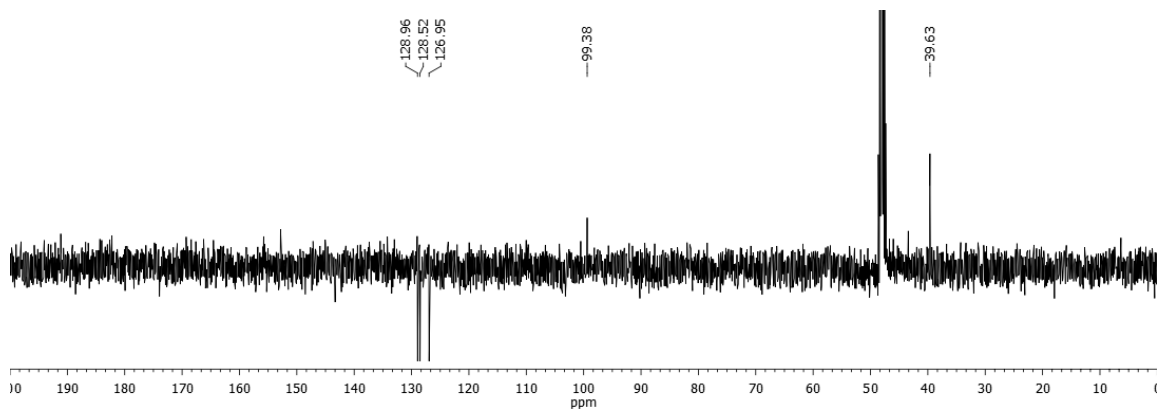
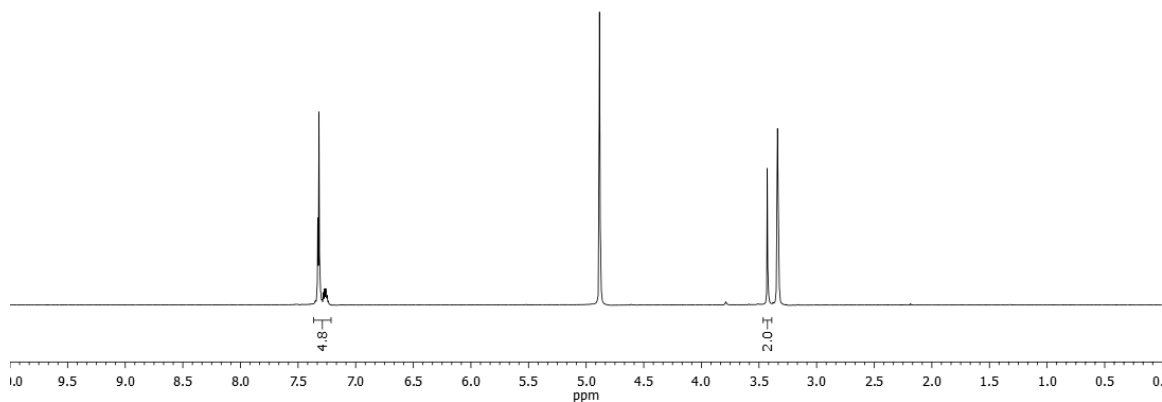


Chemical Formula:  $C_8H_9NO_2$

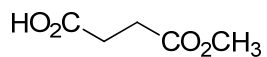
Exact Mass: 151.0633

Molecular Weight: 151.1626

$^1H$  NMR 400 MHz,  $^{13}C$  NMR 100.6 MHz,  $d_4$ -MeOD

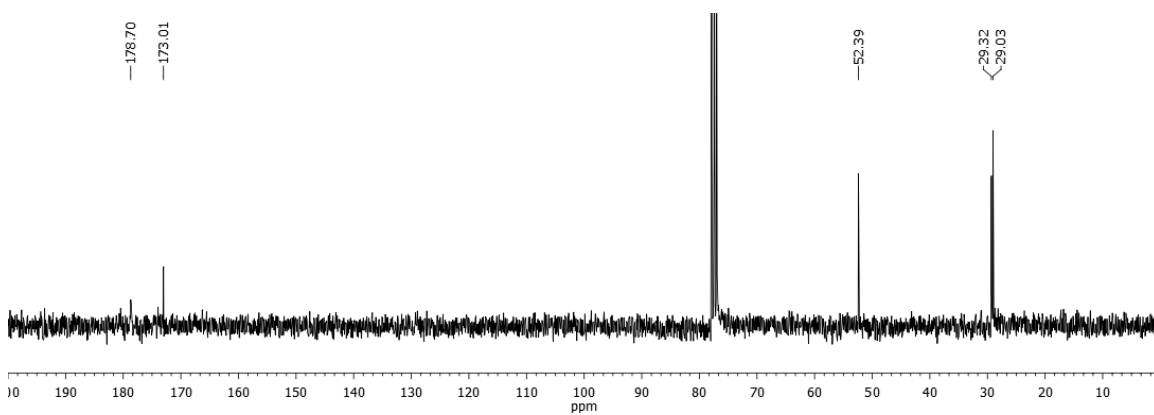
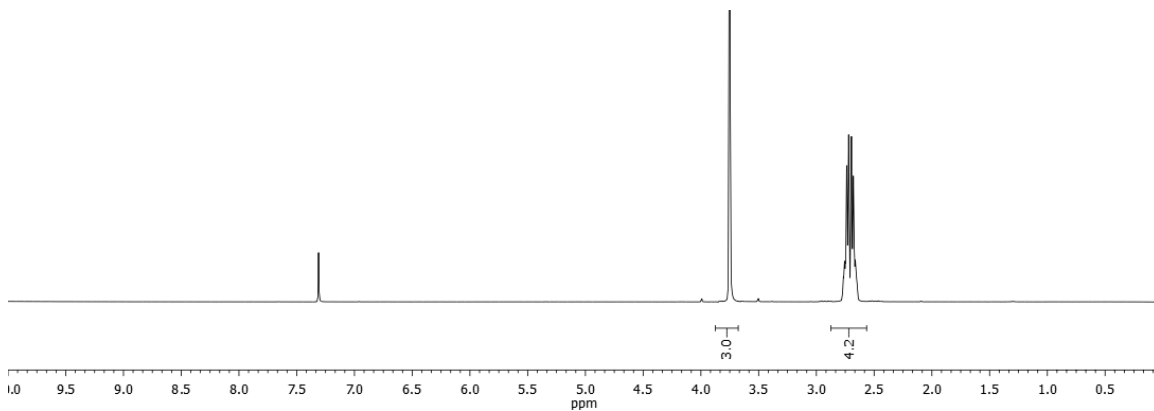


## Monomethyl succinate

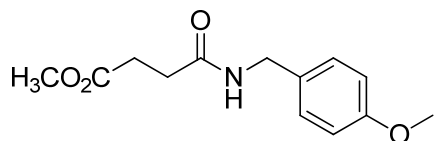


Chemical Formula: C<sub>5</sub>H<sub>8</sub>O<sub>4</sub>  
Exact Mass: 132.0423  
Molecular Weight: 132.1146

<sup>1</sup>H NMR 300 MHz, <sup>13</sup>C NMR 75.5 MHz, CDCl<sub>3</sub>



### Methyl 4-((4-methoxybenzyl)amino)-4-oxobutanoate

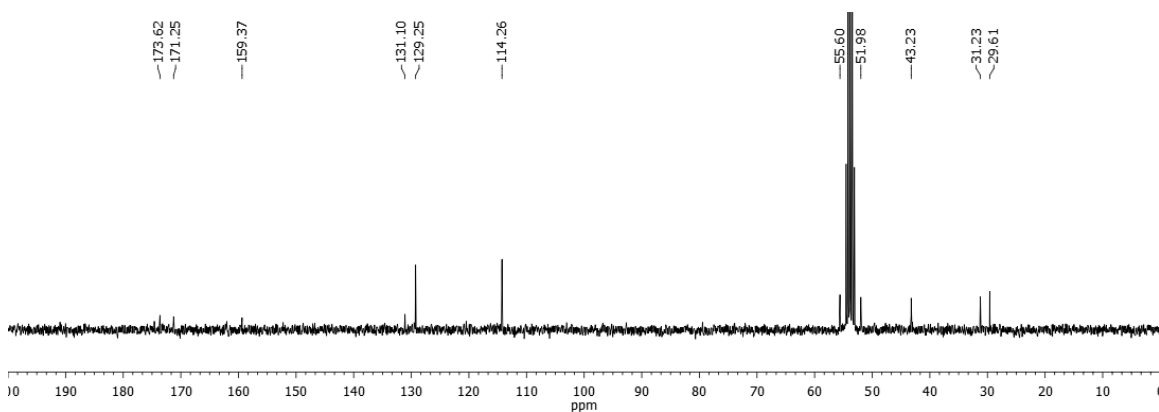
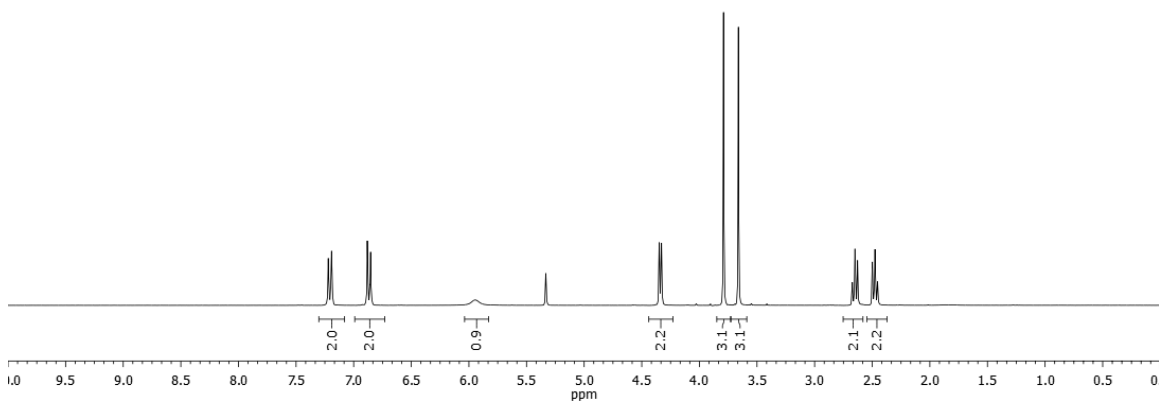


Chemical Formula: C<sub>13</sub>H<sub>17</sub>NO<sub>4</sub>

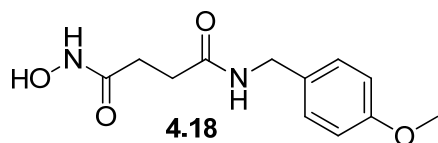
Exact Mass: 251.1158

Molecular Weight: 251.2784

<sup>1</sup>H NMR 300 MHz, <sup>13</sup>C NMR 75.5 MHz, CD<sub>2</sub>Cl<sub>2</sub>



***N*<sup>1</sup>-Hydroxy-*N*<sup>4</sup>-(4-methoxybenzyl)succinamide (4.18)**

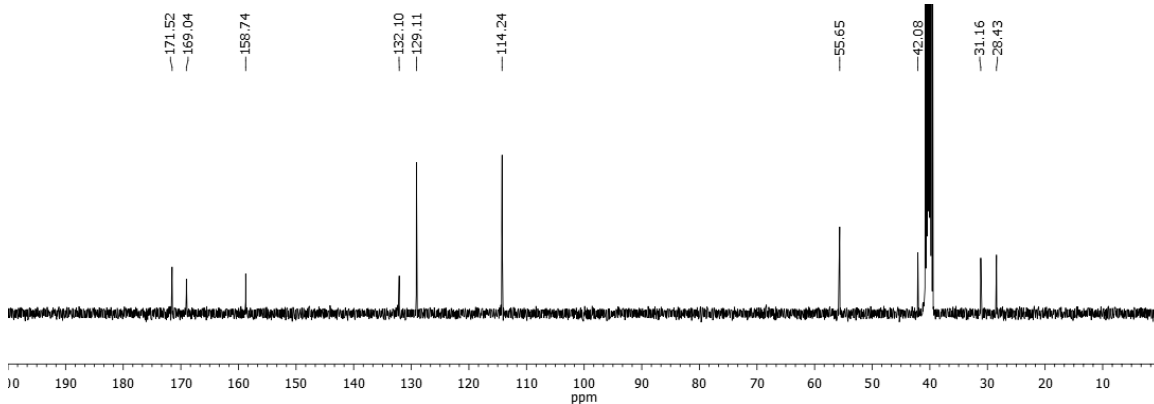
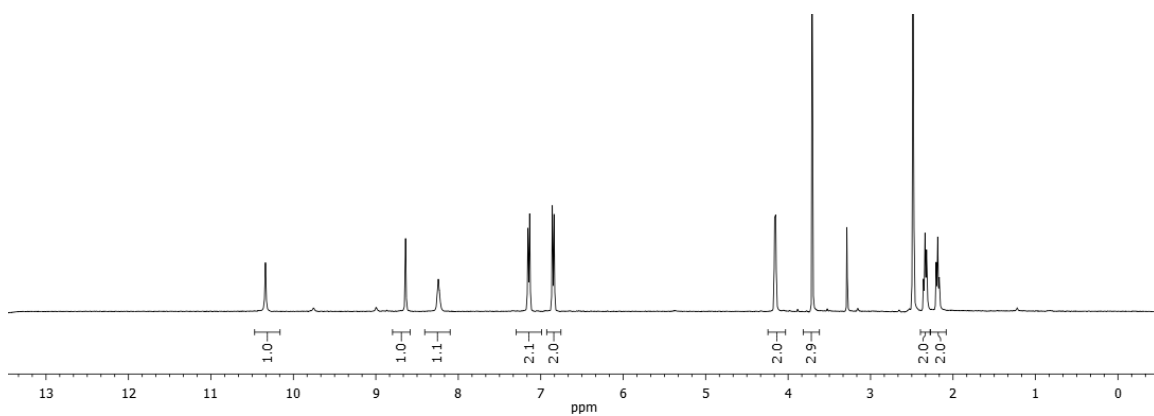


Chemical Formula: C<sub>12</sub>H<sub>16</sub>N<sub>2</sub>O<sub>4</sub>

Exact Mass: 252.1110

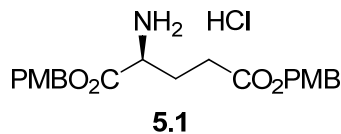
Molecular Weight: 252.2664

<sup>1</sup>H NMR 400 MHz, <sup>13</sup>C NMR 100.6 MHz, *d*<sub>6</sub>-DMSO



## Appendix E.4. NMR spectra for Chapter 5

### H-(L)-Glu(OPMB)-OPBM·HCl (5.1)

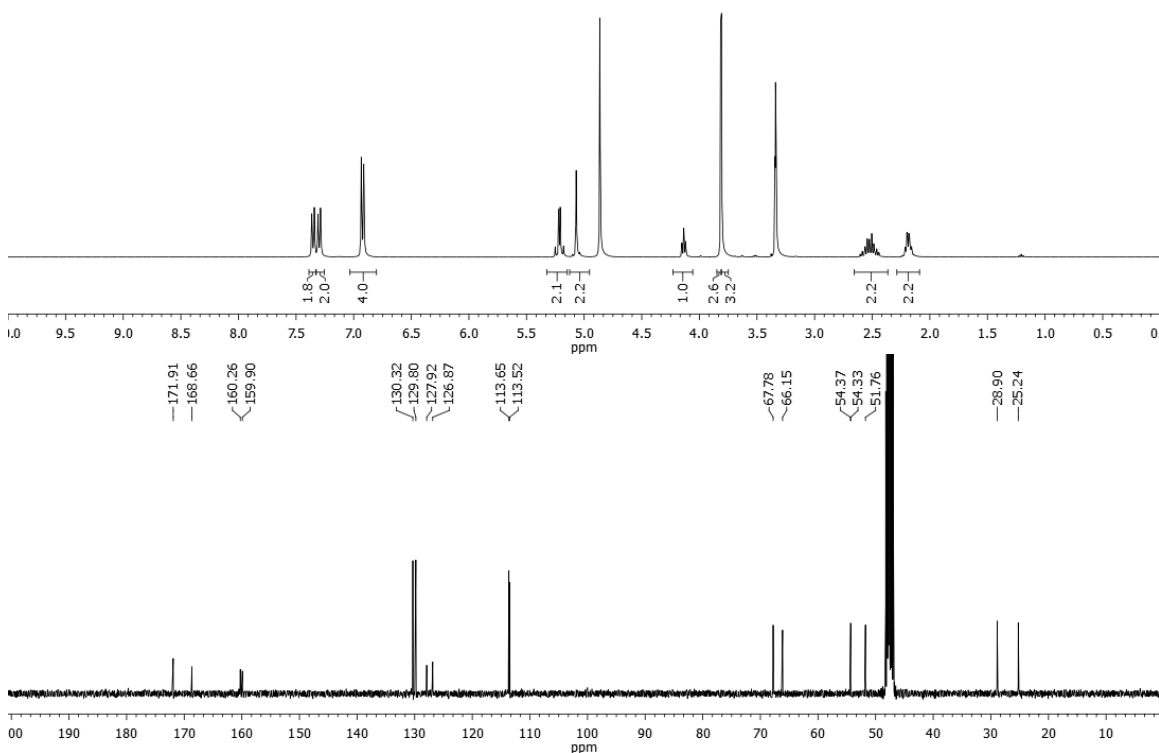


Chemical Formula: C<sub>21</sub>H<sub>26</sub>ClNO<sub>6</sub>

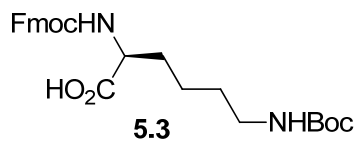
Exact Mass: 423.1449

Molecular Weight: 423.8872

<sup>1</sup>H NMR 400 MHz, <sup>13</sup>C NMR 100.6 MHz, *d*<sub>4</sub>-MeOD



### Fmoc-(L)-Lys(Boc)-OH (5.3)

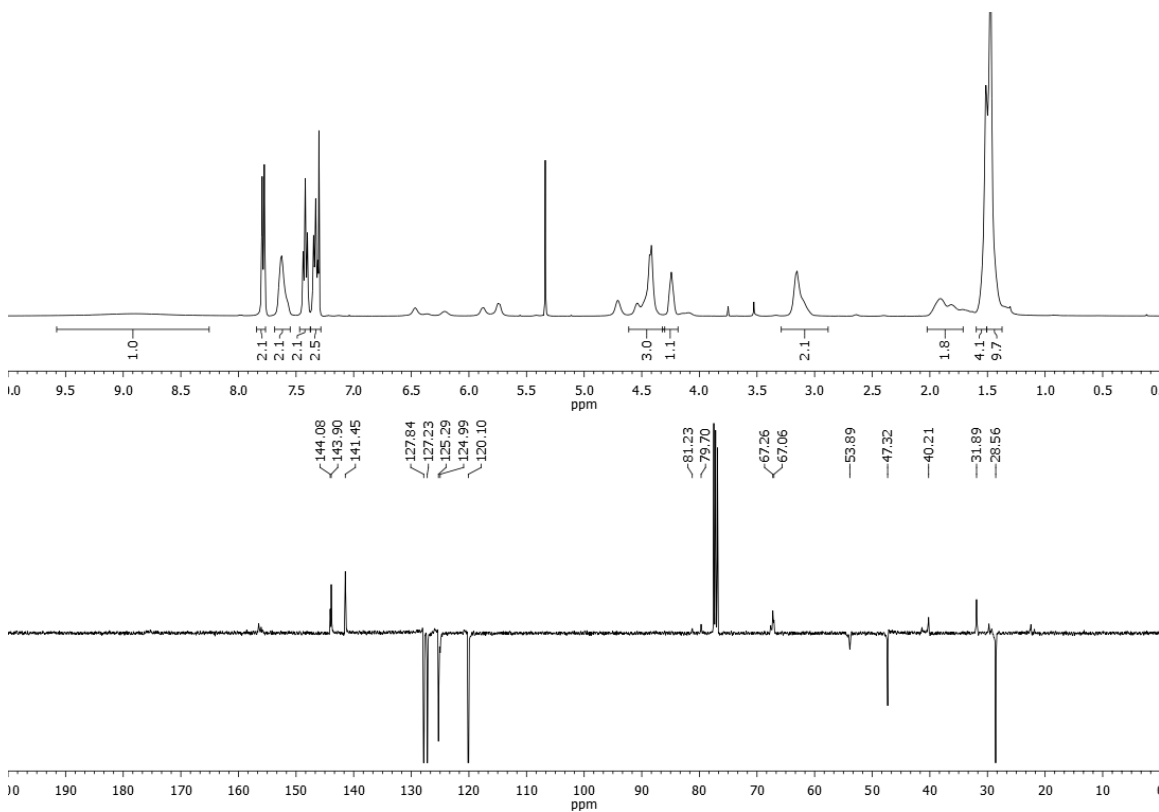


Chemical Formula:  $C_{26}H_{32}N_2O_6$

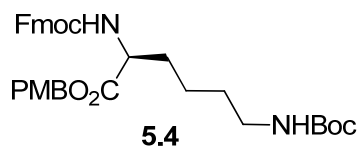
Exact Mass: 468.2260

Molecular Weight: 468.5421

$^1H$  NMR 400 MHz,  $^{13}C$  NMR 100.6 MHz,  $CDCl_3$



### Fmoc-(L)-Lys(Boc)-OPMB (5.4)

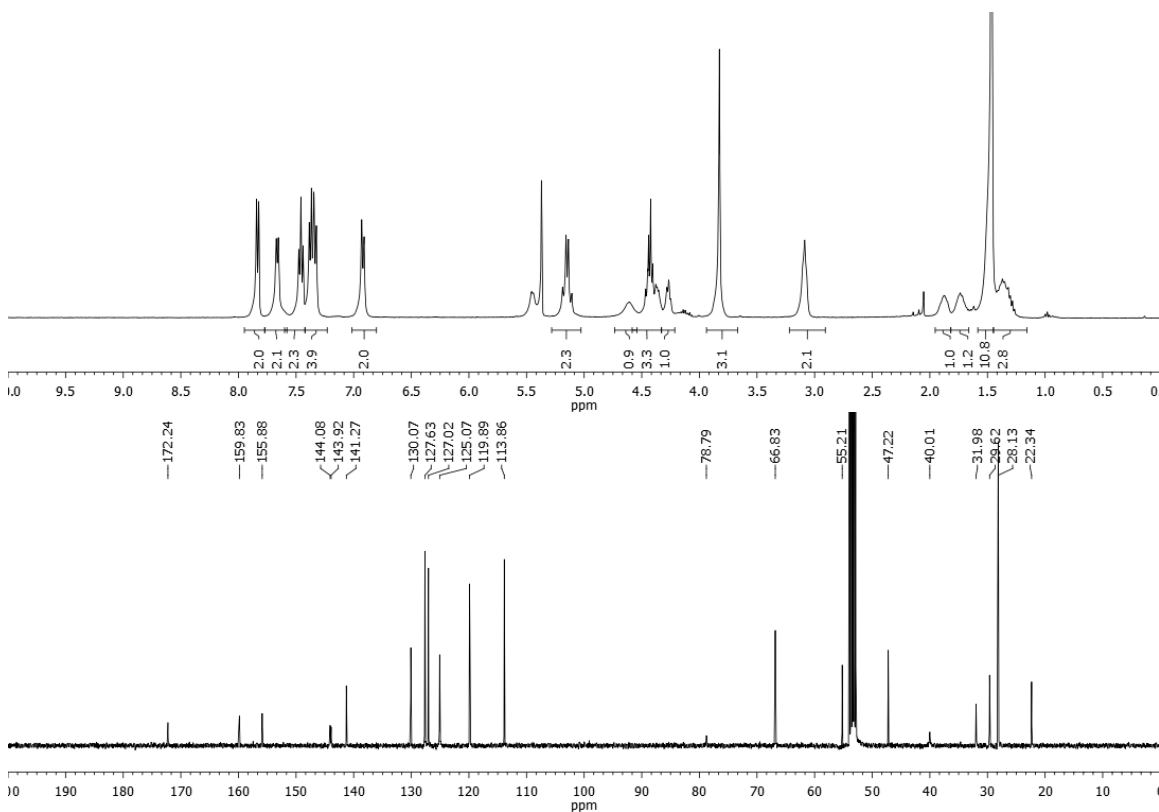


Chemical Formula:  $C_{34}H_{40}N_2O_7$

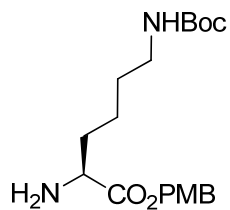
Exact Mass: 588.2836

Molecular Weight: 588.6906

$^1H$  NMR 400 MHz,  $^{13}C$  NMR 100.6 MHz,  $CD_2Cl_2$



## H-(L)-Lys(Boc)-OPMB(5.5)



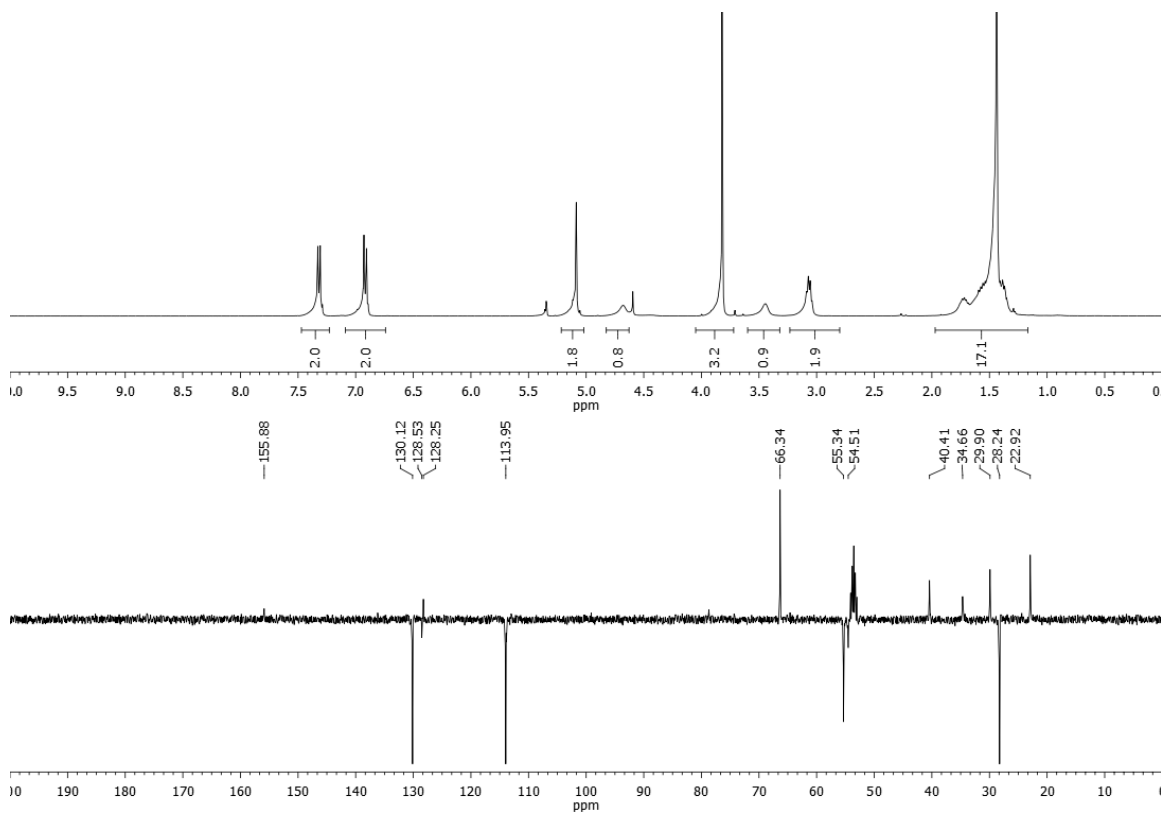
Chemical Formula:  $C_{19}H_{30}N_2O_5$

Exact Mass: 366.2155

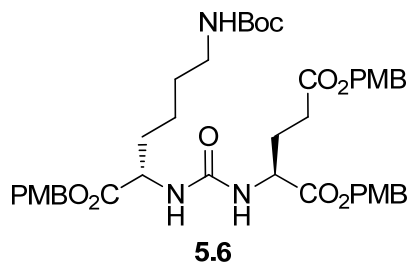
Molecular Weight: 366.4519

5.5

$^1\text{H}$  NMR 400 MHz,  $^{13}\text{C}$  NMR 100.6 MHz,  $\text{CD}_2\text{Cl}_2$



### PMBO-Lys(Boc)-C(O)-Glu(OPMB)-OPMB (5.6)

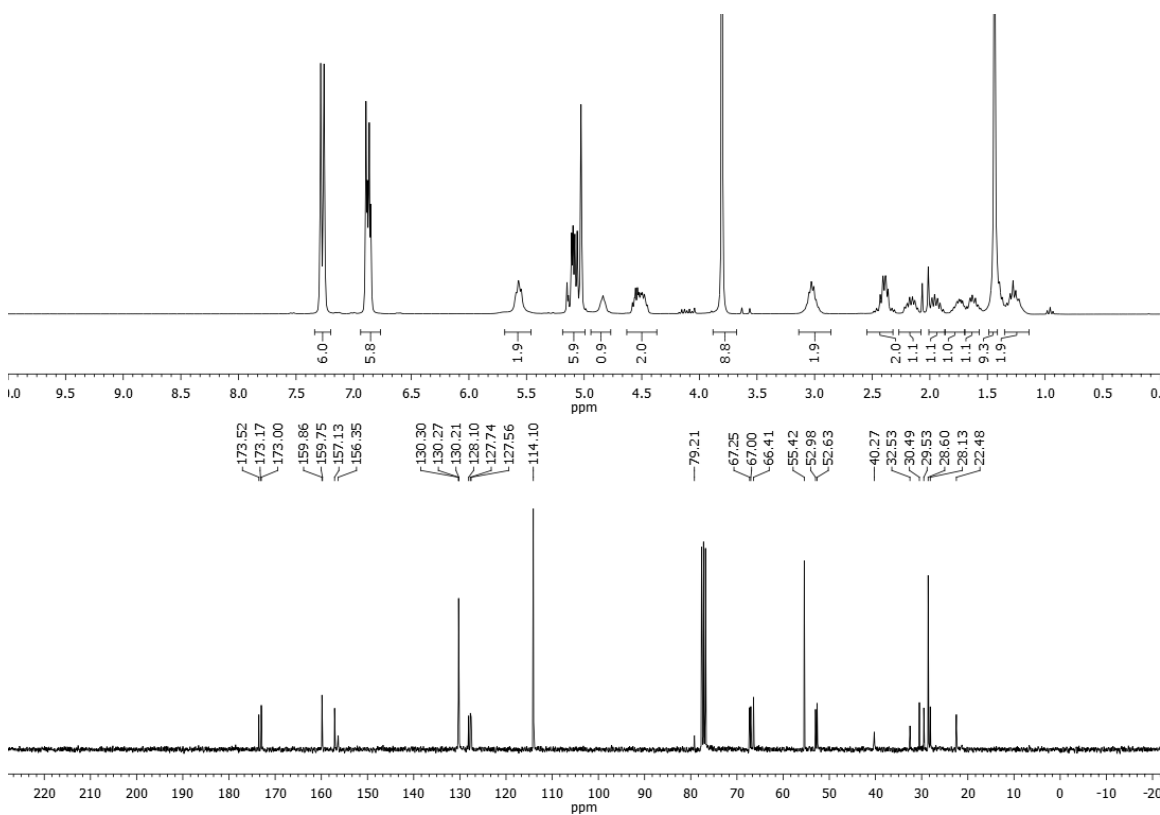


Chemical Formula:  $C_{41}H_{53}N_3O_{12}$

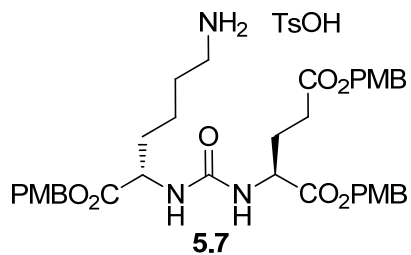
Exact Mass: 779.3629

Molecular Weight: 779.8724

$^1H$  NMR 300 MHz,  $^{13}C$  NMR 75.5 MHz,  $CDCl_3$



### PMBO-Lys-C(O)-Glu(OPMB)-OPMB-TsOH (5.7)

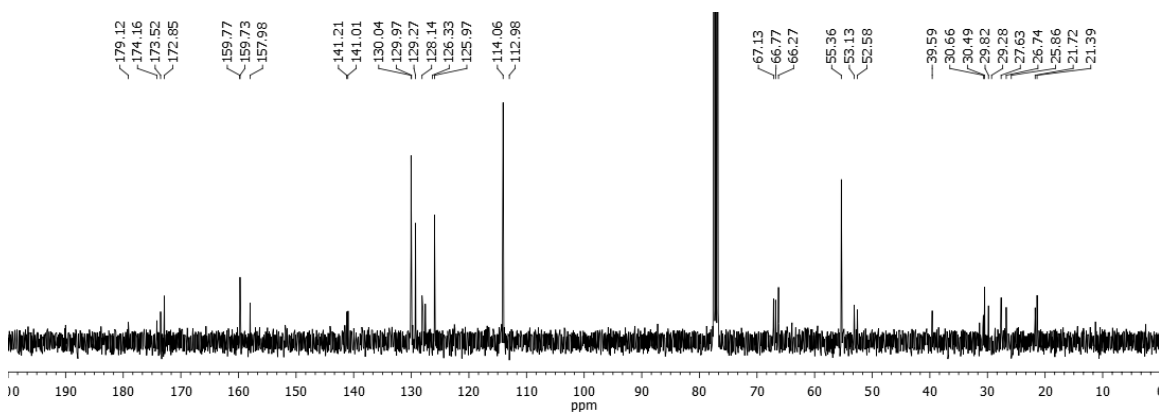
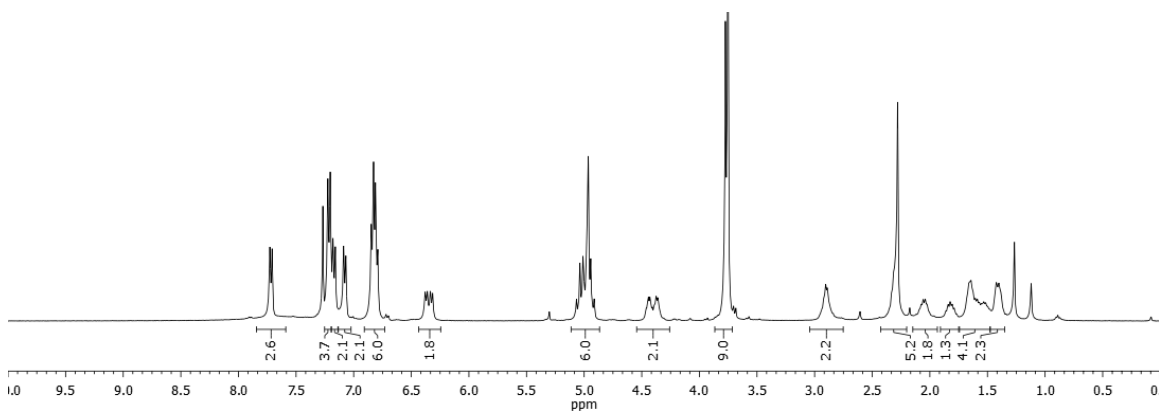


Chemical Formula:  $C_{43}H_{53}N_3O_{13}S$

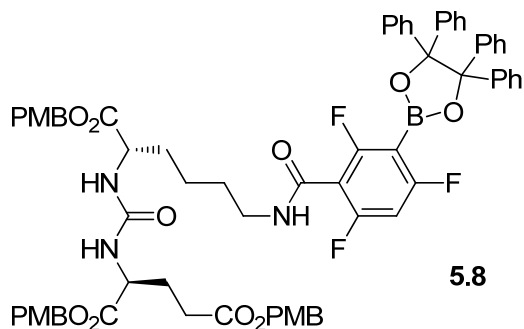
Exact Mass: 851.3299

Molecular Weight: 851.9582

$^1H$  NMR 400 MHz,  $^{13}C$  NMR 100.6 MHz,  $CDCl_3$



**PMBO-Lys(boronate)-C(O)-Glu(OPMB)-OPMB (5.8)**

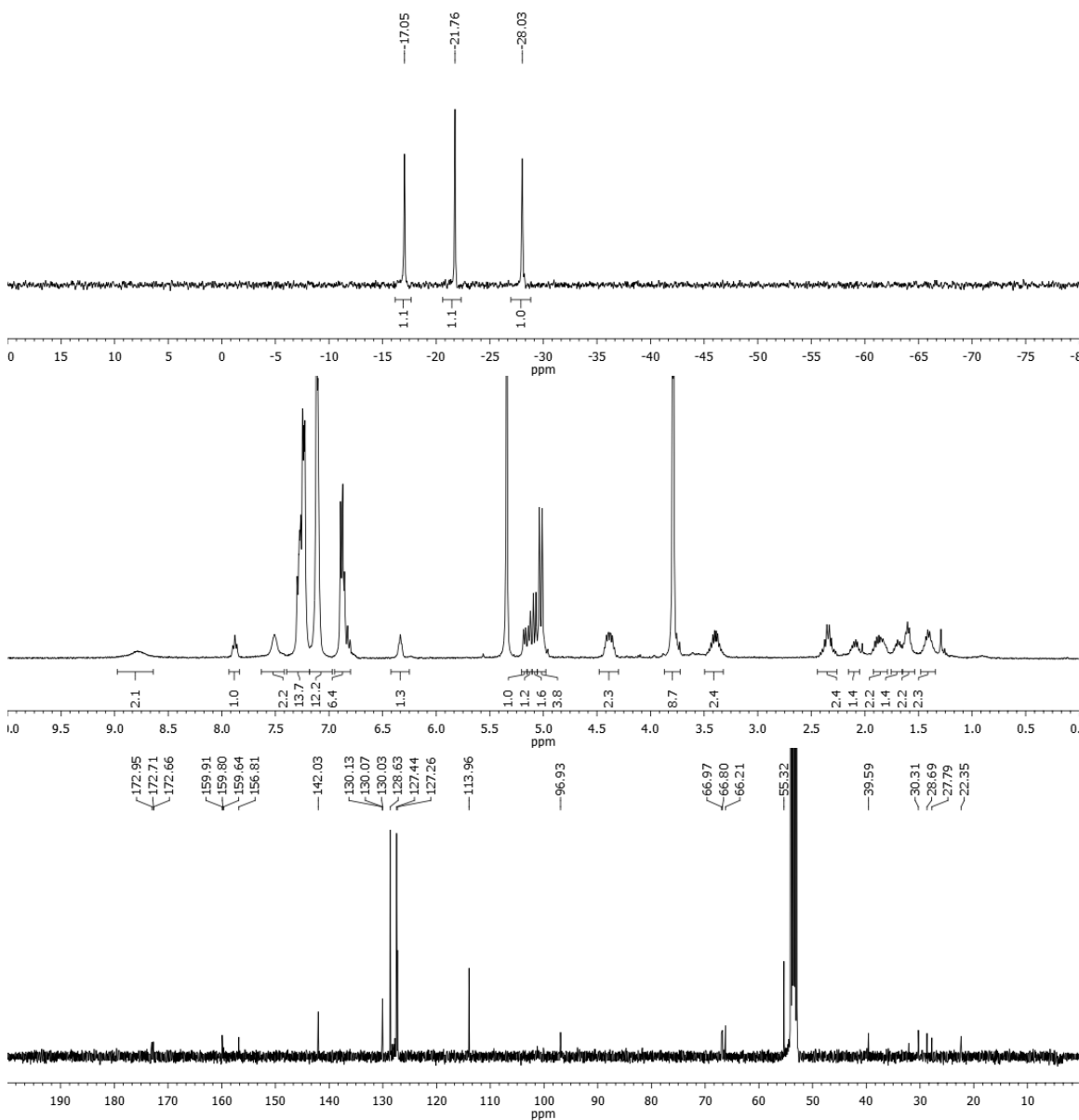


Chemical Formula:  $C_{69}H_{65}BF_3N_3O_{13}$

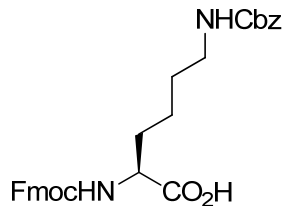
Exact Mass: 1211.4563

Molecular Weight: 1212.0729

$^{19}F$  NMR 282.4 MHz,  $^1H$  NMR 400 MHz,  $^{13}C$  NMR 100.6 MHz,  $CD_2Cl_2$



### Fmoc-(L)-Lys(Cbz)-OH (5.12)



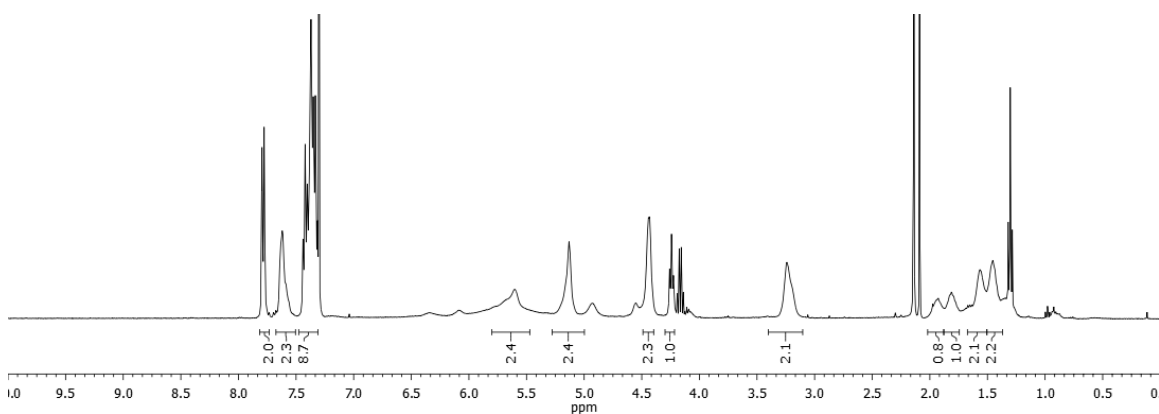
Chemical Formula:  $C_{29}H_{30}N_2O_6$

Exact Mass: 502.2104

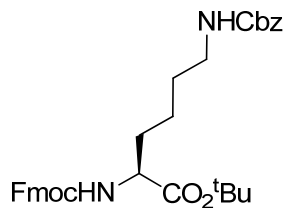
Molecular Weight: 502.5583

5.12

$^1H$  NMR 400 MHz,  $CDCl_3$



### Fmoc-(L)-Lys(Cbz)-O<sup>t</sup>Bu (5.13)



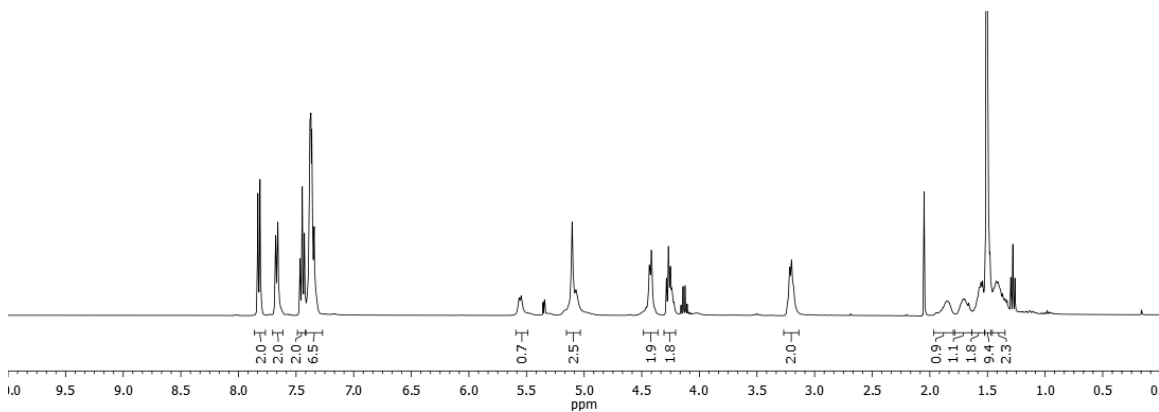
Chemical Formula:  $C_{33}H_{38}N_2O_6$

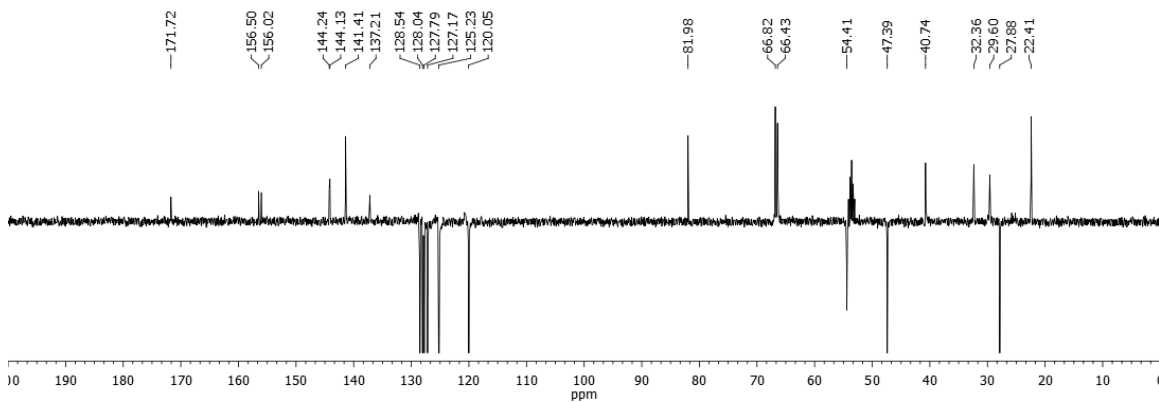
Exact Mass: 558.2730

Molecular Weight: 558.6646

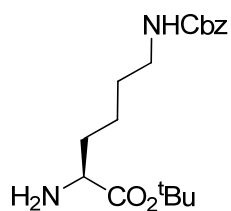
5.13

$^1H$  NMR 400 MHz,  $^{13}C$  NMR 100.6 MHz,  $CD_2Cl_2$





**H-(L)-Lys(Cbz)-O<sup>t</sup>Bu (5.14)**



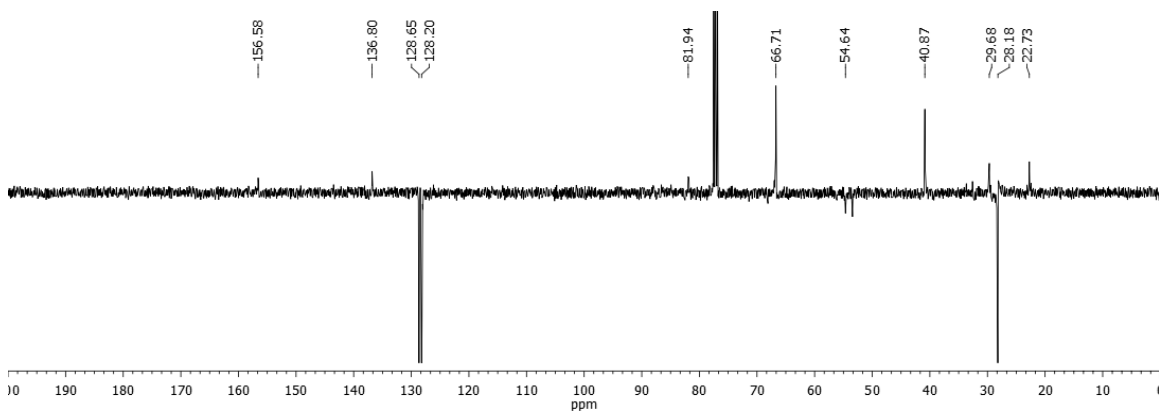
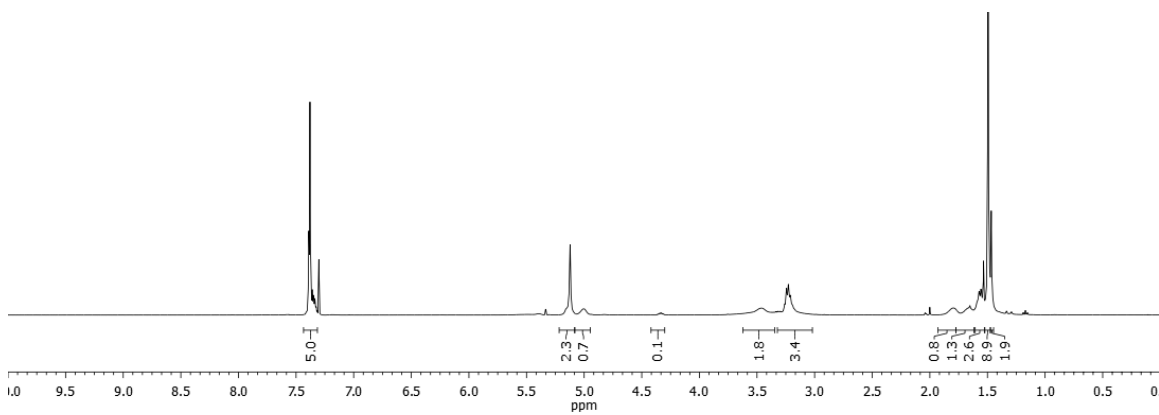
**5.14**

Chemical Formula: C<sub>18</sub>H<sub>28</sub>N<sub>2</sub>O<sub>4</sub>

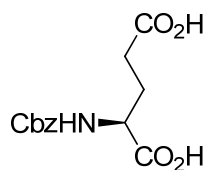
Exact Mass: 336.2049

Molecular Weight: 336.4259

<sup>1</sup>H NMR 400 MHz, <sup>13</sup>C NMR 100.6 MHz, CDCl<sub>3</sub>



### Cbz-(L)-Glu-OH (5.15)



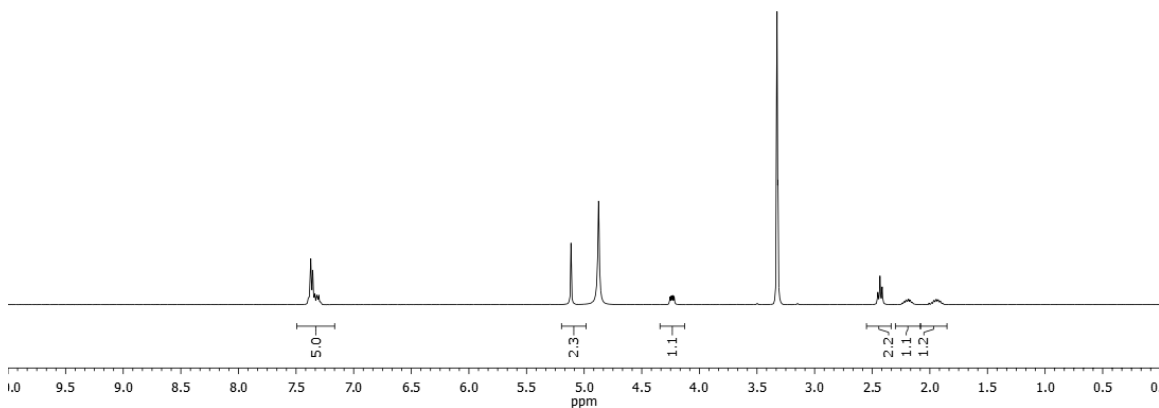
Chemical Formula: C<sub>13</sub>H<sub>15</sub>NO<sub>6</sub>

Exact Mass: 281.0899

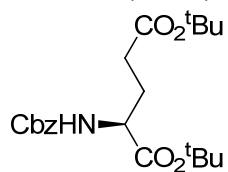
Molecular Weight: 281.2613

#### 5.15

<sup>1</sup>H NMR 400 MHz, *d*<sub>4</sub>-MeOD



### Cbz-Glu(O<sup>t</sup>Bu)-O<sup>t</sup>Bu (5.16)



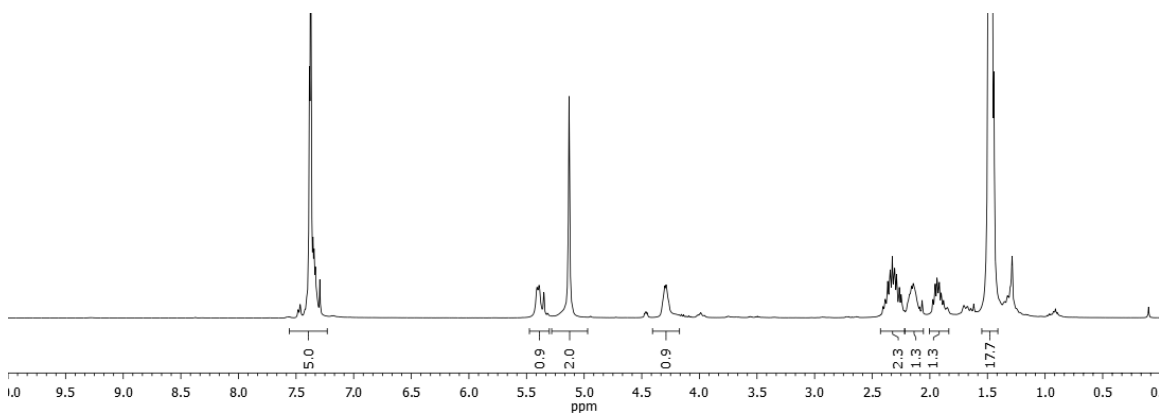
Chemical Formula: C<sub>21</sub>H<sub>31</sub>NO<sub>6</sub>

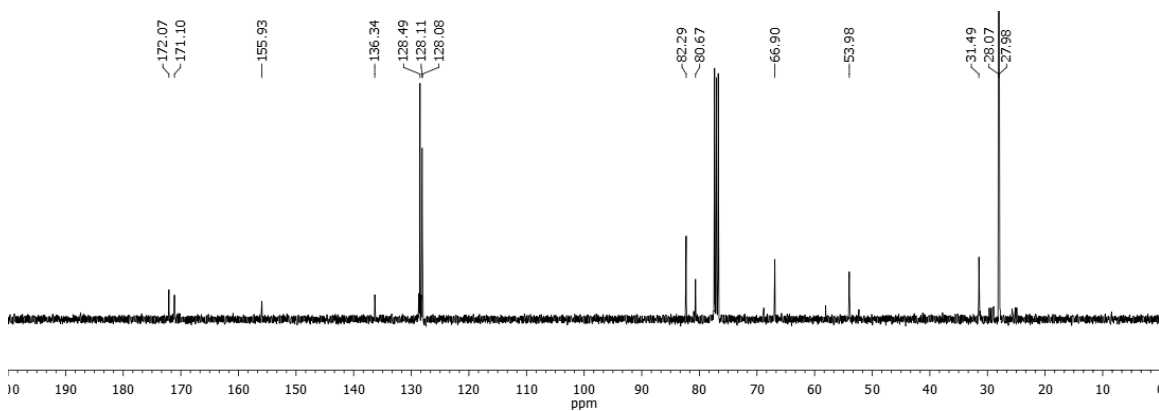
Exact Mass: 393.2151

Molecular Weight: 393.4739

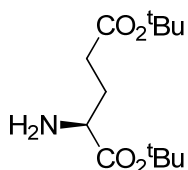
#### 5.16

<sup>1</sup>H NMR 400 MHz, <sup>13</sup>C NMR 100.6 MHz, CDCl<sub>3</sub>





### H-Glu(O<sup>t</sup>Bu)-O<sup>t</sup>Bu (5.17)



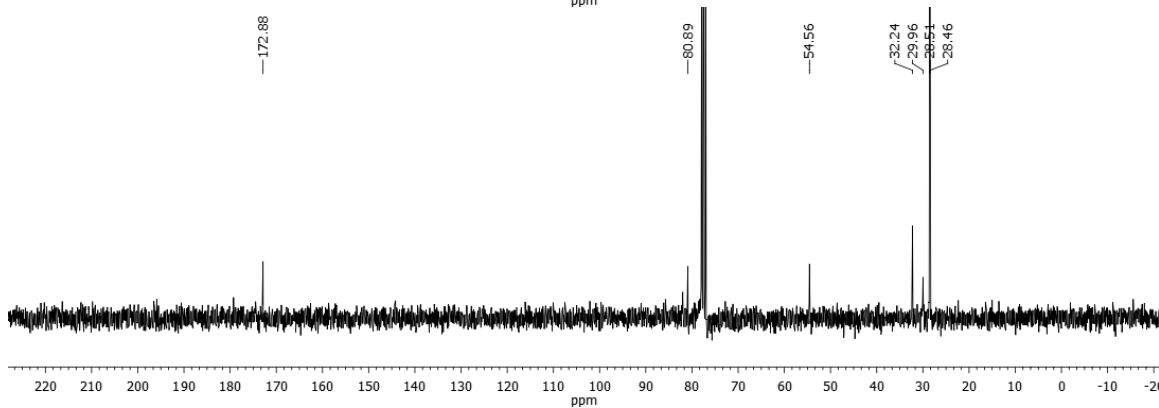
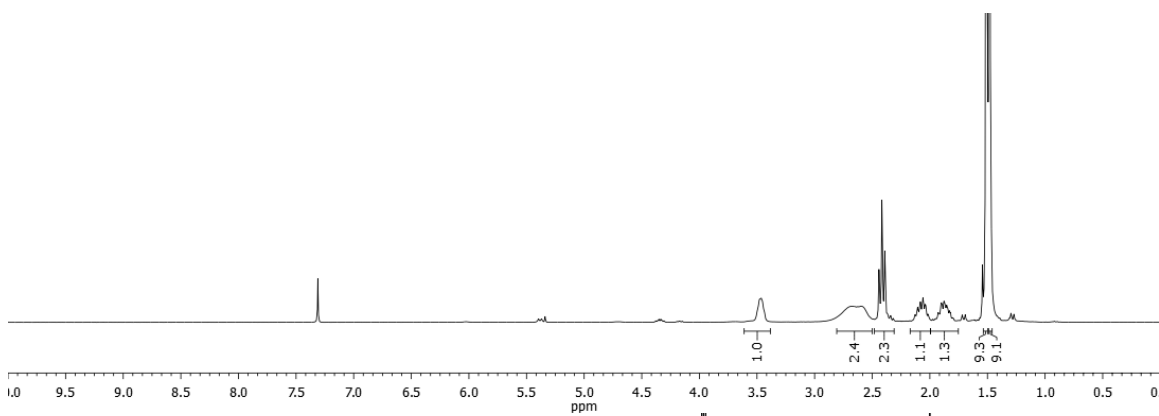
Chemical Formula: C<sub>13</sub>H<sub>25</sub>NO<sub>4</sub>

Exact Mass: 259.1784

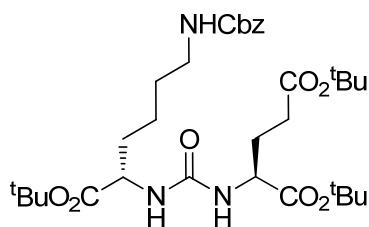
Molecular Weight: 259.3419

#### 5.17

<sup>1</sup>H NMR 300 MHz, <sup>13</sup>C NMR 75.5 MHz, CDCl<sub>3</sub>



**<sup>t</sup>BuO-Lys(Cbz)-C(O)-Glu(O<sup>t</sup>Bu)-O<sup>t</sup>Bu (5.18)**



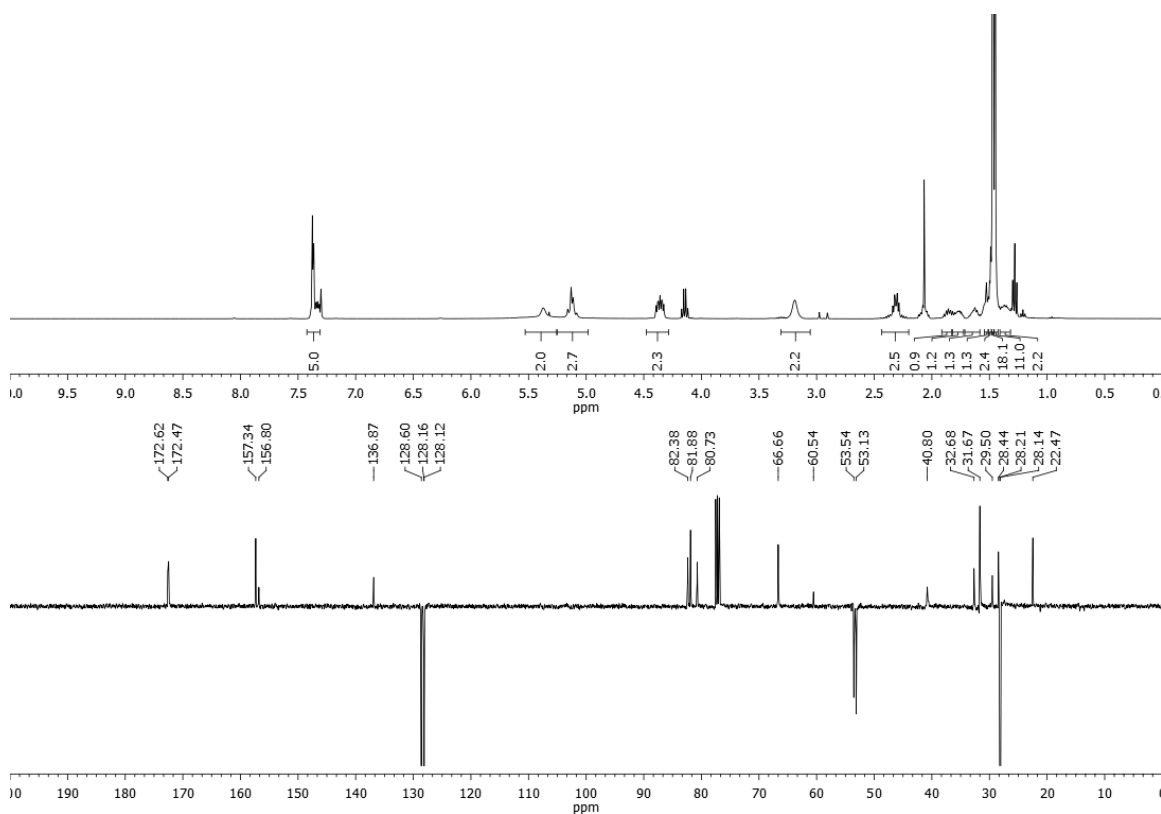
Chemical Formula: C<sub>32</sub>H<sub>51</sub>N<sub>3</sub>O<sub>9</sub>

Exact Mass: 621.3625

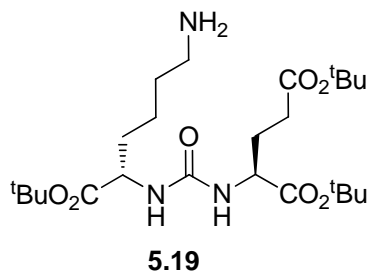
Molecular Weight: 621.7620

**5.18**

<sup>1</sup>H NMR 400 MHz, <sup>13</sup>C NMR 100.6 MHz, CDCl<sub>3</sub>



**<sup>t</sup>BuO-Lys-C(O)-Glu(O<sup>t</sup>Bu)-O<sup>t</sup>Bu (5.19)**

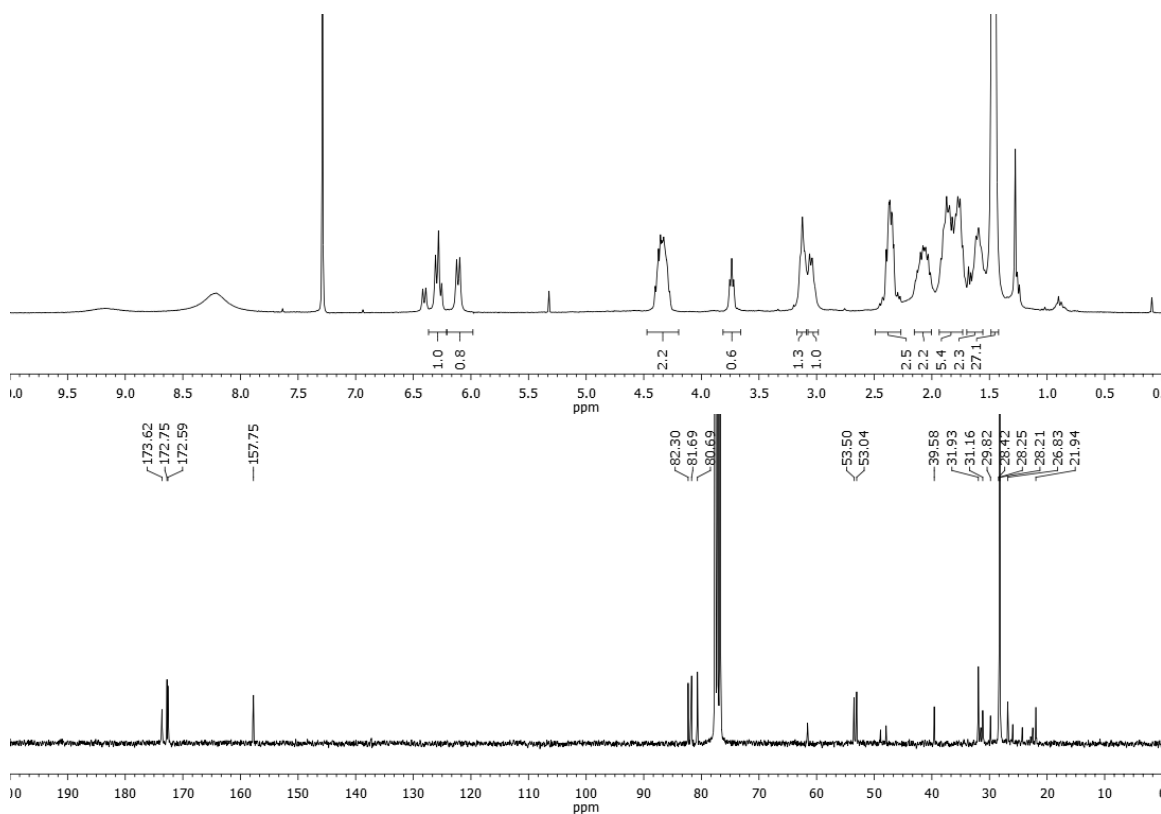


Chemical Formula: C<sub>24</sub>H<sub>45</sub>N<sub>3</sub>O<sub>7</sub>

Exact Mass: 487.3258

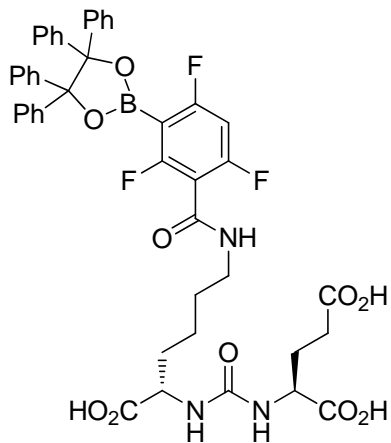
Molecular Weight: 487.6300

<sup>1</sup>H NMR 300 MHz, <sup>13</sup>C NMR 75.5 MHz, CDCl<sub>3</sub>





### HO-Lys(boronate)-C(O)-Glu(OH)-OH (urea-boronate) (5.9)



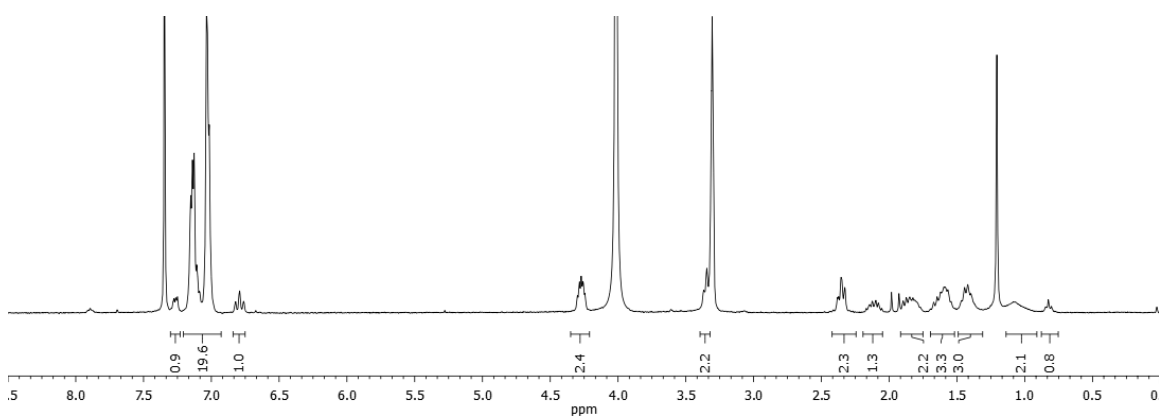
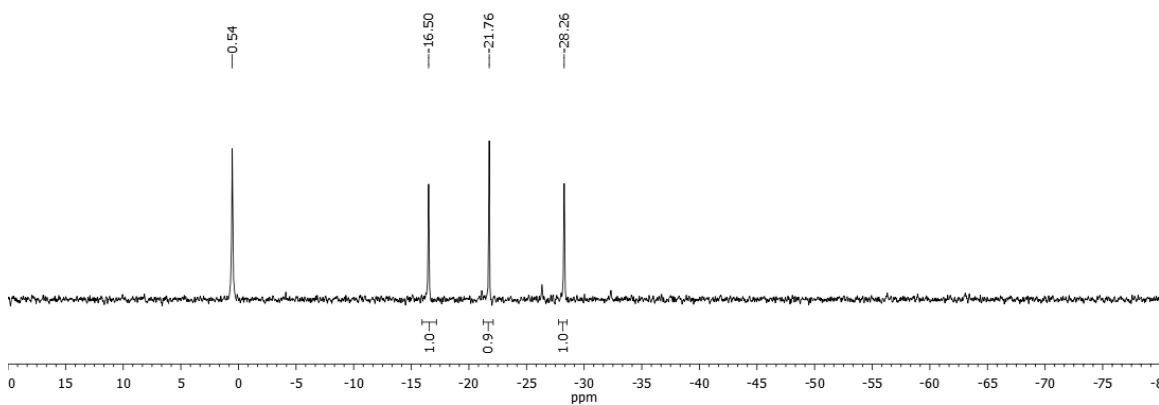
Chemical Formula:  $C_{45}H_{41}BF_3N_3O_{10}$

Exact Mass: 851.2837

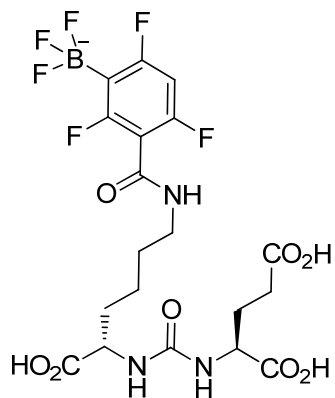
Molecular Weight: 851.6273

**5.9**

$^{19}F$  NMR 282.4 MHz,  $^1H$  NMR 300 MHz,  $d_4$ -MeOD/ $CDCl_3$



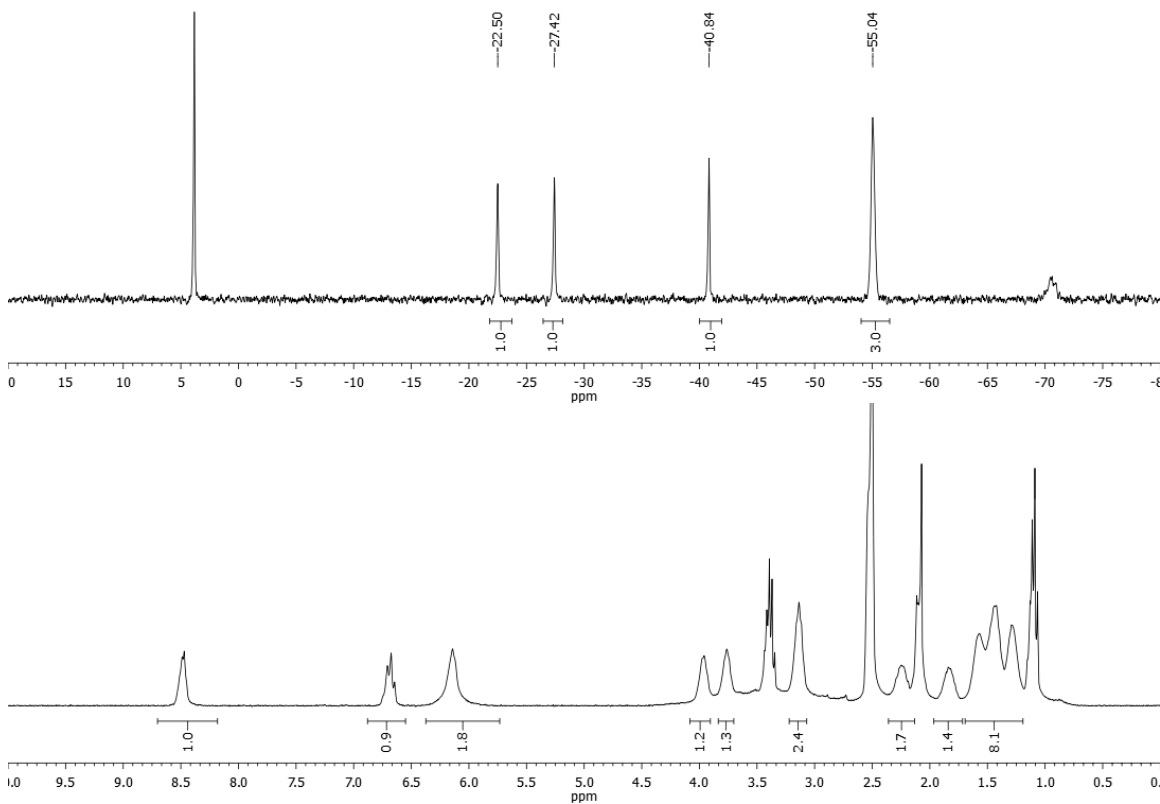
### Urea-ArBF<sub>3</sub> (5.10)



Chemical Formula: C<sub>19</sub>H<sub>21</sub>BF<sub>6</sub>N<sub>3</sub>O<sub>8</sub>  
Exact Mass: 544.1331  
Molecular Weight: 544.1873

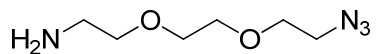
5.10

<sup>19</sup>F NMR 282.4 MHz, <sup>1</sup>H NMR 300 MHz, d<sub>6</sub>-DMSO



## Appendix E.5. NMR spectra for Chapter 6

### 2-(2-(2-Azidoethoxy-ethoxy)ethanamine (6.1)



6.1

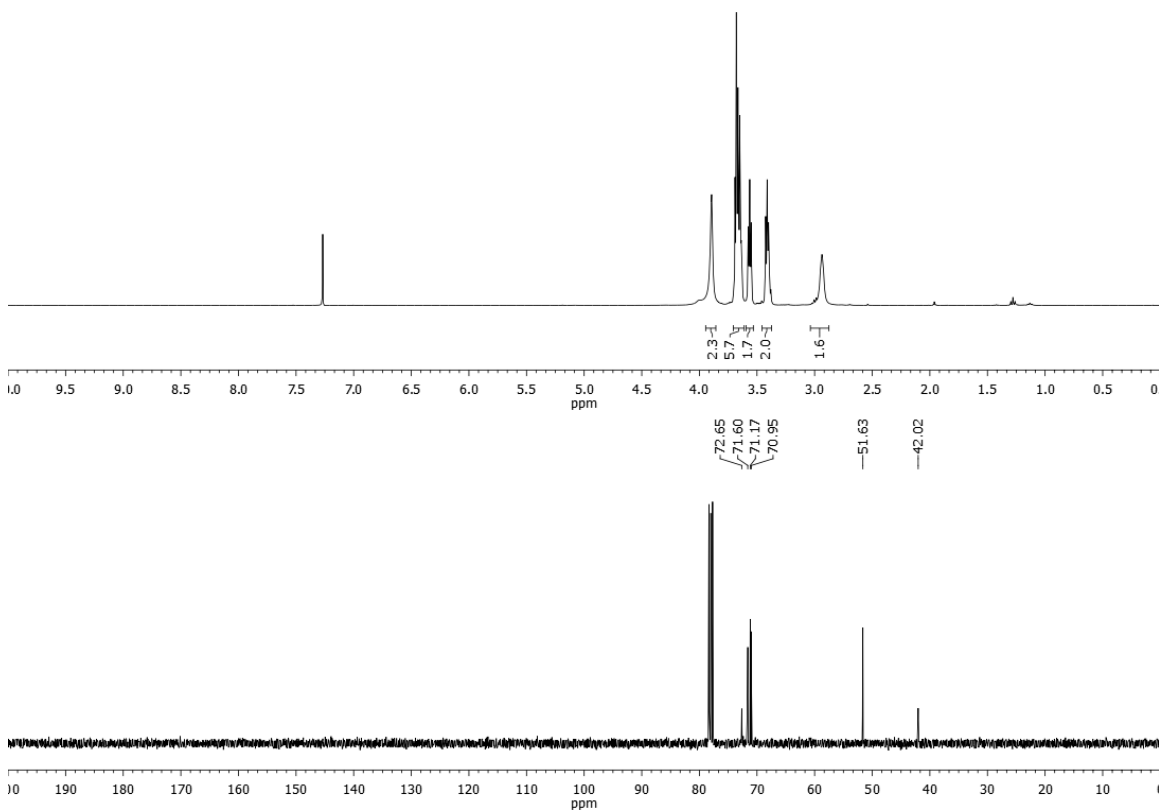
Chemical Formula:

$C_6H_{14}N_4O_2$

Exact Mass: 174.1117

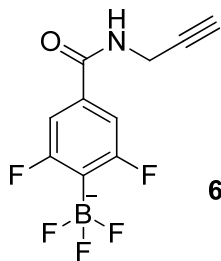
Molecular Weight: 174.2010

$^1H$  NMR 400 MHz,  $^{13}C$  NMR 100.6 MHz,  $CDCl_3$



**(2,6-Difluoro-4-(prop-2-yn-1-ylcarbonyl)phenyl)trifluoroborate (alkynylArBF<sub>3</sub>)**

**(6.2)**



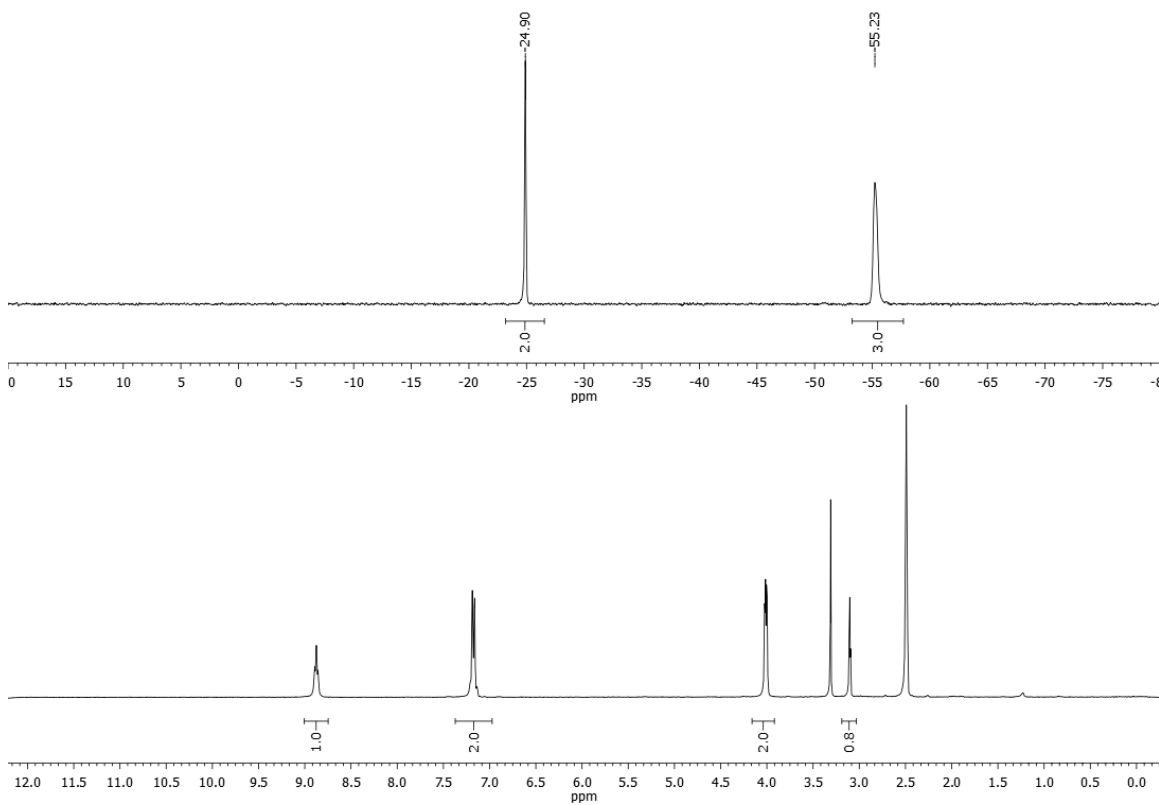
**6.2**

Chemical Formula: C<sub>10</sub>H<sub>6</sub>BF<sub>5</sub>NO<sup>-</sup>

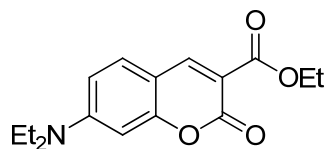
Exact Mass: 262.0468

Molecular Weight: 261.9643

<sup>19</sup>F NMR 282.4, MHz <sup>1</sup>H NMR 300 MHz, *d*<sub>6</sub>-DMSO



### Ethyl 7-diethylaminocoumarin-3-carboxylate (6.3a)



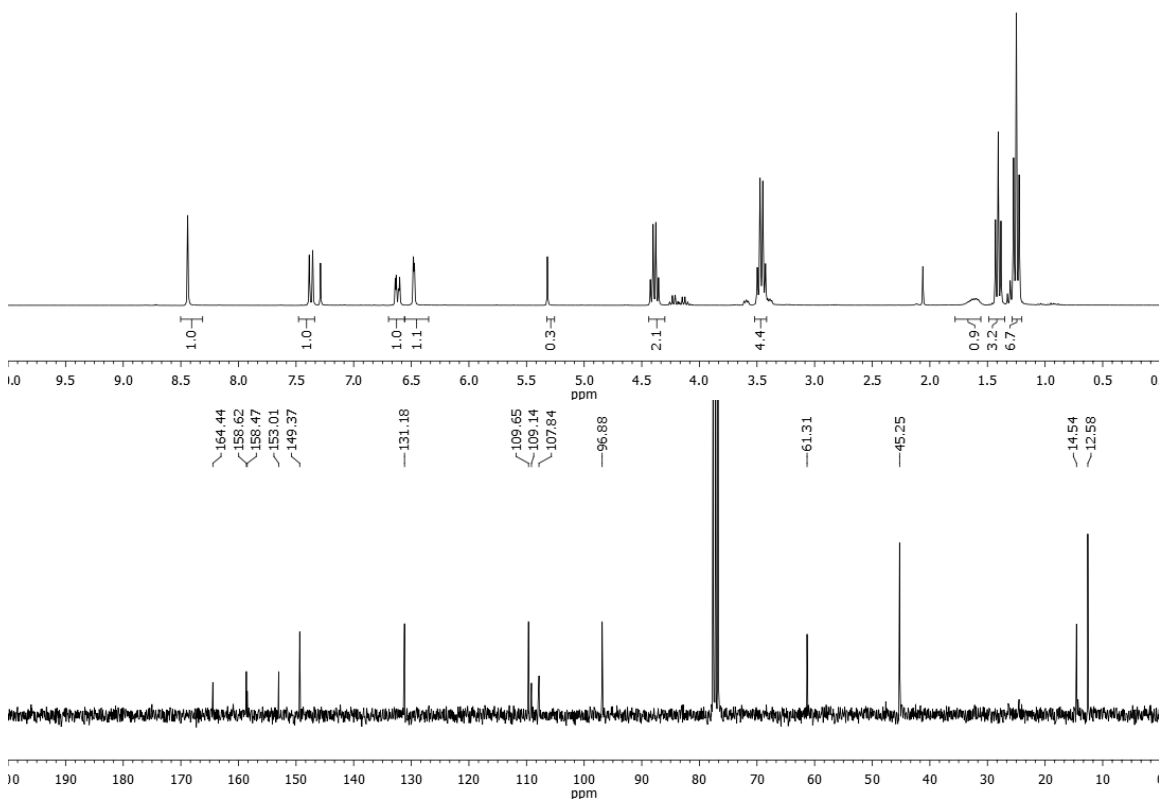
**6.3a**

Chemical Formula: C<sub>16</sub>H<sub>19</sub>NO<sub>4</sub>

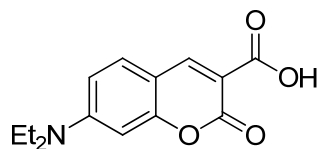
Exact Mass: 289.1314

Molecular Weight: 289.3264

<sup>1</sup>H NMR 300 MHz, <sup>13</sup>C NMR 75.5 MHz, CDCl<sub>3</sub>



## 7-Diethylaminocoumarin-3-carboxylic acid (6.3b)



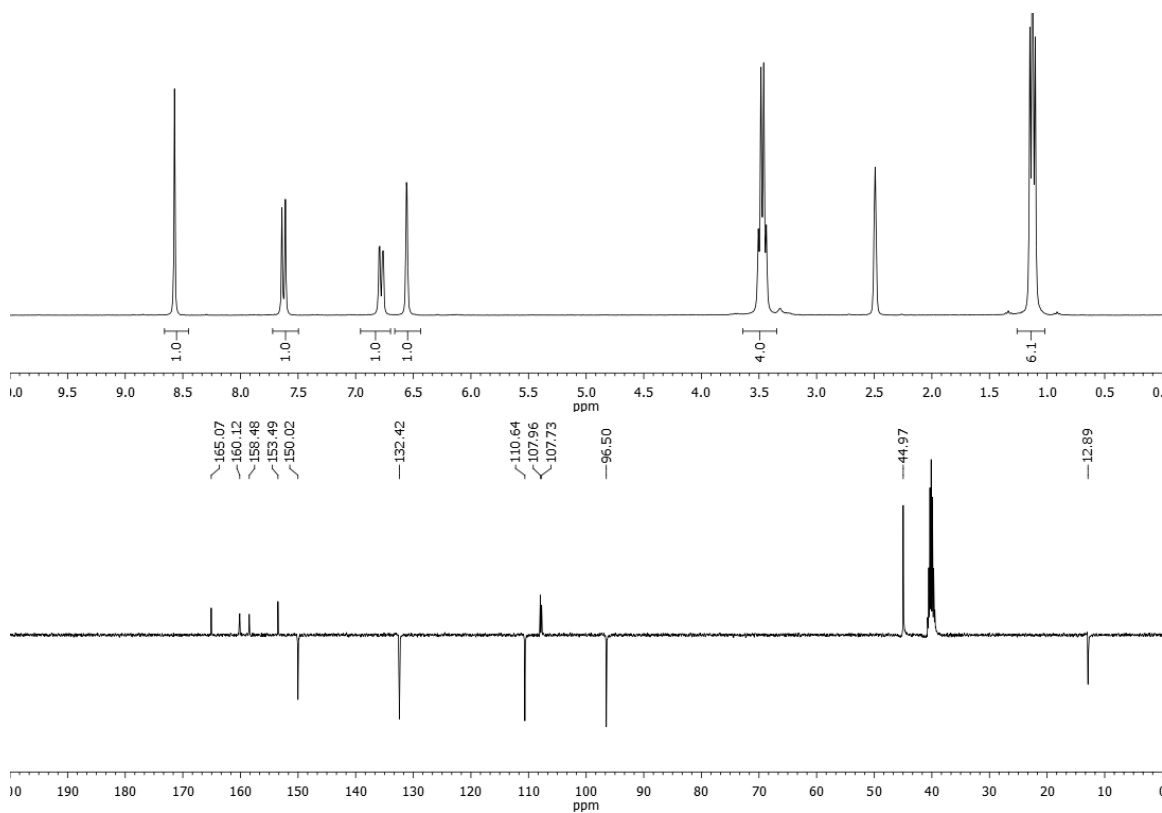
**6.3b**

Chemical Formula: C<sub>14</sub>H<sub>15</sub>NO<sub>4</sub>

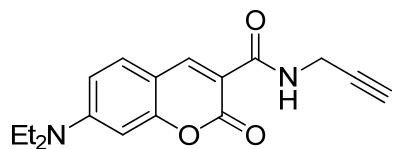
Exact Mass: 261.1001

Molecular Weight: 261.2732

<sup>1</sup>H NMR 300 MHz, <sup>13</sup>C NMR 100.6 MHz, *d*<sub>6</sub>-DMSO



7-(Diethylamino)-2-oxo-N-2-propyn-1-yl-2H-1-benzopyran-3-carboxamide (6.4)



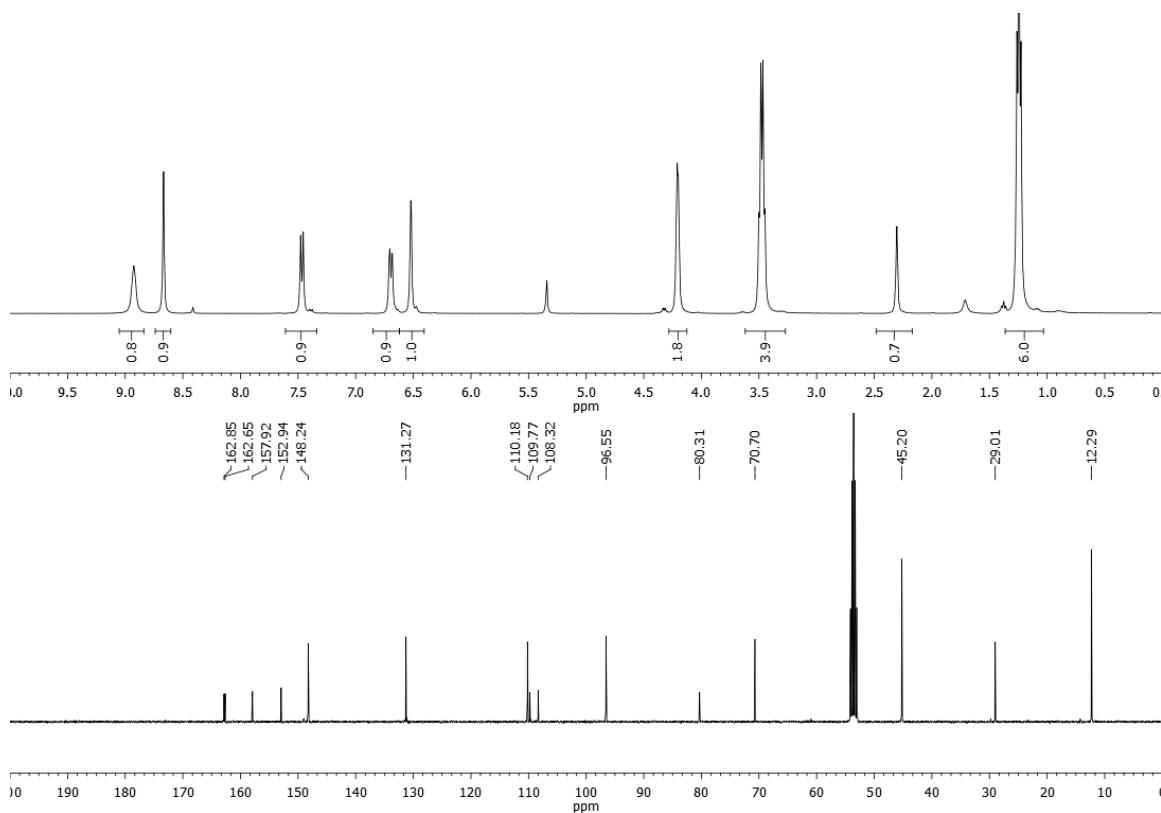
6.4

Chemical Formula: C<sub>17</sub>H<sub>18</sub>N<sub>2</sub>O<sub>3</sub>

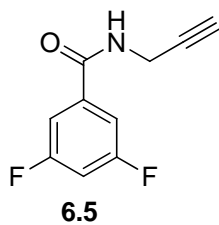
Exact Mass: 298.1317

Molecular Weight: 298.3364

<sup>1</sup>H NMR 400 MHz, <sup>13</sup>C NMR 100.6 MHz, CD<sub>2</sub>Cl<sub>2</sub>

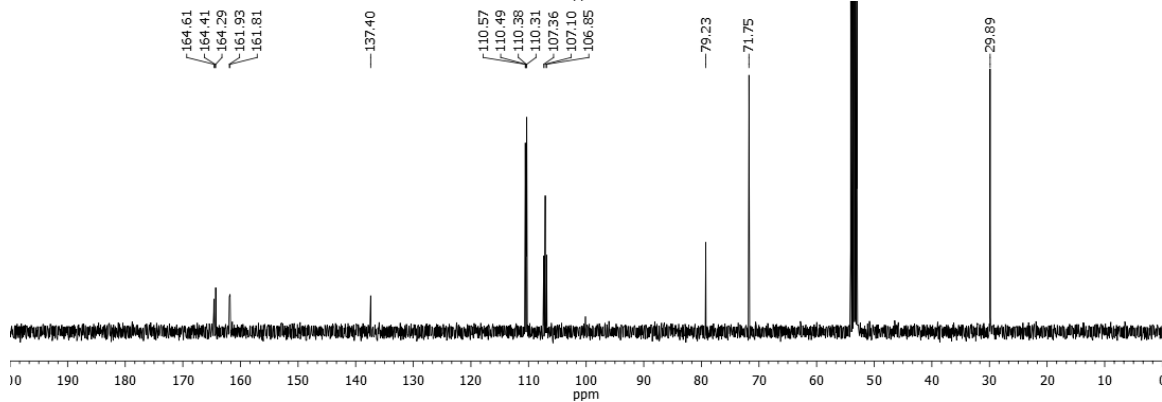
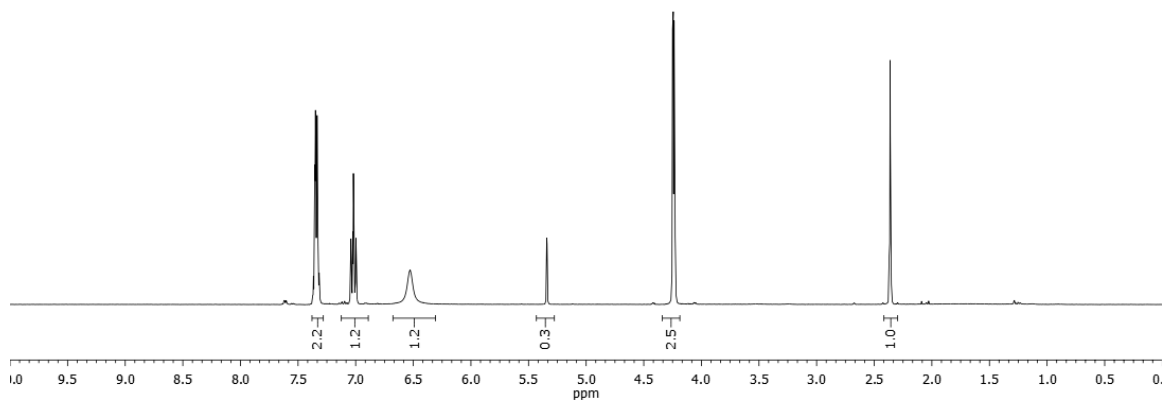
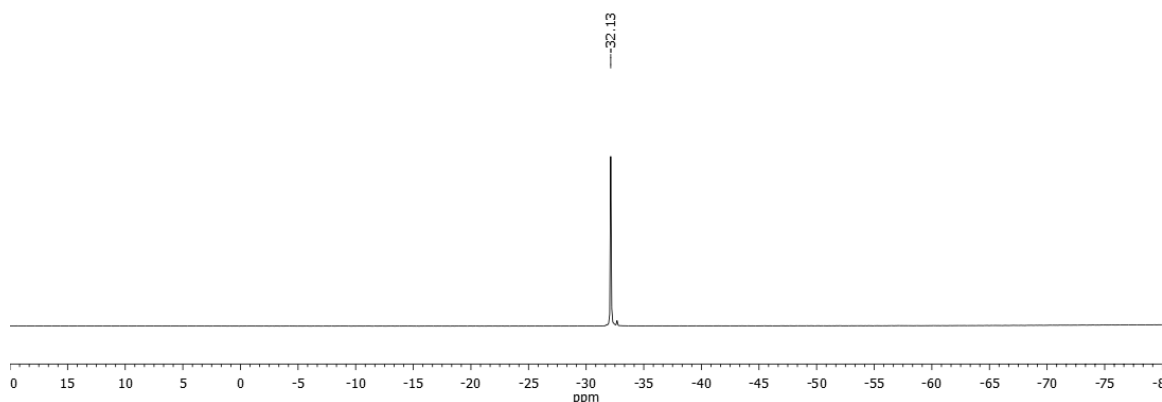


### 3,5-Difluoro-*N*-(prop-2-yn-1-yl)benzamide (6.5)

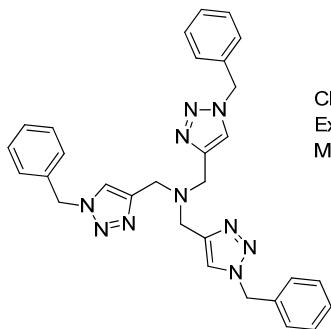


Chemical Formula:  
 $C_{10}H_7F_2NO$   
Exact Mass: 195.0496  
Molecular Weight:  
195.1655

$^{19}F$  NMR 282.4 MHz,  $^1H$  NMR 300 MHz,  $^{13}C$  NMR 100.6 MHz,  $CDCl_3$

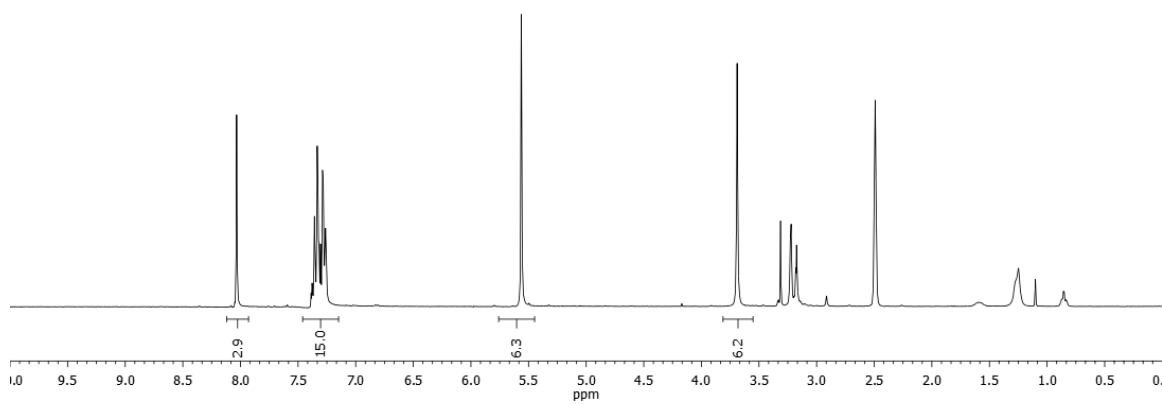


## Tris-(benzyltriaazolylmethyl)amine (TBTA)



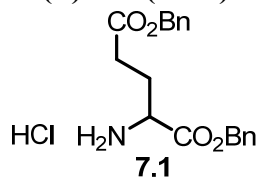
Chemical Formula:  $C_{30}H_{30}N_{10}$   
Exact Mass: 530.2655  
Molecular Weight: 530.6262

$^1\text{H}$  NMR 300 MHz,  $d_6$ -DMSO



## Appendix E.6. NMR spectra for Chapter 7

### H-(L)-Glu(OBn)-OBn·HCl (7.1)

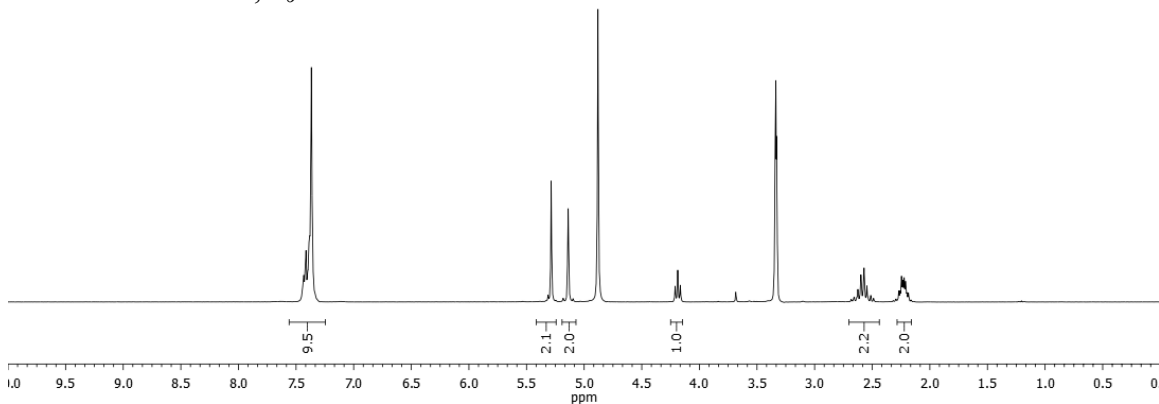


Chemical Formula: C<sub>19</sub>H<sub>22</sub>ClNO<sub>4</sub>

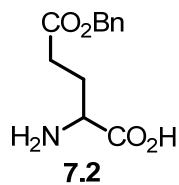
Exact Mass: 363.1237

Molecular Weight: 363.8353

<sup>1</sup>H NMR 300 MHz, *d*<sub>6</sub>-MeOD



### H-(L)-Glu(OBn)-OH (7.2)

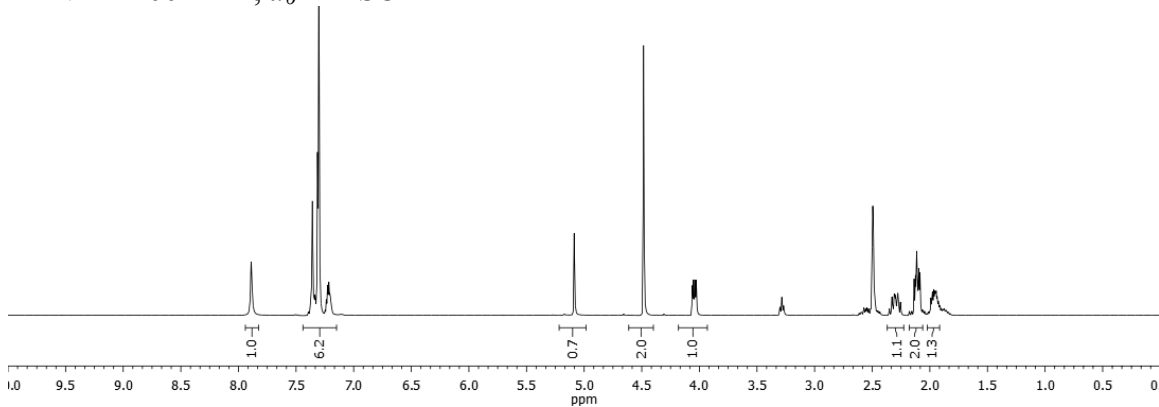


Chemical Formula: C<sub>12</sub>H<sub>15</sub>NO<sub>4</sub>

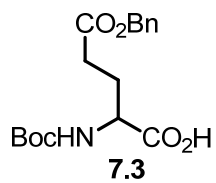
Exact Mass: 237.1001

Molecular Weight: 237.2518

<sup>1</sup>H NMR 400 MHz, *d*<sub>6</sub>-DMSO



### Boc-(L)-Glu(OBn)-OH (7.3)

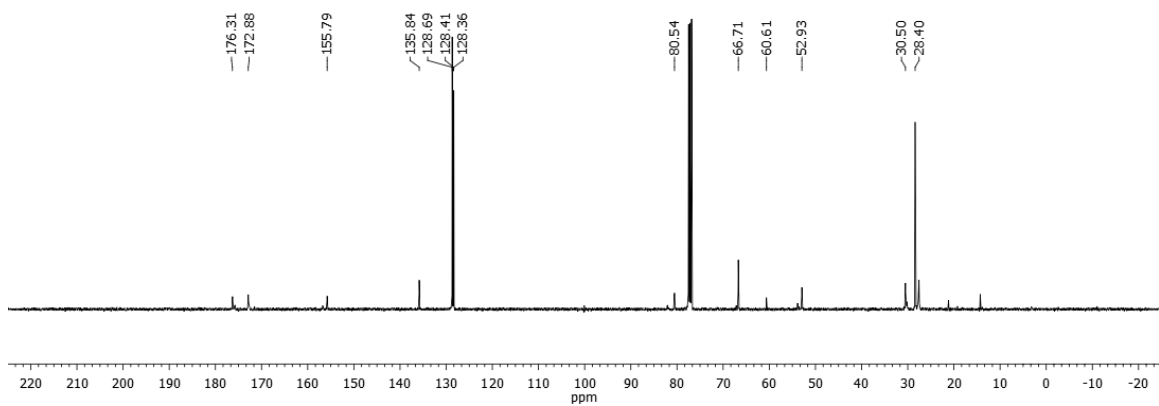
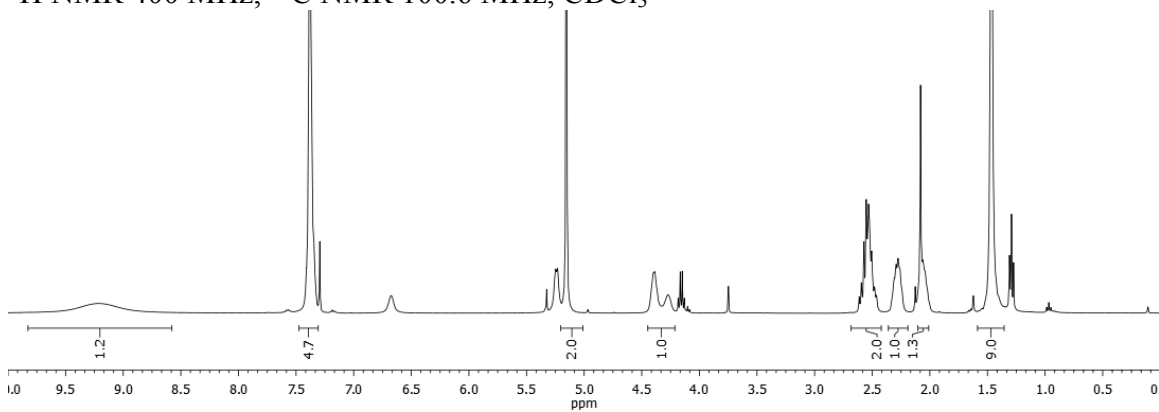


Chemical Formula: C<sub>17</sub>H<sub>23</sub>NO<sub>6</sub>

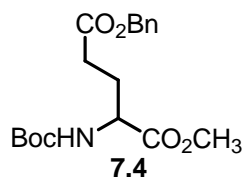
Exact Mass: 337.1525

Molecular Weight: 337.3676

<sup>1</sup>H NMR 400 MHz, <sup>13</sup>C NMR 100.6 MHz, CDCl<sub>3</sub>

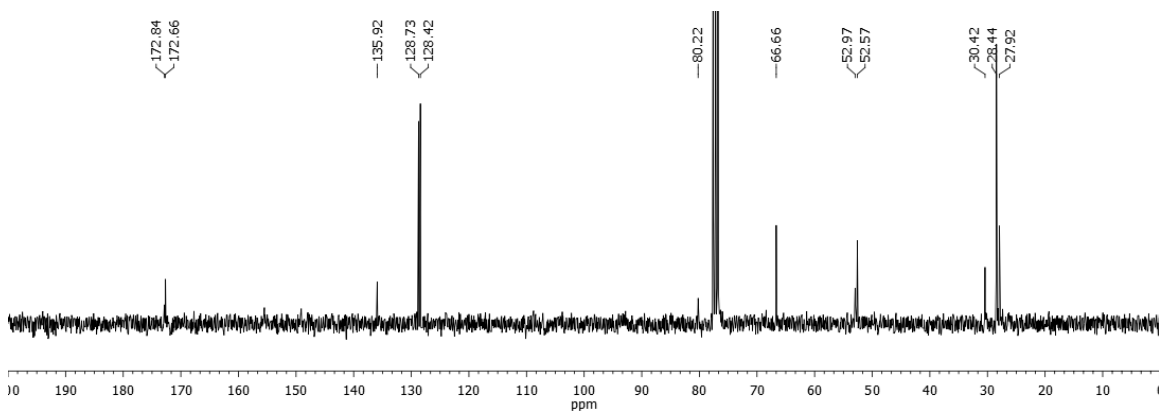
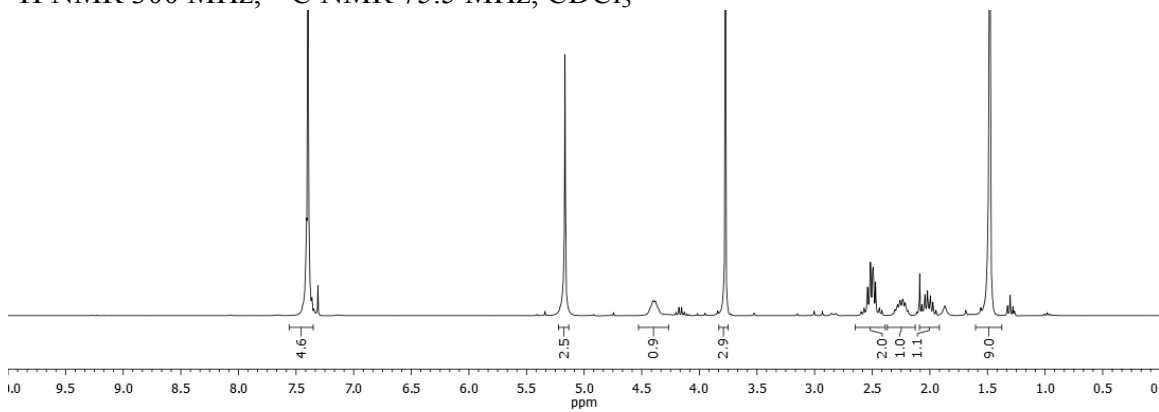


### Boc-(L)-Glu(OBn)-OCH<sub>3</sub> (7.4)

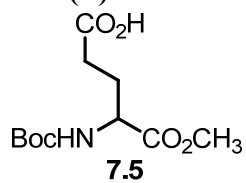


Chemical Formula: C<sub>18</sub>H<sub>25</sub>NO<sub>6</sub>  
Exact Mass: 351.1682  
Molecular Weight: 351.3942

<sup>1</sup>H NMR 300 MHz, <sup>13</sup>C NMR 75.5 MHz, CDCl<sub>3</sub>



**Boc-(L)-Glu-OCH<sub>3</sub> (7.5)**

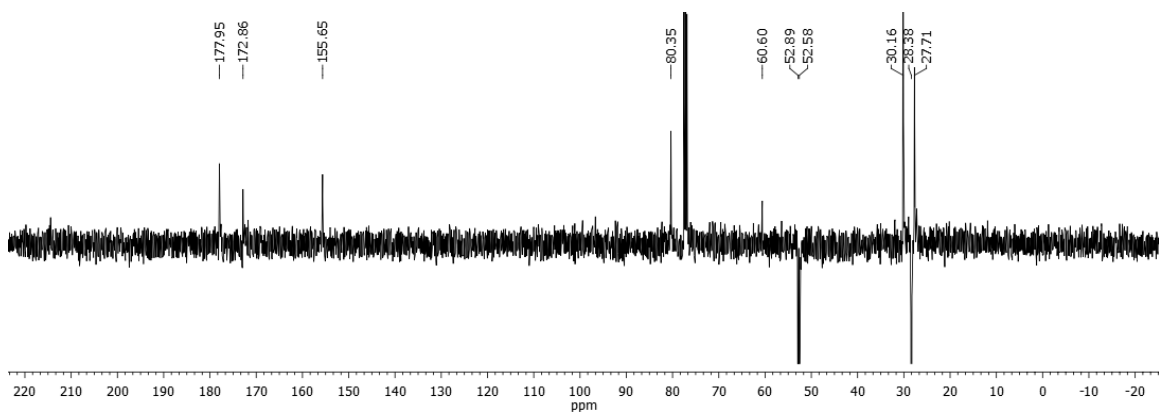
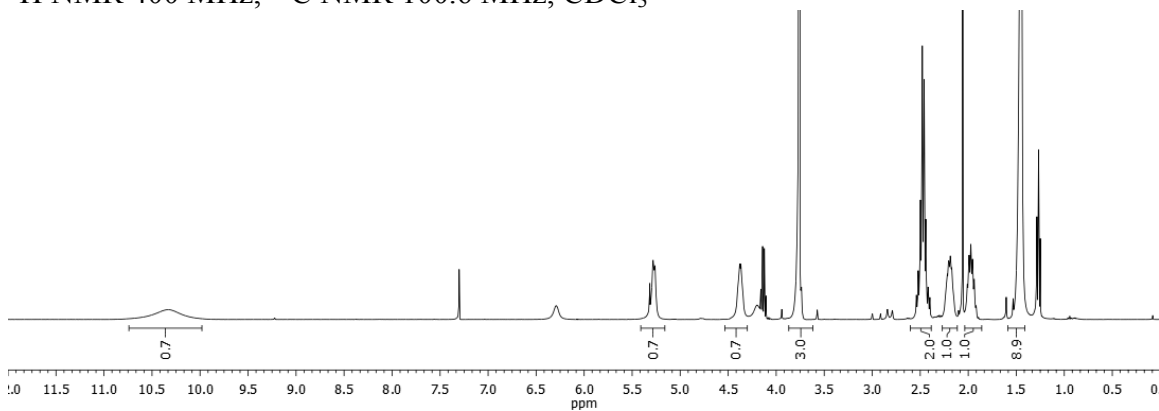


Chemical Formula: C<sub>11</sub>H<sub>19</sub>NO<sub>6</sub>

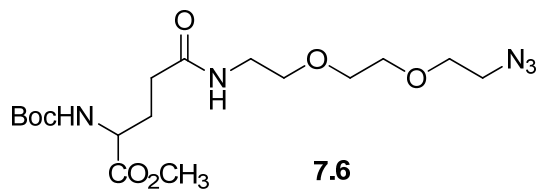
Exact Mass: 261.1212

Molecular Weight: 261.2717

<sup>1</sup>H NMR 400 MHz, <sup>13</sup>C NMR 100.6 MHz, CDCl<sub>3</sub>



### Boc-(L)-Glu[(PEG)<sub>2</sub>N<sub>3</sub>]-OCH<sub>3</sub> (7.6)

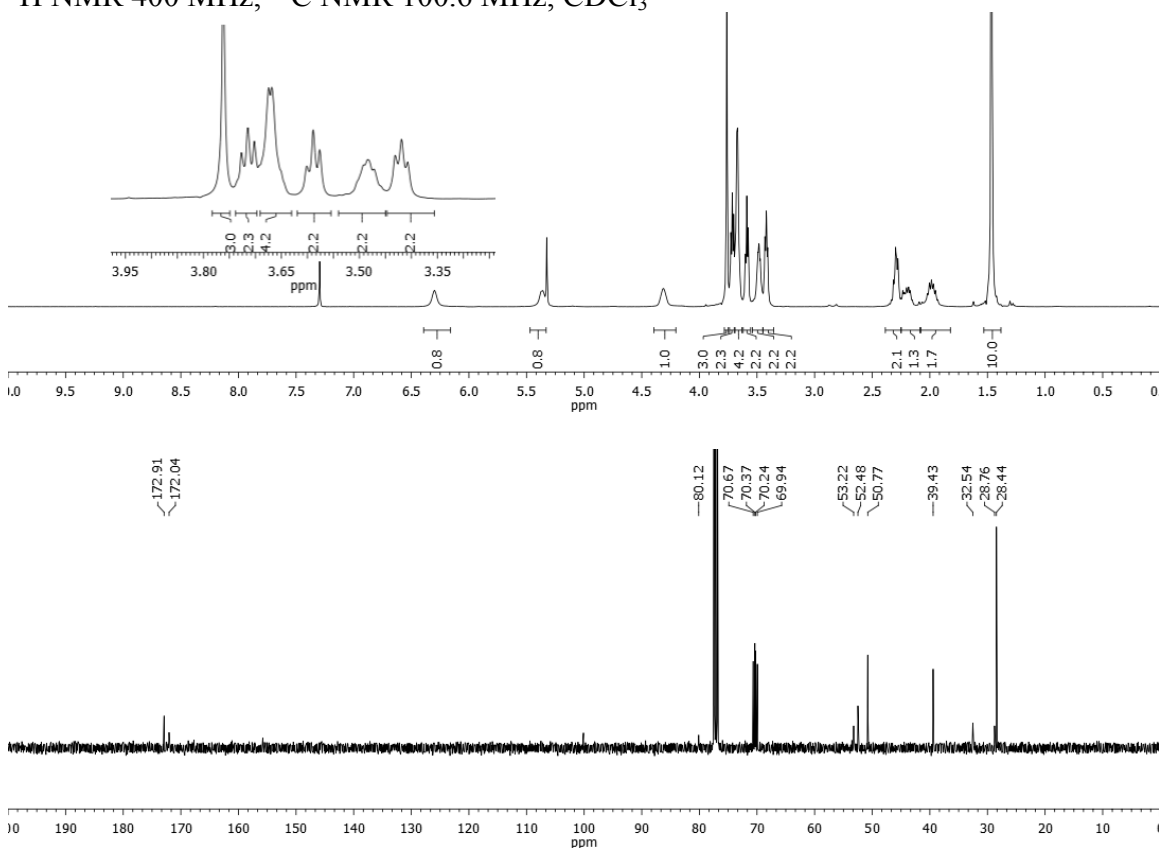


Chemical Formula: C<sub>17</sub>H<sub>31</sub>N<sub>5</sub>O<sub>7</sub>

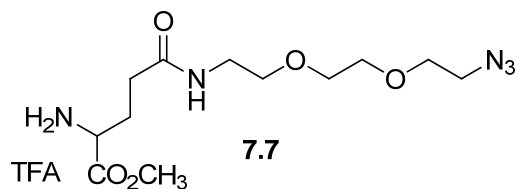
Exact Mass: 417.2223

Molecular Weight: 417.4573

<sup>1</sup>H NMR 400 MHz, <sup>13</sup>C NMR 100.6 MHz, CDCl<sub>3</sub>



# H-(L)-Glu[(PEG)<sub>2</sub>N<sub>3</sub>]-OCH<sub>3</sub> · TFA (7.7)

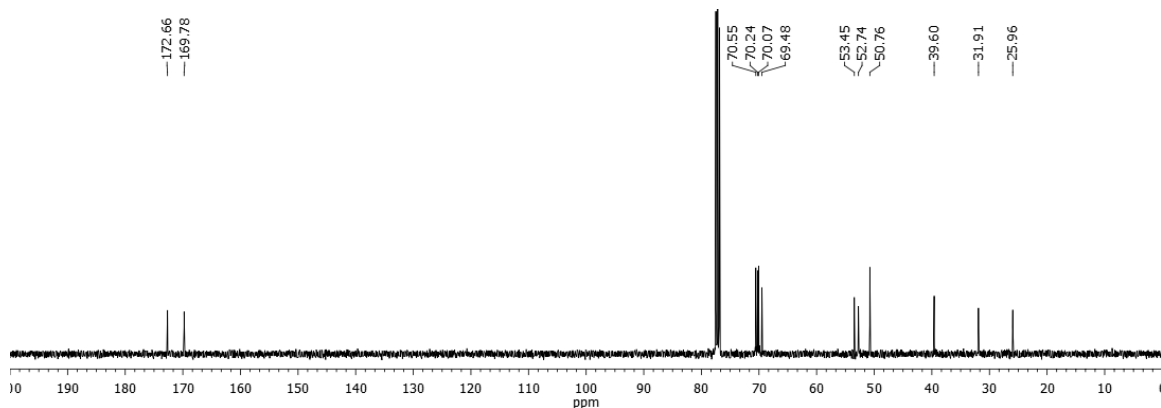
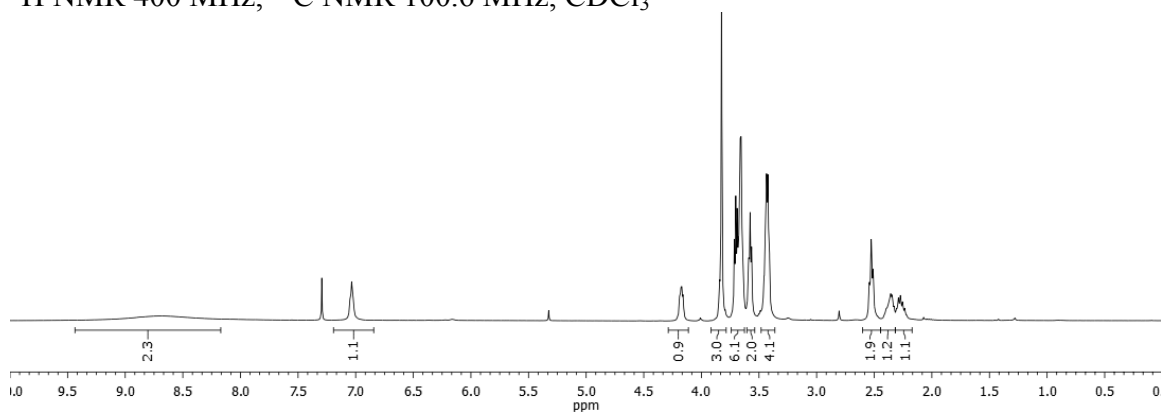


Chemical Formula: C<sub>14</sub>H<sub>23</sub>F<sub>3</sub>N<sub>5</sub>O<sub>6</sub>

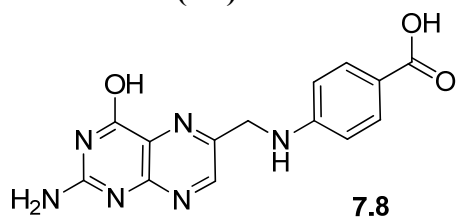
Exact Mass: 414.1600

Molecular Weight: 414.3575

TFA  
<sup>1</sup>H NMR 400 MHz, <sup>13</sup>C NMR 100.6 MHz, CDCl<sub>3</sub>



**Pterotic acid (7.8)**

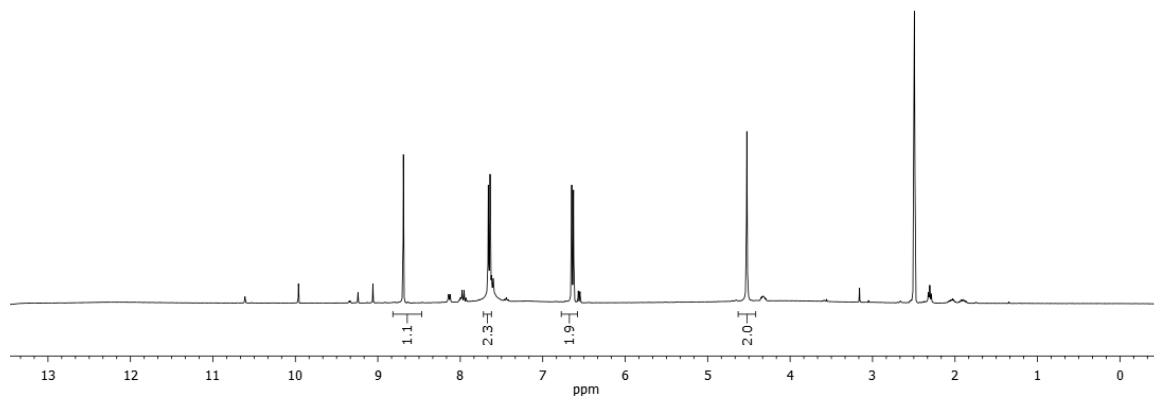


Chemical Formula:  $C_{14}H_{12}N_6O_3$

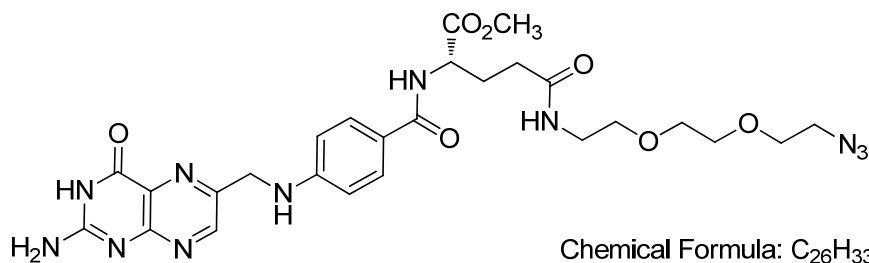
Exact Mass: 312.0971

Molecular Weight: 312.2835

$^1H$  NMR 400 MHz,  $^{13}C$  NMR 100.6 MHz,  $d_6$ -DMSO



**Pte-Glu[(PEG)<sub>2</sub>N<sub>3</sub>]-OCH<sub>3</sub> (7.9)**



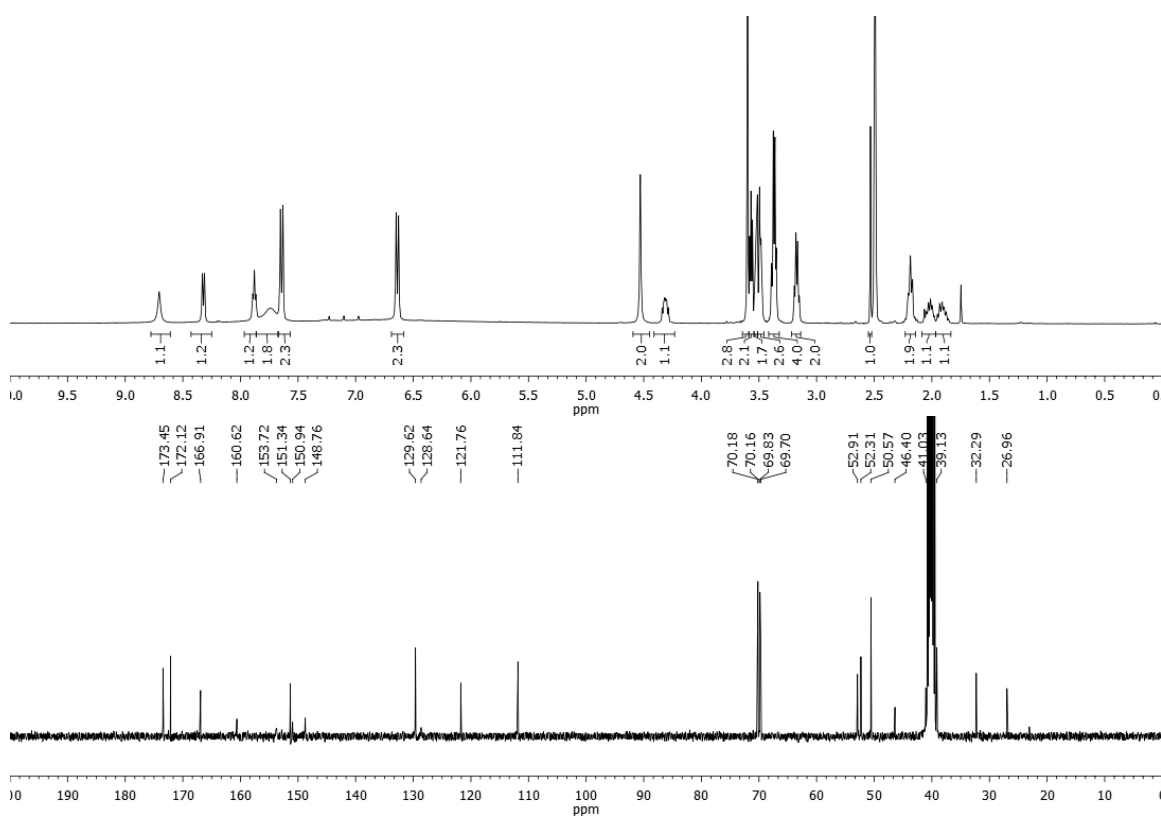
**7.9**

Chemical Formula: C<sub>26</sub>H<sub>33</sub>N<sub>11</sub>O<sub>7</sub>

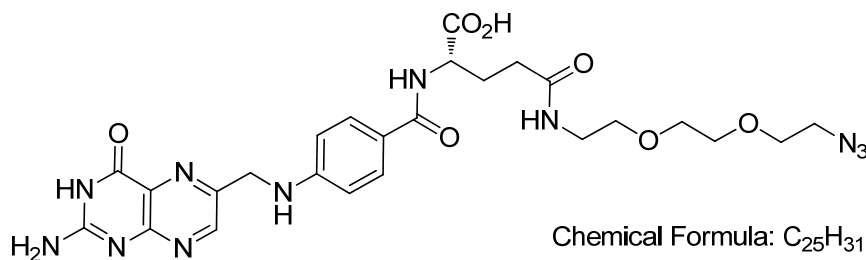
Exact Mass: 611.2564

Molecular Weight: 611.6097

<sup>1</sup>H NMR 400 MHz, <sup>13</sup>C NMR 100.6 MHz, *d*<sub>6</sub>-DMSO



**Pte-Glu[(PEG)<sub>2</sub>N<sub>3</sub>]-OH (7.10)**



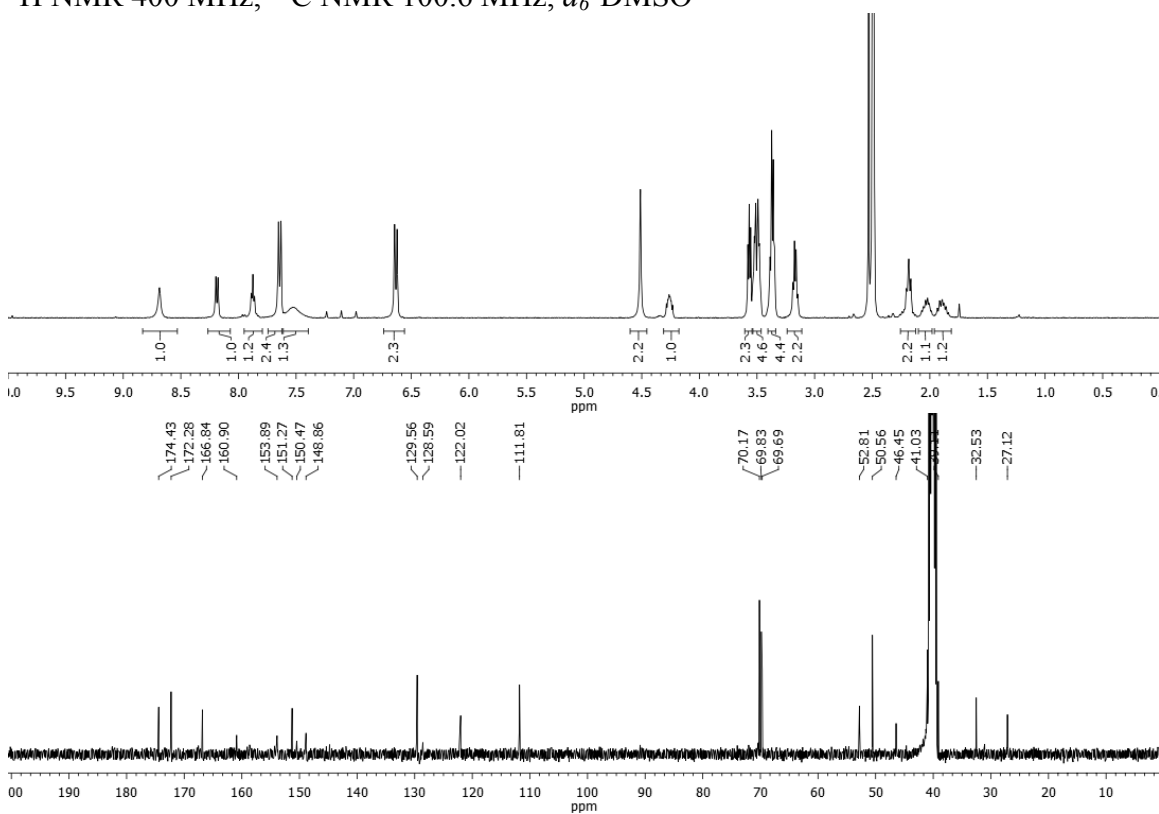
**7.10**

Chemical Formula: C<sub>25</sub>H<sub>31</sub>N<sub>11</sub>O<sub>7</sub>

Exact Mass: 597.2408

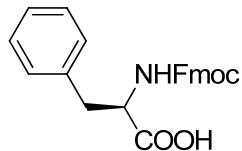
Molecular Weight: 597.5831

<sup>1</sup>H NMR 400 MHz, <sup>13</sup>C NMR 100.6 MHz, *d*<sub>6</sub>-DMSO



## Appendix E.7. NMR spectra for Chapter 8

### Fmoc-D-Phe-OH

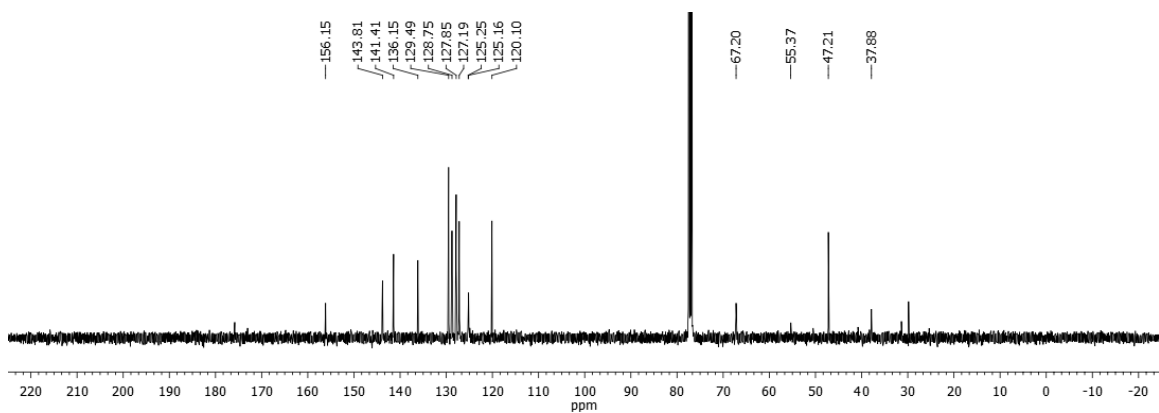
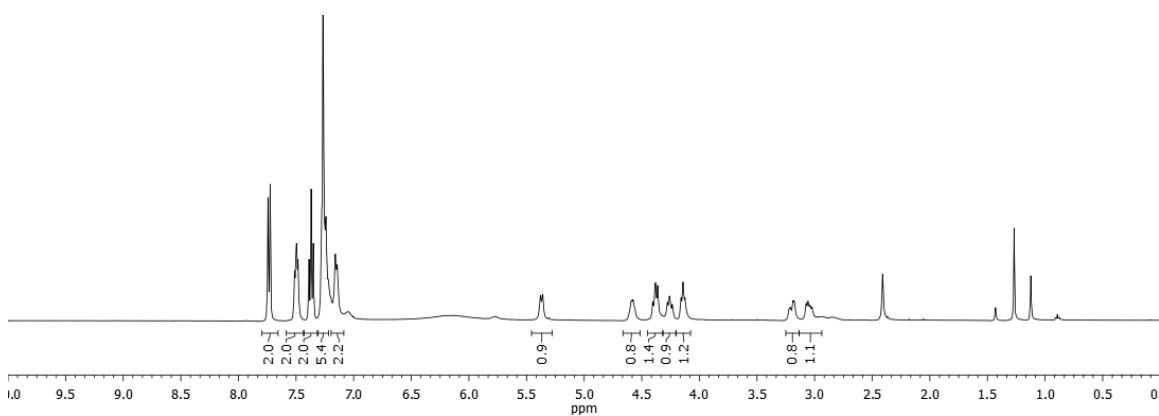


Chemical Formula:  $C_{24}H_{21}NO_4$

Exact Mass: 387.1471

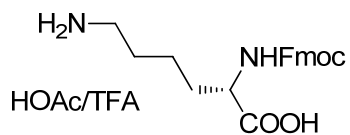
Molecular Weight: 387.4278

$^1H$  NMR 400 MHz,  $^{13}C$  NMR 100.6 MHz,  $CDCl_3$



### Fmoc-(L)-Lys-OH·xTFA/HOAc

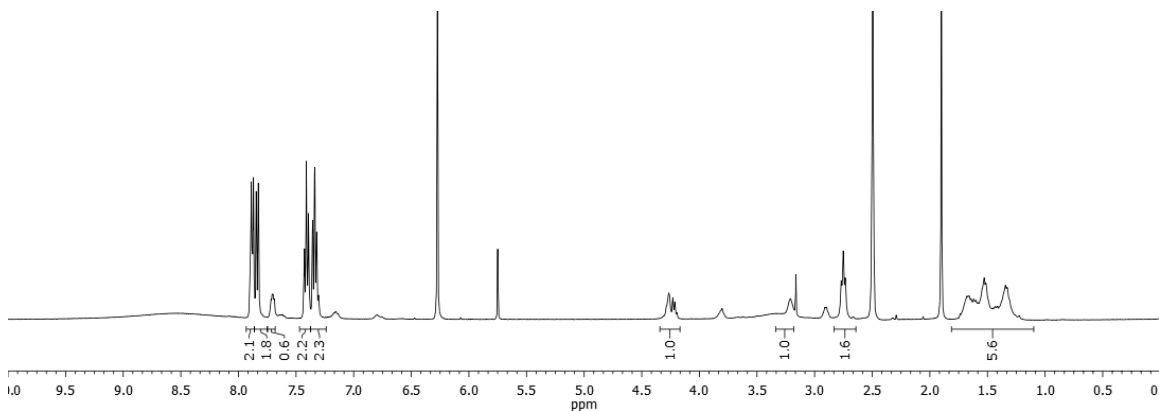
$^1\text{H}$  NMR 400 MHz,  $d_6$ -DMSO



Chemical Formula:  $\text{C}_{21}\text{H}_{24}\text{N}_2\text{O}_4$

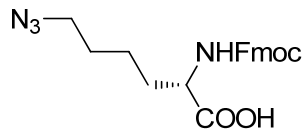
Exact Mass: 368.1736

Molecular Weight: 368.4263



### Fmoc-(L)-Lys(N<sub>3</sub>)-OH

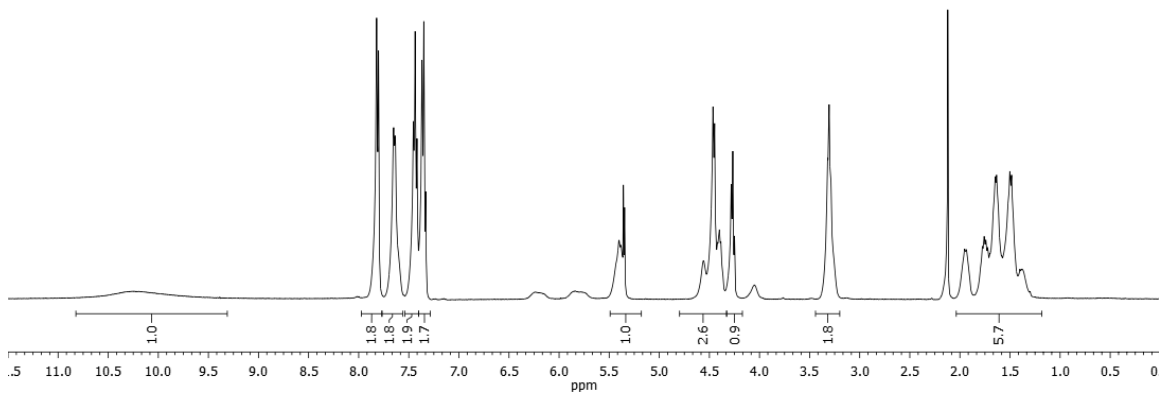
$^1\text{H}$  NMR 400 MHz,  $^{13}\text{C}$  NMR 100.6 MHz,  $\text{CD}_2\text{Cl}_2$

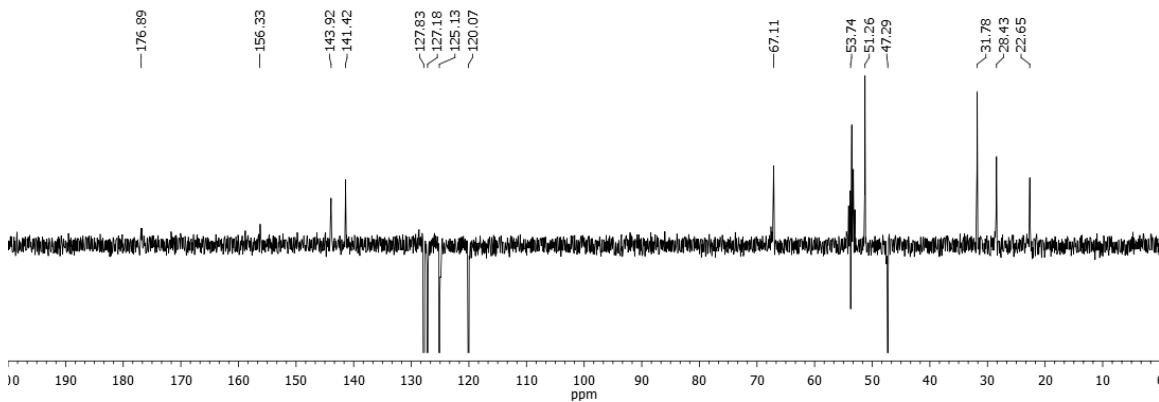


Chemical Formula:  $\text{C}_{21}\text{H}_{22}\text{N}_4\text{O}_4$

Exact Mass: 394.1641

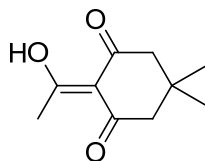
Molecular Weight: 394.4238





### Dde-OH

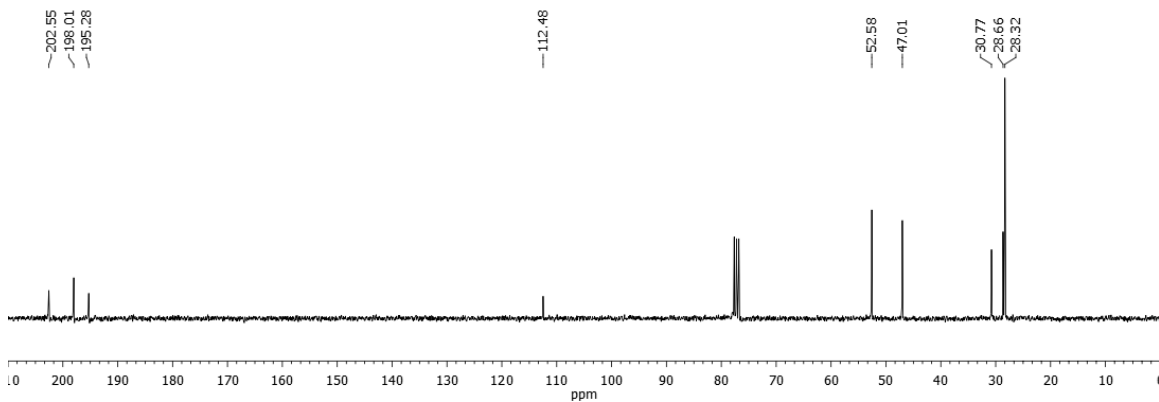
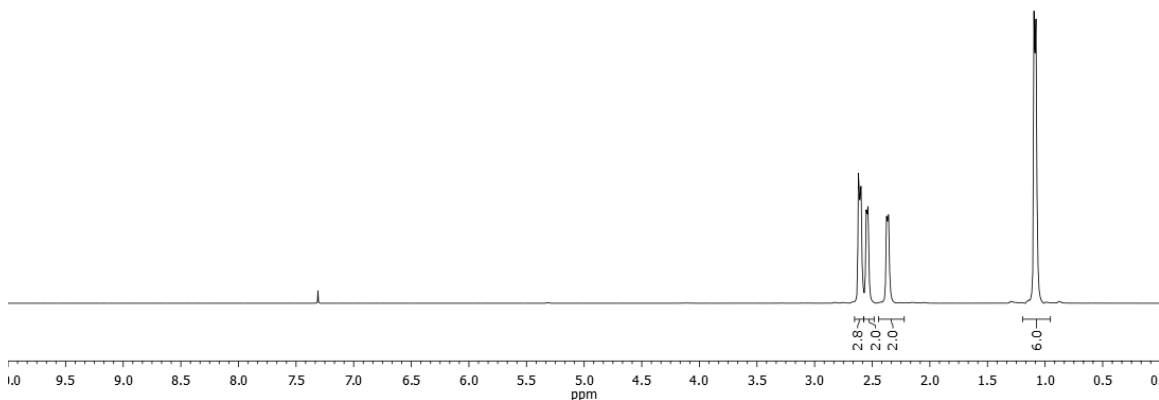
$^1\text{H}$  NMR 300 MHz,  $^{13}\text{C}$  NMR 75.5 MHz,  $\text{CDCl}_3$



Chemical Formula:  $\text{C}_{10}\text{H}_{14}\text{O}_3$

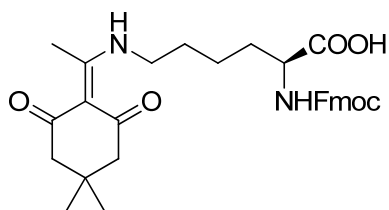
Exact Mass: 182.0943

Molecular Weight: 182.2164



# Fmoc-(L)-Lys(Dde)-OH

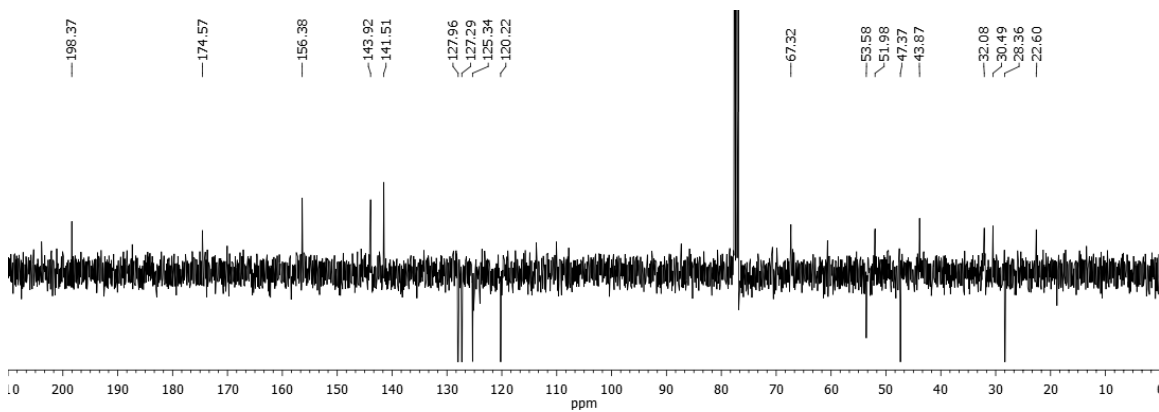
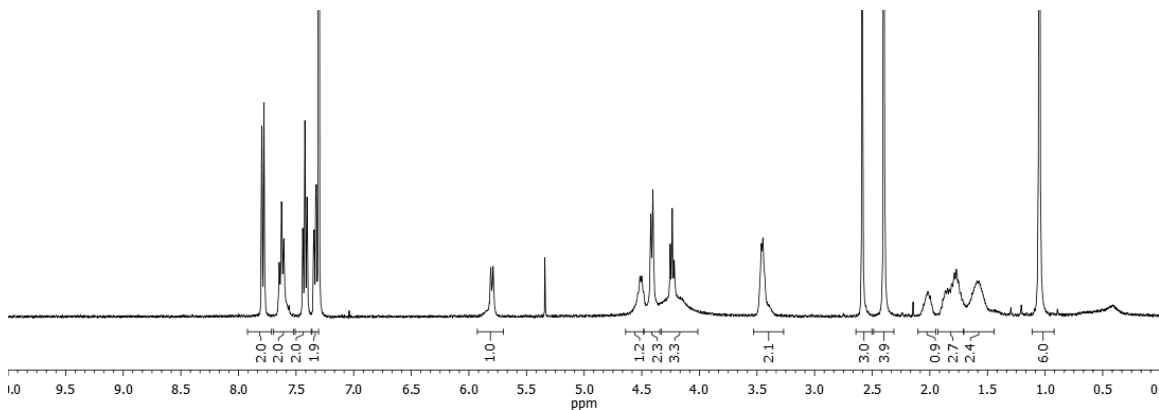
$^1\text{H}$  NMR 400 MHz,  $^{13}\text{C}$  NMR 100.6 MHz,  $\text{CDCl}_3$



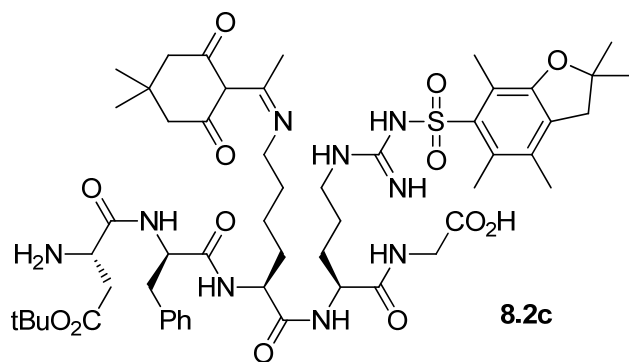
Chemical Formula:  $\text{C}_{31}\text{H}_{36}\text{N}_2\text{O}_6$

Exact Mass: 532.2573

Molecular Weight: 532.6273



### H-Asp(O<sup>t</sup>Bu)-D-Phe-Lys(Dde)-Arg(Pbf)-Gly-OH (8.2c)

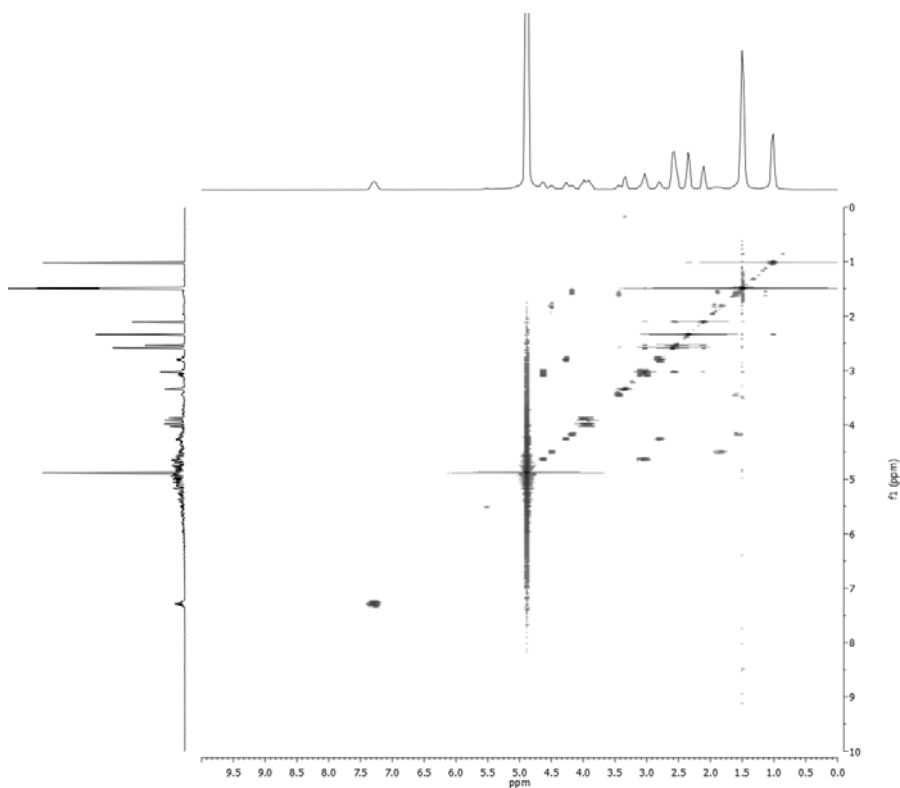
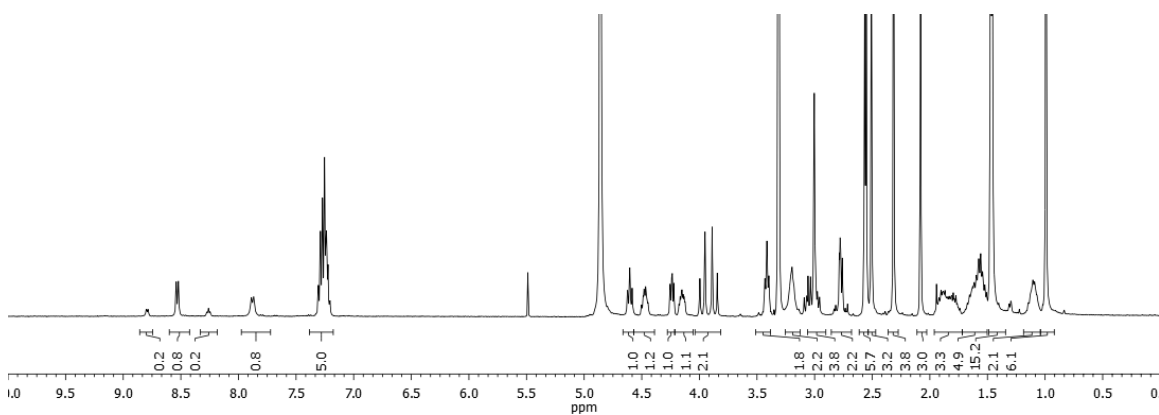


Chemical Formula: C<sub>54</sub>H<sub>79</sub>N<sub>9</sub>O<sub>13</sub>S

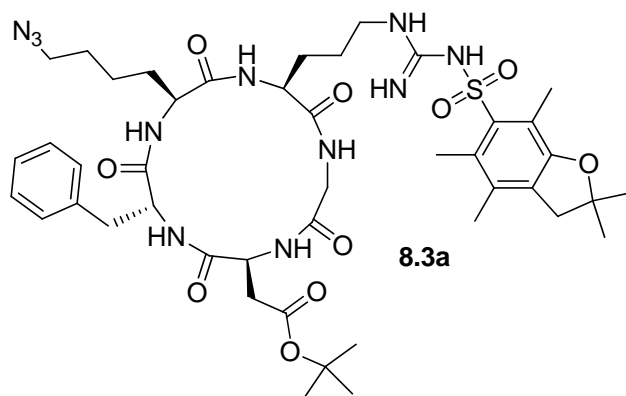
Exact Mass: 1093.5518

Molecular Weight: 1094.3226

<sup>1</sup>H NMR 400 MHz, <sup>1</sup>H-<sup>1</sup>H-COSY, d<sub>4</sub>-MeOD



**Cyclo[Arg(Pbf)-Gly-Asp(O<sup>t</sup>Bu)-D-Phe-Lys(N<sub>3</sub>)] (8.3a)**

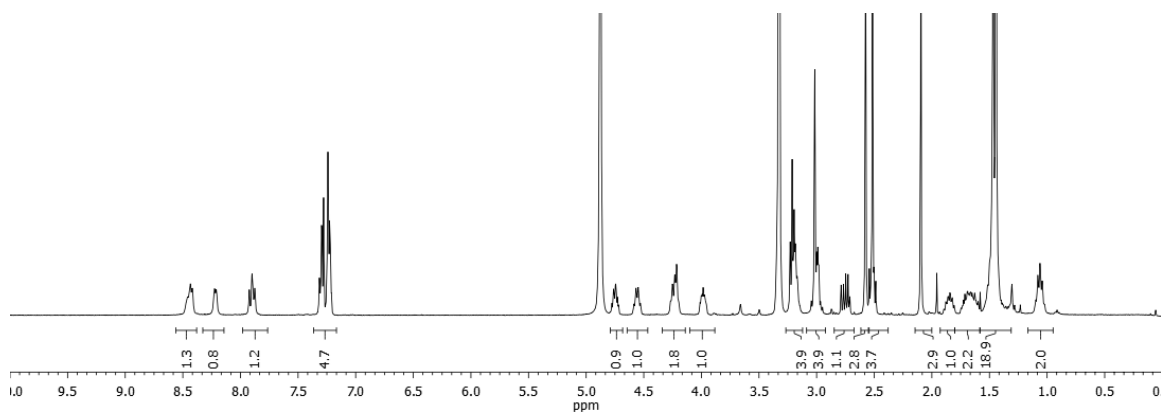


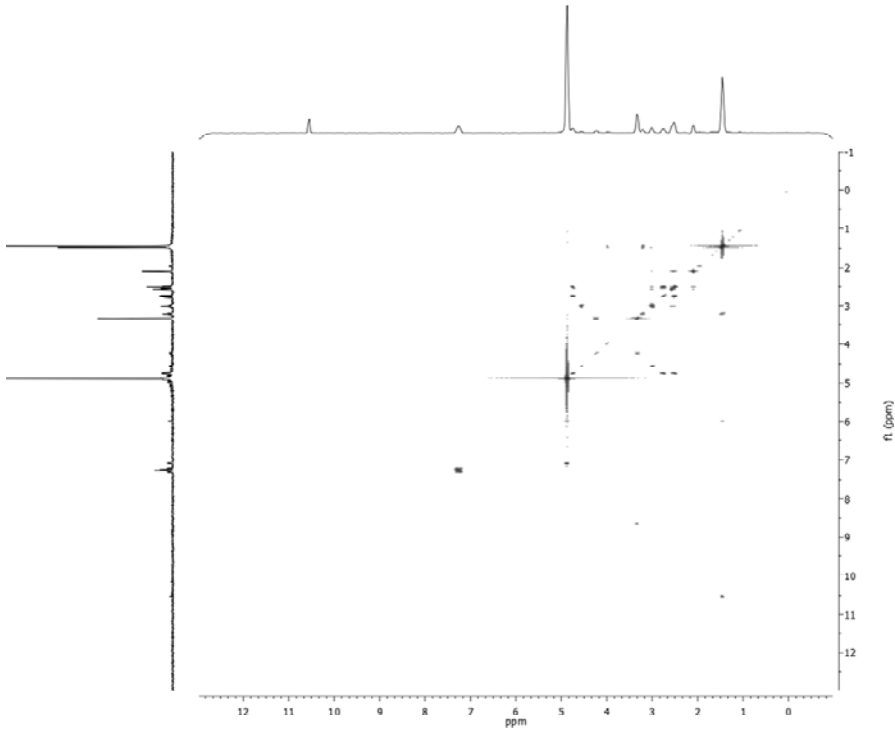
Chemical Formula: C<sub>44</sub>H<sub>63</sub>N<sub>11</sub>O<sub>10</sub>S

Exact Mass: 937.4480

Molecular Weight: 938.1037

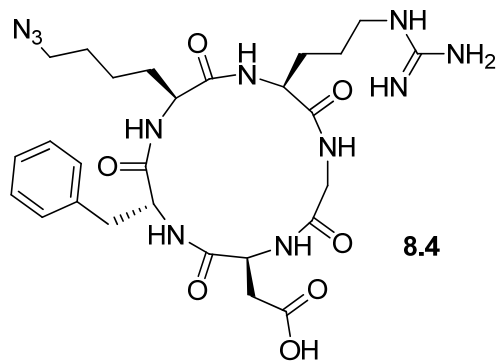
<sup>1</sup>H NMR 400 MHz, <sup>1</sup>H-<sup>1</sup>H-COSY, d<sub>4</sub>-MeOD



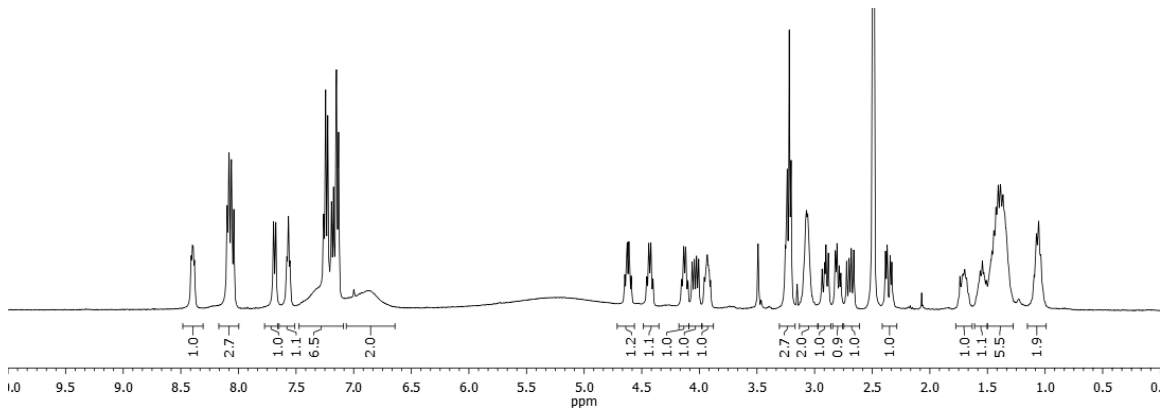


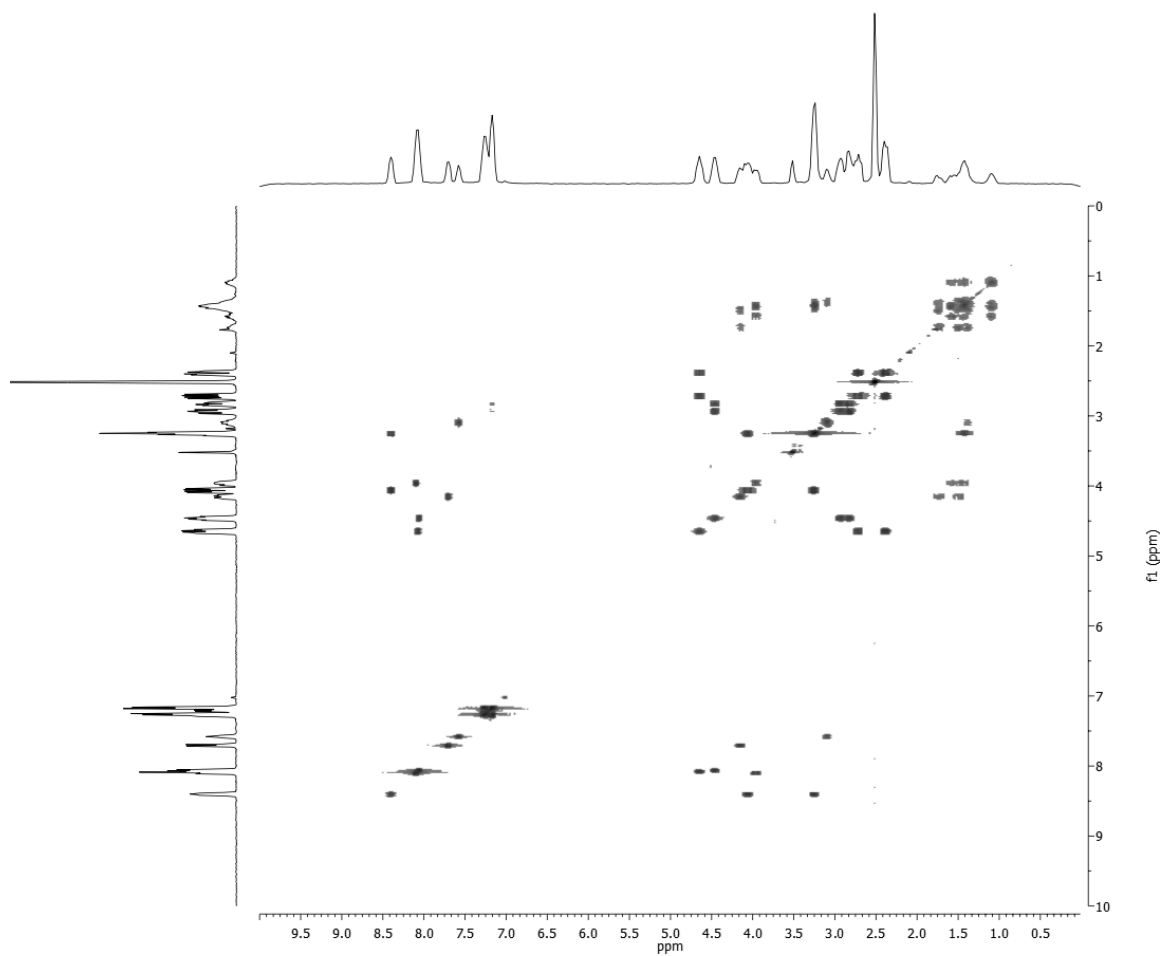
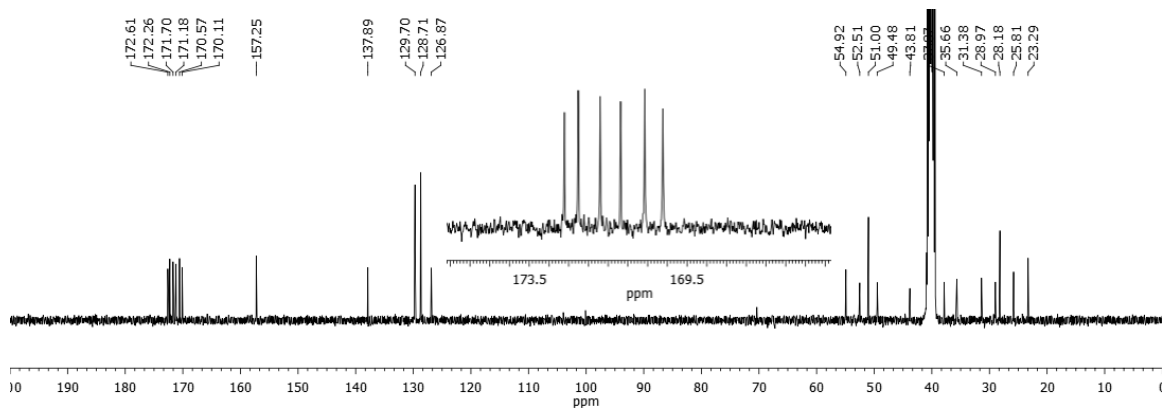
**Cyclo[Arg-Gly-Asp-D-Phe-Lys(N<sub>3</sub>)] (8.4)**

<sup>1</sup>H NMR 400 MHz, <sup>13</sup>C NMR 100.6 MHz, <sup>1</sup>H-<sup>1</sup>H-COSY, *d*<sub>6</sub>-DMSO

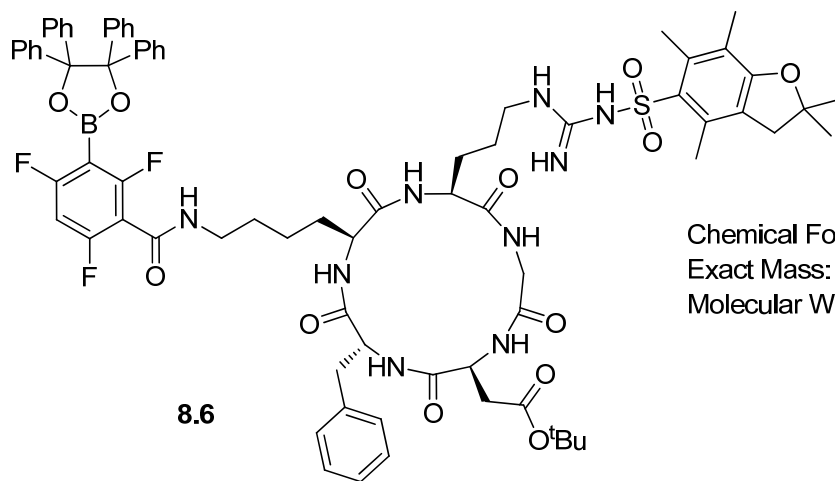


Chemical Formula: C<sub>27</sub>H<sub>39</sub>N<sub>11</sub>O<sub>7</sub>  
Exact Mass: 629.3034  
Molecular Weight: 629.6681



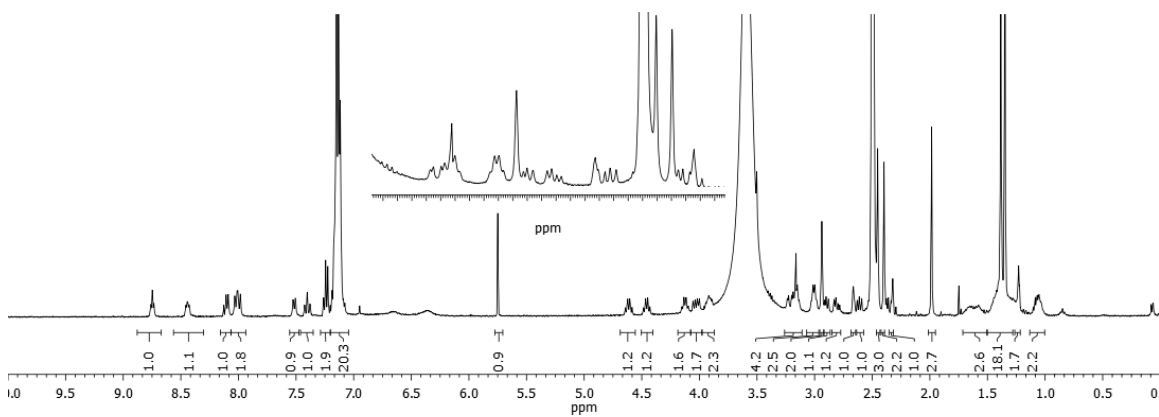
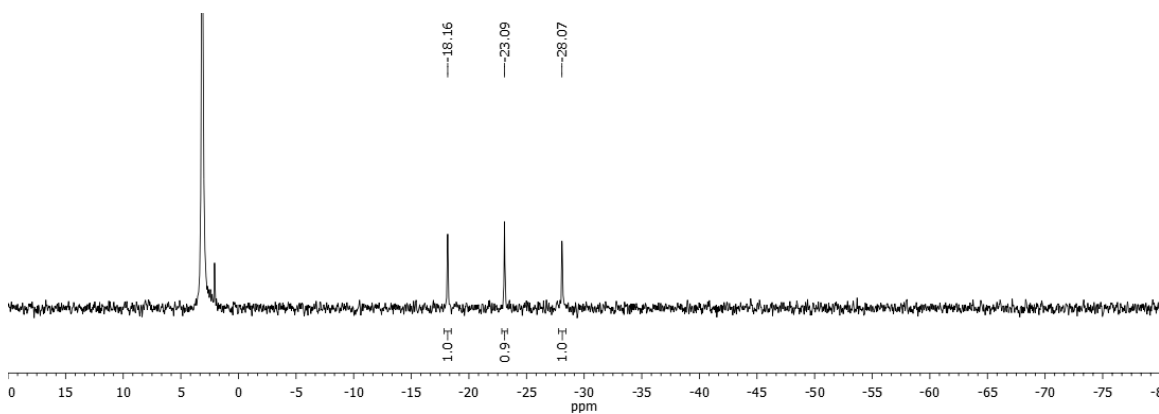


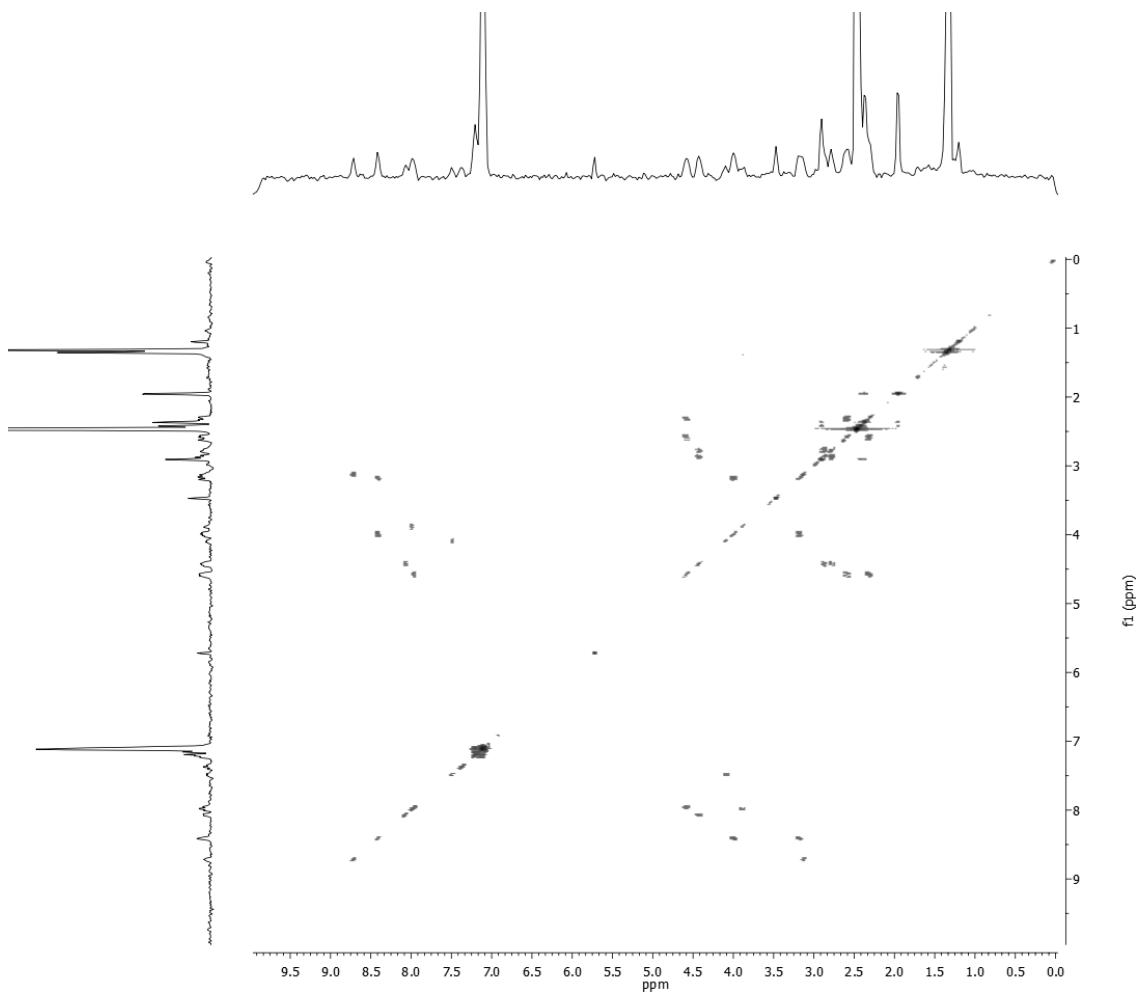
**Cyclo[Arg(Pbf)-Gly-Asp(O<sup>t</sup>Bu)-D-Phe-Lys]-boronate (8.6)**



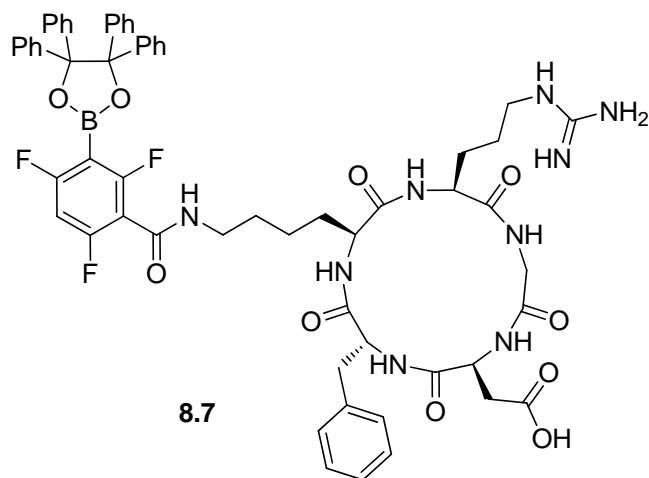
Chemical Formula: C<sub>77</sub>H<sub>85</sub>BF<sub>3</sub>N<sub>9</sub>O<sub>13</sub>S  
 Exact Mass: 1443.6033  
 Molecular Weight: 1444.4225

<sup>19</sup>F NMR 282.4 MHz, <sup>1</sup>H NMR 400 MHz, <sup>13</sup>C NMR 100.6 MHz, *d*<sub>6</sub>-DMSO



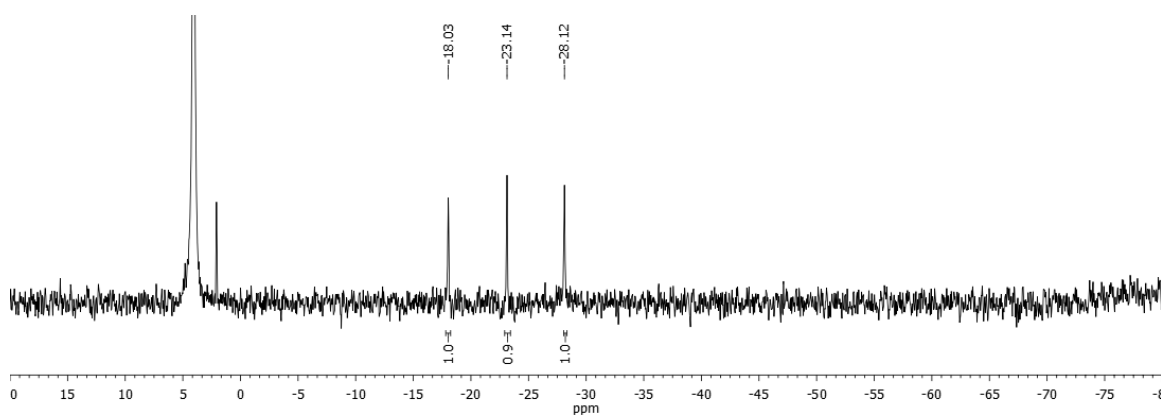


**Cyclo[Arg(Pbf)-Gly-Asp(O<sup>t</sup>Bu)-D-Phe-Lys]-boronate (8.7)**



Chemical Formula: C<sub>60</sub>H<sub>61</sub>BF<sub>3</sub>N<sub>9</sub>O<sub>10</sub>  
Exact Mass: 1135.4587  
Molecular Weight: 1135.9868

<sup>19</sup>F NMR 282.4 MHz, d<sub>6</sub>-DMSO



## *N*-Tritylpiperazine (8.8)



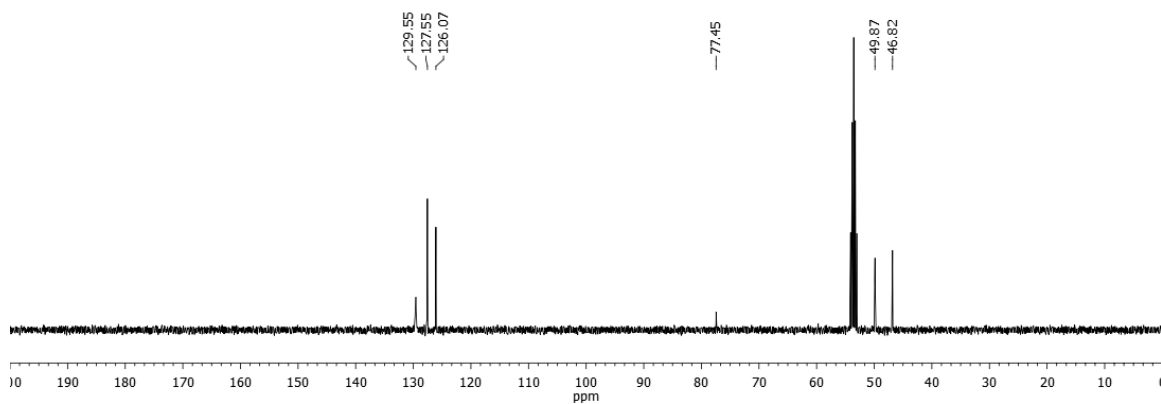
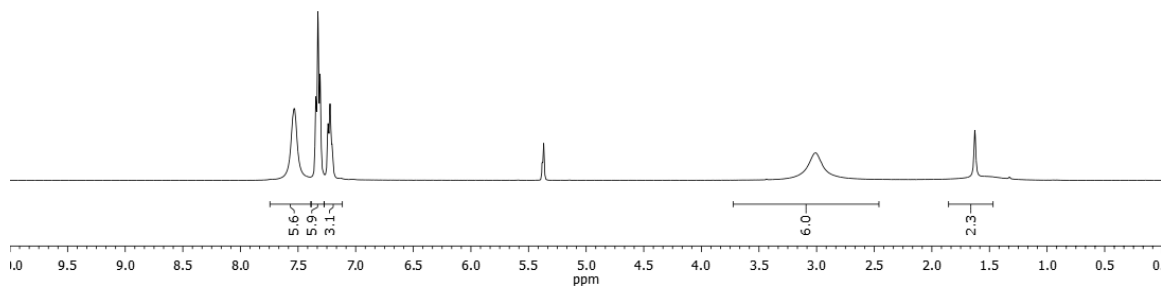
8.8

Chemical Formula: C<sub>23</sub>H<sub>24</sub>N<sub>2</sub>

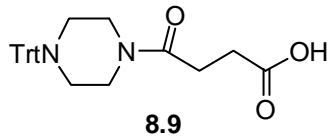
Exact Mass: 328.1939

Molecular Weight: 328.4501

<sup>1</sup>H NMR 400 MHz, <sup>13</sup>C NMR 100.6 MHz, CD<sub>2</sub>Cl<sub>2</sub>



### 4-Oxo-4-(4-tritylpiperazin-1-yl)butanoic acid (8.9)

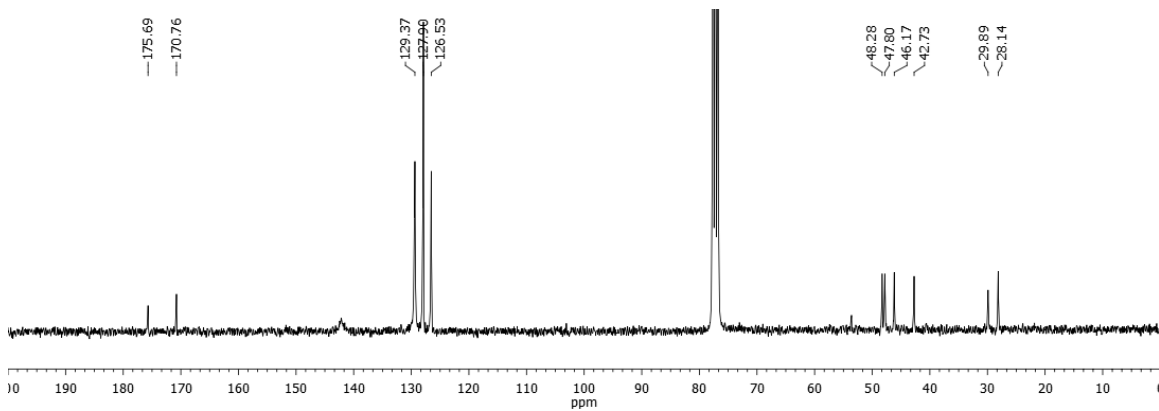
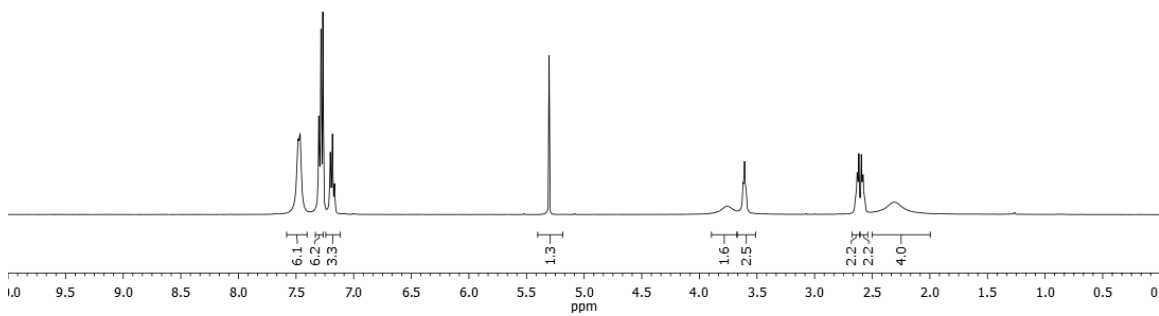


Chemical Formula:  $C_{27}H_{28}N_2O_3$

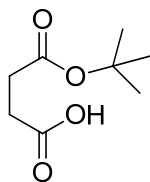
Exact Mass: 428.2100

Molecular Weight: 428.5228

$^1H$  NMR 400 MHz,  $^{13}C$  NMR 75.5 MHz,  $CDCl_3$



## Mono-*tert*-butyl succinate

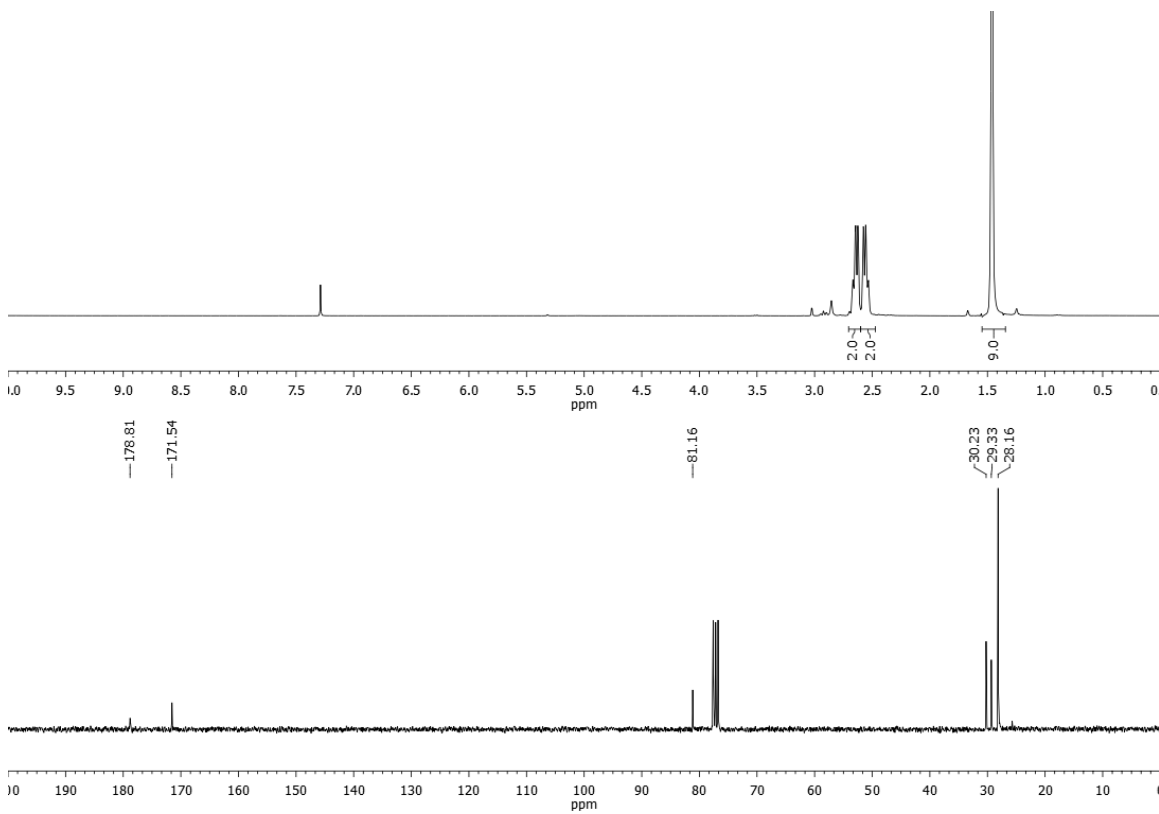


Chemical Formula: C<sub>8</sub>H<sub>14</sub>O<sub>4</sub>

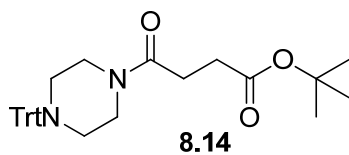
Exact Mass: 174.0892

Molecular Weight: 174.1944

<sup>1</sup>H NMR 300 MHz, <sup>13</sup>C NMR 75.5 MHz, CDCl<sub>3</sub>



**Tert-butyl 4-oxo-4-(4-tritylpiperazin-1-yl)butanoate (8.14)**

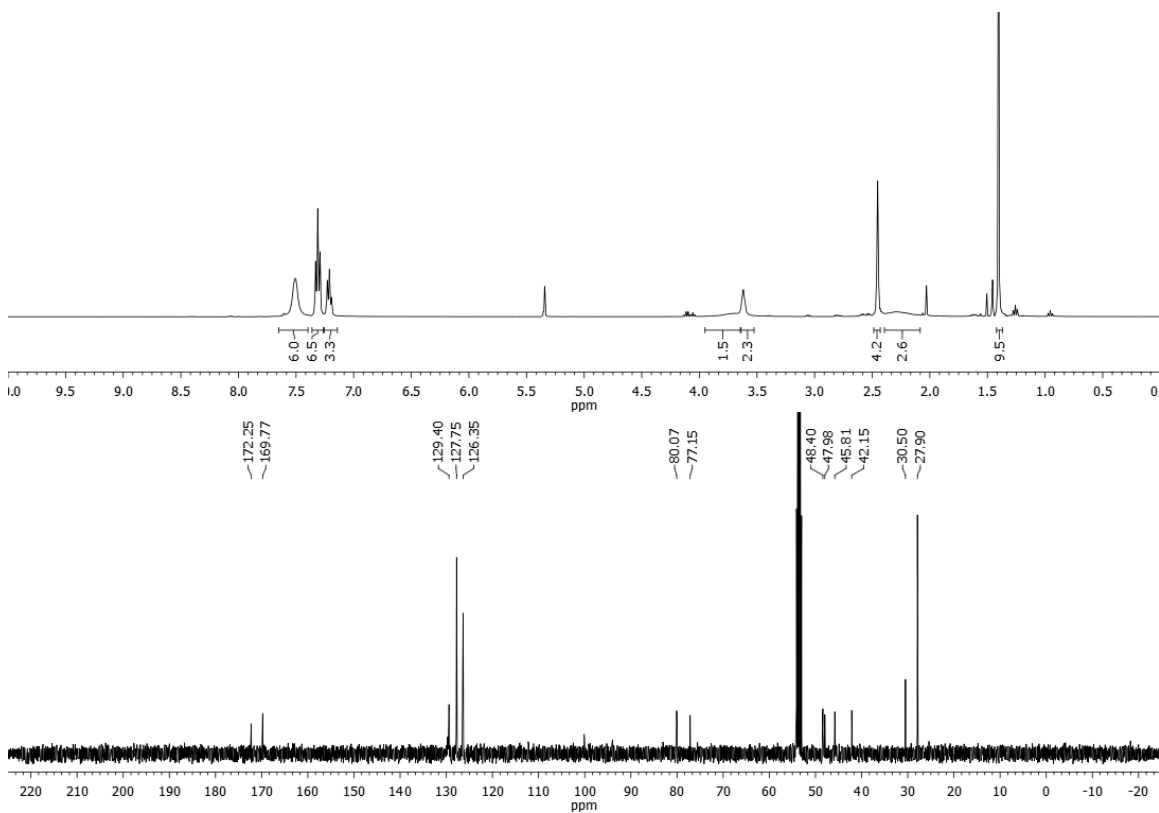


Chemical Formula: C<sub>31</sub>H<sub>36</sub>N<sub>2</sub>O<sub>3</sub>

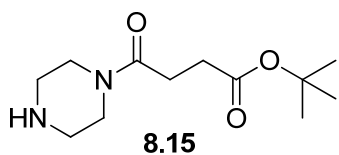
Exact Mass: 484.2726

Molecular Weight: 484.6291

<sup>1</sup>H NMR 400 MHz, <sup>13</sup>C NMR 100.6 MHz, CD<sub>2</sub>Cl<sub>2</sub>



**Tert-butyl 4-oxo-4-(piperazin-1-yl)butanoate (8.15)**

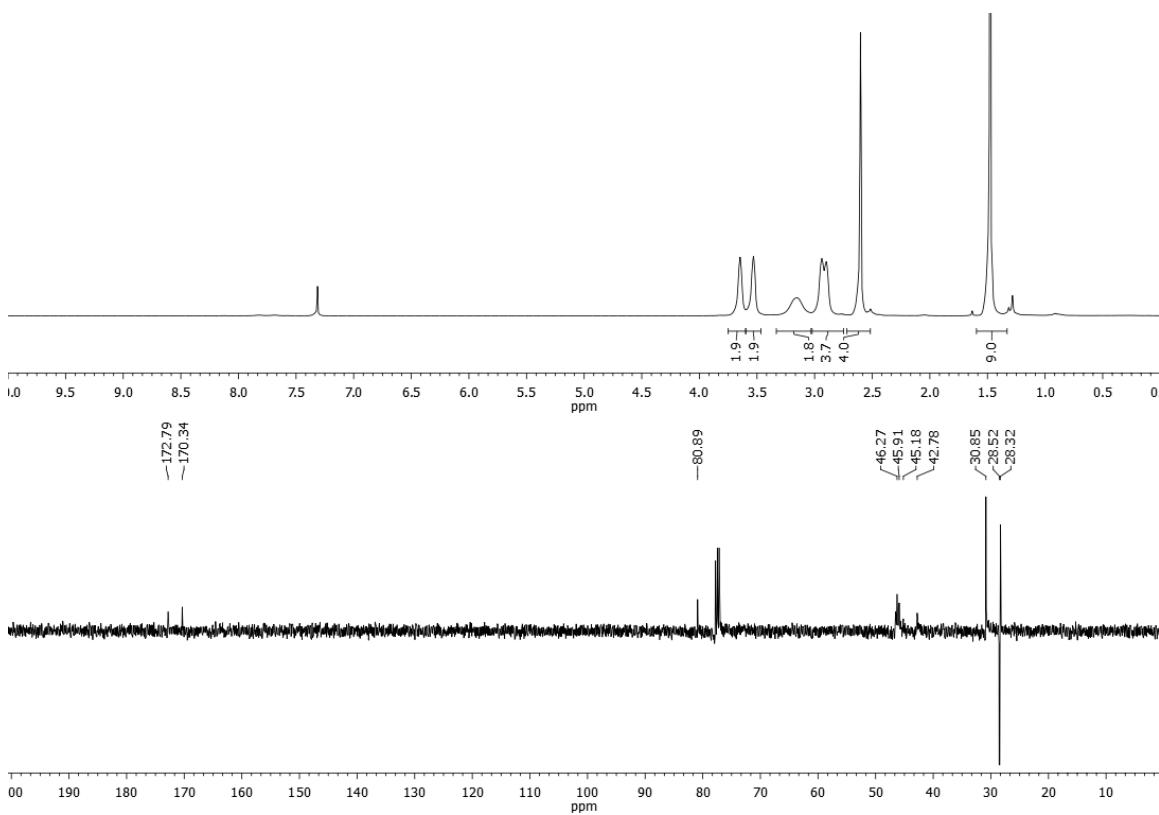


Chemical Formula:  $C_{12}H_{22}N_2O_3$

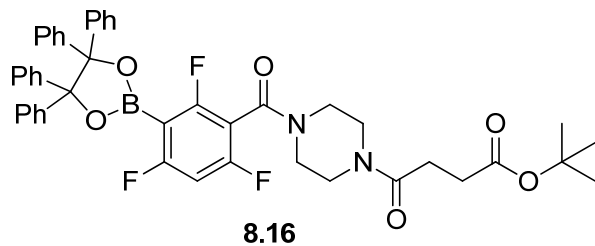
Exact Mass: 242.1630

Molecular Weight: 242.3147

$^1H$  NMR 400 MHz,  $^{13}C$  NMR 100.6 MHz,  $CDCl_3$

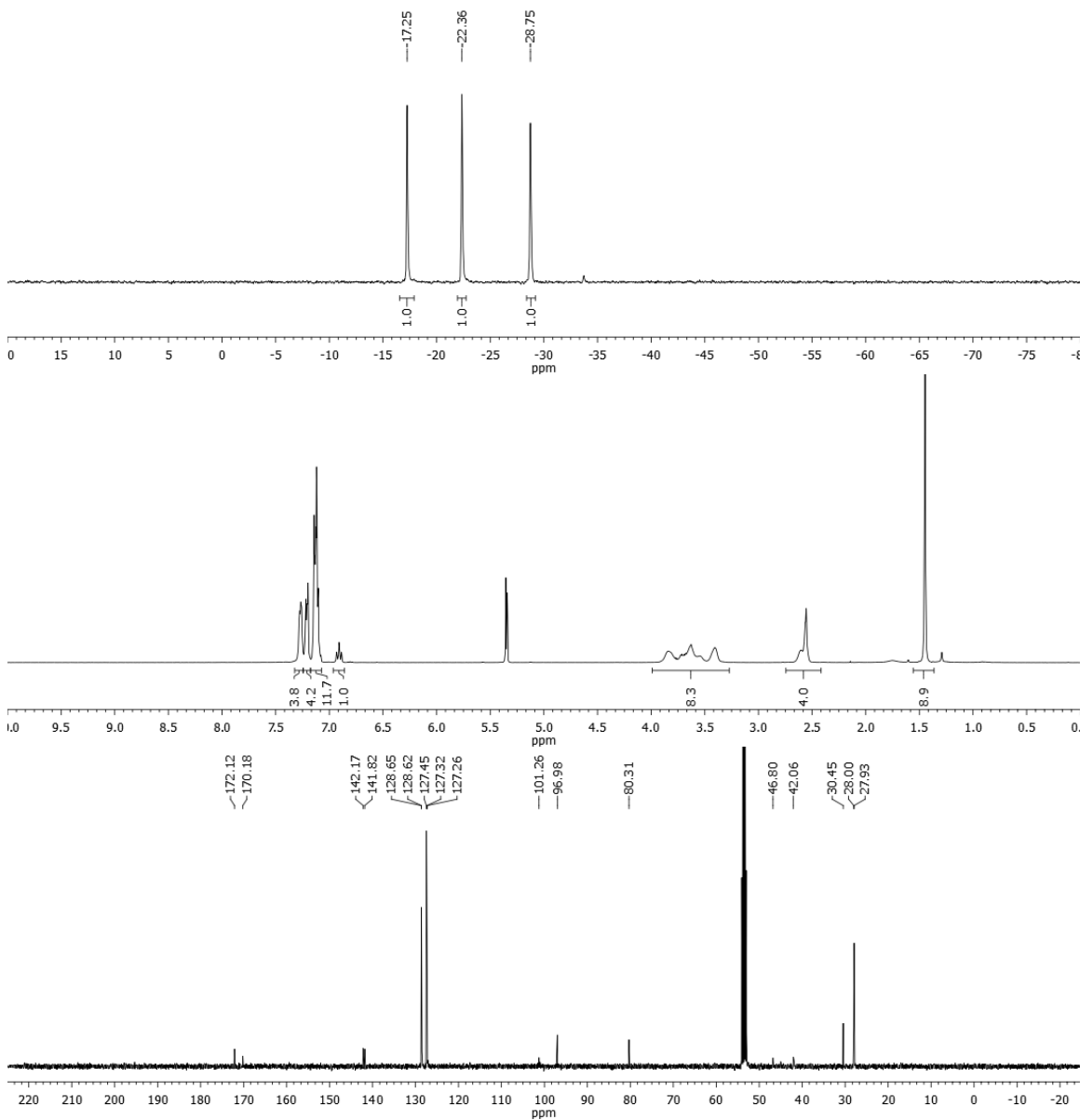


**Tert-butyl 4-oxo-4-(4-(2,4,6-trifluoro-3-(4,4,5,5-tetraphenyl-1,3,2-dioxaborolan-2-yl)benzoyl)piperazin-1-yl)butanoate (8.16)**

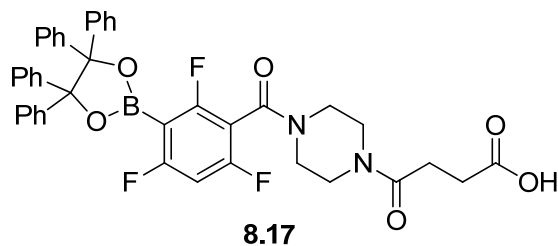


Chemical Formula: C<sub>45</sub>H<sub>42</sub>BF<sub>3</sub>N<sub>2</sub>O<sub>6</sub>  
 Exact Mass: 774.3088  
 Molecular Weight: 774.6310

<sup>19</sup>F NMR 282.4 MHz, <sup>1</sup>H NMR 400 MHz, <sup>13</sup>C NMR 100.6 MHz, CD<sub>2</sub>Cl<sub>2</sub>

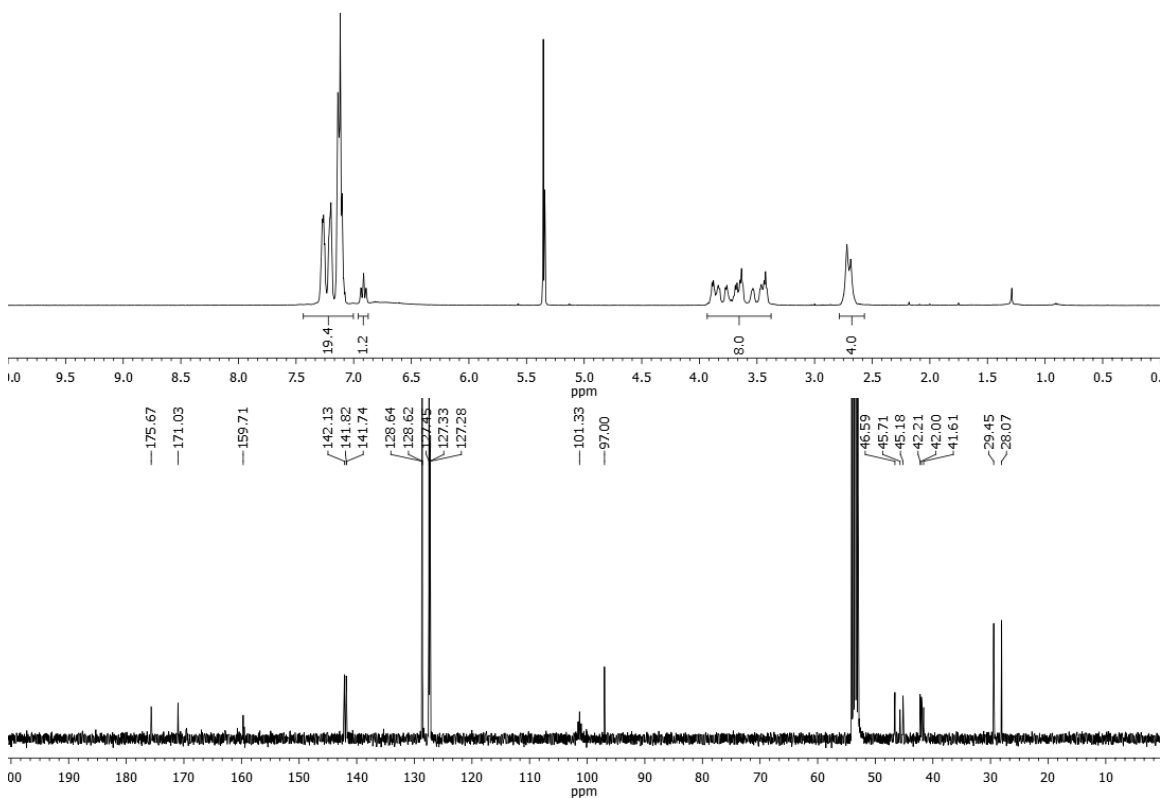
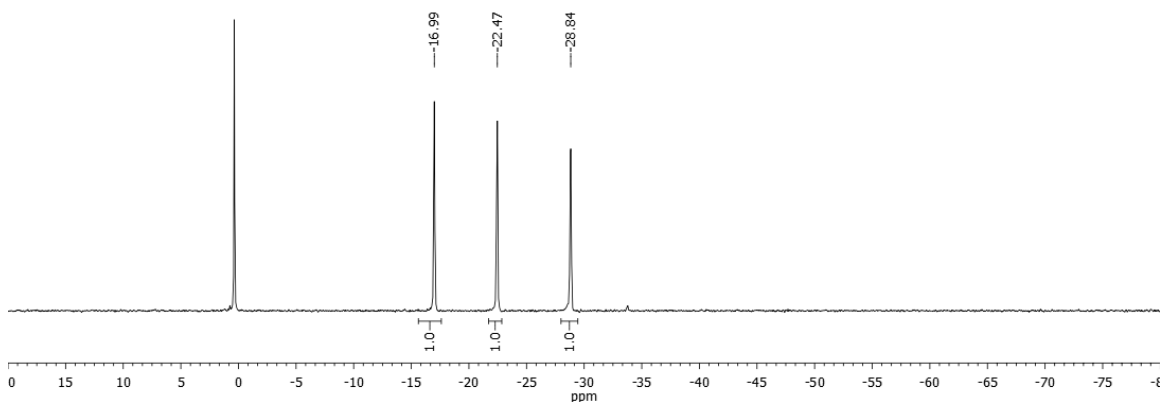


**4-Oxo-4-(4-(2,4,6-trifluoro-3-(4,4,5,5-tetraphenyl-1,3,2-dioxaborolan-2-yl)benzoyl) piperazin-1-yl)butanoic acid (8.17)**

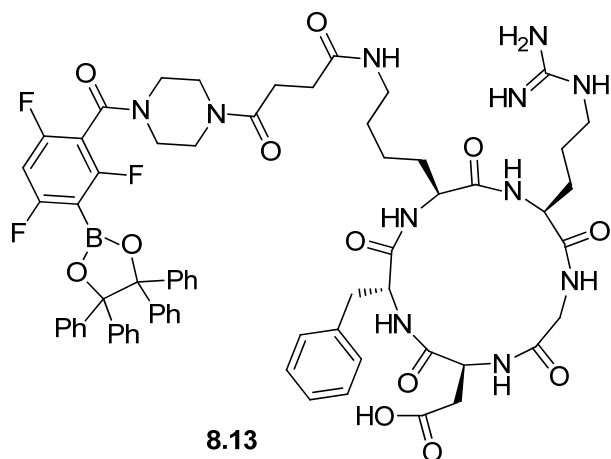


Chemical Formula:  $C_{41}H_{34}BF_3N_2O_6$   
 Exact Mass: 718.2462  
 Molecular Weight: 718.5247

$^{19}F$  NMR 282.4 MHz,  $^1H$  NMR 400 MHz,  $^{13}C$  NMR 100.6 MHz,  $CD_2Cl_2$



**Cyclo[Arg-Gly-Asp-D-Phe-Lys(piperazinyl-boronate)] (8.13)**

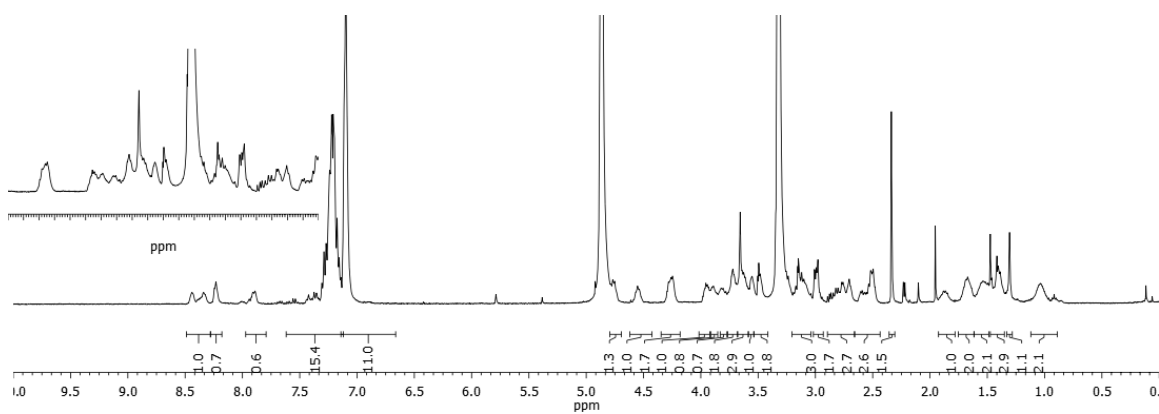
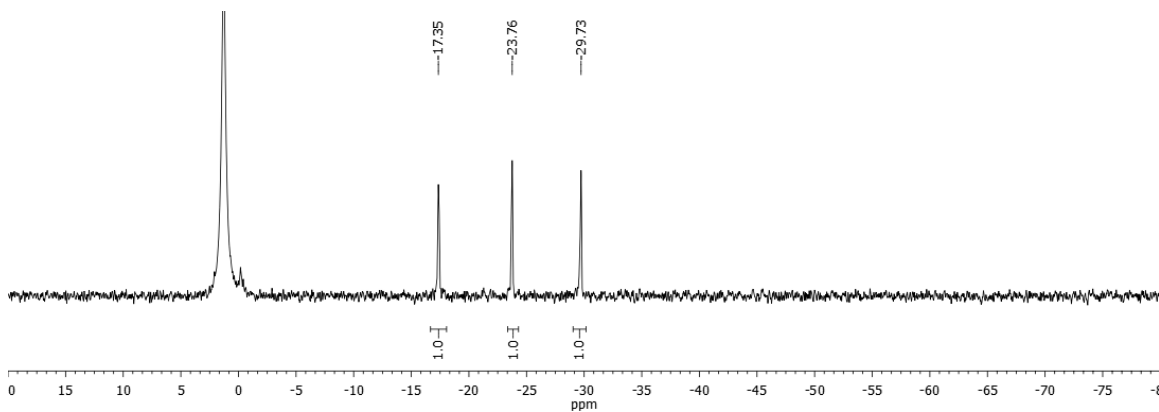


Chemical Formula:  $C_{68}H_{73}BF_3N_{11}O_{12}$

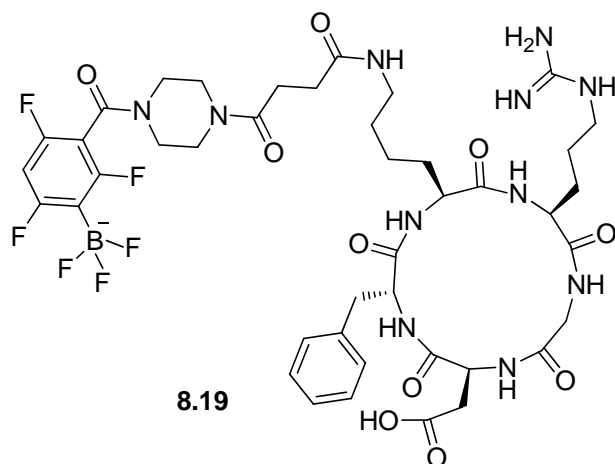
Exact Mass: 1303.5485

Molecular Weight: 1304.1799

$^{19}F$  NMR 282.4 MHz,  $^1H$  NMR 400 MHz,  $^{13}C$  NMR 100.6 MHz,  $d_4$ -MeOD



**Cyclo[Arg-Gly-Asp-D-Phe-Lys(suc-piperazinyl-ArBF<sub>3</sub>)] (8.19)**



**8.19**

Chemical Formula: C<sub>42</sub>H<sub>53</sub>BF<sub>6</sub>N<sub>11</sub>O<sub>10</sub><sup>-</sup>

Exact Mass: 996.3980

Molecular Weight: 996.7399

<sup>19</sup>F NMR 282.4 MHz, d<sub>6</sub>-DMSO

